AEOLIAN DUST EMISSION, TRANSPORT AND DEPOSITION IN WESTERN LIBYA

by

Mokhtar Salem Elatrash

Thesis submitted to the University of Nottingham
for the degree of Doctorate of Philosophy

September 2003

Memory

In memory of my beloved baby daughter Dunia who was born prematurely on the 12th of October 2001 at the City Hospital in Nottingham and died ten days later.

ACKNOWLEDGEMENT

I take this opportunity to offer my sincere gratitude at this privileged site to all the persons who has provided me with their academic assistance and moral support throughout the course of my study. While acknowledging the academic gains from being a research student at the University of Nottingham, I give most credit to my academic supervisors Professor Sarah O'Hara and Dr Michele Clarke who provided me with their unconditional guidance and support. Special thanks to Dr Robert Bryant from the School of Geography at the University of Sheffield for his generous assistance in processing satellite aerosol data needed for this project.

My appreciation also to Graham Morris, the chemist at the Geography chemistry laboratory and David Clift, the Radiation Officer at the School of Mineral and Environmental Engineering at the University of Nottingham for their endless assistance in carrying out the experimental part of this research successfully.

None the less over the last four years I have received much assistance that is impossible to acknowledge it all, and to those I have overlooked my apologies and thanks.

ABSTRACT

Of numerous aeolian studies around the world, few have been dedicated to dust trapping in the Saharan regions and none is known in Libya. This research aims to explore the extent of dust activities in the western part of Libya, the main factors that influence dust entrainment and deposition, the likely regional emission sources transporting aerosol to this part of the country and ultimately to establish base line information in space and time based on a study area larger than the size of the UK. Dust trapping was carried out at thirty sites on a monthly basis starting from the beginning June 2000 until the end of May 2001. A physical characterization of 274 aeolian sediments were based on grain size distribution analysis and the mineral composition was based on XRD testing of 24 dust samples taken from extreme locations near the Mediterranean Sea and about 800 km inland.

An assessment of dust emissions within the area of study, the vertical deposition rates in relation to The Total Ozone Mapping Spectrometer (TOMS) data have been investigated. Moreover, an attempt identify potential Saharan dust emission sources that have impacted the study area has also been made utilizing TOMS data. The area of study has been divided into three regions northern, central and southern according to the dominant factors controlling mobilization of dust particles on the bed surface.

This study concludes that deposition rates in the northern coastal region are largely dominated by human activities. Rates in the central region were strongly affected by topographic irregularities whereas in the south deposition rates were less affected by topography and anthropogenic activity. However, deposition rates and particle size distributions are strongly controlled by wind regimes and correlate with the average atmospheric temperatures. Local sediments seem to be strongly affected by saltating particles in most of the study area and no evidence of long range aerosol emission from western Libya was found. Nevertheless, fine dust (<10 μm) is wide spread in the local atmosphere, however it is more pronounced during late spring and summer. TOMS data and the prevailing wind directions reveal that the depressions of the Libyan Desert and the Bodele Depression in Chad were the main sources of

aerosol transported over the study area during the highest months of emission, transport and deposition, July and April.

It is hoped that this baseline information can pave the way for future studies on dust impacts on soil fertility, human health, desertification, climate change and the validation of present day computer models.

CONTENTS

LIST OF FIGURES

LIST OF TABLES

CHAPTER 1

INTRODUCTION

1.1. INTRODUCTION

In recent years there has been an increasing interest in atmospheric dust, most of which is derived from the arid regions of the world. Due to the arid conditions and poor vegetation cover in these regions, high velocity winds tend to mobilize predominantly silt particles from susceptible surfaces. Human activities such as grazing, ploughing and automobile driving are considered to be causes of destabilising topsoil and making the surface more vulnerable to wind erosion (Middleton and Goudie, 2001). However, recent satellite imagery shows that human impacts are probably much smaller than previously thought (Prospero, et al., 2002). Satellite data show that the largest and most persisting sources of dust on the global scale are natural and located in the northern hemisphere in regions that are essentially uninhabited. These regions are North Africa, Middle East, Central and South Asia and China (Goudie and Middleton, 2001, Middleton and Goudie, 2001, Prospero, et al., 2002).

North Africa has been identified as the strongest and the most persisting source of dust in the world (Prospero, et al., 2002; Middleton and Goudie, 2001). Nearly a half of desert dust deposited in the world's oceans has been derived from the Sahara (Middleton and Goudie, 2001). Saharan aerosols have been linked to changes in soil fertility and erosion, increased rates of morbidity and mortality of humans and marine species and climatic changes through a range of possible mechanisms (Middleton and Goudie, 2001). Because of the long range transport of Saharan aerosols, these implications extend as far as the western regions of the Atlantic such as the Caribbean Sea and the southeastern United States (USGS, 2000).

Despite the fact that the Sahara Desert is recognised as being the world's largest source of aeolian dust, ground data remain very limited and most available information is based on satellite measurements. During the spring months, aerosols transported from the Sahara, northward and northeastward, largely occur along trajectories over Libya. In addition, the Libyan Desert has been identified from satellite imagery as one of the major Saharan sources, which indicates the importance of this region on the world map of dust activity (Prospero, et al., 2002). Therefore, this project has been designed to investigate aeolian dust emission, transport and deposition in the western part of Libya.

The main objective of this project is to qualify and quantify the nature and scale of dust deposition within the study area over a twelve month period and using these data, in combination with satellite derived data, to identify the Saharan sources that relate to deposition in western Libya. Moreover, the project involves an assessment of the physical nature of deposited sediments in the study area within a spatial and temporal frame.

The product of this work is expected to provide a more quantitative description of the actual dust activity on the ground and should prove important in verifying present day numerical ground models.

1.2. AEOLIAN DUST

A commonly used term in literature to indicate wind action is *aeolian* which is a derivative of the word *Aeolus,* the Greek God of winds (Pye and Tsoar, 1990). Dust can be defined as a suspension of solid particles in gas, or a deposit of such particles (Pye, 1987). Therefore, *aeolian dust* can be defined as particles entrained from the Earth's surface, transported in the air and deposited on the surface under the effect of wind action. Dust is composed of particles of matter smaller than 0.07 mm (70 μm) carried in suspension by the wind (Thomas *et al.*, 2000). Wind blown dust falls into two major grain size groups; coarse and fine. Grains larger than 20 μm fall out of suspension as the deriving winds decrease whereas smaller particles can remain in the atmosphere for longer periods of time, days or even weeks, held aloft by turbulent eddies (Pye, 1987). The very fine size grains, smaller than 10 μm, constitute the world's aerosol dust, a type of dust that remains suspended in the air until brought down by rain fall onto the land surface and water (Péwé, 1981).

1.3. SIGNIFICANCE OF AEOLIAN DUST STUDIES

Aeolian dust emission, transport and deposition are topics of considerable interest within the scientific community (e.g. Reheis and Kihl, 1995; Middleton and Goudie, 2001, Augusti *et al.*, 2001) and the effects of aeolian processes are of considerable importance at the global level for several reasons related to agricultural soil fertility, human health and environmental change.

1.3.1. Aeolian dust and soil fertility

On a global scale, transported dust has profound effects on soil fertility and plant growth. On the one hand, soil nutrients transported by dust storms lead to the loss of soil productivity at the source (Larney *et al.*, 1997) while on the other hand, transported nutrients may serve as a renewal factor by upgrading the topsoil where dust is deposited (Simonson, 1995; Ramsperger *et al.*, 1998; Reynolds *et al.*, 2001). Wind erosion physically removes the lighter constituents of the topsoil (organic matter, clays, and silts), thus removing the most fertile part of the soil and impairing the productive capacity of the land (USDA and ARS, 2000). One third of soil erosion is attributed to wind action (World Resources Institute, 2001), and topsoil loss has been reported from different parts of the world (e.g. Larney, *et al.* 1995). The removal and destruction of the vegetation cover in the Sahel region, for example, has resulted in the breakdown of soil organic matter and thus soil structure is lost enabling even gentle winds to remove those fine particles of soil that are essential to soil fertility (MacLeod, 1998).

1.3.2. Aeolian dust implications on human health

The impact of airborne dust on the human population has been investigated in different parts of the world and numerous studies have highlighted the potential implications of inhaled dust particles on human health. Inhaled aeolian particles of less than 10 μm have been related to an increase in the rates of human morbidity and mortality (Pye, 1987). Several respiratory, allergic, cardiovascular and skin infection illnesses are attributed to fine aeolian dust inhalation (e.g. Leather, 1981; Richards *et al.*, 1993; Pop, 1996; Corbett, 1996; Rubio *et al.*, 1998). Inhaled dust particles of larger than 10-15 μm are trapped by cilia and mucus in the upper respiratory tract, however, particles smaller than 10 μm have a higher chance of being inhaled and reaching the lower respiratory tract. Lung damage caused by inhaled dust is of two types. The first is the scarring of alveolar walls (fibrosis) and the second is the distension of the alveoli resulting in formation of large spaces and disruption of the alveoli walls (emphysema) (Pye, 1987).

An area of current concern is the transport of heavy metals within fine dust (USGS, 2000; Krolak, 2000). African dust particles of sizes of the order of one micrometer collected during an extraordinary dust event on 26th of February, 2000 along the western Atlantic Ocean region (Figure 1.1) were found to contain 2 parts per million of the element mercury, which is many times greater than normal concentration in the air. The mercury component in the dust is believed to have originated from Algerian Mercury mines. Furthermore, the North African and the Sahel countries are believed to apply excessive amounts of pesticides such as those banned in the USA (USGS, 2000).

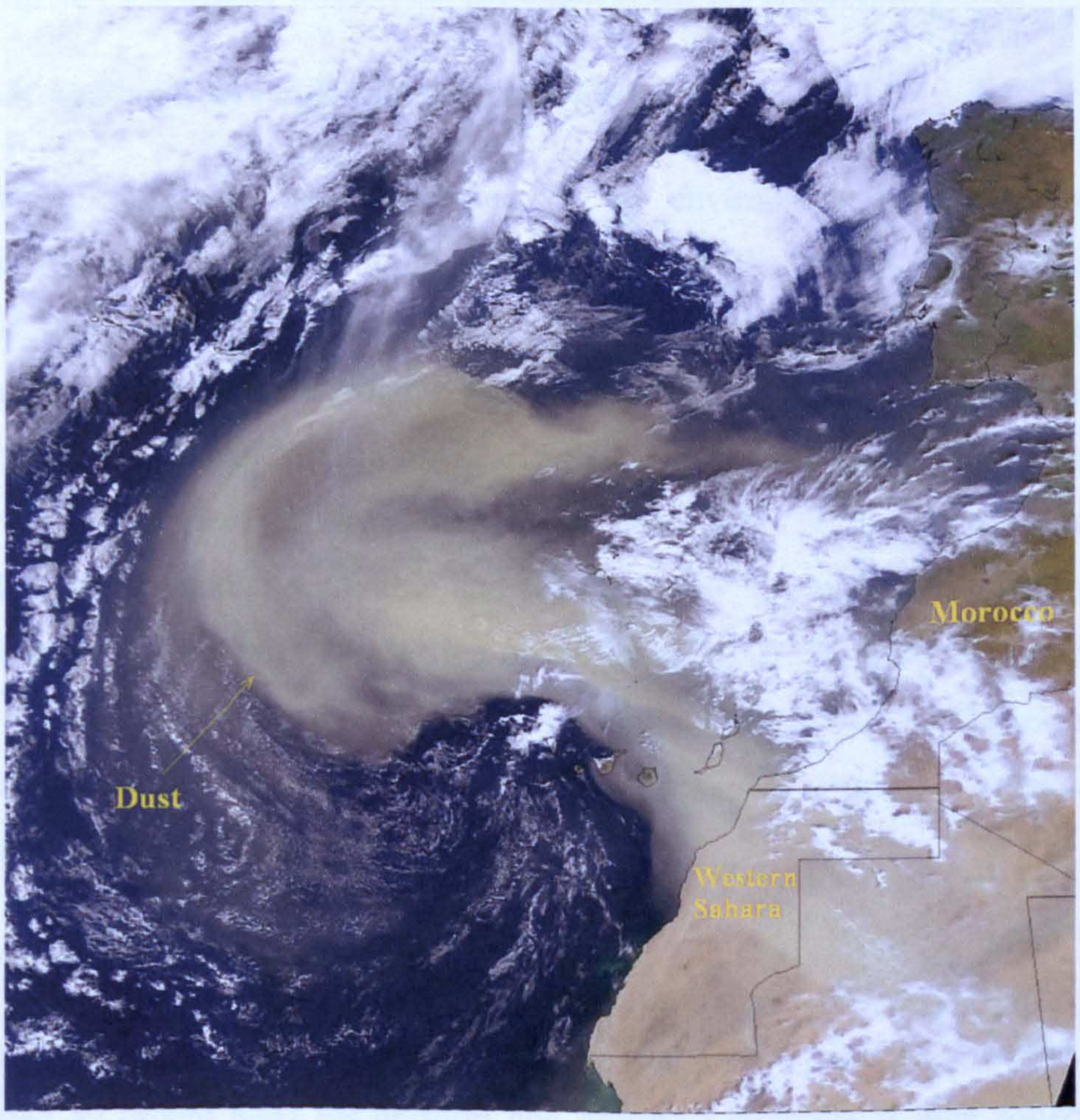

Figure 1.1 A Saharan dust storm over the Atlantic on 26 of February 2000 acquired by NASA/Goddard Spaceflight Center's SeaWiFS Project and ORBIMAGE (*from* USGS 2002)

A joint study sponsored by the USGS and NASA concluded that North African dust reaching the western Atlantic Ocean region is responsible for increasing

the occurrence of asthma in the Caribbean region, especially in Puerto Rico and Trinidad, as hundreds of viable microorganisms in each gram of dust make and survive their journey across the Atlantic, protected within the particles or shielded by overlaying dust clouds (USGS, 2000). African dust samples collected in St. John's in the U.S. Virgin Islands on dusty and clear days, as indicated by satellite images, all contained microbes. But, samples taken on dusty days contained nearly 9 times as many bacteria and at least 10 times as many viruses as did those taken on clear days (Raloff, 2001). The extent of health effects of dust depends on the nature of dust sources and it involves a spatial and a temporal component (Milligan et al., 1998; Corbett, 1996).

1.3.3. Aeolian dust implications on marine life

Airborne dust has been identified as an environmental hazard and a contributory cause of environmental changes. North African dust outbreaks have been blamed for increased amphibian diseases and increased coral mortality in the western Atlantic region. USGS scientists have monitored the Caribbean coral reef vitality for nearly four decades have noticed that corals have been in decline since the 1970s. Moreover, other marine species, including the grazing sea urchin and sea fans, have experienced a widespread demise coinciding with the decline of the coral population. Recent studies at the University of South Carolina have linked the death of the Caribbean corals to several species of soil fungus, *Aspergillus*, which were found in African dust samples collected in the region (USGS, 2000).

1.3.4. Soil erosion by wind

The interrelation between soil erosion by wind and dryland degradation has created an urgent need for uniform and objective methods of data collection relating to the characteristics and status of soils and for the evaluation of such data on an integrated basis. An extensive international monitoring network to collect baseline data relevant to all aspects of desertification is also needed (Williams, 2001). As yet, our understanding of the magnitude and frequency of wind erosion in drylands is still very patchy and, for some regions, is deficient (Williams, 2001). Progressive degradation of vegetative cover especially in

arid and semi arid regions of the world has resulted in climatic impacts. These impacts include increased albedo leading to decreased precipitation, which in turn results in impoverished vegetative cover and increased dust entrainment (Carbon Dioxide Information Analysis Centre, 1990).

Until recently, scientists had believed that airborne dust was a result of reduced rainfall. Recent research carried out at the Hebrew University and the Weizmann Institute in Israel, however, has indicated that airborne dust would be a cause rather than a result of decreased rainfall. Prior to this finding, scientists believed that large airborne dust particles would enhance the formation of rain by forming large cloud condensation nuclei and large cloud droplets, whereas (NASA, 2001) has shown that when a lot of dust enters a cloud it causes water to be spread into many small droplets and as such increases evaporation. Therefore, when more dust penetrates rain clouds less rainfall is produced, thereby exacerbating drought and contributing to the desertification of the landscape (NASA, 2001; Perkins, 2001).

1.3.5. Dust clouds and climatic change

Aerosols effect both solar and thermal radiation. Since solar radiation has wavelengths ranging from 0 to ~ 4 μm and most aerosol particles are < 4 μm, aerosol particles tend to scatter radiation most efficiently at wavelengths near their sizes, therefore most radiation scattering by dust clouds falls within the solar spectrum. Thermal radiation, on the other hand, is emitted from the surface of the earth and has wavelengths within 4-20 μm that can be absorbed by aerosol particles of > 2 μm, such as sea salt (Penner *et al.*, 2001). By scattering and absorbing incoming solar and outgoing infrared radiation, airborne dust particles can alter the Earth's radiative balance. The extent of this influence varies according to the chemical composition and particle size distribution of dust that tends to modify short wave and long wave solar radiation (Arimoto, 2001; Goudie and Middleton, 2001, Harrison *et al.*, 2001).

Atmospheric dust has been linked to the reduction of Earth's surface warming by intercepting sunlight intended for the surface causing the same effect as rain clouds. While solar radiation is reduced beneath the dust cloud, the absorption

of sunlight by dust particles raises the temperature of the cloud itself. The dust cloud therefore displaces heating from the earth's surface into the atmosphere. The displacement of solar heating away from the surface by dust aerosols changes the earth's climate. It has been reported that temperatures at the surface beneath dust cloud are typically reduced by 1°C (Miller and Tegen, 2003). However, in some regions, the atmosphere adjusts to this cooling by transporting heat from surrounding warmer regions and restoring the temperature to its original value (Miller and Tegen, 2003). An example of this phenomenon occurs over the Arabian Sea, where the temperature remains unchanged under the dust cloud, despite the large reduction in surface radiation. Further downwind the dust cloud originated in the Arabian Peninsula, a vast region extending from northern Asia to the Pacific and North America experiences cooling. Such cooling is attributed to the atmospheric circulation that connects regions beneath the dust cloud to regions downwind. Furthermore, the winds that extend this cooling to regions far beyond the dust cloud can also transport warm air beneath the cloud itself, thus offsetting the effect of diminished sunlight. It is believed that dust can provide an adverse action to global warming which is attributed to increasing greenhouse gases, such as CO_2 (Miller and Tegen, 2003).

1.4. DUST PRODUCTION

1.4.1. Sources of atmospheric dust

Atmospheric dust is attributed to several sources such as cosmic dust, volcanic ash, industrial emissions, fire smoke, sea salt, gas to particulate conversion and deflated sediments and soils (Pye, 1987). These sources contribute various quantities of dust to the atmosphere. Disintegrated meteorites in the outer space enter the Earth's atmosphere to supply the planet with an estimated amount of 0.02-0.2 $\times 10^6$ t/yr (Hidy and Brock, 1971). These particles are black magnetic spherules within 2-60 μm size range (Handy and Davidson, 1953). Volcanic eruptions inputs range from 4 to 25×10^6 t/yr (Hidy and Brock, 1971) and dust or ash clouds travel around the globe before settling out on land. Emissions from industrial installations, waste dumps and mines contribute an estimated amount of 38-112$\times 10^6$ t/yr (Hidy and Brock, 1971). Fire generates organic and

inorganic dust, estimated to be 148×10^6 t/yr (Hidy and Brock, 1971). Sea salt particles in the atmosphere are a result of wave breaking and bubble bursting in the oceans (Heathershaw, 1974; Fairall et al., 1983). The total estimated production of sea salts ranges from 508 to 1113×10^6 t/yr (Peterson and Junge, 1971; Hidy and Brock, 1971). Conversion of gases such as SO_2 and NO_x produce particles smaller than 1μm (Fennelly, 1976). An estimated production of converted industrial gases reaches 284×10^6 t/yr and of converted natural gases ranges from 478 to 2113×10^6 t/yr (Peterson and Junge, 1971). Deflated sediments and soils of the Earth's surface represent the main source of atmospheric dust and constitute an estimated amount of up 5000×10^6 t/yr (Schütz, 1980).

1.4.2. Contemporary global aeolian dust production

1.4.2.1. Global aeolian dust sources

Regions where most aeolian dust originates from eroded sediments are predominantly arid and semi-arid lands. These include the major deserts of the world shown in Figure 1.2 (Pye, 1987; Péwé, 1981; Livingstone and Warren, 1996).

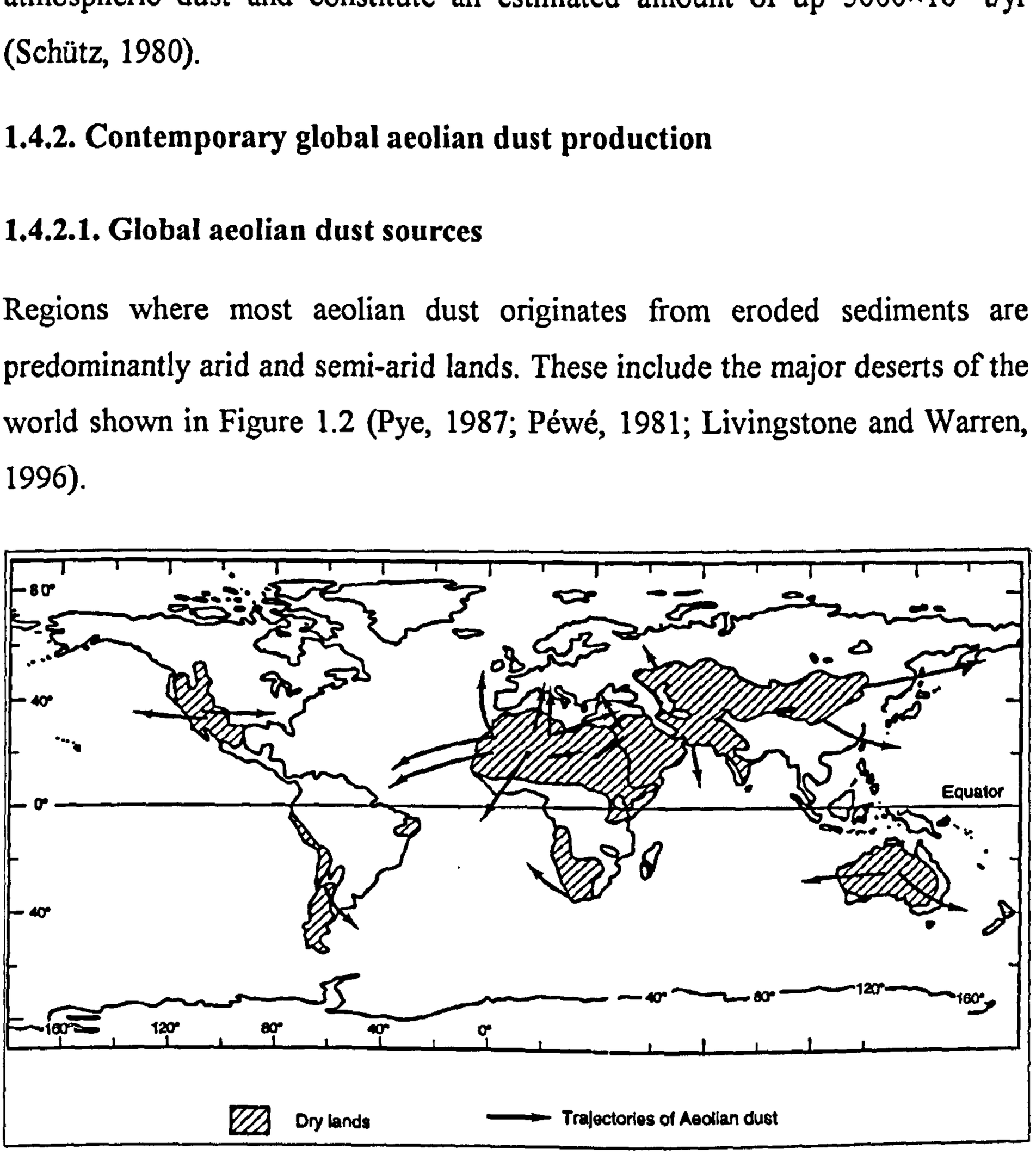

Figure 1.2 World major aeolian dust sources and trajectories (*from* Livingstone and Warren 1996)

Most dust is transported hundreds of kilometres, although much of the fine dust can travel thousands of kilometres (Péwé, 1981). The major sources are central Australia, north and western China, central Asia, the lower Volga and North Caucasus, the Arabian Peninsula, north western Sudan, the Sahara, the semi-arid coastal region of the Mediterranean, the Kalahari of south west Africa, the US Great Plains, the American south west, the dry regions of Argentina, Chile and Peru (Péwé, 1981).

Attempts to assess the amounts of produced dust have been numerous. An estimate of total world dust reaches 5000 million tonnes per year of which 300 million tonnes come from the Sahara (Schütz, 1980). An estimated total transport from the Sahara varies between 600×10^6 and 700×10^6 t/yr with 190×10^6 t/yr travelling across the Atlantic and an estimate between 7.6×10^6 and 10×10^6 t/yr is transported to Europe (D'Almeida, 1986; Livingstone and Warren, 1996). An estimated 25×10^6 t/yr are transported from the Sahara to Israel (Yaalon and Ganor, 1979).

Experimental studies have concluded that the nature of the land surface determines the susceptibility to dust entrainment, but a high clay and silt content does not ensure large-scale dust entrainment. Some of these studies included a deployment of wind tunnels to determine the minimal wind velocities (threshold velocities) required to dislodge different size particles from the surface (Malina, 1941; Zingg, 1951; Clement *et al.*, 1963; Gillette, 1978a,b; Gillette *et al.*, 1980). A number of other studies considered mineralogical composition, analyses of grain size distributions and photographic interpretation (Clement *et al.*, 1963; Gillette *et al.*, 1982). More recently, numerical models have been used to predict threshold velocities of dust entrainment and these have constructed dust emission maps (e.g. Callot *et al.*, 2000). Terrain susceptibility to dust entrainment is dependent on a number of factors. Bare surfaces of loose and mobile sediments, high in sand and silt, but low in clay content are regarded to be the most favourable surfaces for dust production. Surfaces of high clay content are not favourable due to the presence of cohesion bonding between the fine particles, particularly, if the soil is compacted or cemented (Pye, 1987). The favourable terrain types for dust

production that exist in arid and semi-arid regions are dry wadi beds, dry lake beds and playas, surfaces of coastal sabkhas, alluvial fans, stony deserts with high weathering rates, areas of exposed argillaceous bedrock, areas of löess where vegetation cover is shallow, area of weathered regolith of reduced vegetation cover because of climatic change and human activities, alluvial flood plain sediments, reactivated formerly stabilised dunes (Pye, 1987). Wadis serve as carriers of sediments during very short periods of time. Flooded wadis bring considerable amounts of sediments; some of these sediments are transported further by water and discharged at sea, while the remaining sediments in wadis become poorly sorted (Pye, 1987). Occasional floods in the stable desert surfaces and rock slopes of North Africa and the Near East desert transport sediments and deposit them onto alluvial pediments where they become subject to entrainment and transport by moderate winds elsewhere (Yaalon and Ganor, 1973). Loess transported to northern Negev in Israel has mostly been transported by wind from the wadi El Arish deposits in the Sinai desert (Yaalon, 1969). Wadi deposits in Israel and Sinai contain 80-90% sand, 10-15% silt and 1-5% clay in the non-gravel part (Gerson *et al.*, 1985). Inland shallow basins, playas, are rich in fined grained material. These are usually surrounded by sheets of cohesive saline and alkaline crust which reduce deflation unless it is not continuous. Dry salt lakes in arid areas such as the chotts in southern Tunisia and north eastern Algeria as well as the salt dry lakes extend south east of the Gulf of Sirt in Libya are all regarded as major emission areas at a global level (Prospero *et al.*, 2002). Shallow basins found near coastal areas (sebkhas) are similar to playas where sediments are more than 70% silt and clay. Examples of this terrain are found on the coastal zones of the Red Sea, the Arabian Gulf (Pye, 1987) and the southern coastal zones of the Mediterranean Sea (Secretary of Planning, 1978).

In stony deserts where gravel covers the surface and fine particles present in the underlying material the amount of deflated dust is limited unless the action of wind is high. The Gobi desert in northern China and Mongolia is an example of this terrain (Chao and Xing, 1982; Walker, 1982). The outcrops of weathered argillaceous bedrocks, which are largely composed of clay minerals, can easily disintegrate under the effect of wind due to the presence of shales,

silt and marls in its composition. An example of this type of terrain is found in Borku in Chad (Mainguit, 1968). Deeply weathered regolith, incoherent and loose rock waste overlying a bedrock and palaesols (ancient soil profiles), which is believed to have been formed by weathering during humid periods are experiencing erosion under present semiarid and arid conditions as in the case of some parts of Egypt and Sudan (Pye, 1987). Another potential source of dust is loess, which is a type of deposited dust largely composed of particles ranging between 10 and 50 μm and its mineral suite is dominated by quartz. The estimated total area of the globe covered by löess is as high as 10 percent (Figure 1.3) (Pye, 1987; Livingstone and Warren, 1996).

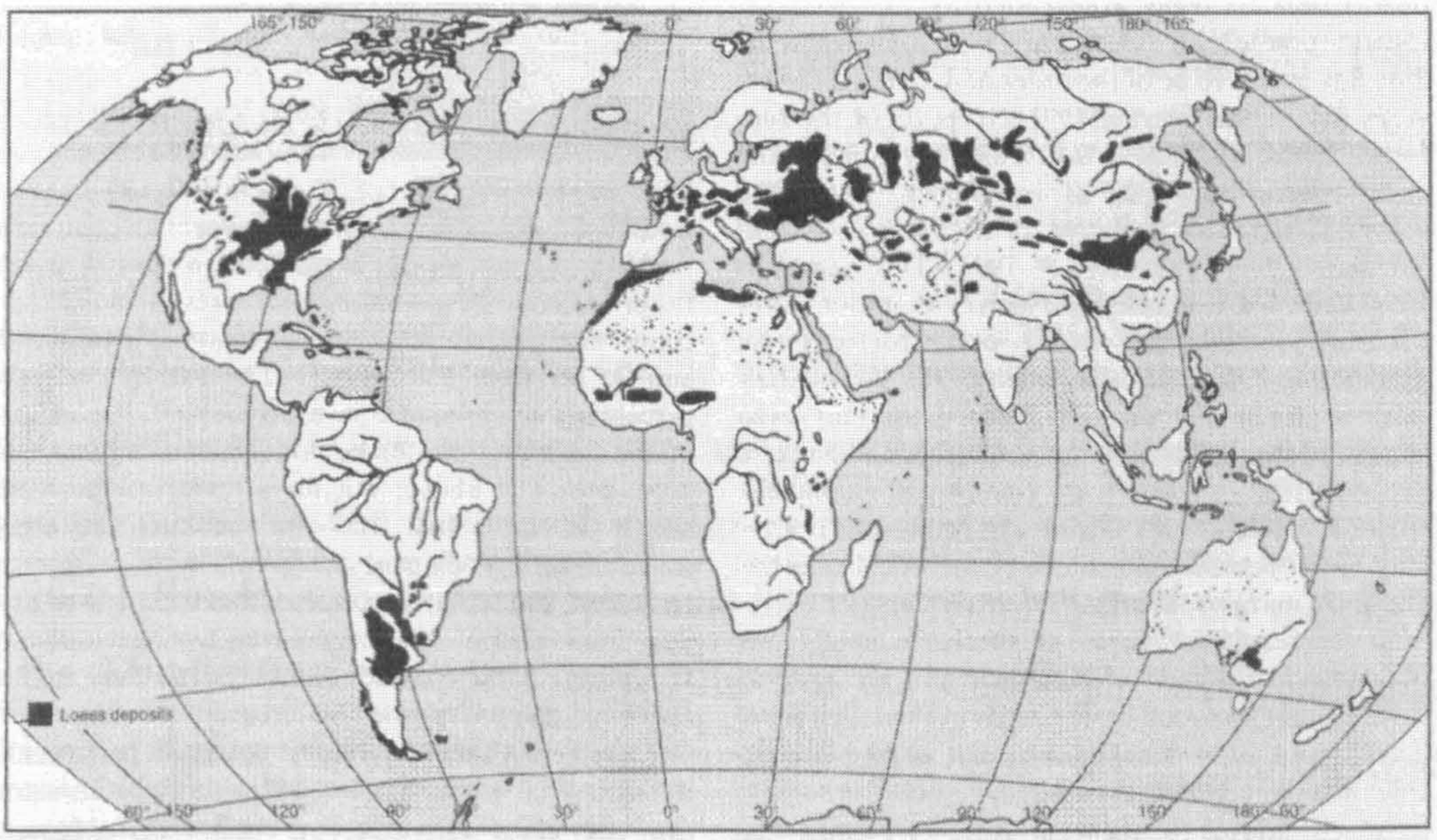

Figure 1.3 Major loess covered regions of the world (*from* Livingstone and Warren 1996)

Alluvial flood plain sediments represent another source of fine dust where deflation occurs on unvegetated channels when flows are low. Examples of these sediments occur near the Tigris and Euphrates rivers in Iraq and are believed to constitute most fallout in Kuwait (Khalaf *et al.*, 1985). Sand dunes disturbed by human activities represent a dust source of a lesser importance where fine dust is believed to have been generated by abrasion during saltation of sand in active dune fields and partially transported by wind and infiltrated into the dunes by rain (Whalley *et al.*, 1982, 1987). Stabilised desert dunes may have up to 15% clay and silt (Goudie *et al.*, 1973; Tsoar and Moller, 1986) representing aeolian dust addition to existing dune fields and desert surfaces

(Goossens, 1985; Amit and Gerson, 1986). In Crete, trapped dust samples were found to be rich in quartz and these have been attributed to the Libyan Desert (Pye, 1992), implying long distance transport of desert-derived dust.

1.4.2.2. Global aeolian dust sinks

Fine dust is dispersed in the atmosphere and transported great distances by the wind and deposited in regions known as dust sinks. Some dust sinks are oceanic and others are continental. The most important oceanic sinks are the northwestern Pacific and the eastern equatorial Atlantic. Smaller sinks occur in the eastern equatorial Pacific in the Tasman Sea, south west Indian Ocean, the Arabian Gulf, the Mediterranean and the north west Indian Ocean (Pye, 1987). An estimate of 1000 t/yr of Asian aerosol is deposited in the pacific and about one third of this estimate is deposited in the western north Pacific between 25 and 50° N west of 150° E (Unluata, 2001). African dust deposits in the Caribbean basin have received special attention from the scientific community in recent years due to their increasing understanding of the subsequent implications on the ecological system in that region (USGS, 1998; USGS, 2002). Similarly, Saharan mineral dust has been found in different regions of the Middle East, Europe, South America, the Caribbean, and continental United States. North African dust incursions have been tracked, characterized, and quantified across much of the eastern half of the United States (Perry *et al.*, 1997). Aerosol deposits were found in Central Asia in the southern slopes of the eastern Himalaya, the Karakoram, southeastern Tibetan Plateau, northern/western Tibetan Plateau were mainly attributed to Asian sources (Wake, *et al.*, 1994). The presence of dust fallout has also been reported from northern Greenland, Alaska and Ellesmere in Canada (Darby *et al.*, 1974; Rahn *et al.*, 1981). The influx of brownish insoluble deposits in the Arctic is believed to have come from the Gobi deserts of Asia. An estimated rate of the amount of dust being transported to from Asian sources the region was 6000 t/yr (Rahn *et al.*, 1977).

1.4.3. Past dust flux

The geologic record of dust is regarded as source of information that can be used to test dust simulation models. Records of dust can be obtained from polar and tropical ice cores and marine sediments (Kohfeld and Harrison, 2001; Harrison *et al.*, 2001). Dust sediments at the Late Glacial Maxima (LGM) and for the Late Holocene show that the LGM was an interval of much higher atmospheric dust loadings than today, but they also reveal that were some regions of the world experienced much more deposition than others (Harrison, *et al.*, 2001).

1.4.3.1. Ice core evidence

Dust records in ice cores provide useful records of dust deposition from regions that are currently ice-covered and the total amount of dust present in the core provides a record of dust deposition rates through time. The mineralogy and chemical composition of the sediments can be used to identify the source areas from which the aeolian material is derived and provide reconstruction evidence of the atmospheric circulation regime during deposition. Changes in the grain size of dust can be interpreted as an indicator of changes in source area proximity, wind strength and/or changes in the type of deposition processes (Kohfeld and Harrison, 2001). Ice core evidence shows that aeolian deposition rates were greater during glacials than interglacials and it is worth noting that concentrations of dust in the ice cores are significant because of low precipitation rates during the glacial periods (Harrison, *et al.*, 2001).

1.4.3.2. Deep sea sediments

Aeolian dust represents a major contributor to oceanic sediments, and in some areas this concentration can reach up to 80 % of the total accumulated sediments (Pye, 1987). Accumulations of dust sediments in the oceans have provided important clues on changes on global wind systems and environmental changes on land during the Quaternary. The eastern Atlantic, northwest Pacific, the northwest Indian ocean, southwest Pacific and east equatorial Pacific are regarded as the most important regions of aeolian dust input (Pye, 1987). The interpretation of material in marine sediments is more

complicated than interpreting the ice core records, because they contain materials of non-aeolian sources (Kohfeld and Harrison, 2001).

Variations in African aridity during the Pliocene-Pleistocene have been reconstructed from deep sea sediment records off West and East Africa. These sediments have provided the most compelling evidence for progressive increase in African aridity during the Late Neogene (deMenocal, 1995). Sediments collected in the Arabian Sea revealed that aeolian fluxes during glacial maxima were three to five times higher than those occurred during interglacial periods (deMenocal, 1995). Analysis of aeolian sediments from a number of sites in the Arabian Sea, the Gulf of Aden and off subtropical West Africa have made researchers believe that the occurrence of large amplitude regional aridity cycles were closely linked to the development of high latitude glacial cycles (deMenocal and Rind, 1993; Tiedemann *et al.*, 1994; deMenocal, 1995).

Whilst past dust flux may have been greater during glacial climates, detailed evidence for contemporary terrestrial dust flux is still lacking in some regions of the globe. The following section focuses on the state of current knowledge on dust flux in North Africa.

1.4.4. Saharan dust

1.4.4.1. Saharan dust plumes and sources

Reconstructed dust plume trajectory events in the western Mediterranean indicate that mountainous regions and wadis in the central Sahara are source areas as shown in Figure 1.4 (Yaalon, 1997).

Yaalon (1997) argued that an intermediate stage of Saharan dust transport to southern Europe via the pre desert area is feasible. Re-entrainment of deposited dust by consecutive dust storms can lead to insignificant amounts of loess deposits in North Africa. On the contrary, some mathematical models suggest that two thirds of the Saharan dust settles out during the first 2000 km down wind from its sources (Jaenicke and Schultz, 1978; Ganor and Mamane, 1982).

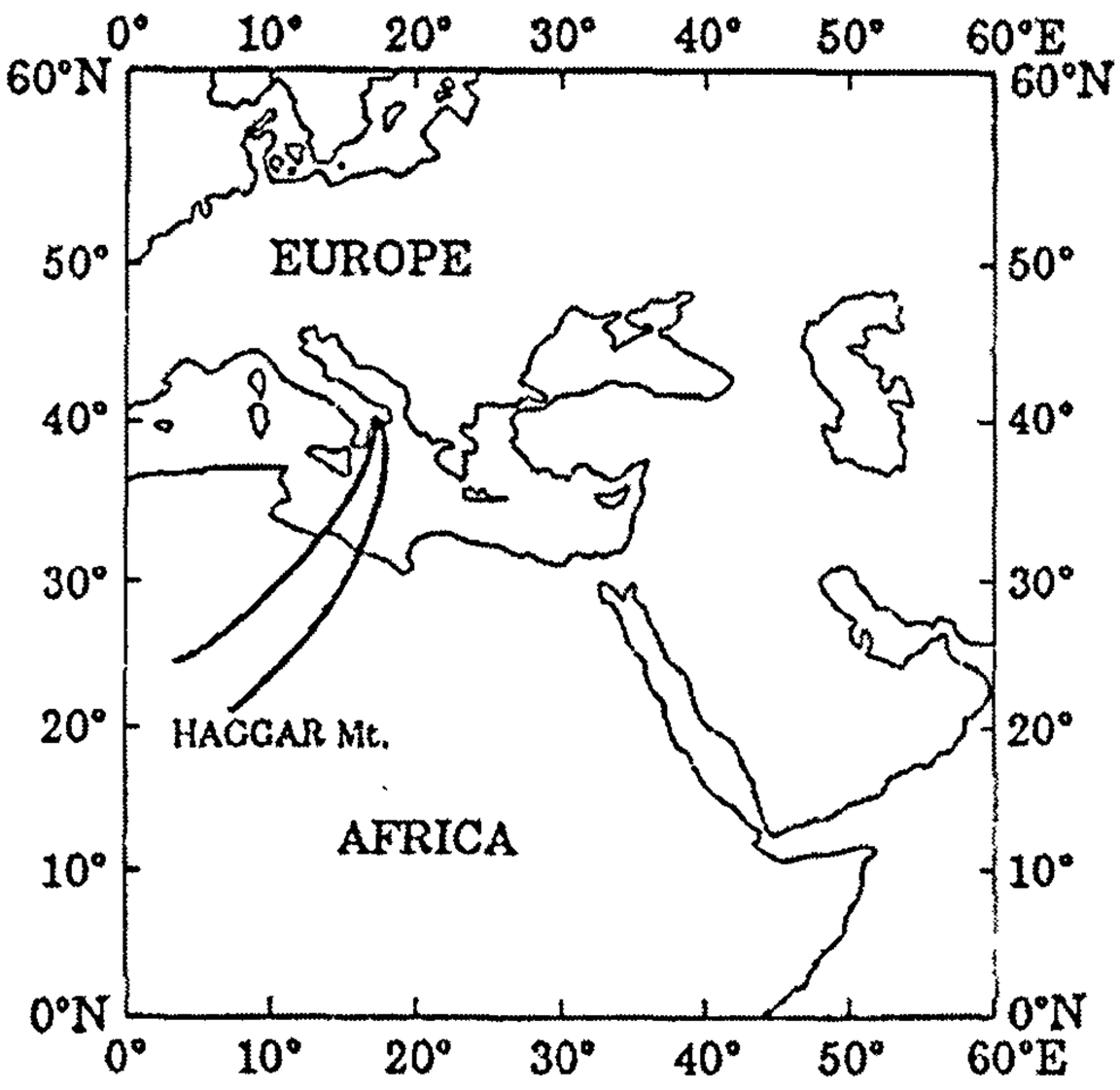

Figure 1.4 Reconstructed jet stream above 1500 m altitudes originating in the Ahaggar Mountains and crossing the Mediterranean (*from* Yaalon, 1997)

This implies that dust input along the most populated and productive lands of north Africa can be significant. Meteosat infra-red (IR) images, the Total Ozone Mapping Spectrometer (TOMS) Aerosol Index (AAI) and back trajectories were used to study the vertical structure of dust plumes to the Mediterranean Basin and these reveal that dust layers of a single event originated in more than one area of the Sahara; in south and west Algeria, north and south Tunisia, north and south Morocco and north and south Libya (Hamonou, *et al.*, 1999).

Satellite data based studies have been increasingly used to identify the major dust sources and temporal changes in their emission intensities (e.g. Goudie and Middelton, 2001; Middelton and Goudie, 2001; Prospero *et al.*, 2002; Goudie, 2003). Prospero *et al.* (2002) have described the major emission sources in North Africa based on satellite aerosol index maps. A summary of this work in relation to this Ph.D. project is presented and supported by a regional map showing the sources and their main trajectories of seasonal transport (Figure 1.5).

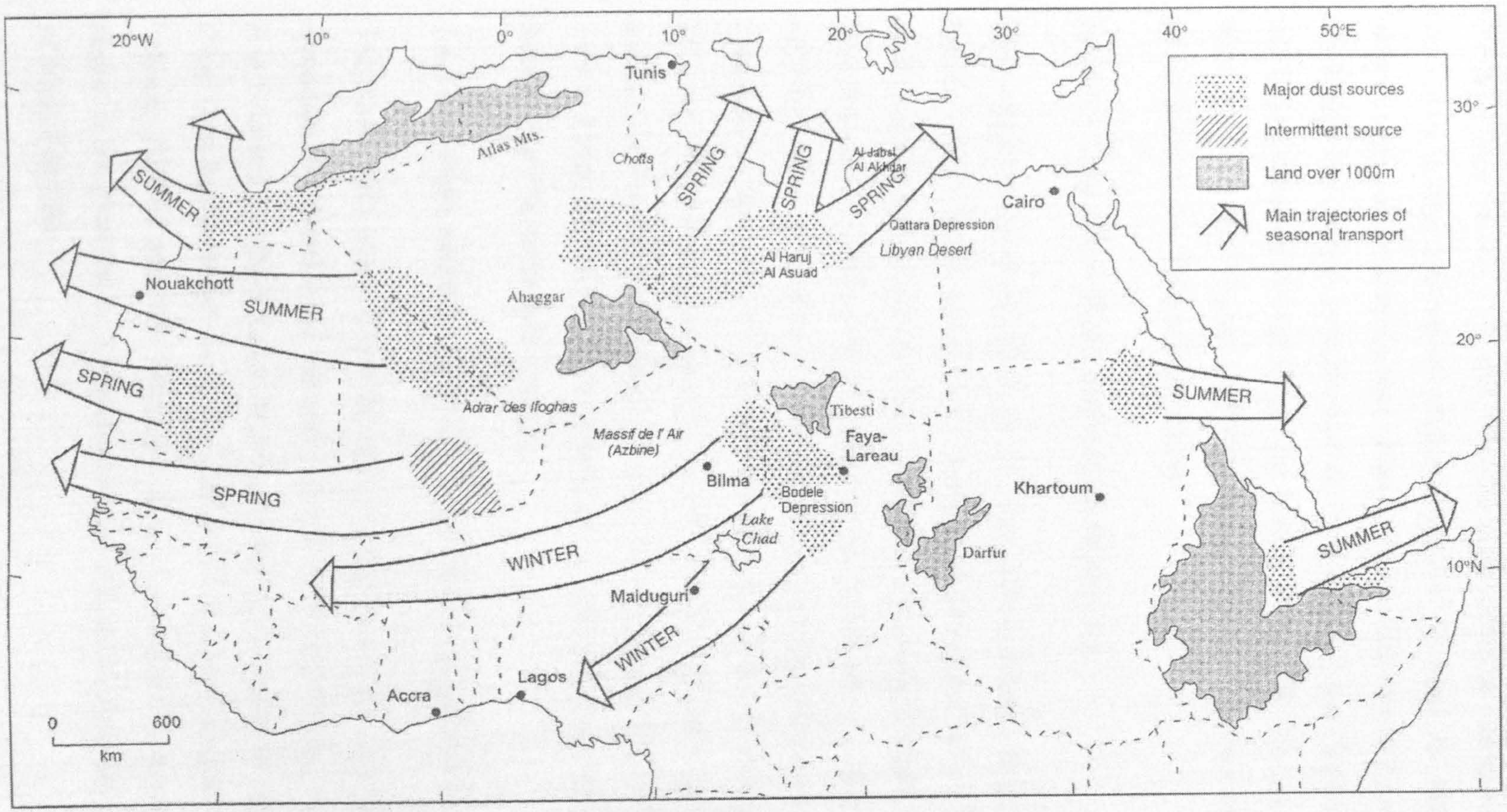

Figure 1.5 Saharan dust sources and major trajectories of seasonal transport (*modified from* Goudie 2003)

1.4.4.1.1. Eastern Libyan Desert

A major Saharan emission area which is most intensive during the summer, is located in a large depression situated south of Al Jabal Al Akhdar in north eastern Libya and extending into western Egypt. The dust source areas extend southwest in a narrow corridor east of Al Haruj Al Asuad highlands as far as the Tibesti Mountains foothills on the border with Chad. The main features of these areas are wadi systems and salt/dry lakes stretching from the coast south of Benghazi to the Qattara Depression.

1.4.4.1.2. Lake Chad Basin and Bodélé Depression

This region has been described as the most intense source of dust in the world based on both space and ground observations (Prospero *et al.*, 2002). TOMS AAI monthly and annual average values have been the highest of any region (Prospero *et al.*, 2002) and the meteorological data show a high frequency of visibility reduction during all seasons except autumn (Mbourou *et al.*, 1997). Diagnosis of satellite aerosol maps show that the centre of activity lies between 16° and 18°N and extends from 15° to 19°E in the centre of Bodélé Depression and Erg du Djourab. Topographical maps show considerable drainage from the Tibesti Mountains to the north carried into the Bodélé Depression by seasonal flood planes that terminate in wadis.

1.4.4.1.3. Niger and the Southern Flanks of the Ahaggar Mountains

The dust source area within this region consists of low terrain nested between mountain slopes and lying between 18° and 23°N and 6°E in the west of Niger. It is bounded by the Ahaggar Mountains in Algeria from the north, Massif de l'Air (Azbine) in Niger from the east and Adrar des Ifoghas on the border between Algeria and Mali from the west. A prominent characteristic of this region is the presence of a system of ephemeral rivers especially on the slopes of Massif de l'Air.

1.4.4.1.4. Mali, Mauritania, and the Western Flanks of the Ahaggar Mountains

The dust emission areas within this region experience a complete obscuration by aerosols during the summer but the intensity of aerosols is reduced during the other months. The presence of several active areas within this region results in complex shape of linked plumes that make the constituting sources difficult to identify, however, the active region mainly extends from ~ 17°-18°N, 8°-10°W to ~ 26° along the meridian. This region is defined on the east by the 500-1000 m elevation line of the Ahaggar Mountains which are believed to provide it with extensive drainage.

1.4.4.1.5. Tunisia and Northeast Algeria

The depression situated between ~ 5°-10°E and 30°-35°N south of the northern (Tell) Atlas is an emission region comprised of an extensive system of salt lakes and dry lakes and receives <100 mm of direct rain annually. This region is described as a combination of hillslope, channel, alluvial fan and playa environments. Major dust activities begin in April and May and continue until September. The centre of dust emission, as derived from the satellite images, occurs in the region immediately to the south of the salt lakes that are named chotts. The largest of these of these lakes is 4900 km^2, known as Chott Jerid, centred at 33.7°N, 8.4°E is situated in west Tunisia and Chott Melrhir, 1800 km^2 (34.3°, 6.3°E) lies in northwestern Algeria. The centre of intense and persistent dust emission is identified as an area situated to the south of these chotts and centred at 33.5°N and 7.5°E.

1.4.4.2. Libya a place of dust sources and transport routes

Dust haze episodes monitored in Europe and the eastern Mediterranean are usually associated with southerly or south westerly winds which transport fine sediments from North Africa. As mentioned earlier, it is suggested that dust trapped in Crete was partially derived from sandy deserts and the semiarid soils of Libya (Pye, 1992). Recent NASA satellite images have revealed that the

Libyan Desert is an important source of Saharan dust (e.g. NASA, 2000b; Prospero *et al.*, 2002) as shown in Figure 1.6.

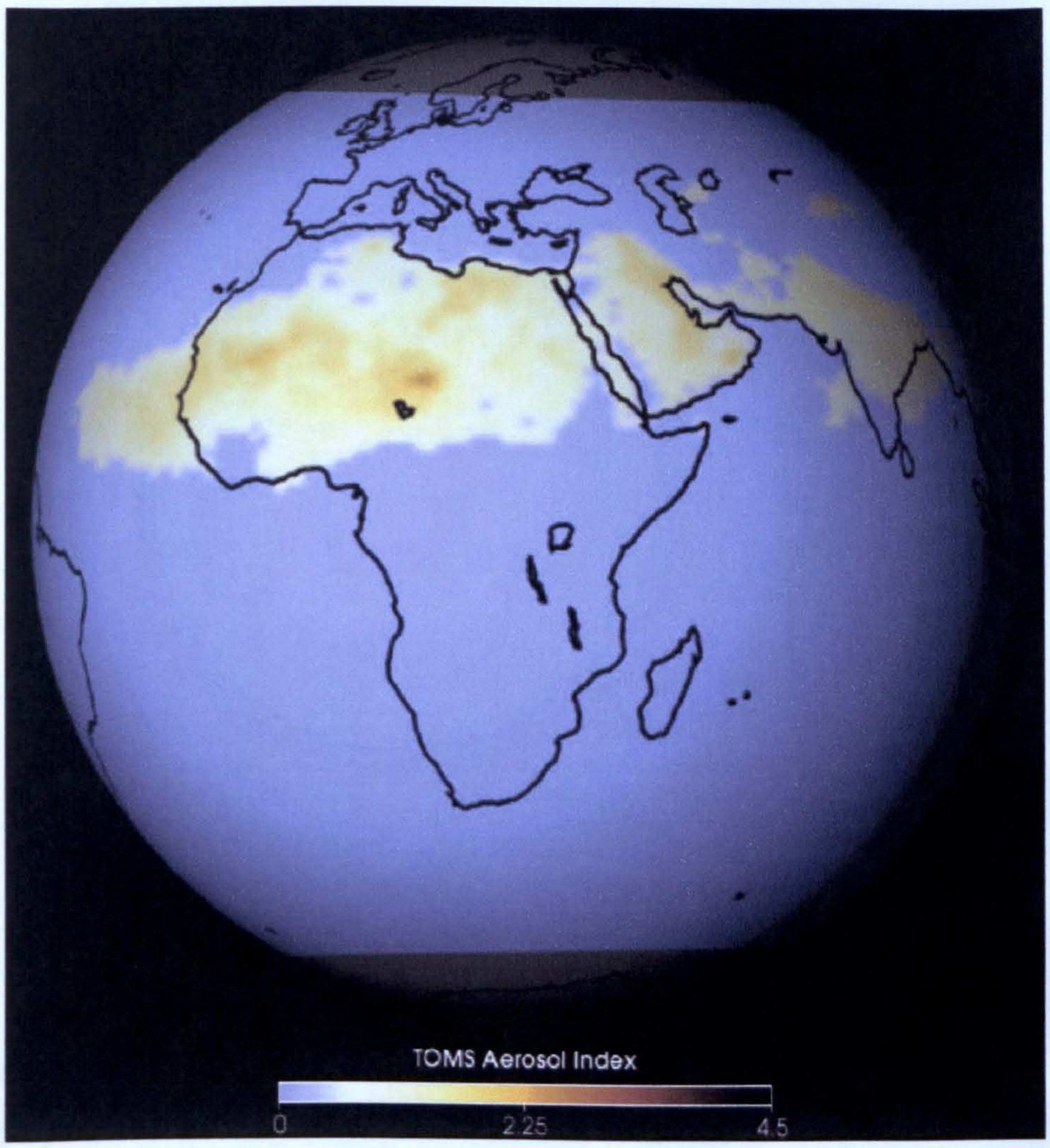

Figure 1.6 A Total Ozone Mapping Spectrometer image from April 2000 shows Saharan dust moving into the Atlantic. In true colour, brown pixels indicate higher aerosol concentrations, yellow pixels indicate lower aerosol concentrations and light blue regions indicate either little or no dust. (*from* NASA 2000b)

A recently developed dust emission model based topographic, geological and climatic data suggests that local emissions in the coastal regions of Libya represent some of the most intense dust emission areas of the Sahara (Callot *et al.*, 2000). Studies investigating the presence of deposited loess in Libya are few; however, the presence of true loess in the country has been established (Assallay *et al.*, 1996). Grain size distribution analysis of topsoil samples taken

from the northwestern coastal region and the southwestern region of the country shows that Libyan loess could be classified into two types: silty loess in the northwestern region and clayey loess in the southwestern region near Ghat as shown in Figure 1.7 (Assallay *et al.*, 1996). The presence of loess deposits implies significant dust depositions in these regions in the past.

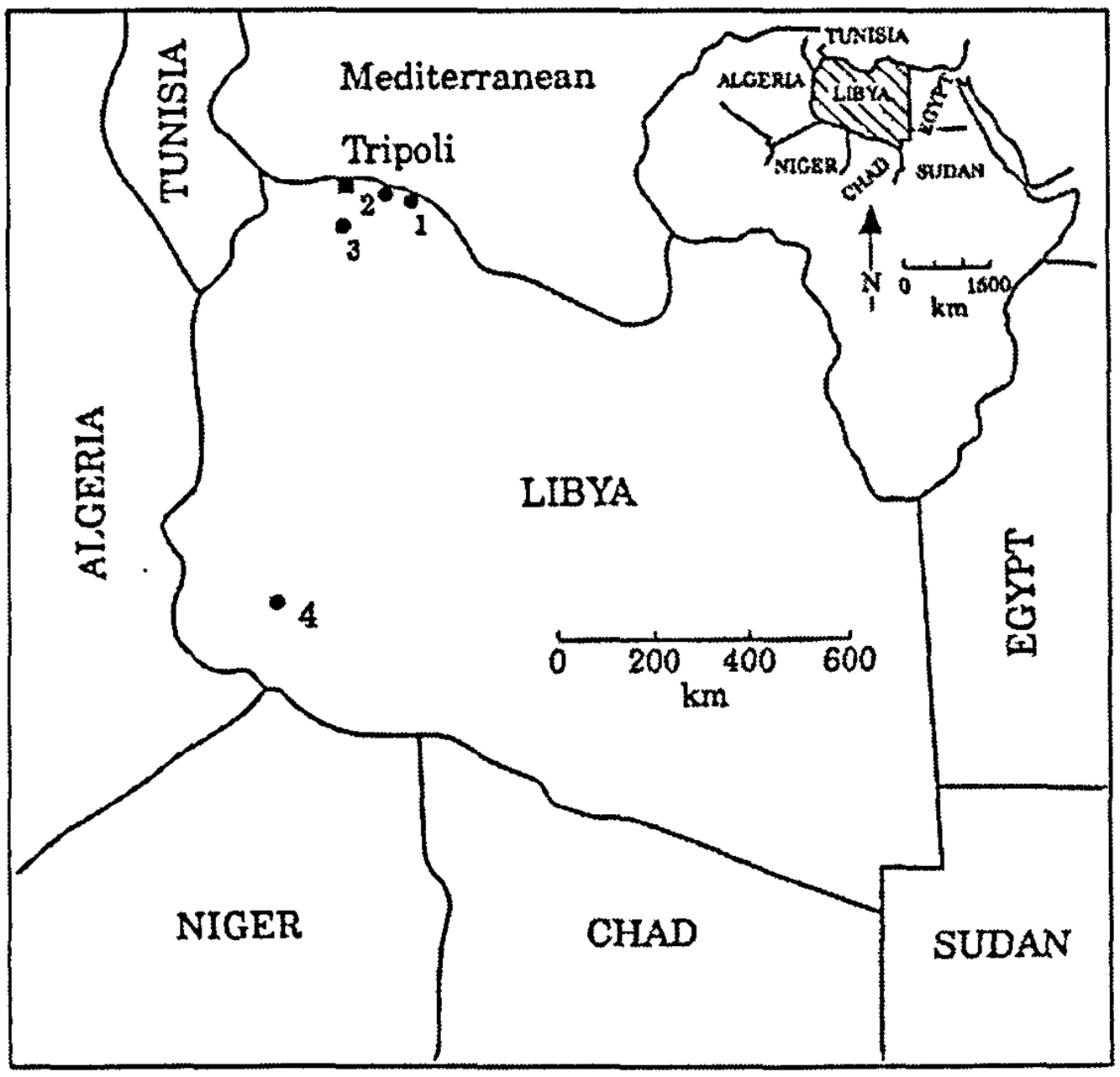

Figure 1.7 Some loess locations in Libya (1) Al Khums; (2) Garabolli; (3) Gharyan; (4) Tahala (Ghat), (*from* Assallay *et al.* 1996)

Dust studies of actual deposition rates, sources, transport routes and dust effects on human health, soil fertility and desertification are still relatively few. Despite its special significance on the world map of aeolian dust sources and trajectories (Figure 1.8), collection of basic data on aeolian dust activities remain relatively scarce except that derived from satellite imagery (Brooks, 1999; NASA, 2000b; Middelton and Goudie, 2001). Therefore, Libya is likely to be an important study area to improve and broaden the present understanding of aeolian activities from ground data gathered from the Saharan regions.

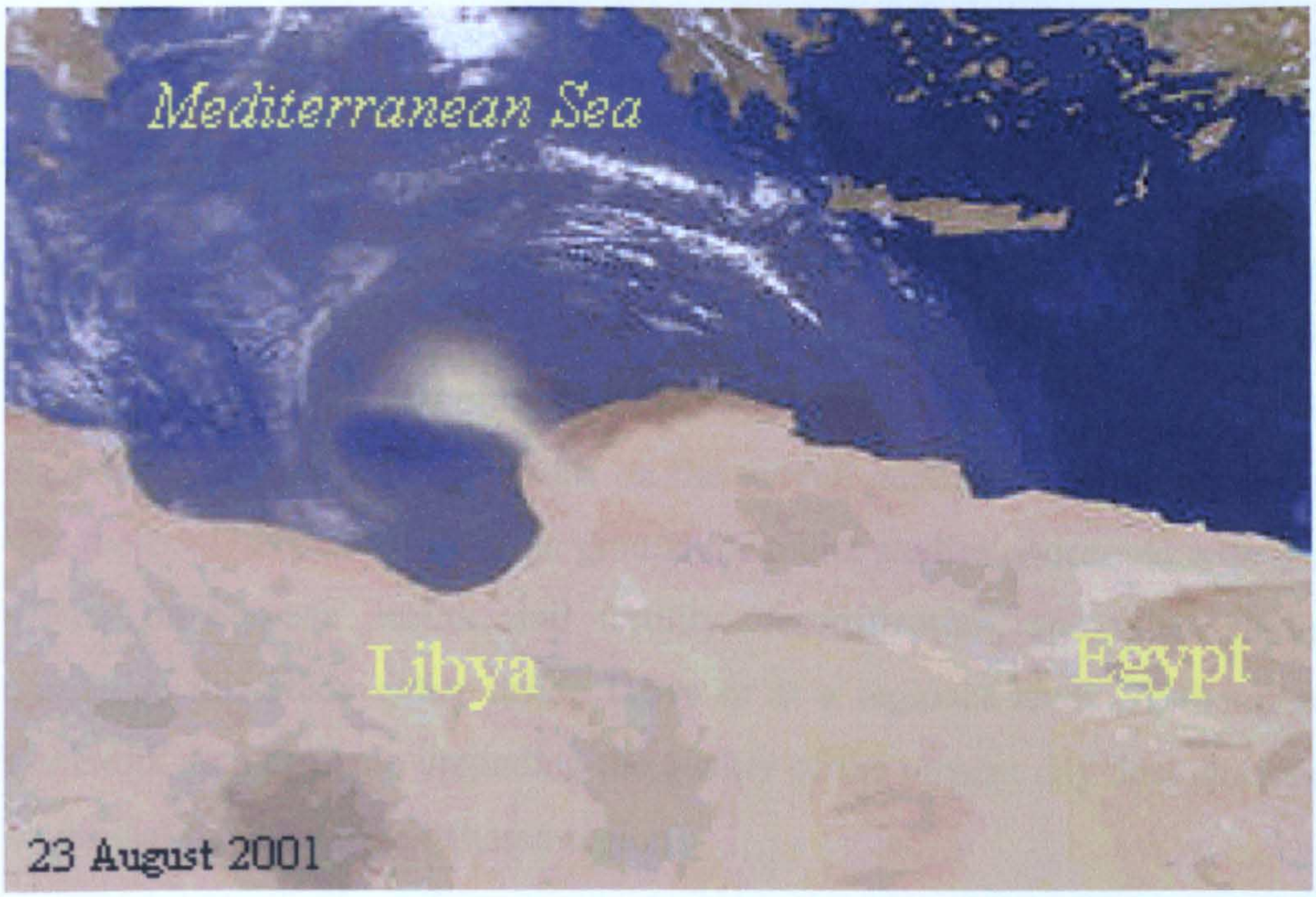

Figure 1.8 Dust storm originated in northeast Libya intruding the Mediterranean on 23/08/2001(*from* NASA 2001a)

1.5. SUMMARY

An apparent shortage of field studies in the most persisting dust source regions in North Africa seems to be a limiting factor in evolving aeolian research in relation to those regions. Many dust studies applied to potential dust source regions such as those based on modelling (e.g. Callot *et al.*, 2000) fall short of validation by direct field observations. A need for information on dust deposition rates, mineral composition in remote and undisturbed desert areas of the world has been recognised (Reheis and Kihl, 1995; Callot *et al.*, 2000).

Despite its significance as the largest source of dust in the world (Prospero *et al.*, 2002; Goudie and Middleton, 2001), field studies in the Saharan regions remain very limited (Callot *et al.*, 2000). Therefore, there is a need for more information in this region. This study aims to fill this gap in knowledge using a monthly dust trapping field study carried out in the western part of Libya from June 2000 until May 2001. Although, a one year field study is not expected provide a long term representative information on average dust activities, especially in a dry year like this, such data can be valuable as they are the first of their kind in that region.

This study aims to provide the first baseline information on dust deposition rates, grain size distribution and mineral composition in west Libya and investigate their spatial and temporal variations in light of the meteorological and geomorphologic effects in the regions of study. The results obtained from laboratory analyses of the collected dust and soil samples are used together with the Total Ozone Mapping Data (TOMS) for the regions of study to assess the effects of local dust emissions on the overall deposition rates. Generally, this project is expected to lay the ground for future studies concerned with dust effects on humans' health, soil fertility, desertification, and other studies similar to this study either inside Libya or at a regional level. Furthermore, fieldwork data can help upgrading the quality of the present day dust emission numerical models of the Saharan regions.

This thesis is organised into 6 further chapters which focus on the study area (chapter 2), aeolian entrainment and transport in Libya and surrounding regions (chapter 3), trapping methodology and methods of quantifying aeolian sediment transport (chapter 4). The results are presented as monthly rates of dust deposition (chapter 5) and the nature and characteristics of the sediments are discussed in relation to their source areas (chapter 6). Chapter 7 provides conclusions and suggestions for further study.

CHAPTER 2

INTRODUCTION TO THE AREA OF STUDY

2.1. THE STUDY AREA

2.1.1. Location and area

Libya is situated in the central part of North Africa between 9° and 25° E and 20° and 33° N. It has a 1,900 km long coast along the southern basin of the Mediterranean Sea, and it shares borders with Tunisia and Algeria to the west, Egypt and Sudan to the east and Niger and Chad to the south as shown in Figure 2.1. The total area of the country is 1,759,540 km^2, most of which is dominated by desert (CIA, 2002).

2.1.2. Population

Due to its inhospitable environment, the desert has always been inhabited by a small fraction of the total population, who either live a nomadic life style across communal lands or a sedentary life around the oases and some governmental agricultural project sites. Over 90 % of the population live along the coastal region, where the country's two largest cities, Tripoli and Benghazi are situated (Figure 2.1; Lawless, 1989). The discovery of oil in 1950s and the subsequent exploitation of this reserve has resulted in a considerable growth of the local economy causing a rapid population growth and dramatic demographic changes (Lawless, 1989; Mclachlan, 1989). In 1964 the population stood at 1,564,369 (Armandi, 1976) while the latest official estimates reveal that the population size had reached 5.4 million people in 1994 (Haub and Yanagishita, 1996; Fisher, 1998). An increasing polarisation of the population in the northeast and northwest regions started in mid 1970s and created by strong rural-to-urban migration is the most important demographic change, with the concentration of development programmes in certain urban areas being a major cause of migration of Bedouins toward the main cities (Lawless, 1989).

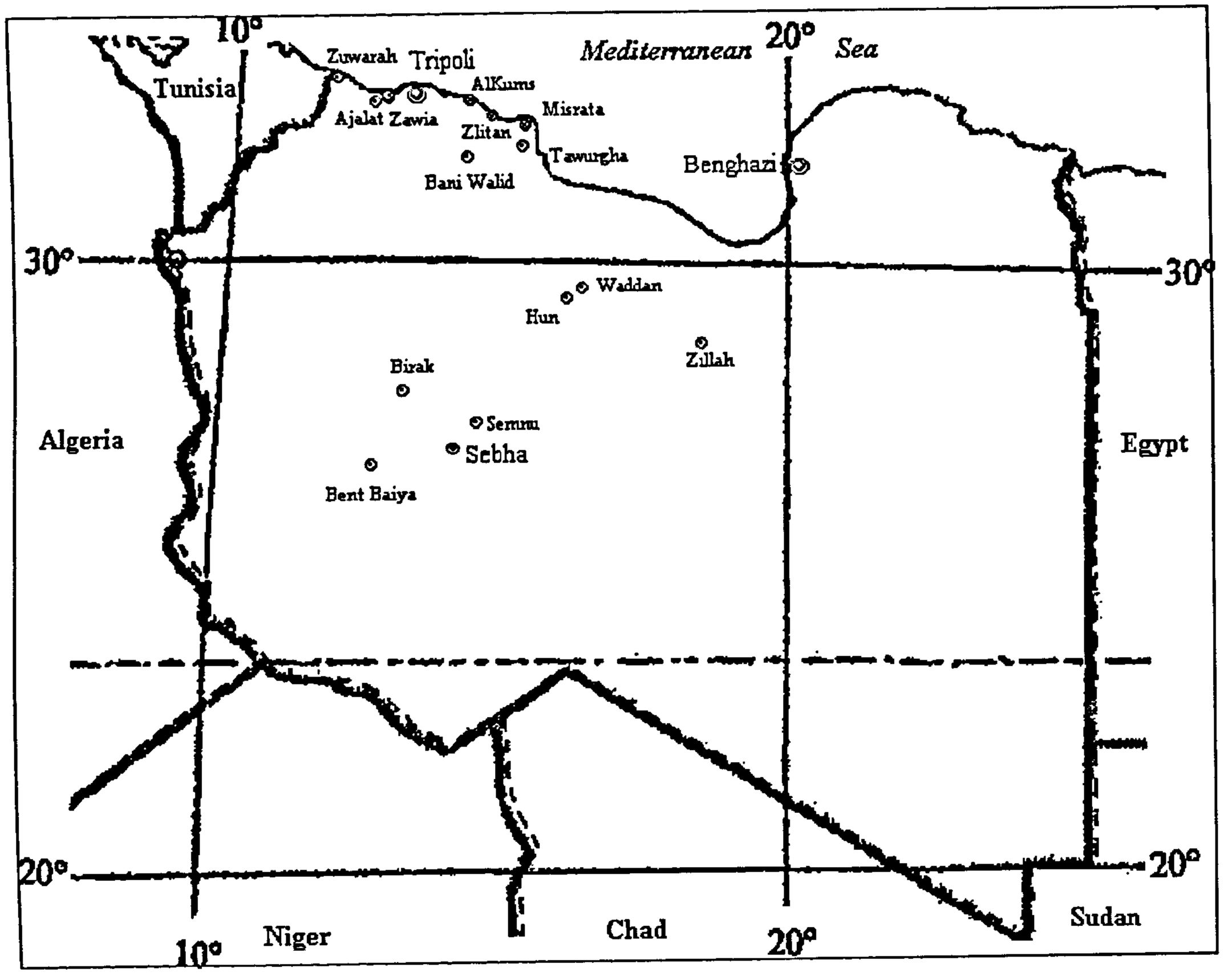

Figure 2.1 Political map of Libya (*after* Reed Int'l Ltd. 1993 *modified*)

2.1.3. Water resources

The arid climate imposes certain constraints on any future economic developments. Increased demand for ground water over the last three decades has resulted in a serious problem of water shortage. Ground water is the main source of water for both domestic and agricultural use. Over exploitation of ground water has led to a marked ground water deficit, especially, in the two most populated cities, Tripoli and Benghazi. In turn, this has led to seawater intrusion into underground aquifers. During the 1970s the average water salinity in wells supplying the town of El Abiar near Benghazi reached 1,800 ppm exceeding the international standard of 1,500 ppm (Kezeiri, 1987). Similar problems of increased salinity have been noted in other cities and towns along the coastal region such as Tukrah, east of Benghazi, Sirt, Zilitan, Al Aziziyah, Al Qarabulli, Surman, Ezhra, Sabratah, Zuwarah and other towns and cities (Kezeiri, 1987). Water shortage has remained a pervasive problem along the coastal region despite the efforts of the government to remedy the problem through building dams across several wadis in the north and erecting several water desalination plants (Kezeiri, 1987).

2.2. CLIMATE AND METEOROLOGICAL DATA

2.2.1. Climatic regimes of North Africa

The climate of North Africa is controlled by two opposing climatic regimes: the Mediterranean and the Saharan regime.

2.2.1.1. The Mediterranean regime

The Mediterranean regime is transitional, controlled by westerlies in winter and subtropical anticyclones in summer (Barry and Chorley, 1998; Figure 2.2). Incursions of continental arctic (cA) and marine arctic (mA) air are relatively infrequent (6-9 invasions/year) but, marine polar (mP) air incursion is much more common and critical in the formation of Mediterranean depressions (Figure 2.3). Atlantic depressions entering the western Mediterranean bring rainfall, but the Saharan depression south of the Atlas Mountains (Algeria) is the most important source of late winter and spring rainfall. The Saharan

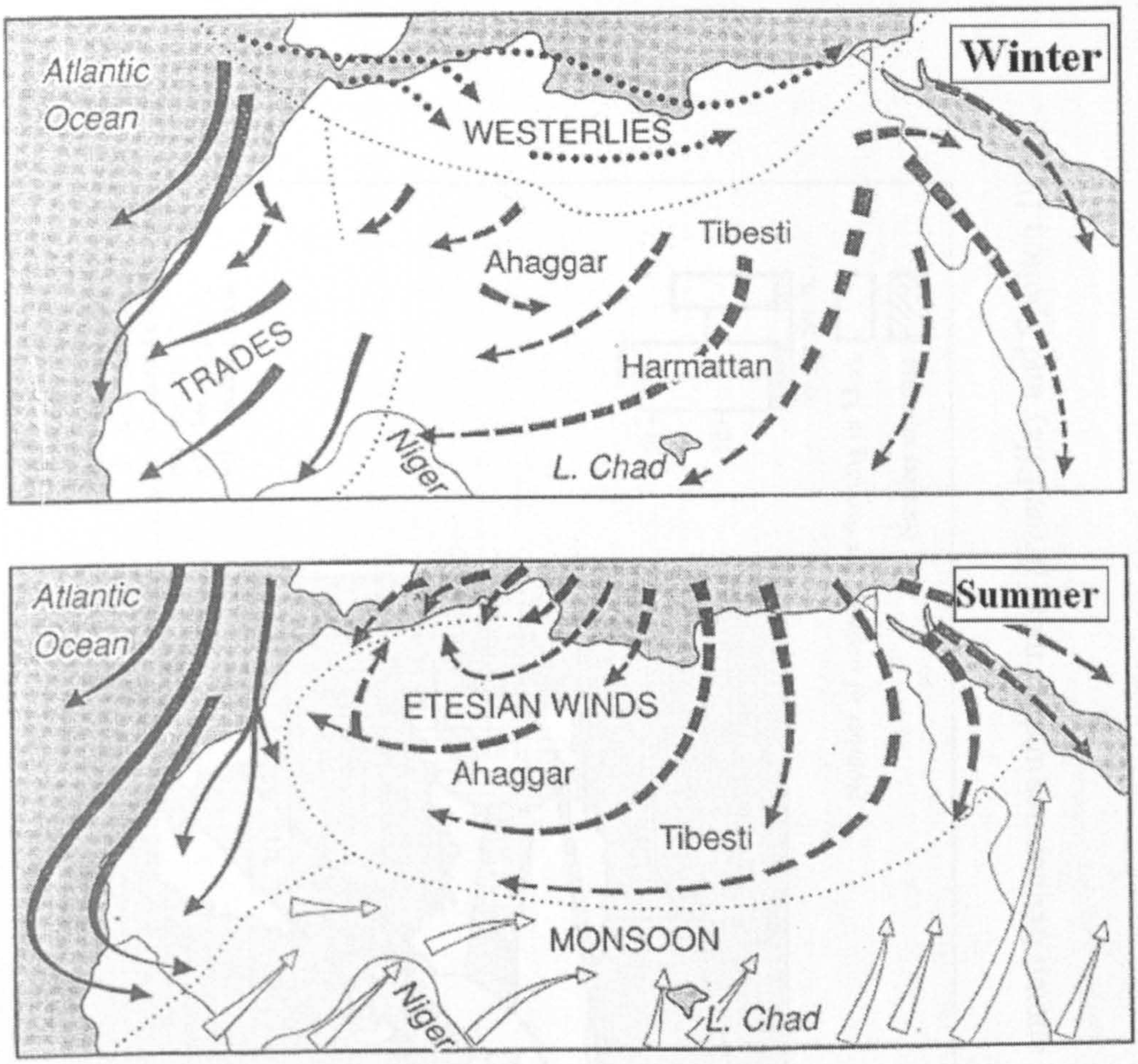

Figure 2.2 Saharan winter and summer wind systems (*from* Goudie 2003)

depression and those from the western Mediterranean move eastwards creating a low pressure belt and often draw continental tropical (cT) air from the south northward as warm and dusty winds known as Sirocco especially in the spring and autumn (Barry and Chorley, 1998).

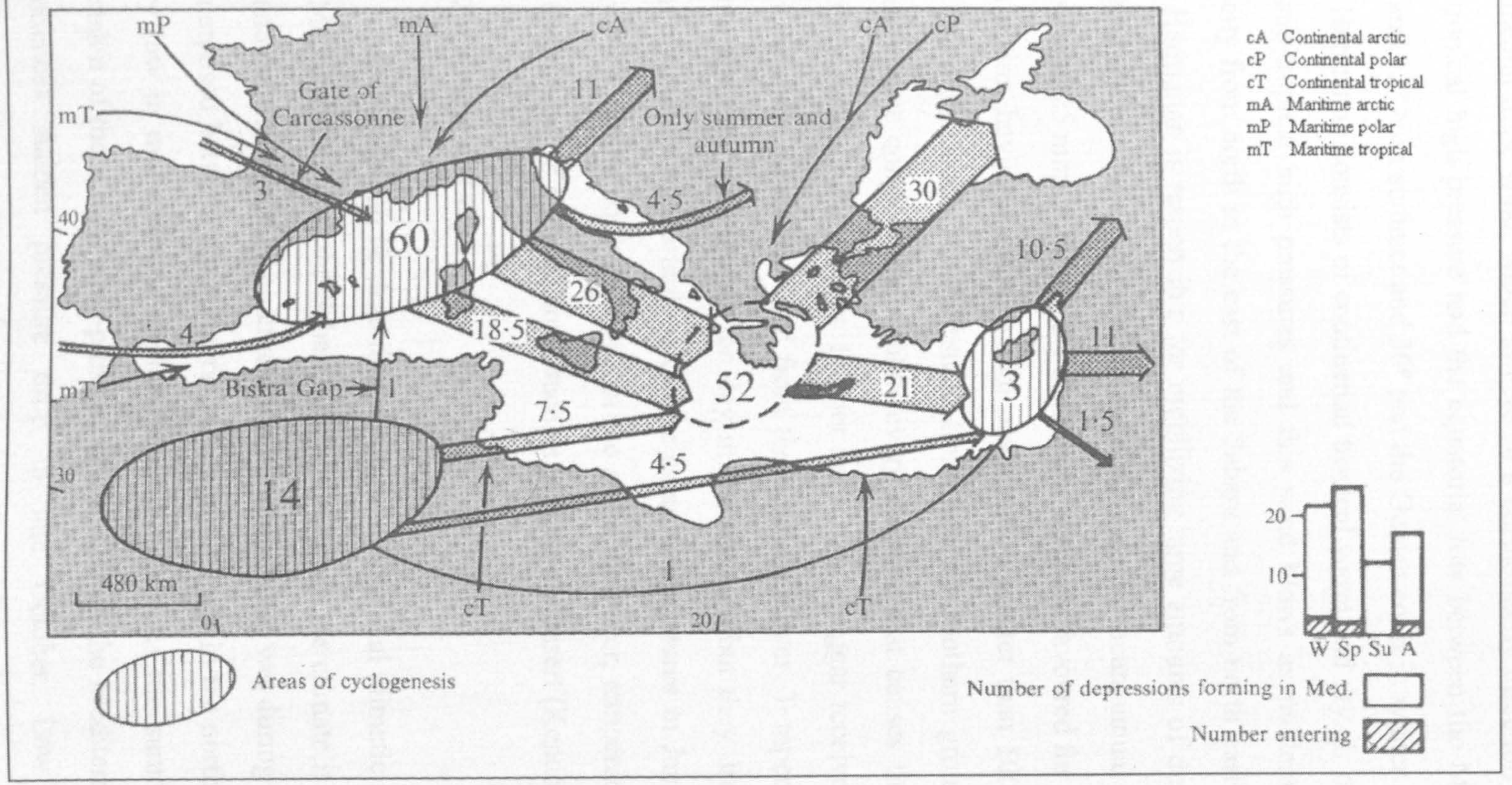

Figure 2.3 Tracks of the Mediterranean depressions, their annual frequencies and air mass *(from* Riley and Spolton 1982)

2.2.1.2. The Saharan regime

The main features of the Saharan climate are imposed by the Harmattan, the continental trade wind, which sweeps in a northeasterly direction between the sub-tropical high pressure and the equatorial low between the Mediterranean Sea and 17° N in summer and 30° and the Guinea coast in winter (Figure 2.2). The Harmattan consists of continental tropical warm and dry air originating in the sub-tropical high pressures and this wind blows as moderate to strong velocity from north in the east of the Sahara and from north east in the west. The Harmattan is responsible for mobilizing large amounts of dust across the Saharan region. Over most of the central Sahara, the mean annual precipitation is less than 25 mm, however, the mountains are more favoured for precipitation than plains, having a mean annual precipitation greater than 100 mm (Barry and Chorley, 1998). The Tibesti in Chad and the southern groups of Air in Niger receive considerable rainfall every summer that causes the ephemeral wadis to flood in some years. Further north, the Ahaggar receives more rain, from the south in summer and from the north in winter. Temperatures in the Sahara are very high during the day in the summer but they drop rapidly at night. Winter is comfortably cool, the mean temperatures in January ranging from 10° C in the north to 21° C in the south, however, temperatures at night can drop below 0° C in the north such as the Libyan Desert (Kendrew, 1953).

2.2.2. Climate of Libya

The local climate can be described through the regional climatic regimes over the Mediterranean and the Sahara. Along the coast, the climate is described as hot and dry during the summer and mild and relatively wet during the winter. It is interposed between the temperate maritime climate in the north and the arid (very low in moisture) subtropical desert climate. As the summer eastward extension of the Azores high-pressure cell collapses, the Mediterranean region experiences sudden pressure drop in late October. Low pressure is accompanied by an increase in the probability of precipitation and the region experiences the first invasion of cold fronts (Riley and Spolton, 1982; Barry and Chorley, 1998). The highest precipitation rates over the coastal region of

Libya occur in December and January when the mean sea surface temperature is higher than the mean air temperatures by about 2°C. On average, precipitation is only six days per month during winter in northern Libya (Barry and Chorley, 1998). The generally wet, windy and mild winter of northern Libya is succeeded by spring lasting from March to May, with some interrupting days of false summer (Barry and Chorley, 1998). The coastal districts experience very hot and dusty ghibli (Sirocco) winds from March to June. These winds come from the desert and the incursion of warm air raises temperatures in the north of the country up to 50° C. Such conditions can last up to four days and carry high levels of dust across the Mediterranean to Europe (Pearce and Smith, 1993). Inland, the climate is characterised by very hot summers and large diurnal temperature ranges (see next section).

2.2.3. Climatic data of Libya

Libya's coastal strip has a Mediterranean climate with some rainfall between October and March, reaching its peak in December and January year (Secretary of Planning, 1978). The highest rainfall in the country occurs in the hill and plateau region of Al Jabal al Akhdar (The Green Mountain) between Benghazi and Darnah, where land is over 500 m above sea level and rainfall reaches 600 mm a year (Figure 2.4).

In the north western coastal region between Misratah and the Tunisian border, the annual average rainfall ranges between 200 and 400 mm. Along the Gulf of Sirt between Misratah and Benghazi, where the desert reaches the coast, the rainfall is limited, ranging between 100 and 200 mm a year (Secretary of Planning, 1978). Beyond the 160 km or less from the coast, annual rainfall drops below 100 mm and the average rainfall is 30-50 mm, which falls mostly during the autumn and spring (Secretary of Planning, 1978). During winter, the vast area of desert inland receives very little rain brought by the Mediterranean depression (Pearce and Smith, 1993). Along the coast, the average annual relative humidity ranges from 60 to 80 % that falls gradually inland reaching 30% (Secretary of Planning, 1978).

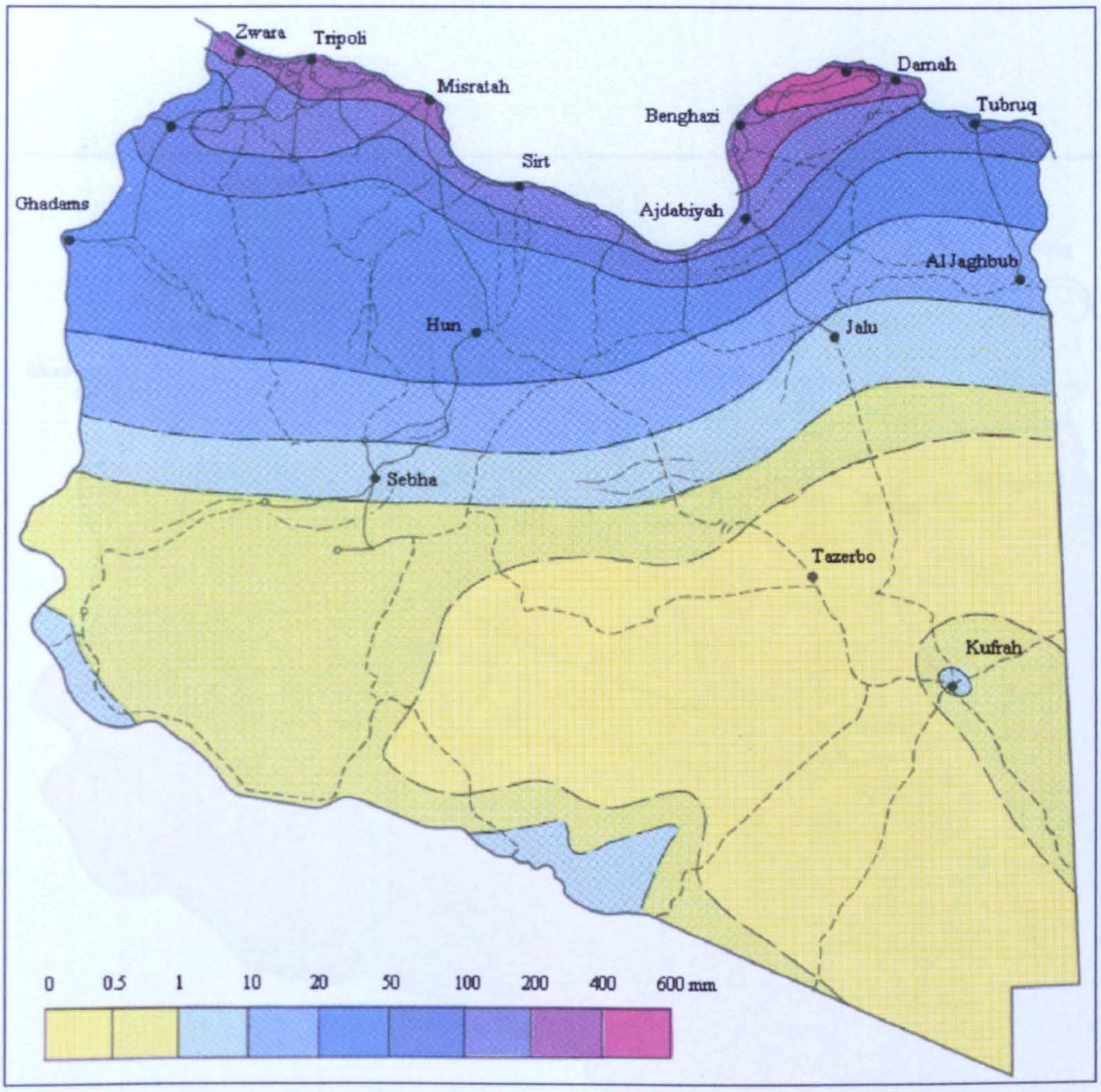

Figure 2.4 Annual average precipitation across Libya (*after* The Secretary of Planning 1978)

The coastal strip is characterised by warm summers and mild winters. Climate in the desert interior is characterized by very hot summers and extreme diurnal temperature ranges. An average temperature distribution during July and January, based on 30 years of climatic records, is shown in Figure 2.5 and 2.6. The coastal areas are affected in the period March to June by very high temperatures reaching 50 °C for a day or two associated with the southerly winds of ghibli transporting significant amounts of dust (Pearce and Smith, 1993).

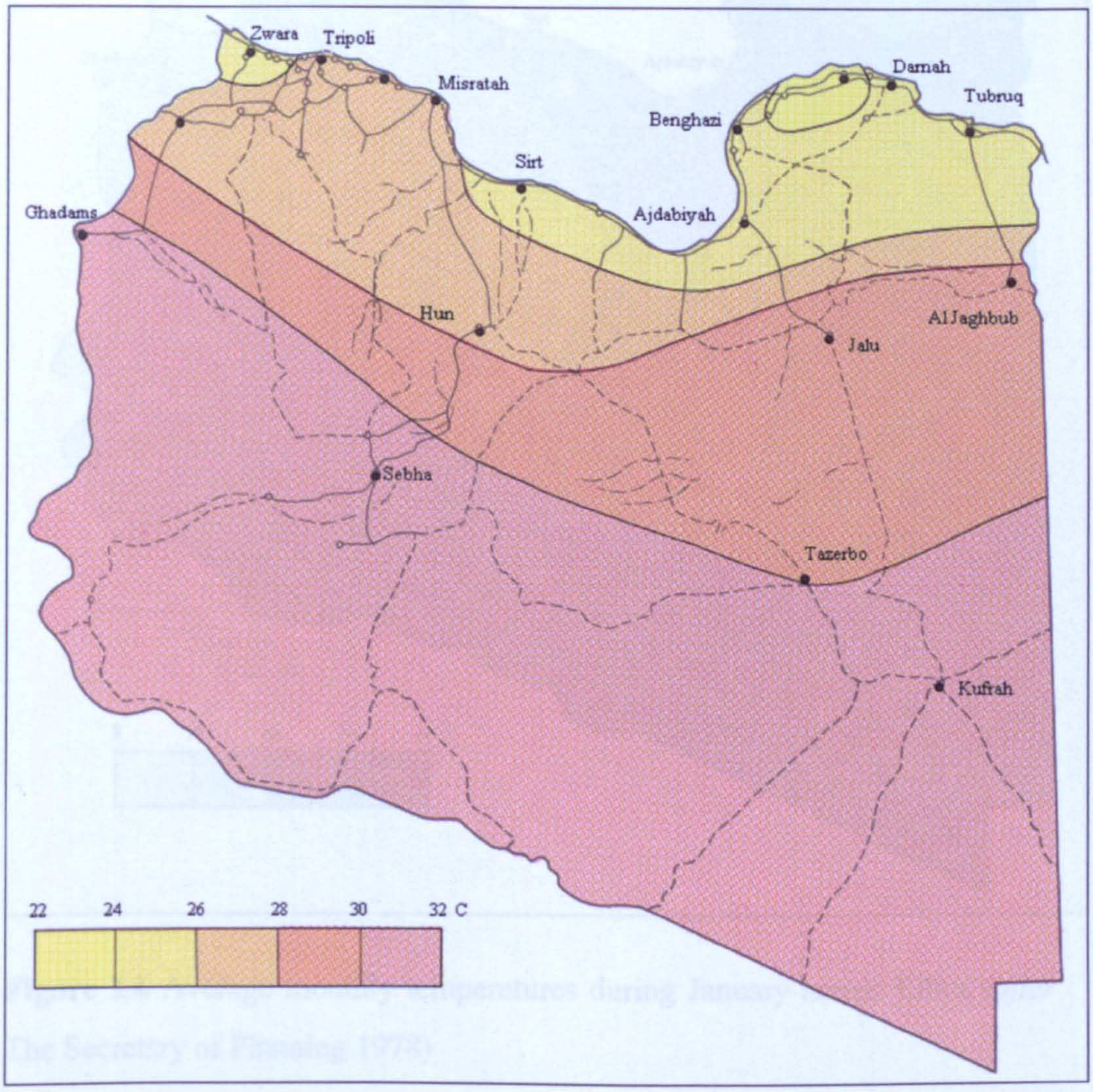

Figure 2.5 Average monthly temperatures during July across Libya (*after* The Secretary of Planning 1978)

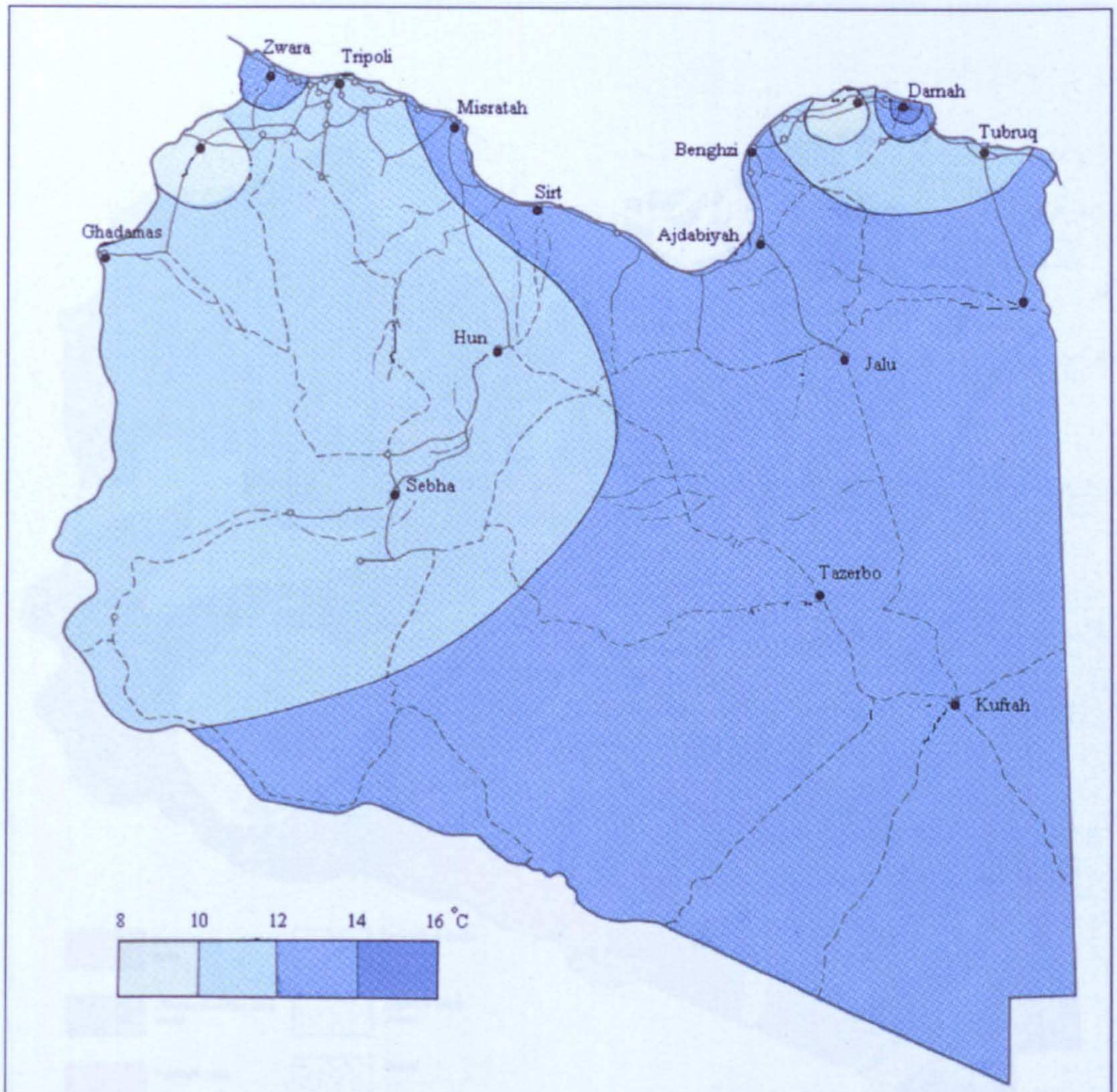

Figure 2.6 Average monthly temperatures during January across Libya (*after* The Secretary of Planning 1978)

2.3. GEOMORPHOLOGY OF LIBYA

The land formations of Libya are diverse ranging from low lands to mountainous regions and from sandy deserts to rocky plateaux. A landforms map of the country is shown in Figure 2.7.

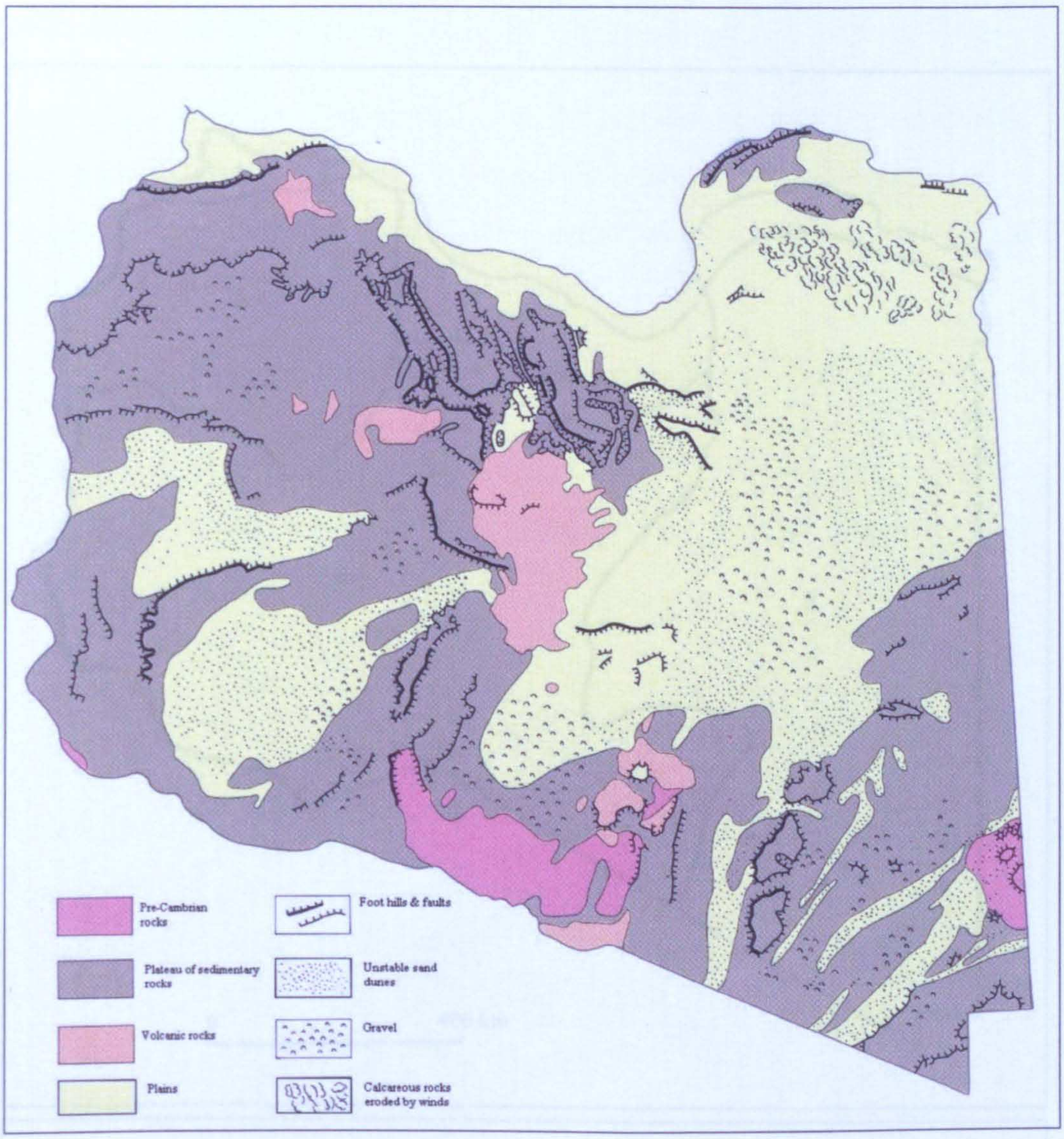

Figure 2.7 Landforms of Libya (*after* Secretary of Planning 1978)

[Scale 1: 12,000,000]

The description of geomorphology is simplified by deviding the country into six main regions (Figure 2.8).

- The Jifarah Plain and the foothills of Jabal Nafusah.
- The Hammadah Al Hammrah Plateau and Eastern Tripolitania valleys.
- The coastal region along the Gulf of Sirt from Al Khums to Ajdabiya.
- Northern Cyrenaica.
- Fezzan region.
- Southern Cyrenaica (The Libyan Desert).

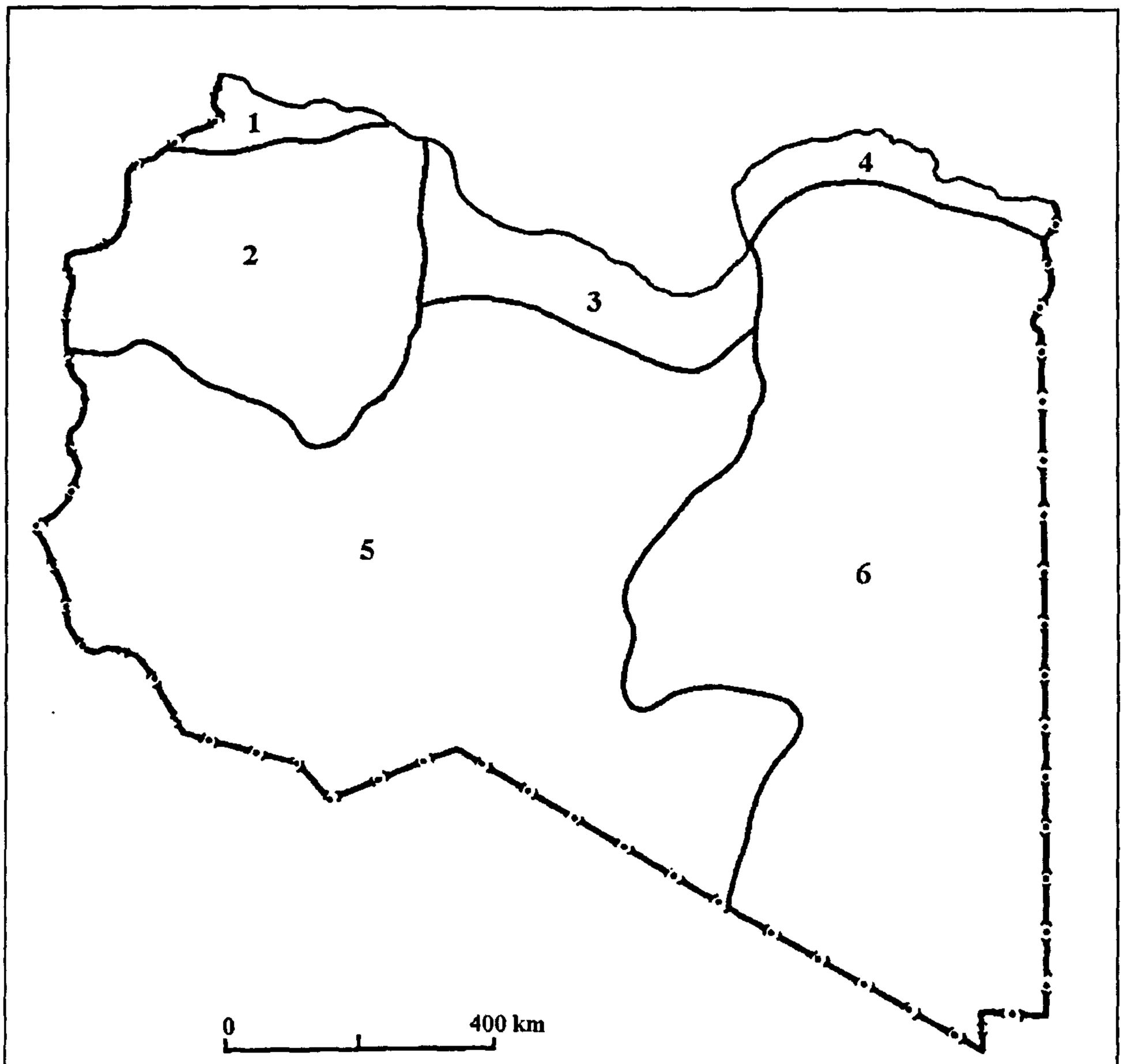

1. The Jifarah Plain and the foothills of Jabal Nafusah.
2. The Hammadah Al Hammrah Plateau & Eastern Tripolitania valleys.
3. The coastal region along the Gulf of Sirt from Al Khums to Ajdabiya.
4. Northern Cyrenaica.
5. Fezzan region.
6. Southern Cyrenaica (The Libyan Desert).

Figure 2.8 Map of natural regions (*derived from* Armandi 1976)

2.3.1. Northern Libya

North of the 30th parallel along the coast, the northern lands can be subdivided into four regions from west to east. Anketell (1989) has provided a geomorphologic review of three of these regions and the following is based on his work.

2.3.1.1. The Jifarah Plain and the foothills of Jabal Nafusah

A triangular region bounded to the north by the Mediterranean Sea and to the south by Jabal Nafusah, known as Jifarah Plain (Figure 2.9), comprises Mesozoic limestones and sandstones.

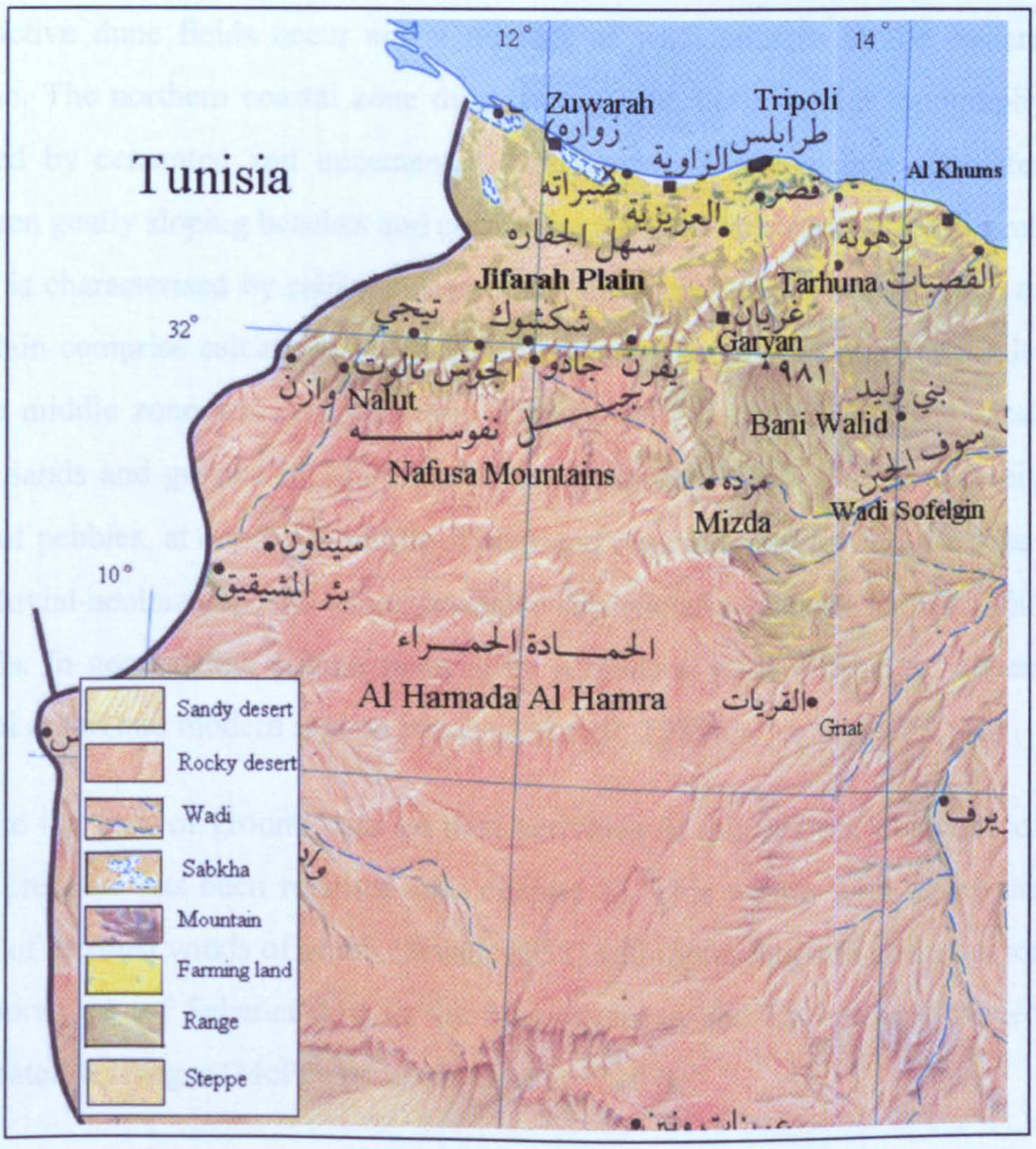

Figure 2.9 Geomophological features of Jifarah Plain and Al Hammadah Al Hamrah (*after* The Secretary of Planning, 1978)

The Jifarah Plain stretches westwards from Al Khums over a distance of 300 km and is widest near the Libyan Tunisian border (about 100 km). The escarpment of the plain drops to meet the sea in Al Khums and rises steadily southwards from the coast to reach 250 m at the base of the escarpment which rises sharply to about 600 m. The Jifarah Plain can be subdivided into three main zones, a coastal zone of a maximum 3 km in width, followed by a 50 km wide middle zone and a southern zone which abuts the escarpment. The southern zone has an irregular topography consisting of a blanket of Quaternary deposits and outcrops of calcareous Mesozoic rocks, incised by a number of wadis which reach the coast. The wadis constitute a major geomorphological feature in the vicinity of Al Khums in the eastern part of the plain. The middle zone is mainly flat with limited topographical changes where some stabilised and active dune fields occur and a number of wadi courses in the eastern Jifarah. The northern coastal zone displays a gentle, but irregular topography created by cemented and uncemented sand dunes. The coastline alternates between gently sloping beaches and cliffs. The northwestern zone of the Jifarah Plain is characterised by sabkahs near Zuwarah. Facies in the coastal zone of the plain comprise calcarenites and red silts which change into sands and silts in the middle zone and conglomeratic deposits in the foothills and the Jabal area. Sands and gravels in Jifarah comprise yellowish, aeolian sand and thin beds of pebbles, at depth, in middle Jifarah and pass laterally toward the Jabal into fluvial-aeolian deposits which comprise superficially cemented alluvial fan gravels. In general, the Jifarah plain is by a modern wadi fill, active dunes, coastal dunes and modern sabkah beach (Anketell, 1989).

Despite the lack of ground data on dust activities in this region, evidence of loess presence has been reported (see chapter 1). This region falls under the effect of the dust winds of ghibli (Sivall, 1957) and represents one of the major transport roots of Saharan dust to the Mediterranean and Europe as revealed from satellite images (McPeters, 2002; Goudie, 2003).

2.3.1.2. The Al Hammadah Al Hamrah Plateau and Eastern Tripolitania Valleys

This plateau is mainly comprised of Mesozoic and Tertiary limestones, shales and substantial basalt lava fields between Gharyan and Beni Walid (Figure 2.9). In the west, the plateau descends gently to the south and southeast from the Jabal Nafusah escarpment and is dissected by a number of wadis. In the east, in the region of Mizdah and Beni Walid, the plateau is cut by deep, well-defined ephemeral wadi systems draining northwards to the Mediterranean Sea. Deposits on the plateau are aeolian red sands rich in iron hydroxides. Fluvio-aeolian deposits reach up to ten metres in thickness occur in major wadis, regional depressions and on the plateau but, they are thinner and of a lesser gravel content on the plateau. Large vegetated barchan dunes overlie the fluvio-aeolian deposits and unconsolidated mobile dunes are reported on the plateau and in the wadis. Recent wadi deposits from silts to gravel are found across the whole region (Anketell, 1989).

The local aeolian activities in this region may be higher than those in the Jifarah Plain and the foothills of Jabal Nafusah due to poorer vegetation cover and the presence of a large number of ephemeral wadis; however, this region falls under the same effects created by regional dust storms.

2.3.1.3. The coastal region along the Gulf of Sirt from Al Khums to Ajdabiya

This area is predominantly low lying and underlain by limestones and marls. One of the largest sabkhas in the country stretches along the coast from south Misratah to Bu'ayrat and about 30 km inland (Figure 2.10). In the eastern zone of this region, large areas of sabkha lands can be found along the coast between Ras Lanuf and Ajdabiya and about 70 km toward the south (Figure 2.11). These sabkhas are a main feature of the land surface in this region. The region comprises aeolian dunes, beaches, wadis and fluvio- aeolian deposits (Anketell, 1989; USGS, 1962). This region may have a significant contribution of dust due to the presence of the Sabkhas.

Figure 2.10 Sabkhat Tawurgha along the western coast of the Gulf of Sirt

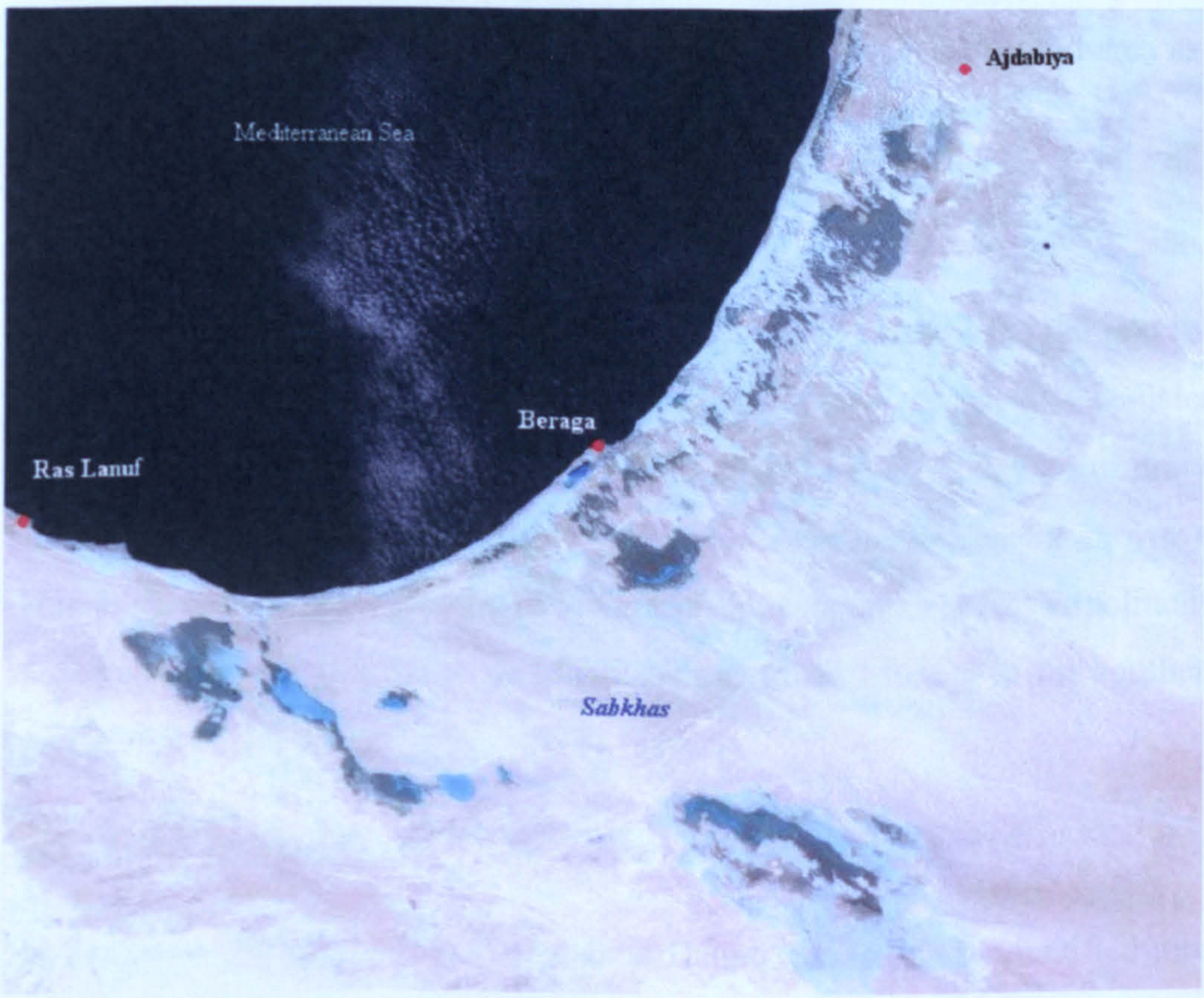

Figure 2.11 Sabkhas along the southeastern coast of the Gulf of Sirt. Enhanced Thematic Image Mapper Plus (Landsat 7) in true colour (*from* US Geological Survey 2002) [11/12/2002]

2.3.1.4. Northern Cyrenaica

Along the coast of Cyrenaica from Benghazi to Darnah, stretch the high lands of Al Jabal al Akhdar which form an anticline oriented east/northeast to west/ southwest. The rocks here are largely composed of Cretaceous and Tertiary limestones. In some places land surface height reaches 882 m above sea level. On its northern side, the Jabal consists of two nearly parallel escarpments which are cut by a number of wadis. A terrace ranging from 3 to 25 km in width lies between the two escarpments. Generally, the terrace has a gentle seaward slope. The upper escarpment extends over a distance of about 300 km. The wadis on the southern and western slopes end at the coastal plain or the semi-arid region to the west (Hasan, 1997). The Jabal topsoil is largely formed of terra rossa (Blake *et al.*, 1987). Although, this region is more vegetated than any other region in the county which makes the topsoil less vulnerable to entrainment by wind; the ephemeral wadis in this region are believed to be of a great significance in transporting fluvial sediments to the northern areas of the Libyan Desert, a well recognised area as a major source of dust (Prospero *et al.* 2002) as described in chapter 1.

2.3.2. Southern Libya

South of the 30th parallel, the southern land surfaces can be subdivided into two natural vast regions, the Fezzan region and the southern region of Cyrenaica. The desert is named according to the nature of its surface. A surface of gravel is known as Sarir, such as Sarir Tibesti and a desert pavement is known as Hamadah such as Al Hamadah al Hamra in the southern part of Tripolitania. Sandy regions are referred to as Idhan such as Idhan Murzug in the southern part of Fezzan region (Armandi, 1976).

2.3.2.1. Fezzan region

In Fezzan to the south of Al Hamadah al Hamra, the region is identified most by two sand seas known as Idhan Ubari and Idhan Murzuq. These two are separated by a plateau known as Hamadat Murzuq, extending from southwest to northeast across Fezzan as shown in Figure 2.12.

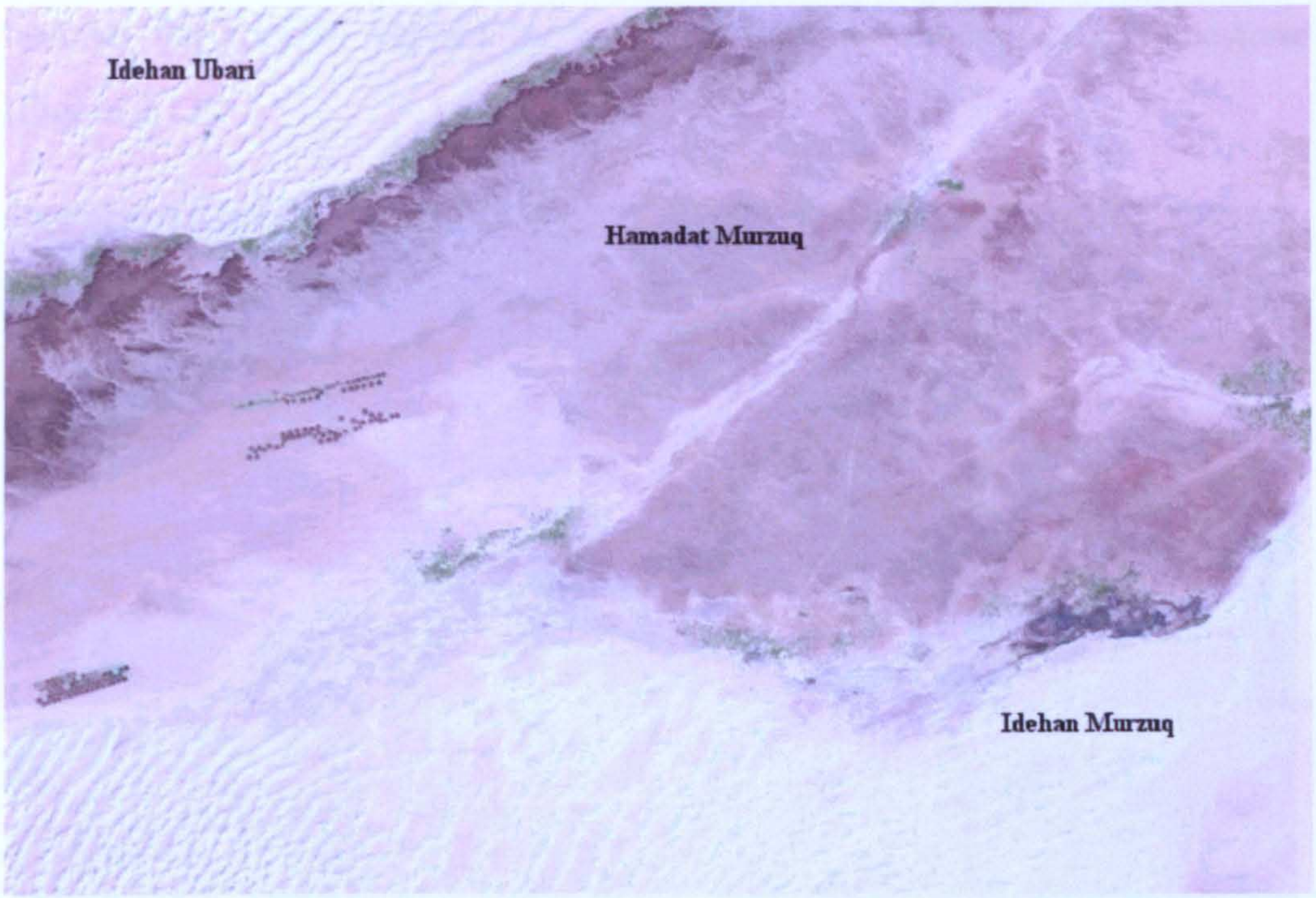

Figure 2.12 Enhanced thematic image of Landsat 7 in true colour of the central region of Fezzan (*From* US Geological Survey) [Accessed 09/12/2002]

In this region, fine silt particles are preferentially eroded and separated from sand by wind and transported out of the region reducing the landscape to a nearly level plain (Fookes and Gahir, 1995). In the vicinity of Sebha, the capital of the south, seif (or linear) dunes seem to originate where either small rock masses or vegetation, or both create sand traps above the general level of the sand sea (Pitty, 1971). Simple crescentic sand dunes (barchans) lie transverse to the dominant wind direction with their 'horns' pointing down wind, occur in locations where the wind direction and sand supply remain constant. Wadis constitute the major geomorphologic feature of Fezzan, their width in the south reaching 2 km with a very gentle slope towards a narrow central channel in which some natural vegetation can grow. In the northern part of Fezzan where precipitation is slightly higher (10-20 mm/yr), the wadis are narrower and more vegetation can be found. These wadis and the complex network of dry channels are believed to have been formed during Quaternary times (Fookes and Gahir, 1995). The wadis are dry and recorded flow of water is less than 1 % of the time (Reid, 1994). The dry weather has caused hills and stepped plateau to

become flat topped, capped by more resistant accumulations of limestone (Figure 2.13).

Figure 2.13 Residual hills in Fezzan

In the southeastern part of Fezzan lies Sarir Tebesti, which comprises gravel plains with scattered sand and rock outcrops. This part of desert is situated about 500 m above sea level. To the north of Fezzan and south of the volcanic Jabal As Soda, basalt lava can be found in the flat central areas which occurs as fields of boulders and cobbles as a result of weathering (Fookes and Gahir, 1995). Further to the east of Fezzan in central Libya, nearly between 26°-28° N and 16°-19° E, stretches the highlands of Al Haruj al Asuad which rise nearly up to 1200 m above sea level and comprises lava and volcanic debris (Figure 2.14).

The soils of Fezzan largely comprise fluvial deposits, playa sediments, colluvial deposits, wadi sediments and aeolian deposits. The soils typically are carbonate rich sediments. Exposed terraced sediments of 3-5 m thick can be observed in some wadis where two distinct units of fluvial deposits are visible, a lower unit of weakly cemented gravels and carbonate rocks overlaid by an upper unit of yellowish sand. Playa deposits are less than 1 m

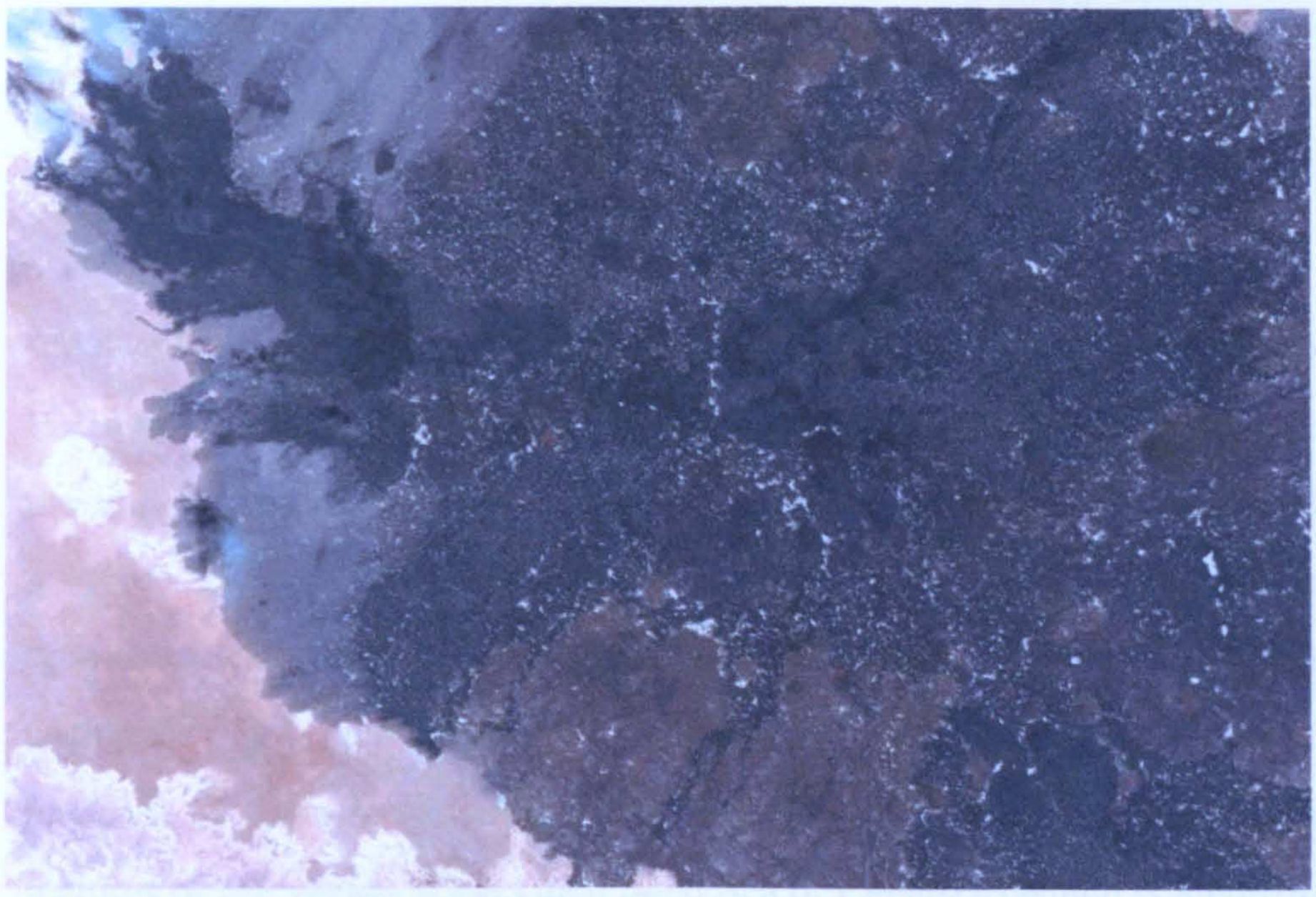

Figure 2.14 The volcanic high lands of Al Haruj al Asuad from space. Enhanced thematic image of Landsat 7 in true colour of (*From* US Geological Survey 2002) [Accessed 09/12/2002]

thick of salt rich sand, silt and clay accumulations. The playas are incised by present day wadis and locally overlain by Colluvial deposits. Colluvial deposits are small fans that occur adjacent to rock exposures, along wadi slopes and across rock plateaux. These deposits are composed of clastic debris of carbonate rock and chert loosely bound by gypsiferous sand clay. Wadi deposits are found on the bottom of most wadis, and consist of weakly cemented gravel with some sand. The surfaces layers are locally gypsiferous. Aeolian deposits in the form of barchan dunes have been formed by transporting sand from local unconsolidated deposits and sand seas in the south west of Fezzan. These dunes are mainly composed of fine and medium sand grains dominated by quartz (approximately 95 %) and the rest is feldspar or carbonate rocks. The heights of the barchans range between 3 to 5 m (Fookes and Gahir, 1995).

Despite its hyperarid nature, satellite spectrometers have never detected any major dust emission areas in this region (McPeters, 2002). Since Fezzan is situated in the central part of the Sahara where the presence of loess has been

reported (Assalley *et al.*, 1996), deposition of dust originating in the surrounding regions is feasible.

2.3.2.2. Southern Cyrenaica (The Libyan Desert)

This region is bounded by the eastern skirts of the volcanic highlands of Al Haruj al Asuad from the west and the Egyptian and the Sudanese frontiers to the east. It stretches toward the south to the skirts of Sarir Tibesti and the junction of the Egyptian-Sudanese-Chadi borders. This region is largely dominated by sand and sand dunes which are mostly consist of quartz (Armandi, 1976; Fisher, 1998). In additon, Bagnold (1941) reported the presence of ferrous oxides in the Libyan Desert. One of the most important features of this region is the Great Sand Sea of Calanscio which is identified by its sand dunes and linear ridges. West of the sand sea, beyond the 22nd parallel, stretches Sarir Calanscio, which is largely comprised of gravel plains with scattered sand. Occasional rock outcrops and wadis bisect the eastern escarpments of Al Haruj al Asuad. Sarir Calanscio rises from about 50 to 300 m above sea level at the eastern lower escarpments of Al Haruj al Aswad. It is dominated by linear dunes trapped by rock outcrops as the land surface rises toward Al Haruj. Further south, more sand dunes form the Rebiana Sea Sand. South of the Calanscio Sea Sand and south of Al Kufrah, the desert consists of gravels, scattered sand, some rock outcrops and barchan dunes. This region lies between the Egyptian frontier, the skirts of Jabal Arkanu and Al Uwaynat at the junction of the Egyptian-Sudanese frontiers and Sarir Rebiana (USGS, 1962; Armandi, 1976; Fisher, 1998).

The northern and western areas of this region have been recognised in recent aeolian studies as one of the most persisting sources of dust especially during the spring (e.g. Goudie and Middelton, 2001; Prospero *et al.* 2002) as described in chapter 1.

2.4. VEGETATION COVER

The northeastern and northwestern coastal regions are the most vegetated parts of Libya. The central northern coastal region along the Gulf of Sirt and some parts of the south are covered with sparse desert shrubs. Regions dominated by sand dunes in the east and southwest lack vegetation cover which make them potential sources of dust. The north eastern highlands of Al Jabal al Akhdar where rainfall is the highest in the country, vegetation consists of maquis Mediterranean scrub and steppe. Maquis can be found in the wetter northern slopes of the Jabal. East of the Jabal al Akhdar, beyond Darnah and south of the Jabal where rainfall is less the climatic conditions are more suitable for the growth of steppe vegetation (Hasan, 1997). Woodland maquis species which are largely xerophytic occur on the northern slopes of the Jabal and include rosemary [*Rosmarinus officinalis*], lentisc [*Pistacia lenticus*], deadnettle [*Phlomis floccosa*], prickly burnet [*Poterium spinosum*], sea squill [*Urginia maritime*], juniper [*Juniperus phoenicea*], kermes oak [*Quercus coccifera*], Libyan strawberry tree [*Arbustus pavarii*], *Thapsia garganica,* wild sumach [*Rhus oxyacantha*], jasmine box [*Phillyrea media*], carob [*Ceratonia siliqua*] and thorny lotus jujube [*Zizyphus lotus*]. On the southern slopes, the more drought resistance species can be found such as rosemary [*Rosmarinus officinalis*], sage [*Artemisia herba-alba*] and deadnettle [*Phlomis floccosa*] (Johnson, 1973). The Jabal al Akhdar is the only real forest to be found between Lebanon and Tunisia (Armandi, 1976). Similar species can also found in northwestern Libya. The chief species occur in Tripolitania are desert pistachio [*Pistacia atlantica*], umbrella thorn [*Acacia tortilis*], sumach [*Rhus*] and thorny lotus jujube [*Zizyphus lotus*] and some patches of Mediterranean scrub vegetation (Armandi, 1976). Drought resistant shrubs cover the coastal strip along the Gulf of Sirt where camel grazing is widely practised. South of the 30th parallel, shrubs are sparser due to low precipitation. Localised denser vegetation covers occur in the remote south near the oases particularly in central Fezzan and Jalu and Al Kufrah in Cyrenicia.

2.5. METEOROLOGICAL PATTERNS

2.5.1. Interannual variability of precipitation

Drylands are characterised by scarcity of precipitation, long time intervals between two successive rains, high interannual variability, increased aridity and more aggressive rains. The highest irregularities correspond to the tropical deserts. The Saharan region exhibits a variability between 80 and 100 % in its central parts and even higher than 100 % in the Libyan Sahara (Mainguet, 1998).

2.5.2. Bioclimatic aridity index

The FAO and UNESCO classify drylands on a quantitative basis using the Thornthwaite or bioclimatic aridity index P/PET, in which P is the annual precipitation and PET is the potential evapotranspiration (total moisture loss from soil and plant cover) (Mainguet, 1998). Drylands are classified into four classes, each class is defined by the interannual variability of precipitation and the bioclimatic aridity index (Table 2.1).

zones	Average rainfall	P/PET	Interannual var. precip.
hyper-arid	10 - 50 mm/yr	< 0.03	100%
arid	50 - 150 mm/yr	0.03 - 0.20	50 - 100 %
semi-arid	150 - 500 mm/yr	0.20 - 0.50	25 - 50 %
sub-humid	500 - 800 mm/yr	0.50 - 0.75	< 25 %

Table 2.1 Aridity classification by UNESCO 1979 (Bruins and Lithwick 1998)

The bioclimatic index values at different sites across Libya, as calculated from climatic data records over a thirty year period (FAO, 1984), reveal that Libya falls in three climatic zones: hyper-arid, arid and semi-arid. Different degrees of bioclimatic aridity at several sites in Libya are shown in Figure 2.15 and provided in Table 2.2.

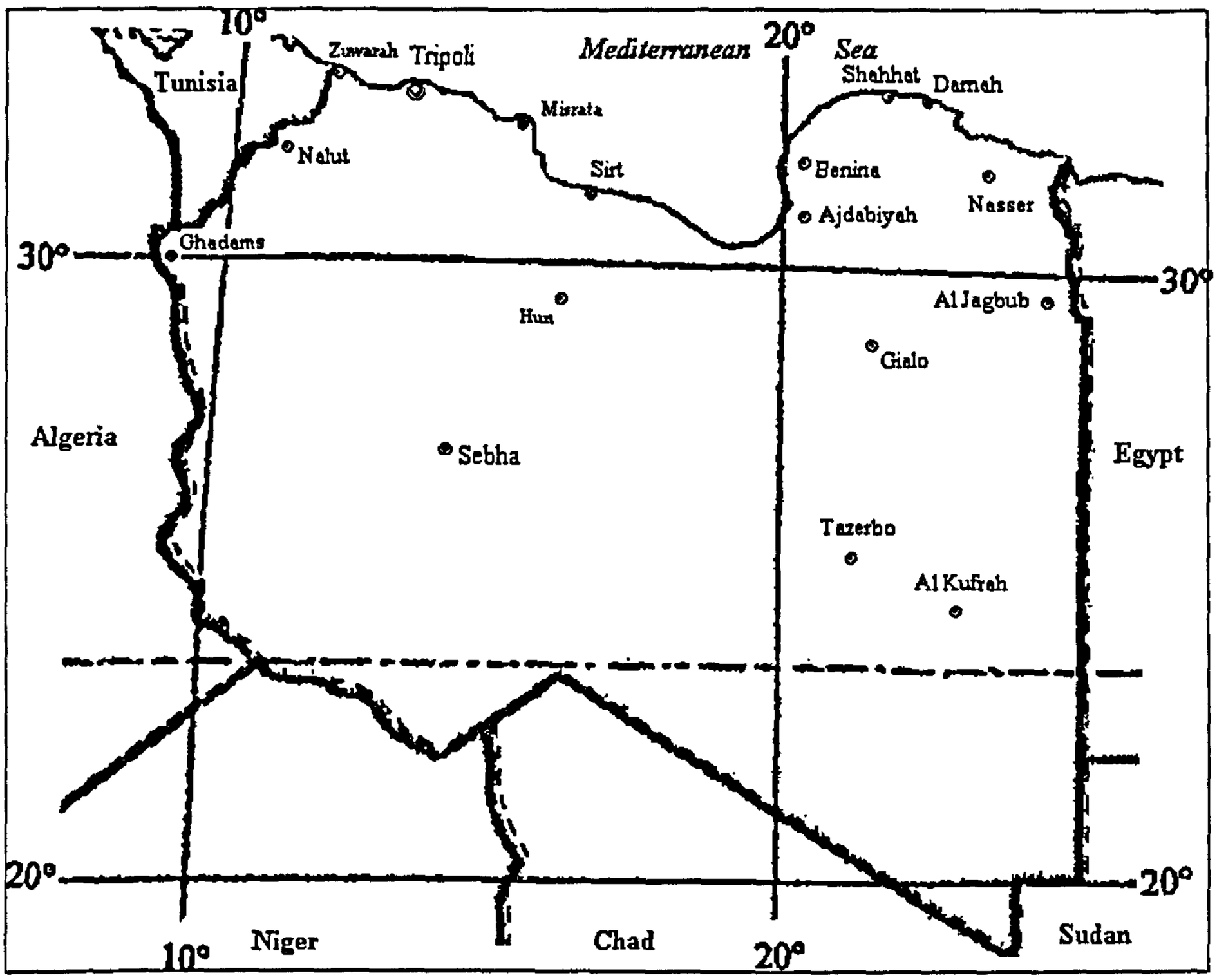

Figure 2.15 Sites of different degrees of aridity in Libya (*modified* Reed Int'l Ltd. 1993)

STATION	LATITUDE	LONGITUDE	ALTITUDE	P/PET	CLIMATIC ZONE
Nalut	N 31.52	E 10.59	620 m	0.06	arid
Zuwarah	N 32.55	E 12.05	3 m	0.18	arid
Tripoli	N 32.54	E 13.11	20 m	0.22	semi-arid
Misratah	N 32.25	E 15.06	6 m	0.19	arid
Sirt	N 31.12	E 16.35	22 m	0.15	arid
Benina	N 32.05	E 20.16	132 m	0.23	semi-arid
Ajdabiyah	N 30.43	E 20.10	6 m	0.08	arid
Shahhat	N 32.49	E 21.51	625 m	0.45	semi-arid
Darnah	N 32.44	E 22.38	9 m	0.20	arid
J. A. Nasser	N 31.51	E 23.55	155 m	0.06	arid
Ghadams	N 30.08	E 9.30	338 m	0.00	hyper-arid
Sebha	N 27.01	E 14.26	434 m	0.01	hyper-arid
Hun	N 29.08	E 15.57	261 m	0.02	hyper-arid
Gialo	N 29.02	E 21.34	62 m	0.00	hyper-arid
Al Jaghbub	N 29.45	E 24.32	-1 m	0.00	hyper-arid
Tazerbo	N 25.48	E 21.08	260 m	0.00	hyper-arid
Al Kufrah	N 24.13	E 23.18	418 m	0.00	hyper-arid

Table 2.2 Bioclimatic aridity in Libya (*calculated from meteorological data published by* FAO 1984)

2.6. CONCLUSION

This chapter draws together literature dealing with the land surface conditions in Libya and provides essential background needed to facilitate the physical interpretation of the spatial and temporal variations in dust deposition rates and mineral composition. It also highlights the importance of this country on the world map of aeolian dust. The aridity of the study area is one of the factors on which the applied dust trapping method in this project was based (see chapter 4), the geomorphological, meteorological and demographic factors constitute the elements in interpreting the results in the subsequent chapters.

CHAPTER 3

AEOLIAN ENTRAINMENT AND TRANSPORT OVER LIBYA

3.1. INTRODUCTION

This chapter presents a review of particle entrainment mechanisms, transport modes and present day methods of measuring dust flux. A TOMS data set of the average monthly emissions inside Libya and the surrounding regions and their effects on the study area is also presented. Transported aerosols over the study area are linked to the more likely source(s) based on the general climatic patterns of North Africa.

3.2. AEOLIAN ENTRAINMENT MECHANISMS AND TRANSPORT MODES

Soil and sediment particles at rest on a bed surface can be moved by wind by one or more of four mechanisms: air drag; aerodynamic lift; ballistic impacts caused by rolling or bouncing particles and disturbance created by humans and animals. Once a particle is dislodged from the surface it is transported in the atmosphere in a horizontal mode by mechanisms known as saltation and modified saltation, or in a vertical mode by suspension. The mode in which particles are transported determines the range of their transport (Pye, 1987).

3.2.1. Aeolian entrainment mechanisms

3.2.1.1. Drag

Drag is classified into types, surface and form drag. Surface drag is the skin friction between the particle surface and the air, whereas form drag is the difference in pressure between the windward and the leeward side of the particle. Surface drag causes particles to roll, whilst form drag causes particles to roll and slide (Cooke *et al.*, 1993). The flow of wind over a stable bed is opposed by friction created by the roughness of the surface that reduces the wind velocity profile to zero near the surface. The roughness height of the zero velocity plane (z_o) is about $1/30^{th}$ of the particle diameter on the bed surface (Bagnold, 1941). In the presence of non-erodible roughness elements, the zero velocity plane is displaced upwards to some height determined by the flexibility and permeability of these elements. Above this plane, the average forward velocity (U_z) of the wind increases as the height above the surface increases due to the decreasing effects of surface shear. The relationship is defined by von

Kármán-Prandtl logarithmic velocity profile law (Pye and Tsoar, 1990; Cooke *et al.*, 1993; Nickling, 1994; Wiggs, G.F.S., 1997):

$$u_* = k\, U_Z / \ln (z/z_\circ) \qquad [3.1]$$

where

k is the von Kármán constant, a temperature dependent constant but, is usually is taken to be 0.4

U_Z is the average time wind velocity at a height z

$z_\circ$ is the zero velocity plane height

u_* is the shear velocity

The shear or drag velocity is related to the horizontal force exerted by the wind at the surface, the shear stress (τ), and air density (ρ_a) by the equation [3.2] (Pye, 1987).

$$u_* = \sqrt{\tau / \rho_a} \qquad [3.2]$$

The velocity at which aerodynamic forces are sufficient to dislodge particles from the soil and initiate movement is referred to as the threshold velocity (Bagnold, 1941) and defined by the relationship

$$u_{*t} = A \sqrt{(\rho_p - \rho_a / \rho_a)\, g\, D} \qquad [3.3]$$

where

u_{*t} is the fluid threshold velocity

ρ_p is the relative density of the grains (g/cm)

ρ_a is the relative density of the air (1.22×10^{-3} gm/cm^3)

g is the gravity (980 cm/s^2)

D is the mean grain diameter (cm)

A is an empirical coefficient equals 0.1 for Reynolds numbers, Re > 3.5 ($Re = u_* D/\nu$) where ν is the kinematic viscosity of the air, a temperature dependent parameter. Reynolds numbers are a measure of flow turbulence.

The relationship between u_{*t} and D as shown in Figure 3.1 reveals that a 0.06 mm mean grain size particle is associated with the minimum threshold velocity (Wiggs, 1997). Particles larger than 0.06 mm require greater wind speed, probably because of their greater weight.

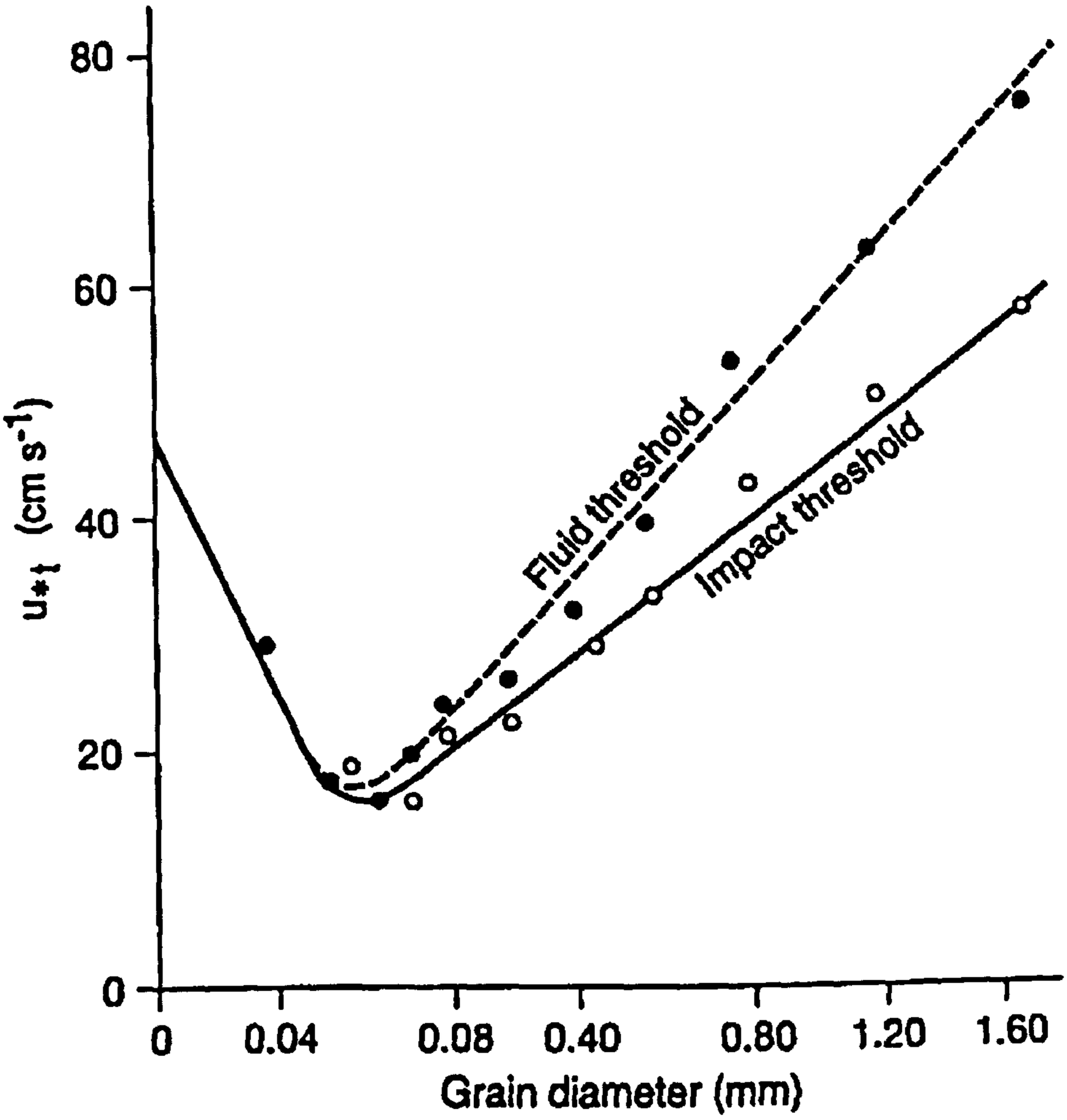

Figure 3.1 Fluid threshold velocity and impact velocity versus median particle diameter (*from* Wiggs, 1997)

The finer the particle the stronger the interparticle contact by moisture and electrostatic charges is. These fine particles require larger pressure fluctuation to overcome the interparticle cohesiveness and dislodge from the bed surface. Once particle movement begins, momentum is transferred from a moving particle to a resting one which results in more dislodged particles from the

surface (Gillette, 1981; Pye and Tsoar, 1990). The stability of a soil surface and the bonding between its particles is attributed to several factors. These factors include, moisture, salt content, algae and fungi and the presence of non-erodile cover such as large grains (gravel) and shrubs. The denser the non-erodible cover, the higher the threshold velocity required to activate erosion (Pye, 1987). The moisture content can be a very effective factor in increasing the required threshold velocity to dislodge fine particles. An experimental study has shown that 0.6 % moisture (by volume) could double the threshold velocity if compared to dry sand (Belly, 1964). Similar conclusions have also been reported by others (e.g. Chepil, 1956; Svasek and Terwindt, 1974; Bisal and Hsieh, 1966). Equation [3.3] has been modified to include the effect of moisture content on the threshold velocity (Belly, 1964; Nickling, 1994).

$$u_{*tw} = A[(\rho_p - \rho_a / \rho_a)\, g\, D]^{0.5} (1.8 + 0.6 \log_{10} W) \quad [3.4]$$

where

u_{*tw} is the threshold velocity for wet soil

W is the percentage of moisture content

A linear relationship between air threshold velocity and moisture content for grain size range 0.2- 0.8 mm was experimentally concluded by (Horikawa *et al.*, 1982; Hotta *et al.*, 1985):

$$u_{*tw} = u_{*t} + 7.5\, W \quad [3.5]$$

When evaporation rates are high, the surface dries rapidly causing a lower threshold velocity (Hotta *et al.*, 1985):

$$u_{*tw} = u_{*t} + 7.5\, W\, I_w \quad [3.6]$$

Where I_w is a function of the evaporation rate and given values range between 0 and 1.

3.2.1.2. Aerodynamic lift

Once the threshold velocity requirement is met and the grain starts to move, the particle begins to roll and then bounce under the effect of the velocity pressure exerted by the air on the upwind side of the grain and the negative viscosity pressure on the down wind side (Bagnold, 1941). Others noted that sand grains begins to rock backwards and forwards and then are lifted into the flow due to the instantaneous variation of the air pressure near the surface (Bisal and Nielsen, 1962). Lifting occurs as the static pressure at the top of the grain decreases with respect to the bottom which is known as the Bernoulli effect (Figure 3.2; Chepil, 1945). A discontinuous lift is attributed to fluctuation in the above the surface pressure created by a turbulent eddy motion (Lyles and Krauss, 1971). Lift is important only to the fist ejections and can raise particles only slightly (Cooke *et al.*, 1993). Instantaneous fluctuations in drag and lift enhance the mechanisms of dust entrainment (Chepil, 1959). Drag and lift become negligible once bombardment begins (Cooke *et al.*, 1993).

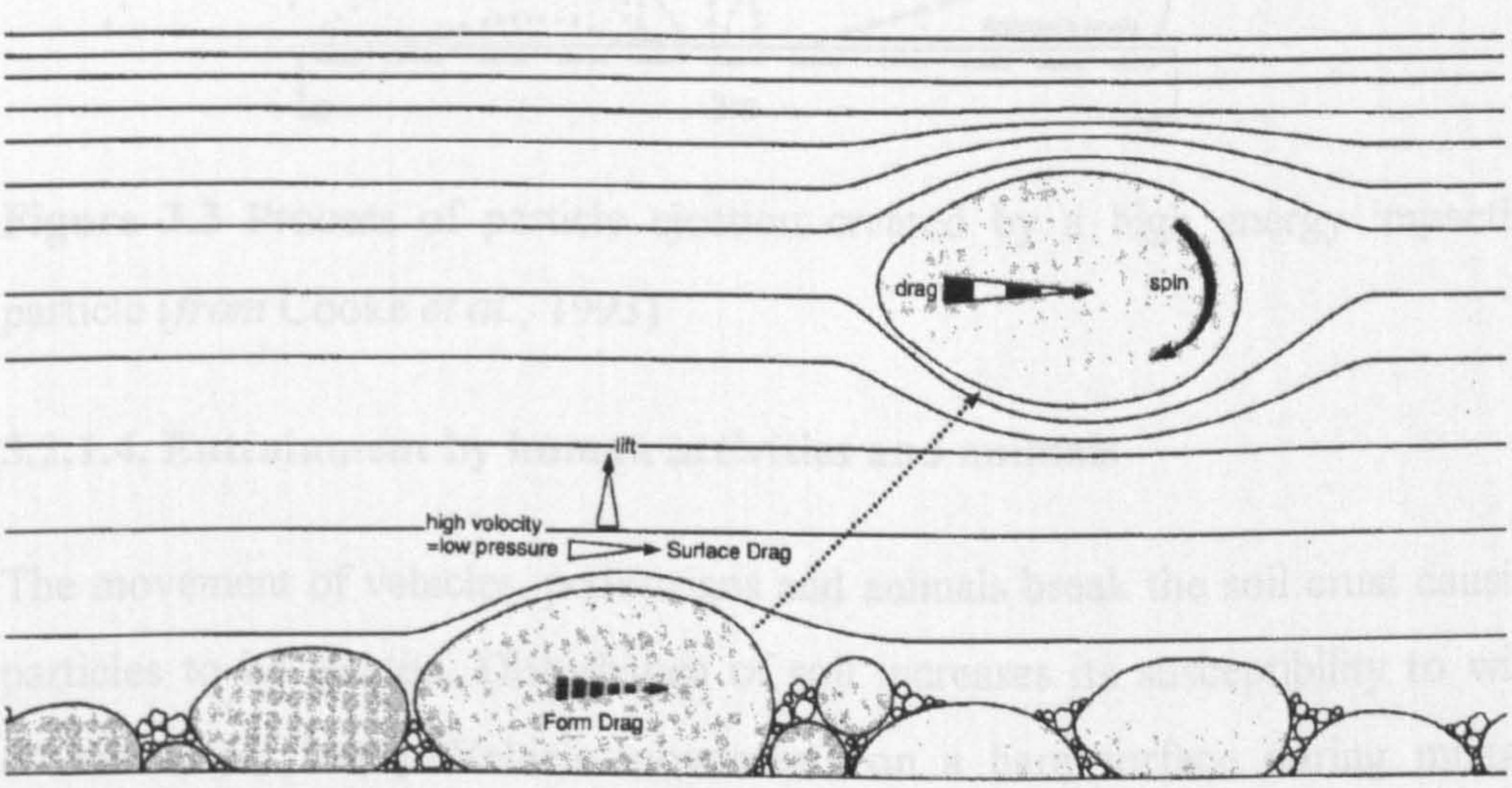

Figure 3.2 Lift, shear and spin of an entrained particle (*from* Cooke *et al.*, 1993)

3.2.1.3. Ballistic impact

Once the particles movement begin, the settled particles on the surface become subjected to impacts by the entrained particles which cause them to eject. The minimum velocity of the moving particles to entrain particles at rest is called the impact threshold (Bagnold, 1941). The relationship between the impact

threshold velocity and the particle size is illustrated in Figures 3.1 (Bagnold, 1941). The size and the number of the ejected particles from the surface depend on the speed, trajectory of the impacting particles and the nature of the impact (Pye, 1987). Once a descending particle collides with the bed, its energy is imparted to other particles that results in the ejection of about 10 particles with velocities of about 10 % of the impact velocity (Figure 3. 3).

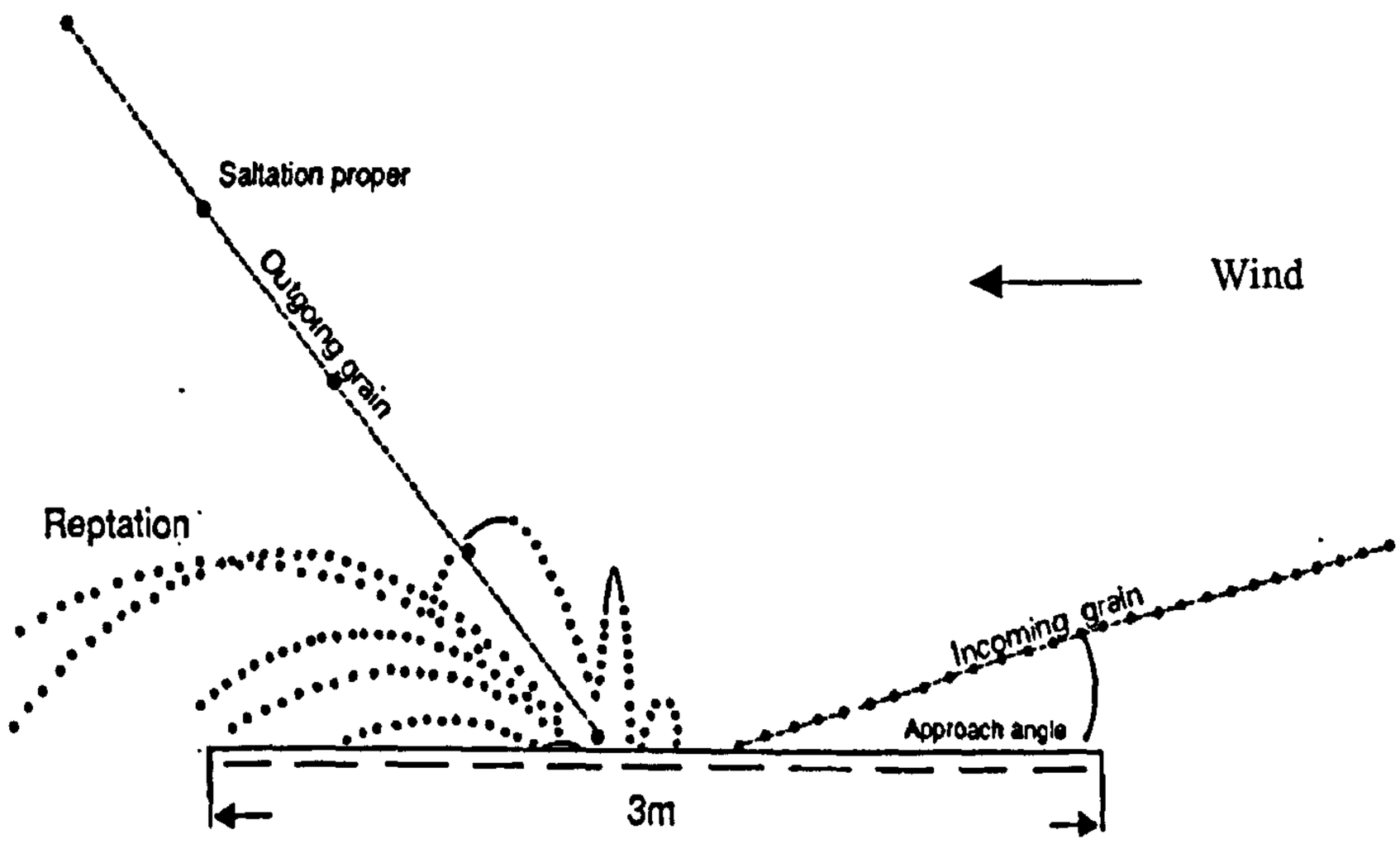

Figure 3.3 Process of particle ejection created by a high energy impacting particle (*from* Cooke *et al.*, 1993)

3.2.1.4. Entrainment by human activities and animals

The movement of vehicles, pedestrians and animals break the soil crust causing particles to be ejected. Disturbance of soil increases its susceptibility to wind erosion (Pye, 1987). Vehicle movements on a bare surface during military manoeuvres in a desert area can raise large amounts of dust into the atmosphere (Wilshire, 1980). The movement of vehicles on unpaved roads can also generate significant amounts of dust (Rubio *et al.*, 1998). It has been estimated that a 4-wheel vehicle travelling at 60 km/h along a dirt road containing 12% silt can raise 3-7 kg/km of dust (Hall, 1981). Furthermore, human activities in arid regions of the world where vegetation cover is limited tend to enhance wind erosion. In Libya and Egypt, grazing is blamed for reducing land cover and

inducing deflation of topsoil in the coastal areas which regarded as a pervasive. In the coastal areas of Western Cape, South Africa, erosion is attributed to intensive mechanised agriculture (UN Environmental Programme, 1997).

3.2.2. Particle transport modes

The physical characteristics of the deflated particle, the velocity and the turbulent structure of the wind define transport mechanisms of dust particles. All modes of particle transport have higher chances to develop simultaneously on a multi-grain size soil surface. Once removed from the soil surface, a particle either returns immediately to the surface a short distance down wind of the entrainment point or remains suspended in the atmosphere for a longer period of time as shown in Figure 3.4 (Pye, 1987).

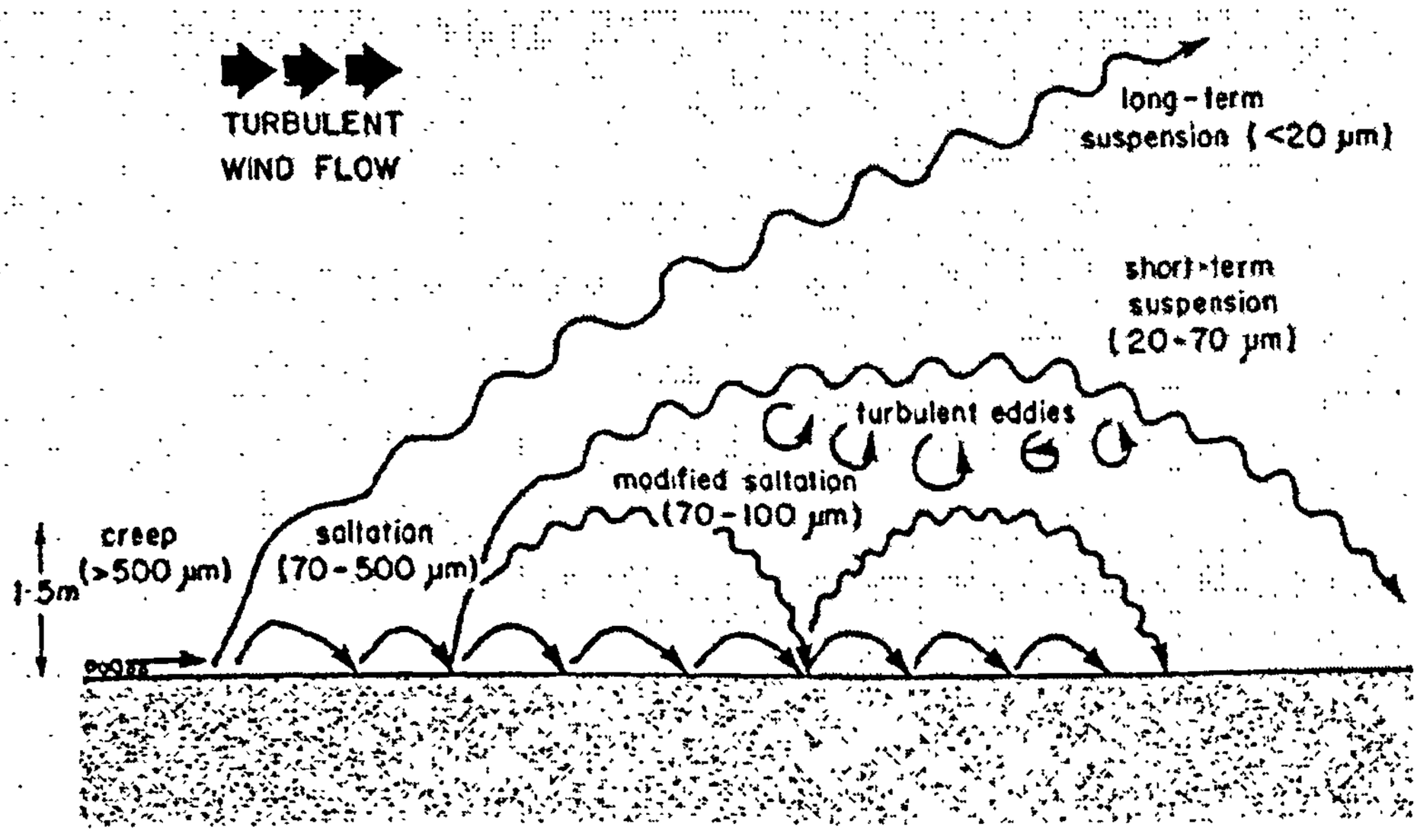

Figure 3.4 Particle transport modes and corresponding particle size ranges of a moderate windstorm (*after* Pye, 1987)

3.2.2.1. Horizontal flux component

Dislodged grains from the bed surface move forward either by series of jumps which is known as *saltation* or by rolling or sliding along the surface which is known as *surface traction.* The movement of grains near the bed surface is known as *bedload* transport. This type of transport mechanism constitutes the horizontal flux component. Grain sizes between 0.1 and 0.3 mm in diameter

constitute most of the saltating grain sizes in a typical windstorm. Bedload transport is the main mechanism in sand dune formation (Pye and Tsoar, 1990).

3.2.2.2. Vertical flux component

Some of the dislodged soil particles can be lifted by wind from the surface, driven long distances, remain suspended in the atmosphere for several days and fall out of suspension as wind velocity declines or if washed out by rain. The vertical velocity component of the wind must exceed the settling velocity, the downward velocity, of the particle so it remains in suspension otherwise, it returns to the surface (Pye and Tsoar, 1990). The settling velocity of a particle depends on its mass and shape and can be calculated from Stoke's Law (Green and Lane, 1964):

$$U_f = K. D^2 \qquad [3.7]$$

where

U_f is the settling velocity (cm/s)

D is the particle diameter (cm)

$K = \rho_p\, g/18\, \mu$ (cm-1 s-1)

Where (ρ_p) is the particle density, (g) is the gravity constant and (μ) is the dynamic viscosity of the air.

Wind blown suspended dust can be divided into two types based on the travelling range. Dust initiated by local dust storms can travel distances of less than 100 km and result in widespread loess deposits in the world. This type of dust consists of particles within the range 5 to 50 μm in diameter. The other type is the fine aerosol that is composed of particle sizes ranging between 2 and 10 μm. This fine aerosol remains in suspension and in motion in the troposphere until brought down to the surface by rain (Péwé, 1981). It was noted that Saharan dust collected in the Caribbean was composed of more than 98 % fine particles (< 10 μm) (Prospero *et al.*, 1970). Central Asian dust has been detected over Alaska, consisting of 2 μm median particle radius and was believed to have travelled more than 5000 km (Rahn *et al.*, 1981).

3.2.2.3. Total dust

The vertical flux component becomes insignificant when the particle mean settling velocity is much larger than the mean drag velocity (U_f / u_* >> 1) and most of the grains are moved by a pure bed load transport. If the particle mean settling velocity is reduced with respect to the drag velocity such that U_f / u_* << 1, the transport becomes a pure suspension. In an intermediate range between these two modes where $U_f/u_* \leq 1.25$ and $U_f/u_* \geq 0.7$, particles display random trajectories throughout the flow in an alternating behaviour between saltation and suspension in a transport mode known as modified saltation (Nalpanis, 1985; Gillette *et al.*, 1974). Modified saltation is a part of the horizontal flux component. Total flux is a combination of both component horizontal and vertical. There is no sharp division between a bed load and a suspended load; it is rather a gradual transition (Nickling, 1983).

3.3. MEASURING DUST FLUX

Aeolian particle flux rates are estimated either by using satellite imagery based techniques (see section 3.4), ground modelling (see section 3.5) or quantified near the ground surface using sand and dust traps (see chapter 4).

3.4. DUST EMISSION AND TRANSPORT FROM SATELLITE IMAGERY

3.4.1. Overview

Data sets collected from different satellite sensors have been utilised to identify source areas of major dust events. These include the North Atlantic Oscillation (NAO) index, the Infra-red Difference Dust Index (IDDI) and the Total Ozone Mapping Spectrometer Aerosol Index (TOMS AI).

TOMS is a device carried on board the Earth Probe satellite, designed to provide data regarding ozone levels. Unlike its predecessors, TOMS is the first sensor detecting aerosol and smoke over land. It is also capable to discriminate between light absorbing and light reflecting aerosols. Thirty-five measurements in every 8 seconds are executed by this sensor which make TOMS capable of monitoring dust storms and biomass burning around the globe (Smith, 2003).

3.4.2. Atmospheric modelling using TOMS data

In recent years, the relative amounts of aerosols have been measured using the Earth Probe Total Ozone Spectrometer (EP-TOMS). The measurements represent the amount of ultra-violet radiation absorbed by the atmosphere and the amount reflected back into space (Prospero *et al.*, 2002). Differences in pixel colours indicate differences in aerosol concentration that is quantitatively described by the TOMS aerosol index. The TOMS aerosol index is a measure of how much fine airborne particles are prevented from passing through a column of the atmosphere. Aerosols tend to absorb or reflect incoming sunlight that result in reduced visibility, increased optical depth and higher aerosol index. An aerosol index of less than 0.1 indicates clear sky, while an index of 4.2 indicates a very high density of aerosols making sunlight difficult to see at mid-day (Figure 3.5).

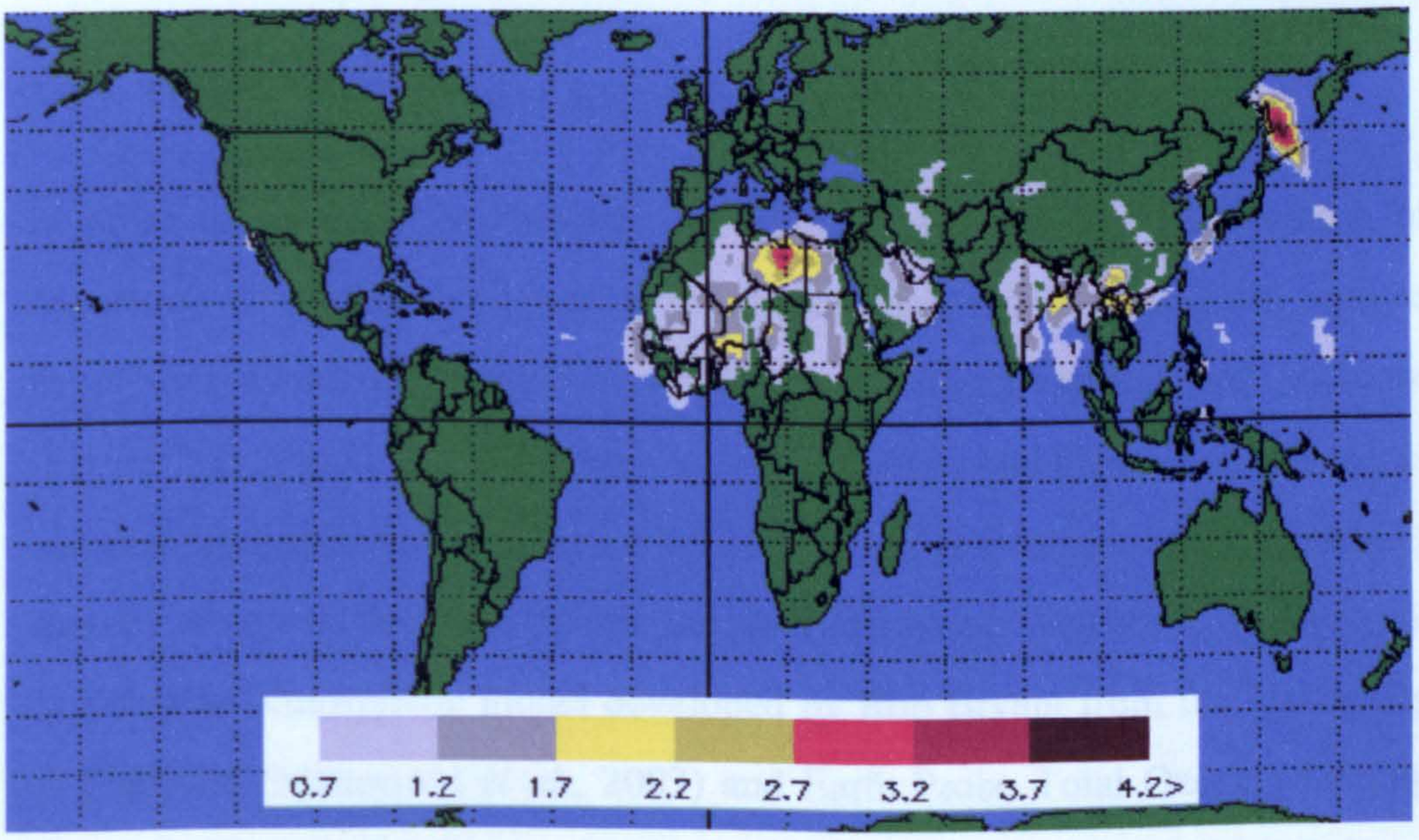

Figure 3.5 TOMS AI for 10 April 2000 (*from* McPeters 2002)

The daily TOMS measurements have a spatial resolution of 50 × 50 km at nadir and 150 × 250 km at extreme off nadir. The satellite-based spectrometer utilizes backscattered UV radiance measured in six bands (313, 318, 331, 340, 360 and 380 nm). Aerosol measurements are made in the longest wavelengths (340, 360 and 380 nm) where gaseous absorption is weak and where the backscattering of

radiation is mainly controlled by molecular scattering, scattering from aerosol and clouds, and surface reflection (Prospero *et al.*, 2002). The radiative effect of aerosols is measured in terms of an aerosol index (AI): The aerosol index as described by Herman *et al.* (1997) and Torres *et al.* (1998) is

$$AI = -100 \log_{10} [(I_{340}/I_{380})_{meas} - (I_{340}/I_{380})_{calc}]$$

where I_{meas} is the measured backscattered radiance at given wavelength and I_{calc} is the calculated radiance at the same wavelength using an atmospheric model that assumes an aerosol free atmosphere. Dust and smoke are characterized by their absorption of UV which yields positive AI values. Non-absorbing aerosols such as sea salt particles yield negative values where AI values for clouds are nearly zero. The positive values of AI are also known as TOMS index or the absorbing aerosol index 'AAI'. TOMS index values range from 0.7 to 4.2 (representing the dustiest atmospheric conditions).

3.4.3. TOMS data applied to Libya and surrounding regions

In order to simplify the description of TOMS data and the presentation of deposition data (chapter 5) and their analysis (chapter 6), three main regions have been identified within the study area, northern, central and southern (Figure 3.1), based on differences in their geomorphological, meteorological and demographical conditions (see chapter 2). An assessment of the persisting sources of aerosol in North Africa and their effects on Western Libya is made by using an atmospheric model developed by Rob Bryant from the University of Sheffield (Mahowald *et al.*, 2003) and Earth Probe Total Ozone Mapping (EP-TOMS) data (McPeters, 2002) recorded during the study period (June 2000-May 2001).

Emission in western Libya was undetectable from space indicating that deposited aeolian sediments in this part of the country were largely created by aeolian activities at low altitudes of few hundred meters and possible partial rain out from dust trajectories of aerosol derived from Saharan sources situated outside the study regions. The TOMS data show that the highest densities of aerosols transported over the study regions have occurred during summer 2000

and spring 2001. EP-TOMS data have been plotted into contour maps using ARCVIEW 3.3 which provides a picture of the spatial and temporal variations of average monthly emissions of some major Saharan sources during the study period. Contour maps based on average monthly EP-TOMS data reveal that aerosol transported over Libya reached its maximum density during the summer season while the winter months were aerosol free.

3.4.3.1. Summer months

Emissions at all the Saharan sources during summer 2000 represent the highest emission rates during the whole year of study (Figures 3.7-3.9). The highest AAI values during the summer coincide with the western flanks of the Ahaggar, reaching maximum values of 2.2, 2.3 and 2.2 during June, July and August over this source. Since the climatic system during summer is characterized by easterly winds (Figure 3.6), sources in the Libyan Desert seem to be the most influential on the western regions of Libya.

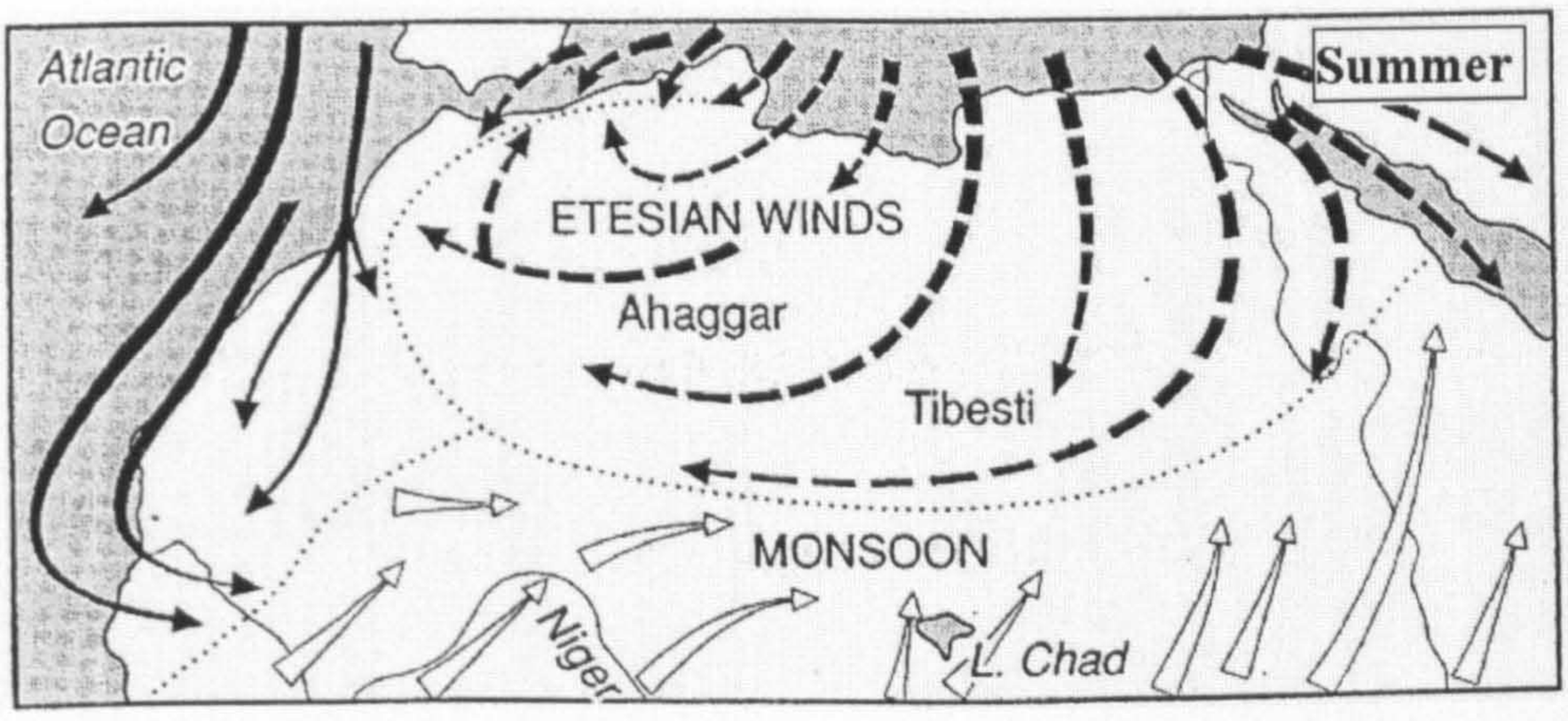

Figure 3.6 Saharan summer wind directions (*from* Goudie 2003)

Aerosol densities over the northern region were very low on the aerosol index with average monthly AAI values 0.058, 0.19 and 0.0. These values seem to correspond to plumes originated at the Chotts in northeastern Algeria (Figures 3.7-3.9). The central region, the nearest of the three study regions to any major Saharan dust source, the Libyan Desert, appears to be the largest sink in western Libya. AAI values of detected aerosol over the central region were 0.5, 0.73 and 0.3 during June, July and August respectively. Tracing the contours in Figures 3.7-3.9 shows that Eastern Libyan Desert and the corridor between the

Great Sand Sea and the AL Haruj Al Asud are the most likely aerosol supplying sources to the central region. Aerosol densities over the southern region were higher than those of the northern region, but lesser than those of the central region. The monthly AAI averages over the southern region were 0.37, 0.38, 0.0 which seem to be largely attributed to the Libyan Desert, however, partial effects from the Bodélé Depression and the Ahaggar plumes are also probable.

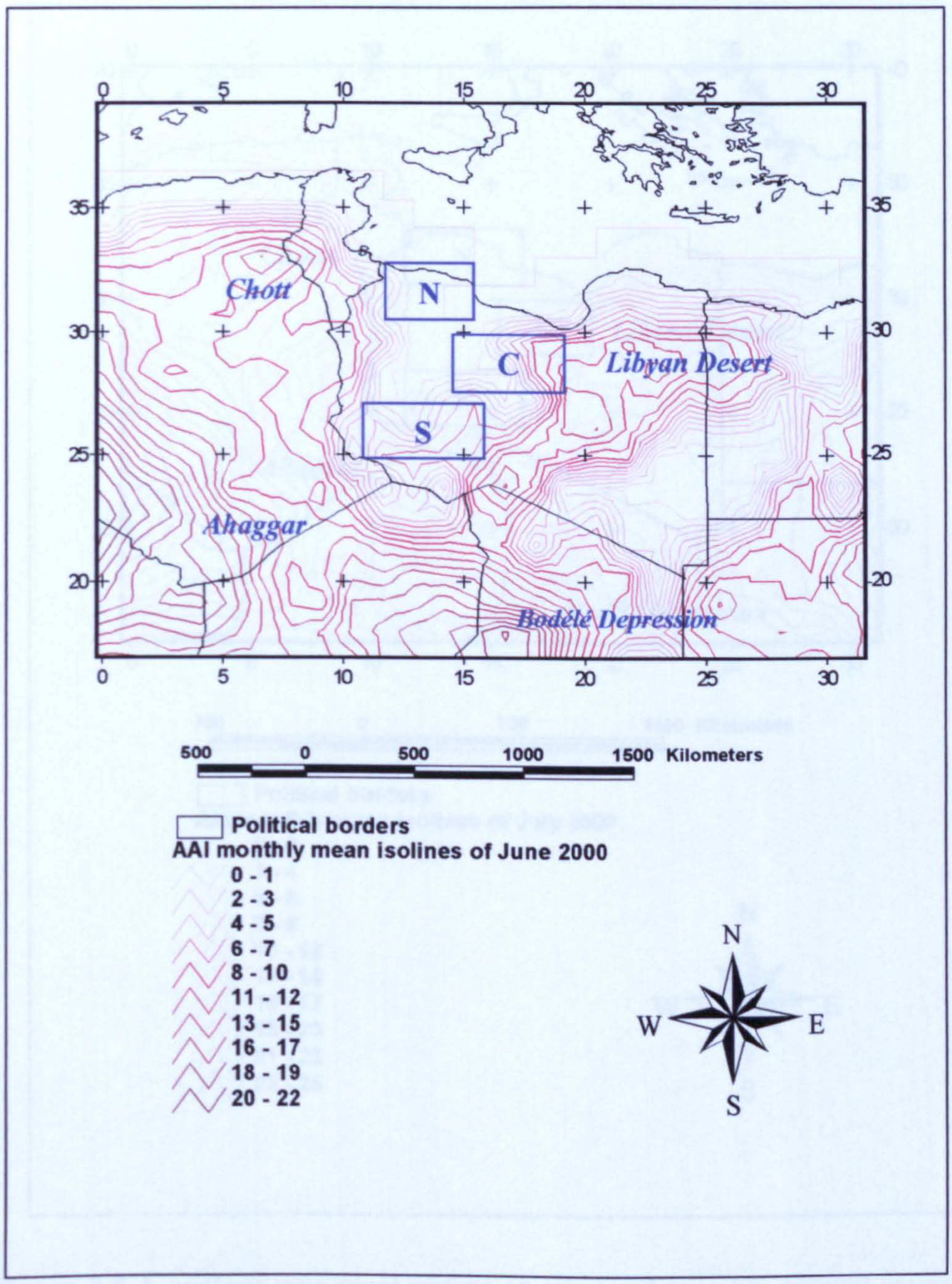

Figure 3.7 A contour map representing an averaged monthly aerosol emission over Libya during June 2000 and, some major Saharan sources and the three regions of field study, northern (N), central (C) and southern (S). AAI values on this map are 10 times greater than the actual values.

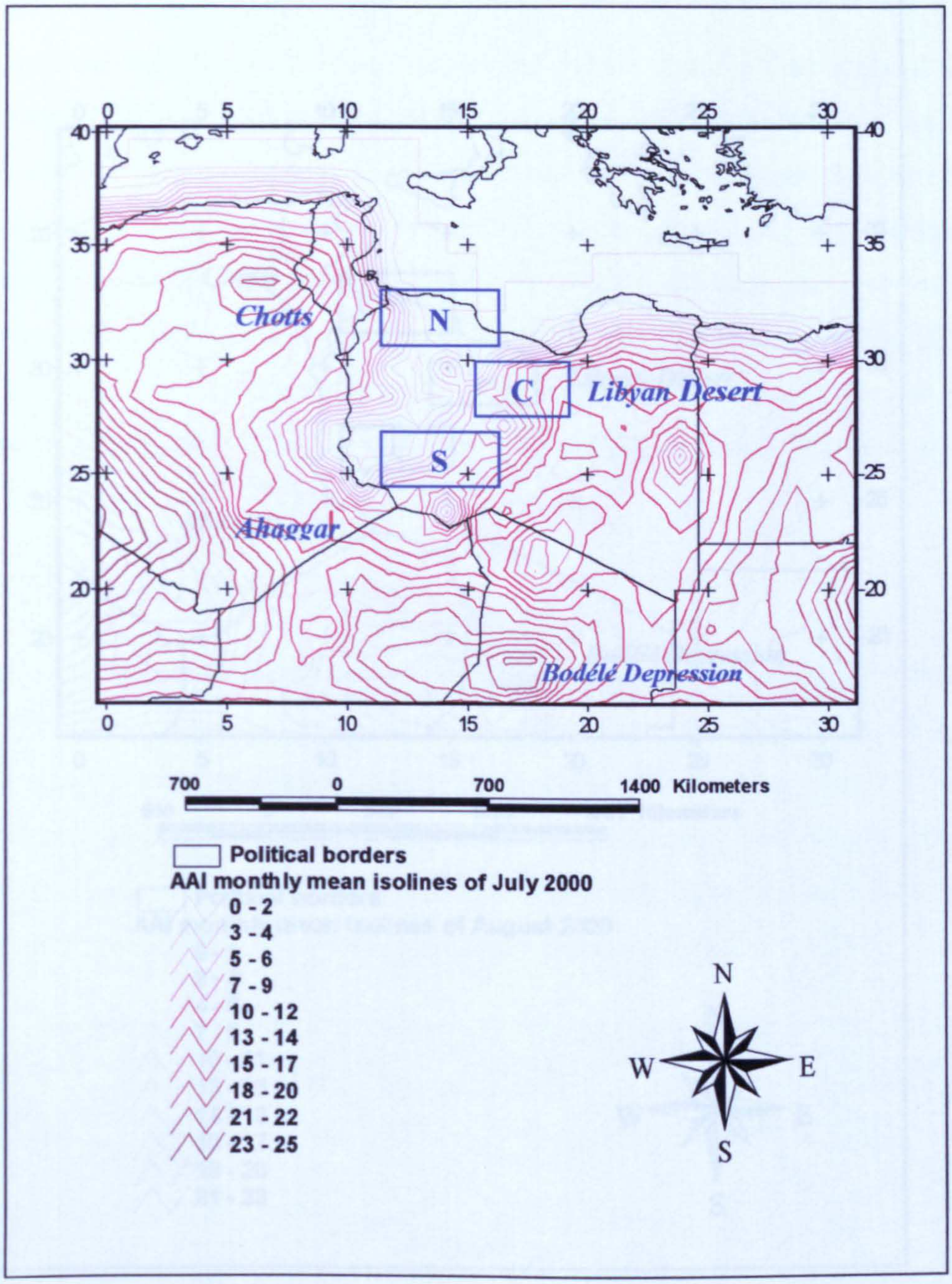

Figure 3.8 A contour map representing an averaged monthly aerosol emission over Libya during July 2000 and, some major Saharan sources and the three regions of field study, northern (N), central (C) and southern (S). AAI values on this map are 10 times greater than the actual values.

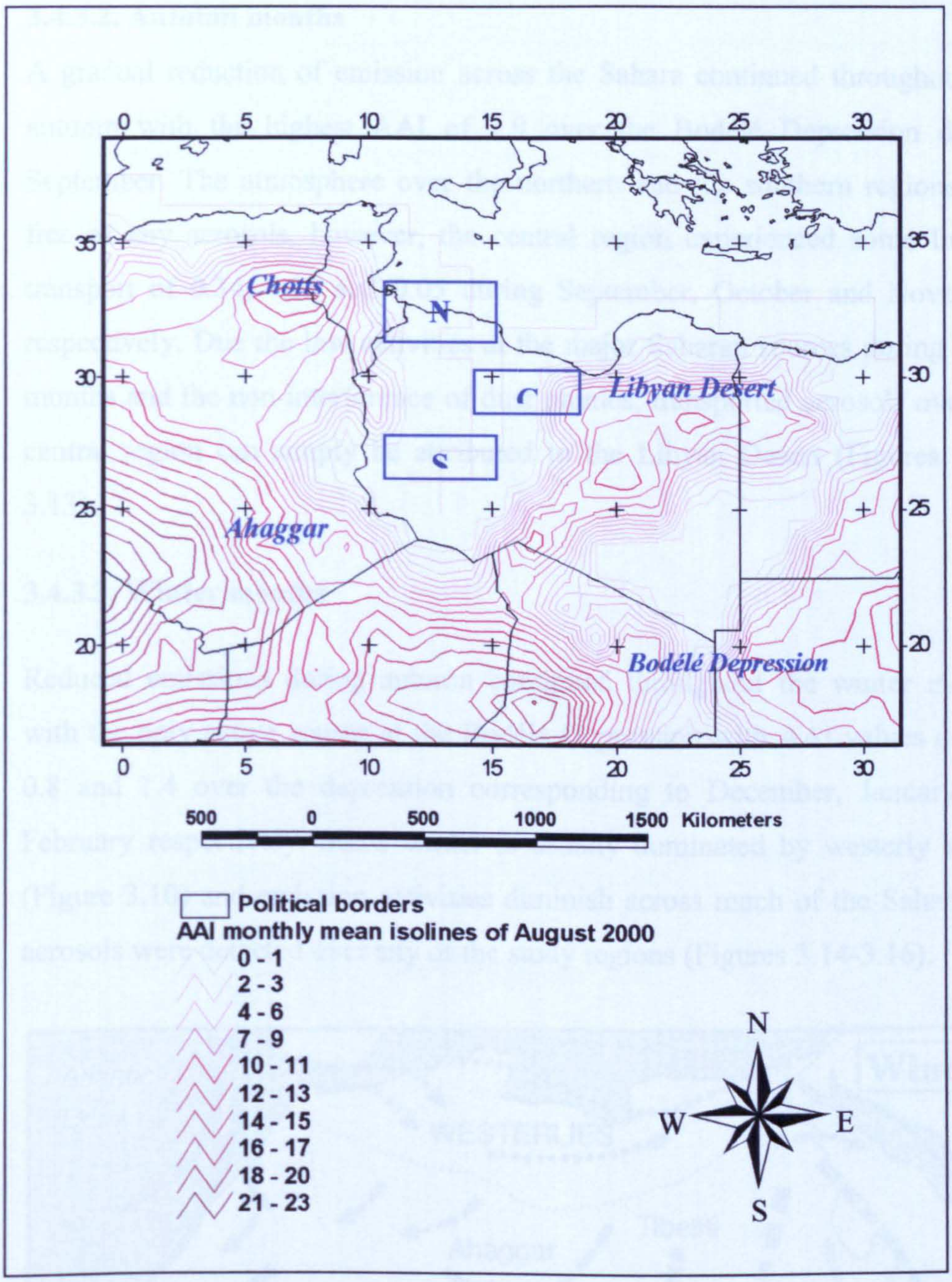

Figure 3.9 A contour map representing an averaged monthly aerosol emission over Libya during August 2000 and, some major Saharan sources and the three regions of field study, northern (N), central (C) and southern (S). AAI values on this map are 10 times greater than the actual values.

3.4.3.2. Autumn months

A gradual reduction of emission across the Sahara continued throughout the autumn with the highest AAI of 1.9 over the Bodélé Depression during September. The atmosphere over the northern and the southern regions was free of any aerosols, however, the central region experienced some limited transport of 0.34, 0.15 and 0.05 during September, October and November respectively. Due the low activities at the major Saharan sources during these months and the non-interference of dust plumes, transported aerosols over the central region can simply be attributed to the Libyan Desert (Figures 3.11-3.13).

3.4.3.3. Winter months

Reduced emissions during autumn continued throughout the winter months with the only active source at the Bodélé Depression with AAI values of 0.9, 0.8 and 1.4 over the depression corresponding to December, January and February respectively. Since winter is usually dominated by westerly winds (Figure 3.10) and emission activities diminish across much of the Sahara, no aerosols were detected over any of the study regions (Figures 3.14-3.16).

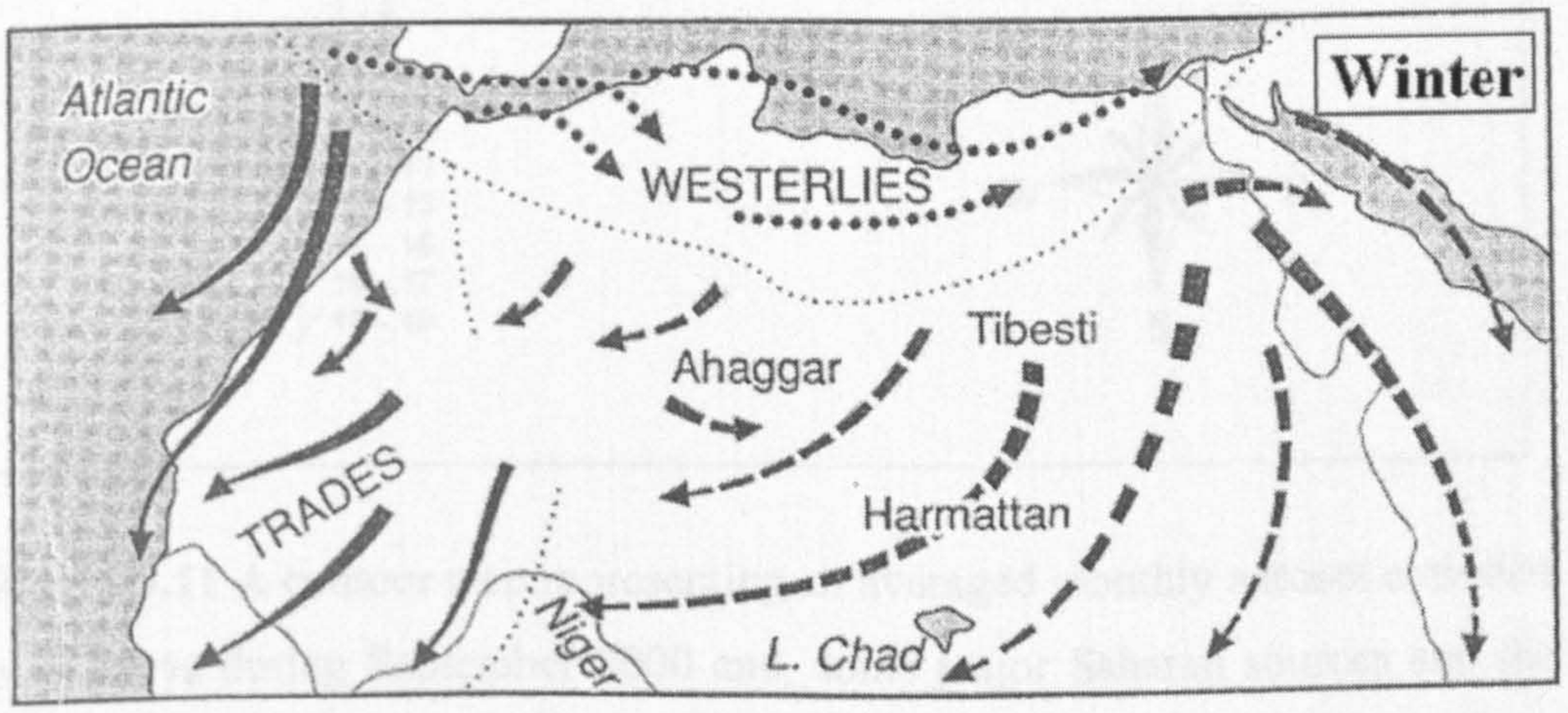

Figure 3.10 Saharan winter wind systems (*from* Goudie 2003)

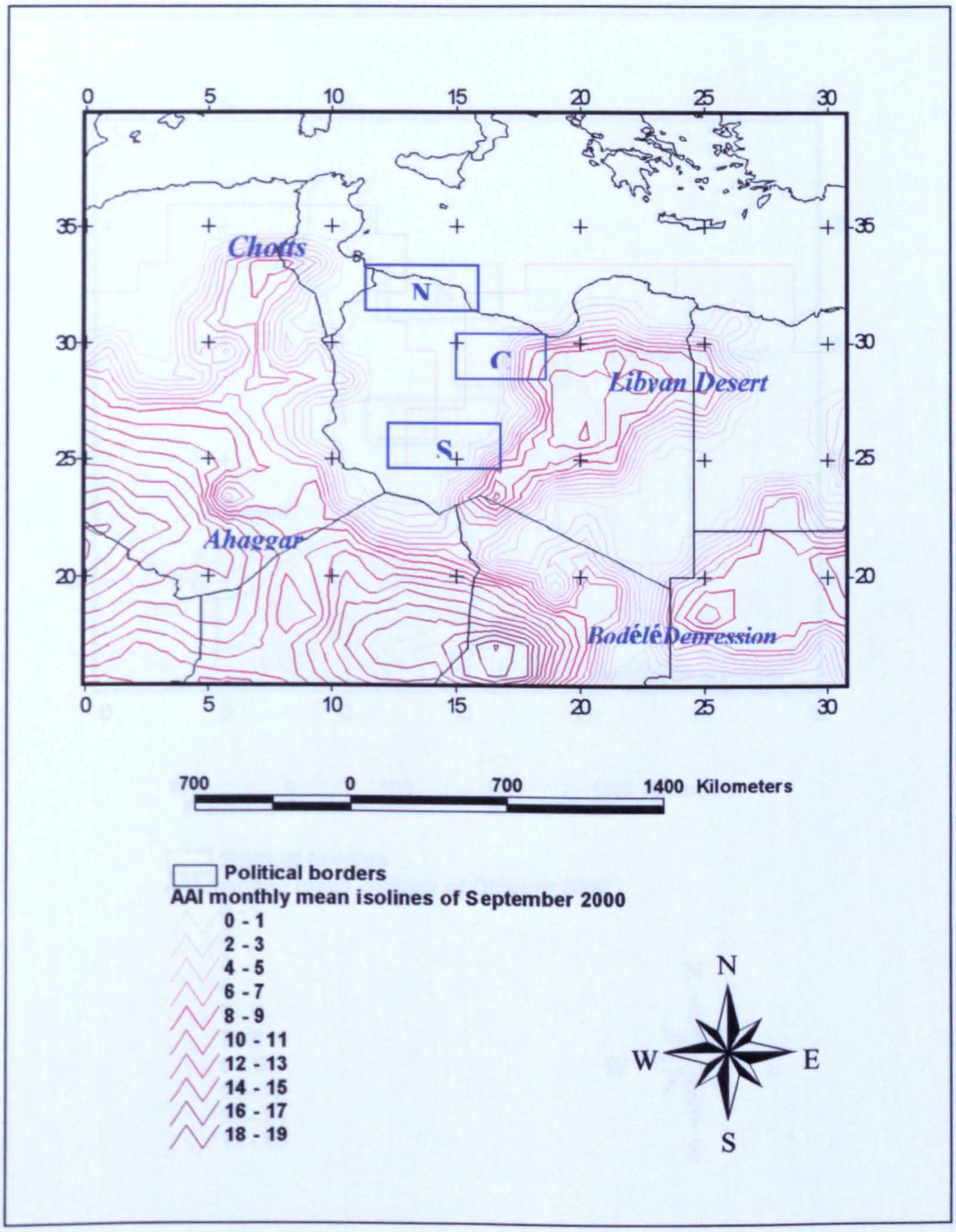

Figure 3.11 A contour map representing an averaged monthly aerosol emission over Libya during September 2000 and, some major Saharan sources and the three regions of field study, northern (N), central (C) and southern (S). AAI values on this map are 10 times greater than the actual values.

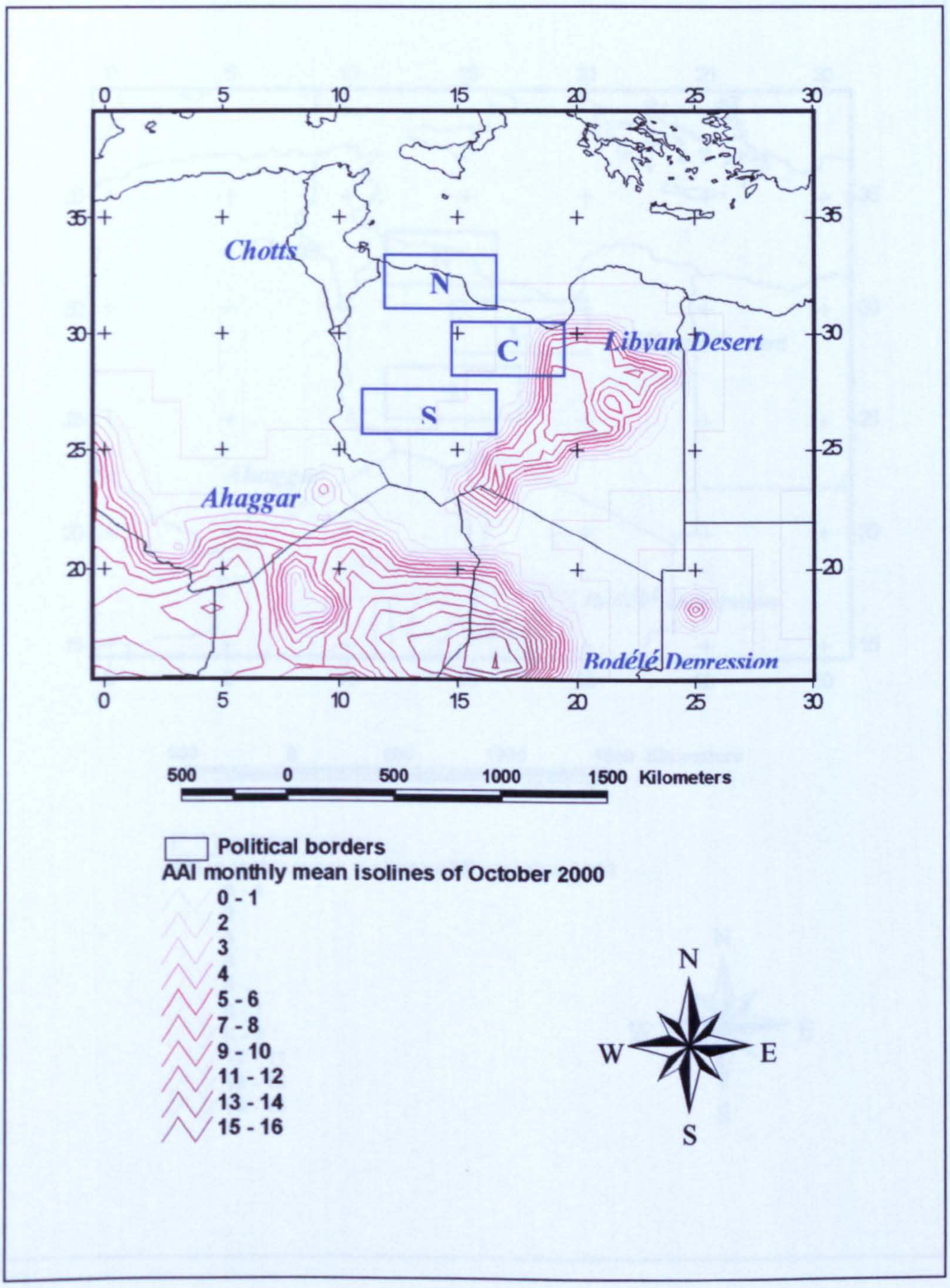

Figure 3.12 A contour map representing an averaged monthly aerosol emission over Libya during October 2000 and, some major Saharan sources and the three regions of field study, northern (N), central (C) and southern (S). AAI values on this map are 10 times greater than the actual values.

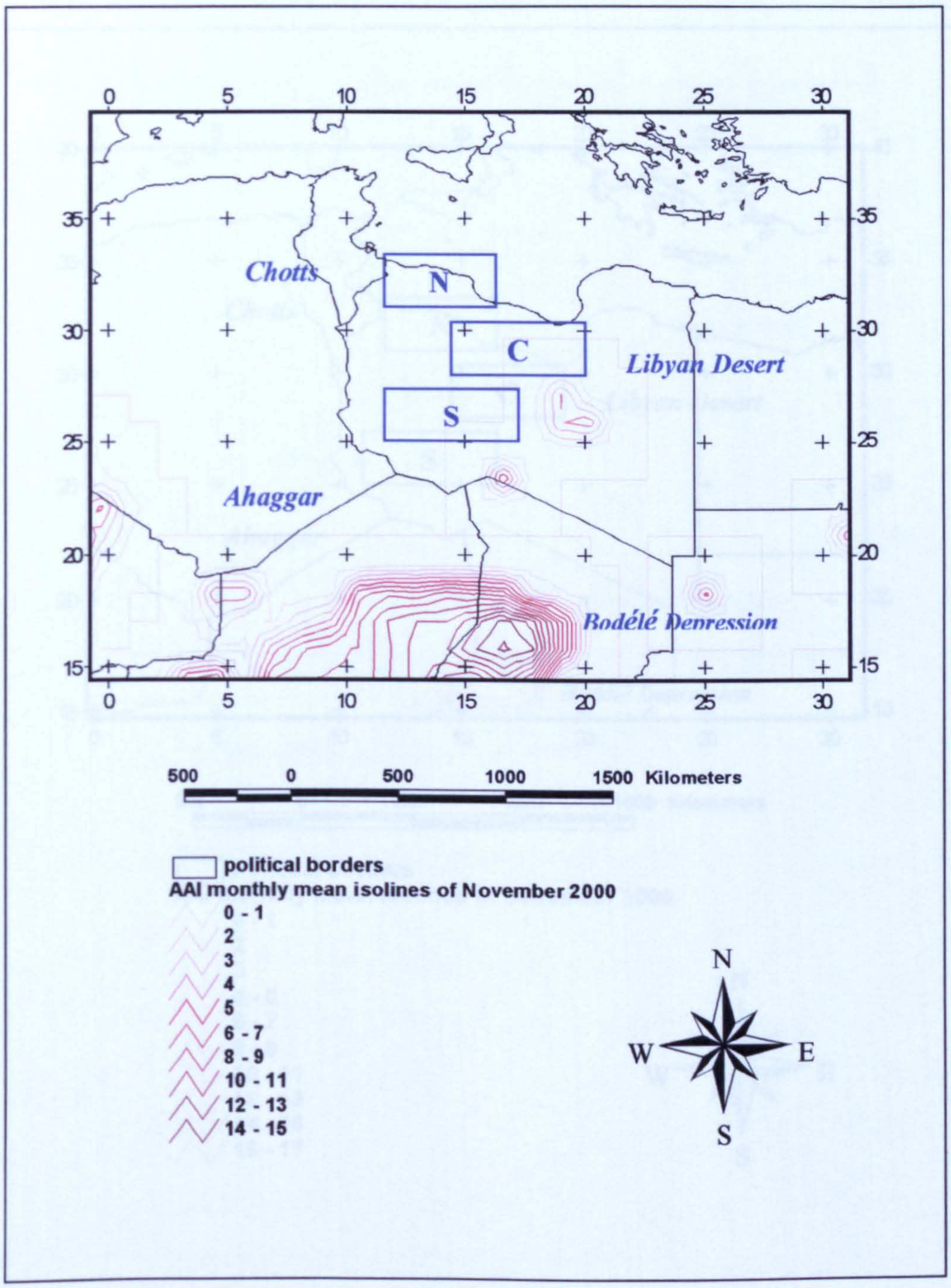

Figure 3.13 A contour map representing an averaged monthly aerosol emission over Libya during November 2000 and, some major Saharan sources and the three regions of field study, northern (N), central (C) and southern (S). AAI values on this map are 10 times greater than the actual values.

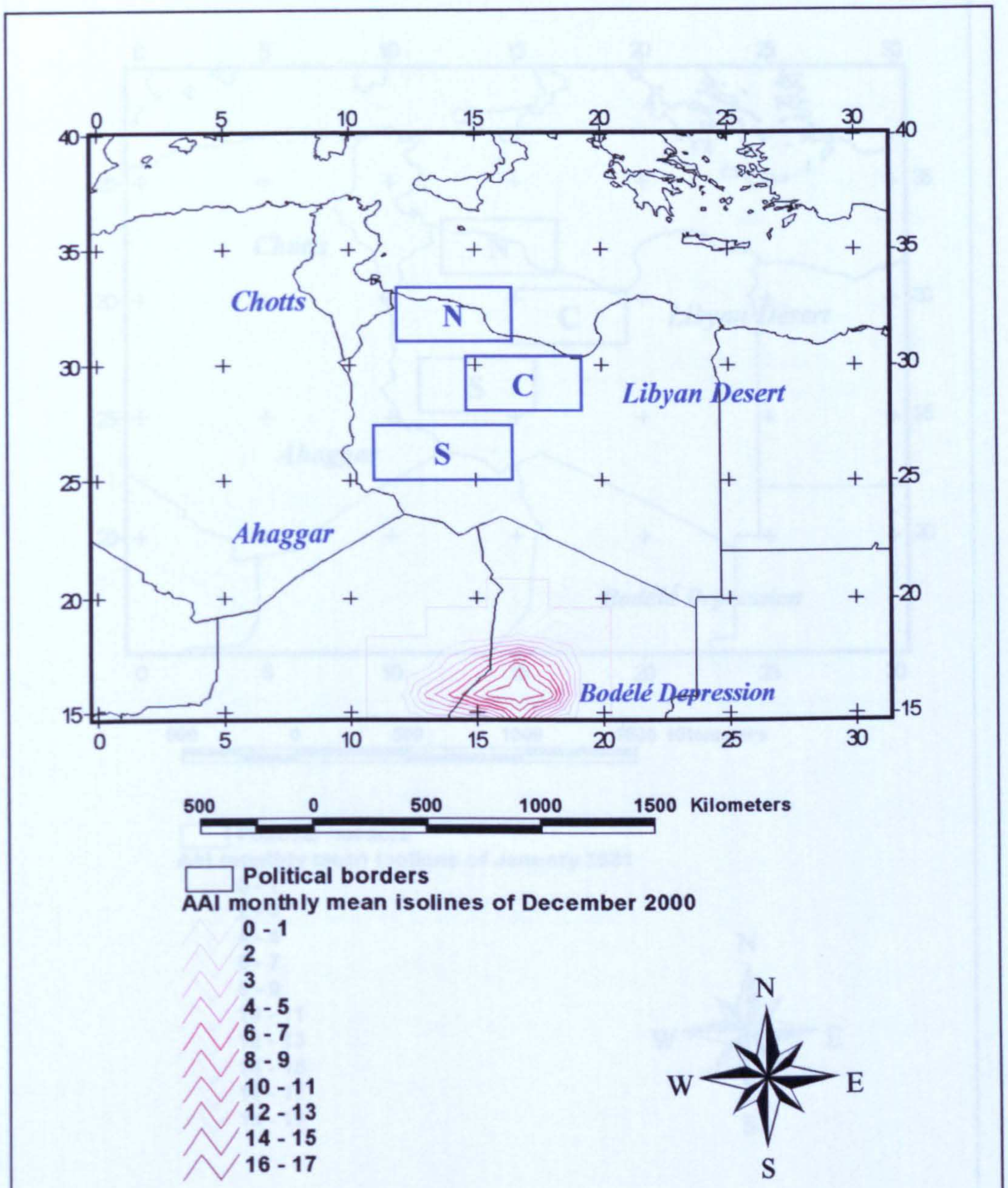

Figure 3.14 A contour map representing an averaged monthly aerosol emission over Libya during December 2000 and, some major Saharan sources and the three regions of field study, northern (N), central (C) and southern (S). AAI values on this map are 10 times greater than the actual values.

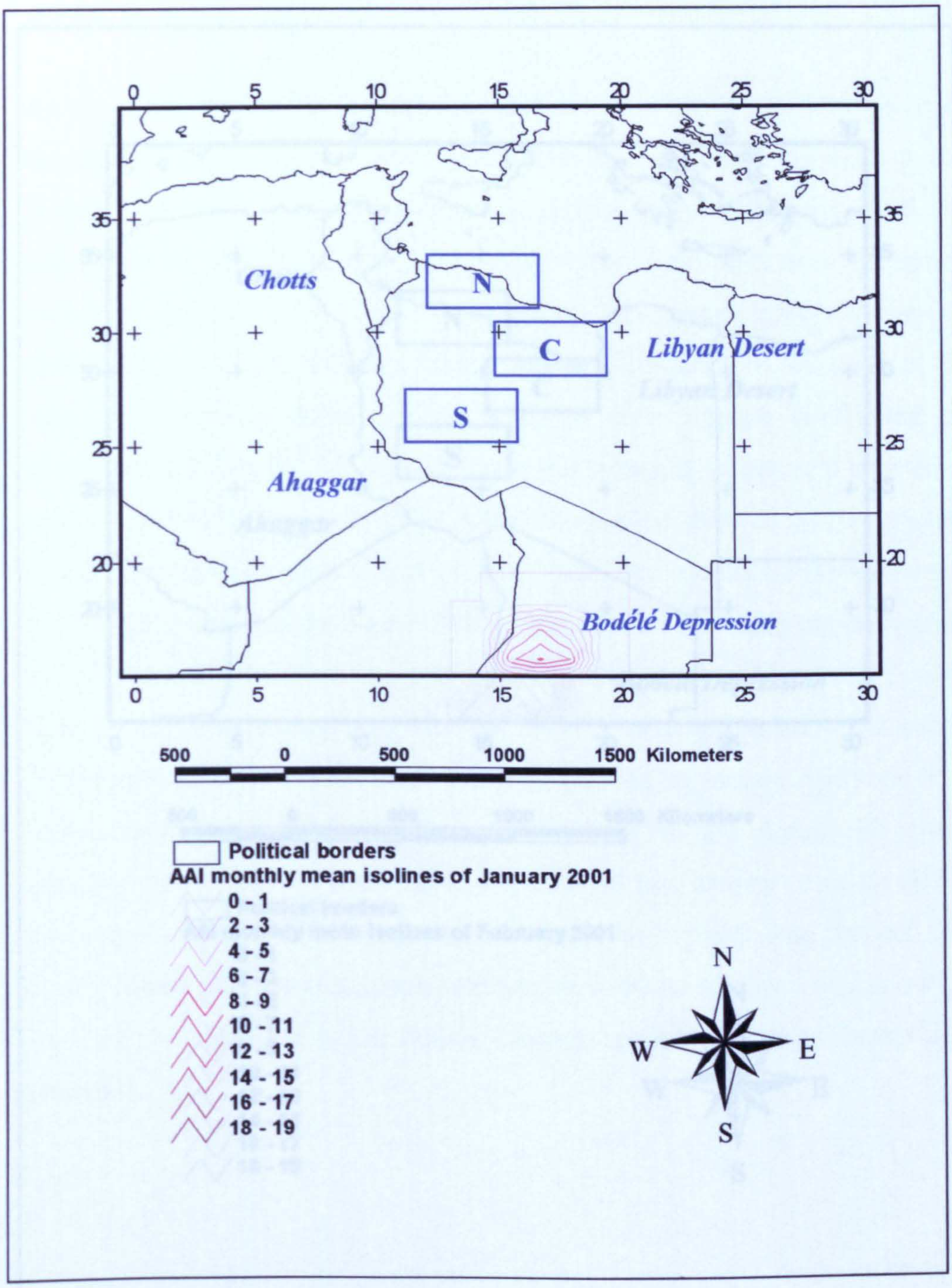

Figure 3.15 A contour map representing an averaged monthly aerosol emission over Libya during January 2001 and, some major Saharan sources and the three regions of field study, northern (N), central (C) and southern (S). AAI values on this map are 10 times greater than the actual values.

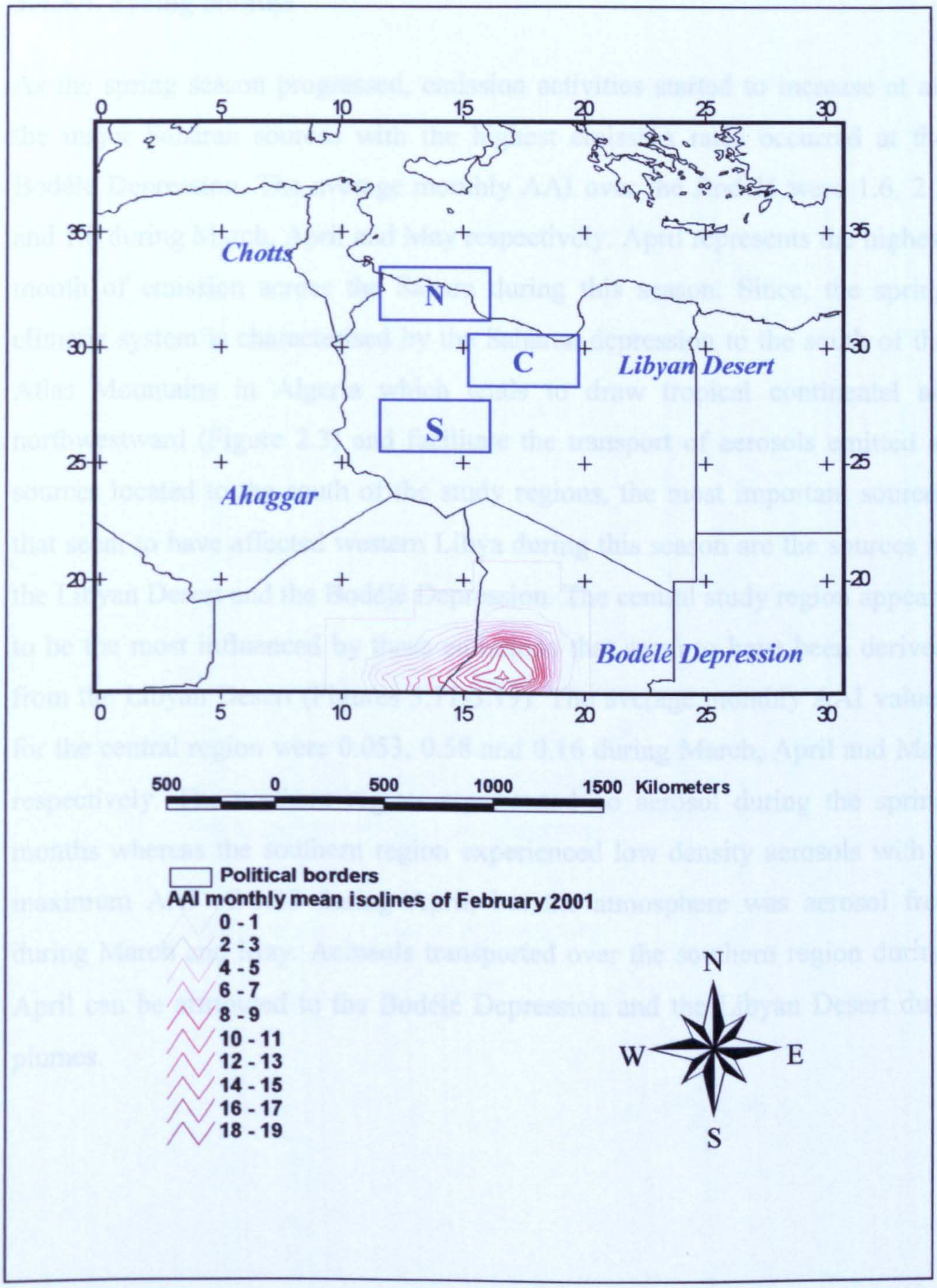

Figure 3.16 A contour map representing an averaged monthly aerosol emission over Libya during February 2001 and, some major Saharan sources and the three regions of field study, northern (N), central (C) and southern (S). AAI values on this map are 10 times greater than the actual values.

3.4.3.4. Spring months

As the spring season progressed, emission activities started to increase at all the major Saharan sources with the highest emission rates occurred at the Bodélé Depression. The average monthly AAI over the Bodélé were 1.6, 2.1 and 1.8 during March, April and May respectively. April represents the highest month of emission across the Sahara during this season. Since, the spring climatic system is characterised by the Saharan depression to the south of the Atlas Mountains in Algeria which tends to draw tropical continental air northwestward (Figure 2.3) and facilitate the transport of aerosols emitted at sources located to the south of the study regions, the most important sources that seem to have affected western Libya during this season are the sources in the Libyan Desert and the Bodélé Depression. The central study region appears to be the most influenced by these emissions that seem to have been derived from the Libyan Desert (Figures 3.17-3.19). The average monthly AAI values for the central region were 0.053, 0.58 and 0.16 during March, April and May respectively. The northern region experienced no aerosol during the spring months whereas the southern region experienced low density aerosols with a maximum AAI of 0.33 during April, but the atmosphere was aerosol free during March and May. Aerosols transported over the southern region during April can be attributed to the Bodélé Depression and the Libyan Desert dust plumes.

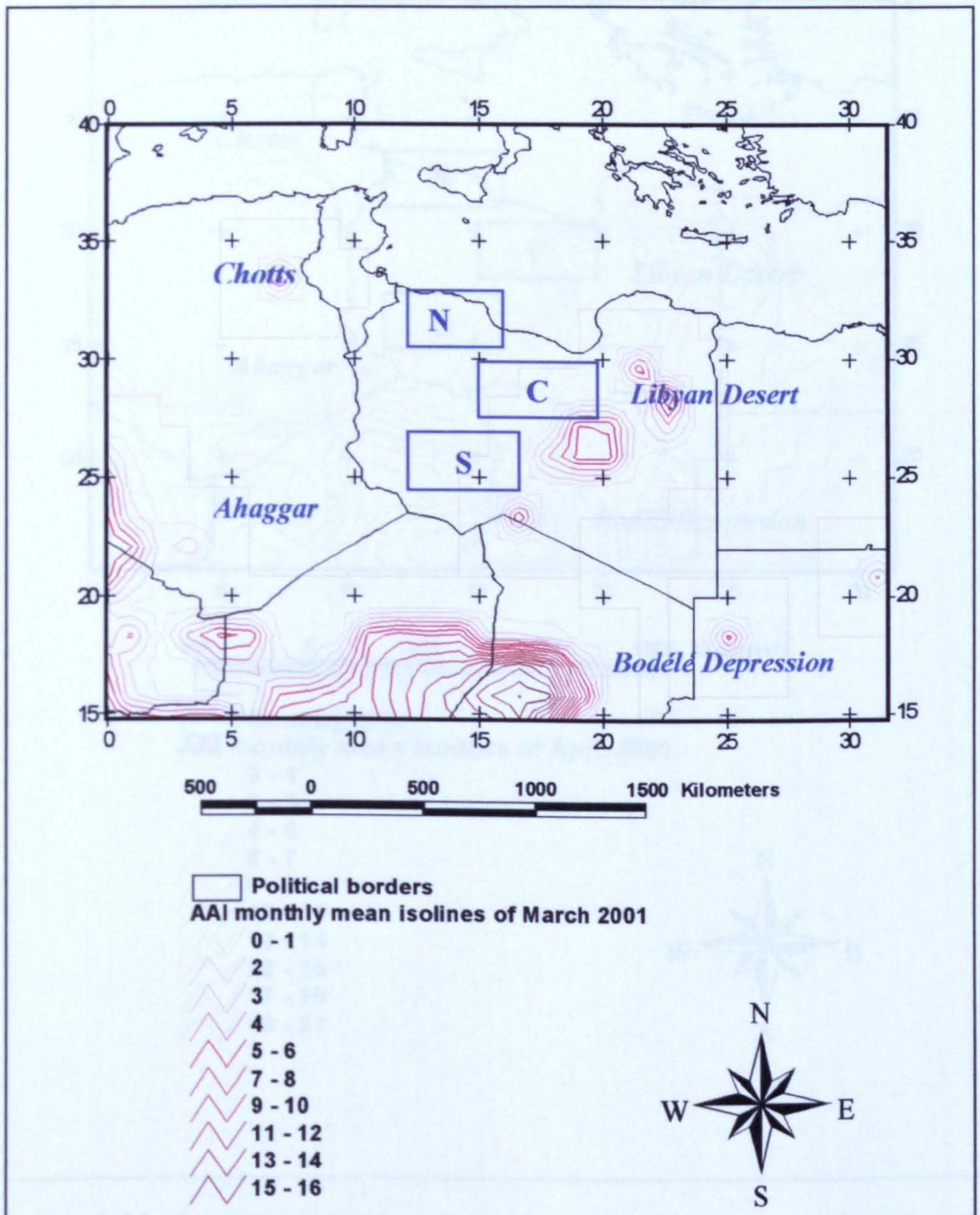

Figure 3.17 A contour map representing an averaged monthly aerosol emission over Libya during March 2001 and, some major Saharan sources and the three regions of field study, northern (N), central (C) and southern (S). AAI values on this map are 10 times greater than the actual values.

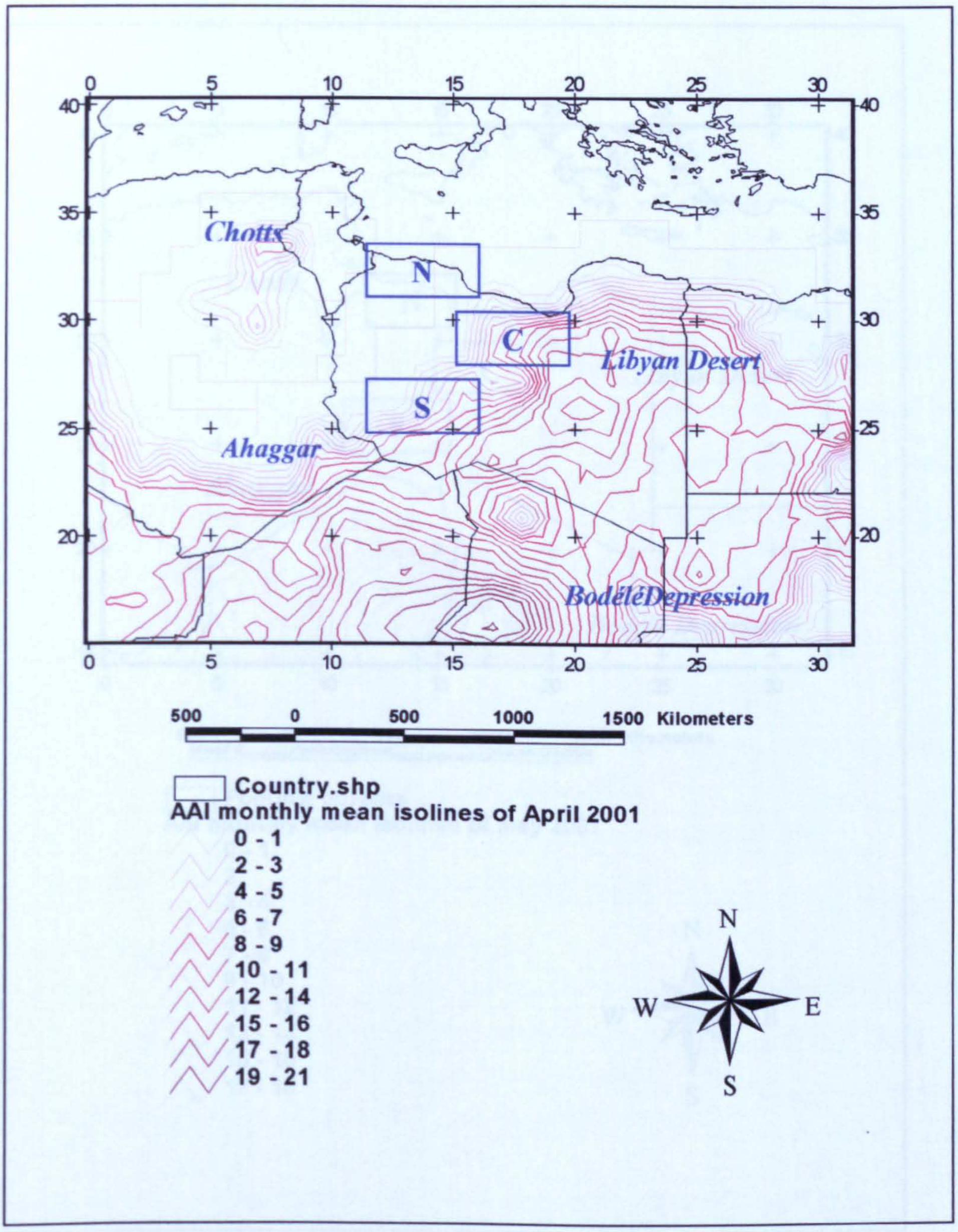

Figure 3.18 A contour map representing an averaged monthly aerosol emission over Libya during April 2001 and, some major Saharan sources and the three regions of field study, northern (N), central (C) and southern (S). AAI values on this map are 10 times greater than the actual values.

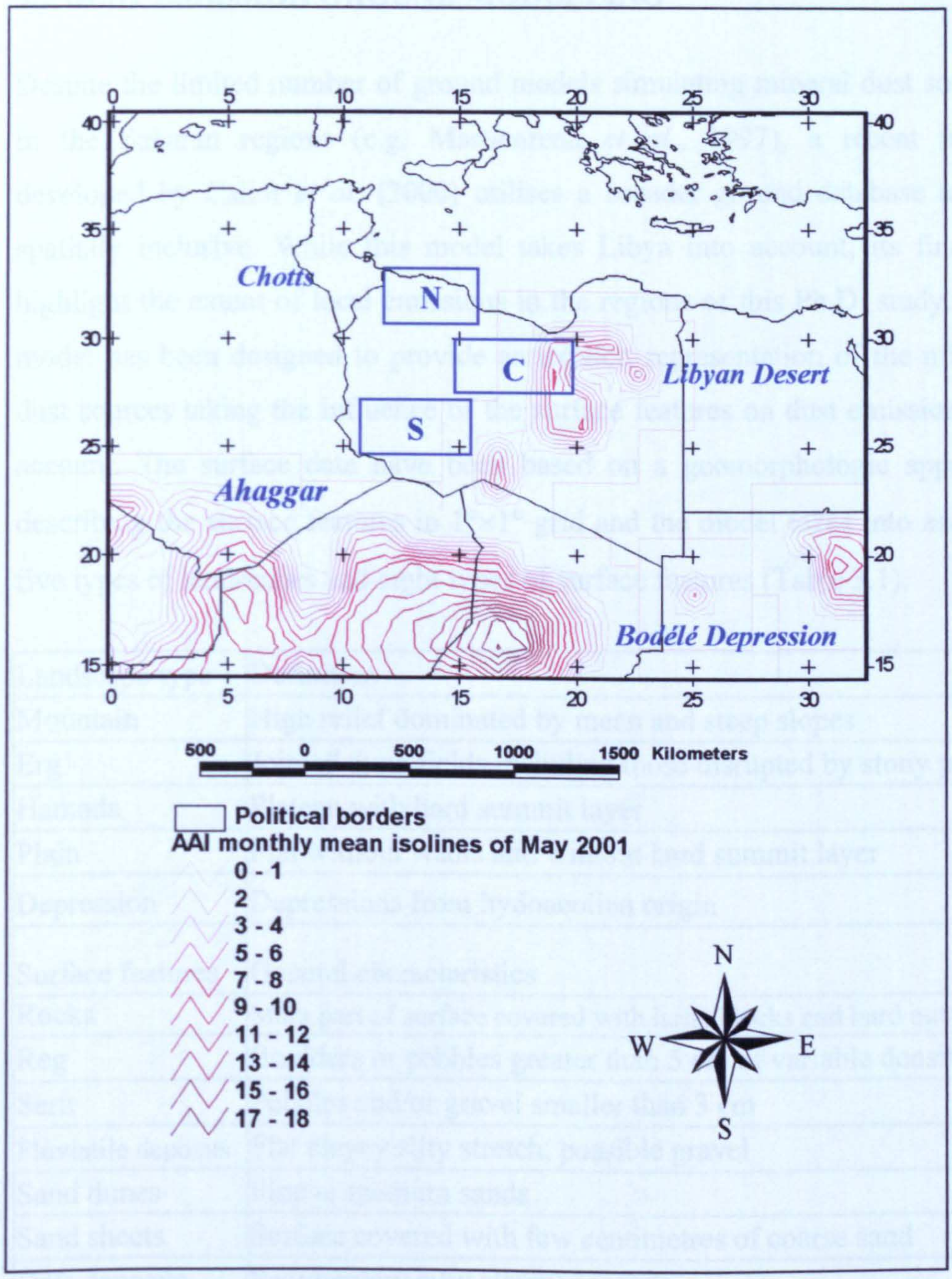

Figure 3.19 A contour map representing an averaged monthly aerosol emission over Libya during May 2001 and, some major Saharan sources and the three regions of field study, northern (N), central (C) and southern (S). AAI values on this map are 10 times greater than the actual values.

3.5 DUST EMISSION GROUND MODELLING

Despite the limited number of ground models simulating mineral dust sources in the Saharan regions (e.g. Marticorena *et al.*, 1997), a recent model developed by Callot *et al.* (2000) utilises a broader ground database and is spatially inclusive. While this model takes Libya into account, its findings highlight the extent of local emissions in the regions of this Ph.D. study. This model has been designed to provide an explicit representation of the mineral dust sources taking the influence of the surface features on dust emission into account. The surface data have been based on a geomorphologic approach describing the surface features in 1°×1° grid and the model takes into account five types of landscapes and eight types of surface features (Table 3.1).

Landscape type	Definition
Mountain	High relief dominated by mean and steep slopes
Erg	Jointed dune fields including those disrupted by stony places
Hamada	Plateau with hard summit layer
Plain	Flat without wadis and without hard summit layer
Depression	Depressions from hydoaeolian origin
Surface features	General characteristics
Rocks	Main part of surface covered with large blocks and hard outcrops
Reg	Boulders or pebbles greater than 5 cm of variable density
Serir	Pebbles and/or gravel smaller than 3 cm
Fluviatile deposits	Flat clayey silty stretch, possible gravel
Sand dunes	Fine or medium sands
Sand sheets	Surface covered with few centimetres of coarse sand
Daia deposits	Sedimentary silty clayey deposits
Sabkha deposits	Sedimentary salty deposits with various surface features

Table 3.1 Landscape and surface feature types deployed in Callot's *et al.* model (*from* Callot *et al.* 2000)

The daily fluxes are averaged over three years to obtain mean annual dust emission per degree as shown in Figure 3.20. This model was used to simulate dust emissions for 1990, 1991 and 1992 and found to be in agreement with 74% of satellite observations (Callot *et al.*, 2000). It is evident from the dust emission map that western Libya represents some of the highest dust emission

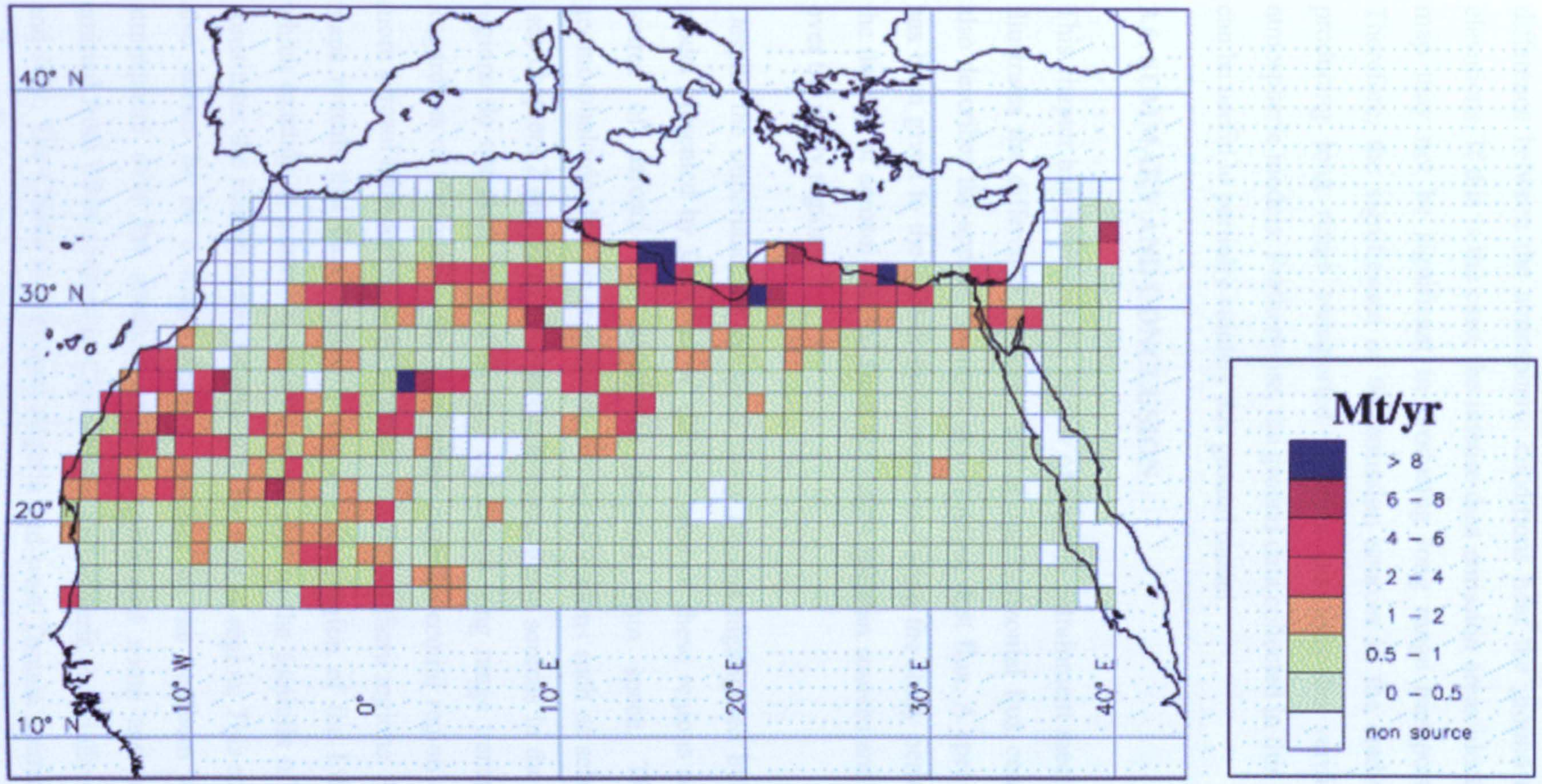

Figure 3.20 Map of the average annual dust emission for the Saharan regions (*from* Callot *et al.* 2000)

rates in the Sahara. This map, however, does not seem to be a true representation of dust intensity in the upper layers of the atmosphere due to the difference between the atmospheric conditions near the ground and at high elevations. If this is the case, the intense dust emission areas identified on the map may not be significant in producing long range transported aerosol. Therefore, the significance of the emission sources in the study regions in producing long range transported aerosols can only be verified through atmospheric models. Furthermore, the ground data collected in this Ph.D. study can be useful to partially validate this ground model.

3.6. SUMMARY AND CONCLUSION

This chapter has presented the review of particle entrainment mechanisms and illustrates the difference between vertical and horizontal flux components. It also describes the applied methods in measuring dust flux. A special attention has been given to the TOMS measurements during the study period to assess the density of aerosol emitted from the major Saharan sources and transported over the study regions.

Despite the importance of the three study regions highlighted by the ground model presented by Callot *et al.* (2000), none of these regions constituted a source of aerosol that could be detected from space. The existing geomorphologic dust sources inside the study regions such as sebkhas, wadis (see chapters 2 and 5) as well as the anthropogenic sources in the three study regions do not seem to produce any substantial long range transported dust. Regardless of seasonality, the atmosphere over the central region experienced more aerosol transport than the northern and the southern regions. AAI contour maps reveals that dust emitted in the northern region of the Libyan Desert which extends in a narrow corridor south east to the foothills of the Tibesti constitutes the nearest potential source to the central region. This source region also seems to be a major aerosol supplier to the southern region. The atmosphere over the southern region experienced some aerosol transport emitted from other sources in Chad, Niger and Algeria especially during June and July. The Chotts in northeast Algeria and west Tunisia seems to play the major role in transporting aerosol to northwestern Libya (northern study

region). Major aerosol activities occurred during the months of July, June and April respectively but no aerosol transport was detected during the winter months. Detected transport during the autumn was limited to the central region. These findings are consistent with the interpretation of EP-TOMS and Nimbus 7-TOMS data (Middleton and Goudie, 2001; Prospero *et al.*, 2002). Since the wind regimes in the upper layers of the atmosphere are unrepresentative of the regimes in the atmosphere near the ground, the actual deposition rates can only be quantified through trapping in the field (see chapter 4).

This chapter has been organized to differentiate between vertical and horizontal flux components in relation to TOMS data during the study period and present day ground model by Callot *et al.*, 2000. The information in this chapter is intended to serve as a background in the analysis of the field data collected for this Ph.D. study (Chapters 5 and 6).

CHAPTER 4

QUANTIFYING AEOLIAN SEDIMENT TRANSPORT

4.1. INTRODUCTION

Sediment trapping is essential in the study of the deposition rates and in the validation of numerical flux models. In addition, it allows for the study of the physical and chemical characteristics of the trapped sediment particles. A need for field data on dust flux has lead to the development of several sediment trapping methods. Whilst sediment transport mechanisms are defined by two major flux components, the vertical and horizontal components, the efficiency of a particular trap depends on the physical nature of trap design, its interaction with the air stream and the type of the targeted flux component. Trap efficiency has been defined as the relative ratio of trapped sediment to the actual quantity of blown sediment (Chepil and Milne, 1941). The efficiency of a trap can be determined experimentally by using a wind tunnel and the following equation (Aren and van der Lee, 1995):

$$\eta_s = (\text{amount trapped / input}) \times (\text{tunnel width / effective trap width}) \times 100 \qquad [4.1]$$

Where

η_s is the trap efficiency (%)

In this type of experiment, a scaled model of the trap being tested is essential to obtain reliable results. Several designs have been deployed in the field, but none of them is known to be efficient in accounting for total dust during long-term investigations.

Better-engineered, highly efficient and electrically powered samplers have been deployed to account for total dust flux. These aspirator samplers operate on the principle of sucking air across a filter of a specific mesh at a known mass rate of collected dust. This type of design is usually used to monitor air pollution for limited periods of time and is regarded to be impractical for a large scale long term dust sampling due to the need to constantly monitor trap operation, undertake intensive maintenance, have a regular power supply and employ frequent filter cleaning. Traps are often classified on the basis of their geometrical shape, either vertical or horizontal, rather than the direction of dust

flux (e.g. Pye and Tsoar, 1990; Wang and Kraus, 1999). This can be misleading because vertical traps cited in literature are primarily designed to account for the horizontal flux component (e.g. Horikawa and Shen, 1960; Leather, 1978; Kubota *et al.*, 1983; Illenberger and Rust, 1986) while other traps of a vertical shape are used to entrap vertical dust flux (e.g. Rabenhorst *et al.*, 1984; Drees *et al.*, 1993). Herein, sediment traps are identified by the targeted sediment flux component.

As yet no standard method has been agreed upon (Livingstone and Warren, 1996), the trap design chosen for this project has basically been decided in accordance with the environmental and logistic conditions in Libya. In this chapter, an assessment of a proper trapping methodology needed to collect dust in Libya is discussed.

4.2. TRAP DESIGNS REVIEW

4.2.1. Horizontal flux traps (sand traps)

With bedload transport, entrained grains move forward by a series of jumps (saltaion and reptation), rolling or sliding (surface traction). These grains make up a flux component parallel to the surface. If the dominant flux mode is characterised by the horizontal flux component and the vertical flux component is insignificant, an efficient trap contains one or more openings on the up wind side to permit particles to enter the trap. A horizontal flux trap must be oriented against the wind direction for maximum performance. A number of trap designs are presented by way of examples.

4.2.1.1. A box and baffles sand traps

Owen (1927) designed one of the early traps of this type (Figure 4.1). The design consisted of a box, 67 cm long and 34 cm high, half buried in the sand. Openings on the upwind and downwind sides were made to permit air to pass through and transverse baffles to entrap the entering particles. Similar designs of different dimensions have been deployed by O'Brien and Rindlaub, 1936; Horikawa and Shen, 1960 and Belly, 1964. The efficiency of this type decreases as the fluctuation in wind direction becomes significant.

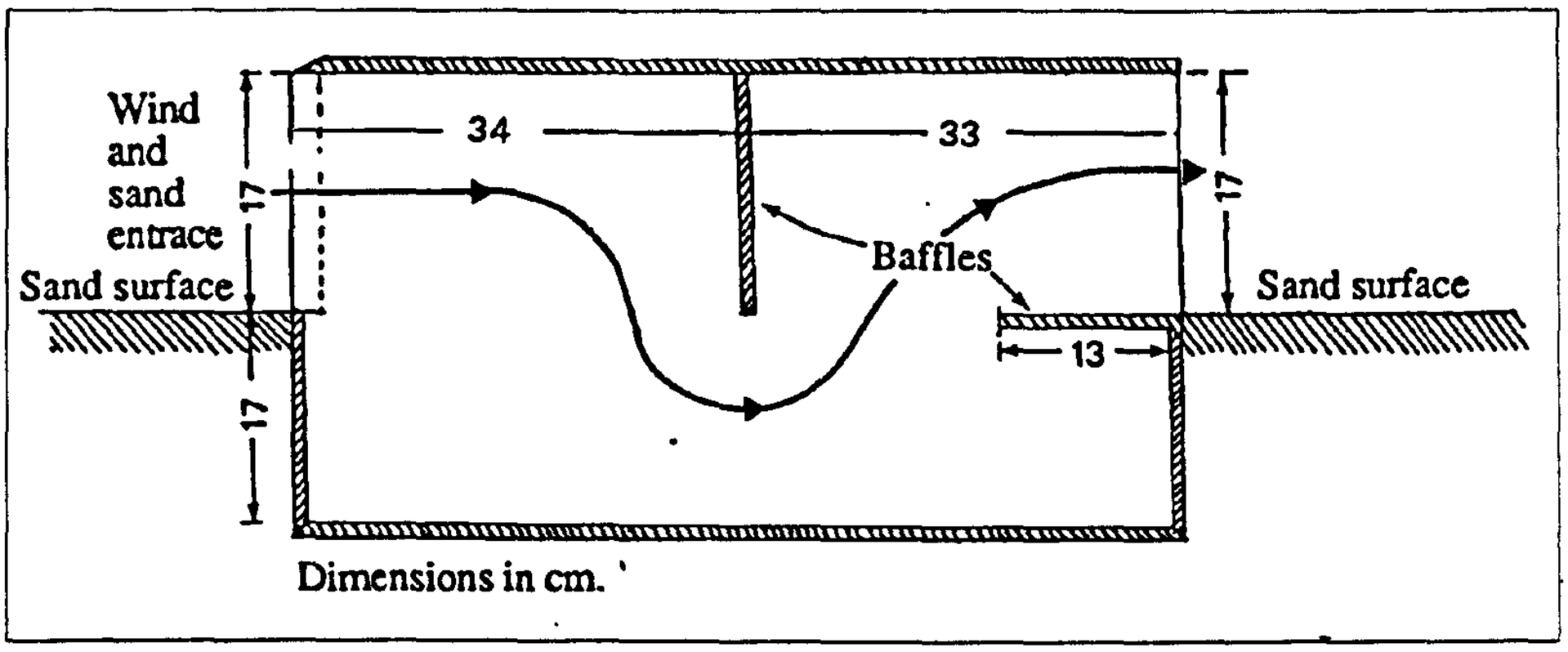

Figure 4.1 A box and baffles trap (*from* Owen 1927)

4.2.1.2. A vertical rod sand trap

Leatherman (1978) introduced another design consisting of a PVC pipe as an outer shell with two slits cut in one end. One slit allows incoming air to pass through while the other slit is covered with a 60 μm mesh screen to let air out. An inner pipe is inserted in the outer pipe and covered at its bottom with a silk screen to retain the collected sand let rainwater infiltrate without sample loss. When used, the trap is buried vertically under the sand surface (Figure 4.2).

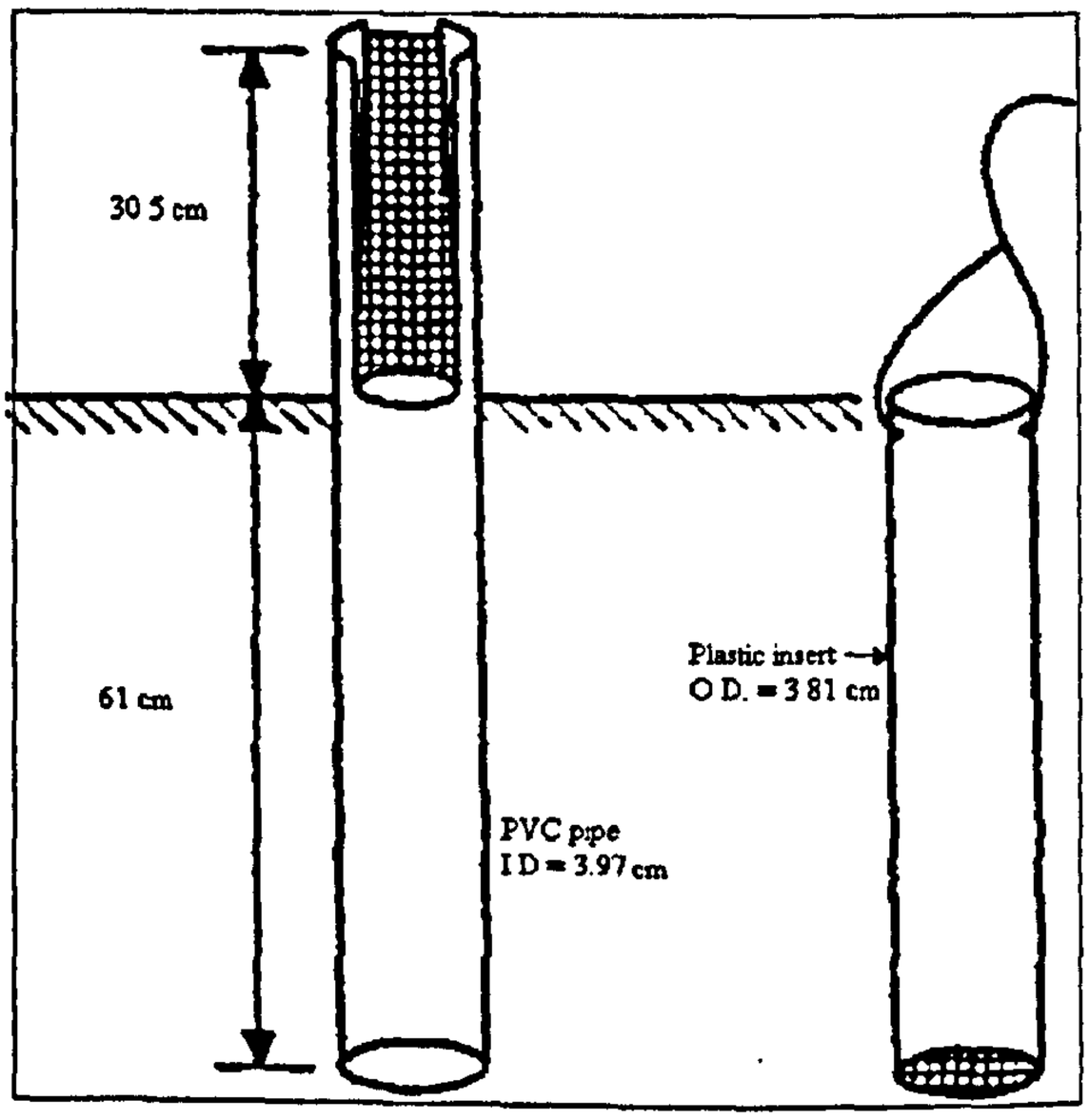

Figure 4.2 A vertical rod sand trap (*from* Leatherman 1978)

A chosen height of 30.5 cm of the outer pipe remains above the surface because most of the saltating grains bounce below this height (Horikawa and Shen, 1960).

4.2.1.3. Automated / buried trap

A different design has provided continuous measurement of sediment flux and wind velocity (Figure 4.3, Jackson, 1996). This design consists of a cylindrical casing buried vertically co-planar with the sediment and accommodates an automatic sample collector device attached to a sensitive load cell to monitor weight changes at a resolution of 1 gram. The collector device consists of two cylindrical containers attached to a central tipping mechanism. During the course of operation, as one container becomes 75% full (200 g), a solenoid signals to tip the load and dumps it in the outer casing. Whilst this mechanism is in progress, the second container replaces the first. The incoming sand enters the containers via a funnel. The collected data are sorted electronically and transferred at the end of the recording period via cabling to a computer. The high cost of this design and the requirement for maintenance make this trap impractical for long-term sampling especially in remote regions of the world.

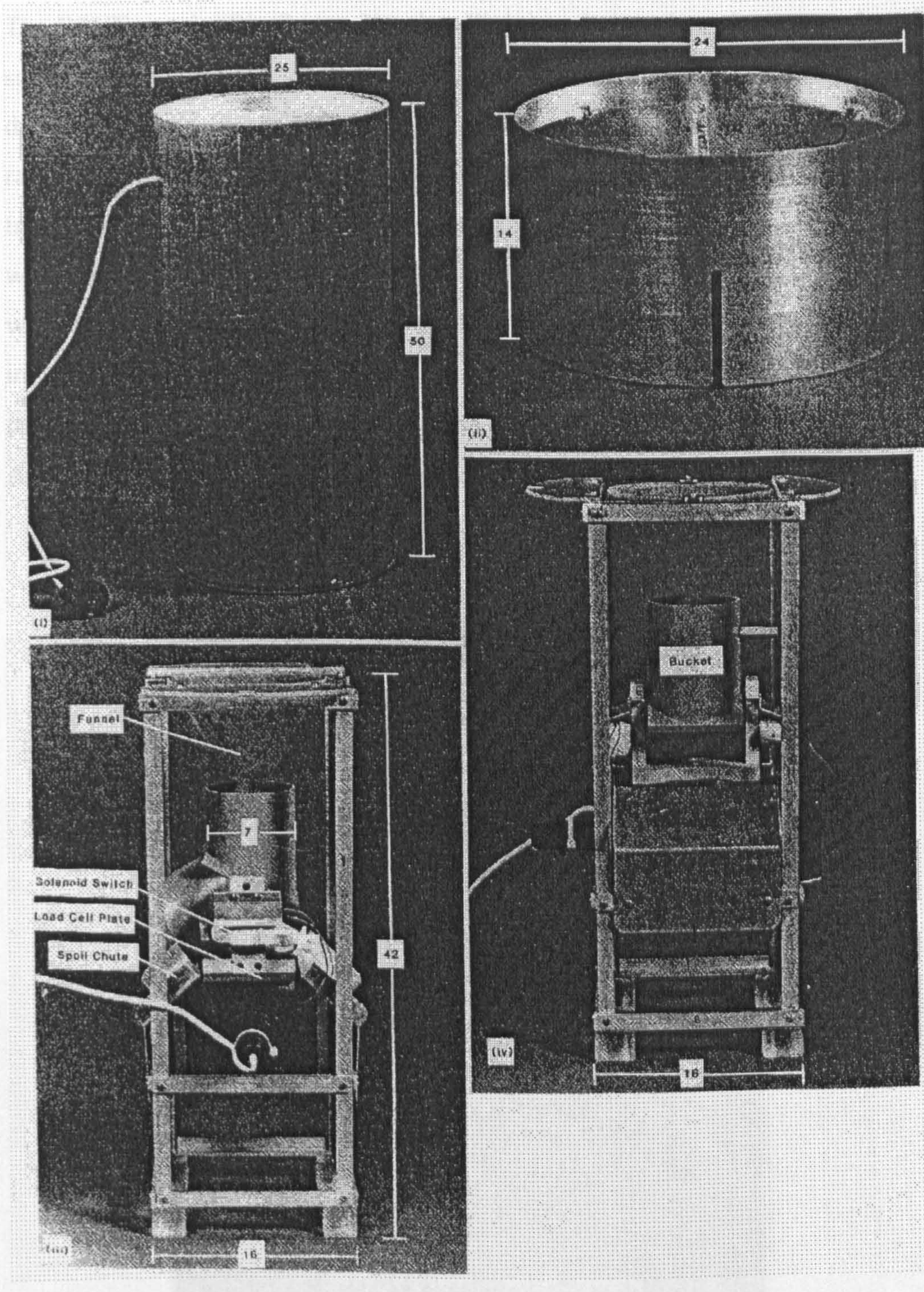

Figure 4.3 Automated/ buried trap (*from* Jackson 1996)

4.2.1.4. BSNE trap

The BSNE trap is (Big Spring Number Eight) is designed to obtain samples of suspended particles at various levels above the surface with varying wind directions. It consists of several rotating canisters mounted to a post at height range of 0.15 to 4.00 m (Figure 4.4). Sediment can be collected on removable trays placed inside each canister. The trap efficiency has been found to be within 88 to 94 % depending on wind speed and particle size. The higher the wind speed, up to 15 m/s, the lower the efficiency. Due to its higher efficiency in retaining coarse particles > 60 μm in size, this trap is more efficient in trapping sandy soils than loamy soils (Fryrear, 1986). It is widely used in North America (Stout and Zobeck, 1996; Stetler and Saxton, 1996).

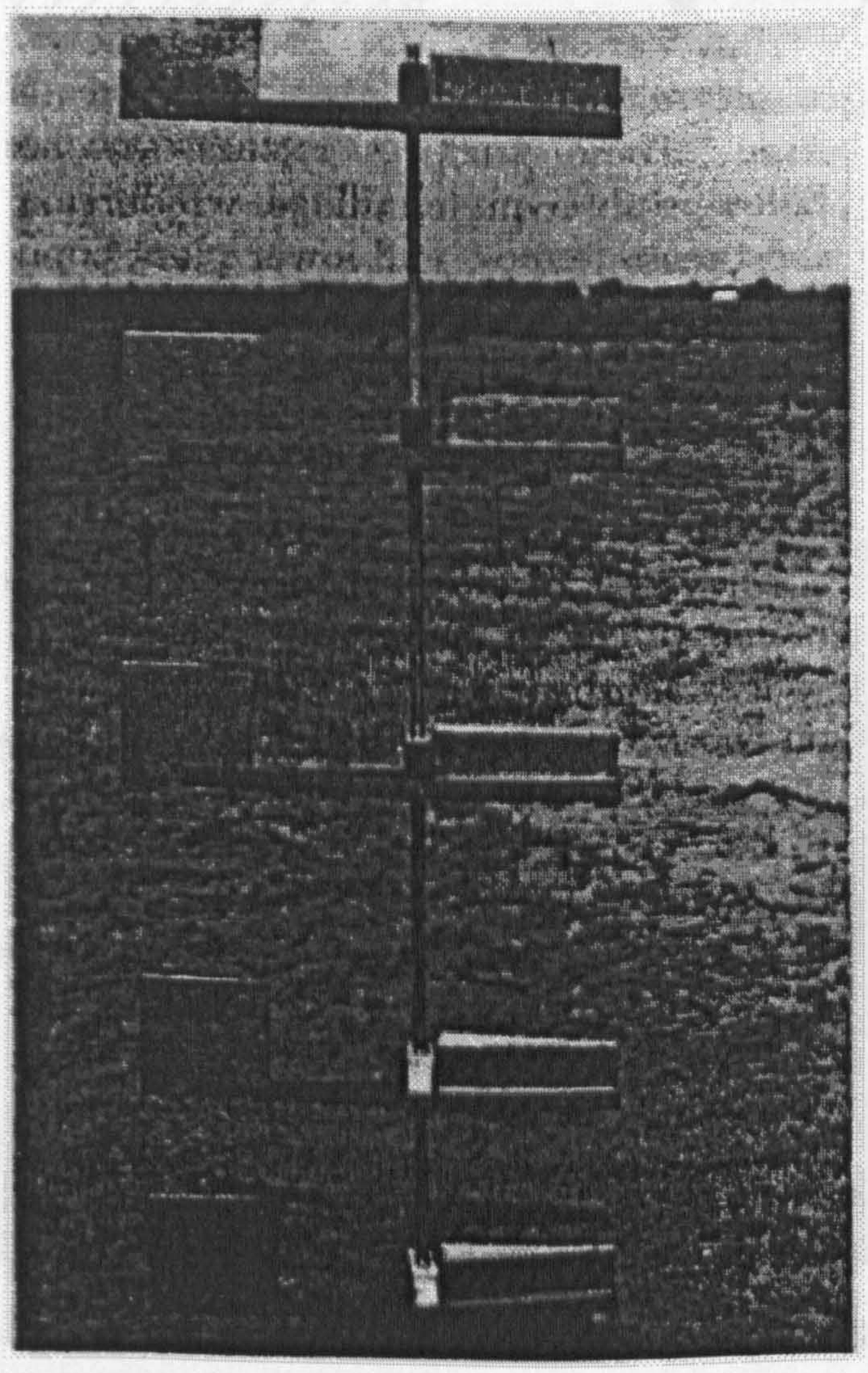

Figure 4.4 BSNE Samplers, mounted at different heights (*from* Fryrear, 1986)

4.2.1.5. Water traps

In water traps, water is used to prevent captured sediment from being re-entrained. Shallow water acts as an alternative to a deep tray in a dry trap. One design of this type (Wang and Kraus, 1999), consists of a rectangular frame of adjustable dimensions (Figure 4.5). It can be adjusted according to the wind speed and surface conditions. The perimeter is formed by plywood or aluminium sheeting assembled in the field and the top 10 cm of sand within the

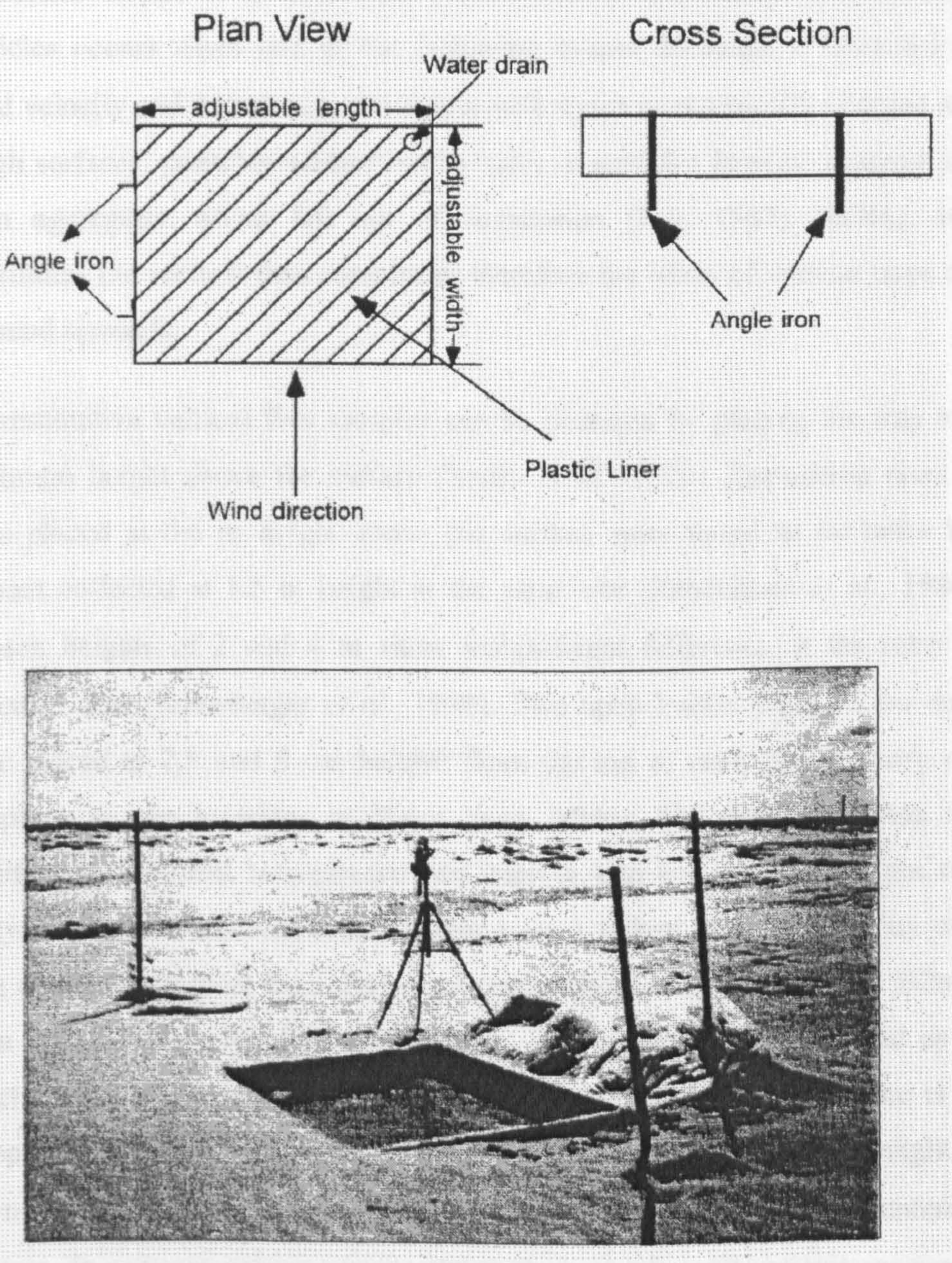

Figure 4.5 Schematic design of water trap (*from* Wang & Kraus 1999)

trap is removed. A plastic liner is placed inside the trap and fitted to the frame by staples to hold water. The disadvantage of this design lies in transporting, drying and weighing large amounts of samples. Under arid climatic conditions, water traps can easily become disfunctional due to the rapid evaporation of water.

4.2.2. Vertical flux traps (dust traps)

Some fine dust carried in suspension can be transported thousands of kilometres before it is deposited (Péwé, 1981). Deposition of suspended particles occurs when one of the following events develops: a reduction in wind velocity and turbulence; a collision with moist or electrically charged and rough surfaces; particles washed out by rain; or particles become charged and form aggregates which fall out of suspension (Pye, 1987). Falling dust constitutes the vertical flux component therefore the inlets of vertical traps are oriented upwards.

Representative vertical flux samples can be obtained by placing the trap at a minimum height above the surface (Smith *et al.*, 1970). Deposition rates in traps placed at 0.6 m height above the surface were found to be twice the amount collected at 1.5 m height at the same site (Rabenhorst *et al.*, 1984). Chosen heights of 2 and 4 m show insignificant difference in the rates of collected dust (Ramsberger *et al.*, 1998). Two open bucket traps 36 cm deep were placed at 2.5 and 5 cm heights from the top of each trap to carry out sampling at two locations in Niger, west Africa. The deposition was not significantly different between the two traps or trap site locations. Grain size analysis revealed that collected samples were a fallout of a vertical flux of a long distance transport from the source area, which is likely to be the Bilma-Faya Largeau alluvial plain (Drees *et al.*, 1993). These examples lead us to conclude that a 2 m height from the top of the trap and the bed surface is an acceptable lower limit to place a vertical flux trap during sampling. A height of $\geq$ 2m can be regarded as convenient to avoid saltating particles from entering the trap. In order to collect representative dust samples and prevent entrapped dust from being re-entrained by convective currents, a number of designs have been developed and presented here by way of example.

4.2.2.1. A bucket and marbles traps

Based on mimicking roughness elements on a natural surface, the design of Rabenhorst *et al.*, (1984) consists of an open plastic bucket and three layers of inert polystyrene balls placed at the bottom of the bucket to prevent entrapped dust from being re-entrained. A similar design was used by Reheis and Kihl (1995) where dust was collected in a cake pan and stabilised by glass marbles. These traps have been proven to be efficient and inexpensive but bulky to use during a long term monitoring. The retrieval of samples requires sufficient amounts of distilled water to wash the marbles at the end of each sampling period that may not be available where needed. Drees *et al.* (1993) have deployed the design of Rabenhorst *et al.* (1984) (Figure 4.6) in Niger, however, dust particles adhered to the balls were removed by a brush rather than distilled water. At the end of each collection period, the buckets were replaced by new ones and the old buckets were returned to a laboratory in Niamey, Niger for sample retrieval. Though this type of trap has been proven to be efficient under dry climatic conditions (Drees *et al.*, 1993), it requires careful collection of samples from the trap, a task that can not be efficiently achieved by workers in the field.

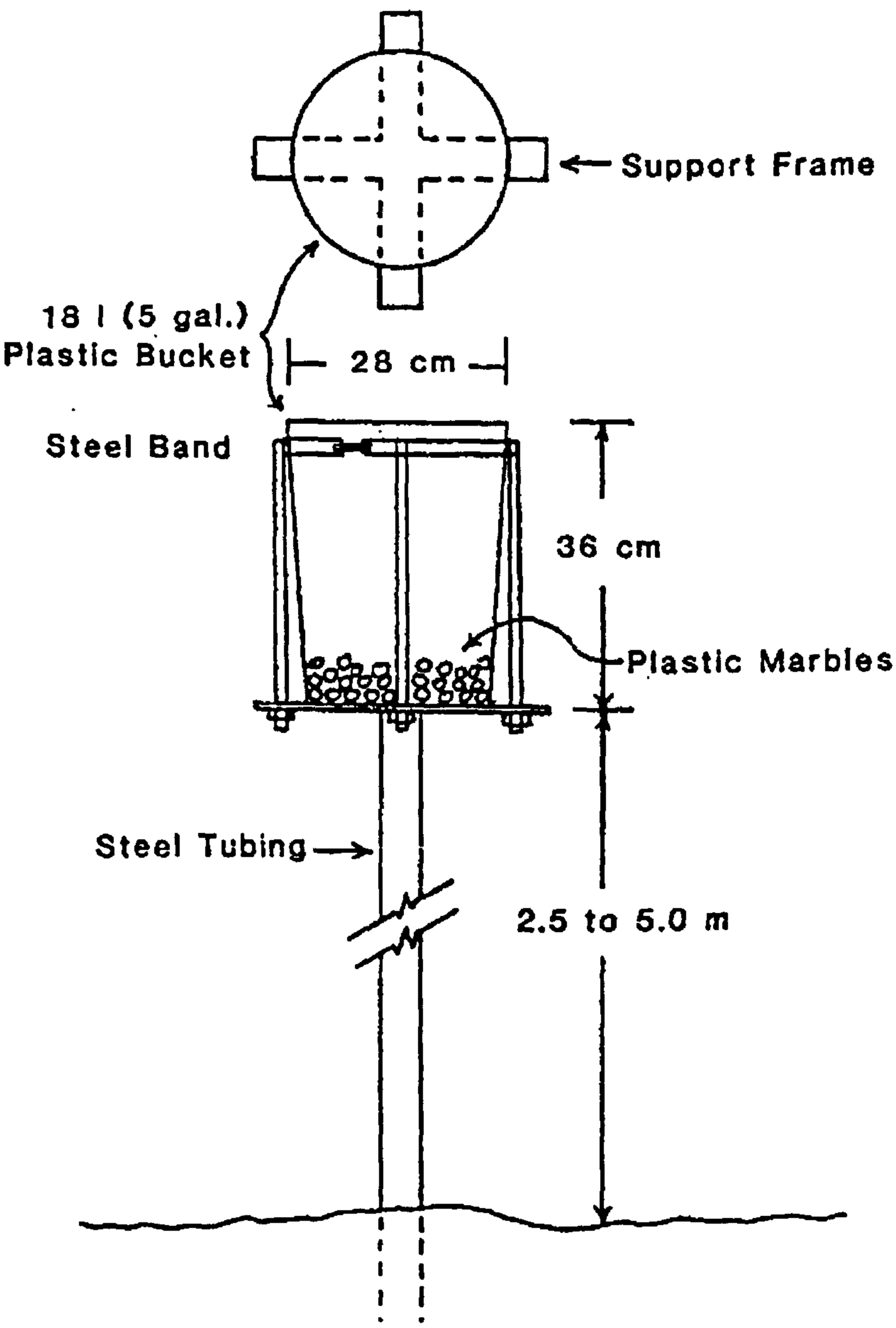

Figure 4.6 A bucket and marbles trap (*from* Drees *et al.* 1993)

4.2.2.2. An open bucket / drained water trap

Herrman (1996) has modified the open bucket design whereby a polyethylene mesh of 2 mm was used as a bucket cover to prevent resuspension of entrapped particles and to prevent insects and leaves from entering the trap (Figure 4.7). A provision was made to drain collected rainwater in the polyethylene bucket. Rainwater could flow off through an aperture and a 63 μm mesh at the bottom of the bucket. Entrapped bulk samples can be collected from the bucket with a paintbrush where the fine fraction of the bulk sediments transported by the drained water can be recovered by evaporation and added to the bulk samples. This design is appropriate for rainy environments.

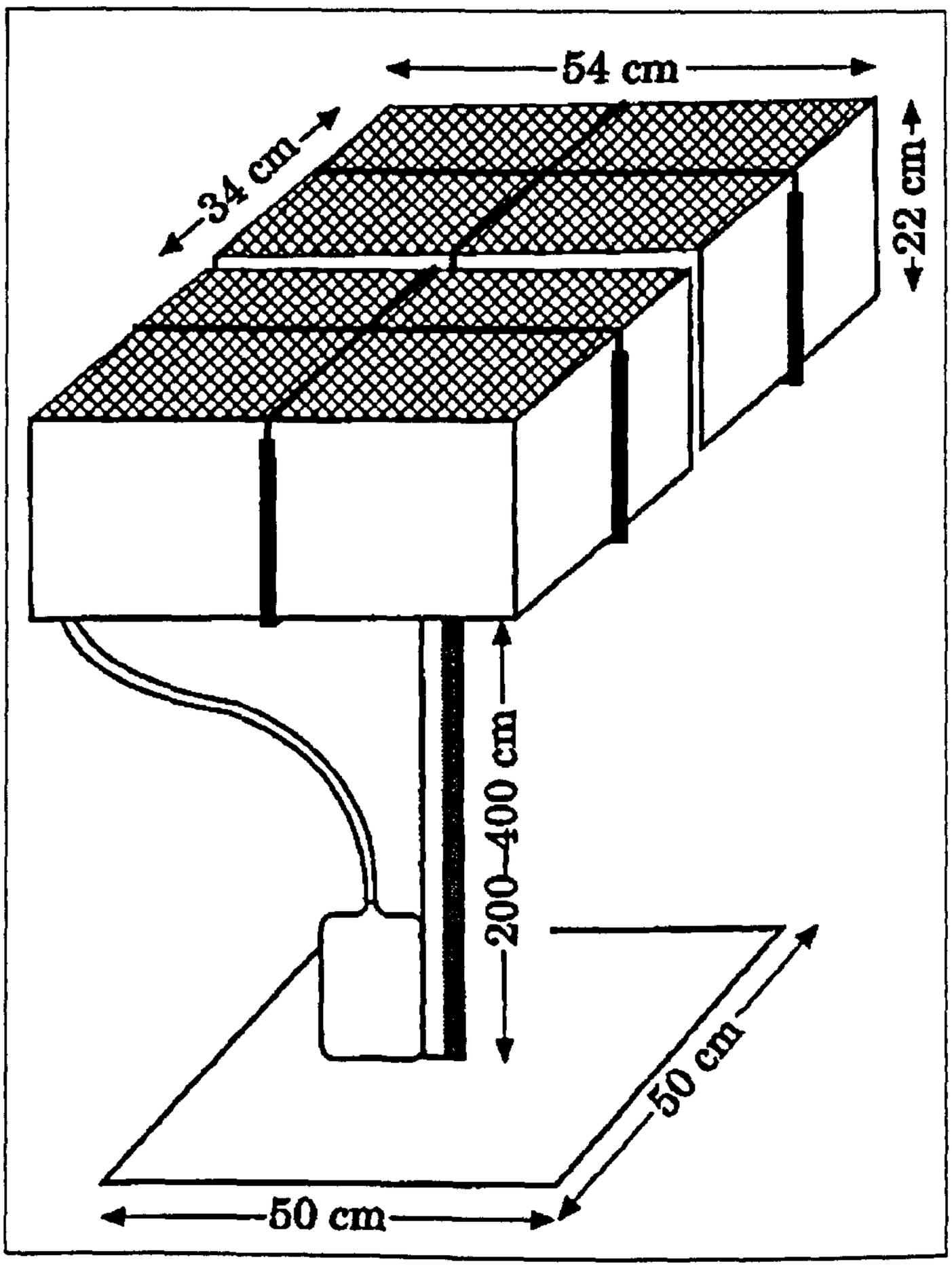

Figure 4.7 Schematic of open bucket/drained water trap (*from* Ramsperger *et al.* 1998)

4.2.2.3. A tray and artificial grass trap

A more recent design by Wiggs and O'Hara (in press) (Figure 3.8) consists of a circular tray (21 cm in diameter and 3 cm deep) and an artificial grass Astroturf insert (20 cm in diameter and 1 cm thick) placed inside the tray to stabilise deposited dust. A stretched net of 1 × 1 cm covers the tray to deter birds and minimise the amount of insect remains, bird droppings and vegetative material from entering the trap. The trap is mounted to a post at 2.5 m height to avoid entrapping saltating particles. This design was deployed in Turkmenistan to

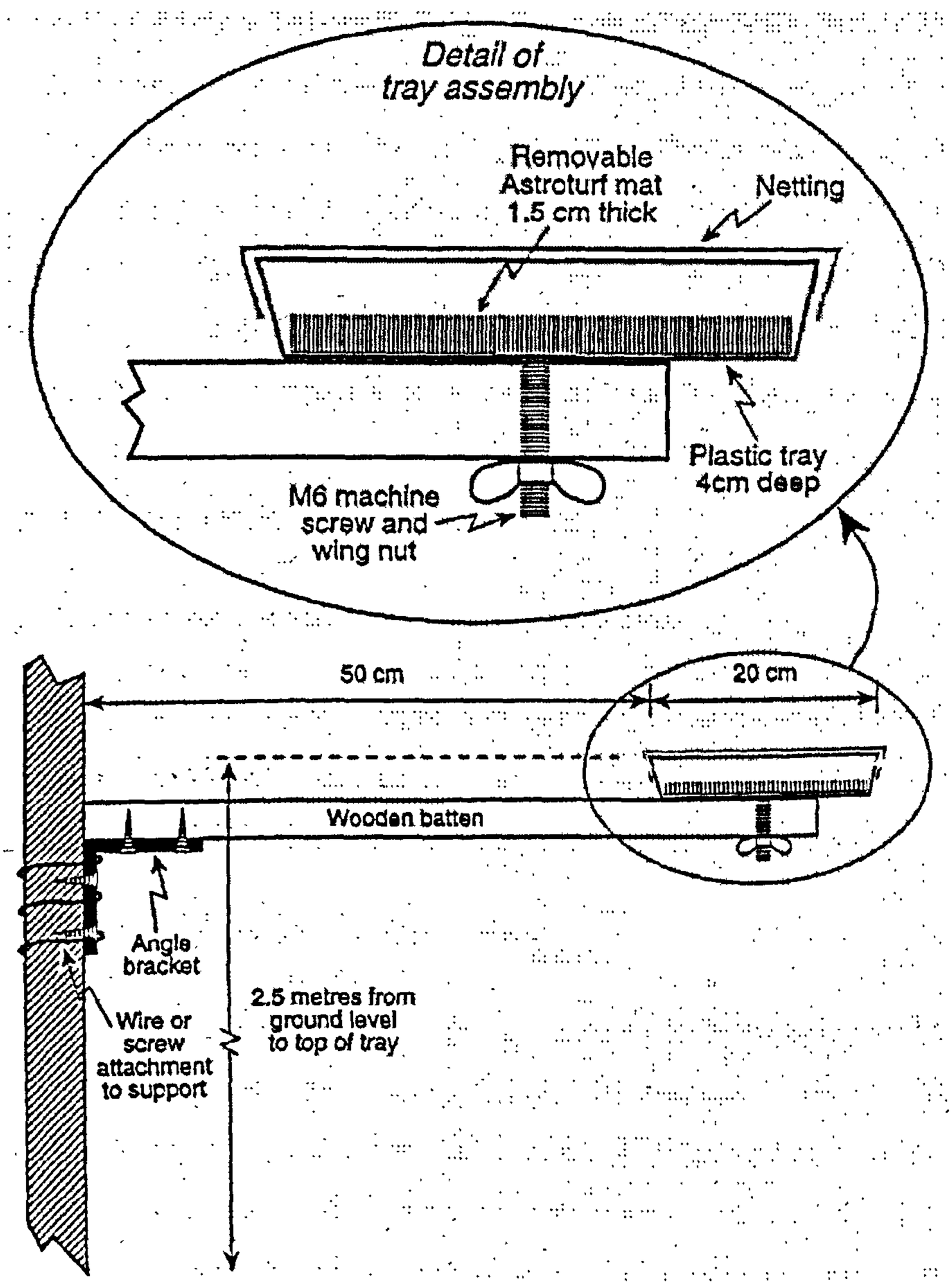

Figure 4.8 Schematic of tray & artificial grass trap (*from* Wiggs & O'Hara in press)

trap dust on monthly basis and it was found to be efficient for trapping fine sediments of < 10 μm. Although this trap is easy to install, inexpensive to build and proven to be effective in dry land environments, the adequacy of this design in rainy environments has not been tested (Wiggs and O'Hara, in press).

4.2.2.4. Water traps

Water traps were deployed to measure vertical dust flux deposition in Kano, northern Nigeria during three Harmattan seasons (McTainsh, 1980). Each trap consisted of a basin of distilled water 20 cm deep with a 0.27 m^2 water collecting surface. The water level was maintained daily, 10 cm below the top of the basin. A second basin was kept full of water to attract birds away from the trap. The trap was elevated 9 m above the ground level to collect the vertical dust component which originated in Faya Largeau, Chad. This type of trap requires daily monitoring of water levels and large amounts of water that may not be available unless transported to the sampling site. Additional labour in the laboratory to separate collected dust from the water is also needed.

4.3. FIELDWORK METHODOLOGY

4.3.1. Fieldwork project design considerations

There are a number of factors on which the fieldwork methodology for this doctoral study was decided. These include technical, spatial, temporal, environmental, meteorological, logistic and financial factors.

4.3.1.1. Trap type selection criteria

An important factor in trap design selection is trapping efficiency. Trap efficiency studies have been limited in number; some were based on comparisons of inconsistent trap designs (sand versus dust traps) (e.g. Goossens and Offer, 2000) and others were dedicated to sand traps (e.g. Li and Ni, 2003). These studies do not recommend a standard trap design. In a two years efficiency evaluation study Goossens and Offer (1994) concluded that a free water trapping surface is more efficient than a marble layered surface, a flat / moist surface or a dry/flat surface (Table 4.1).

Trap type	Relative efficiency % (1^{st} year)	Relative efficiency % (2^{nd} year)
Dry/ Flat	0.40	0.49
Moist	0.49	0.60
Marble	0.71	0.79
Water	1.00	1.00

Table 4.1 Trap efficiency relative to the water trap based on annual deposition (*from* Goossens and Offer 1994)

However, it was suggested by Goossens and Offer (1994) that water traps are actually less efficient as very small particles of dust tend to rebound from the water surface due to the effects of surface tension. Though the water trap had the highest efficiency, Goossens and Offer (1994) recommend use of marble traps as a standard in the future due to their simplicity, handiness and lack of maintenance. For this project, an Astroturf trap was chosen because it requires no distilled water supply to wash the entrapped dust in the field. During the course of trap selection, trap efficiency was a preliminary consideration but, the lack of standardisation in trap design and the shortage of trap efficiency evaluation studies made this consideration of secondary importance. A wind tunnel investigation of potential traps was considered, but was not undertaken due to the financial limitations imposed on this project.

4.3.1.2. Site selection and number of trapping sites

Since the preliminary objective of this project is establishment of baseline data on aeolian dust transport in Libya and since there has been no former dust sampling studies for Libya prior to this work, this leaves the whole country open for fieldwork study. However, the physical constraints in the field overrode the desired trap spatial distribution. These constraints included (1) population distribution and availability of volunteer workers, (2) access to private lands so trapping sites can remain out of any intruder's sight and (3) the existence of roads leading to targeted sites. The total area of Libya at 1,759,540 km^2 (Blake *et al.*, 1987) was considered too great to survey for the purpose of

this study, it was therefore decided to exclude the north eastern and south eastern regions of the country from this study. This decision was based primarily on the fact that personal contacts were needed to facilitate trap positioning and maintenance. Therefore, the study focused on the north western coastal strip of Tripolitania and the south western region of Fezzan. Moreover as the north western coastal region is the most populated part of the country and the fact that most agriculture and industry is located in this region, it was considered appropriate for the purpose of this study.

In a dust trapping study carried out around Be'er-sheva, Israel at several urban and rural sites, Erell and Tsoar, (1999) concluded that there were large spatial and temporal variations in the amounts of dust deposited in the urban sites. Those differences were attributed to the effects of neighbouring buildings and local urban dust sources. Furthermore, the deposited dust in built-up surroundings was coarser and more than twice the weight of the deposited dust in similar traps set in the open countryside. However, the mineral and chemical compositions of dust samples at all locations were similar. These differences in grain sizes and dust amounts were attributed to the properties of the wind field in the vicinity of buildings and the effects of different human activities.

The number of traps placed in the field was determined on the following basis: (1) Sufficient traps to produce a reasonable amount of data taking into account the possibility of losing some traps at the trapping sites and failure of some workers to abide by their promises. (2) Some idea of how many volunteers can be found to take part in the fieldwork before the start date of trapping. (3) Delivery of all traps to the workers before approaching the scheduled trapping deadline. (4) Managing the project at the lowest possible cost. Time is a limiting factor in deciding the number of trapping sites as well as in processing and analysing large amounts of generated data when a large number of traps are deployed.

4.3.1.3. Fieldwork project duration

The duration of the fieldwork is generally limited by the available resources and the timeframe of a given project. Since dust transport and deposition change over time, the longer the trapping period, the more informative the collected data would be. Whilst prevailing wind directions and speeds change from one season to another, representative data of dust deposition variability is best collected through out a full climatic cycle period. A one-year study is expected to provide sufficient deposition data that can be linked to the meteorological data of the sampling period. The duration of the fieldwork is an important element in selecting a practical design, for example, automated samplers require frequent servicing and constant power supply and water traps require regular monitoring of water level if used in dry environments. Therefore, the longer the planned trapping duration, the simpler and more independent the selected trap should be.

4.3.1.4. Dust trapping intervals

Deciding the length of dust collection intervals is a compromise between what may be a short period and a long one. On the one hand, frequent collection of entrapped dust, such as every one or two weeks may not yield a sufficient sample to carry out the necessary laboratory analysis. A weekly sample collection study carried out in Nigeria proved to be adequate, but the sampling was only carried out using a single trap during the Harmattan season which extends from October to April (McTainsh 1980). A short sampling duration can multiply the required amount of work from each worker and that may discourage many locals from volunteering to help with the project. Furthermore, this can raise the cost of the project and produce a large number of samples beyond the capacity of the project to test and analyse. Long periods such as seasonal (3 months) or biannual durations can result in crude and limited amount of data that can be less representative and more difficult to relate to the meteorological data. Furthermore, a loss of few samples can significantly influence the quality of the data.

4.3.2. A comparative assessment of similar dust trapping studies

Some previous studies carried out in similar environments are listed for comparison (Table 4.2) to help understand the reasons for choosing a particular trap for each project and deciding the number of traps for each site and relating these choices to the length of each study. Marble traps have been used for a 12 month sample collection study over a five years period (case 1) and also for a four month sample collection study over a smaller scale of two traps in a four years period (case 2). However, both studies received logistic support from servicing centres in the vicinity of the trapping sites. The Nevada/California project was a product of a collective effort of a number of institutions in that region rather than an individual effort as the case in this project. Water traps require frequent monitoring and dust collection is therefore reduced to one week and conducted during the dustiest days of the year to ensure enough dust input in a very short time (case 3). In an intermediate dust trapping study carried out near the delta of the Aral Sea in Karakalpakstan, Astroturf traps were used at eighteen trapping sites over a period of one year (case 4).

4.3.3. Project specifications

Based on the above studies and considerations, an optimum criterion to bring about a successful fieldwork study was found to be as follows:

- Deployment of 30 Astroturf traps as shown in Figure 4.8.
- Trapping dust for 12 months and collecting samples at the end of each month at all sites.
- The set start date was 1 June 2000 and the end date was 30 May 2001.
- Trap installation at a minimum height of 2.5 m above the ground.
- Two traps were planned for installation on the same post at 2.5 m and 4.5 m to examine the effect of trap height from the surface on its efficiency (Figure 4.9).

Case Number	Trap Design	Area of Study	Number of Traps	Trapping Duration	Sample Collection Duration	Reference
1	Marbles/Pan cake	S Nevada & SE California. Approx. area 217,500 km^2 .	55	5 years	12 months	Reheis & Kihl 1995.
2	Marbles/Bucket	South western Niger, West Africa. Approx. 200 km apart.	2	4 year	4 months	Drees *et al.* 1993.
3	Water Basin	Kano, Nigeria. Only one site.	1	3 Haramattan Seasons	1 week	McTainsh 1980.
4	Astroturf/Tray	Aral Sea, Karakalpakstan. Approx. area 40,000 km^2 .	18	1 year	1 month	O'Hara *et al.* 2001.

Table 4.2 Design specifications of some previous dust trapping studies in desert environments

Figure 4.9 A trapping site at Semnu near Sebha consists of two traps at 2.5 and 4.5 m heights

Selected dust trapping sites, as they seemed to be achievable at the start of this study, were in the regions of: Zuwarah, Ajalat, Surman, Tripoli, Al Khums, Zlitan, Misratah, Tawurgha and inland at Bani Walid, Waddan, Zillah, Sebha, Birak and Bent Baiya (between Sebha and Ubari) (Figure 4.10). The total area of the field area is approximately 300,000 km^2 stretches from north west and

south west regions of the country between 12° E, 18° E and 26° N, 33° N. The 30 traps were distributed unevenly among the chosen sites due to shortage of reliable volunteers at some sites.

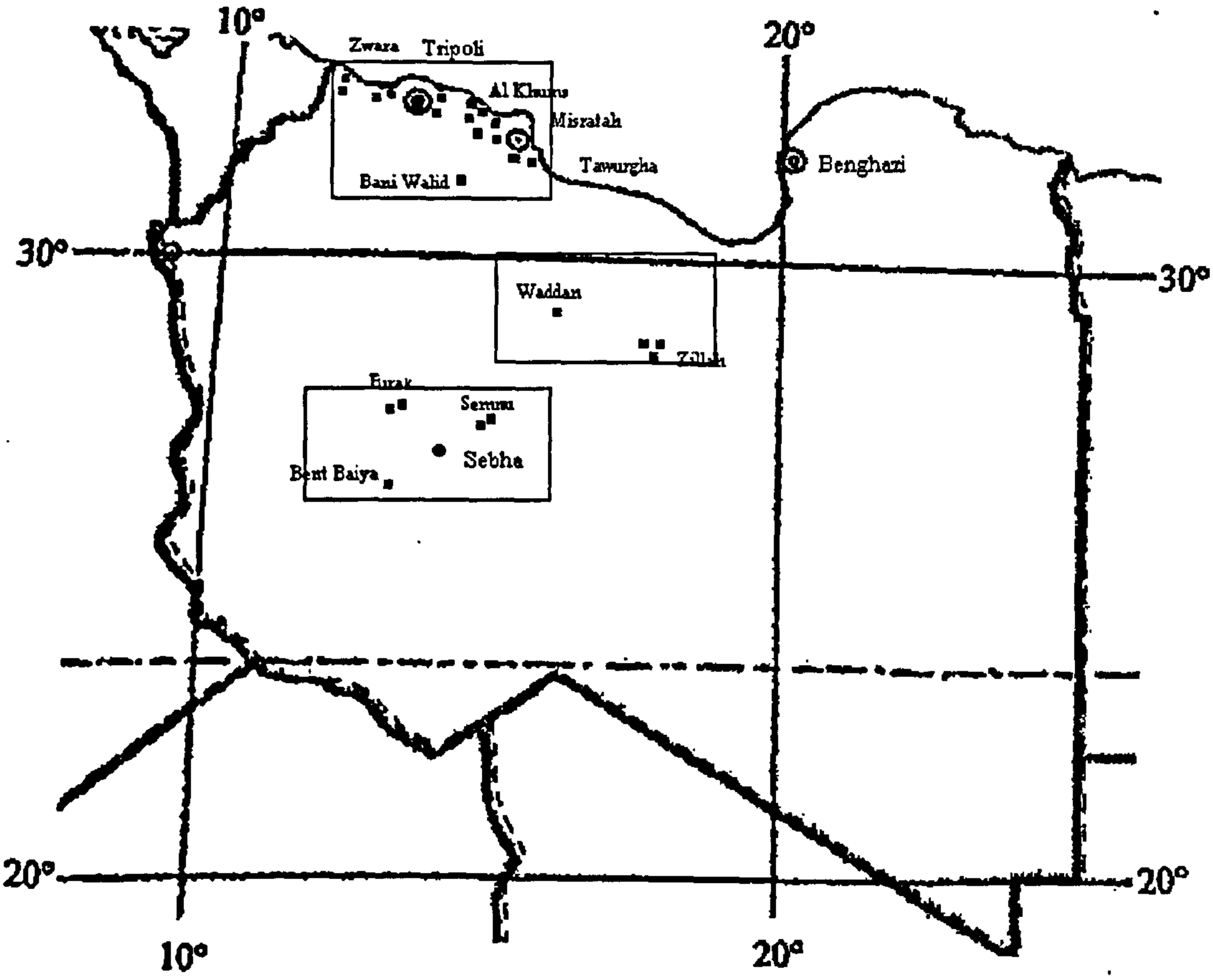

Figure 4.10 Distribution of trapping sites in the regions of study

4.4. SUMMARY

This chapter has focused on the review of aeolian sediment traps available to quantify sediment flux and the fieldwork design. An Astroturf trap for field measurements has been chosen and trapping areas have been identified. The following chapter describes the field and laboratory methods applied to measure the dust flux rates. In addition, locations of field sites and dust flux rates are presented.

CHAPTER 5

MONTHLY DUST DEPOSITION ACROSS LIBYA (2000-2001)

5.1. INTRODUCTION

This chapter involves a description of the creation and maintenance procedures of 30 sediment Astroturf traps, field placement and subsequent laboratory analysis of trapped sediments. It also presents a physical description of field sites and corresponding monthly accretion rates. The temporal variations in total deposition are described for each of the three regions identified in chapter 3 whereas the spatial variations are presented for each month, discussed for each season for the entire study area (3 regions) and compared with TOMS AAI to investigate the spatial variations in total deposition on the ground with respect to the spatial variation of aerosol concentration in the atmosphere.

5.2. PRE-FIELDWORK PREPARATIONS AND FIELDWORK PROCEDURES

- The first procedure of preparation for the fieldwork was fabrication of 360 Astroturf inserts (19.5 cm diameter × 1.5 cm height) and 30 wooden supports (65 cm × 5 cm × 1.5 cm) at the University of Nottingham.
- All the inserts were labelled systematically on the back using water-resistant paint, washed using distilled water and sealed individually in clean plastic bags.
- Packing all the necessary items for the field work which included: (1) thirty PVC trays (20 cm diameter × 3.5 cm height), (2) three hundred and sixty Astroturf inserts, (3) thirty wooden supports, (4) thirty angle brackets, (5) thirty wing nut screws, (6) 3 m^2 of 1 × 1 cm netting, (7) about 400 clean plastic bags, (8) thirty clean kitchen brushes to retrieve adhering dust on the inside surface of the trays, (9) a compass, (10) a camera to photograph the geomorphologic features at the sites and (11) a note book.
- Prior to the start of the fieldwork, some locals were contacted through mutual friends to find volunteers in the vicinity of each primarily targeted place. This assignment was achieved within one month but volunteers were not found in every targeted area. The shortage of volunteers and friends in some areas was a decisive factor in trap site

distribution. Some vast areas are not inhabited and as such had to be excluded from the study.

- At the start of the fieldwork, each site was inspected and in some cases it was necessary to look for an alternative site either because of heavy traffic in the region or the possibility of vandalism at site. Photographs were taken in four directions at each chosen trapping site to maintain a record of the geomorphologic features in the region that may help explain variations in deposition rates.
- Once a volunteer was found and a suitable site identified, a trap was attached to either a pre-existing electric post or a specially erected post for the trap.
- At each site, a terrestrial soil sample of 50 gm or more was taken and each sample was put in a clean bag, sealed and labelled.
- Workers at all sites were instructed on how to change the inserts at the end of each month.
- Frequent contacts were maintained by telephone with most of the workers to remind them of the due dates and instruct them on how to act under any exceptional circumstances. Unfortunately, this was not possible in some cases due to poor telephone connections in some regions.
- Finally, at the end of the fieldwork, all the inserts were collected from the workers and shipped back to the UK.

5.3. LABORATORY ANALYSIS

5.3.1. Dust samples status

Monthly sediments adhering to the Astroturf inserts and inside the plastic bags were recovered and quantified. During the course of sampling, some of the Astroturf inserts were lost to high speed winds, dismantled by intruders or neglected by some of the workers. Twenty traps were properly monitored through out the coarse of this study. Four others were not monitored in a timely fashion as it was planned at the start of the project, while the remaining six traps either were totally neglected by some workers or their reliability is questionable. A comprehensive summary of sampling sites status is provided in Tables 5.1 and 5.2.

LOCATION	NO. SITES	TRAP CODE	JUN 2000	JUL 2000	AUG 2000	SEP 2000	OCT 2000	NOV 2000	DEC 2000	JAN 2001	FEB 2001	MAR 2001	APR 2001	MAY 2001
Zuwarah	1	AA	✓	✓	✓	✓	✓	✓	✓	✓	✓	✓	✓	✓
	2	AB	✓	✓	✓	✓	✓	✓	✓	✓	✓	×	✓	✓
Ajalat	1	AC	✓	✓	✓	✓	✓	✓	✓	✓	✓	✓	✓	✓
Surman	1	AD	✓	✓	✓	✓	✓	✓	✓	✓	✓	✓	✓	✓
Tripoli	1	AF	✓	✓	✓	✓	✓	✓	✓	✓	✓	✓	✓	✓
	2	AE	✓	✓	✓	✓	✓	✓	✓	✓	✓	✓	✓	✓
	3	BB	×	×	×	×	×	×	×	×	×	×	×	×
Al Khums	1	CA	✓	✓	✓	✓	✓	✓	✓	✓	✓	✓	✓	✓
	2	CB	✓	✓	✓	✓	✓	✓	✓	✓	✓	✓	✓	✓
	3	CC	✓	✓	✓	✓	✓	✓	✓	✓	✓	✓	✓	✓
Zlitan	1	BF	✓	✓	✓	✓	✓	✓	✓	✓	✓	×	✓	✓
	2	BA	✓	✓	✓	✓	✓	✓	✓	✓		Q	Q	×
	3	CD	×	×	×	×	×	×	×	×	×	×	×	×
Misratah	1	CE	✓	✓	✓	✓	✓	✓	✓	✓	✓	✓	✓	✓
	2	DD	✓	✓	✓	✓	✓	✓	✓	✓	✓	✓	✓	✓
Tawurgha	1	DE	✓	✓	✓	✓	✓	✓	✓	✓	✓	✓	✓	✓

Table 5.1 Field study report – Dust samples status. [COASTAL REGION]

✓ Collected Q Questionable × Lost

LOCATION	NO. SITES	TRAP CODE	JUN 2000	JUL 2000	AUG 2000	SEP 2000	OCT 2000	NOV 2000	DEC 2000	JAN 2001	FEB 2001	MAR 2001	APR 2001	MAY 2001
Bani Walid	1	BD	✓	✓	✓	✓	✓	✓	×	×	×	×	×	×
	2	BC	Q	Q	Q	Q	Q	Q	Q	Q	Q	Q	Q	Q
	3	BE	Q	Q	Q	Q	Q	Q	Q	Q	Q	Q	Q	Q
Waddan	1	EF	✓	✓	✓	✓	✓	✓	✓	✓	✓	✓	✓	✓
	2	ED	×	×	×	×	×	×	×	×	×	×	×	×
	3	EE	×	×	×	×	×	×	×	×	×	×	×	×
Zillah	1	EA	✓	✓	✓	✓	×	✓	✓	✓	✓	✓	✓	✓
	2	EB	✓	✓	✓	✓	✓	✓	✓	✓	✓	✓	×	✓
	3	EC	✓	✓	✓	✓	✓	✓	×	✓	✓	✓	×	✓
Semnu	1	DF	✓	✓	✓	✓	✓	✓	✓	✓	✓	✓	✓	✓
	2	DC	✓	✓	✓	✓	✓	✓	✓	✓	✓	✓	✓	✓
Birak	1	DA	✓	✓	✓	✓	✓	✓	✓	✓	✓	✓	✓	✓
	2	DB	✓	✓	✓	✓	✓	✓	✓	✓	✓	✓	✓	✓
Bent Baiya	1	CF	✓	✓	✓	✓	✓	✓	✓	✓	✓	✓	✓	✓

Table 5.2 Field study report – Dust samples status. [Inland]

✓ Collected Q Questionable × Lost

5.3.2. Quantification of dust yield

After the completion of the fieldwork, the collected sediments and the terrestrial samples were sent to Nottingham for analysis. In order to ensure an unbiased retrieval of all grain sizes of entrapped dust from the Astroturf inserts, the following procedures were followed:

- The Astroturf insert was removed from the plastic bag and placed inside a 24 cm diameter porcelain dish in an inverted position. The bag was then inverted and flushed with distilled water on its inside surface using a wash bottle.

- Next, the insert was held in an inverted position above the dish and flushed with distilled water carefully to ensure a maximum recovery of adhering dust.

- Then the insert was placed in an inverted position inside the dish and more distilled water added until it was fully immersed under water.

- The porcelain dish was then placed in an sonic bath for 20 minutes to loosen any remaining dust on the Astroturf surface.

- The insert was removed and any remaining sediment washed into the porcelain dish. The contents were then poured into a pre-labelled 20 cm diameter PVC bowl.

- The PVC bowl was placed inside an oven set at about 60 °C and left it until the water was fully evaporated.

- The dry sediment was sprinkled with the least needed amount of distilled water to loosen the adhering sediment particles on the surface of the PVC bowl. The sediment then was gathered by using a washed brush and the contents were poured into a distilled, prelabelled and preweighed 125 ml plastic bottle.

- The bottle was placed open inside the oven at about 60 °C and left until the water was fully evaporated. When the sample became dry, the bottle was weighted (closed) containing the sample. The weight of the sediment was obtained from subtracting the weight of the empty bottle from its weight including the weight of sediment.

5.4. FIELD SITES AND RATIONALE

5.4.1. Introduction

Deposition of dust occurs if the deriving winds experience a reduction in velocity and turbulence, the particles are captured by collision with moist or rough surfaces and when the particles are washed out by rain (Pye, 1987). Short term deposition occurs when coarse and medium silt grains in transport at low heights either settle back to the surface as a result of reduction in wind velocity or are trapped by obstacles such as vegetated surfaces and urban areas that tend to increase the surface roughness and the roughness height (Pye, 1987). Surface roughness plays an important role in dry dust accumulation in rocky deserts especially on concave windward slopes (Goossens, 2000). Deposition of fine dust particles, on the other hand, is less affected by changes in surface roughness and often occurs when particles are washed out by rain (Pye, 1987). The amount of fallout at the regional scale is a function of two sets of variables. First is the rate of production in the source region which is dependent on the rate of weathering, vegetation cover, moisture content and human activities. Second is the transport efficiency from source to sink which is manifested in lifting efficiencies, transporting power and circulation patterns (Livingstone and Warren, 1996). Since entrainment and deposition of dust in arid regions are interchanging and continuous processes, what may be a sink of some transported load can serve as a source of another load. Furthermore, trapped dust samples in arid regions are a mixture of both long range fine aerosol and coarse saltating particles.

5.4.2. Partitioning of the study area

In order to simplify the presentation of deposition data and their analysis, the study area has been divided into three main regions, northern, central and southern (Figure 5.1) based on differences in their geomorphological, meteorological and demographical conditions (see chapter 2). In addition, the northern region is divided into four areas to account for the non-uniform presence of natural dust sources (wadis and sabkhas) and the wide variation in the demographic distribution. Ground modelling has classified the northern western coastal part of Libya (northern region) as one of the highest emission regions of the Sahara (see chapter 3) (Callot *et al.*, 2000), the TOMS aerosol index maps during the study period show that the central region was more frequently affected by higher intensity aerosols of Saharan dust plumes than the other two regions (see chapter 3), where another atmospheric model (Figure 1.5) (Goudie, 2003) highlights the Fezzan region (southern region) as a major source of dust. Furthermore, the main Saharan trajectories during the spring seem to coincide with the locations of the northern and central regions (Figure 1.5).

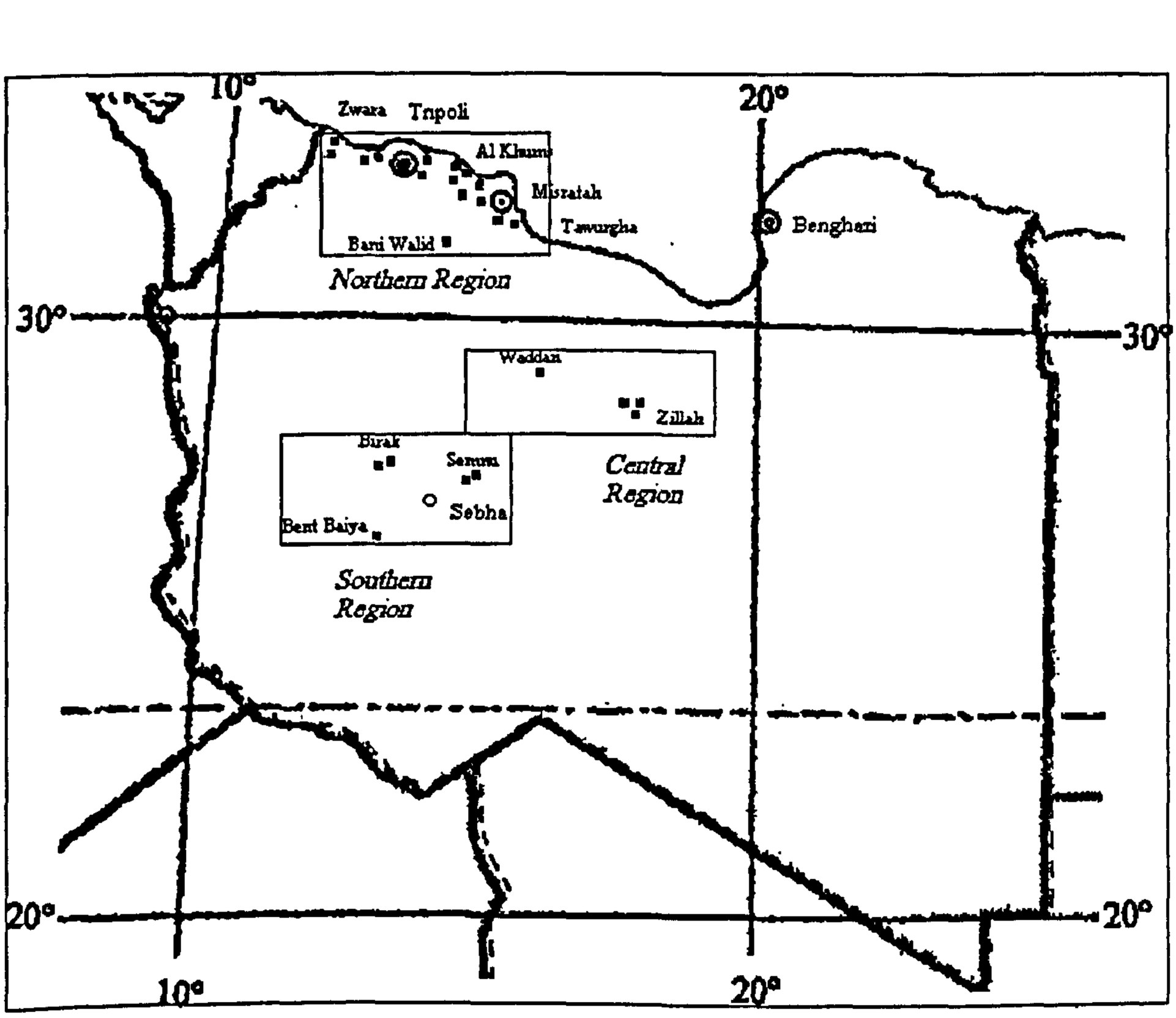

Figure 5.1 Dust trapping sites and regions of study

5.5. NORTHERN REGION

The region situated between 12° and 16° E and 31° and 33° N (Figure 5.2) is bounded by a coastline from the north and comprises sabkhas in the vicinity of Zuwarah and Tawurgha. The foothills of Jabal Nafuse, the southern boundaries of the Jifarah Plain in the west, meet with the coastline at Al Khums and are bisected by a number of wadis. Inland, about 120 km south of Al Khums, a larger seasonal wadi network occurs in the vicinity of Bani Walid. The northern region is one of the most vegetated regions in Libya due to its Mediterranean climate and the most populated region in the whole country. As there are four meteorological stations, a nonuniform demographic distribution, diverse geomorphologic features and different local dust sources, deposition in this region is analysed on the basis of four geomorphological areas (Figure 5.2).

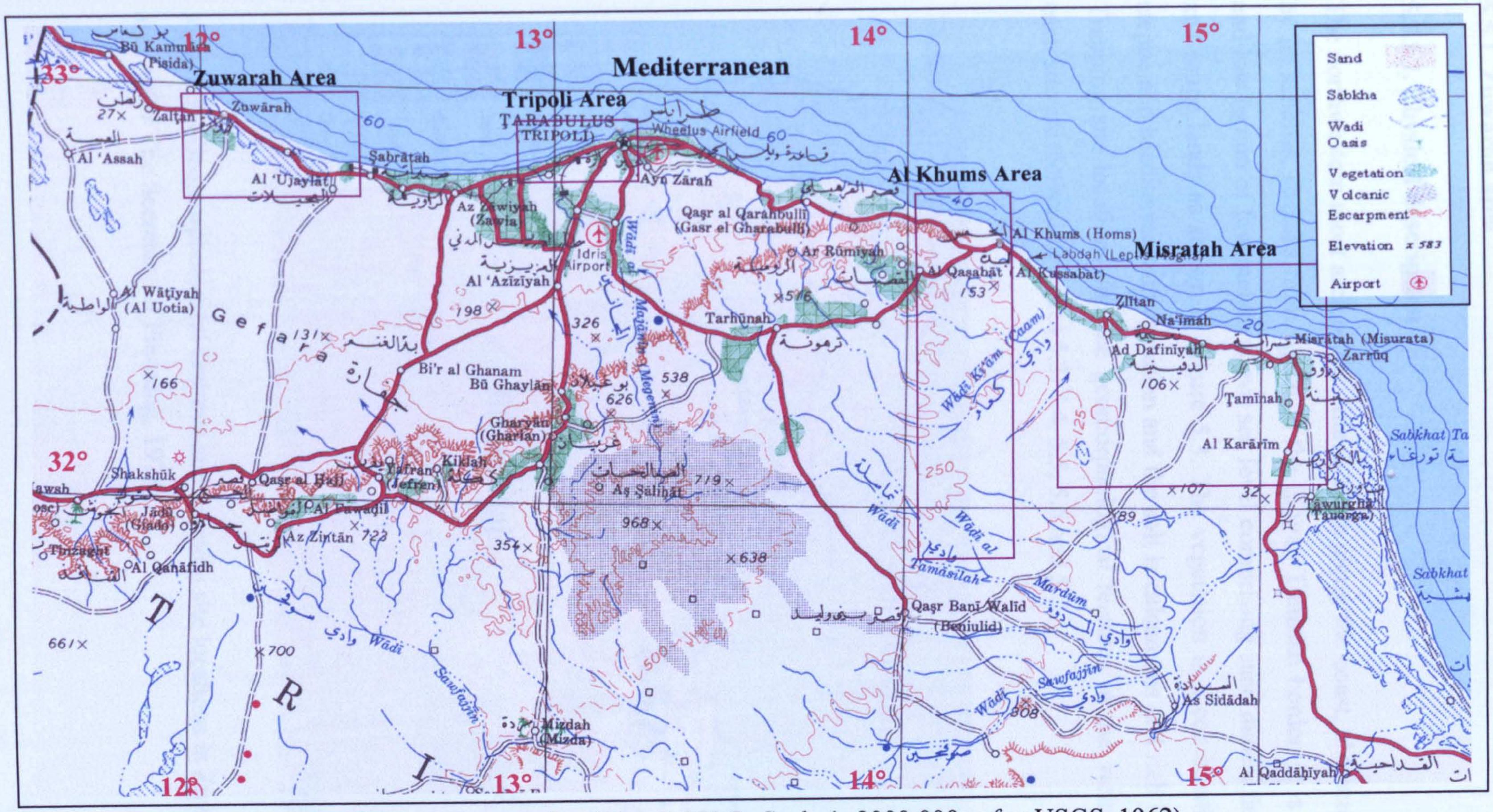

Figure 5.2 Topographic map of the northern region (Plate I-350 B, Scale 1: 2000,000; *after* USGS, 1962).

5.5.1. Zuwarah area

5.5.1.1. Physical description

The northwestern most area of the Jifarah Plain along the coast, characterized by its sabkhas, stretchs from Ajalat to the Libyan Tunisian border. It is a flat and low terrain of few meters above sea level comprising sand dunes, farming and range lands as shown in Figure 5.3. The vegetation is a combination of steppe and Mediterranean vegetation and the soil is calcareous and rich in salt. Trapping site locations and the geomorphological features in the vicinity of each site are shown in Figures 5.3, 5.4, 5.5, 5.6 and 5.7.

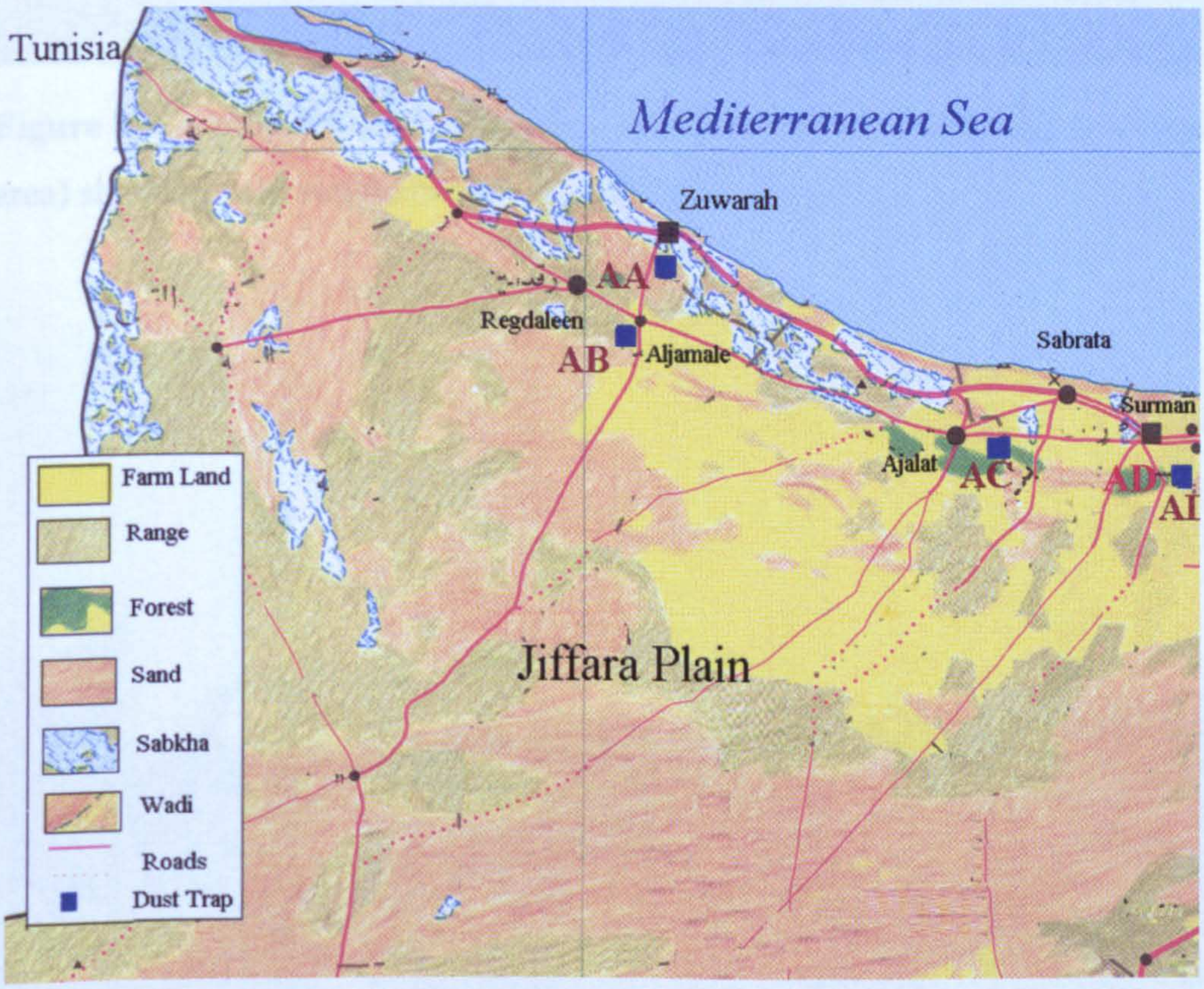

Figure 5.3 Geomorphological features and trapping site locations in Zuwarah area (*after* The Secretary of Planning, 1978)

Figure 5.4 A southern view of trapping site (AA) near Zuwarah city (Zuwarah area) showing poor vegetation cover of salt rich soil

Figure 5.5 A southern view of trapping site (AB) at Aljamale (Zuwarah area) showing newly planted palm trees on the westernmost farming land of the Jiffarah Plain

Figure 5.6 A western view of trapping site (AC) at Ajalat (Zuwarah area)

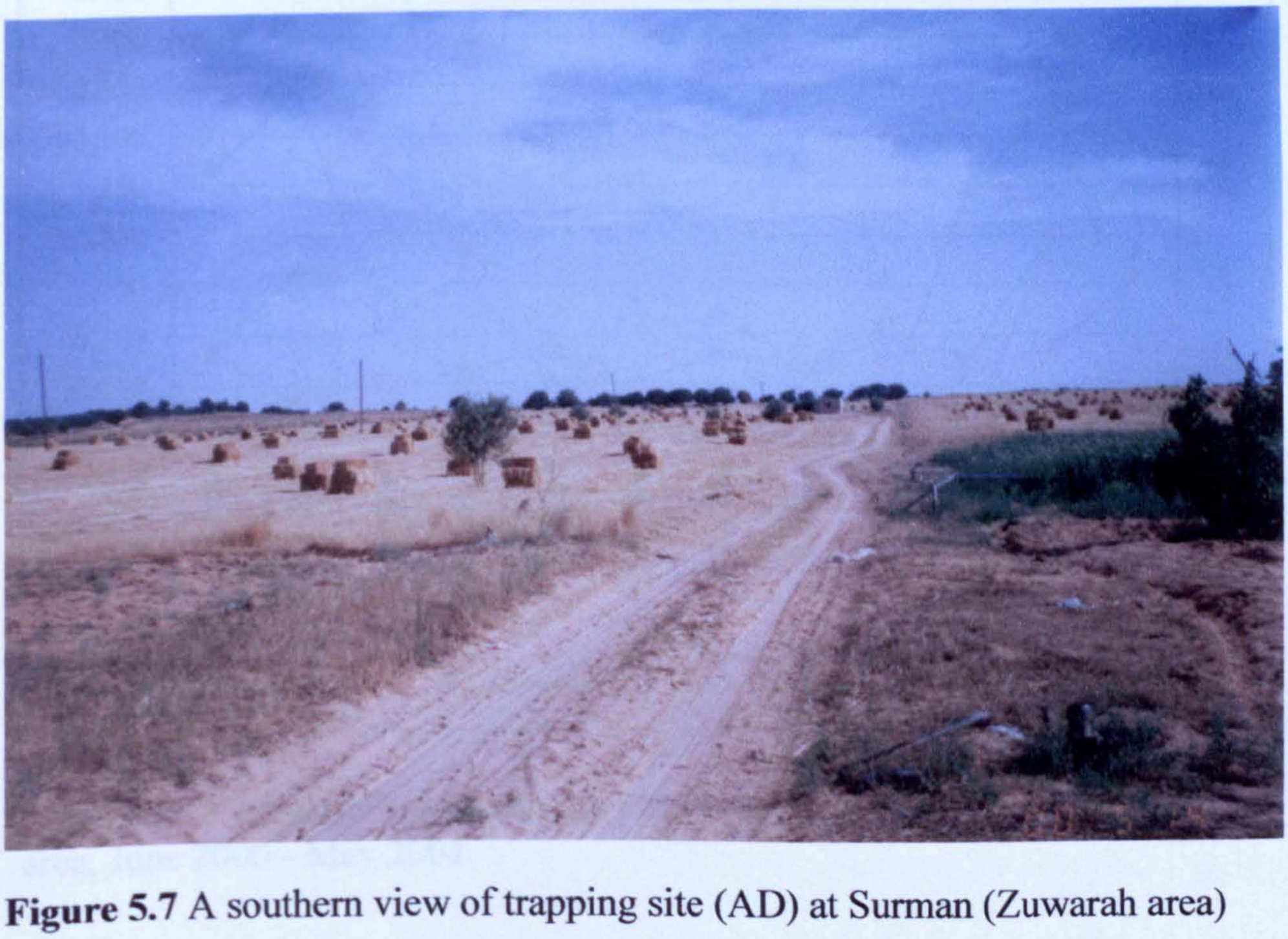

Figure 5.7 A southern view of trapping site (AD) at Surman (Zuwarah area)

5.5.1.2. Dust traps

Deposition rates in the Zuwarah area (Figures 5.8) vary widely from one site to another during the summer and the spring months but, converge in late autumn and winter. Variations in deposition rates show that there is a bi-modal seasonal distribution with one mode corresponds the summer and the other to the spring. The average monthly highest deposition rate corresponds to July (0.235 t/ha). During the period from October until February, this area experienced lower and steady deposition rates of an average ranging from 0.0632 t/ha in October and 0.0780 t/ha in December. In the Spring 2001, higher dust activities resulted in high deposition rates reaching a monthly average of 0.2052 t/ha during April that is comparable to summer.

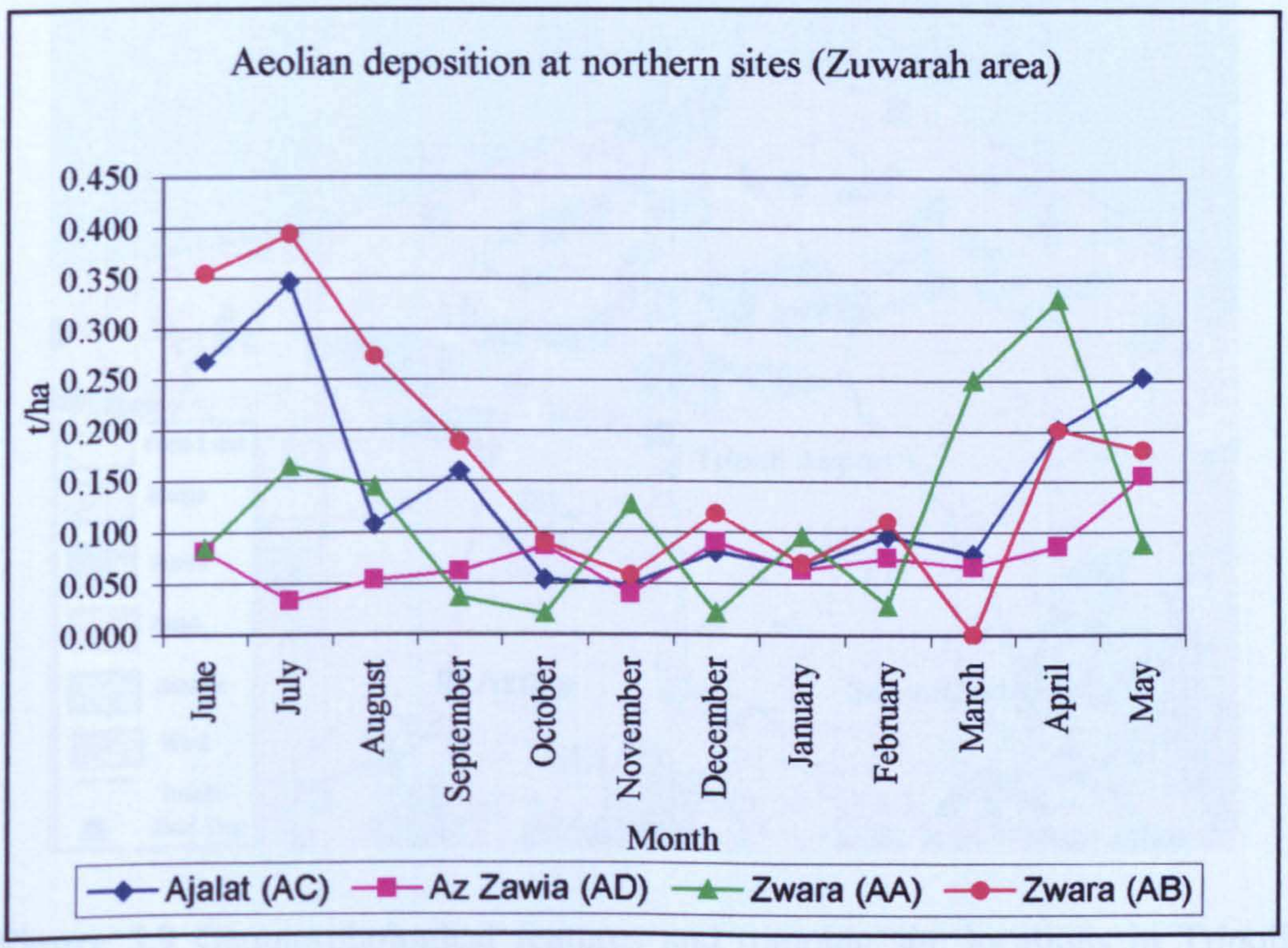

Figure 5.8 Variations in monthly deposition in the northern region, Zuwarah area, June 2000 - May 2001

5.5.2. Tripoli area

5.5.2.1. Physical description

The geomorphologic characteristics of Tripoli are similar to those of Zuwarah, except that Tripoli is free of any sabkhas. The metropolitan area of the city is the largest in Libya and dust sediments re-entrained on the asphalted roads can be an important source of dust as the city experiences the heaviest traffic in the country. More dust may have originated from farms around the city and civil constructions. Trapping locations were selected in areas in which anthropogenic dust sources were minimal. Site locations and the surface landscape at each site are shown in Figures 5.9, 5.10 and 5.11.

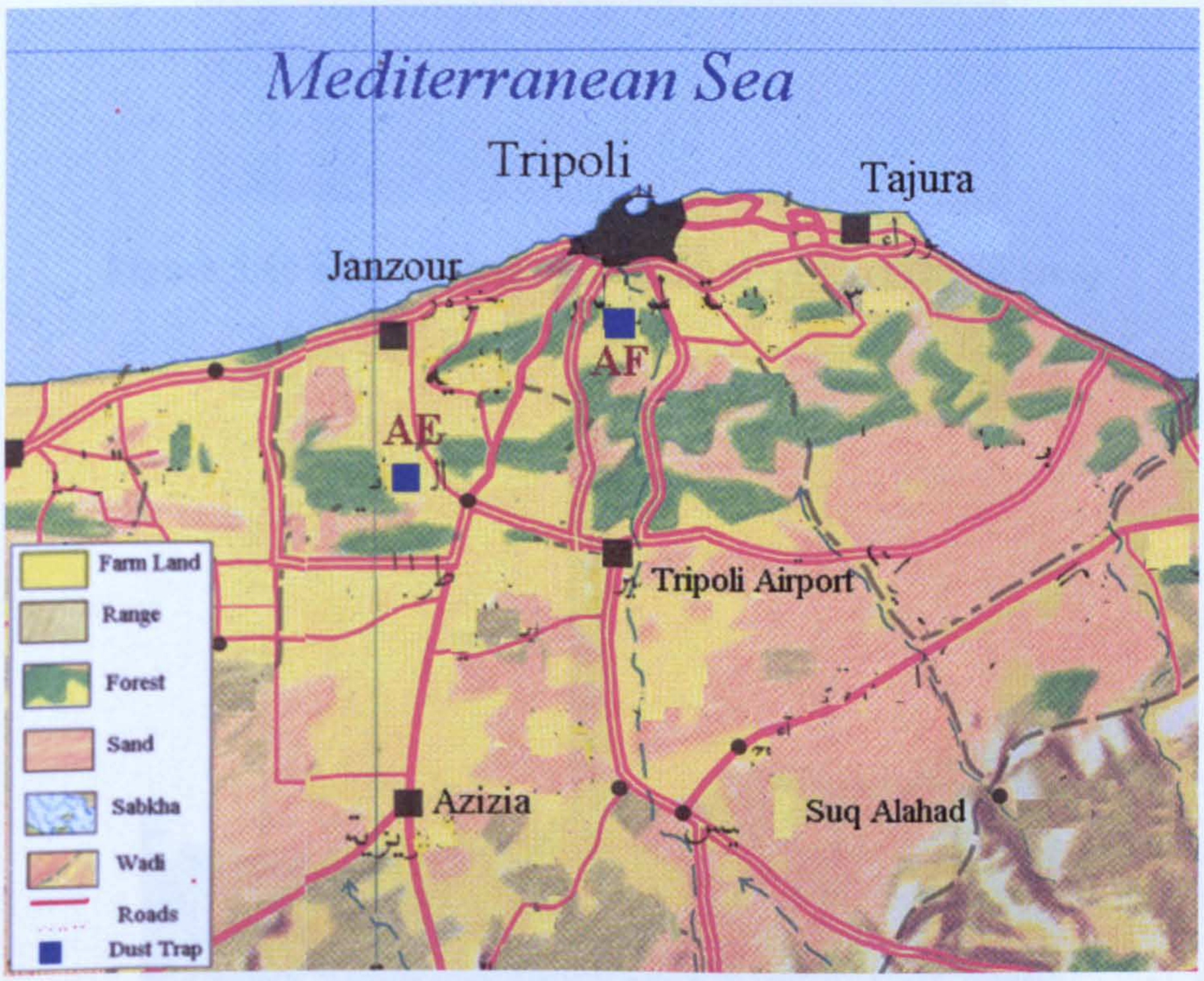

Figure 5.9 Geomorphological features and trapping site locations in Tripoli area (*after* The Secretary of Planning, 1978)

Figure 5.10 Eastern view of trapping site (AF) (Tripoli area)

Figure 5.11 Western view of trapping site (AE) (Tripoli area)

5.5.2.2. Dust traps

Deposition data from individual sites (Figure 5.12) show sudden changes in the weights of the monthly samples resulting in poor temporal patterns. Nevertheless, the averaged monthly data produced a more favourable trend with the highest average deposition of 0.5 t/ha in June and April, however deposition during November, December and January was higher than expected reaching a maximum of 0.317 t/ha during January which exceeds the rates of the dry months of July (0.256 t/ha) and May (0.230 t/ha), the months of a high regional aerosol transport (see chapter 3).

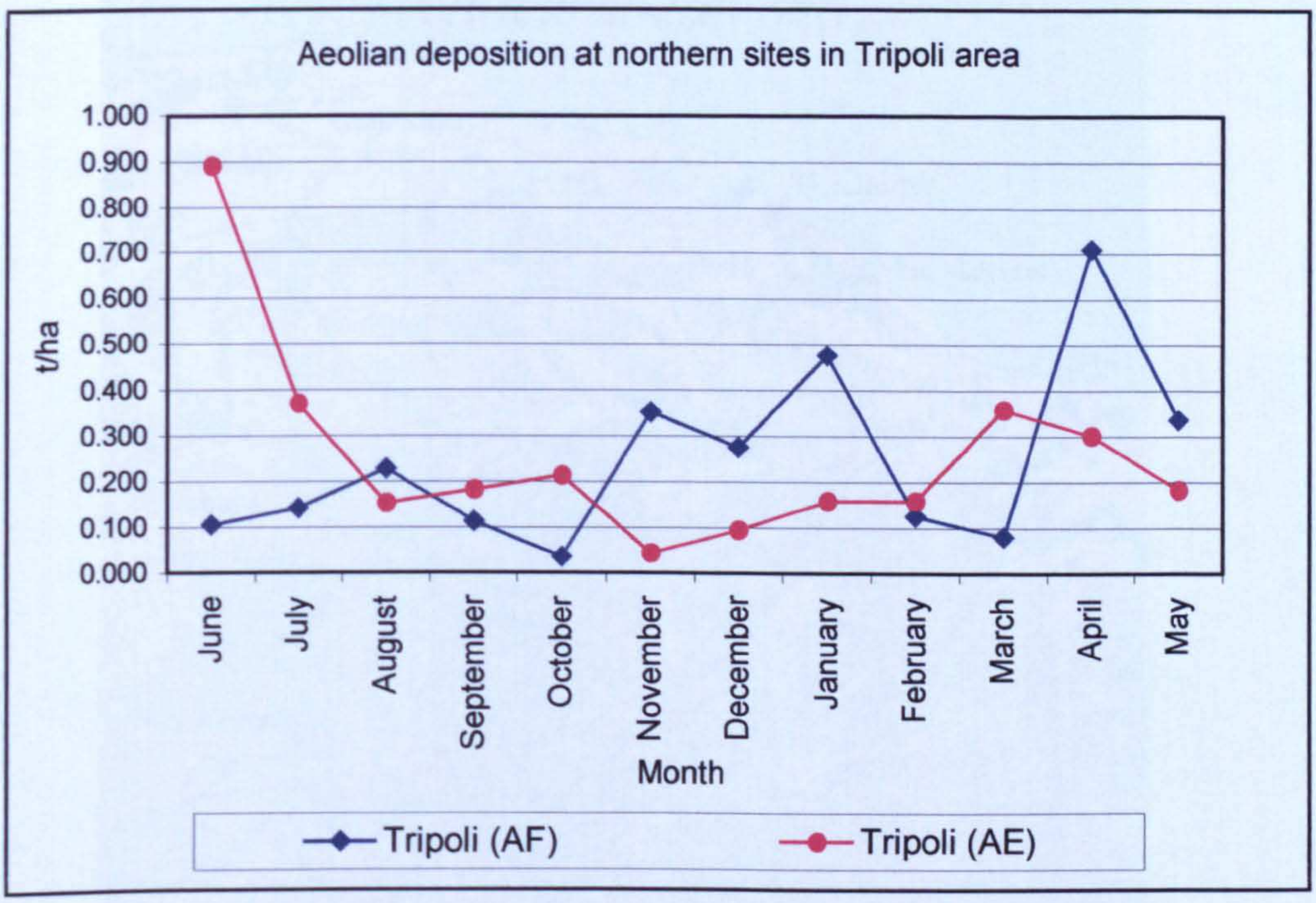

Figure 5.12 Variations in monthly deposition in the northern region, Tripoli area, starting, June 2000 - May 2001

5.5.3. Al Khums area

5.5.3.1. Physical description

Unlike Zuwarah and Tripoli areas, Al Khums is defined by its hilly terrain of altitudes reaching 389 m above sea level. This high plateau, near Bani Walid, is incised by a large number of ephemeral wadis as shown in Figure 5.13. Three traps were installed in the area surrounding Al Khums city as shown in Figures 5.14, 5.15, 5.16 and one other trap was erected near Wadi Memoon southeast of Bani Walid Figure 5.17.

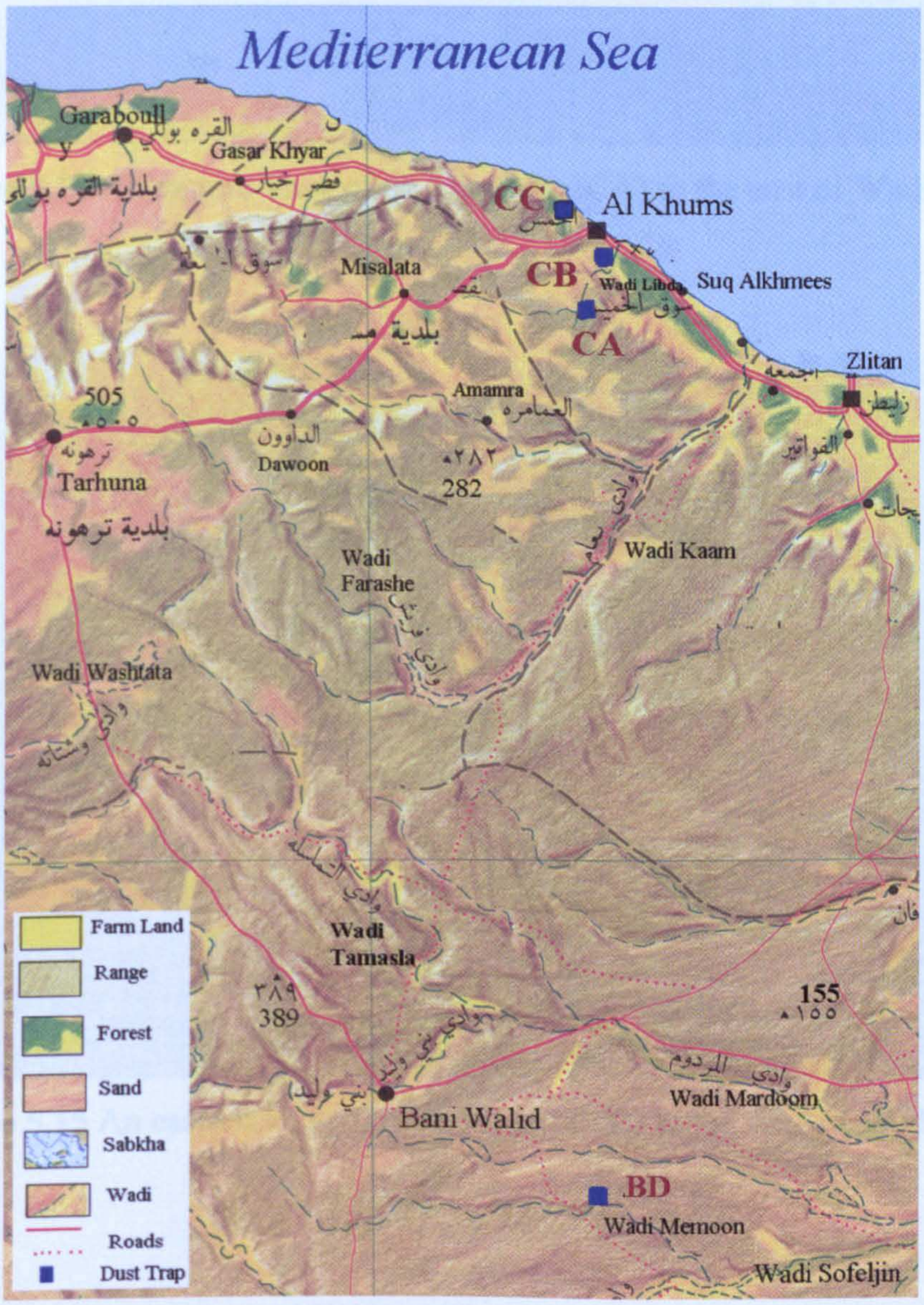

Figure 5.13 Geomorphological features and trapping sites in Al Khums area (*after* The Secretary of Planning, 1978)

Figure 5.14 An eastern view of trapping site (CA) to the east of Wadi Libda

Figure 5.15 An eastern view of trapping site (CB) to the west of Wadi Libda

Figure 5.16 A southern view of trapping site (CC) west of Al Khums city

Figure 5.17 A northern view of trapping site (BD) on the edge of Wadi Mamoon southeast Bani Walid

5.5.3.2. Dust traps

Deposition rates were highest during the summer and the spring reaching an average of 0.1243 t/ha in July and 0.109 t/ha in April as shown in Figures 5.18.

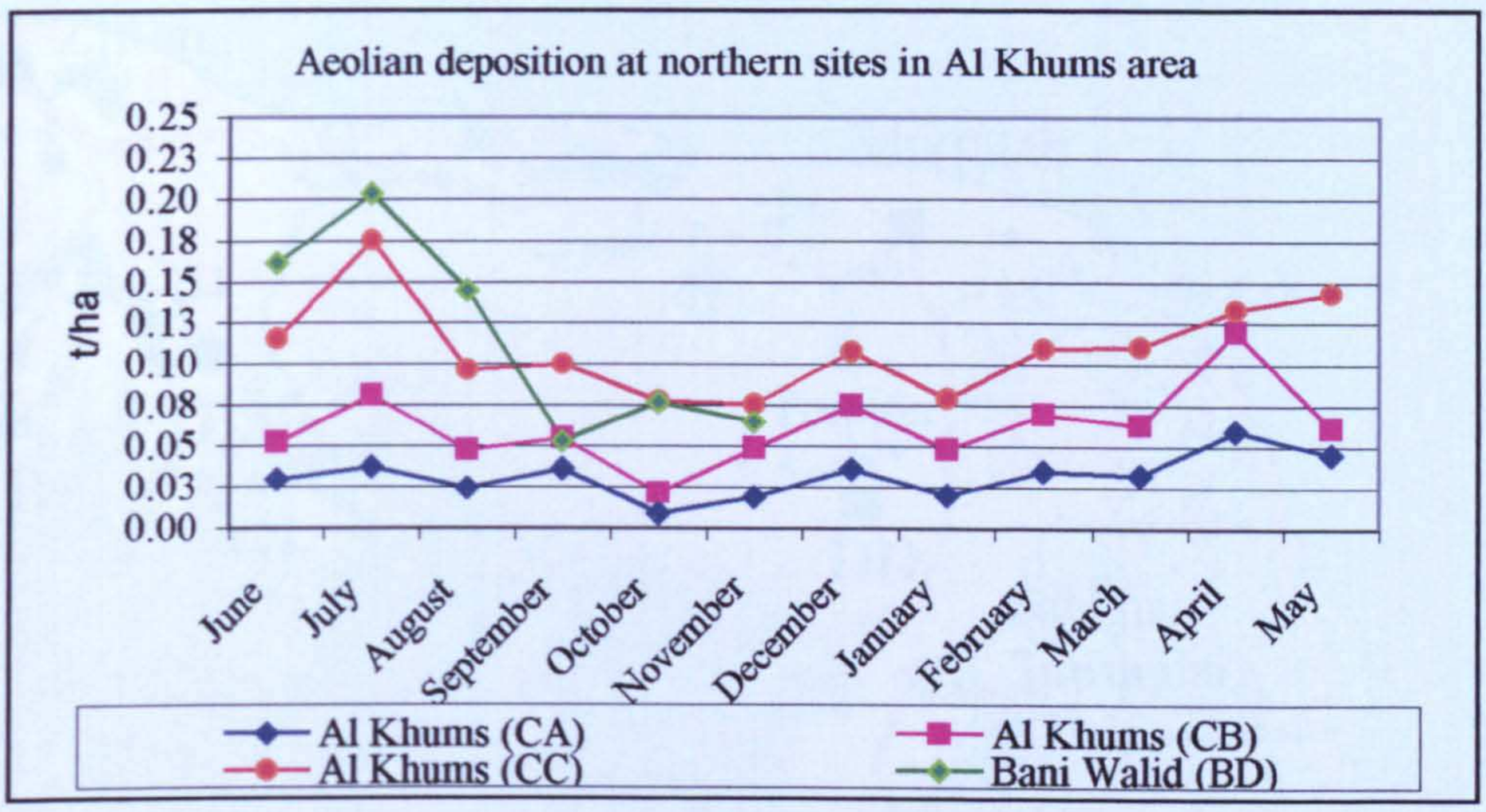

Figure 5.18 Variations in monthly deposition in the northern region (Al Khums area) starting from June 2000 until May 2001

A general trend throughout the sampling period shows that the lowest rates of deposition were found to occur at site (CA) near the coast and the highest at site (BD) which is situated about 130 km inland. The average deposition rate of December (0.0731 t/ha) was higher than the other winter months reaching comparable rates with August. In general, deposition rates create a ti-modal distribution with two major peaks correlate with the dry months of July and April and a minor peak correlates with the traditionally rainy month of December.

5.5.4. Misratah area

5.5.4.1. Physical description

This area is dominated by sabkhat Tawurgha, the largest sabkha in the study area bounded by the Mediterranean to the north and east (Figure 5.19). Further south, major wadi networks such as Wadi Sofeljin merge with a low coastal terrain of few meters above sea level at the sabkha. The geomorphology at the trapping sites is shown in Figures 5.20 - 5-23.

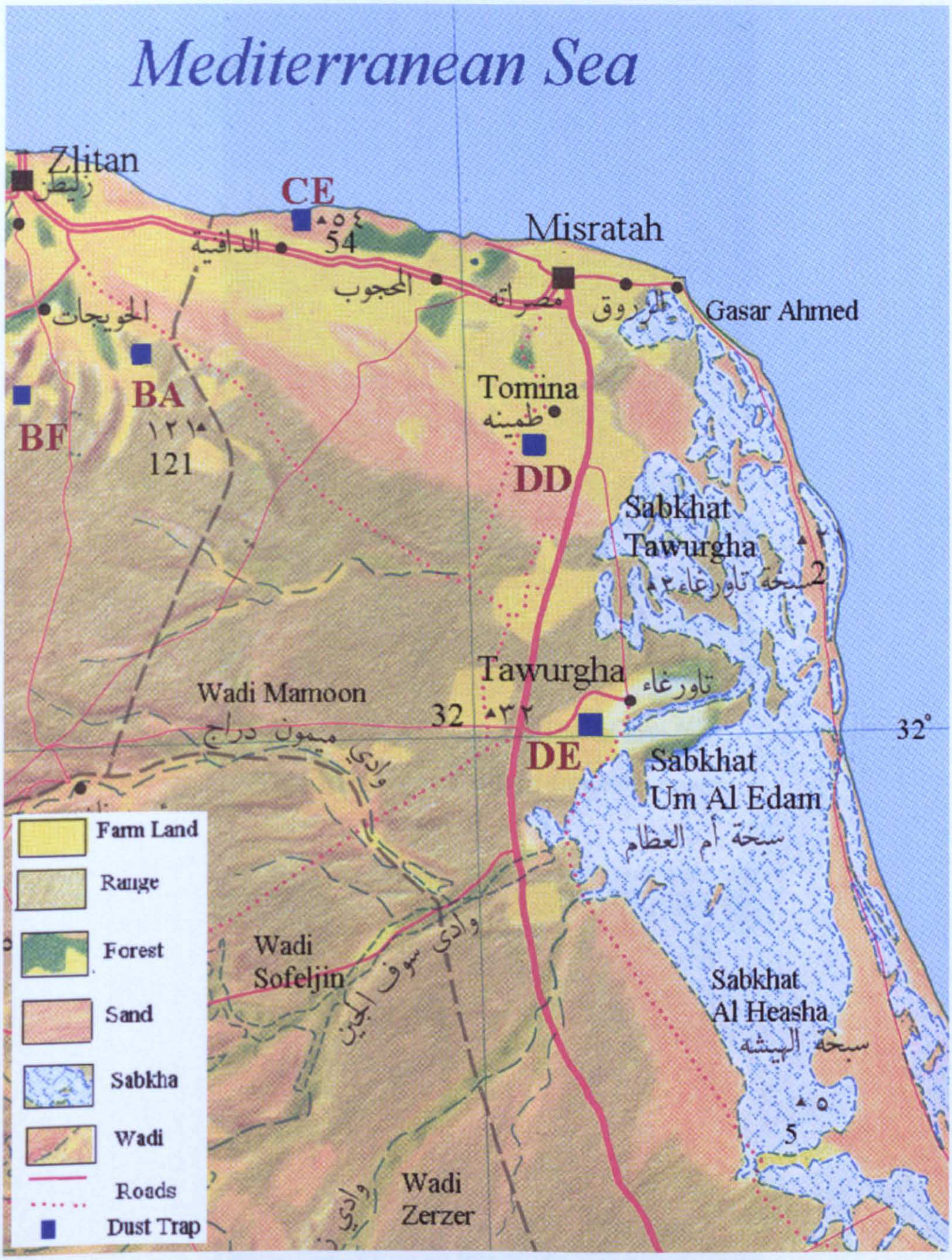

Figure 5.19 Geomorphological features of Misratah area (*after* The Secretary of Planning, 1978)

Figure 5.20 An eastern view at site (CE)

This site is about 300 m from the coast

Figure 5.21 A southern view at site (DD)

Figure 5.22 A northern view at site (BA)

Figure 5.23 A western view at site (BF)

5.5.4.2. Dust traps

Deposition rates (Figure 5.24) at the individual sites are comparable with those recorded at Al Khums area with the largest rates occurred during July and April, however, the general trend of the average monthly deposition seems to represent a bi-modal distribution with a small peak corresponding to December.

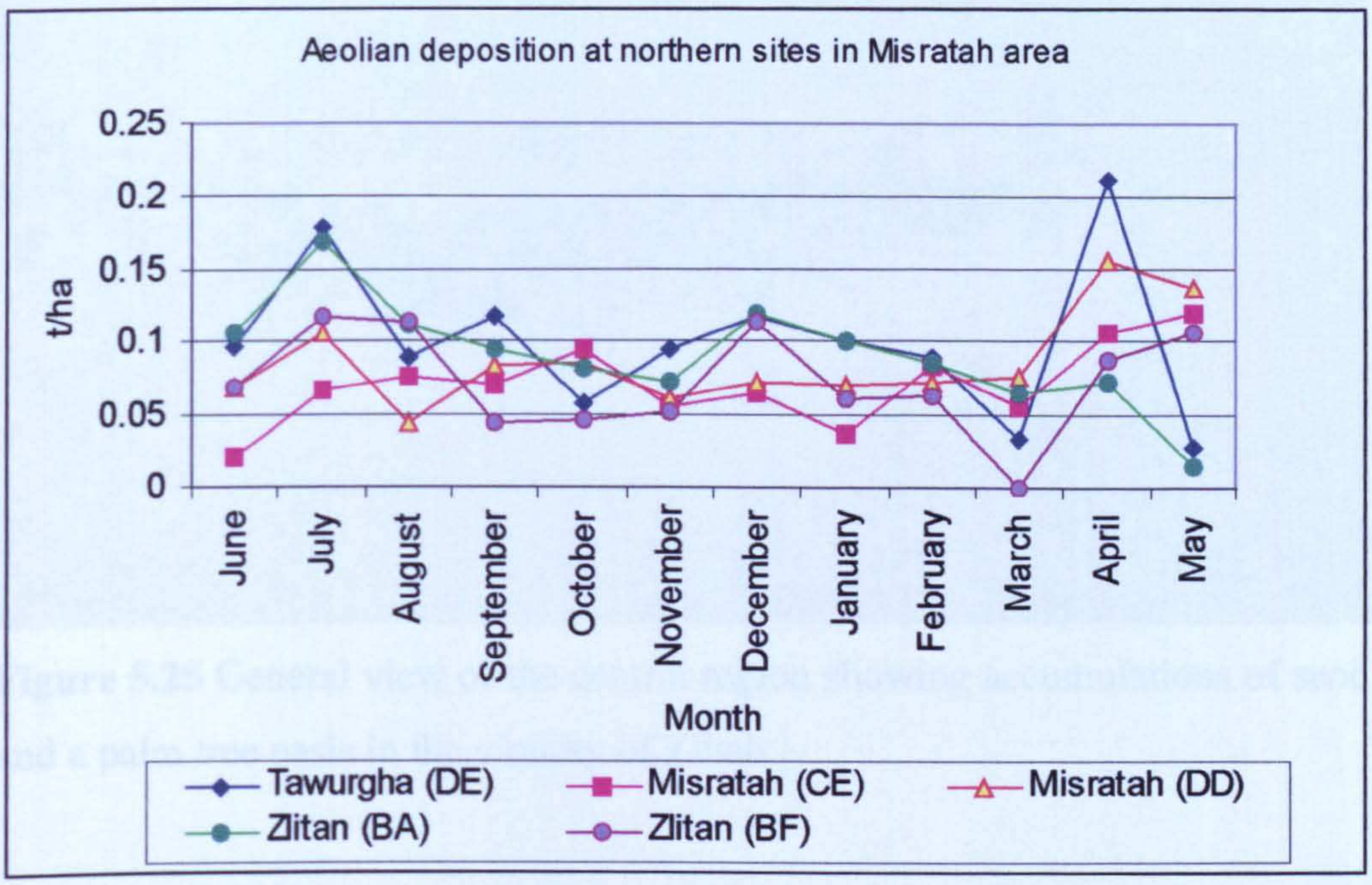

Figure 5.24 Variations in monthly deposition in the northern region, Misratah area, starting from June 2000 until May 2001

5.4. CENTRAL REGION

5.4.1. Physical description

This region has a low density population, is sparsely vegetated and situated in a precipitation belt ranging between 20 and 50 mm/year. The surface comprises scattered hills and accumulations of sand (Figure 5.25) bounded from the south by the volcanic high lands of Al Huruj Al Aswad reaching 1200 m above sea level and to the west and north west, by Jabal Asawda and Jabal Waddan reaching 840 and 671 m above sea level as shown in Figure 5.26. The central region is represented by three sites around Zillah and one site at Waddan (Figures 5.26 - 5.28). Zillah is situated at 168 m above sea level on the northern foothills of Al Huruj Al Aswad where Waddan is situated in a narrow corridor

lies between Jabal Asawda from south and southwest and Jabal Waddan from east and northeast.

Figure 5.25 General view of the central region showing accumulations of sand and a palm tree oasis in the vicinity of Zillah

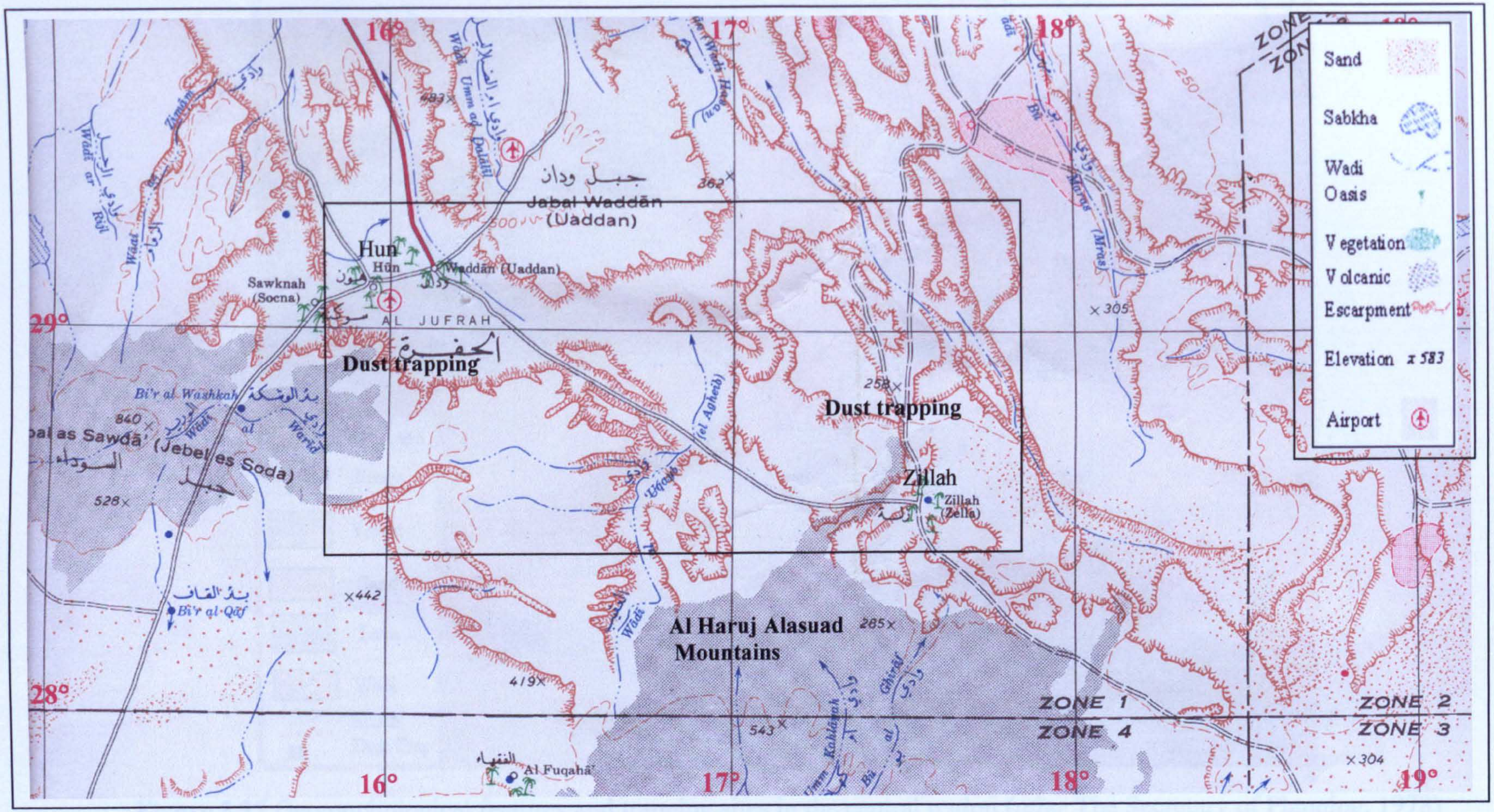

Figure 5.26 Topographic map of the central region (Plate I-350 B, Scale 1: 2000,000). (*after USGS, 1962)*

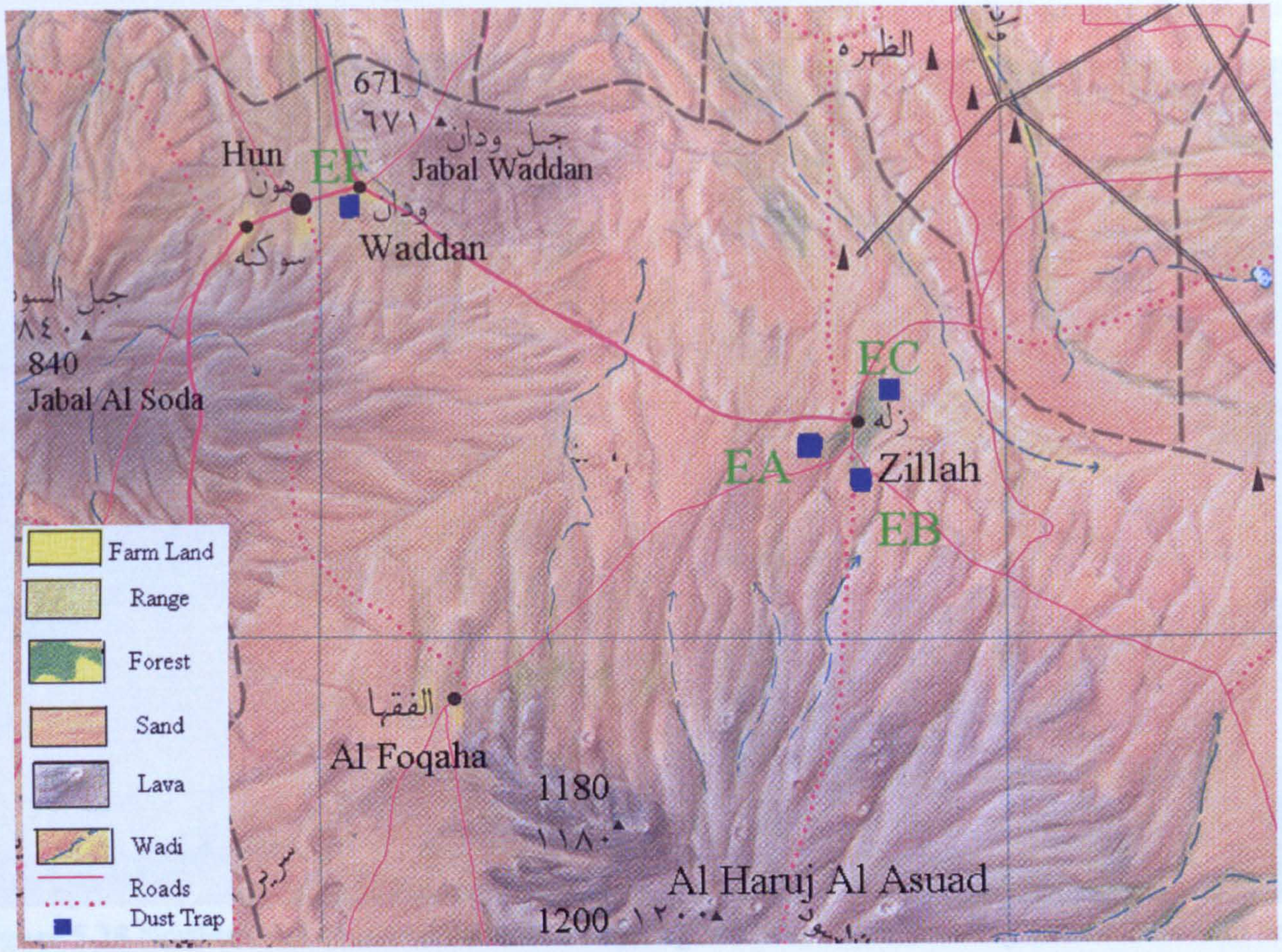

Figure 5.27 Geomophological features and trapping sites in the central region (*after* The Secretary of Planning, 1978)

Figure 5.28 Northern and southern views at a trapping site near Zillah showing accumulations of sand

5.6.2. Dust traps

The monthly deposition plots (Figure 5.29) do not manifest themselves in a clear temporal pattern, however, the largest amounts of the average monthly deposits occurred during April and May. The monthly deposition rates are generally higher than those entrapped in the northern areas except those near Tripoli.

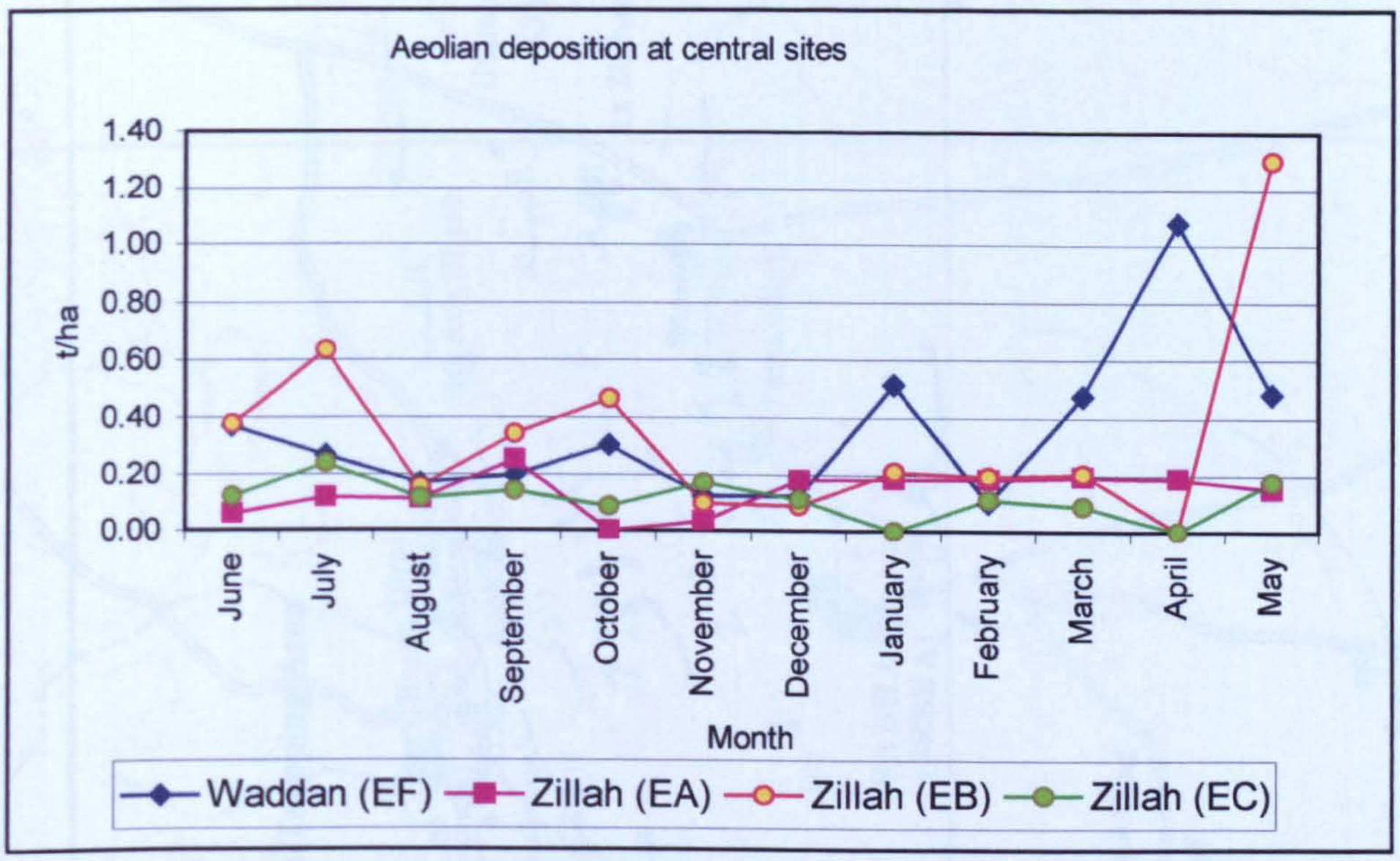

Figure 5.29 Variations in monthly deposition in the central region, June 2000 - May 2001

5.7. SOUTHERN REGION

5.7.1. Physical description

The main geomorphological feature of this region is the Ubari Sand Sea (5.30) which is bounded by plateaux to the north and south. The plateaux are bisected by a number of wadis. This region is situated in the hyper arid part of the country where the vegetation cover is very sparse, mostly, on the fringes of the Ubari Sand sea in areas of very low density population. The wadis are dry and recorded flow of water is less than 1 % of the time (Reid, 1994). The study region is represented by samples gathered by two traps at one site at Semnu, two sites at Birak and one site at Bent Bayia which were all erected on the eastern fringes of the sandy Idhan Ubari (Figures 5.30 and 5.31).

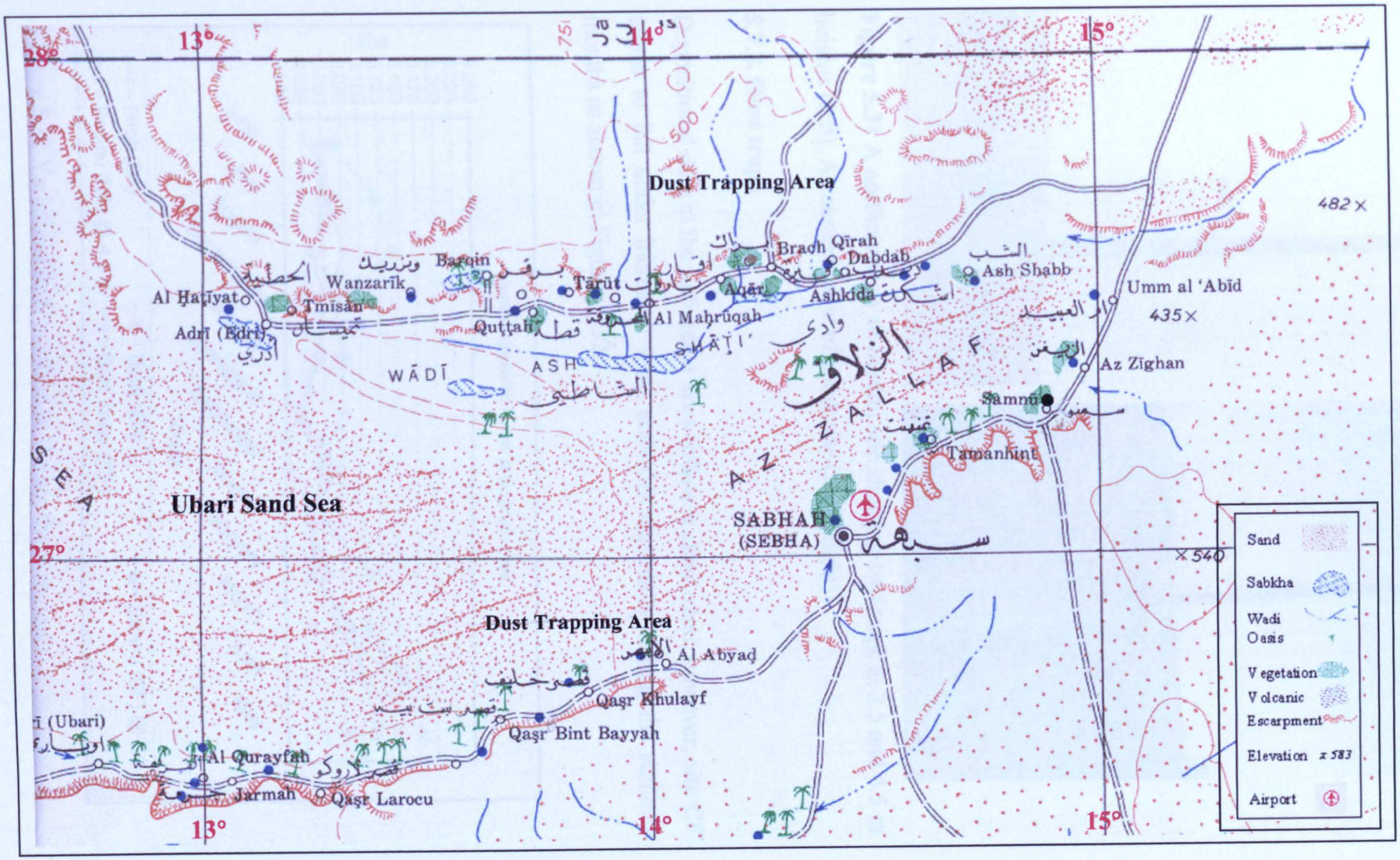

Figure 5.30 Topographic map of the southern region (Plate I-350 B, Scale 1: 2000,000) (*after* USGS, 1962)

Figure 5.31 A northern view of Semnu site showing two traps at 2.5 and 4.5 m heights (left). An eastern view of Birak site (DA) (right)

5.7.2. Dust traps

Depositional data at the individual sites follow a clear trend, however, site CF seems to fall under increased local activities especially during the summer months as shown in Figures 5.32.

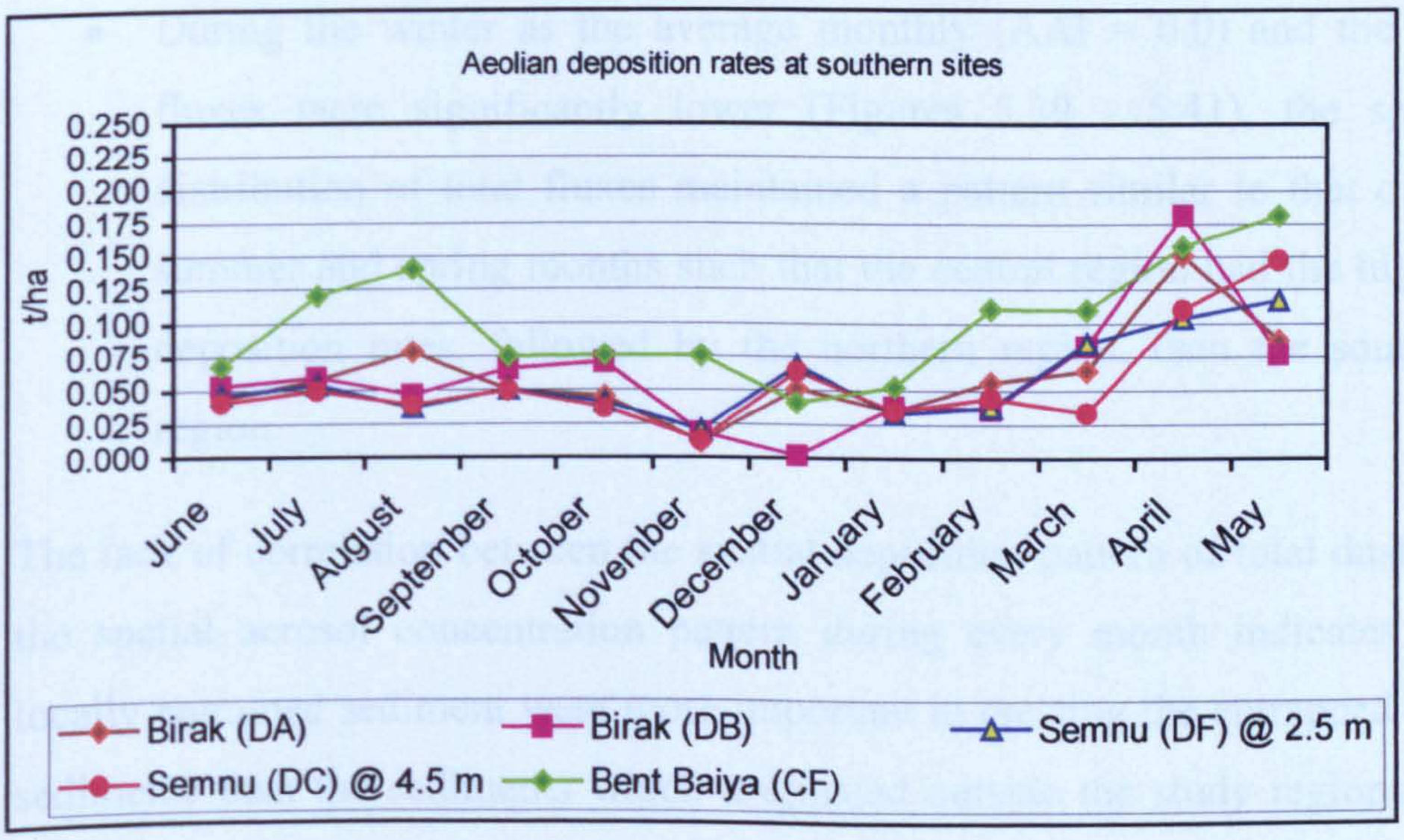

Figure 5.32 Variations in deposition in the southern region

The average monthly deposition rates represent a bi-modal distribution with one peaks correspond to spring and the other to summer. The highest average deposition rates occurred during the spring months and reached their peak in April (0.1409 t/ha) where the peak of the summer occurred equally during June and July with an average monthly rate of 0.0684 t/ha.

5.8. SPATIAL VARIATIONS IN TOTAL FLUX VS. TOMS AAI

Spatial variations in total flux from one region to another seem to be significant regardless of the seasonal changes in climatic conditions and the variations in transported aerosol concentrations over the three regions. Deposited sediments do not seem to represent a response to the spatial variation in the atmospheric loads over the regions of study (Figures 5.33 –5.44). Inconsistency between deposition on the ground and aerosol concentrations in the atmosphere are as follows:

- Throughout the dusty months of summer (Figures 5.33 –5.35) and spring (Figures 5.42 – 5.44), deposition rates were the highest in the central region and so were the aerosol densities whereas the southern region experienced lesser deposition rates than the northern region, but the aerosol indexes for the southern region were always higher than those for the northern region.

- During the winter as the average monthly (AAI = 0.0) and the dust fluxes were significantly lower (Figures 5.39 - 5.41), the spatial distribution of total fluxes maintained a pattern similar to that of the summer and spring months such that the central region had the highest deposition rates, followed by the northern region, then the southern region.

The lack of correlation between the spatial deposition pattern of total dust and the spatial aerosol concentration pattern during every month indicates that locally entrained sediment were more important in creating the entrapped bulk sediments than the sediments which originated outside the study regions and were transported along trajectories over these regions.

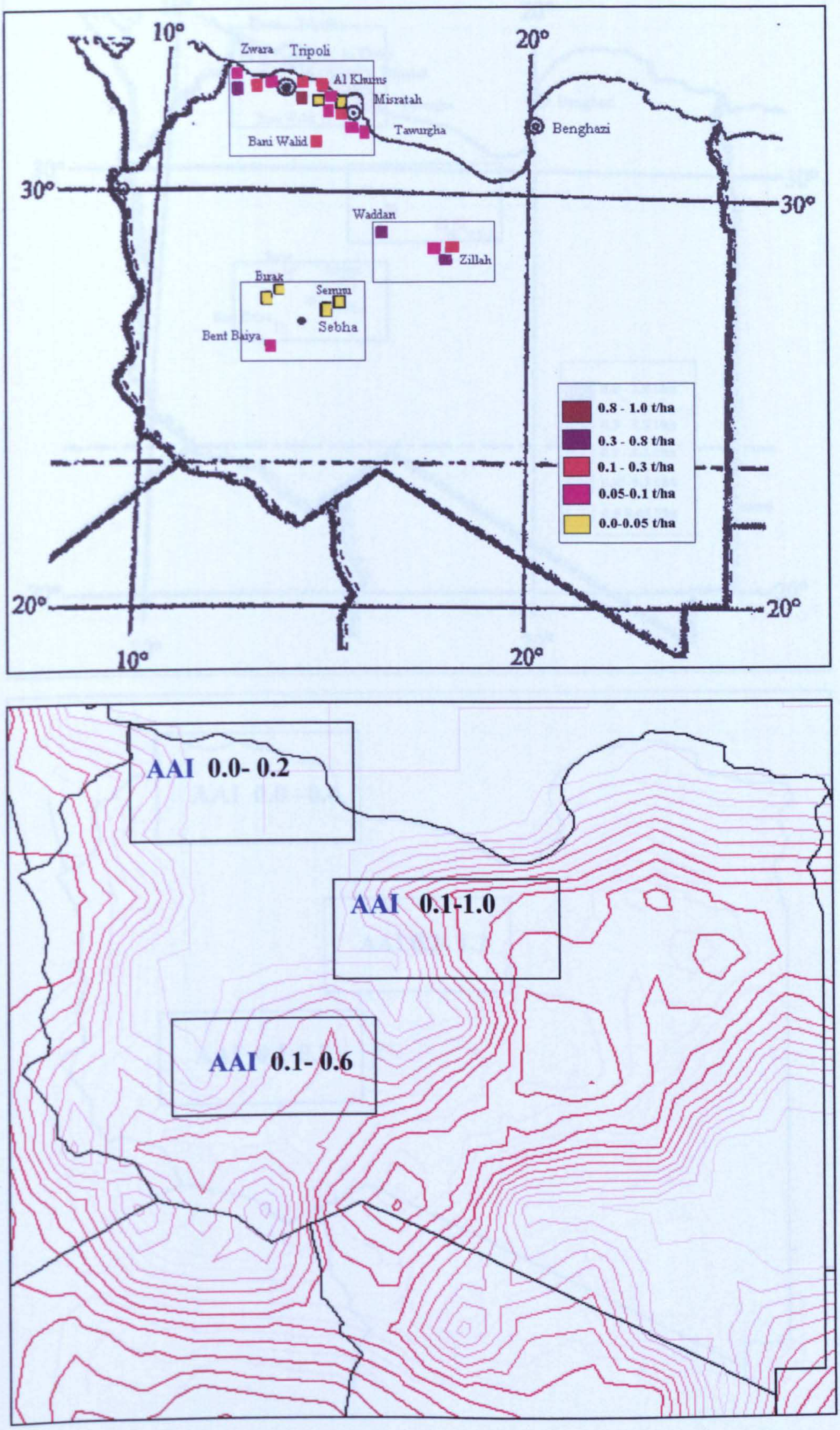

Figure 5.33 Total deposition versus TOMS aerosol index for June 2000

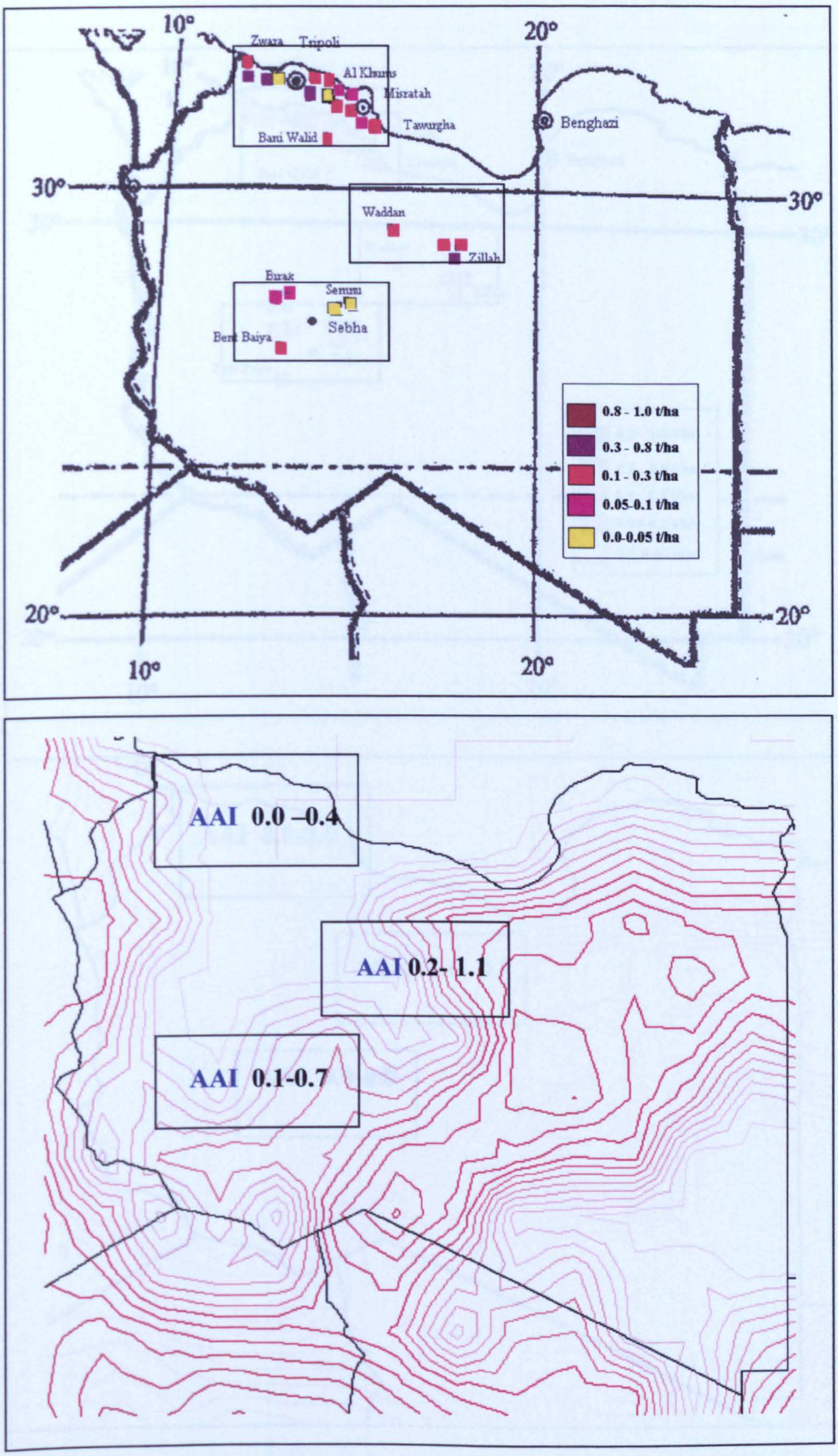

Figure 5.34 Total deposition versus TOMS aerosol index for July 2000

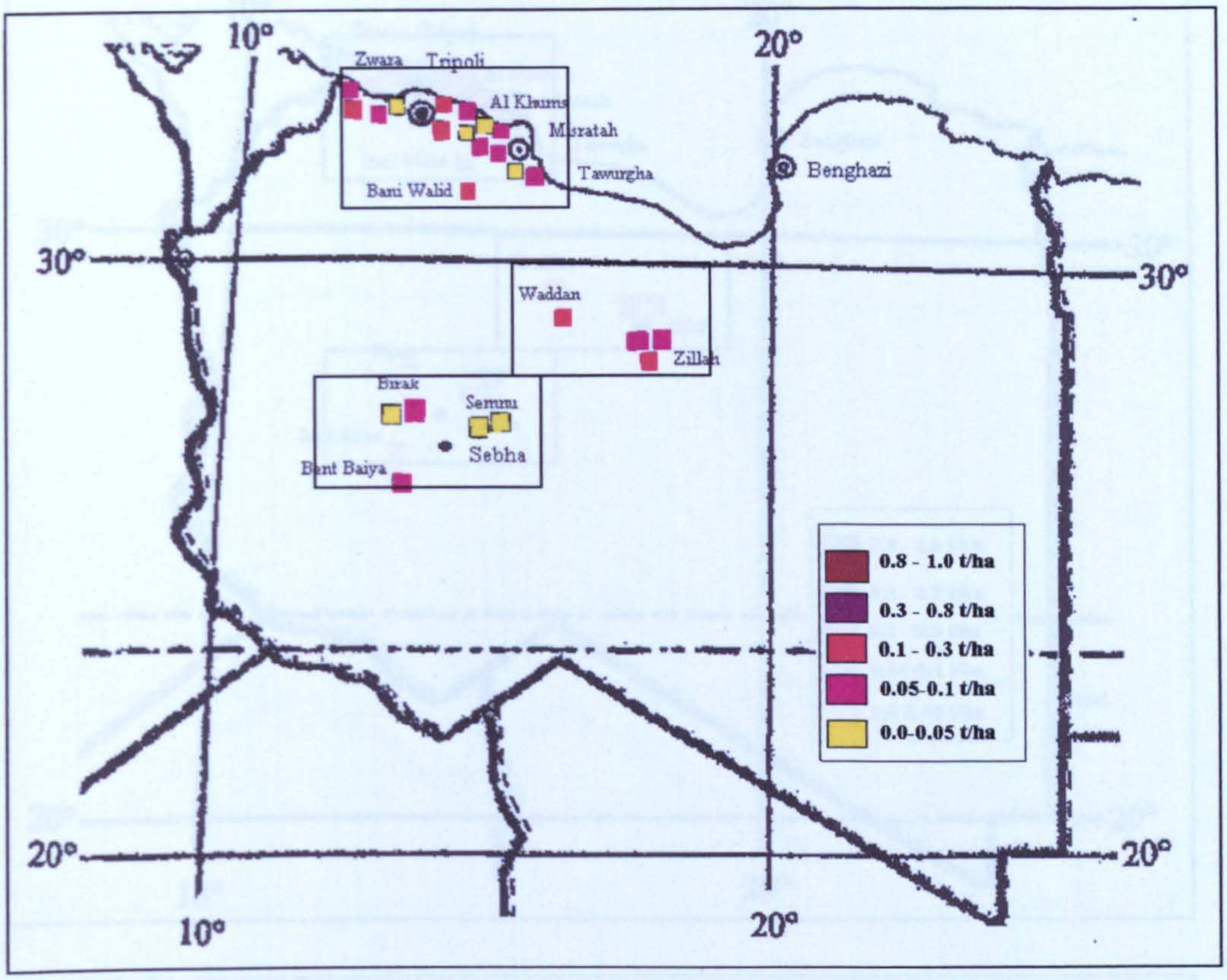

Figure 5.35 Total deposition versus TOMS aerosol index for August 2000

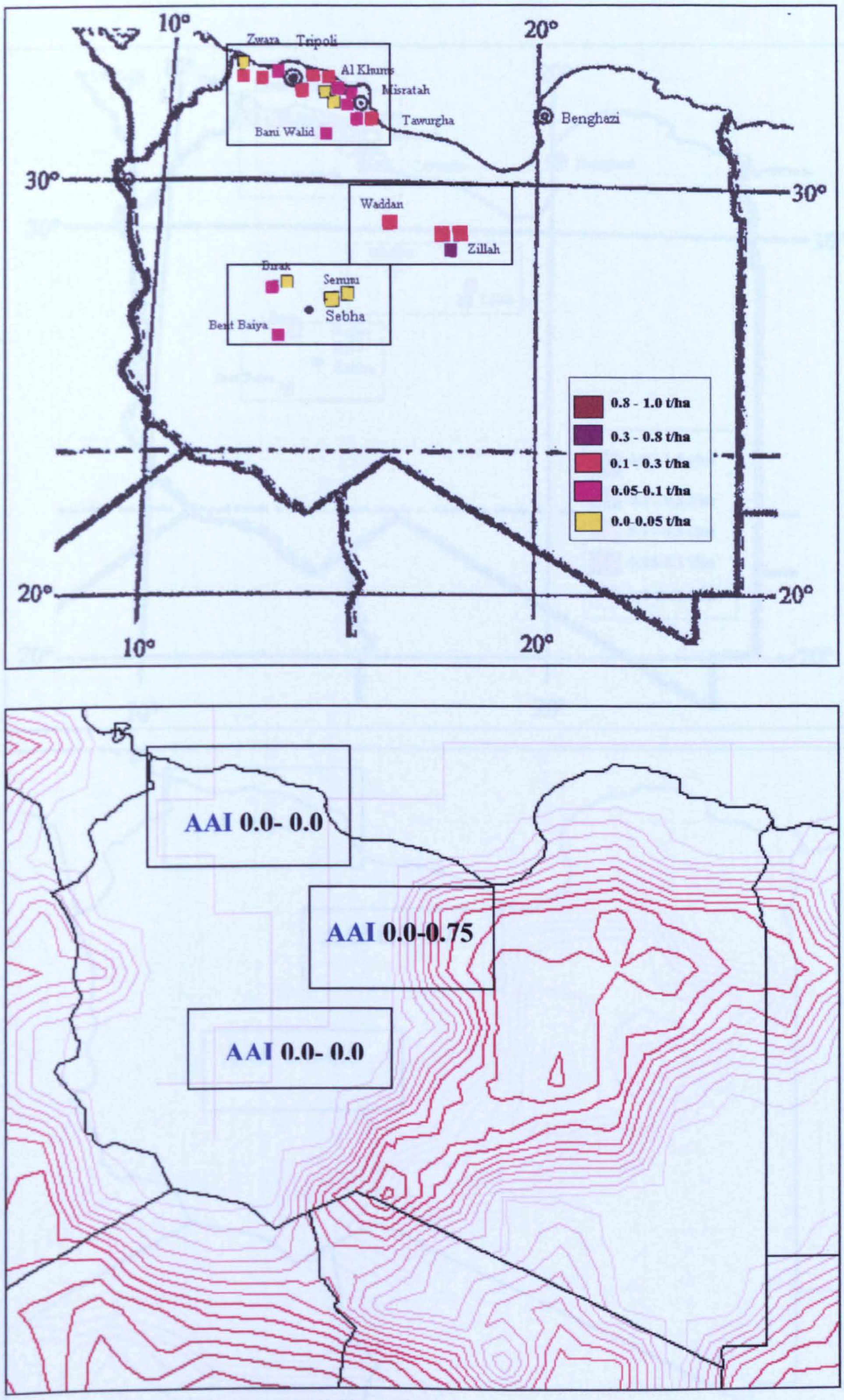

Figure 5.36 Total deposition versus TOMS aerosol index for September 2000

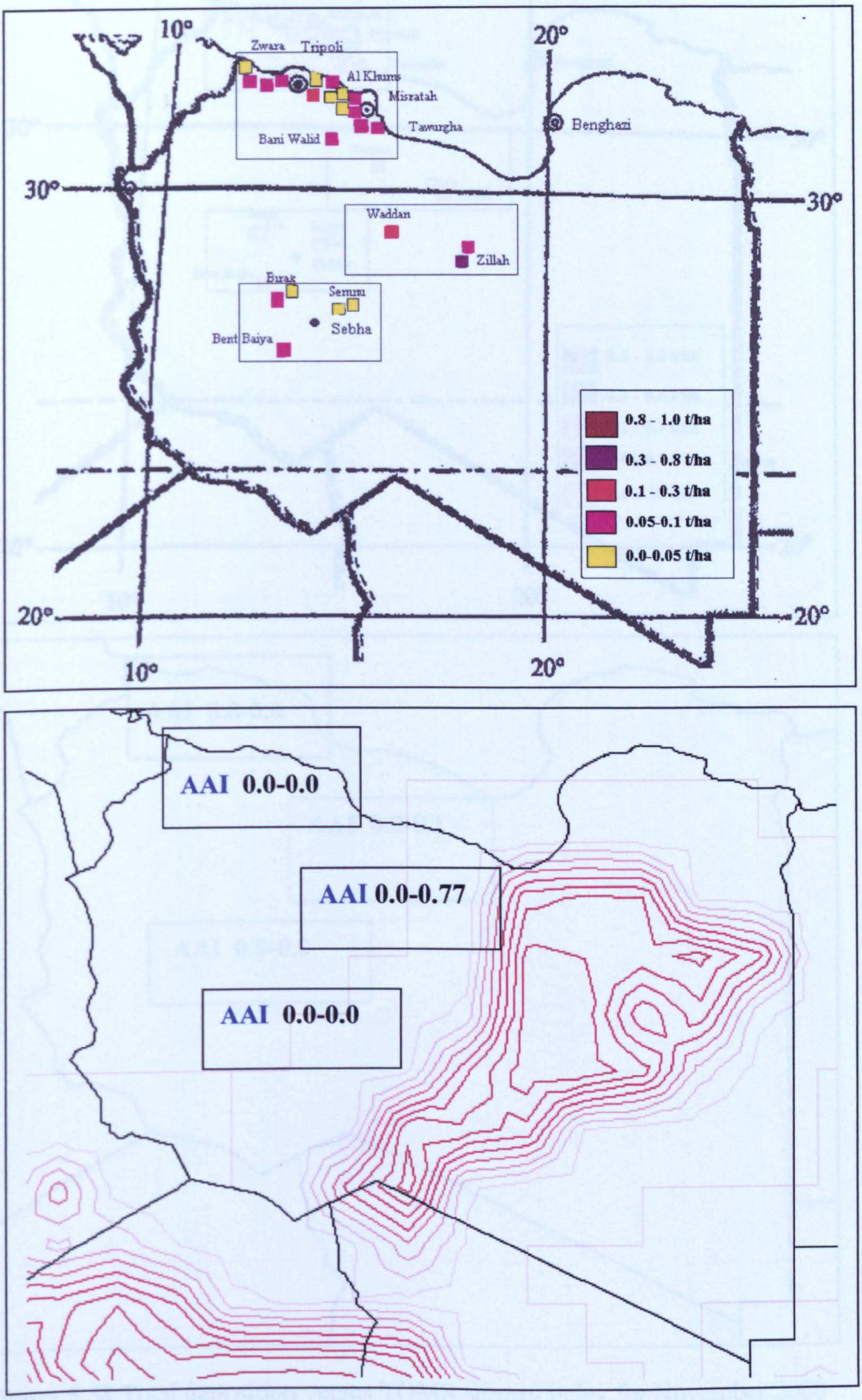

Figure 5.37 Total deposition versus TOMS aerosol index for October 2000

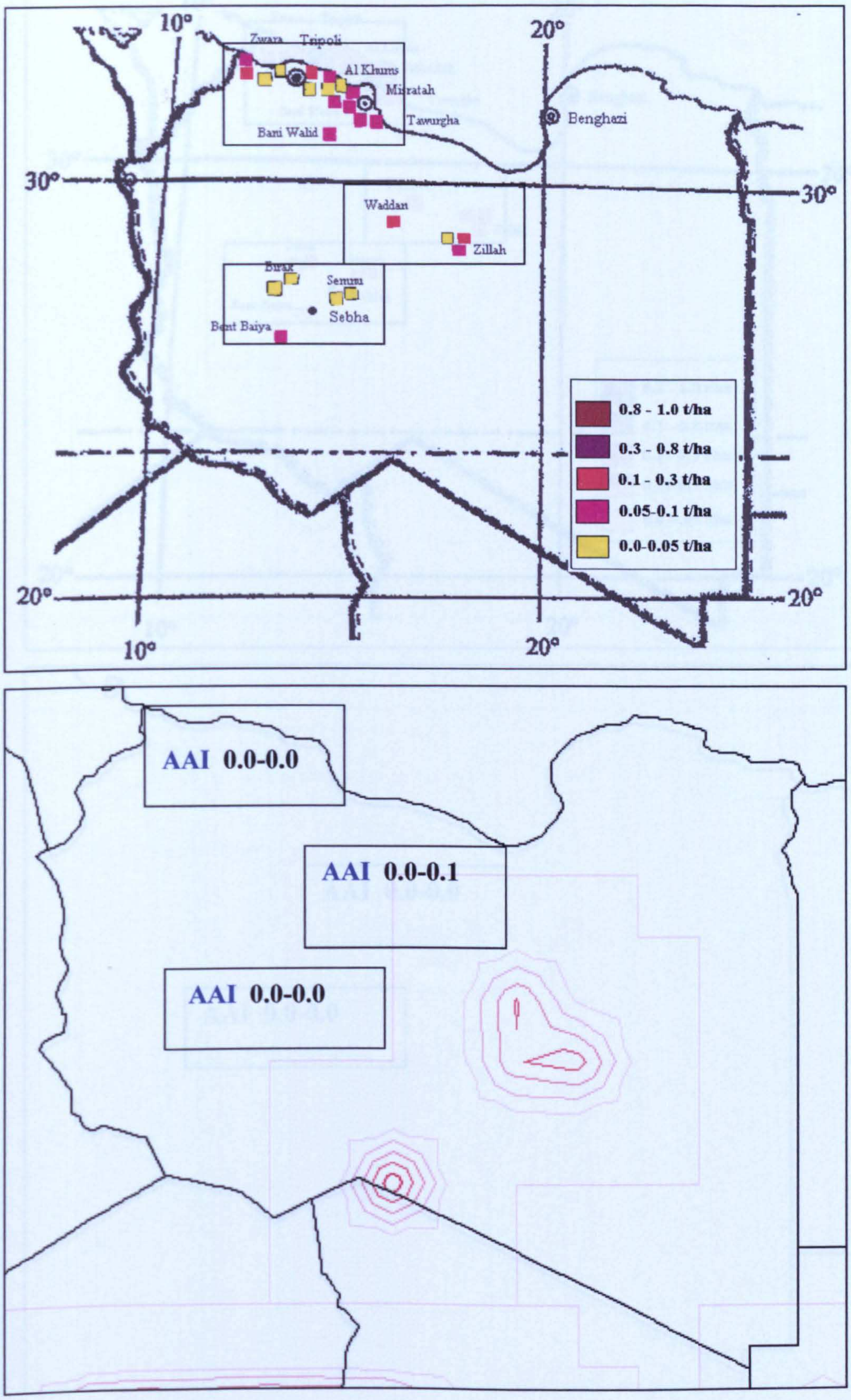

Figure 5.38 Total deposition versus TOMS aerosol index for November 2000

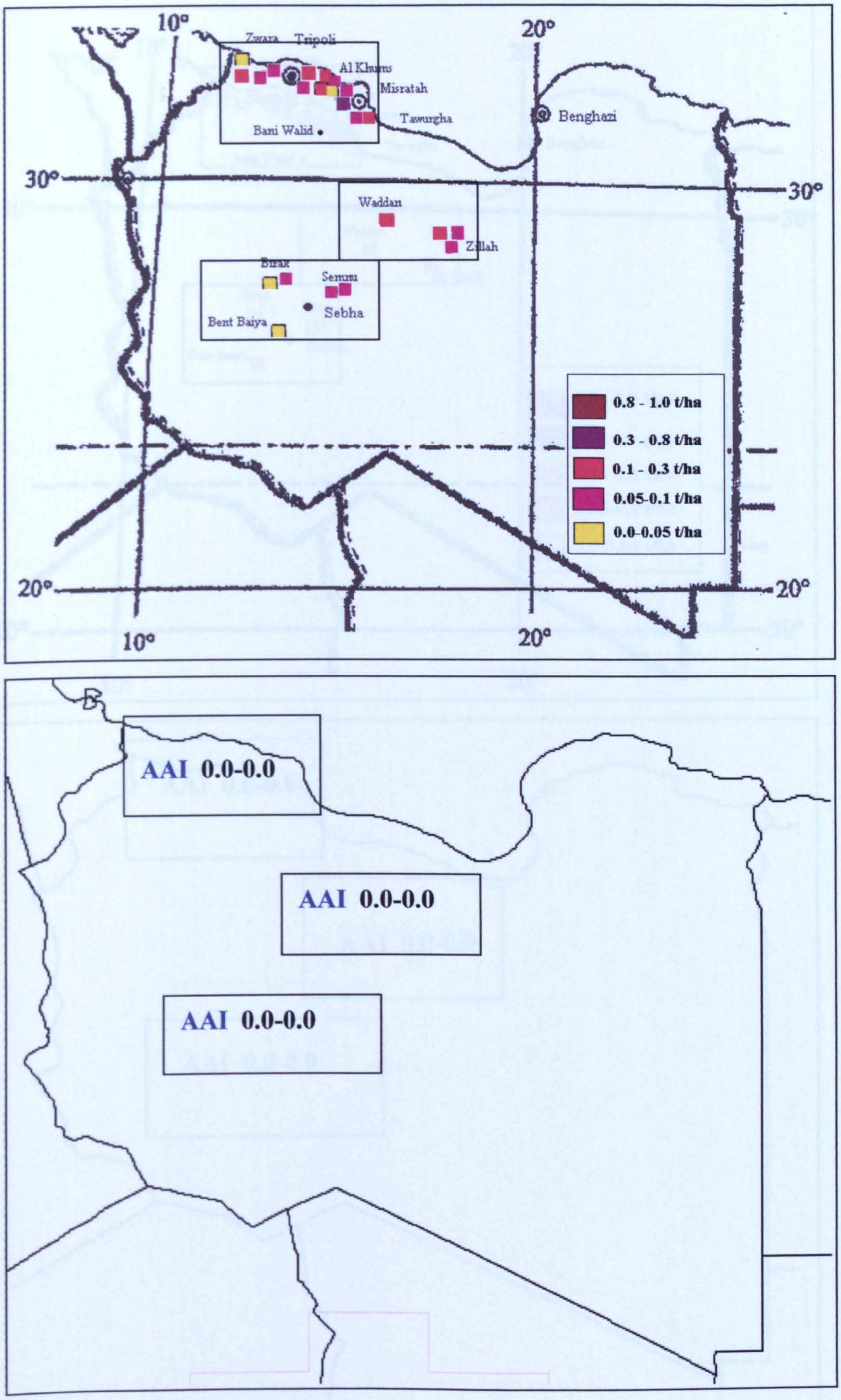

Figure 5.39 Total deposition versus TOMS aerosol index for December 2000

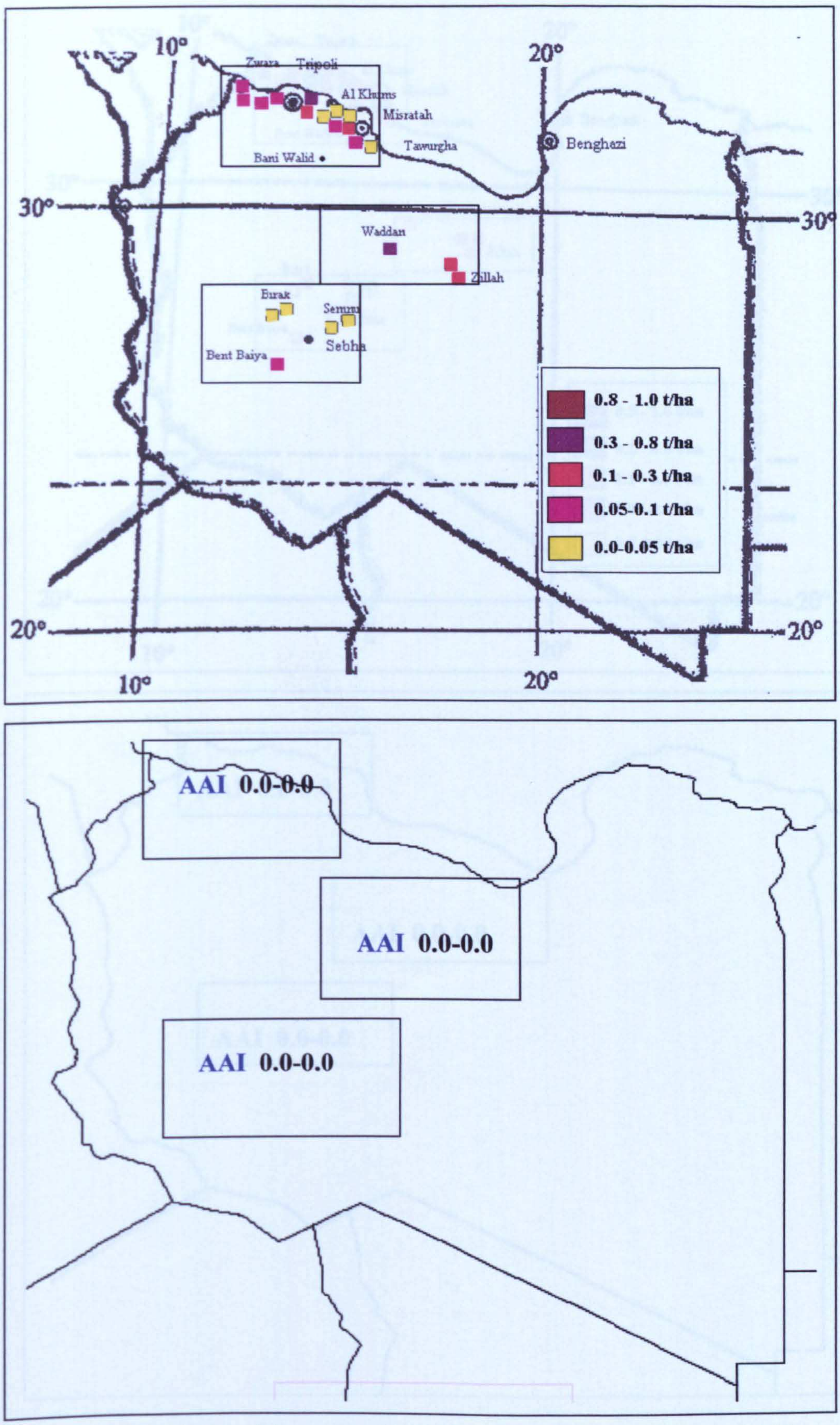

Figure 5.40 Total deposition versus TOMS aerosol index for January 2001

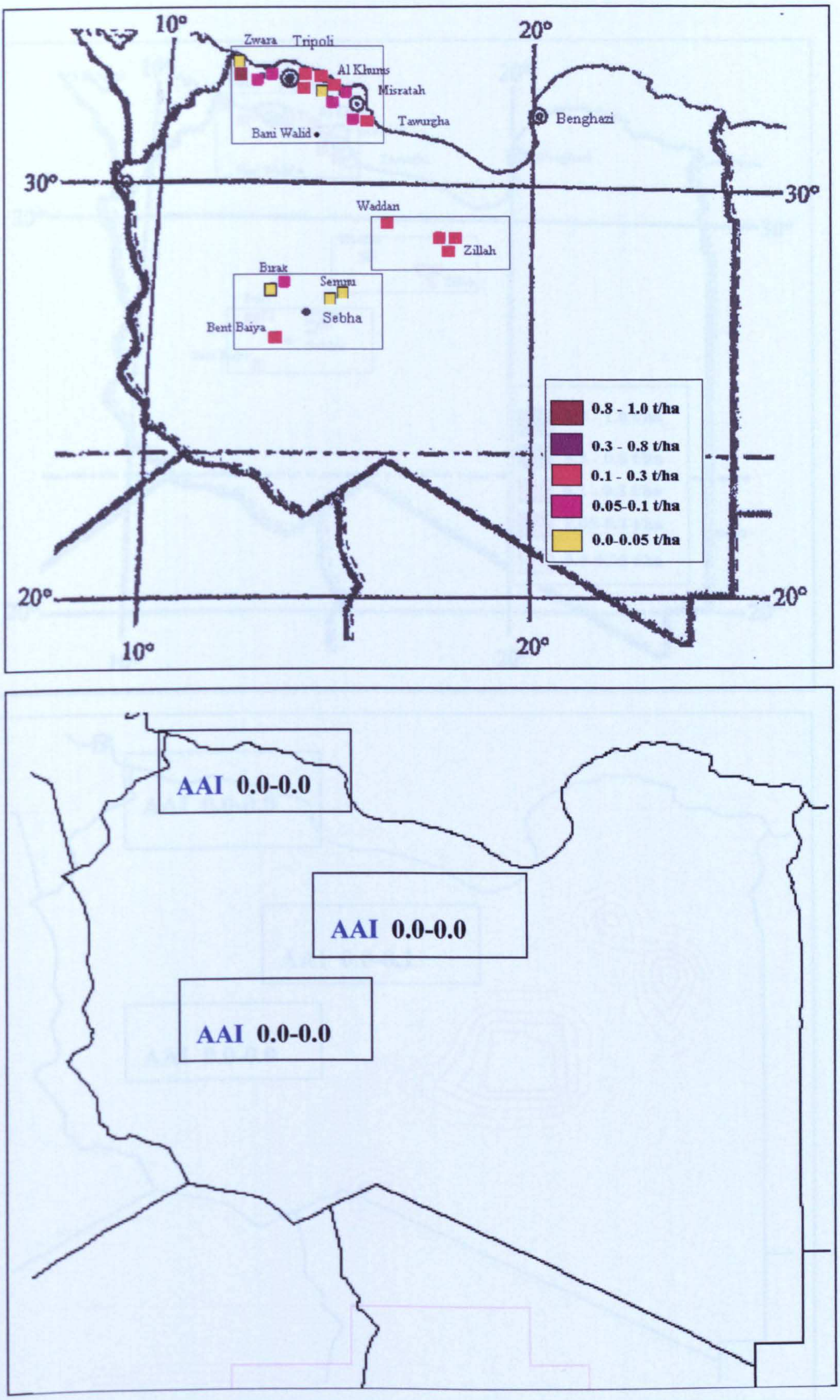

Figure 5.41 Total deposition versus TOMS aerosol index for February 2001

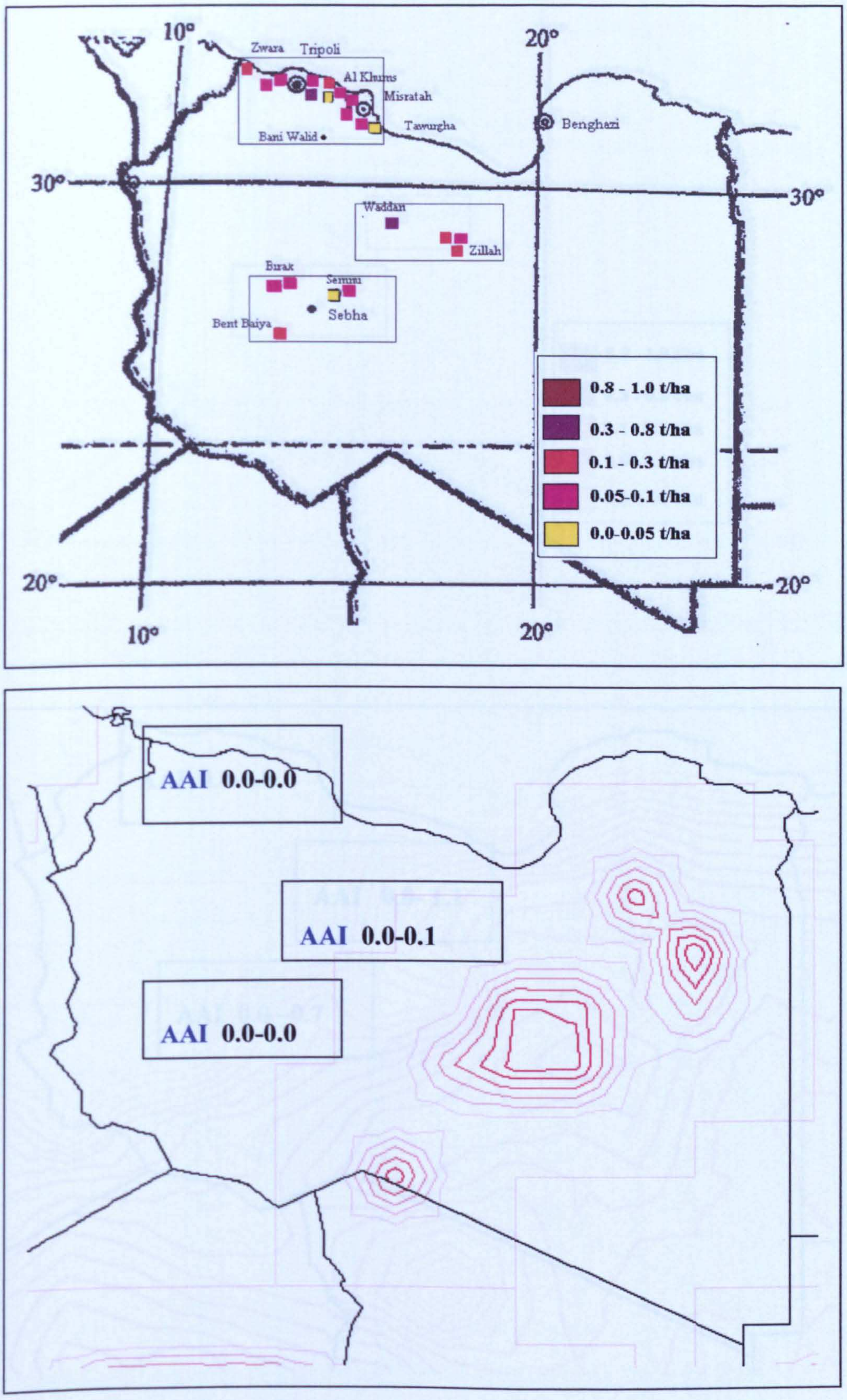

Figure 5.42 Total deposition versus TOMS aerosol index for March 2001

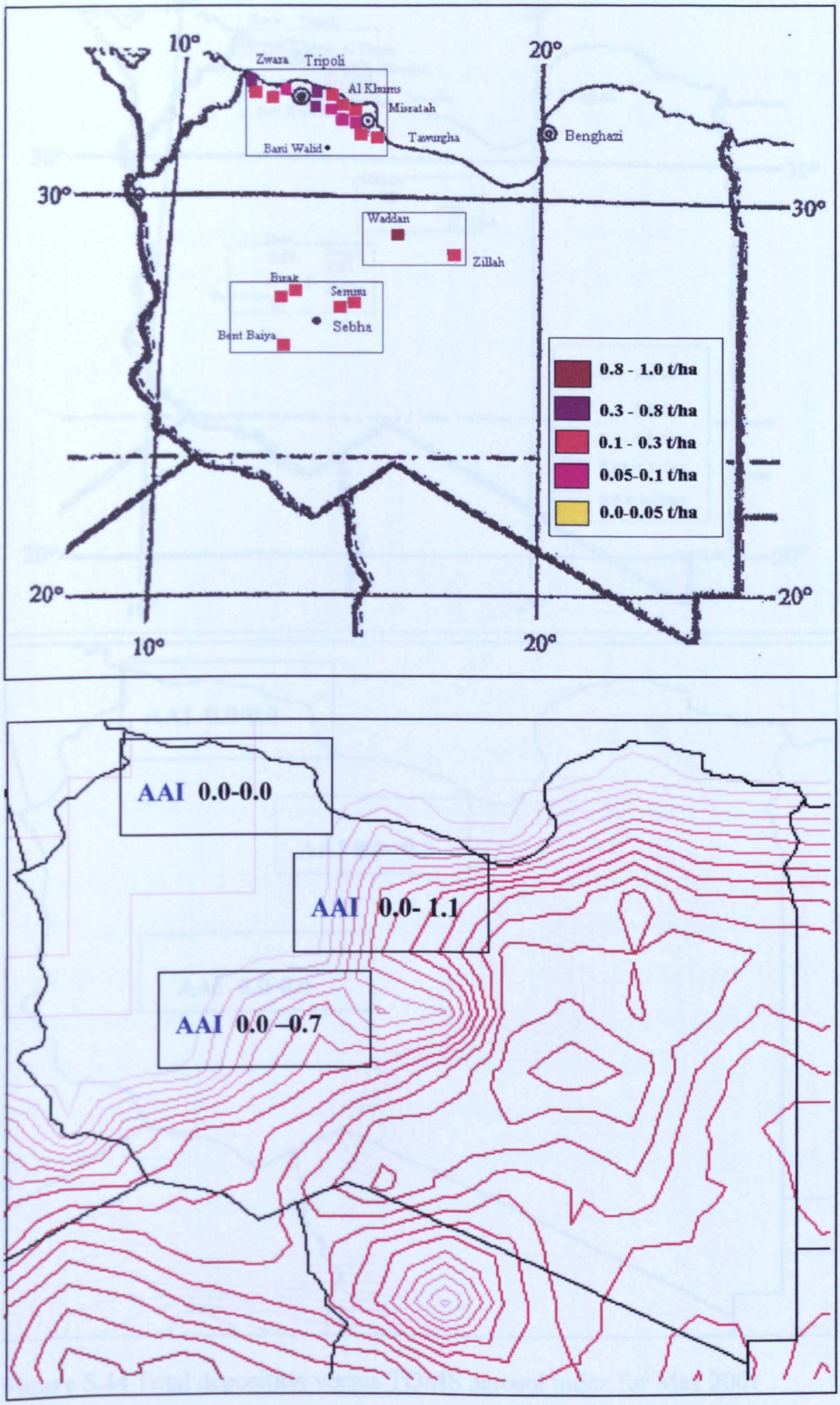

Figure 5.43 Total deposition versus TOMS aerosol index for April 2001

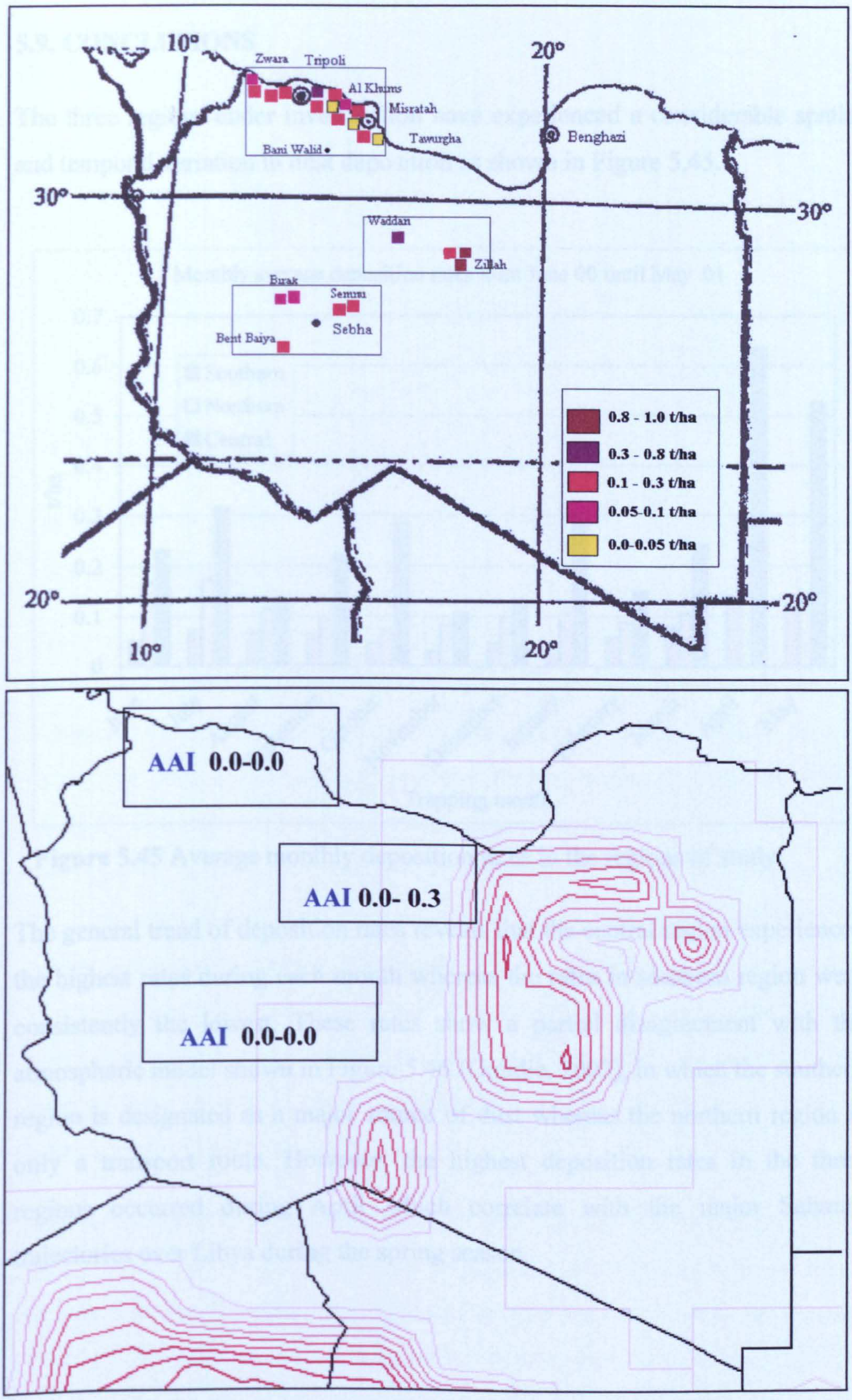

Figure 5.44 Total deposition versus TOMS aerosol index for May 2001

5.9. CONCLUSIONS

The three regions under investigation have experienced a considerable spatial and temporal variation in dust deposition as shown in Figure 5.45.

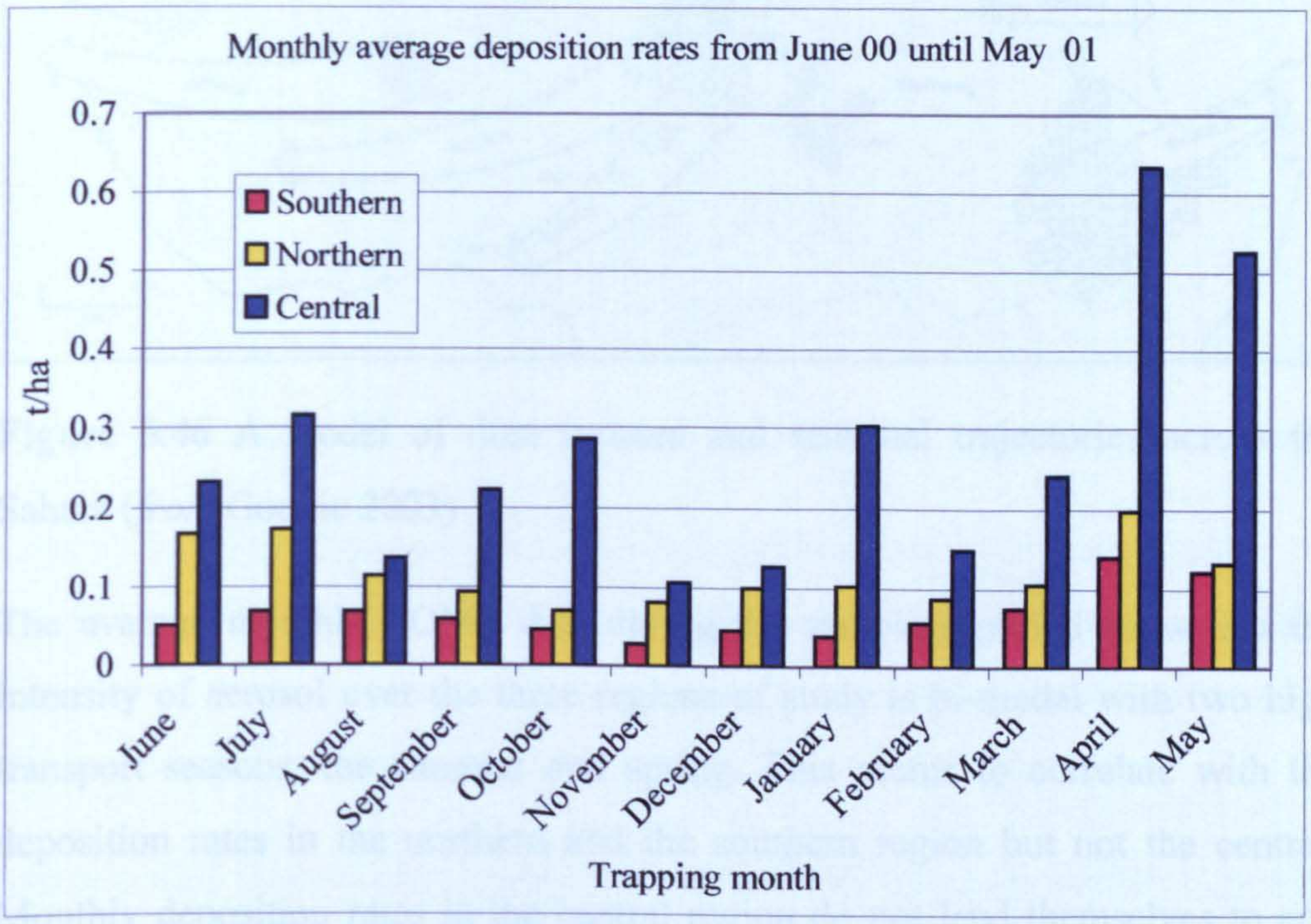

Figure 5.45 Average monthly deposition rates in the regions of study

The general trend of deposition rates reveals that the central region experienced the highest rates during each month whereas the rates in southern region were consistently the lowest. These rates show a partial disagreement with the atmospheric model shown in Figure 5.46 (Goudie, 2003), in which the southern region is designated as a major source of dust whereas the northern region is only a transport route. However, the highest deposition rates in the three regions occurred during April which correlate with the major Saharan trajectories over Libya during the spring season.

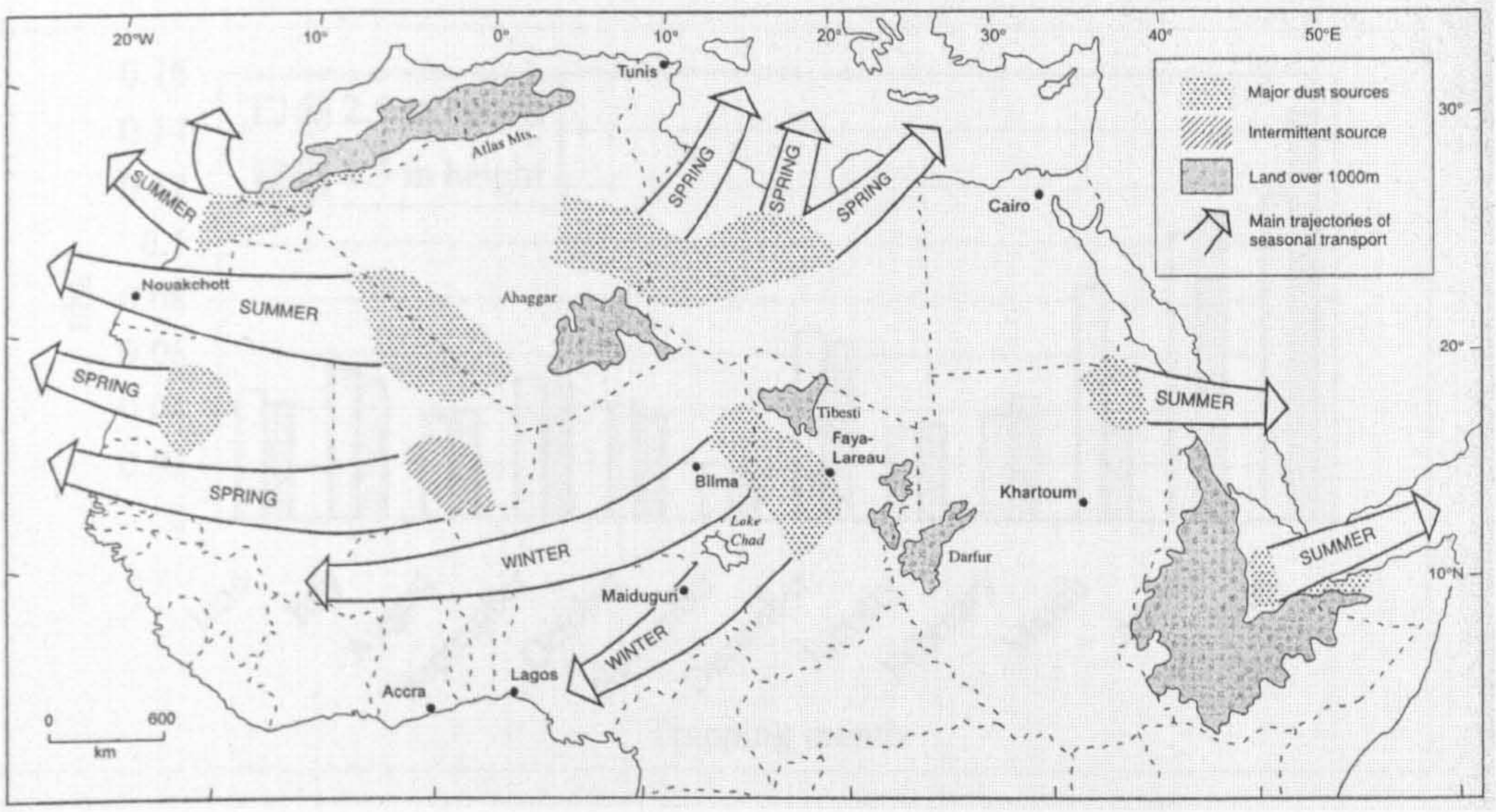

Figure 5.46 A model of dust sources and seasonal trajectories across the Sahara (*from* Goudie 2003)

The average monthly TOMS data during the sampling period show that the intensity of aerosol over the three regions of study is bi-modal with two high transport seasons, the summer and spring. This seems to correlate with the deposition rates in the northern and the southern region but not the central. Monthly deposition rates in the central region do not lend themselves to any clear pattern which is an indication of possible significant contribution from the local soils. Regardless the seasonal differences in aeolian activities, the spatial variations in aerosol distribution over the trapping regions do not seem to mimic the spatial variations in total deposition rates. Deposition rates spatial distributions during the winter months, at times when no aerosols were detected over the whole country, maintained similar patterns to those of the other seasons, but at lower rates.

A comparison of the monthly deposition rates for the two dust traps installed on the same post at 2.5 and 4.5 m heights in the southern region at Semnu reveals that the Astroturf trap is internally very consistent in its performance (Figure 5.47) with an average error of 4.3 % that should not have a significant effect on the quality of the deposition data. Since the Semnu site was uniquely placed in an area that is nearly free of any geomorphologic obstacles and under very limited anthropogenic effects, the variation in deposition rates at other sites seem to vary according to the difference in the environmental conditions

Figure 5.47 Deposition rates based on two traps installed at one site at Semnu

at each site rather than the Astroturf trap performance. The irregularities in total flux created by local wind regimes, geomorphological and anthropogenic effects seem to be more important in effecting the quality of deposition data by adding more of local sediments.

Understanding the nature and extent of near surface deposition in each trapping region requires a quantitative analysis of particle size distribution of the entrapped sediments. Since the horizontal flux seems to be a prevailing component in creating the bulk sediments, an adequate comparison of sediment deposition spatial variations and TOMS AAI variations requires separation of collected sediments according to the their transport mode, vertical and horizontal. Analysing the physical and mineral properties and separation of flux components are expected to bring about an adequate interpretation of the likely dust source(s) influencing deposition in western Libya. Analysis of the physical and mineral properties of dust and variations in deposition rates using the meteorological ground data is discussed in chapter 6.

CHAPTER 6

CHARACTERISTICS OF NEAR-SURFACE SEDIMENT: RELATIONSHIP TO SOURCE AREAS

6.1. INTRODUCTION

The physical and chemical properties of sediment particles partially control particle entrainment, transport and deposition. The individual grain characteristics as well as the grain size distribution, sorting and grain orientation, porosity and cementation of the bulk sediments are among the physical characteristics that control entrainment of grains from the bed (Pye, 1994). During transport in the air stream, particles are sorted according to size, shape and density. In addition, the physical characteristics of particles in motion may undergo changes in shape and size due to inter-particle collisions. These changes are controlled by particle hardness that is dependent on its mineral composition (Pye, 1994). Grain size distribution and mineral composition can be used to provide clues to the materials transport history. The variability of chemical composition of the retrieved dust samples can also be used to evaluate potential dust sources in the region.

This chapter presents the grain size distributions and mineralogical analysis of the sediments collected in the field and discusses the variations in the aeolian sediment physical properties in the light of the ground meteorological data during the study period and the geomorphological conditions at the trapping sites. The objective is to interpret the spatial and temporal variations in deposition rates across the study regions and relate the sediments to the likely sources in the region using TOMS data (2000-2001)

6.2. MATERIAL CHARACTERISTICS

6.2.1. Grain size analysis

Grain size distribution measurements can be achieved in a number of ways. Methods such as the pipette method or using a sedigraph are based on the determination of the settling velocity of the particle, a parameter that depends on the grain density, shape and external dimensions. The grain size distribution of coarse sediments can be determined using a series of progressively finer square mesh sieves to separate particles on the basis of their intermediate axial diameters (Pye, 1994; Kennedy *et al.*, 1985). The most effective method, however, is based on utilizing laser technology for faster processing of samples

and highly accurate measurements. The use of laser was found to be the most appropriate option to process a large number of small quantities of dust samples during a reasonable period of time.

All the grain size analysis methods are to some extent influenced by the variations in grain shape (e.g. Komar and Cui, 1984; Kennedy *et al*, 1985), however, the results obtained from some methods are influenced by grain density and optical properties. Therefore, the results of one method may not be directly comparable to the results obtained from another (Pye, 1994). As the soil surface samples collected at the trapping sites were abundant, they were also analysed by using electro-optical method to ensure consistent results. The aeolian dust and the soil surface samples were analysed using a LS-200 Coulter Laser Particle Size Analyser which operates on the principle of subjecting a specimen of dust suspended in distilled water (with a few drops of calgon solution) to a laser beam such that an obscuration of 8 – 12 % of the incident beam is achieved by the total cross sectional area of dust particles being tested. The suspended dust particles in water scatter the incident laser beam in characteristic patterns that depend on their sizes. The diffracted light is collected by a lens assembly and focused on three sets of detectors. The electronic circuitry executes particle size measurements through 92 channels. The LS-200 is capable of measuring particle sizes within 0.4 to 2000 μm range. A minimum of 1 gm is necessary to achieve the laser beam obscuration percentage and obtain optimum results. In certain cases, this was not achievable as some samples were less than 1 gm.

6.2.2. Bulk mineralogy by X-ray diffraction

The bulk mineralogy of a number of samples was analysed rather than the composition of the constituent grain size classes due to their limited quantities. Each sample was reduced to a fine powder by using a pestle and mortar to ensure enough particle participation in the diffraction process. Grinding of sensitive minerals which may be damaged or undergo alteration during grinding (e.g. calcite or kaolinite) is usually carried out under alcohol in a pestle and mortar (Buhrke *et al*., 1998). Therefore, each sample was ground

under acetone and placed on a brass insert. The mineral composition analysis of a selected number of samples was analysed using a Philips-PW 1050 Powder Diffractometer and the data have been analysed qualitatively and quantitatively using software, TRACES 3.0 and SIROQUANT (version 1) respectively. The X-ray diffraction (XRD) testing was performed on two sets of samples representing two geographically and meteorologically extreme sites. In order to explore the spatial and/or temporal variations in the mineral composition, one set of samples was chosen from the coastal region and another set from the southern region, excluding those sites that seem to be strongly affected by local dust such as those in the area surrounding Tripoli. Some sites were excluded as the samples were totally used during grain size analysis. A combination of samples from the southern region and the northern region (Misratah area); (Figure 6.1) are listed in Table 6.1

Aeolian samples		
Sampling month	Site location	
	Southern region	Northern region
June	Misratah (DD)	Birak (DB)
July	Misratah (DD)	Birak (DB)
August	Zlitan (BA)	Birak (DB)
September	Misratah (CE)	Semnu (DF)
October	Misratah (CE)	Birak (DB)
November	Misratah (CE)	Bent Baiya (CF)
December	Misratah (CE)	Birak (DA)
January	Tawurgha (DE)	Birak (DB)
February	Tawurgha (DE)	Birak (DB)
March	Tawurgha (DE)	Birak (DB)
April	Misratah (CE)	Birak (DB)
May	Misratah (CE)	Birak (DB)
Soil samples		
Site code	Location	Region
CE	Misratah	Northern
DB	Birak	Southern

Table 6.1 Sites of samples tested by XRD for mineral composition

6.3. METEOROLOGICAL DATA

The meteorological data during the fieldwork period was recorded by the Libyan Meteorological Services at six ground stations in the regions under study at Zuwarah, Tripoli, Al Khums, Misratah, Hun and Sebha as shown in Figure 6.1.

Since ground stations across the region of study are few in number and wind data cannot easily be extrapolated as topographic irregularities strongly make surface winds variable (Reheis and Kihl 1995), the meteorological conditions at each trapping site are assumed to be identical to the those recorded at the nearest meteorological station. This assumption can simplify the analysis of deposition patterns in relation to the weather conditions; however, it can also result in false interpretation of dust deposition patterns based on unrepresentative meteorological data taken at distant places from trapping sites. The approximate distances between each trapping site and the nearest ground station are presented in Table 6.2.

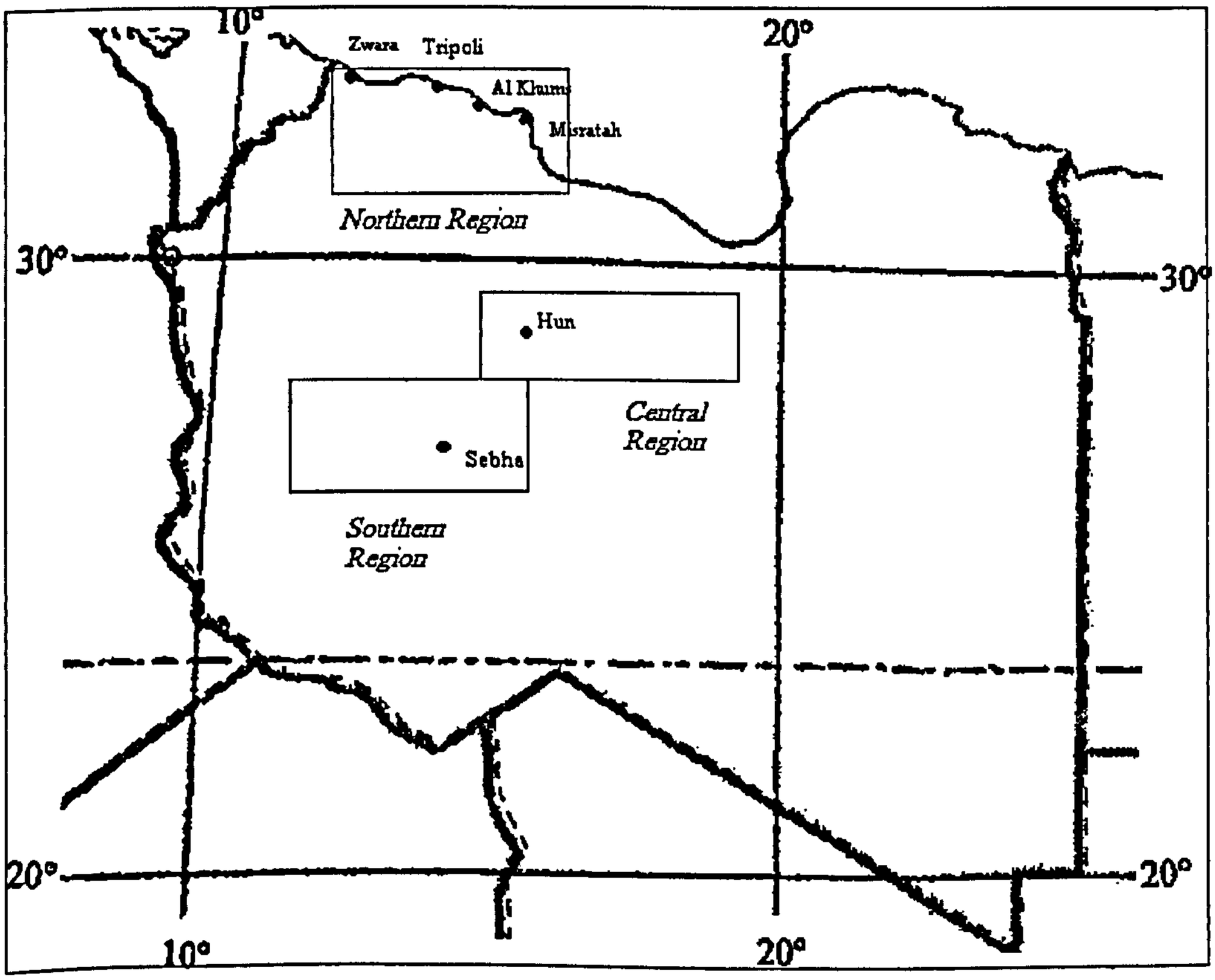

Figure 6.1 Ground meteorological station sites

Trapping location	Site code	Nearest meteo-station	Distance in between (km)
Semnu	DC	Sebha	60
	DF	Sebha	60
Birak	DA	Sebha	50
	DB	Sebha	50
Bent Baiya	CF	Sebha	70
Waddan	EF	Hun	10
Zillah	EA	Hun	160
	EB	Hun	160
	EC	Hun	160
Bani Walid	BD	Al Khums	120
Tawurgha	DE	Misratah	70
Misratah	CE	Misratah	7
	DD	Misratah	10
Zlitan	BA	Misratah	40
	BF	Misratah	40
Al Khums	CC	Al Khums	5
	CB	Al Khums	2
	CA	Al Khums	13
Tripoli	AF	Tripoli	10
	AE	Tripoli	23
Surman	AD	Zuwarah	30
Ajalat	AC	Zuwarah	20
Zuwarah	AA	Zuwarah	3
	AB	Zuwarah	10

Table 6.2 Distance between each trapping site and the nearest meteo-station

A minimum wind shear stress is essential to initiate soil particle movement and result in dust emission. Entrainment of soil particles starts only if wind velocities exceed certain threshold velocities. Wind threshold velocities reported in dust dynamics studies range from 4 to about 20 m/s (Helgren and Prospero, 1987; Nickling and Gillies, 1989; Chomette *et al.*, 1999; Callot *et al.*, 2000).

Studies simulating the atmospheric dust cycle aimed at explaining the interaction between climatic change and dust emissions (Joussaume, 1990; Joussaume, 1993; Genthon, 1992; Tegen and Fung, 1994) were described as relatively deficient (Callot *et al.*, 2000). In these studies, the non-uniformity in spatial and temporal dust emissions has been attributed to the variability in wind velocity. As surface features play a significant role at the source regions, which in turn effects the dust emission rates (Gillette, 1979; Gillette *et al.* 1982; Nickling, 1988; Nickling, 1994), a better simulation to investigate dust emissions must take surface features into account.

A recently developed geomorphological approach to model surface features and their effects on dust emissions has been used to simulate dust emissions over the central and western Sahara during the years 1990, 1991 and 1992 (Callot *et al.*, 2000). The model has yielded a more comprehensive spatial distribution of threshold velocities across the Sahara ranging from 6.5 to 20 m/s with most of the values lower than 14 m/s. The study concluded that threshold velocities are spatially and highly variable, but homogeneous for a particular area of similar topographic conditions. In addition, this study produced a map of threshold velocities based on a surface features description of $1\times1^{\circ}$ grids (Figure 6.2). Although this grid size is relatively large with respect to the needs of this project, this study seems to be more comprehensive and representative of the study field in this project. Callot *et al.*'s (2000) usage of comprehensive data records which include orographical, geological, climatological, pedological and anthropic data, makes this study a more reliable and a favourable reference to select a threshold velocity needed to draw wind roses.

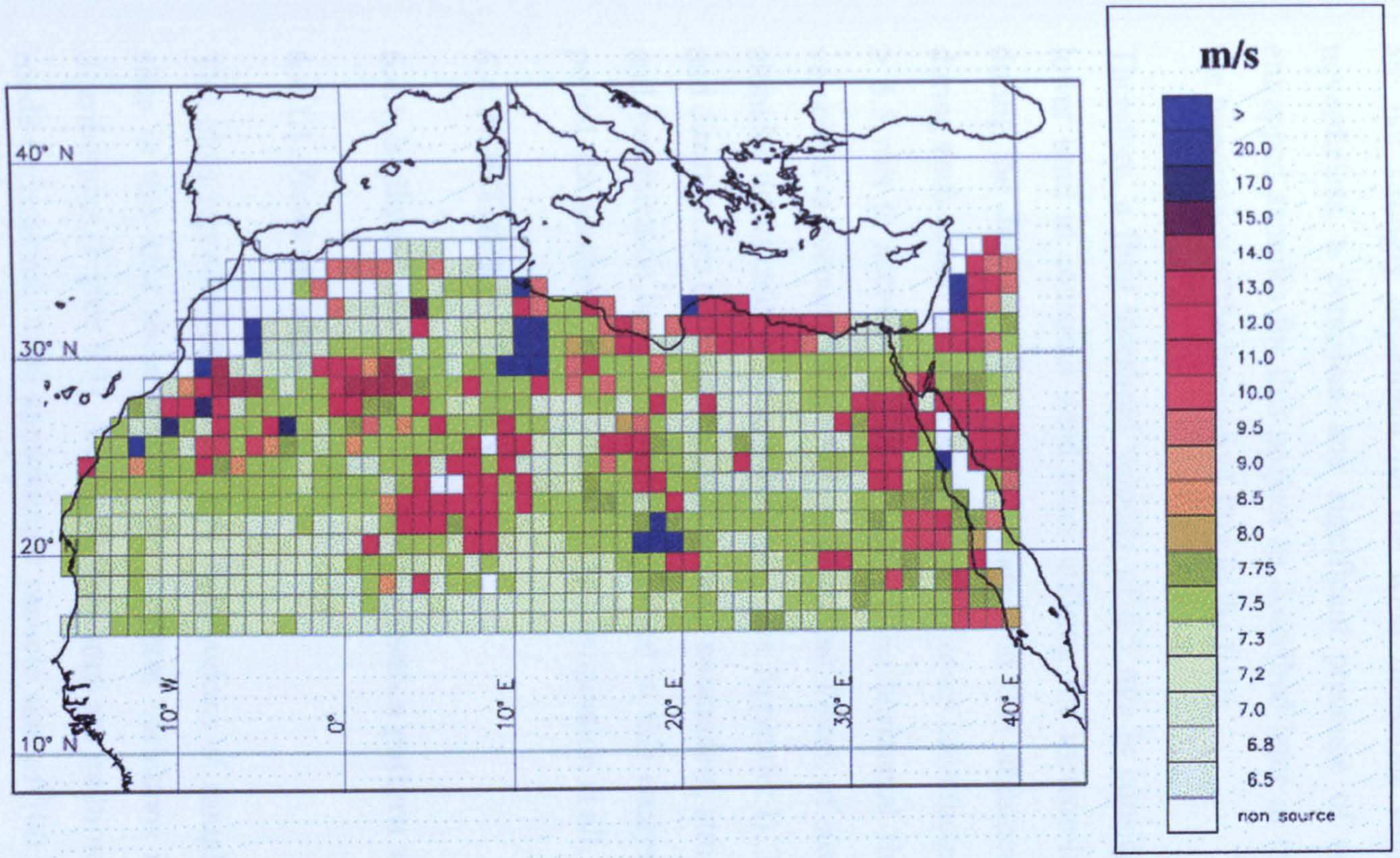

Figure 6.2 Map of fluid threshold velocities at 10 m across the Sahara (*from* Callot *et al.*, 2000)

In spite of the fact that the threshold velocity is an important parameter in dust entrainment assessment, aerosol particles in the upper layers of the atmosphere are in motion at all wind velocities and deposition occurs when the settling velocity of the particle exceeds the vertical component of the wind velocity under calm weather conditions. Although, one can argue that deposition rates are not strongly dependent on the wind threshold velocity at the source, nevertheless, a persistent and significant presence of silt and sand in the entrapped samples for this project as described later in this chapter indicates the importance of the horizontal flux in the field.

Therefore, a fluid threshold velocity of 6.5 m/s is considered as an adequate lower limit to construct wind roses utilising the meteorological data recorded during the dust sampling period. Based on this argument, prevailing winds during each month are represented by wind roses constructed for wind velocities $\geq$ 6.5 m/s to account for the effects of the horizontal flux and for all wind velocities to account for aerosol particles that fallout of suspension from higher altitudes under calm weather conditions (see Appendix I). Though, wind speeds and direction are more important than other parameters, atmospheric temperature and precipitation have also been considered in this analysis. During the study period, the southern region witnessed no precipitation at all, as in most years.

6.4. NORTHERN REGION

6.4.1. Sediment characteristics and deposition pattern analysis

6.4.1.1. Zuwarah area

The plots representing particle size distributions of samples entrapped at four sites in this area show spatial and temporal variations in their particle size distributions (Figure 6.3). All the distributions are multimodal with a dominant mode corresponds to an approximate particle size of 100 μm (very fine sand). Samples collected at sites AB and AC were under greater influence of horizontal particle flux than those collected at sites AA and AD such that the sand fraction ($\geq$ 70 μm) of the bulk sediments from AB and AC represents nearly a half of the total mass of the samples and in some cases dominates their

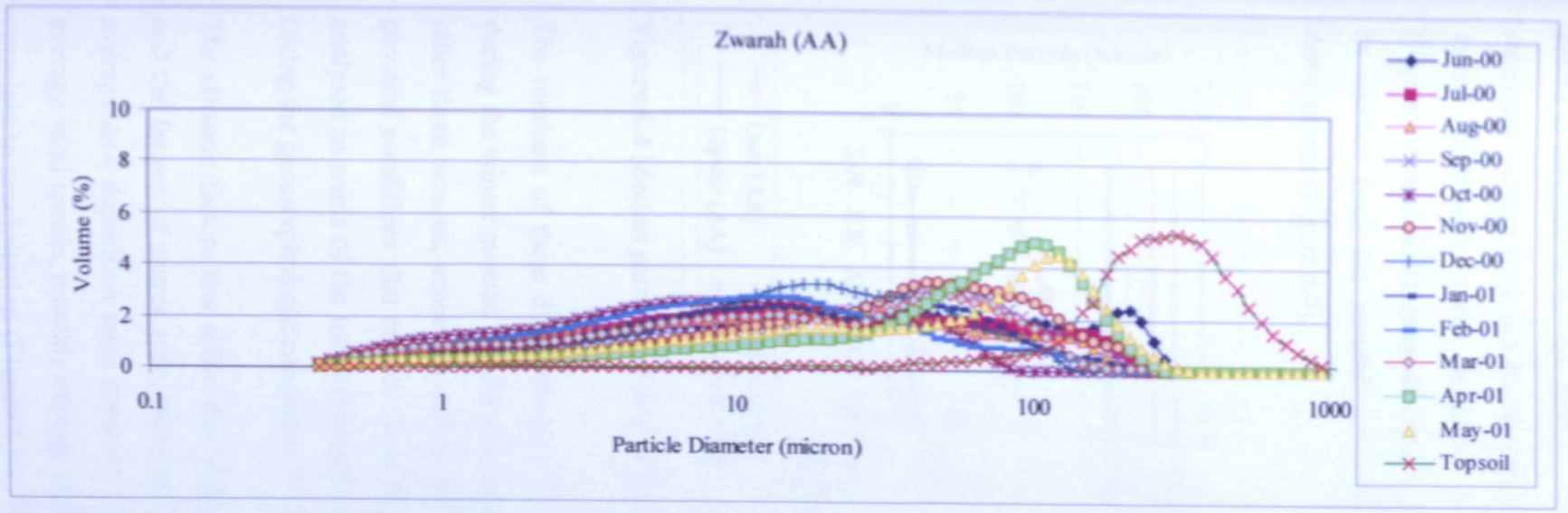

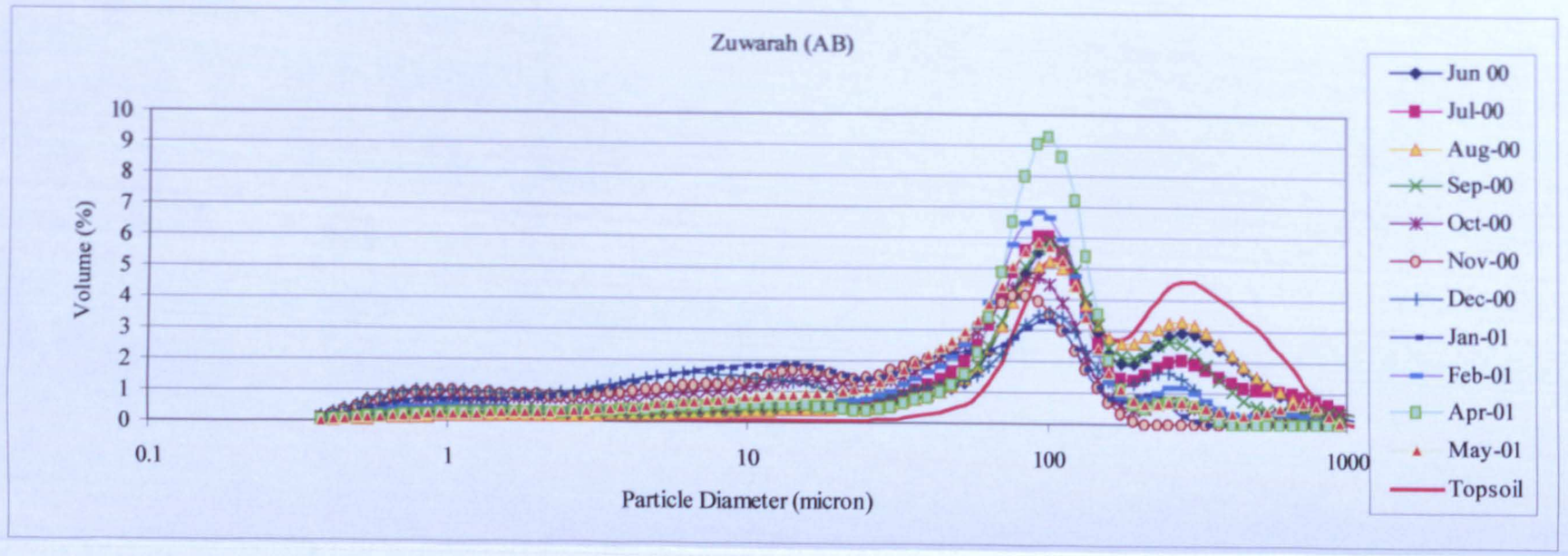

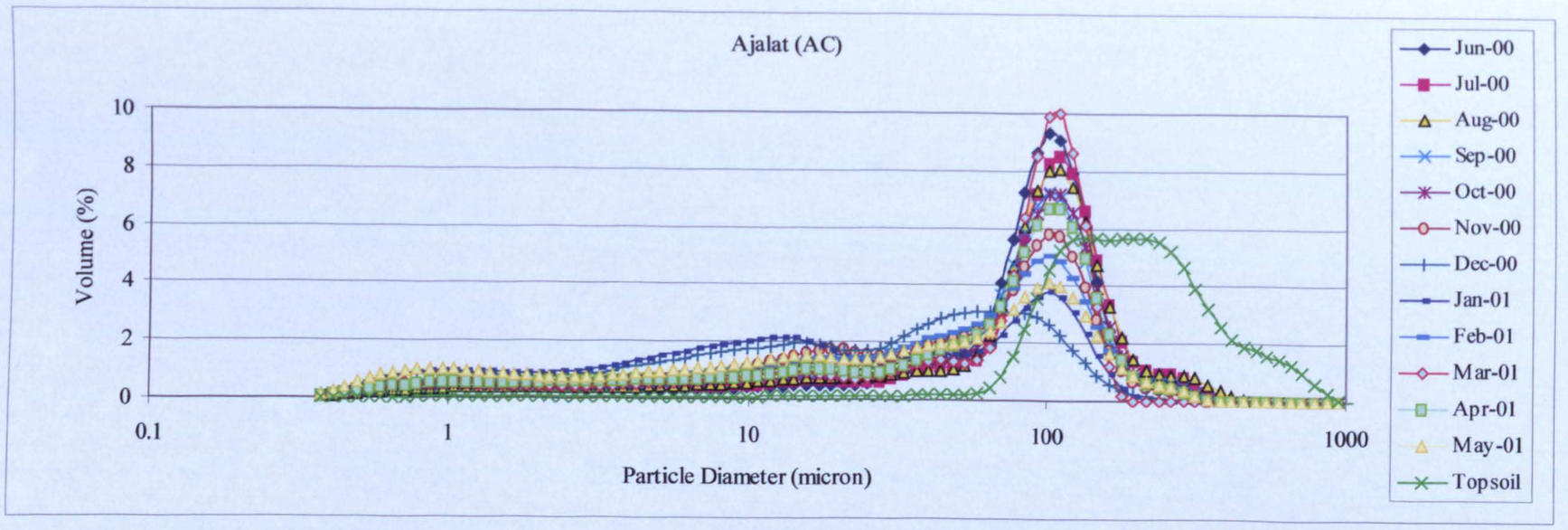

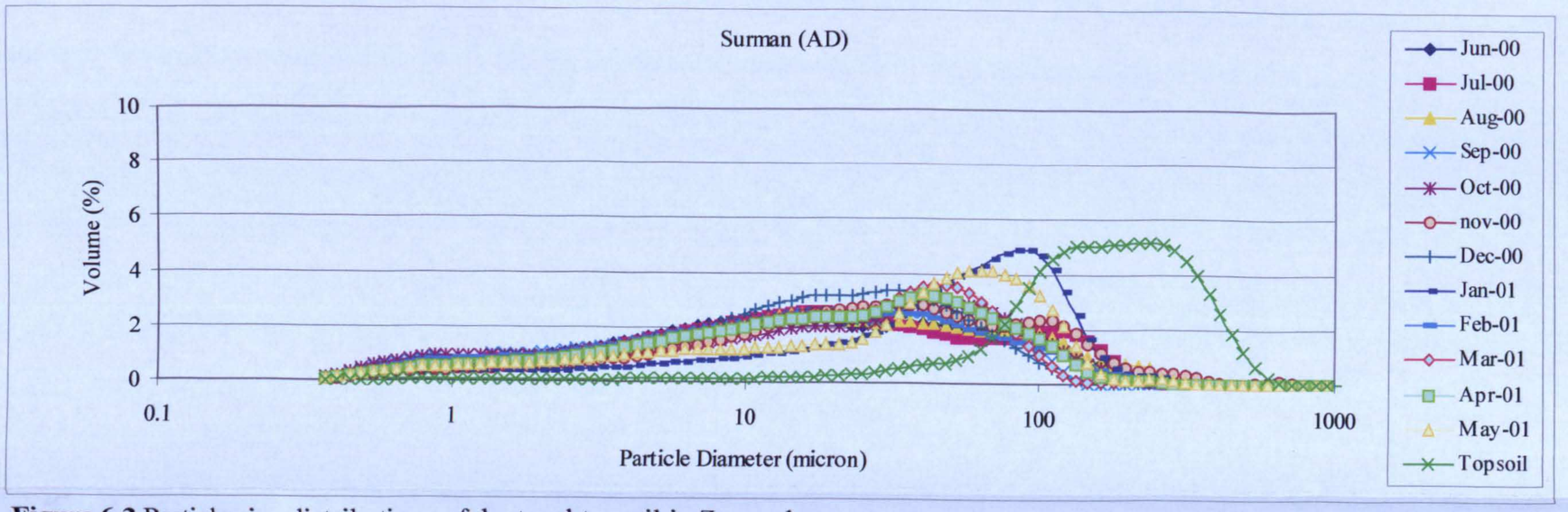

Figure 6.3 Particle size distributions of dust and topsoil in Zuwarah area

weights (Figure 6.4) and (Tables II.2 and II.3) in Appendix II. Increased sand seems to correlate to the dry months of the summer and spring. Although the statistical median may not be an optimum parameter in describing a multi-modal distribution, it can be useful to summarize a large amount of data (Figure 6.3) and facilitate an emergence of a general trend. A general trend can be derived from the monthly variation in median particle sizes of these distributions (Figure 6.4).

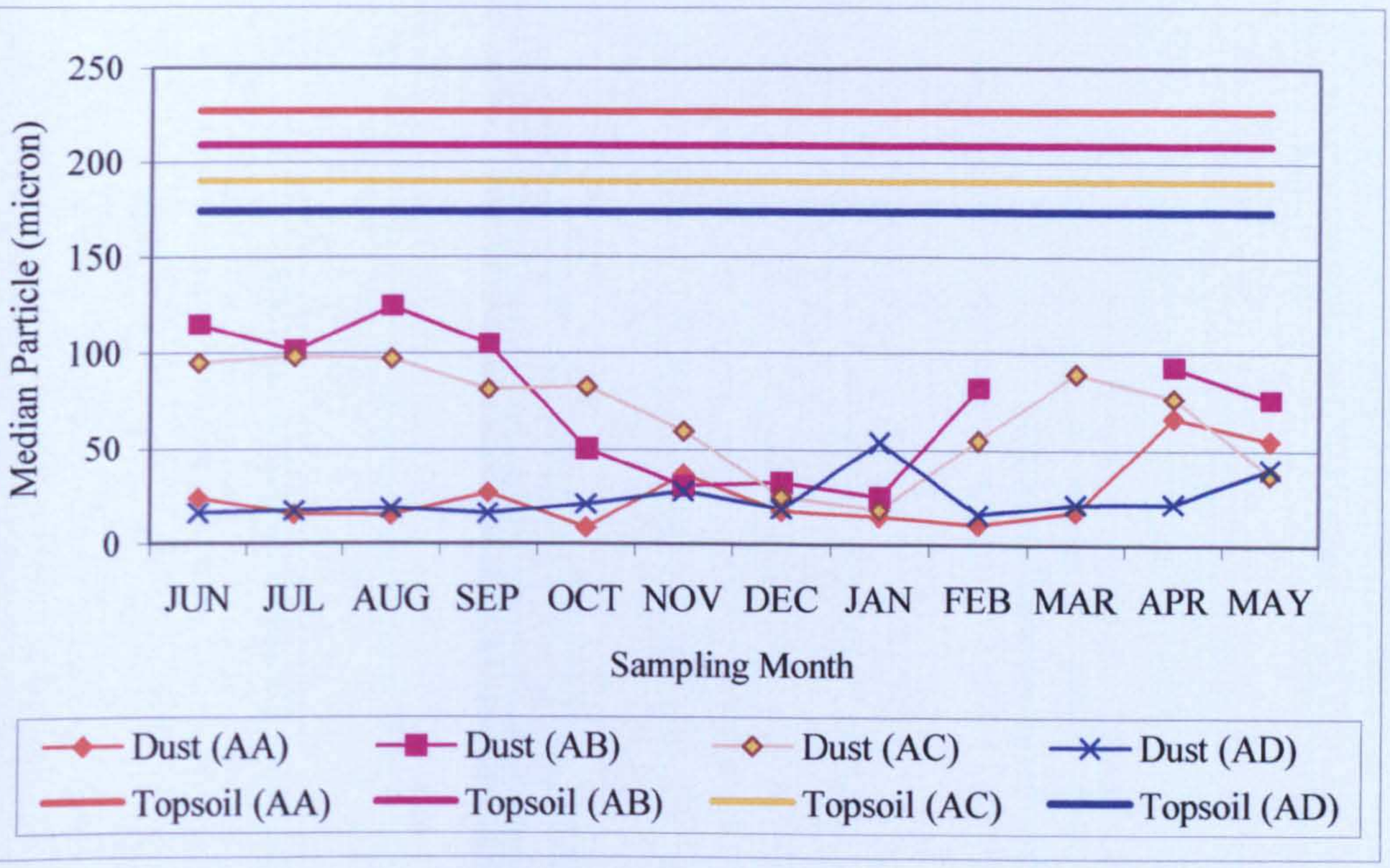

Figure 6.4 Median particles of dust and topsoil

The medians of these distributions tend to converge towards silt size range during the winter months but diverge from medium silt to fine sand during the other three seasons, especially during the summer. In order to understand the physical conditions that created these patterns, particle size distributions are analysed in terms of the meteorological data and deposition rates (Figure 6.5) taking the geomorphologic conditions in this area into consideration.

The climatic factors that affect dust deposition rates interact with each other and the factors of source type, topography and human activity. The monthly average dust deposition rates seem to increase with the increase in monthly average wind speeds, monthly average maximum temperatures, but they do not correlate to precipitation (Figure 6.5). The months of high deposition rates

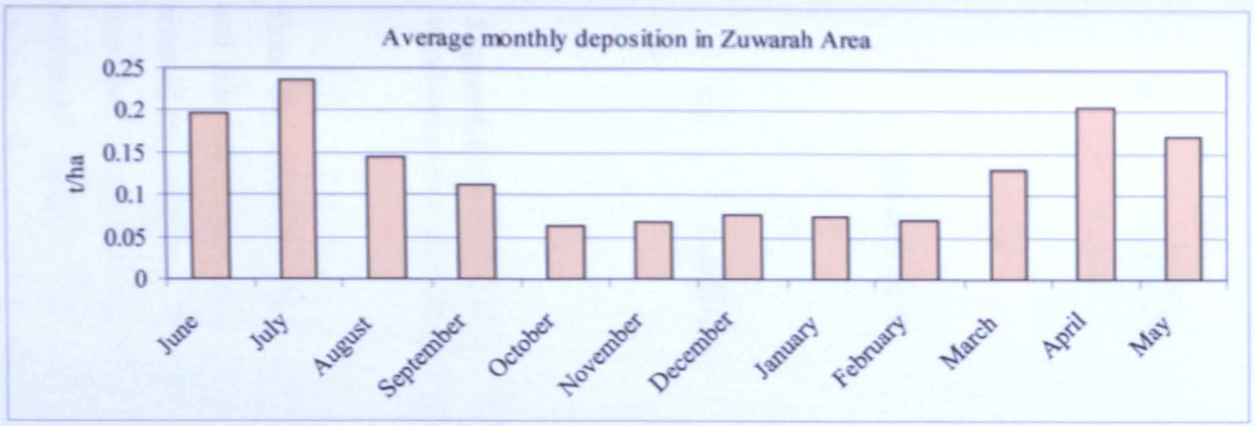

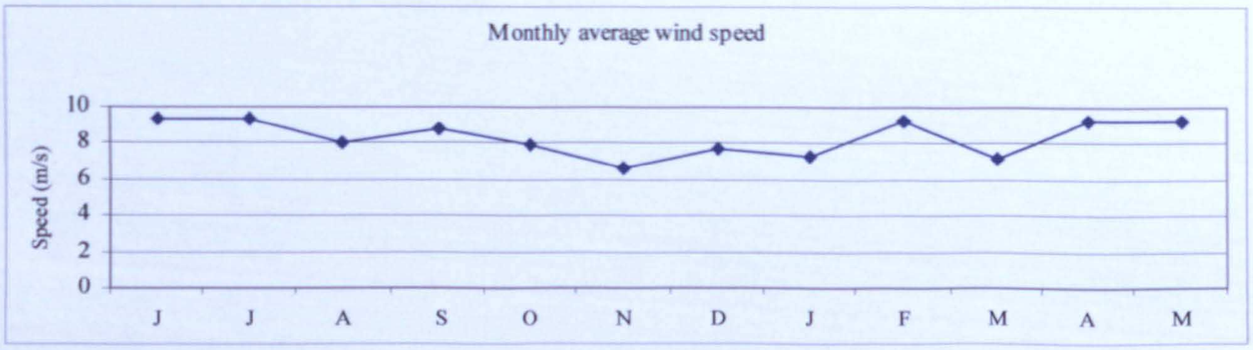

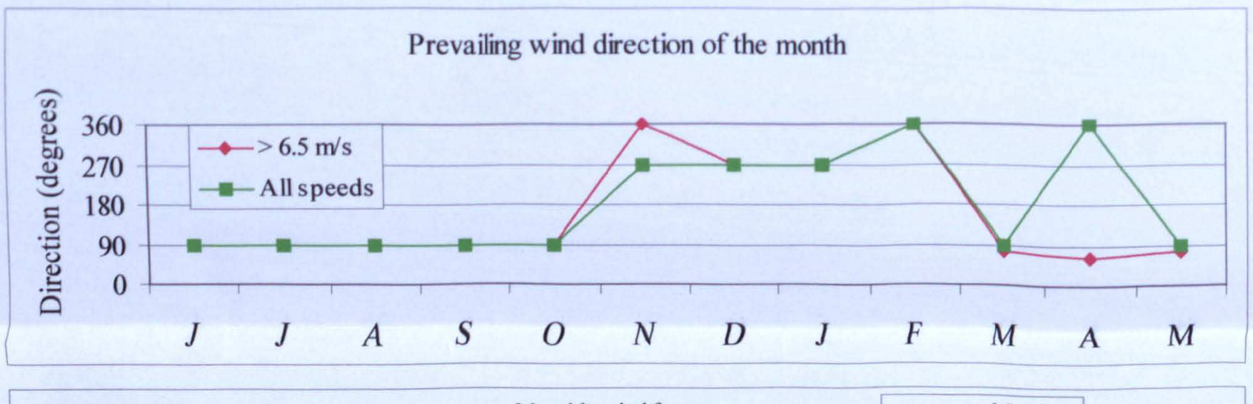

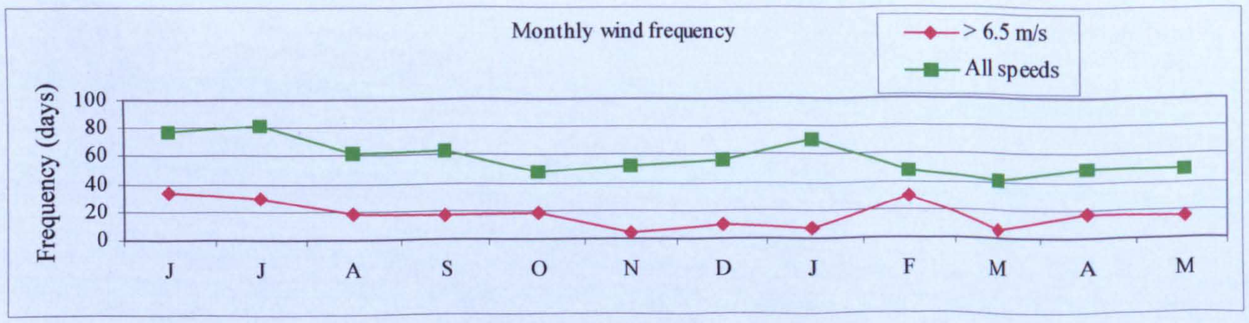

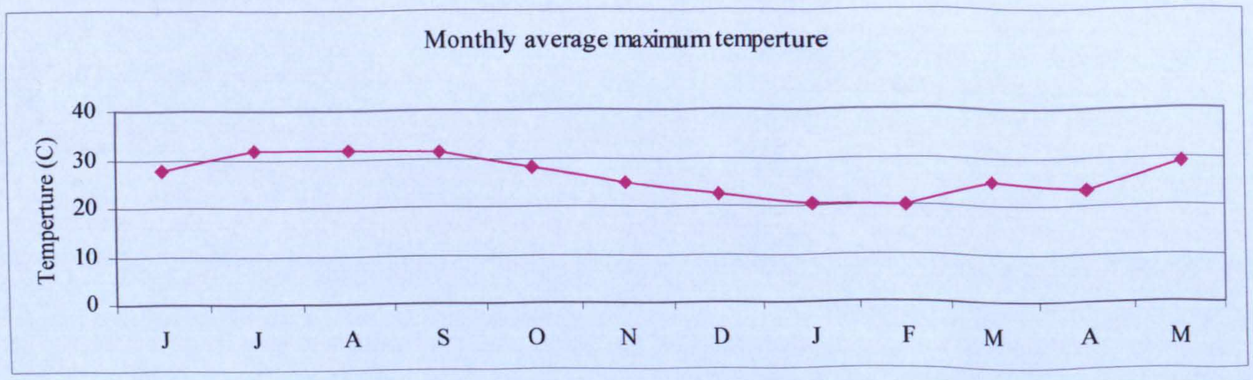

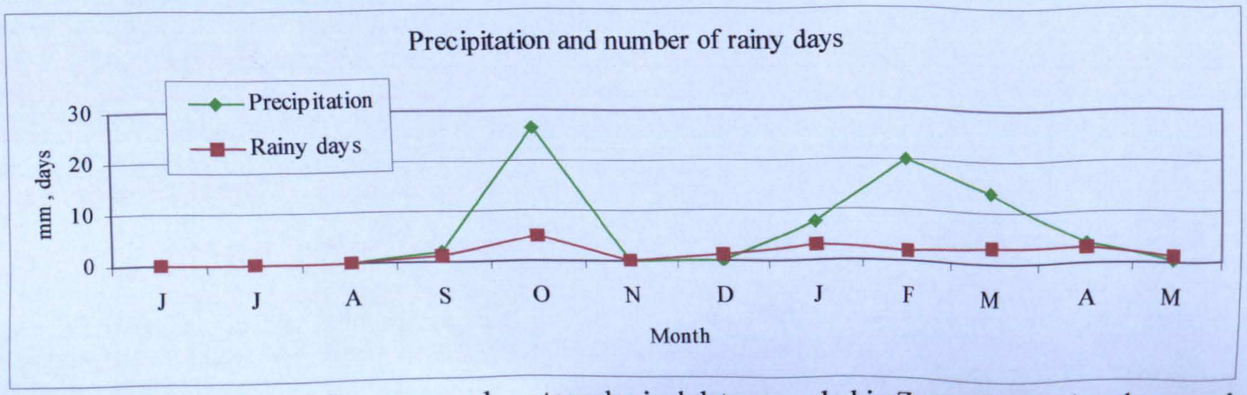

Figure 6.5 Dust deposition rates and meteorological data recorded in Zuwarah area *(northern region)*

correspond more frequently to prevailing easterly winds (Figure 6.6).

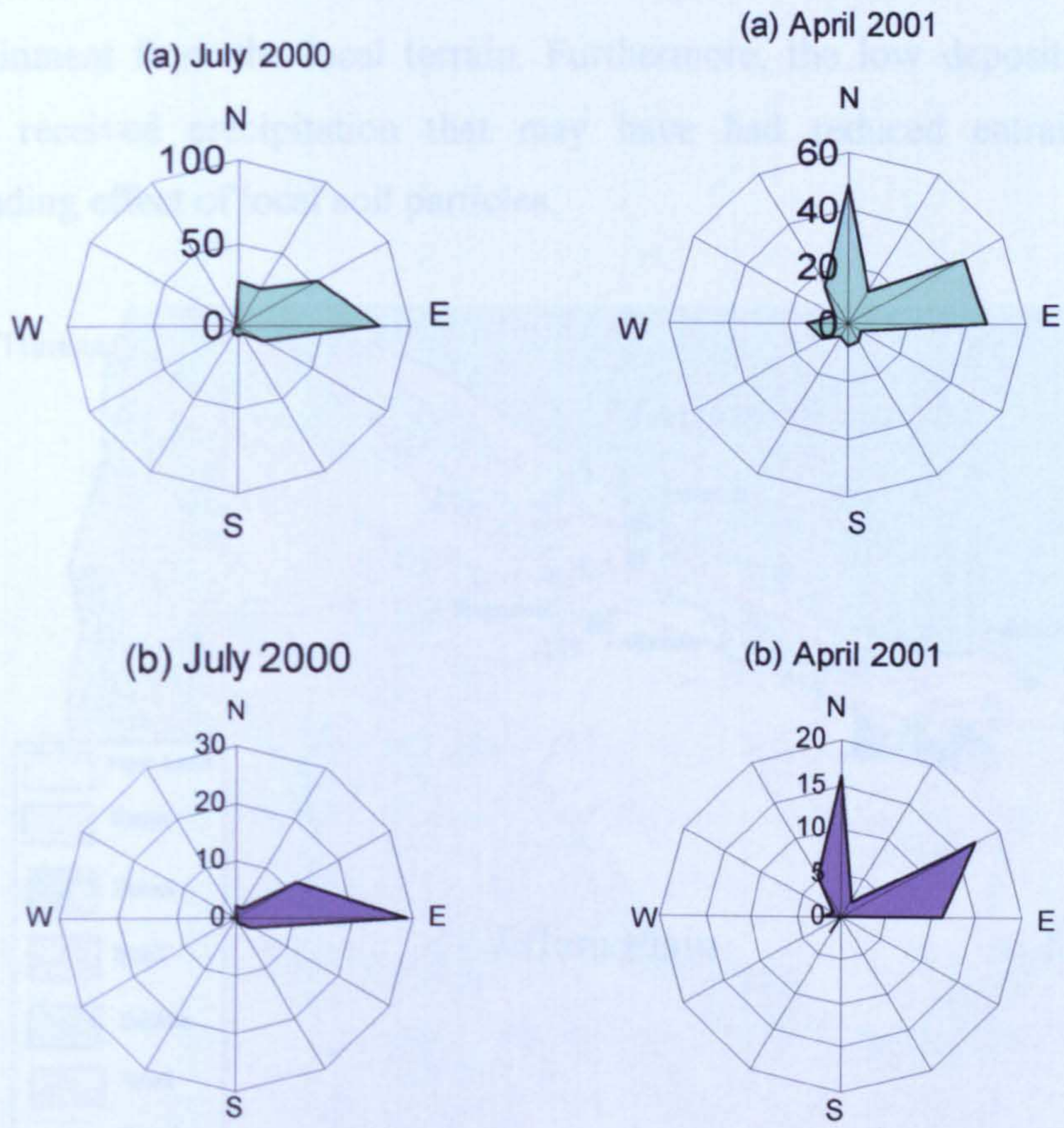

Figure 6.6 Prevailing winds during July 2000 and April 2001 based on (a) all wind velocities, (b) wind velocities ≥ 6.5 m/s

Since the medians of particle sizes of summer samples collected at sites AA and AD fall within a medium to coarse silt whereas the medians of particle sizes of the samples collected at AB and AC during the same season fall in the fine sand range, the last two sites must have undergone a greater influence of horizontal particle flux. Since this area comprises no geomorphological obstacles that can affect the wind regime, the excessive deposition of sand at some sites can only be attributed to entrainment of local soil particles by humans. Finer sediments trapped during the months of October-February (Figure 6.4) correspond to lower deposition rates (Figure 6.5) and coincide with winds ranging from west to north perhaps bringing oceanic aerosols and passing over the sabkhas in this areas before reaching the trapping sites (Figure

6.7). These winds may have played a major role in transporting fine particles from the sabkhas to the trapping sites. Moreover, human activities in the areas to the north and west are very limited which reduces the effect of sand particle entrainment from the local terrain. Furthermore, the low deposition months have received precipitation that may have had reduced entrainment and cascading effect of local soil particles.

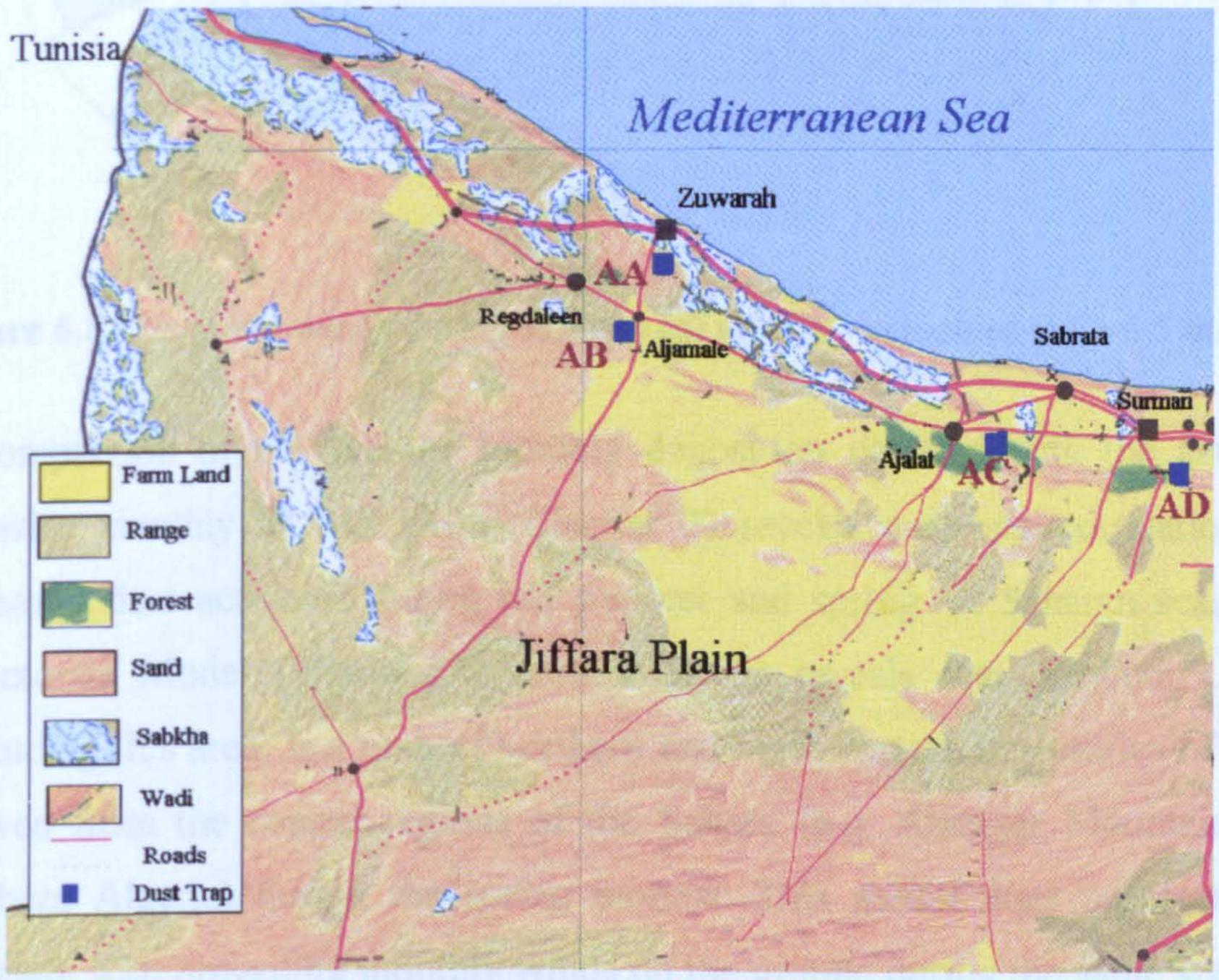

Figure 6.7 Geomorphological features and trapping site locations in Zuwarah area (*after* The Secretary of Planning, 1978).

Increased moisture and lower atmospheric temperatures may have also been other reasons for reduced horizontal dust flux effects during the winter months at times dominated by western and south western low velocity (< 6.5 m/s) winds (Figure 6.8). These winds may have played an important role in drawing dust at high levels (but, not high enough to be detected from space) from southern western areas of the Jiffarah Plain, Al Hamada Al Hamra or the Grand Erg Oriental in southern in Tunisia to this area which may had been washed out by rain and/or fallen out of suspension under calm weather conditions or at times when winds reverse direction at the sea/ land interface.

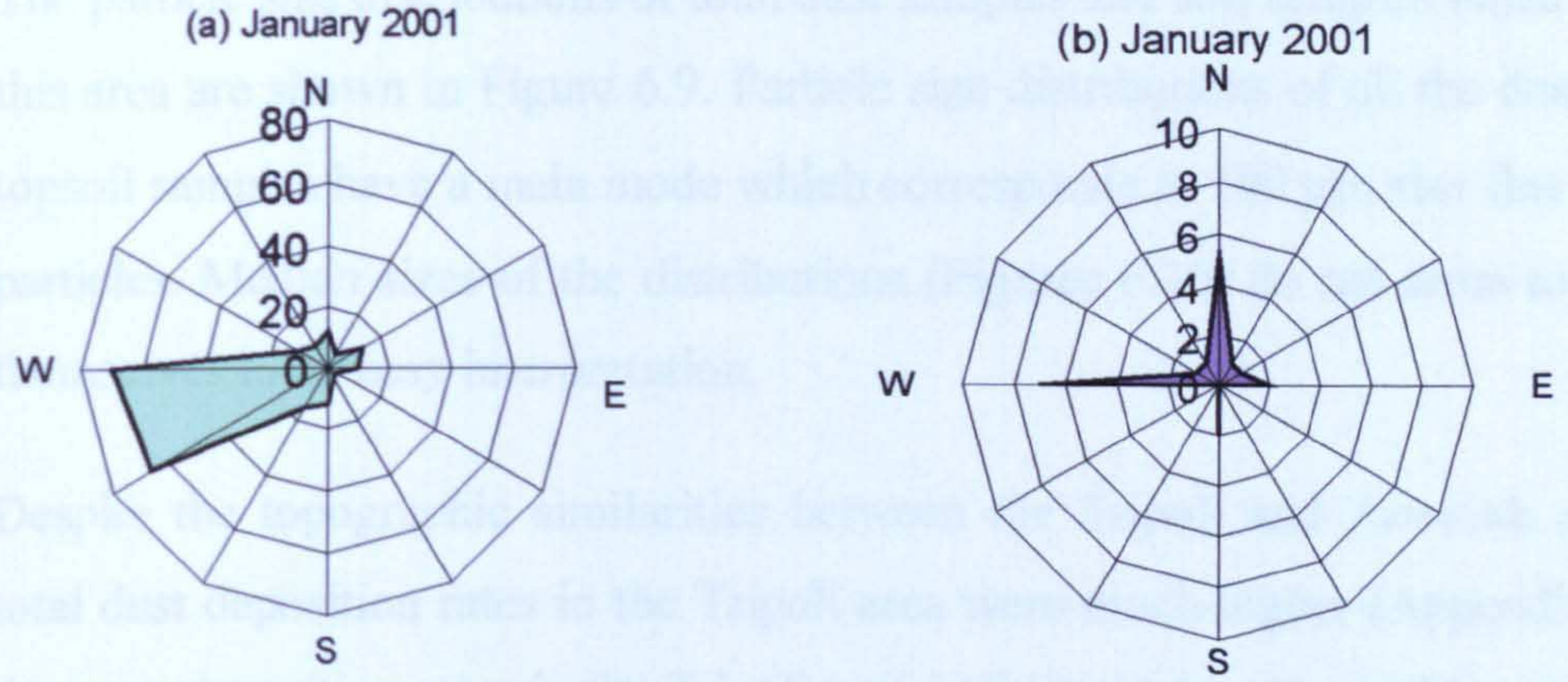

Figure 6.8 Prevailing winds during January (a) all wind velocities (b) ≥ 6.5 m/s

A comparison of the average monthly deposition patterns with the aerosol intensity monthly TOMS plots (Chapter 3) reveals a strong correlation of increased dust activities during the summer and spring. A Saharan seasonal trajectories Model (Figure 1.5; Goudie 2003) reveals that northern Libya (including this area) is a path of northern and north eastern trajectories of dust derived from the central regions of the Sahara (e.g. Ahaggar Mountains in southern Algeria) during the spring months. This model does not seem to correlate with prevailing monthly winds on the ground during the same season. In addition, the median values of the particle size distributions from the spring samples reveal that horizontal particle flux had a significant role in deposition in Zuwarah and TOMS AAI during the spring 2001 months is zero.

Dust originated in the eastern Libyan Desert during the summer, as revealed by TOMS data (chapter 3) and the monthly wind roses (Appendix I), may have constituted a partial source of fine particle deposits in this area. It appears that most dust transported during the dry months of the summer was mainly driven by winds which blew from the east and northeast. Winds during the spring months were from several directions north, east, northeast and south west which is an indication of the relative contributions from different local sources. This may have been the reason for increased deposition during April and May, however, high speed winds ranged from the north to east.

6.4.1.2. Tripoli area

The particle size distributions of total dust samples and soil samples taken from this area are shown in Figure 6.9. Particle size distributions of all the dust and topsoil samples have a main mode which corresponds to 100 μm size fine sand particles. Median sizes of the distributions (Figures 6.10) do not seem to lend themselves to an easy interpretation.

Despite the topographic similarities between the Tripoli and Zuwarah areas, total dust deposition rates in the Tripoli area were much higher (Appendix II). Average deposition rates in the Tripoli area indicate high and variable amounts of deposition that poorly correlate with meteorological factors (Figure 6.11). However, the seasonal modal pattern (Figure 6.11) shows that the highest accretion rates correspond to the months of average maximum higher atmospheric temperatures and average monthly wind speeds.

Since there are no distinctive dust sources in this area, anthropogenic factors such as traffic, farming and construction works in and around Tripoli appear to be the most likely cause of the highly variable and large deposition rates.

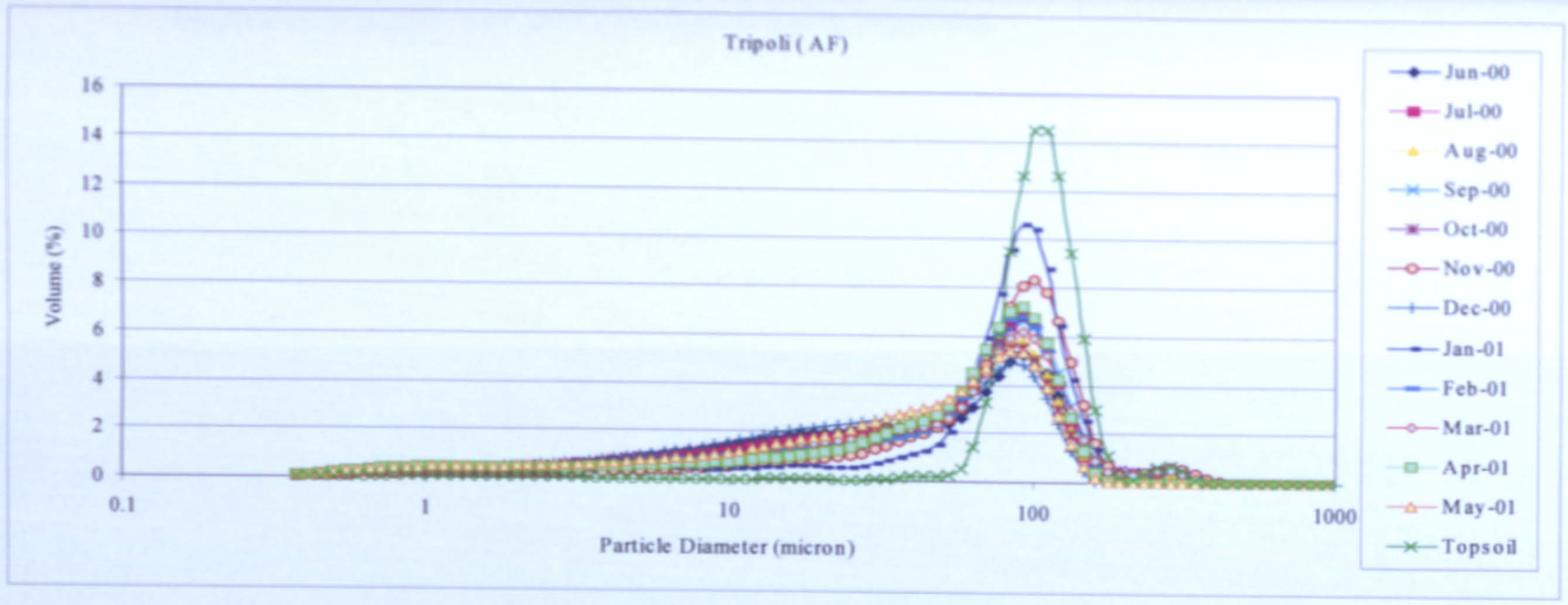

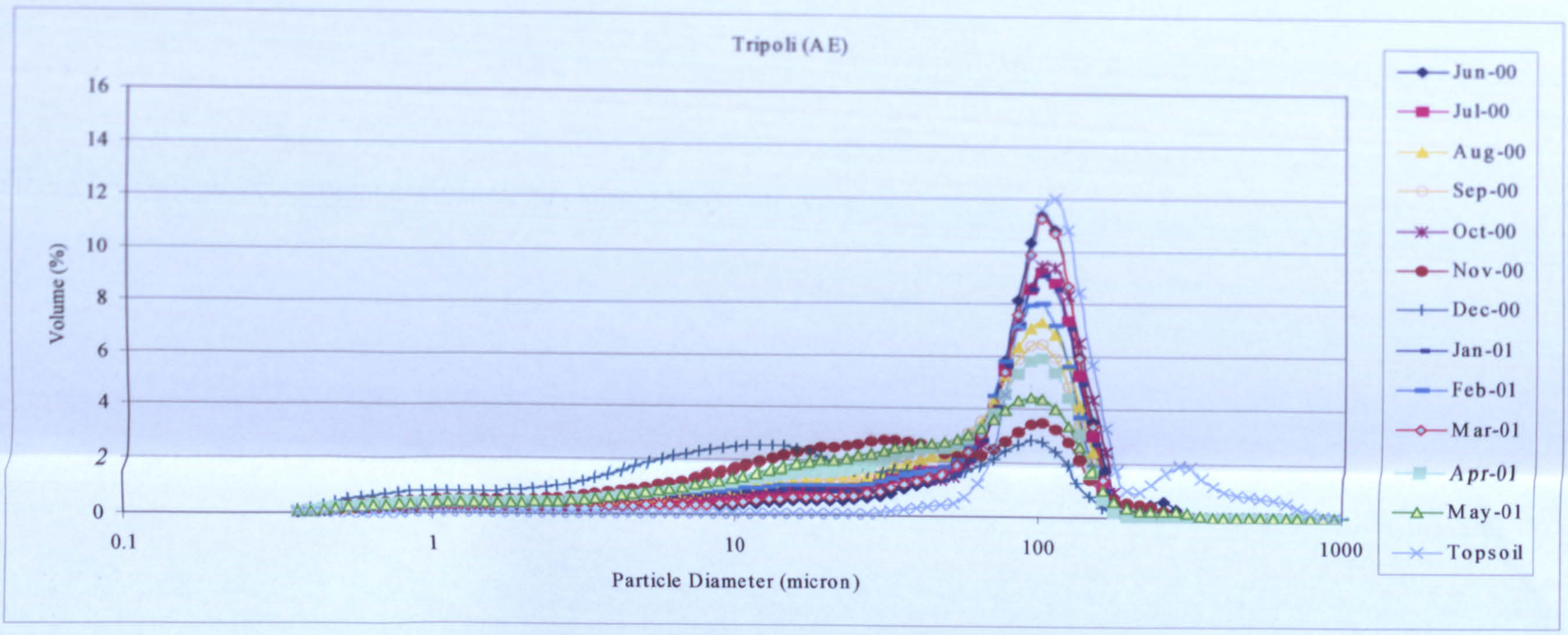

Figure 6.9 Particle size distributions of dust and topsoil in Tripoli area

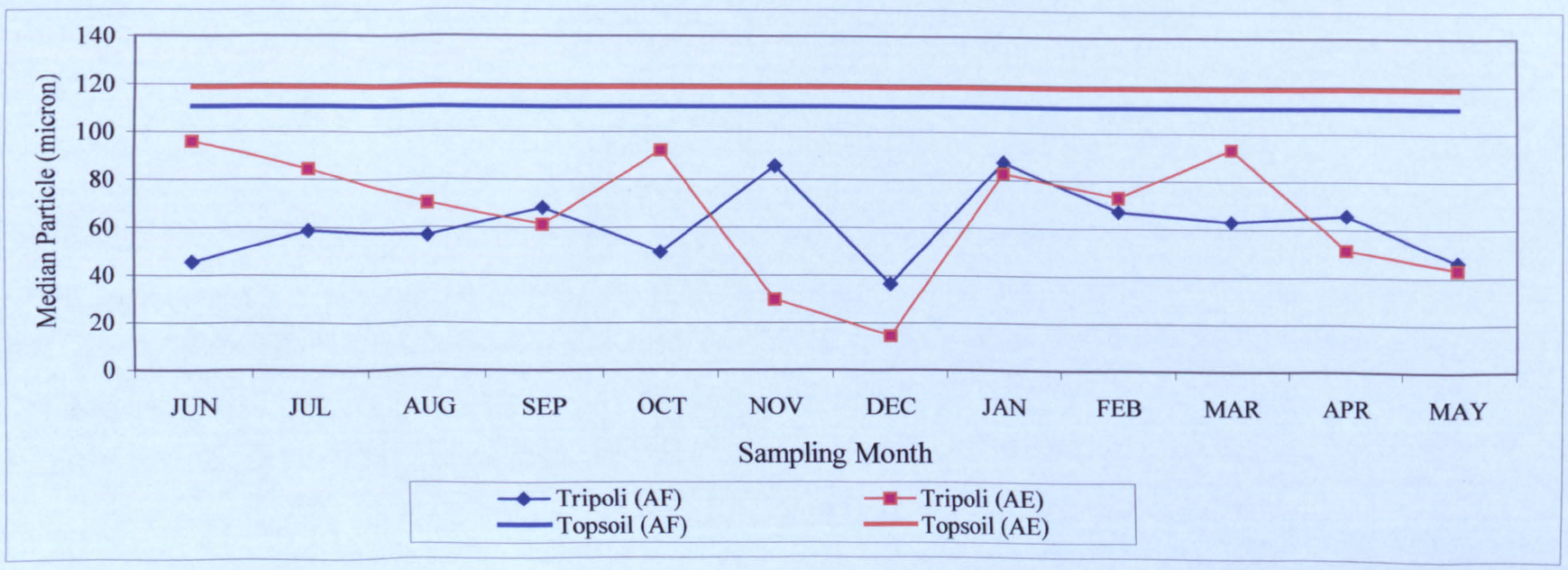

Figure 6.10 Median particles of dust and topsoil

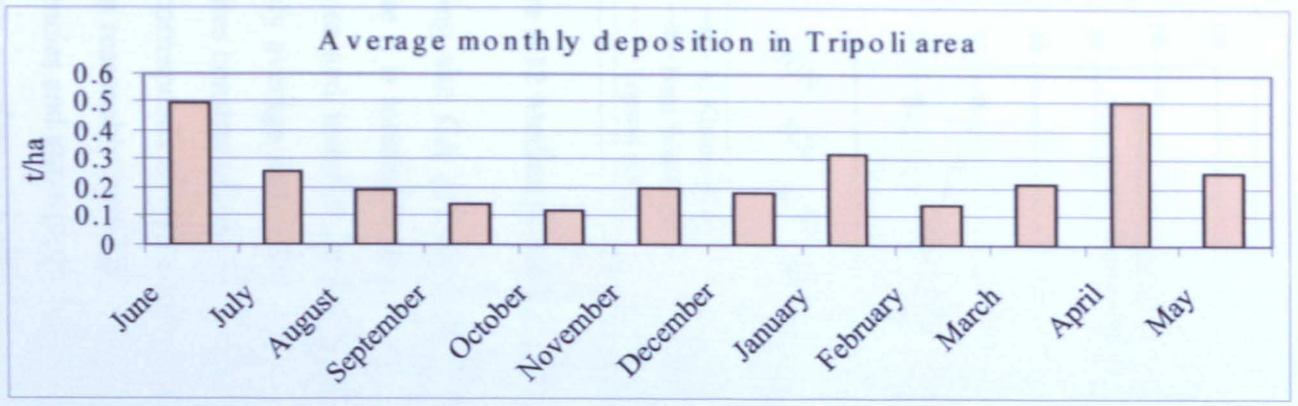

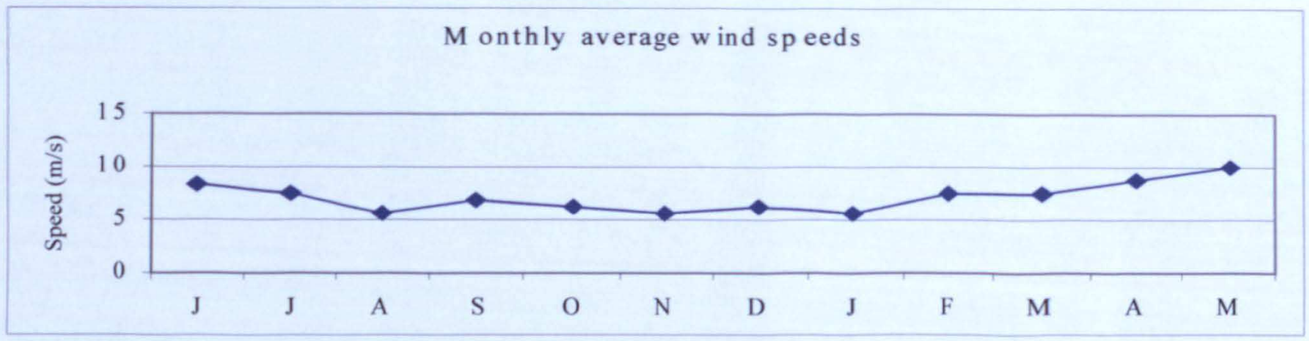

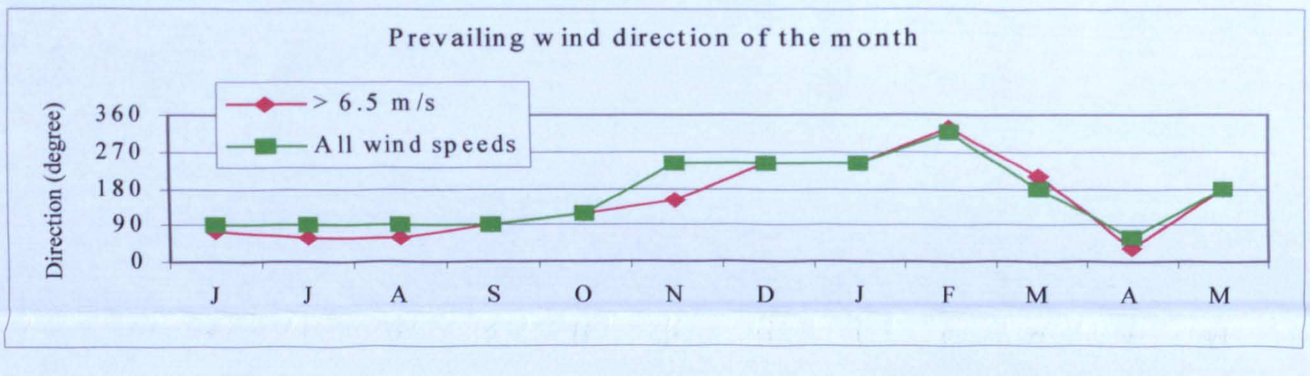

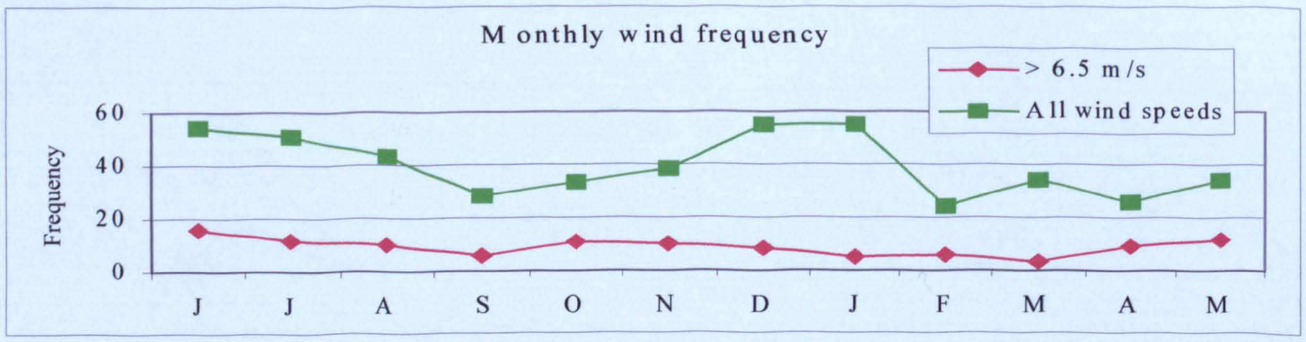

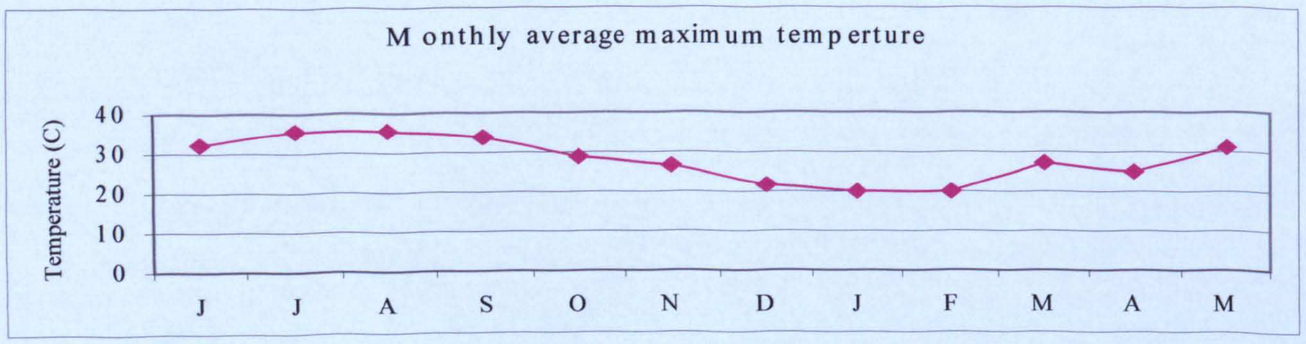

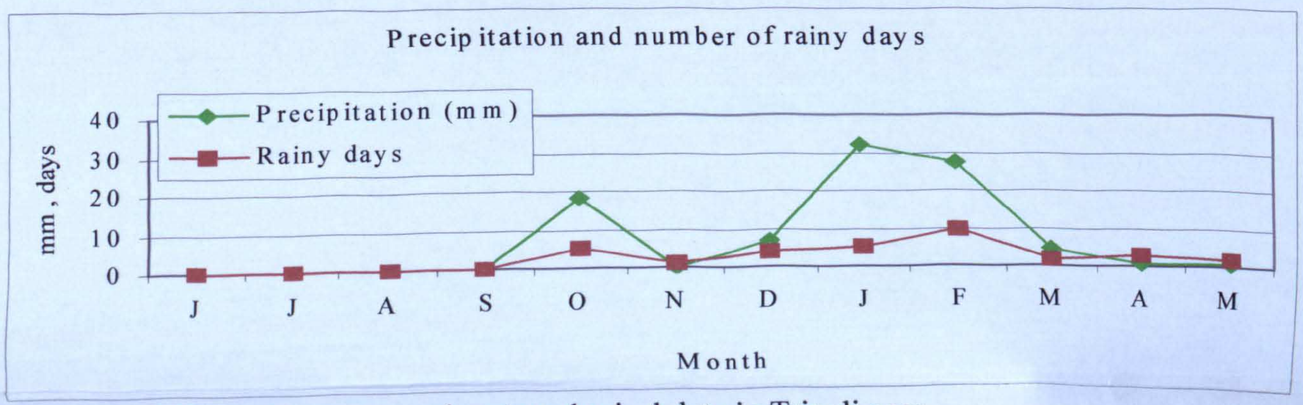

Figure 6.11 Deposition rates and meteorological data in Tripoli area

6.4.1.3. Al Khums area

The particle size distributions in this area (Figure 6.14) show a generally higher proportion of clay and silt and decreased sand contents in all of the aeolian samples in comparison to the Zuwarah and Tripoli areas. This observation can be better revealed from the variation of the median particles (Figure 6.12).

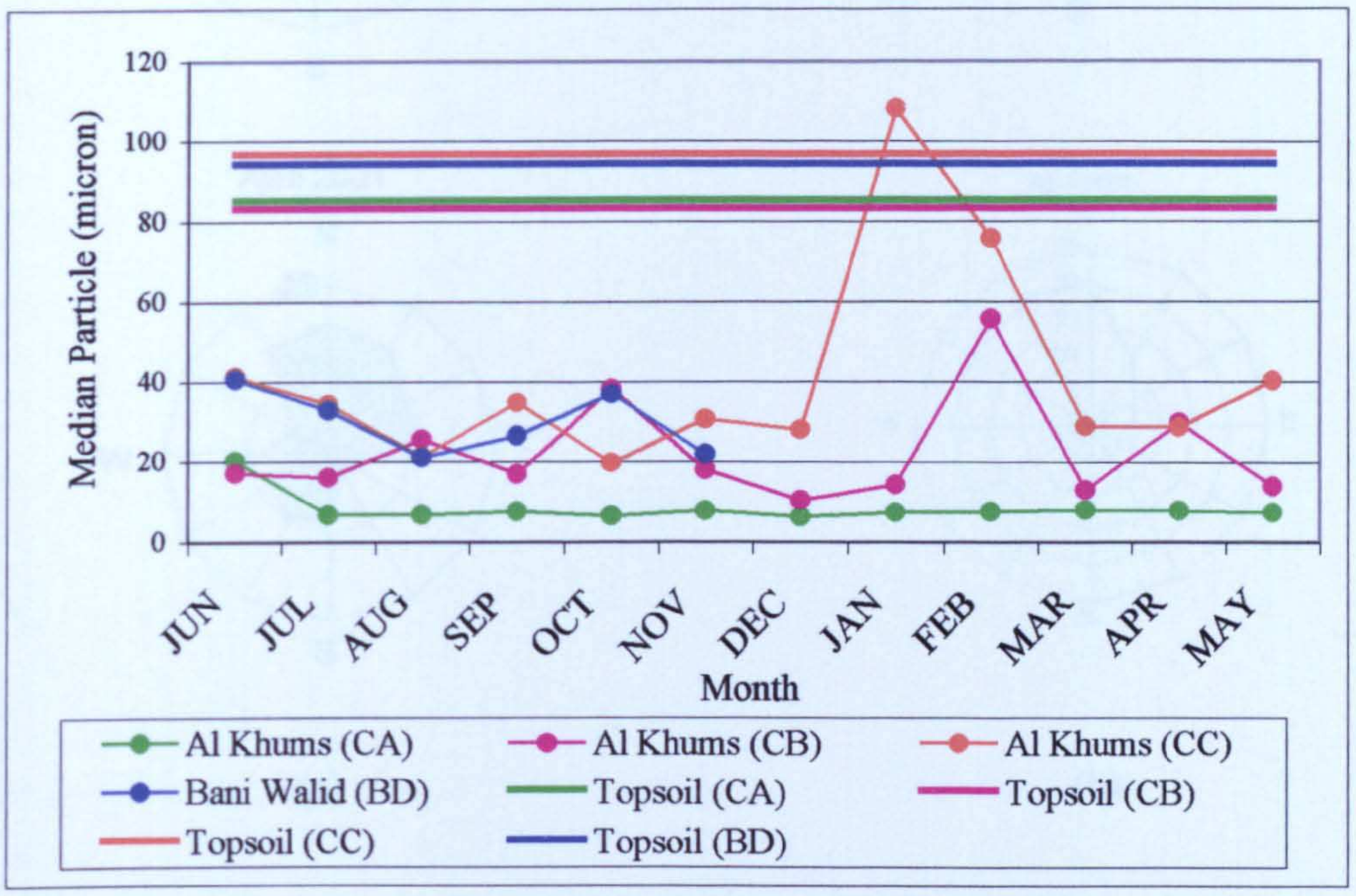

Figure 6.12 Median particles of dust and topsoil

Trapping site CA provided the smallest amounts of trapped dust, probably because it is located further than the other sites from traffic and other human activities and installed on an elevated hilly terrain south of Al Khums. The monthly average deposition rates, a tri-modal seasonal distribution, based on four sites consists of two major peaks correspond to July and April and a small peak corresponds to December (Figure 6.15). The average monthly deposition pattern reasonably correlates with the variation in monthly average velocities, frequencies and atmospheric temperature (Figure 6.15). Precipitation, however, does not correlate with the average deposition pattern. For example, there was more rain during February than December where the latter experienced a similar deposition rate. Oceanic aerosols may have contributed to the clay fraction of dust sediments during the summer and spring, at times of prevailing winds from north (Figure 6.13).

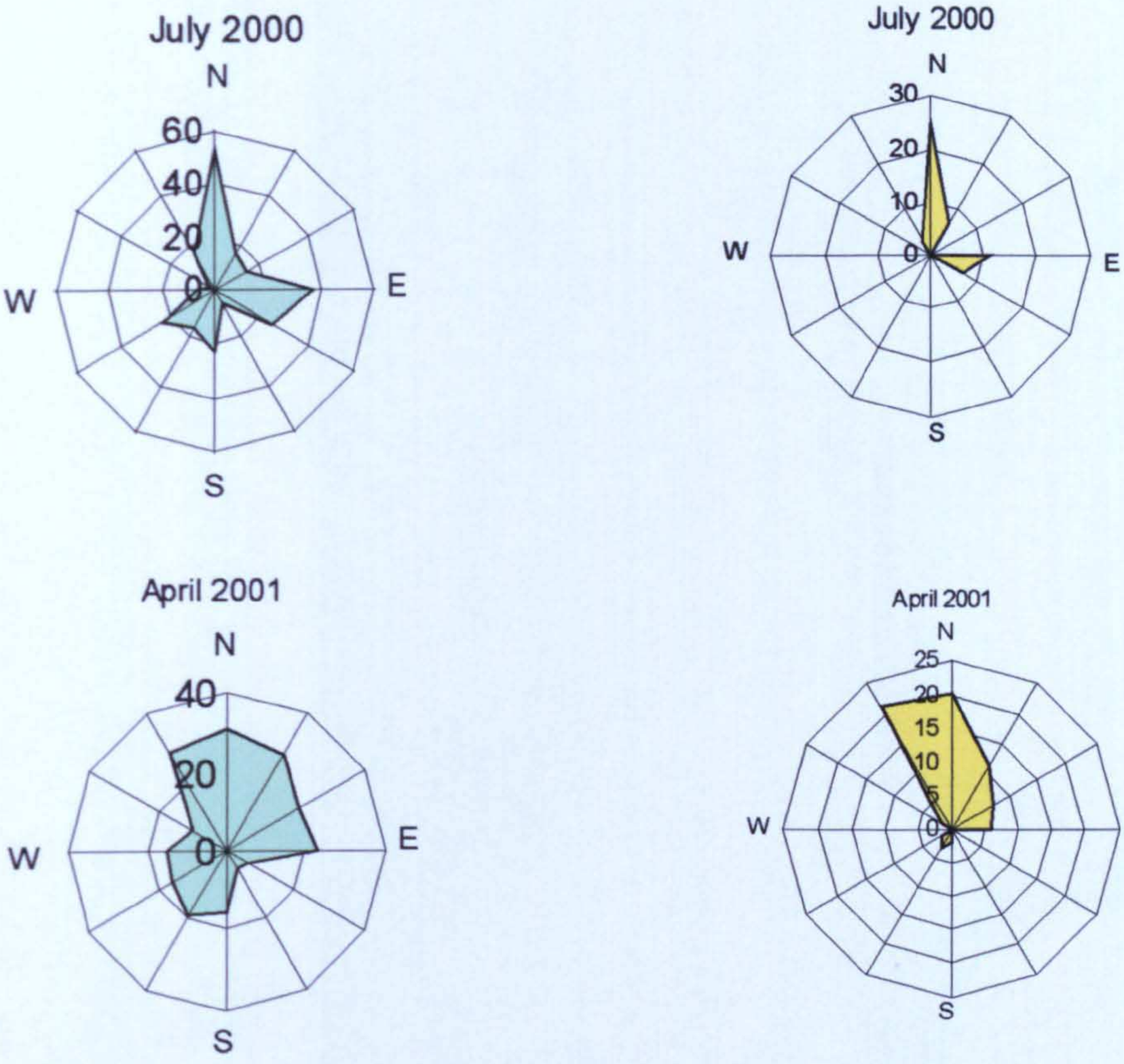

Figure 6.13 Prevailing winds during July and April at Al Khums based on (a) all wind velocities (b) velocities ≥ 6.5 m/s

Since Al Khums area is incised by several major wadis and the general trend of particle size distributions is characterized by a higher content of clay (Figure 14), the fine fractions of deposited aeolian sediments can be attributed to wadi alluvial sediments especially during the dry seasons. In Bani Walid, wadi sediments are probably more significant due to the large number of wadis present there. Rain-out of aerosols derived from the major Saharan sources and transported over this area may not be very significant during the study period (see Chapter 3 and section 6.4.2). In addition to the fact that Al Khums is a farming area, it is a home of open limestone mines supplying two major cement production plants situated in the same area. Emissions from the cement plants can be seen from several kilometres distance (see the calcite content in Figure 6.22). Therefore, anthropogenic dust can be a significant contributor of a wide range of particle sizes.

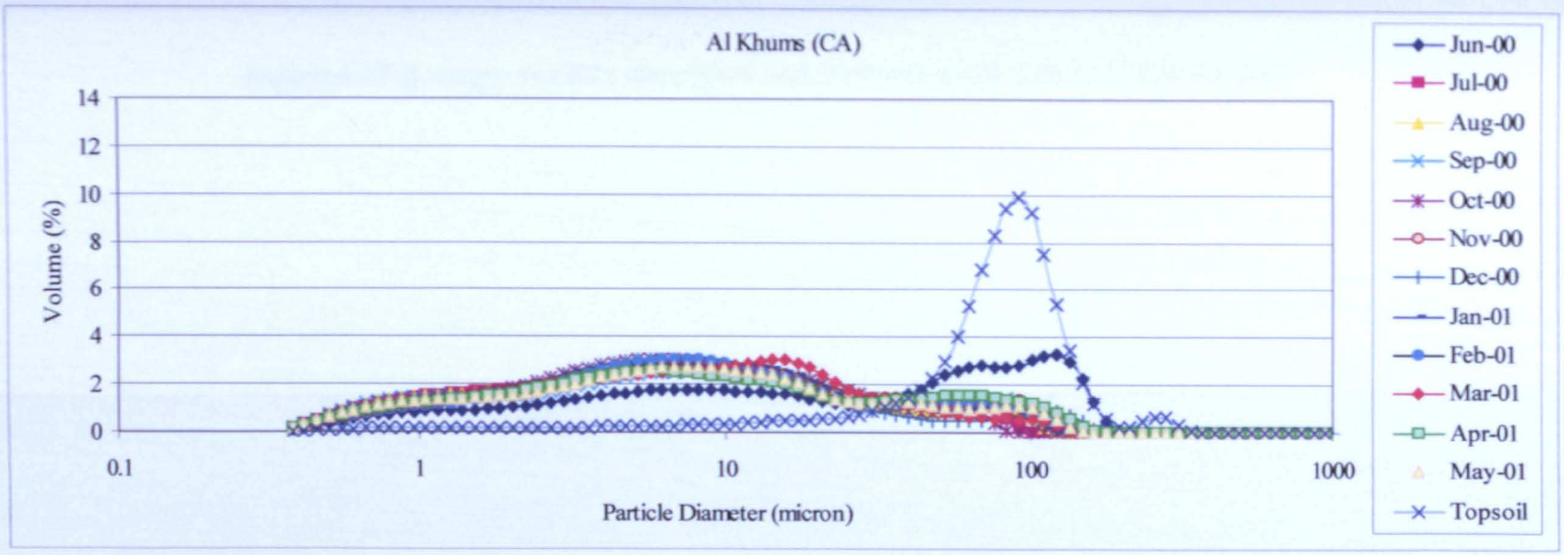

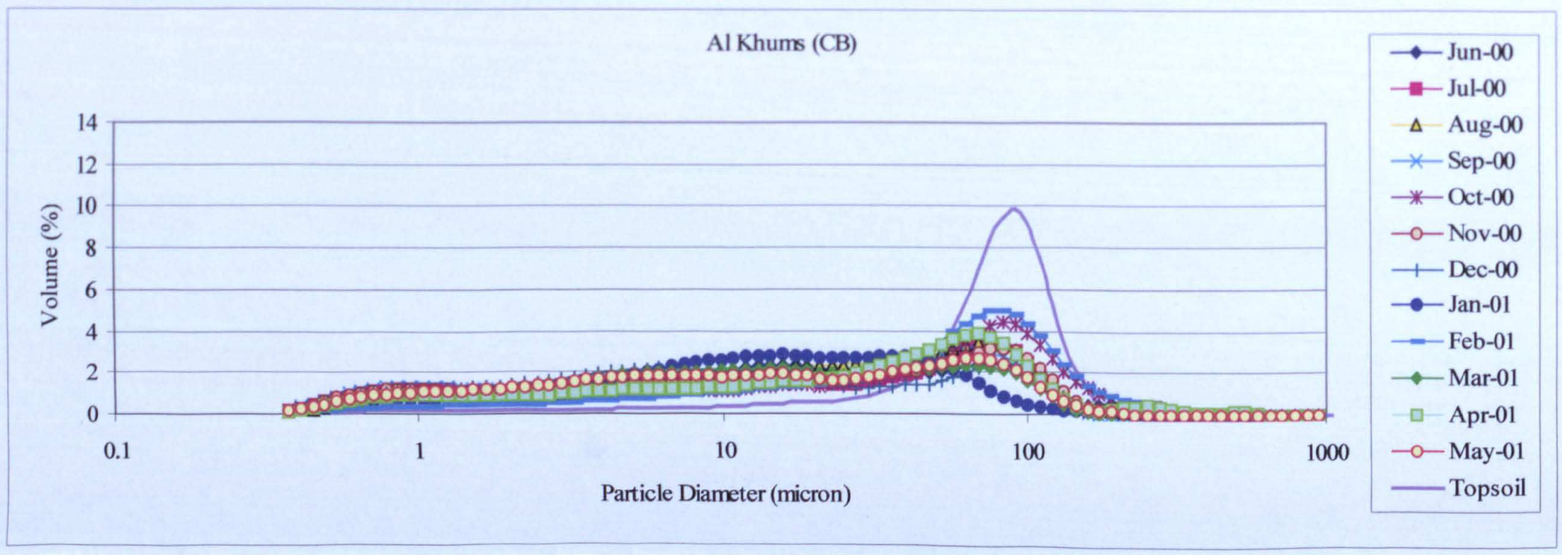

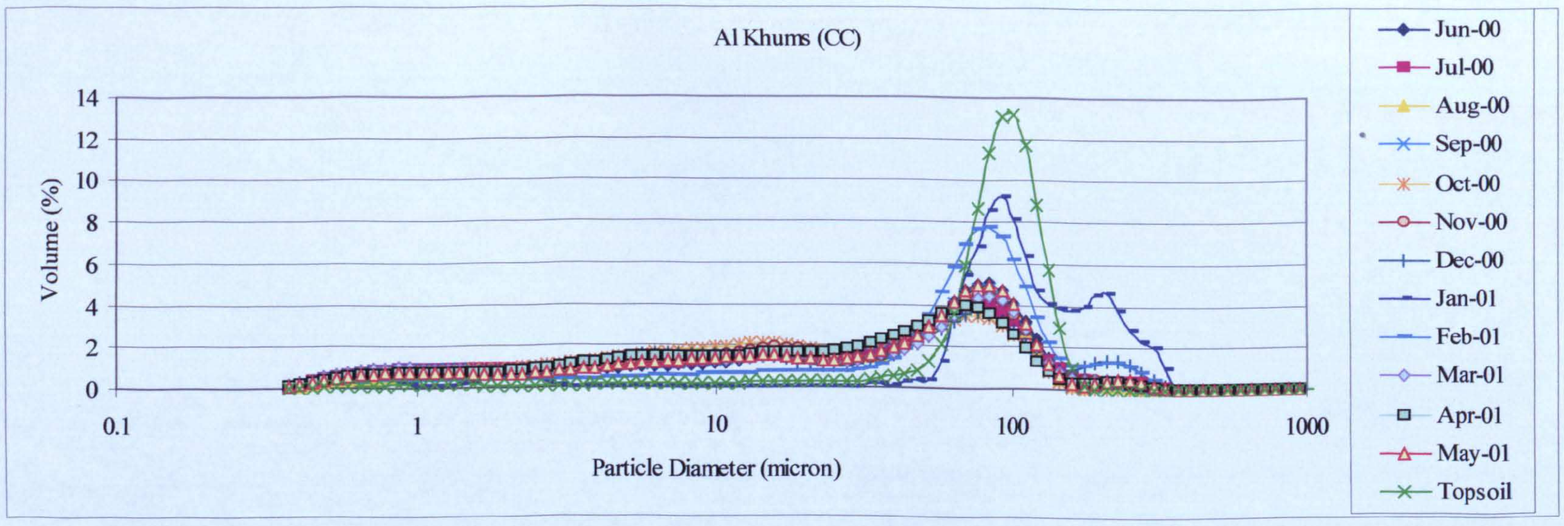

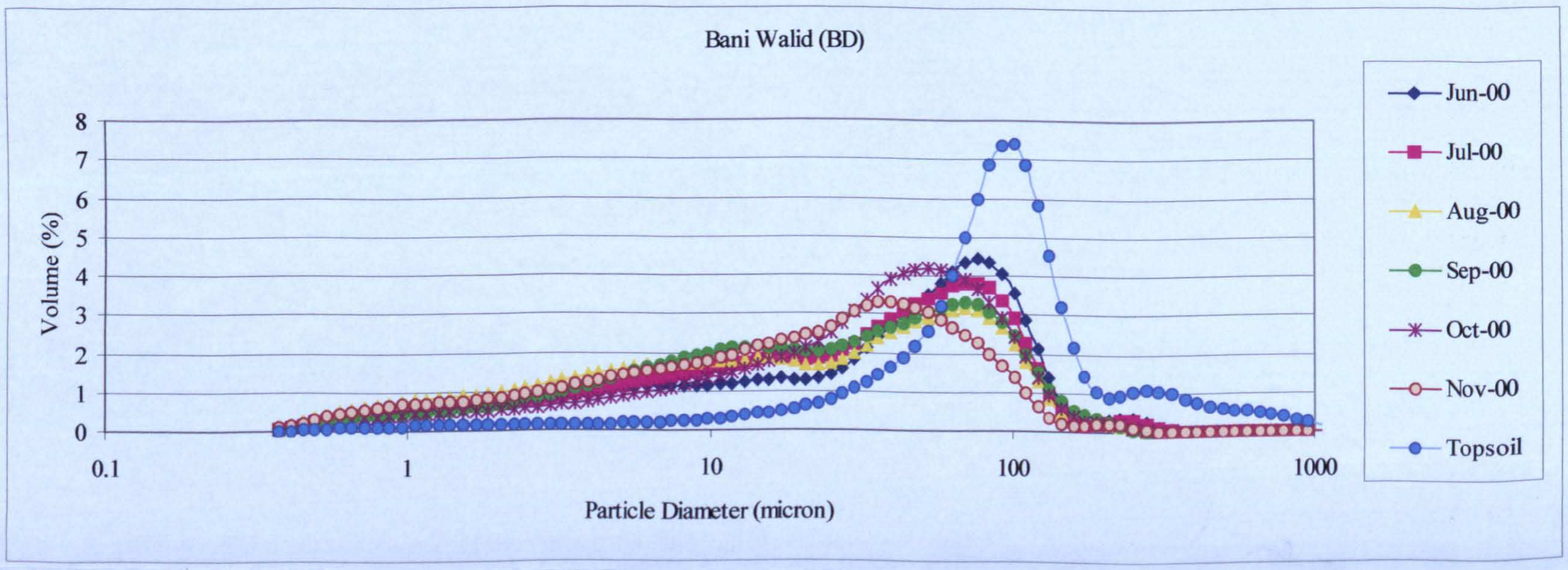

Figure 6.14 Particle size distributions of dust and topsoil in Al Khums area

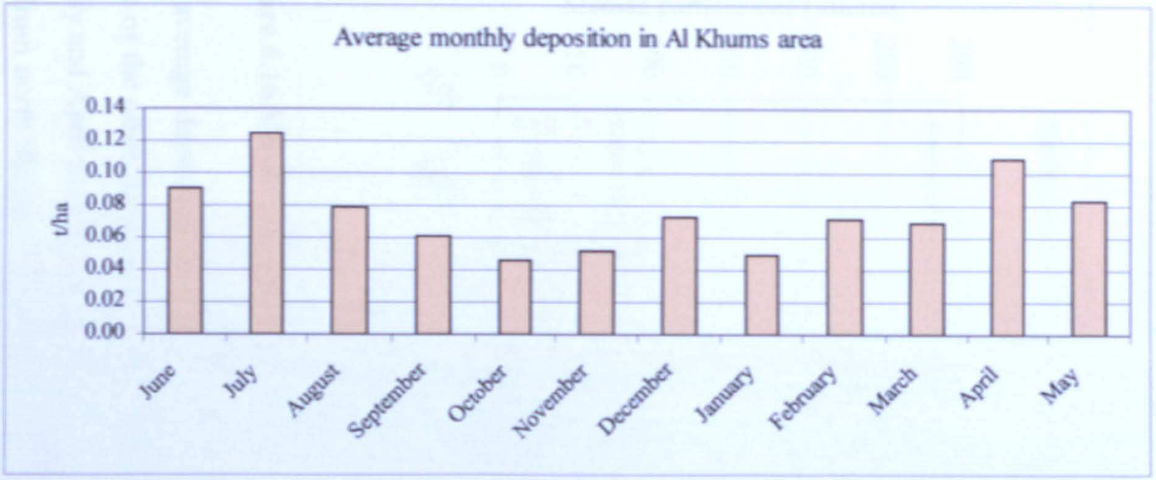

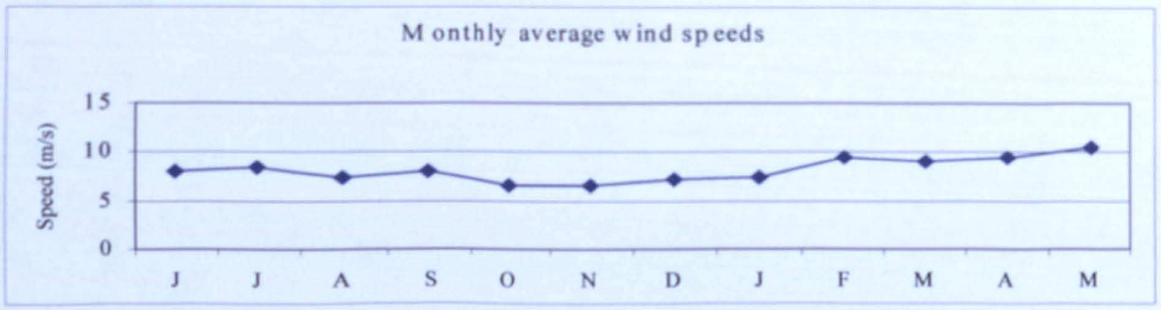

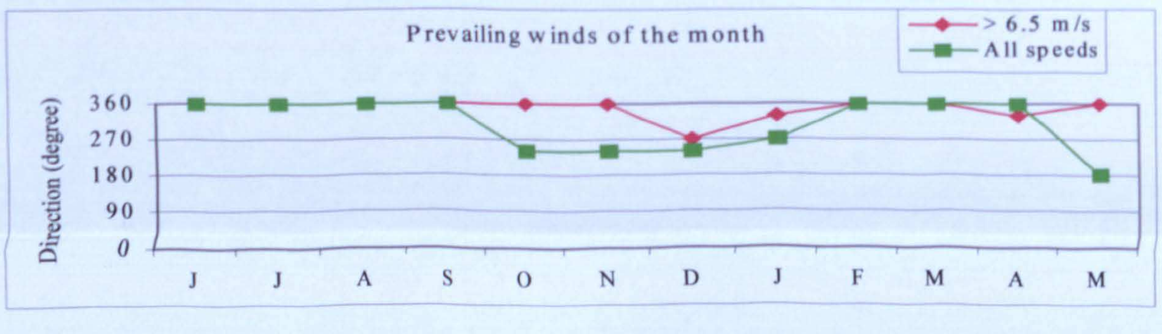

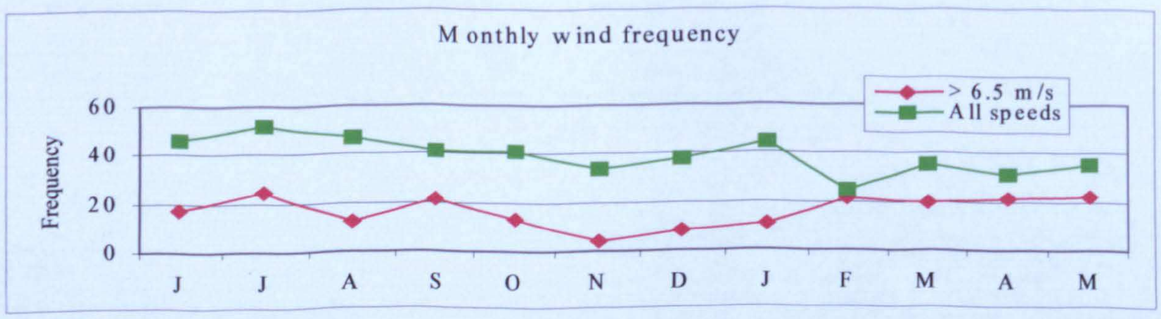

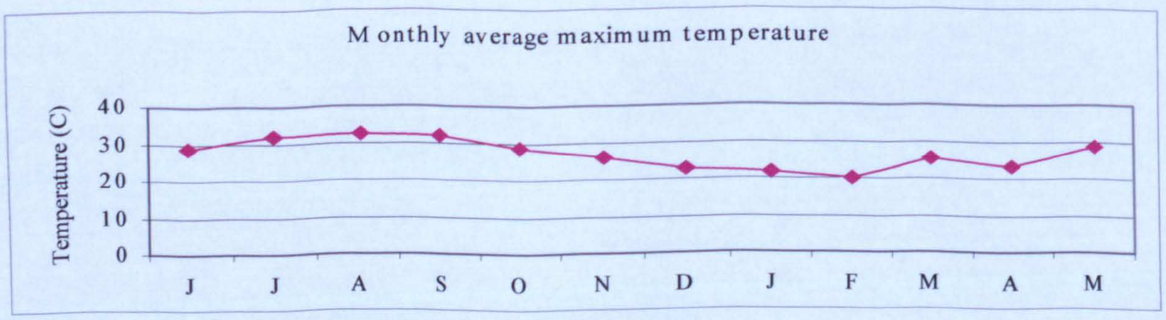

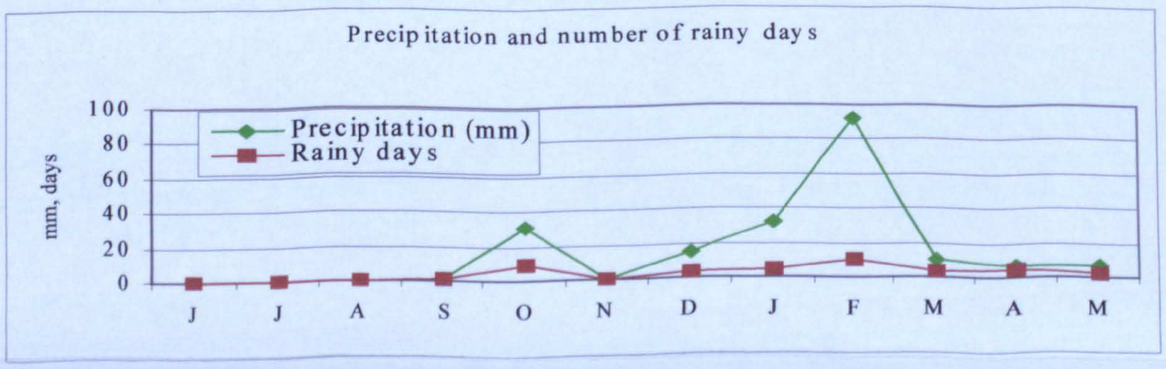

Figure 6.15 Average monthly deposition and meteorological data in Al Khums area

6.4.1.4. Misratah area

The frequency plots of all the aeolian samples (Figure 6.18) are multi-modal distributions with a main mode within 63 to 69 μm. The median particles of the aeolian samples are largely comprised of coarse silt where the topsoil is within very fine to medium sand (Figure 6.16).

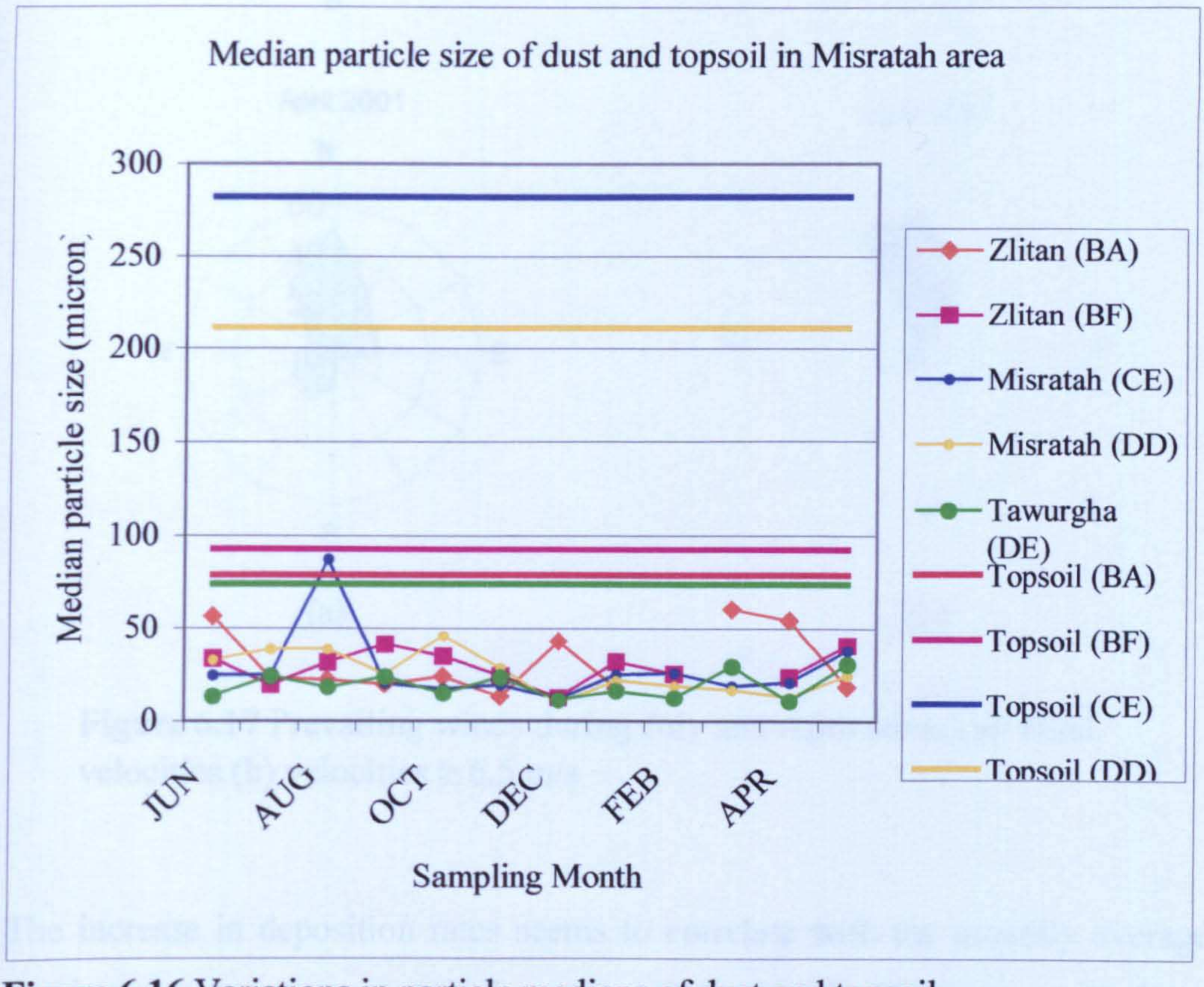

Figure 6.16 Variations in particle medians of dust and topsoil

The average deposition pattern in this area (6.19) follows a similar trend as those of the other three areas in the north with the highest rates corresponding to July and April under prevailing winds ranging from north to east during July and from north during April (Figure 6.17). Although, April was dominated by winds from the north, winds from south west at velocities lower than 6.5 m/s reached 19 events. Despite the absence of aerosols in the troposphere during the spring months (see section 6.4.2), winds from south west during April may have brought some aerosol at altitudes of less than 2 km along north eastern trajectories at times of significant emissions at the major Saharan sources.

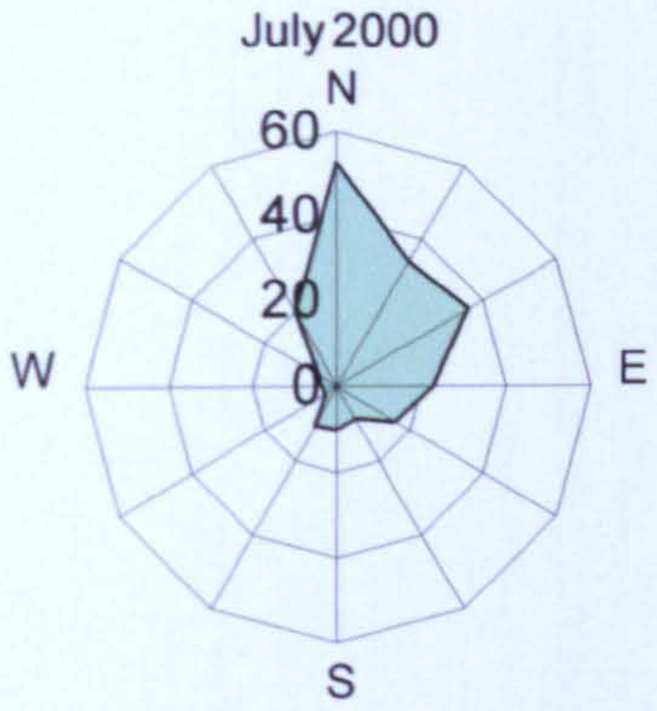

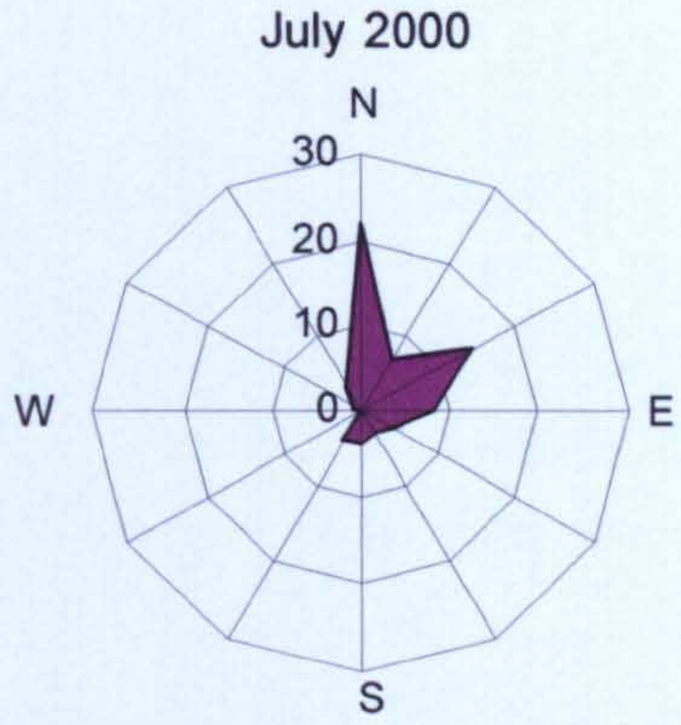

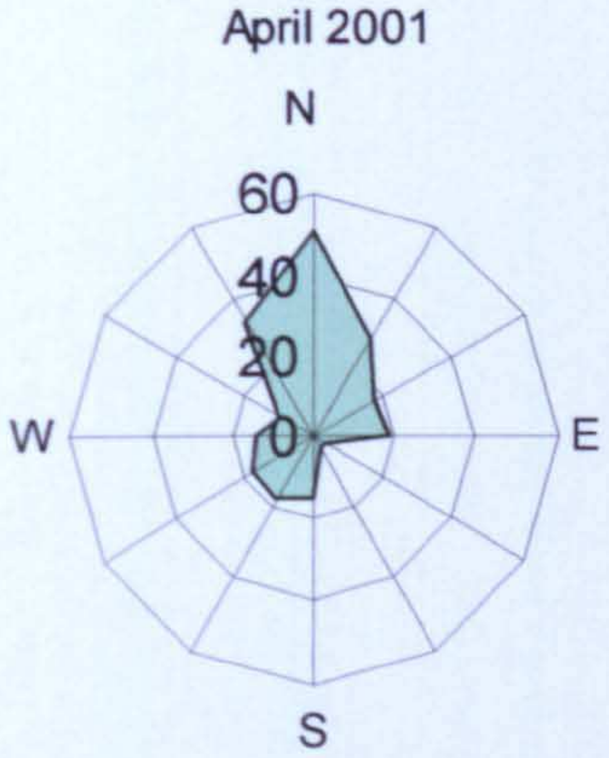

(a)

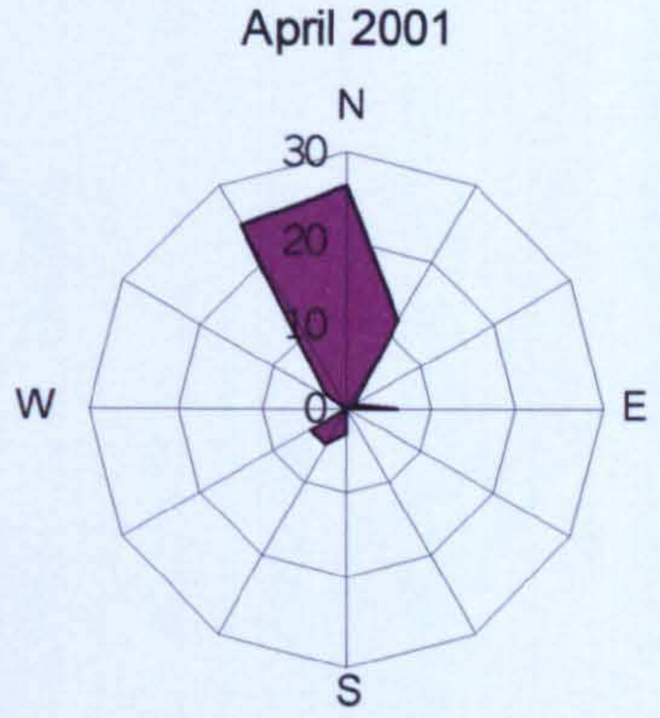

(b)

Figure 6.17 Prevailing winds during July and April for (a) all wind velocities (b) velocities ≥ 6.5 m/s

The increase in deposition rates seems to correlate with the monthly average maximum temperatures and decrease with precipitation that could have cemented topsoil and reduced the effect of horizontal particle flux.

Since this area was under considerable effects of easterly winds during June and July, the only months during which long range transport aerosols were detected by the Earth Probe, any rainout aerosols can mainly be attributed to the Eastern Libyan Desert.

The mineral composition of dust and topsoil in Misratah (Figures 6.20-6.22) show that all dust samples are largely composed of quartz ranging from 28.8 to 60.4 % whereas in the topsoil is 86.8 %. The highest percentages of quartz correspond to the summer months and the highest monthly average temperatures. Winds above the wind threshold velocities during the summer

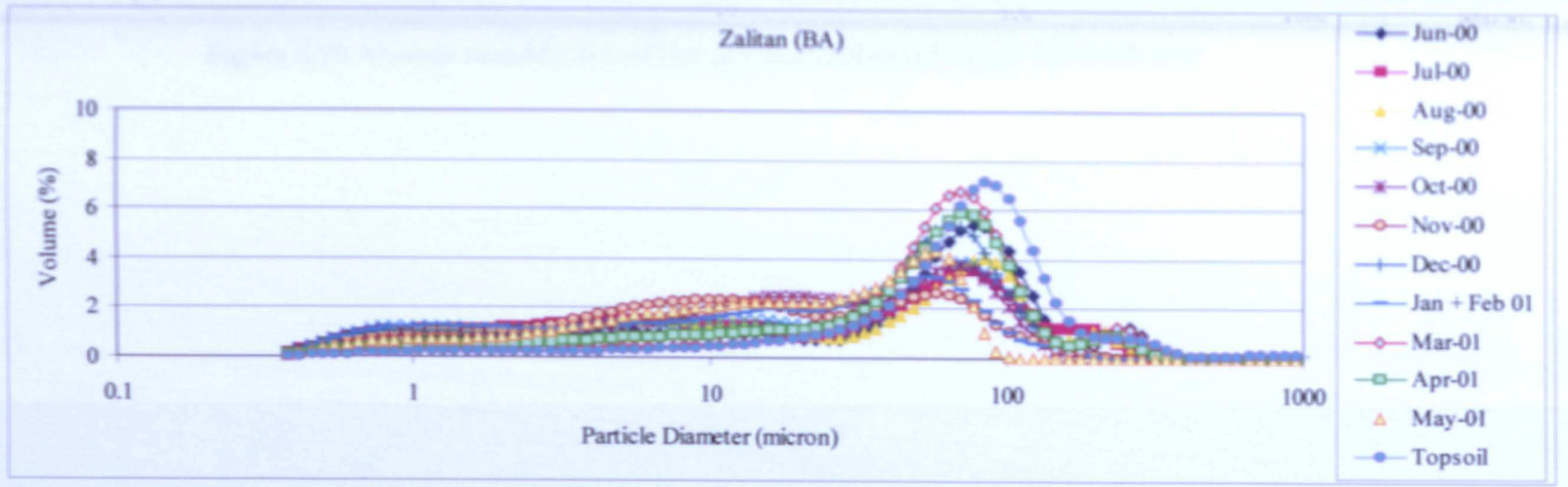

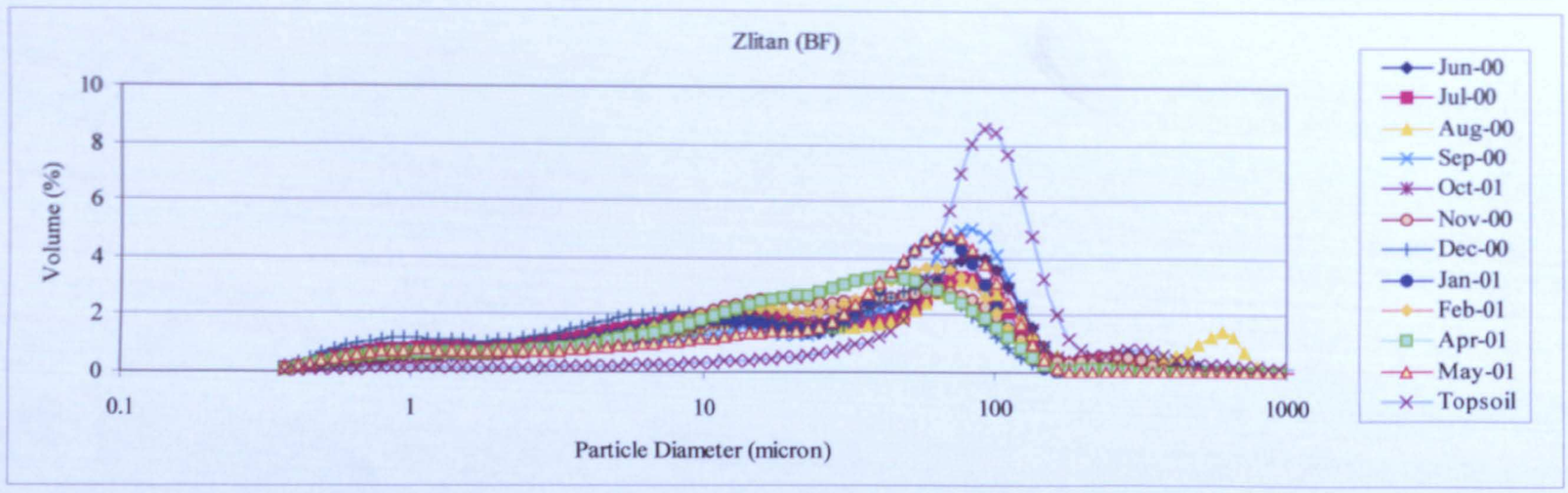

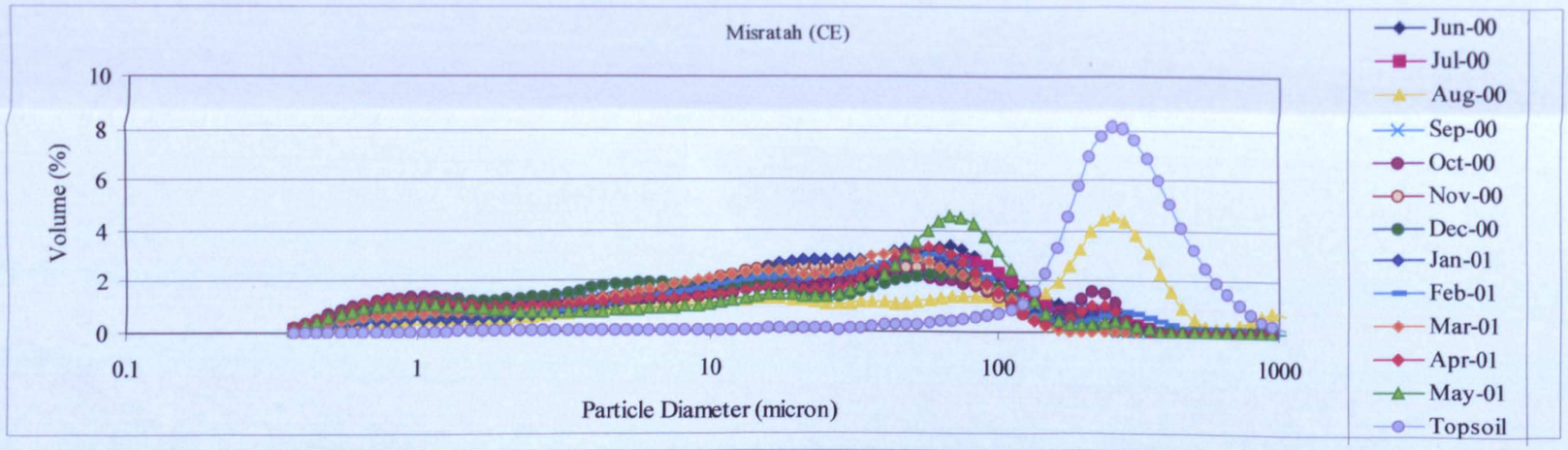

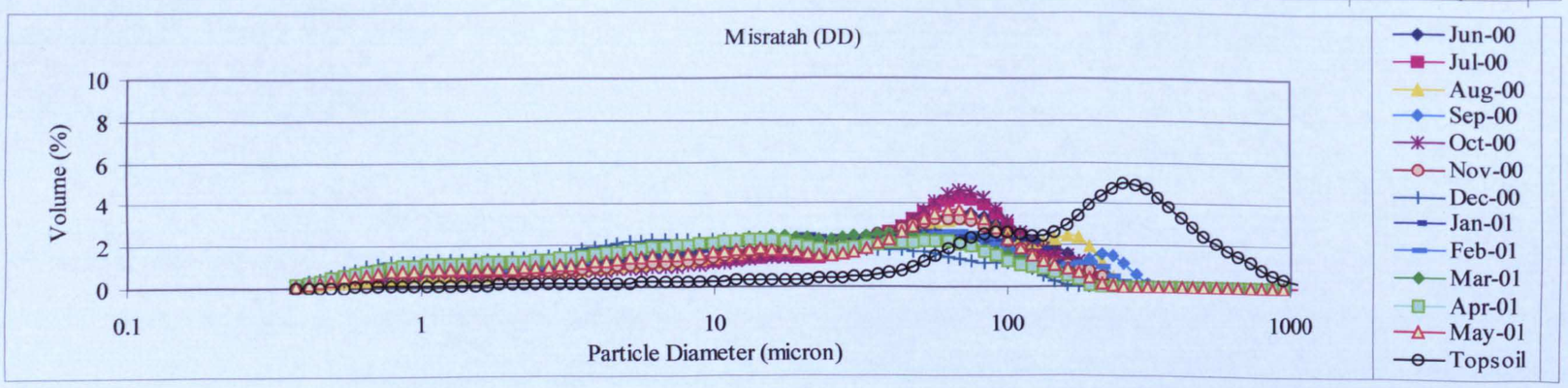

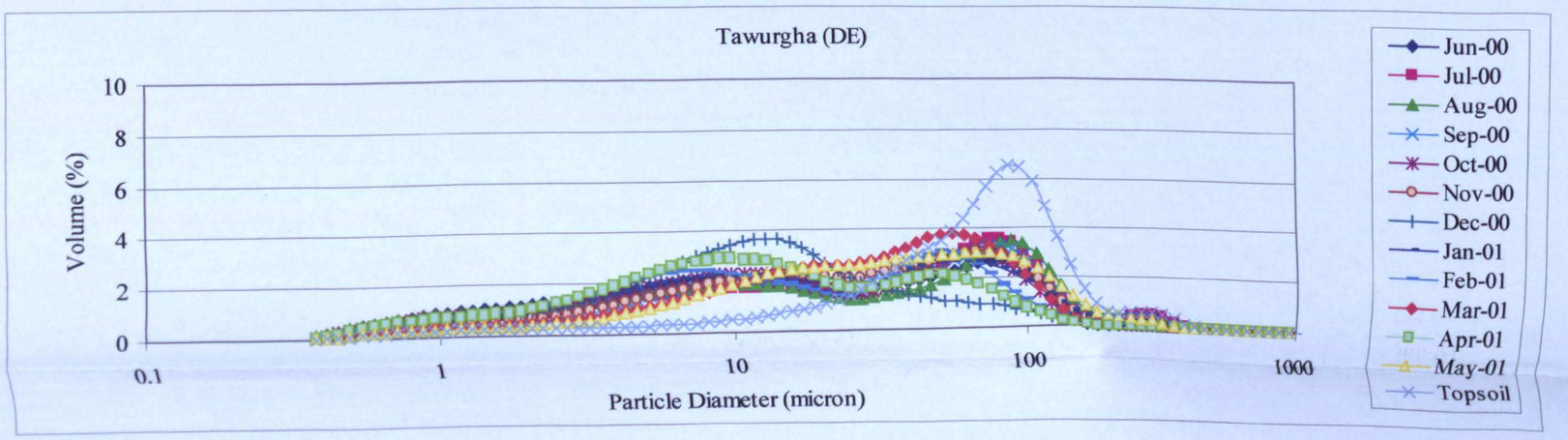

Figure 6.18 Particle size distributions of dust and topsoil in Misratah area

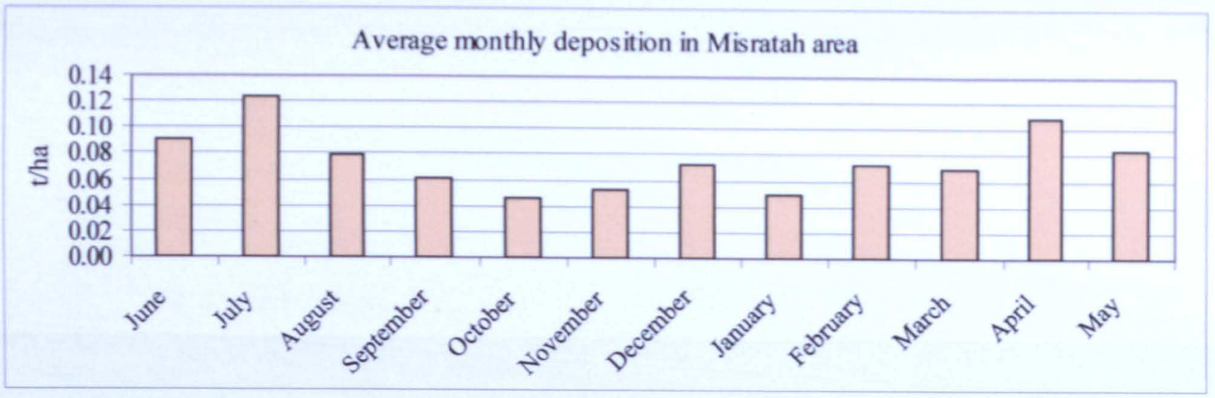

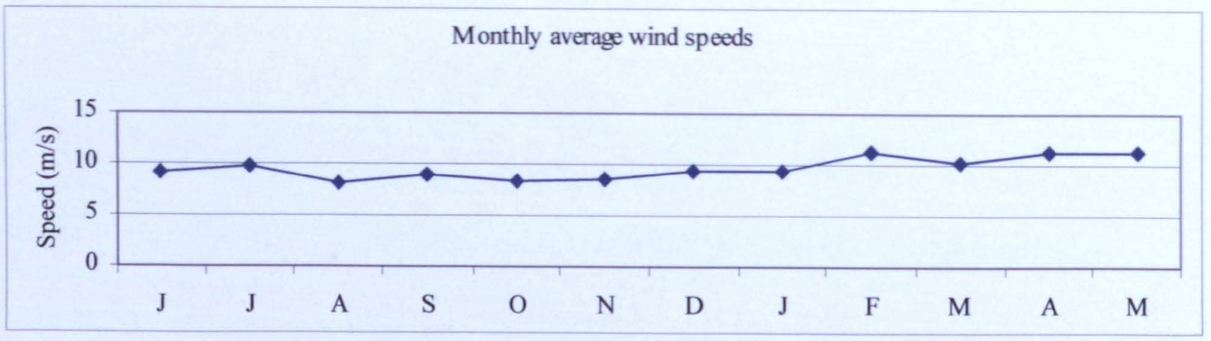

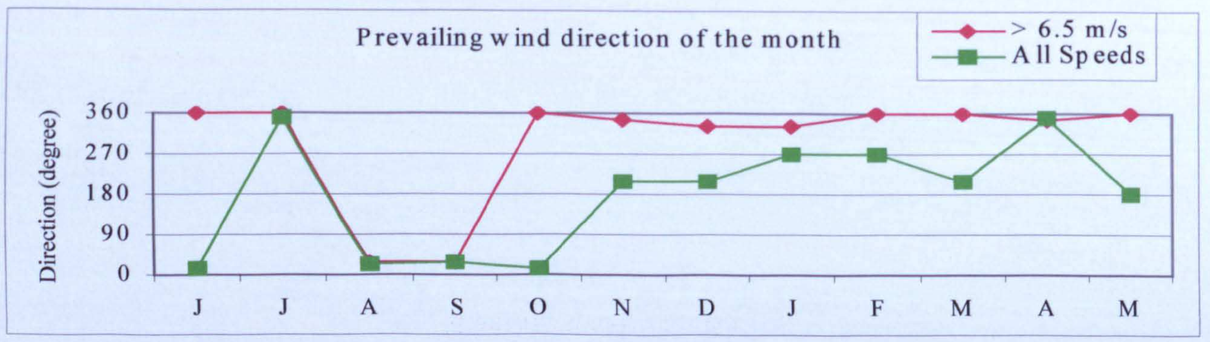

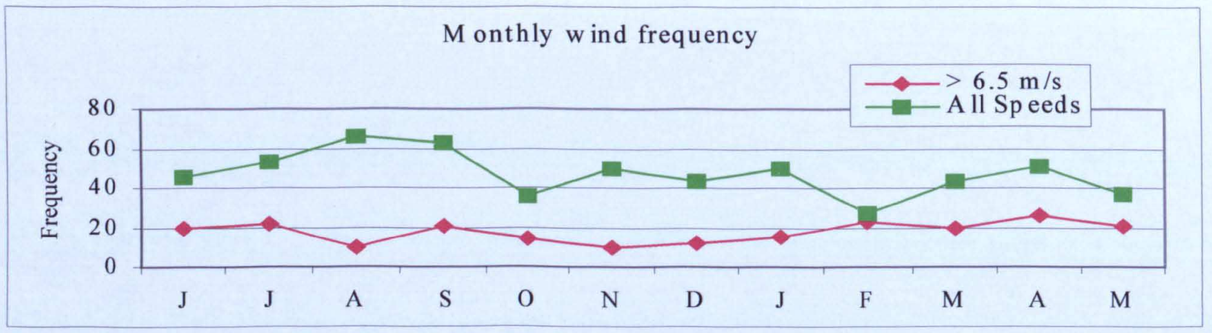

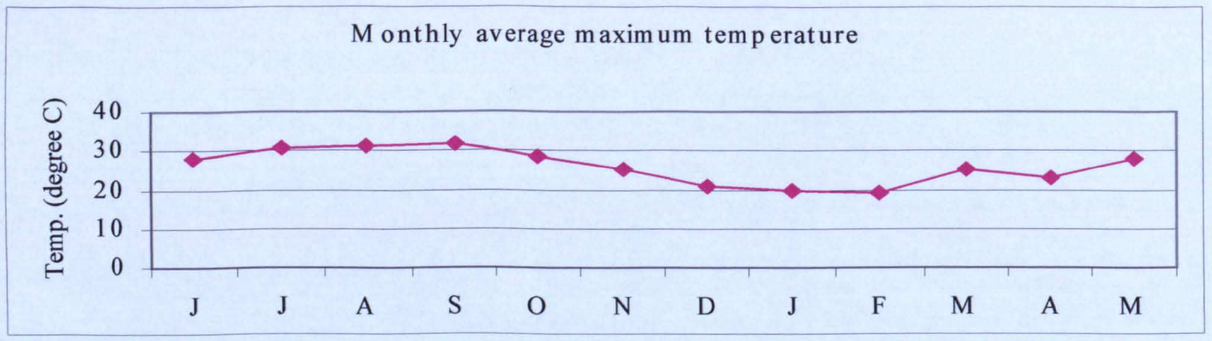

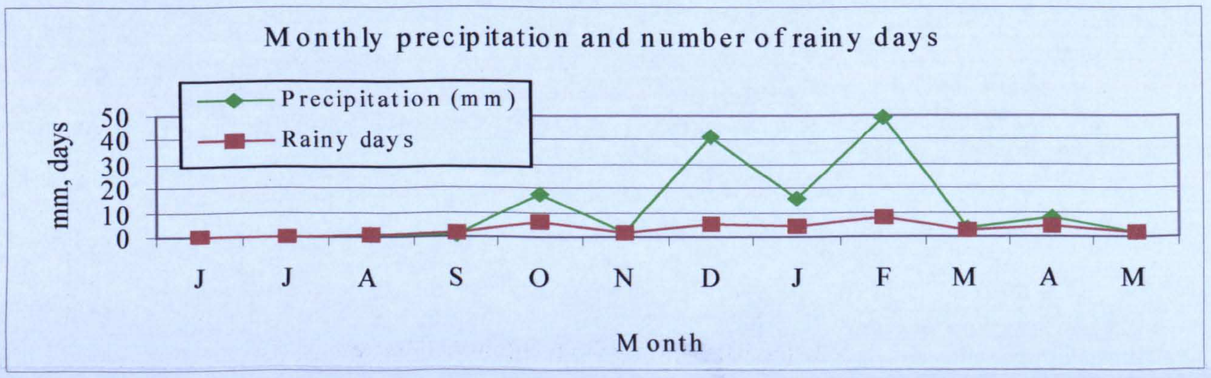

Figure 6.19 Average monthly deposition and meteorological data in Misratah area

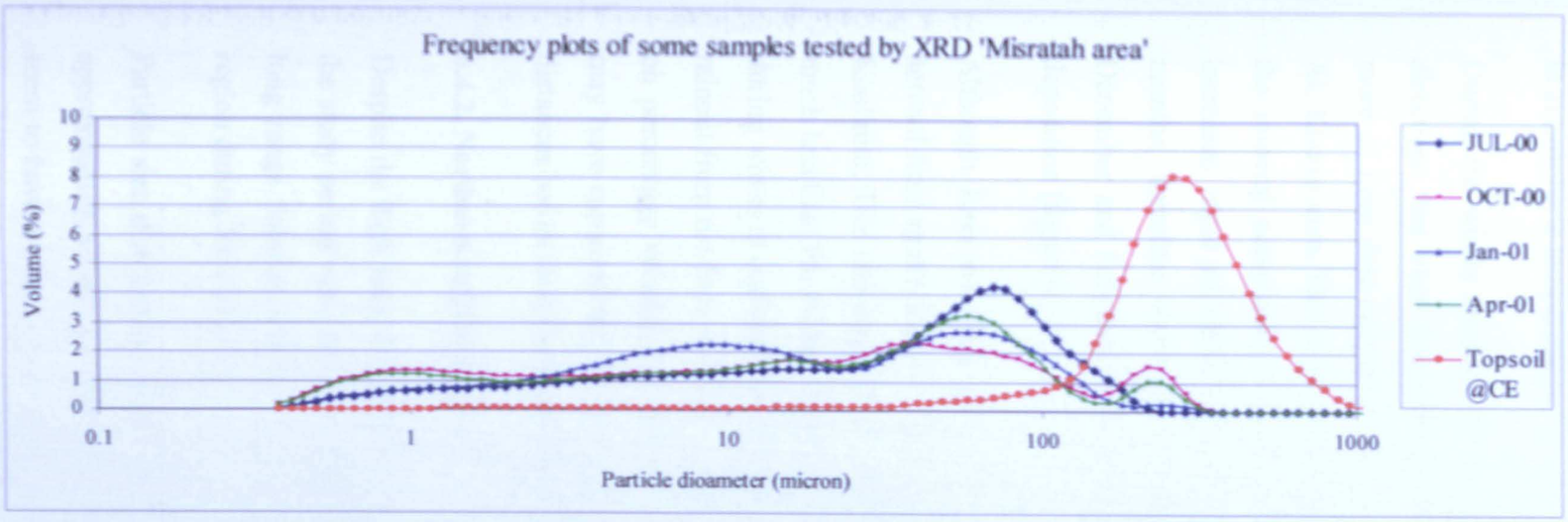

Figure 6. 20 Particle size distributions of dust samples representing four seasons and corresponding topsoil sample test by XRD

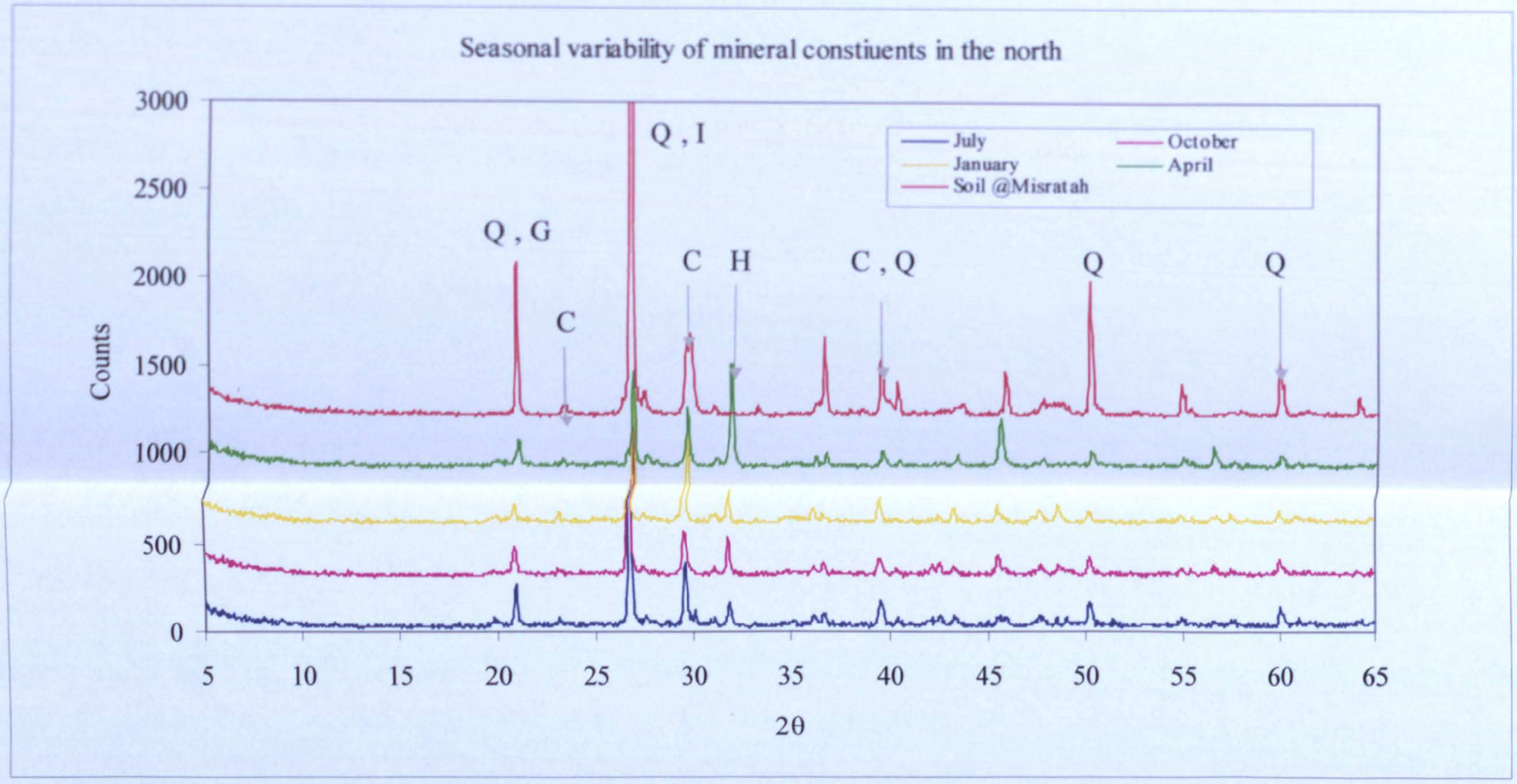

Figure 6.21 XRD of a soil sample and four monthly samples representing the seasonal variability in the mineral constituents of dust deposits in the north for 2 θ between 5 and 65° (Q- quartz, C- calcite, G- gypsum, I- illite, H- halite)

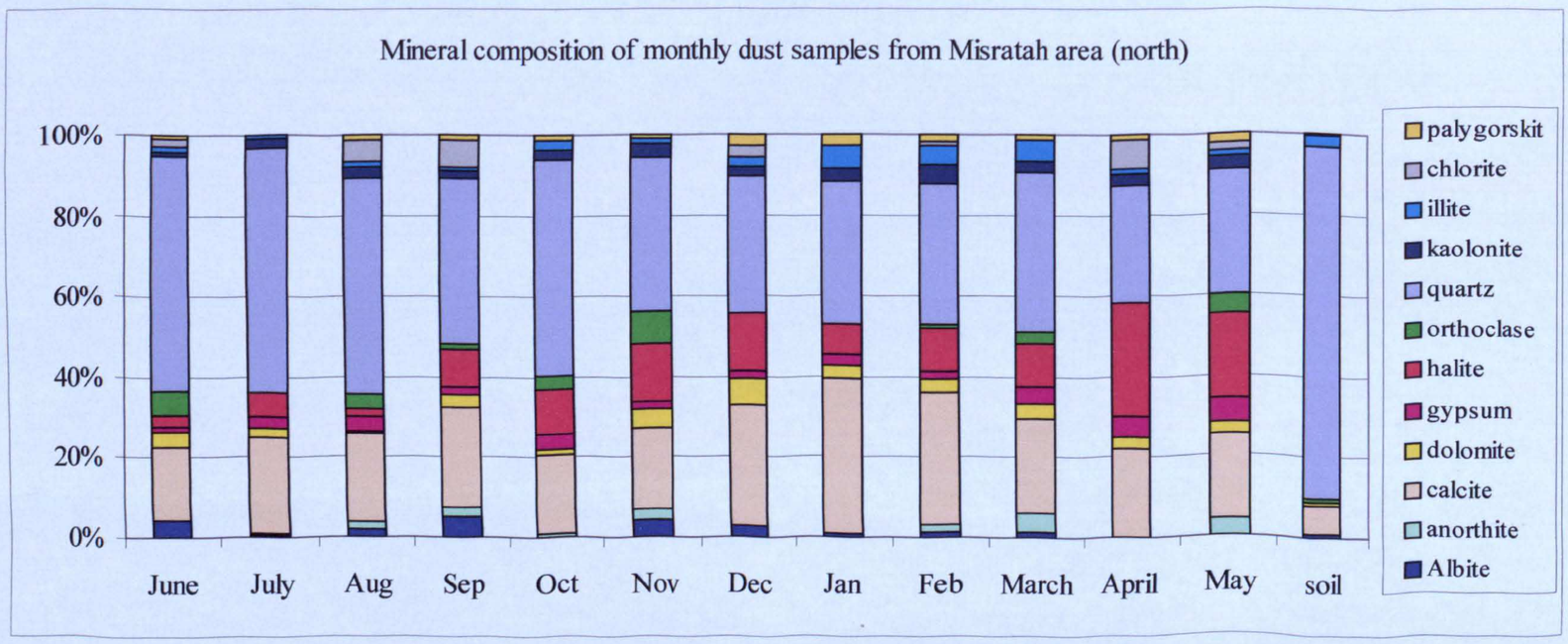

Figure 6.22 Mineral composition of bulk dust and topsoil from Misratah area

months were not more frequent than the other months of the year, therefore the intensive entrainment of local sands was effectively influenced by the increase in atmospheric temperatures.

During the winter months, this area experienced winds from several western directions that were frequently at low speeds which may have drawn some more of finer dust emitted from limestone mines and the cement factories in AL Khums area. This may explain the higher content of calcite and dolomite in the mineral composition of the winter months (Figure 6.22). Furthermore, increased input of calcite and dolomite seems to coincide with the rainy months, therefore wash out of suspended dust in the atmosphere during December and February may have contributed to more calcite and dolomite deposition (figure 6.19).

Although June and July were the only months that experienced detectable aerosol from space (Figure 6.24), Saharan dust diagnostic clay minerals such as Kaolinite, illite and palygorskite in the dust collected during both months were much less than the winter samples. Transport of these minerals from south west during winter at undetectable heights by TOMS may have been greater than the rainout from the June and July plumes. Since the mineral composition is based on percentage volume, the high quartz percentage in June and July samples may have marginalized the percentages of the clay minerals transported long distances before their deposition in this area.

6.4.2. Northern regional trend

Despite the high rates deposited in the northern area, aeolian sediments during the study period were largely emitted from local sources and any rain out from long range Saharan aerosols was in very limited amounts transported to the region during June and July.

Particle size distributions show that a persisting presence of sand particles of approximately within 65 to 100 μm especially in the Tripoli area. Clay and silt seem to have a greater presence in those samples entrapped in the surrounding of Sabkhas, wadis, exposed limestone rocks and emissions from the cement

production facilities. Furthermore, frequent wind from north may have determined the significant contributions of halites. Dust entrained by humans is most pronounced in the samples collected in the Tripoli area, the most populated area of Libya. The grain size distribution of dust collected in the Tripoli area seem to have a very similar trend as the particle size distributions of topsoil samples at the Tripoli sites.

The average deposition rates based on 15 trapping sites in the northern region represent a tri-modal distribution with two major peaks corresponding to July and April, whereas the minor peak corresponds to December and January as shown in Figure 6.23.

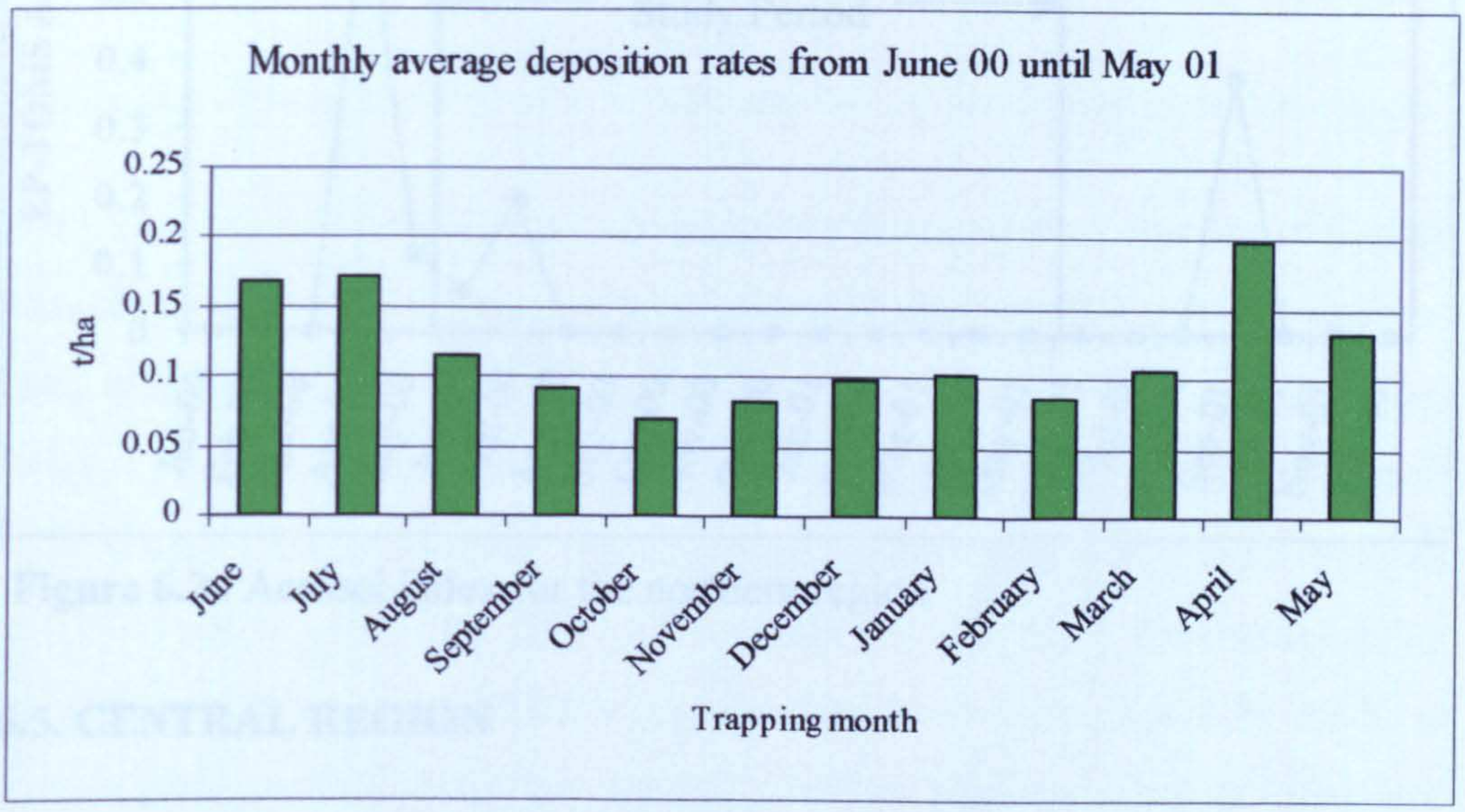

Figure 6. 23 Average monthly deposition rates in the northern region

The highest depositions correspond to an increase in the average maximum temperatures which seem to have boosted the effects of horizontal dust flux. The TOMS data during the study period (Figure 6.24) reveals that aerosol transport over the northern region was limited and occurred only during June and July reaching 0.19 and 0.06 respectively. Although, the highest average deposition rate occurred during April, which coincides with the season of the main Saharan trajectories over this region (Goudie, 2003), TOMS data show that April was aerosol free. While the prevailing winds recorded at all the ground station during June and July were from east, its more likely that the most influential Saharan sources on dust deposition in the northern region is

the Libyan Desert and the narrow strip between the central mountains of Al Haruj Al Asuad and the Libyan Desert. Since the long range transport of dust was very limited and the deposition rates are significant, this region can be regarded as a high emission but, locally transported dust. Although this study is based on a one year data, it highlights the significance of the emission map created by Callot, et al. (2000) (see Figure 3.5) which rates the north western coastal region of Libya as one of the highest emission parts of the Sahara.

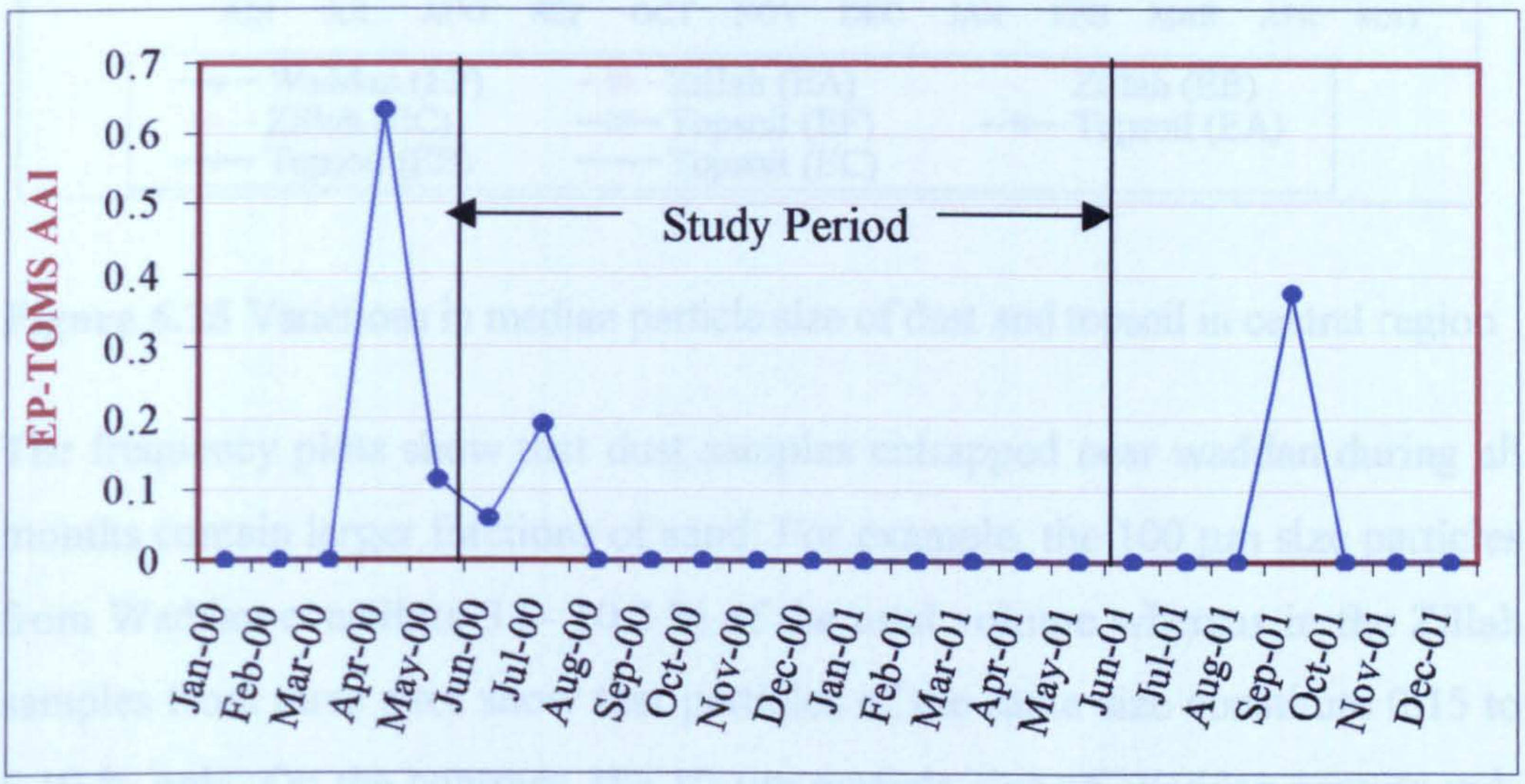

Figure 6.24 Aerosol index for the northern region

6.5. CENTRAL REGION

6.5.1. Sediment characteristics and deposition patterns analysis

The frequency plots (Figures 6.26) and the variations in median particle size of collected dust (Figure 6.25) show that the winter samples contain finer sediments, possibly due to the lesser effect of horizontal flux created by two precipitation events during December and February (Figure 6.27).

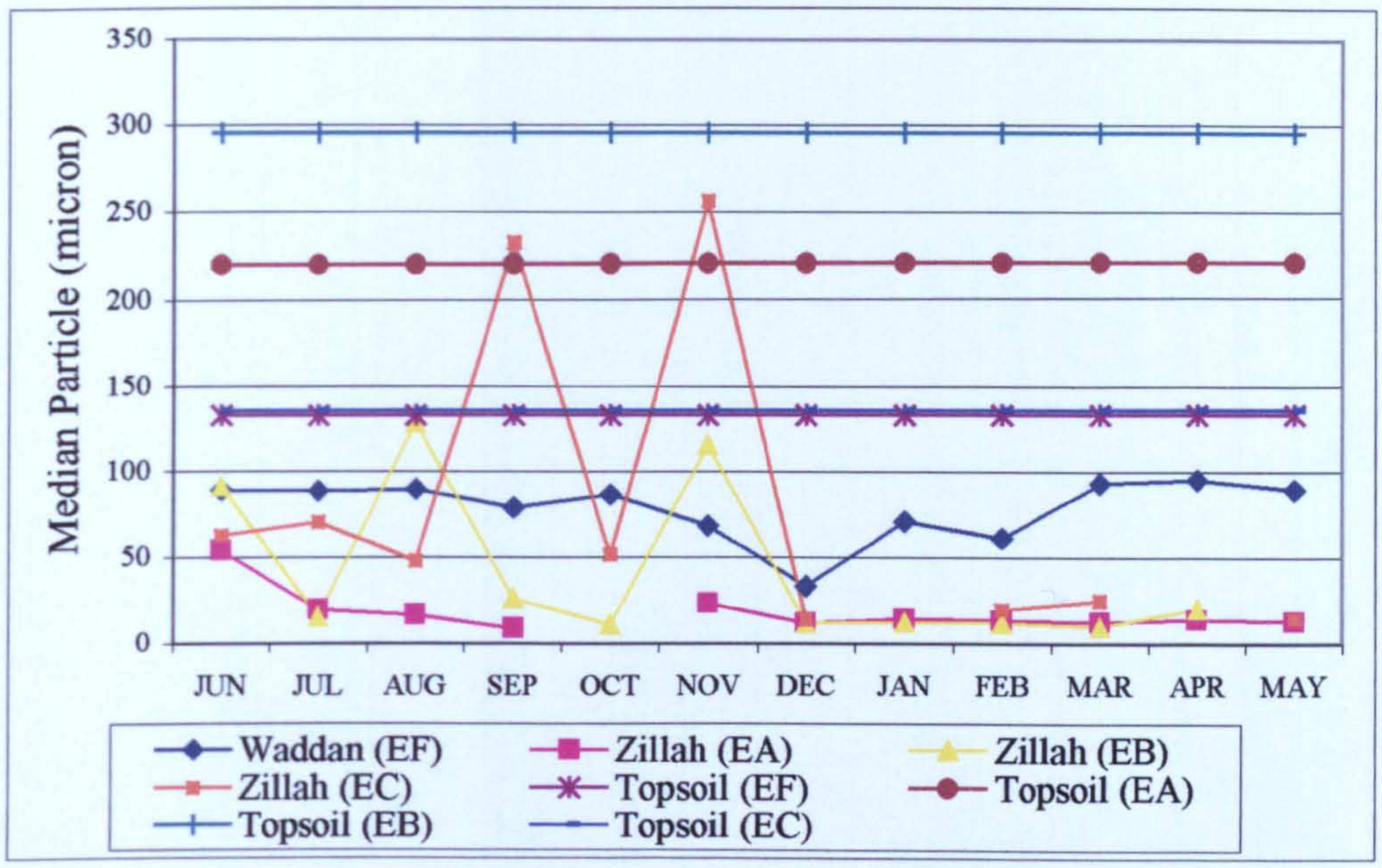

Figure 6.25 Variations in median particle size of dust and topsoil in central region

The frequency plots show that dust samples entrapped near waddan during all months contain larger fractions of sand. For example, the 100 μm size particles from Waddan constitute 3.6- 10.3 % of the total volume whereas in the Zillah samples from three sites show that particles of the same size constitute 0.15 to 6.19 % only. On the contrary, the 10 μm particle size of Waddan corresponds to 0.26- 1.19 % where the Zillah's are within 0.37- 2.75 %. On the one hand, the high sand fraction in Waddan samples may have been caused by the local wind regime controlled by the narrow corridor between Jabal Waddan and Jabal Al soda (see Figures 5.26 and 5.27). On the other hand, Zillah is situated about a 160 km nearer to the Libyan Desert, a persisting Saharan dust source, which may have been the reason for the higher clay fraction volumes in Zillah's samples.

The average monthly deposition (Figure 6.27) represents a distribution with four modes with the highest rates during spring (April and May). The distribution reasonably correlates with the variations in the monthly average winds speeds and the monthly average maximum temperatures. The meteorological data were recorded at 10 km from Waddan, therefore they may not reflect the meteorological conditions at Zillah. Prevailing winds (see wind roses based on ≥ 6.5 m/s) were either from southeast or northwest except during winter months indicating possible funnelling effect by Jabal Al soda and

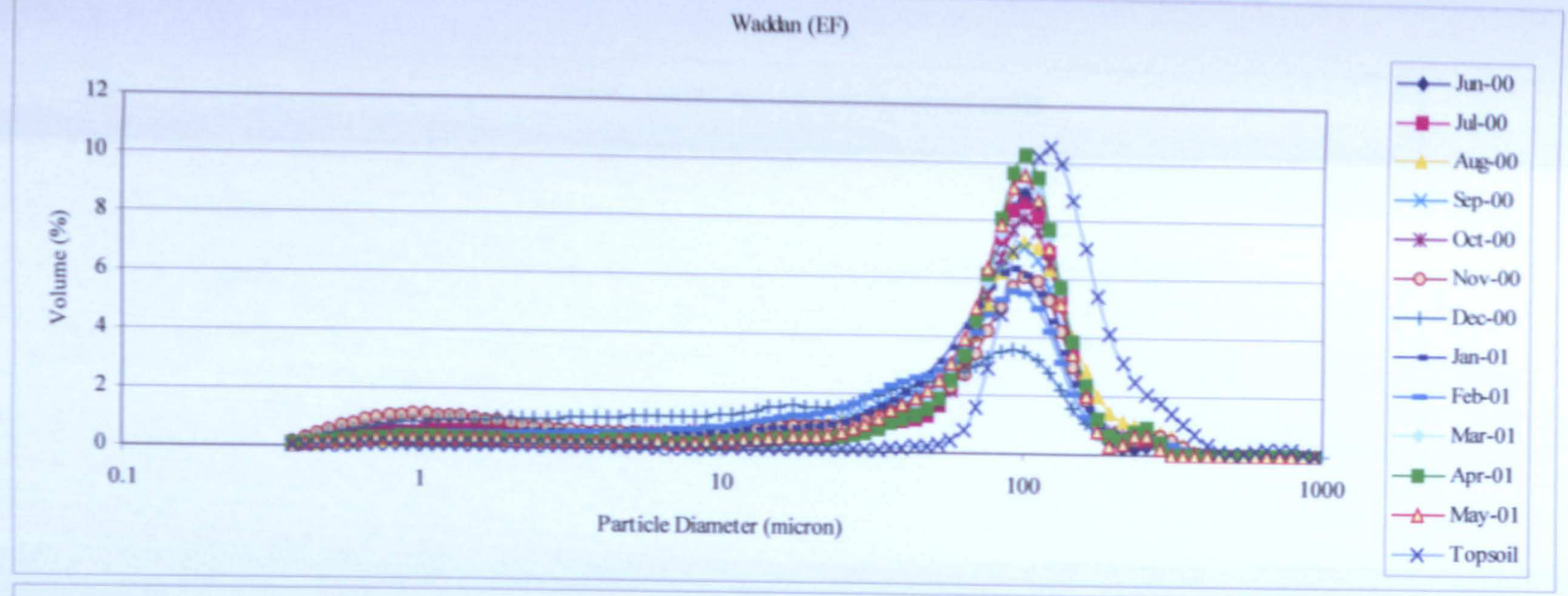

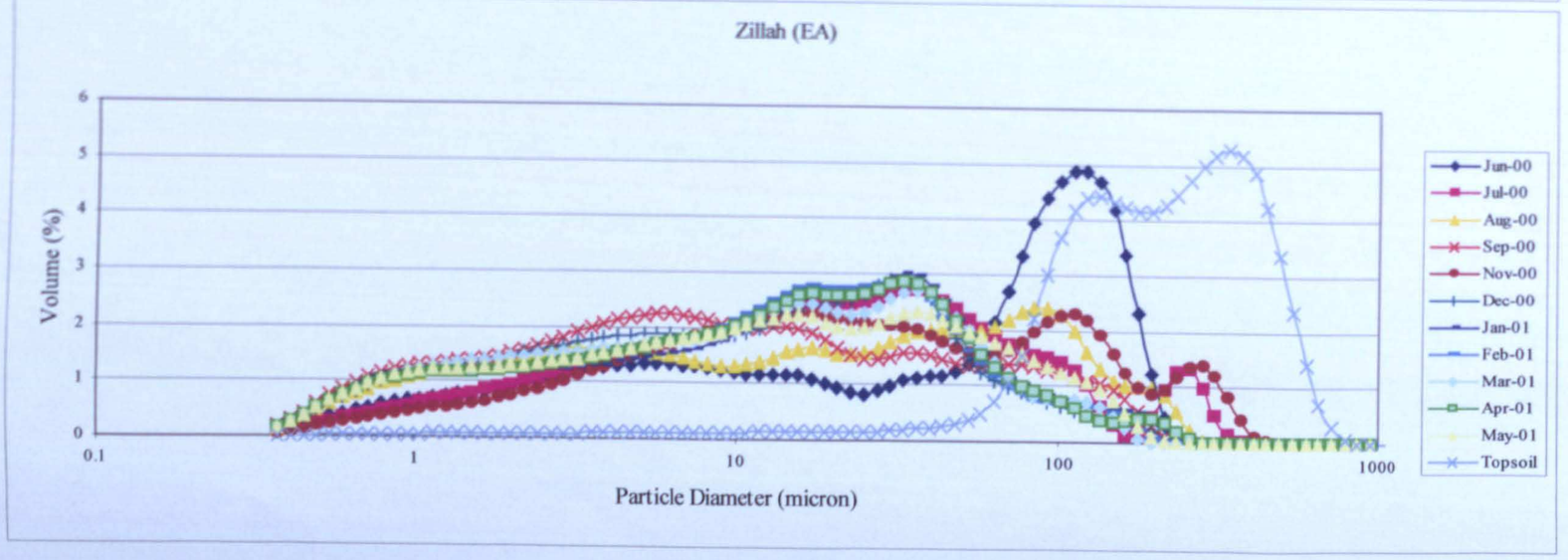

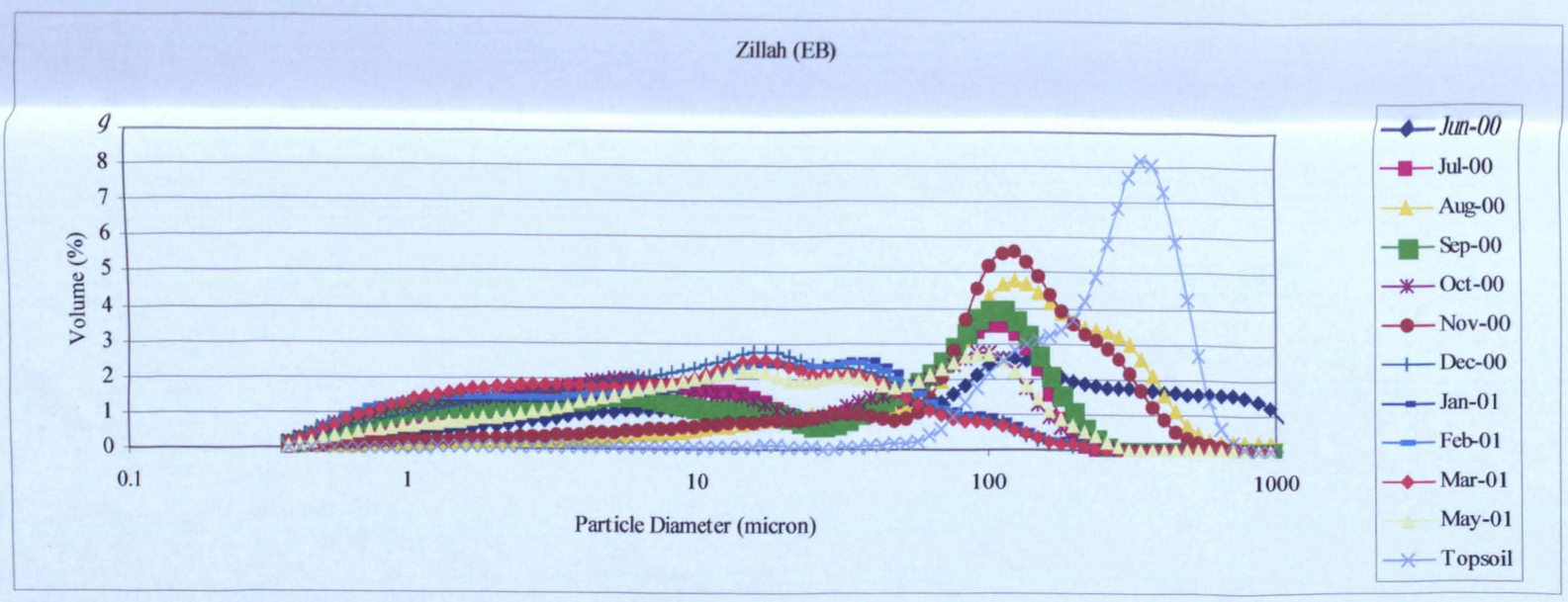

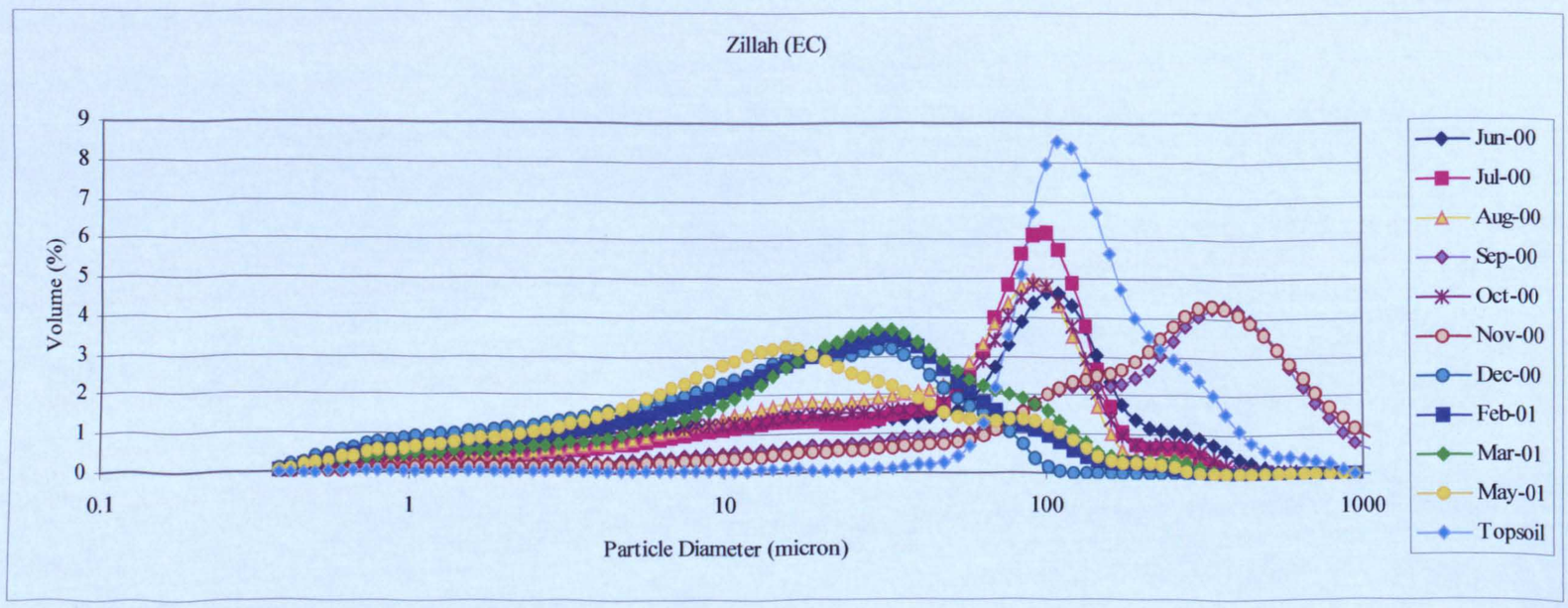

Figure 6.26 Particle size distributions of dust and topsoil in central area

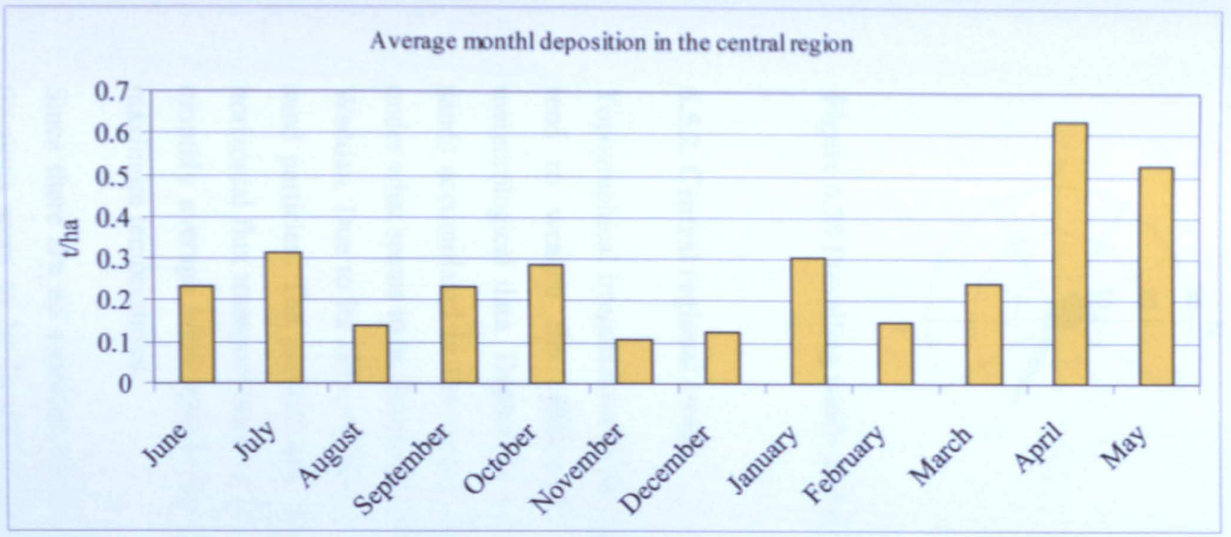

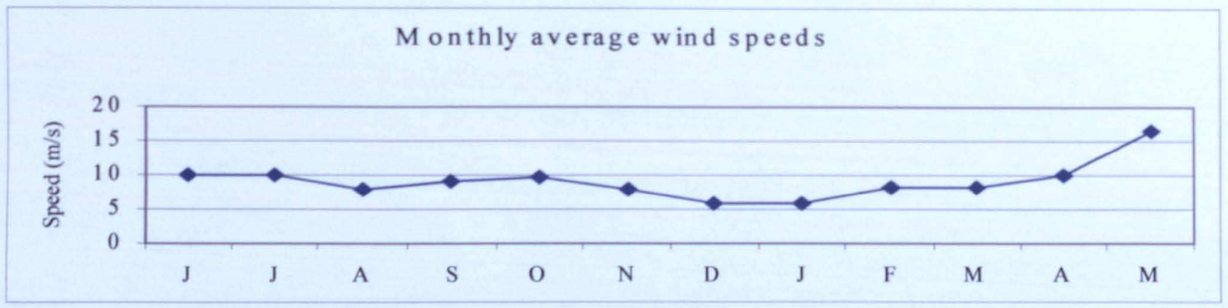

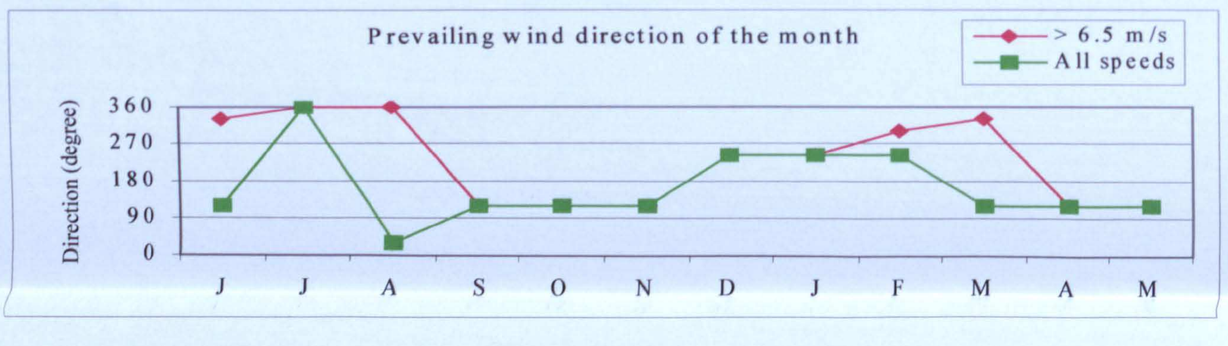

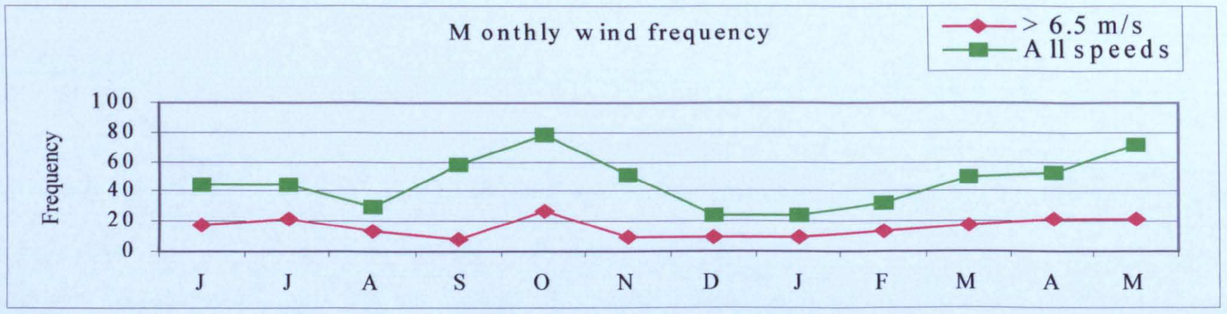

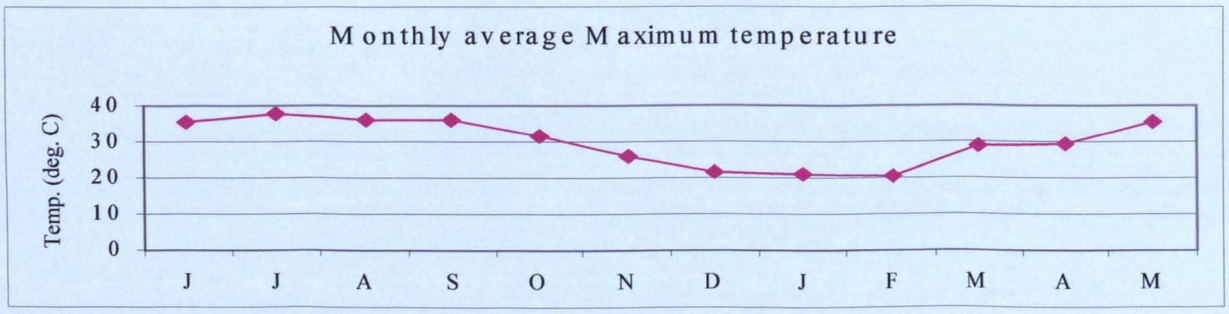

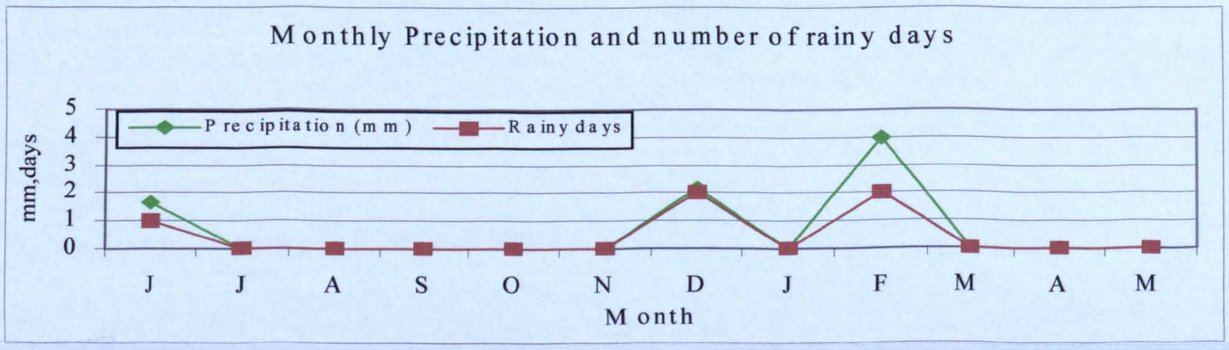

Figure 6.27 Average monthly deposition and meteorological data in central region

Jabal Waddan. This effect, as illustrated by the wind roses, is even more pronounced during the months of highest deposition, April and May (Figure 6.28).

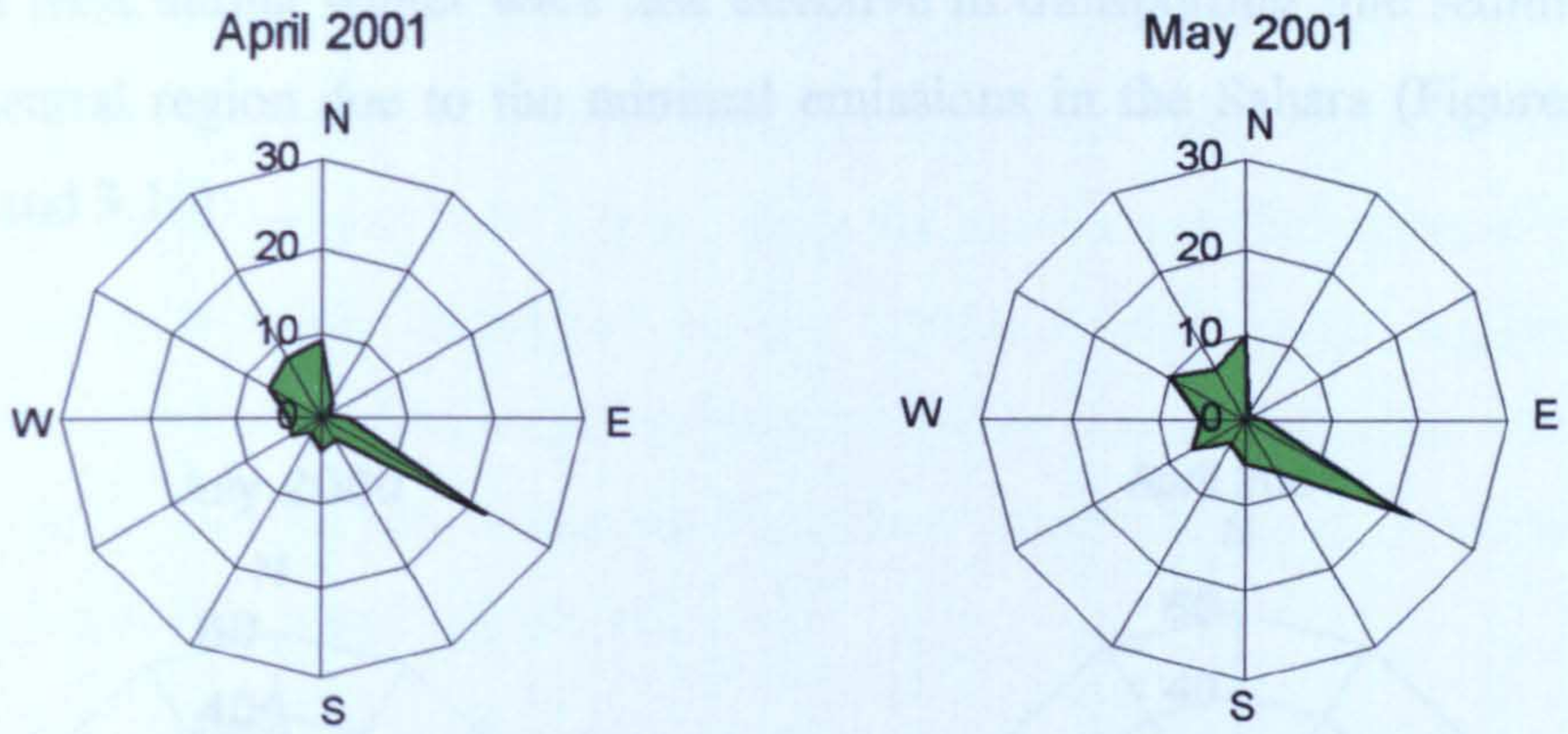

Figure 6.28 Prevailing winds at Hun station (wind velocities ≥ 6.5 m/s)

6.5.2. Central regional trend

Topographical irregularities in the region and the limited meteorological data tend to weaken the relationship between depositional pattern and the meteorological data. Deposition rates seem to be strongly affected by local sands accumulated in the region and re-entrained by the local wind regime under what seems to be funnelling by the inter-mountain corridors especially at Waddan. Due to its hilly nature, this region seems to act as a natural trap of sand particles. The particle size distributions show a persistent presence of horizontal flux transport mode in this region even during months of the lowest monthly average wind speeds, lowest wind frequencies and lowest average maximum temperatures.

Since there are no apparent sources of fine dust inside this region, the clay fractions seem to be largely transported by eastern to south eastern winds during the summer and spring from the Libyan Desert (Figure 6.29). Contributions from wadis in the vicinity of Bani Walid and the coastal Sabkha are also possible. The TOMS data (Figure 6.30) shows that the highest intensity of aerosol occurred during June and April aerosol reaching 0.77 and

0.58 respectively. In addition, TOMS AAI shows that this region may have received aerosol spells throughout the summer, autumn and spring under the effect of winds from east, south east and north west which can largely be linked to the northern and western fringes of the Libyan Desert. Winds from south west during winter were less effective in transporting fine sediments to the central region due to the minimal emissions in the Sahara (Figures 3.14, 3.15 and 3.16)

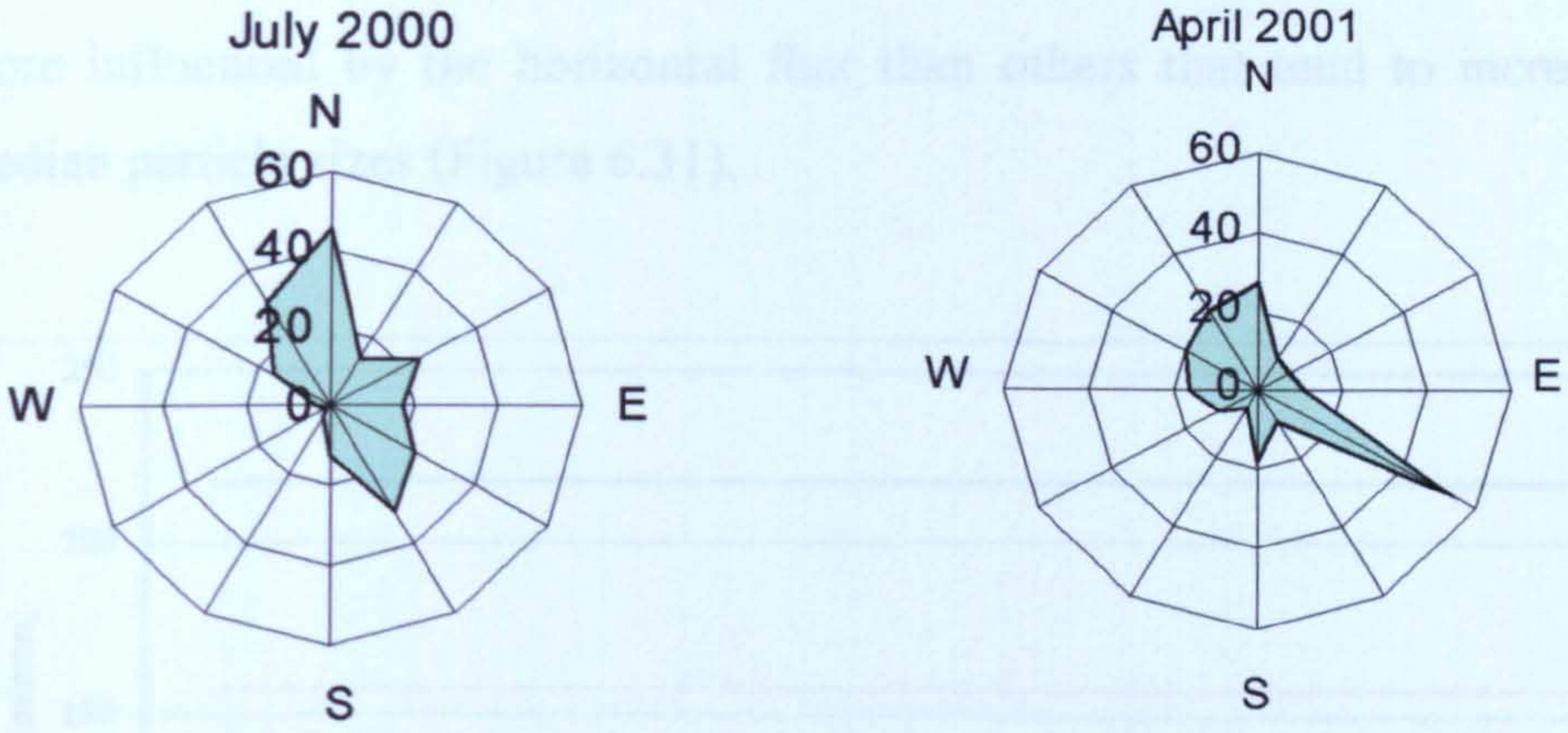

Figure 6.29 Prevailing winds at Hun (based on all wind velocities)

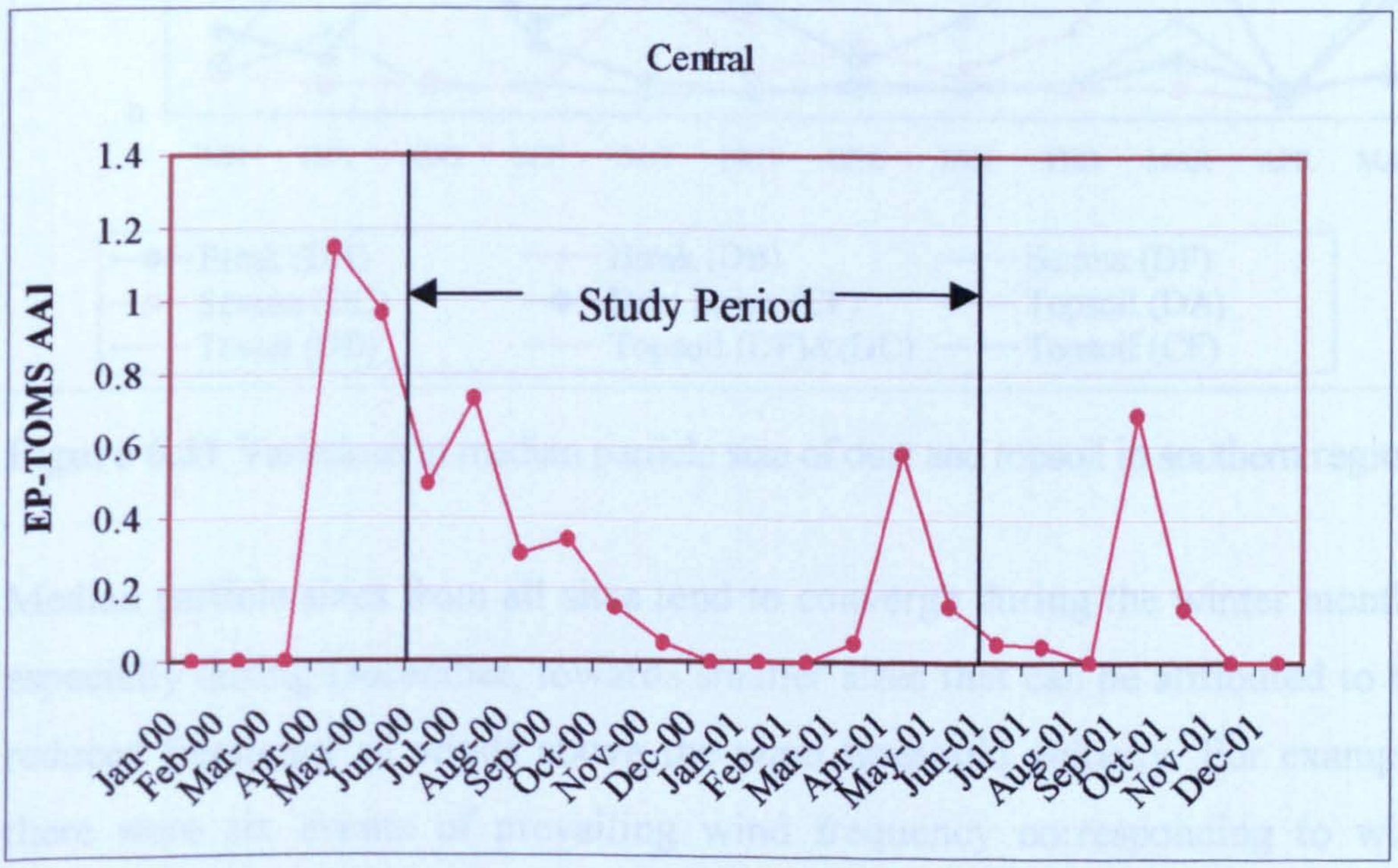

Figure 6.30 Monthly variation in TOMS AAI over the central region

6.6. SOUTHERN REGION

6.6.1. Sediment characteristics and deposition patterns analysis

The particle size distributions (Figure 6.32) show two major modes, one coincides with 100 μm and the other with 10 μm. Since the deposition rates in this region are much less than those in the other two regions, entrapped samples from the southern region seem to have a smaller content of sand particles than those entrapped in the northern and central regions. The variations in the median particle sizes, however, reveal that some sites were more influenced by the horizontal flux than others that tend to increase the median particle sizes (Figure 6.31).

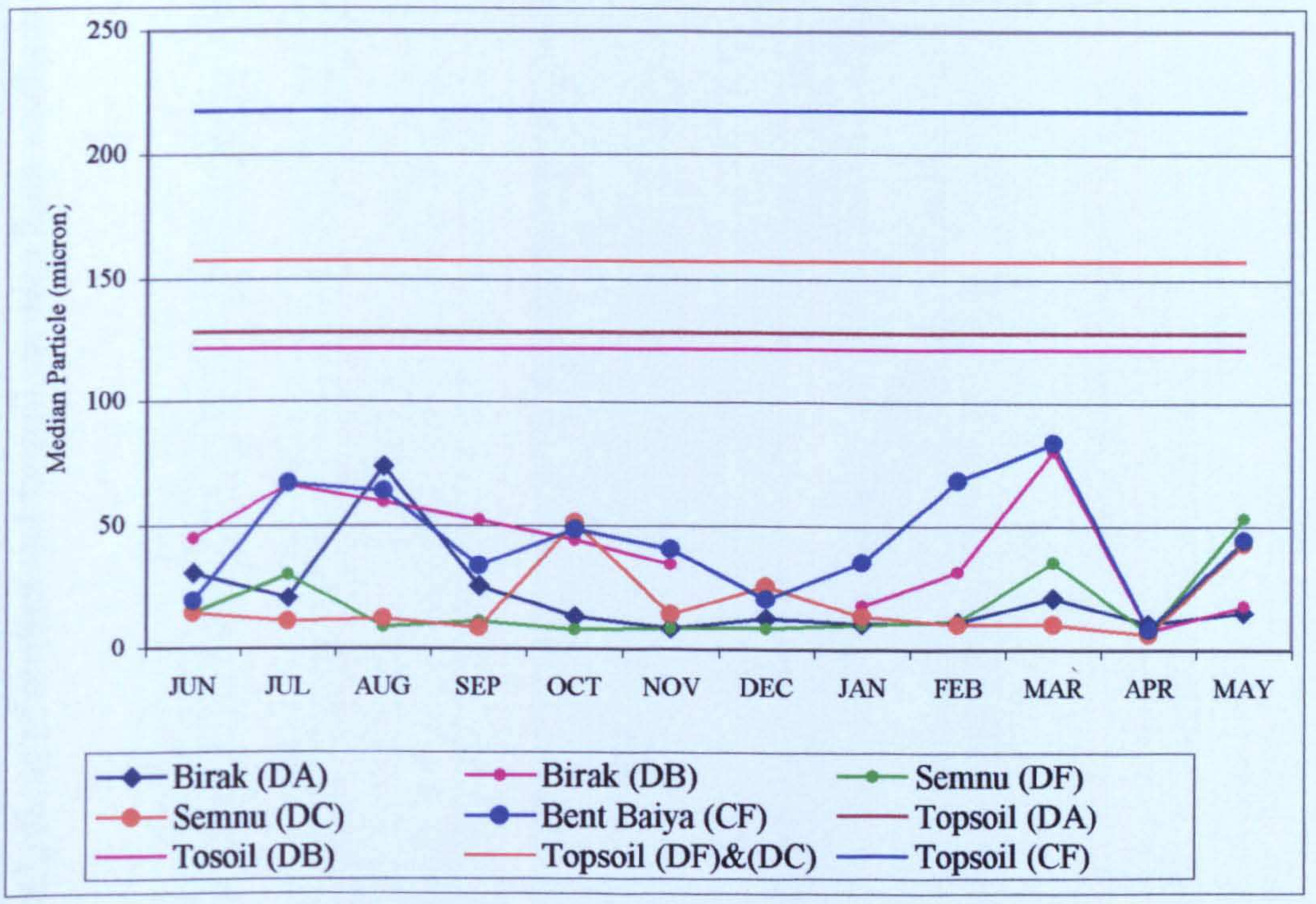

Figure 6.31 Variations in median particle size of dust and topsoil in southern region

Median particle sizes from all sites tend to converge during the winter months, especially during December, towards smaller sizes that can be attributed to the reduced frequency of winds above the wind threshold velocity. For example, there were six events of prevailing wind frequency corresponding to wind velocities ≥ 6.5 m/s during December, the lowest throughout the sampling year (Figure 6. 33). Since this region did not experience any rainfall during the

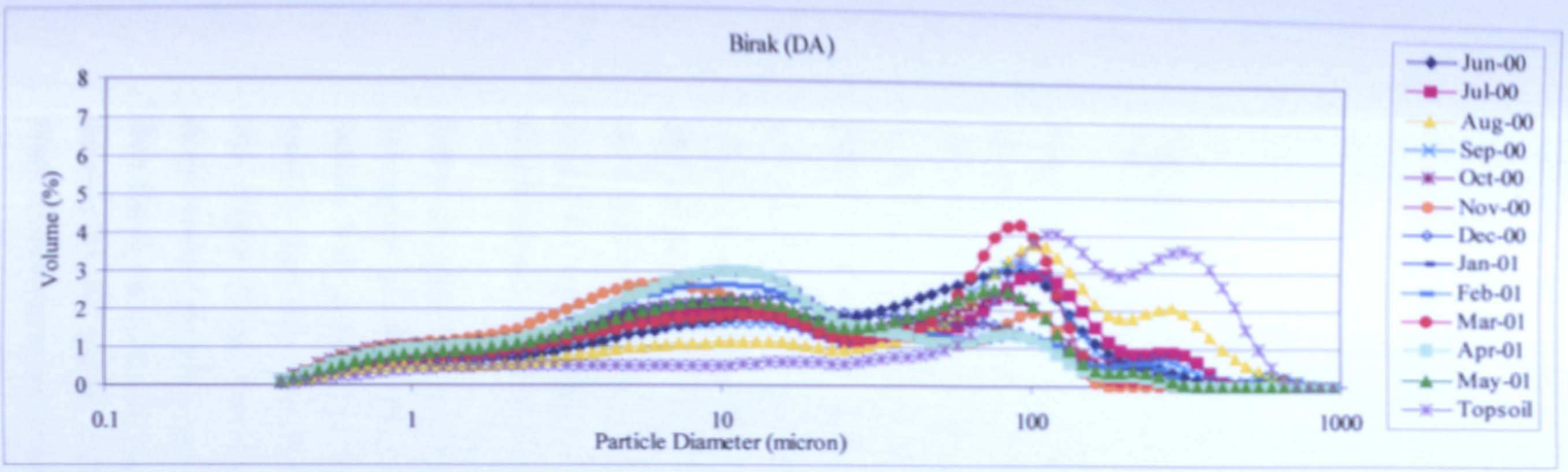

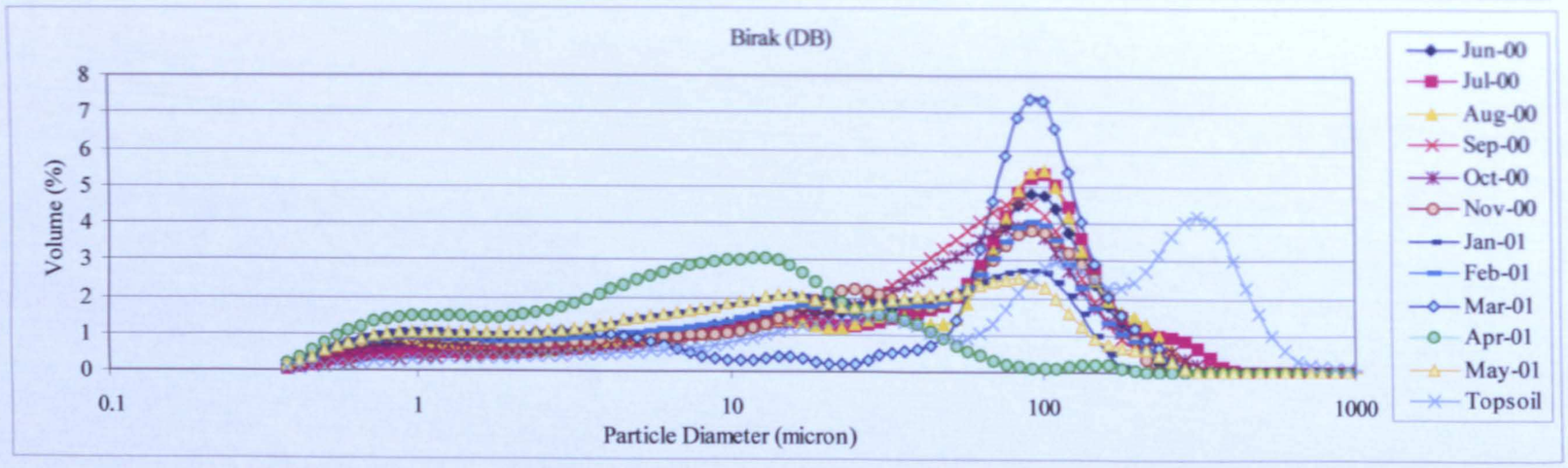

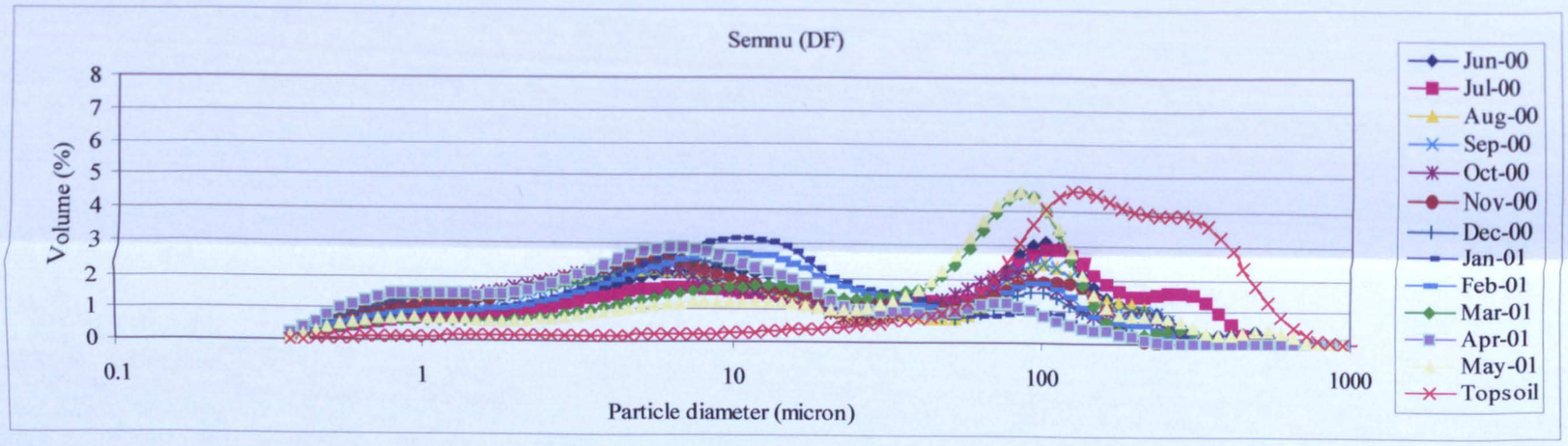

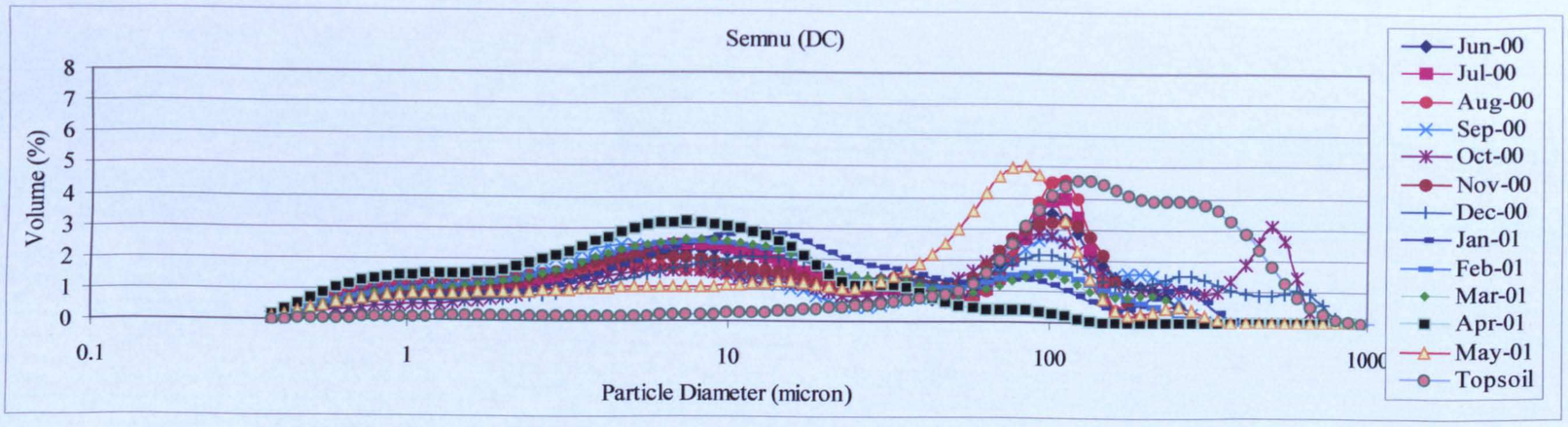

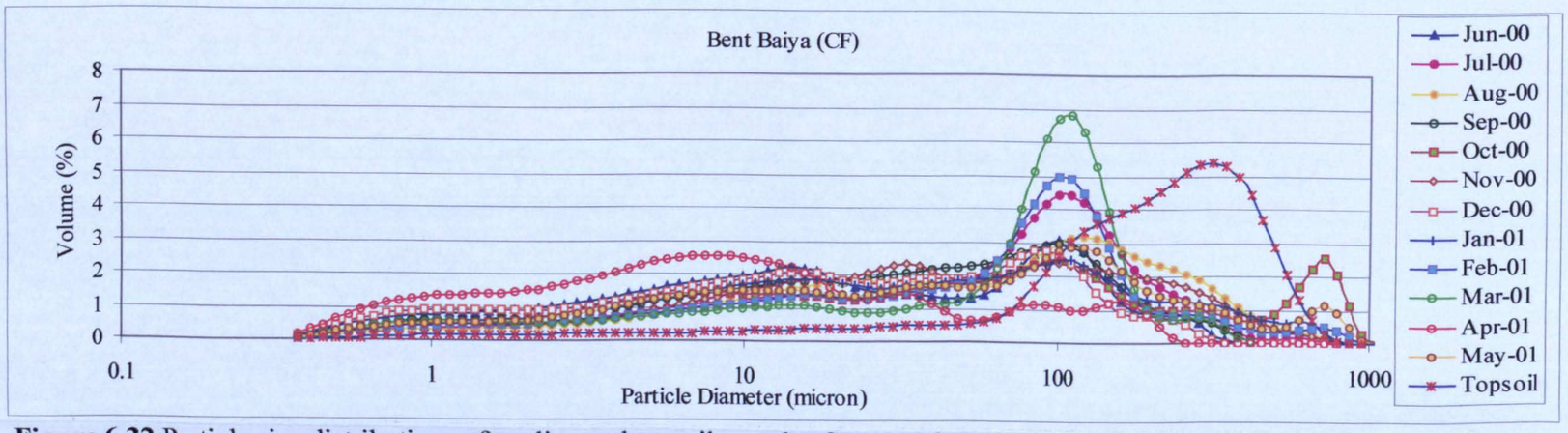

Figure 6.32 Particle size distributions of aeolian and topsoil samples from southern region

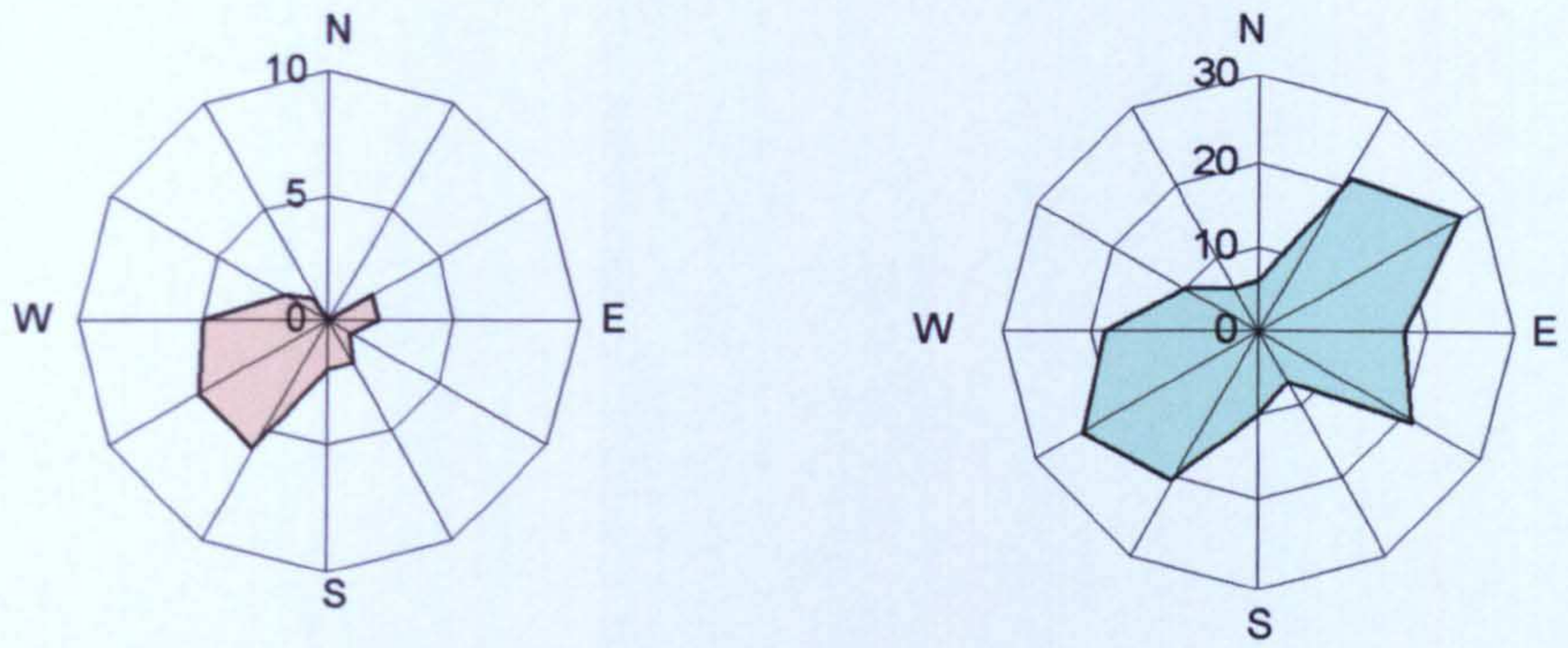

(a) (b)

Figure 6.33 Prevailing winds at Sebha during December for (a) ≥ 6.5 m/s (b) all wind velocities

sampling year, reduction in grain sizes during winter can neither be linked to cementation of topsoil or to wet deposition. Furthermore, a similar trend occurred during April resulting in smaller particle medians ranging from 6.32 to 10.41μm indicating that dry depositions of aerosols derived from major Saharan sources have occurred (Figure 6.38).

In spite of the fact that the highest wind frequencies (e.g. wind speeds ≥ 6.5 m/s) were recorded during May (35 events from SE), October (27 events from SE) and August (22 events from E), the highest recorded deposits at all sites occurred during the months of April and May (Figure 6.34) under an effect of prevailing winds from south eastern direction. Therefore, the emerging deposition pattern cannot be interpreted in meteorological terms only.

Unlike the other three sites in this region, the Birak (DB) and Bent Baiya (CF) sites appear to have experienced excessive activities created by the horizontal particle flux resulting in coarser sediments (Figures 6.31 and 6.32) which seems to have been caused by some topographic irregularities at Bent Baiya (see chapter 5) and some agricultural activities and automobile driving on dusty roads in the vicinity of site (DB) near Birak. The southernmost site at Bent Baiya, received nearly double the annual amount of dust in comparison to the sites DA, DC and DF in this region (Appendix II). Bent Baiya is situated in Wadi Alhaya and bounded from south and west by the escarpment of Hamadat Murzuq (Figures 5.30, 6.35 and 6.36).

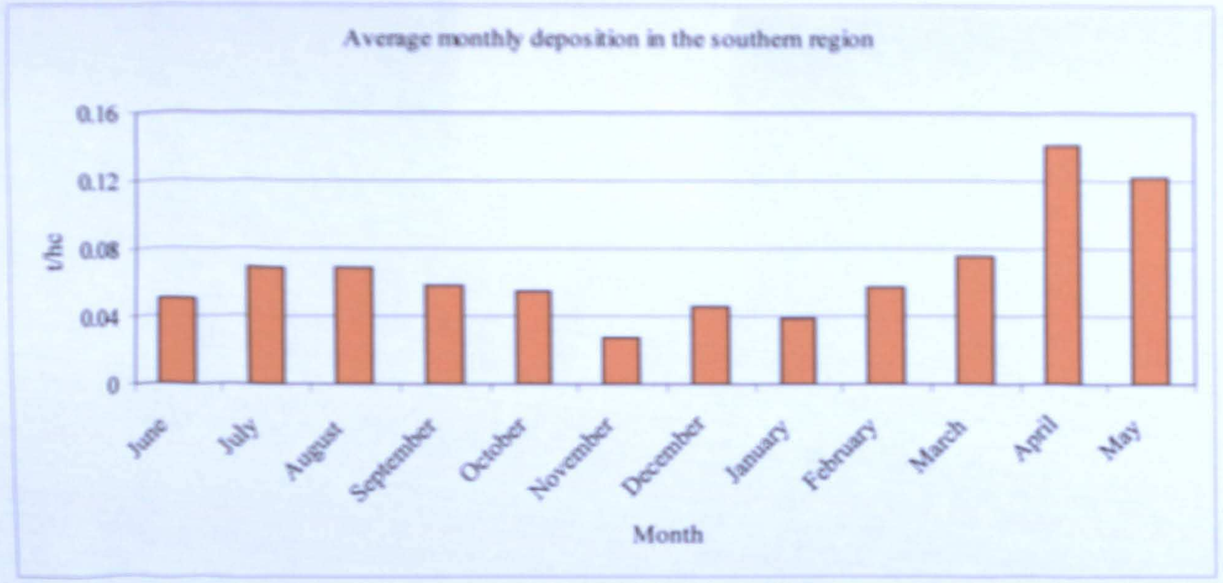

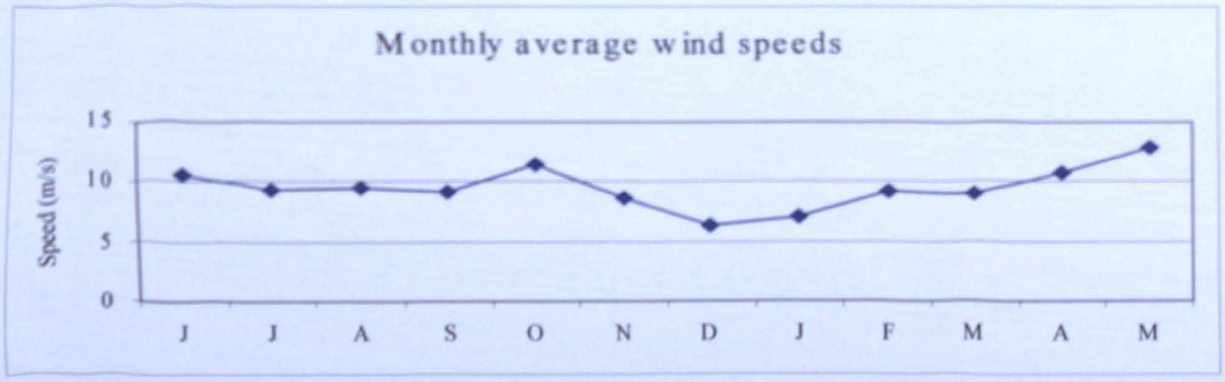

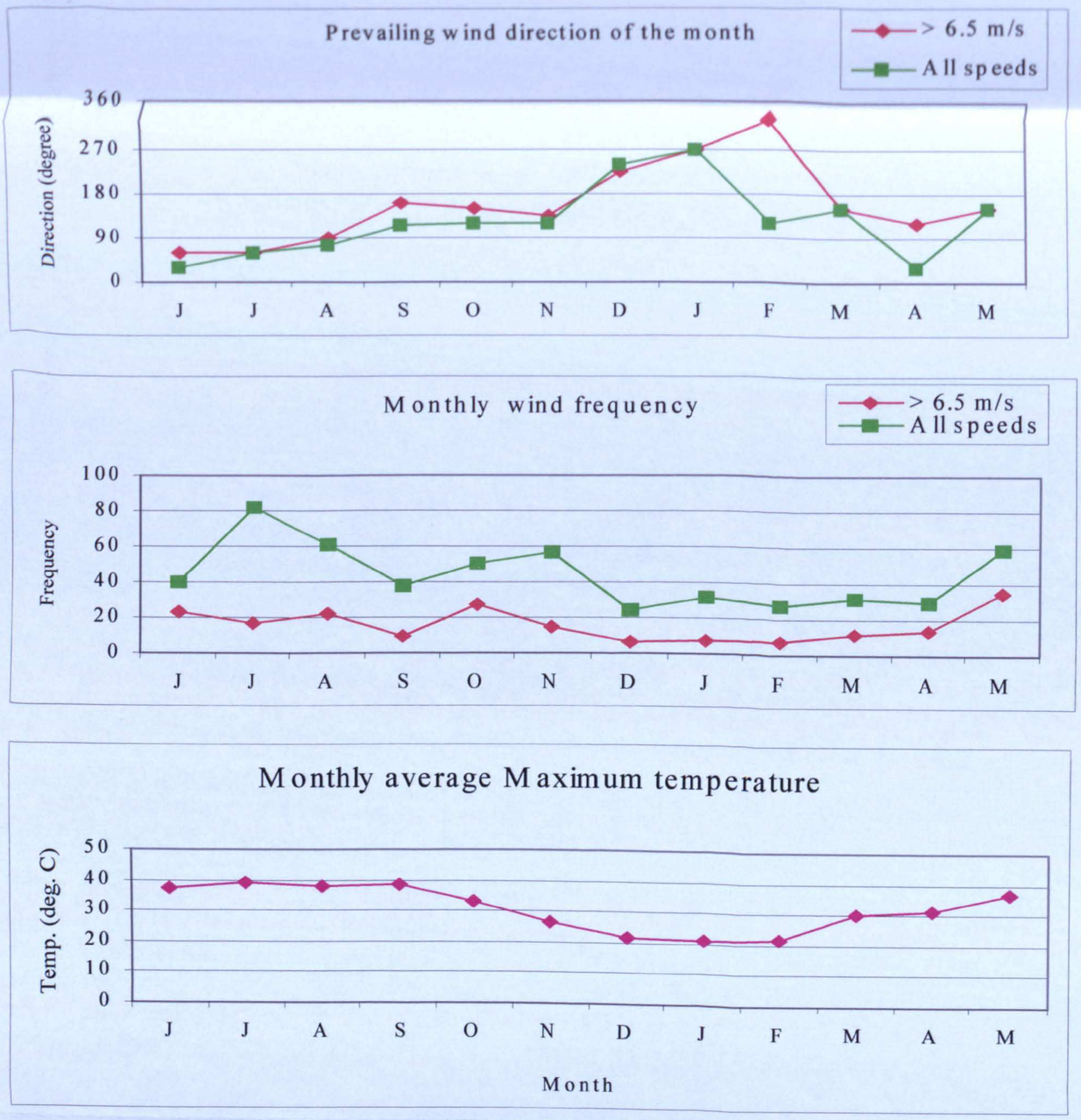

Figure 6.34 Average monthly deposition and meteorological data (southern region)

Figure 6.35 Northern and southern views of Bent Bayia site in Wadi Alhaya.

Figure 6.36 Eastern and western views of Bent Bayia site in Wadi Alhaya.

Studies based on field measurements and modelling have concluded that loess is preferably deposited on the windward than the leeward slopes (Reheis and Kihl, 1995; Goossens, 2000). This may explain the occurrence of higher deposition rates at Bent Baiya site, especially, during July, August and February at times dominated by eastern and northern winds (≥ 6.5 m/s) indicating that dust grains entrained from the wadi bed were deposited on the windward slope. This interpretation has proven to be consistent with the grain size distributions analysis of the aeolian samples collected at the same site.

The mineral composition of the aeolian and topsoil samples show that quartz is a dominant mineral in every samples ranging from 40 to 78.2 % in dust and 85.7 % in topsoil (Figure 6.37). The temporal variation of mineral composition (light and clay minerals) does not lend itself to any interpretation in meteorological terms even in terms of wind velocities and frequencies. Furthermore, the variation of the mineral composition does not seem to correlate with the variation in TOMS AAI (6.38). This probably is a result of transport at low altitudes (e.g. below 1500 m) and transport episodes during few days from non-prevailing monthly wind directions which can not by represented by monthly wind roses and therefore a shorter trapping period may be needed especially during the seasons of intensive emission and transport of aerosol.

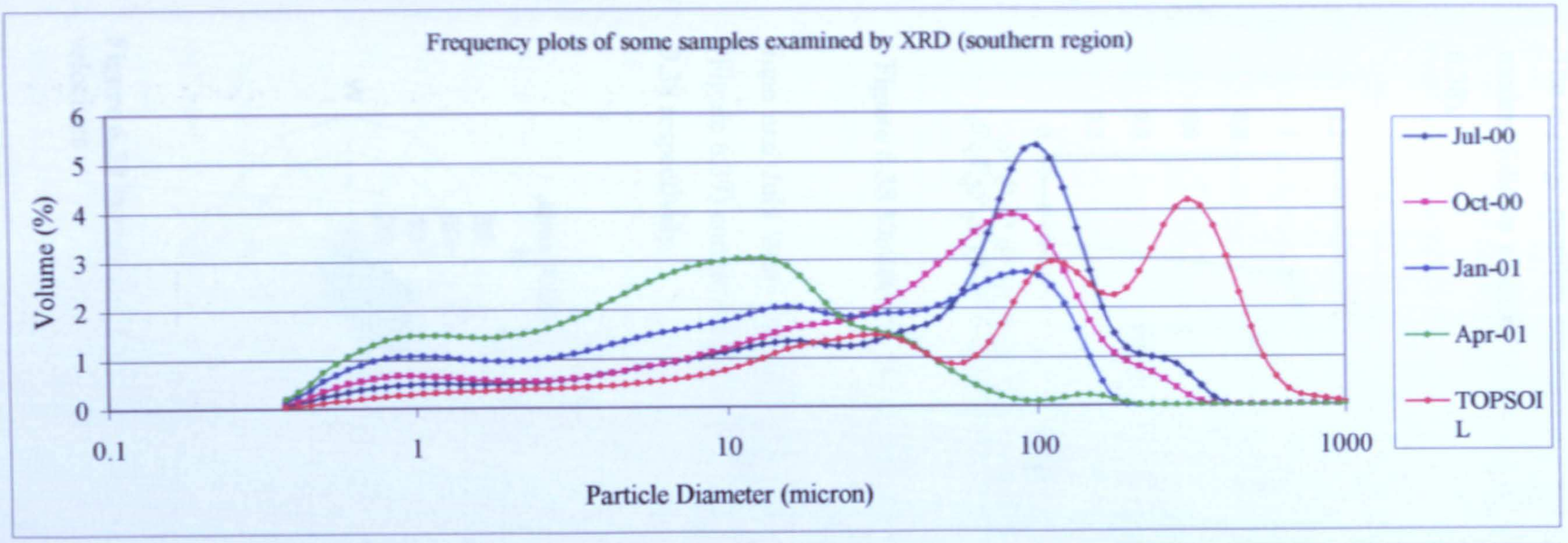

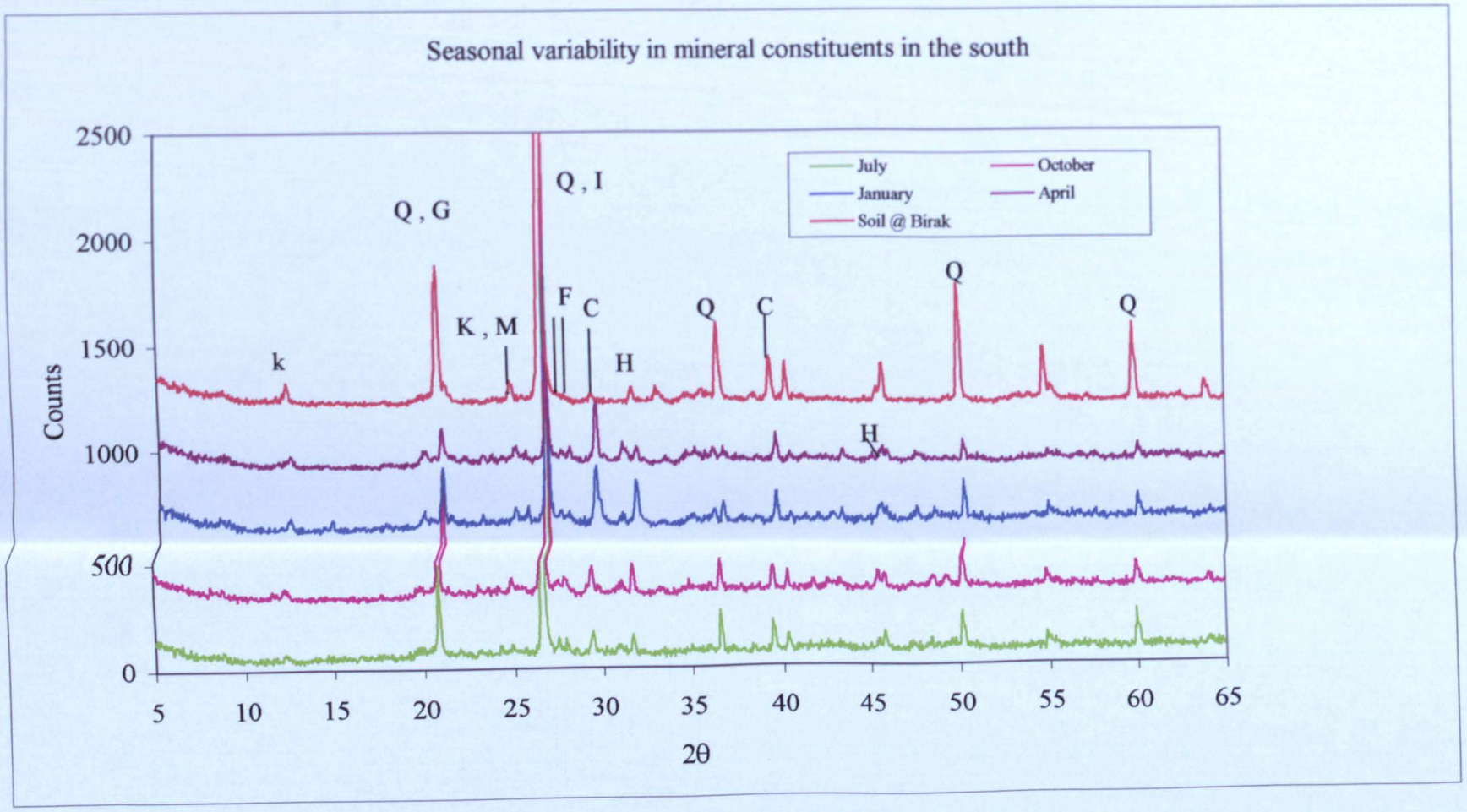

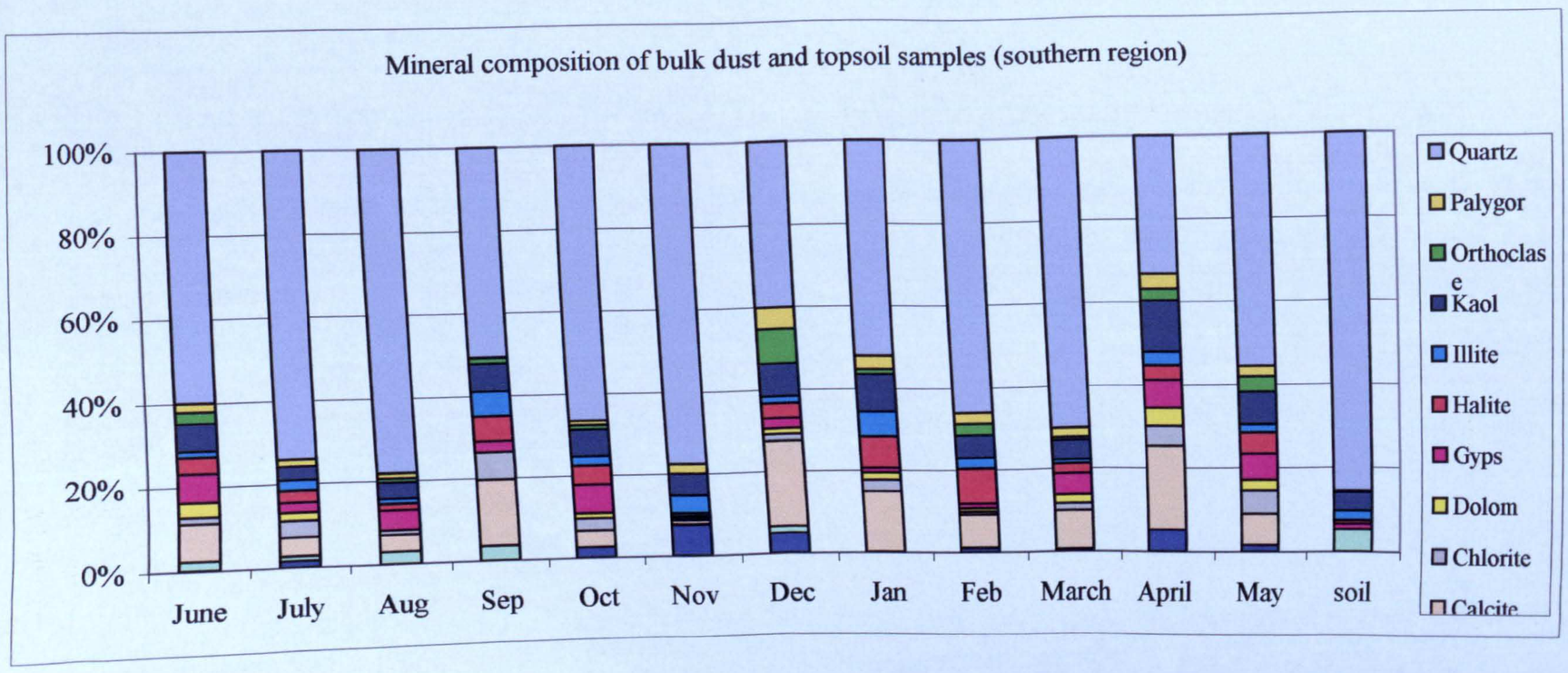

Figure 6.37 Mineral composition of bulk dust and topsoil from southern region

6.6.2. Southern regional trend

The average monthly deposition pattern, a distribution with two well defined modes, follows a similar trend as the monthly average aerosol index (Figure 6.38).

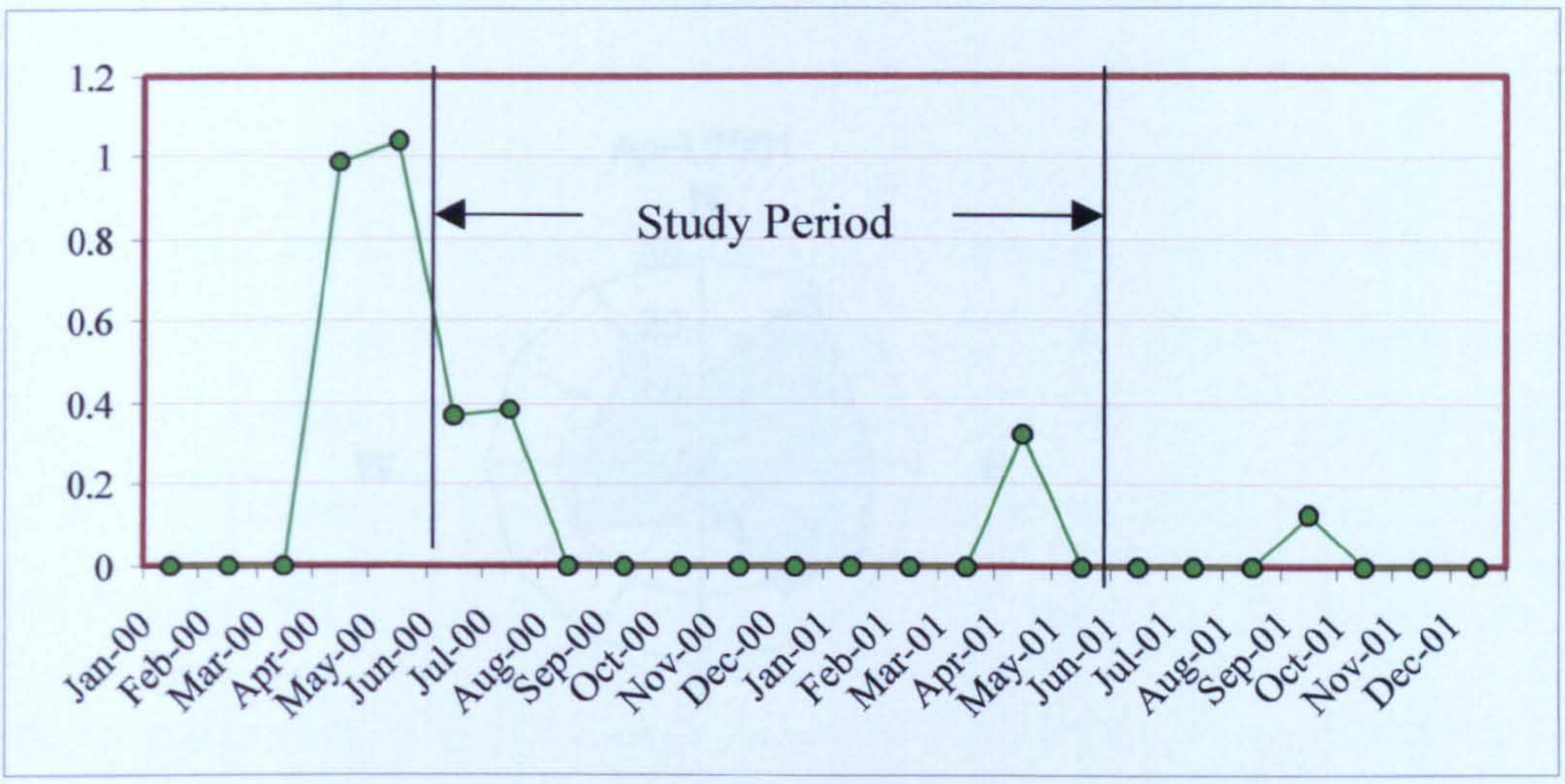

Figure 6.38 Variations in the monthly average TOMS AAI for the southern region

June and July were strongly influenced by prevailing winds from northeast (Figure 6.39) corresponding to 65 and 77 events and an aerosol index 0.36 and 0.38 respectively.

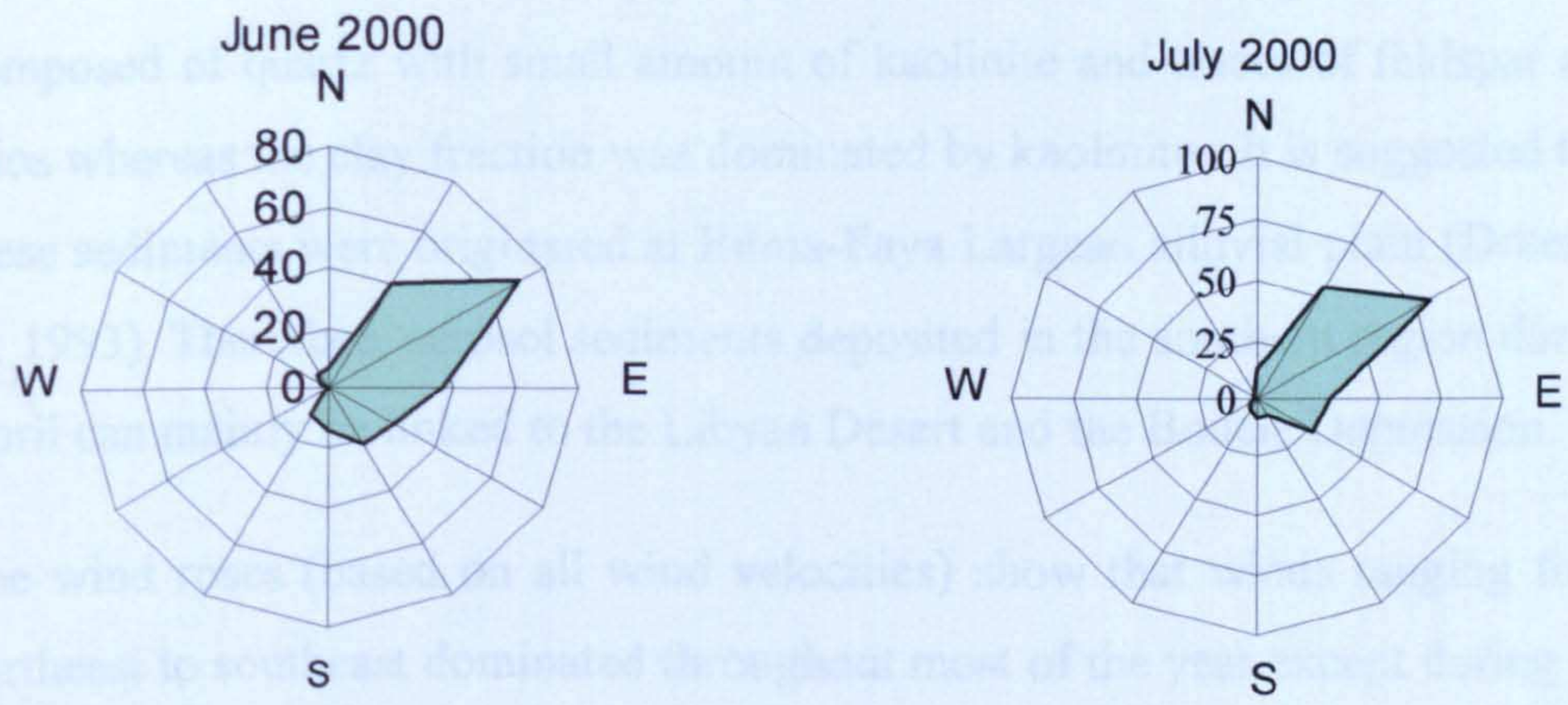

Figure 6.39 Prevailing winds at Sebha during summer 2000 based on all wind velocities

Any rain out of aerosol over the southern region during June and July can be attributed to dust plumes originated in the Eastern Libyan Desert. The April average aerosol index of 0.33 corresponded to prevailing winds ranged from northeast to southeast and a significant frequency of north western to southwestern winds (Figure 6.40).

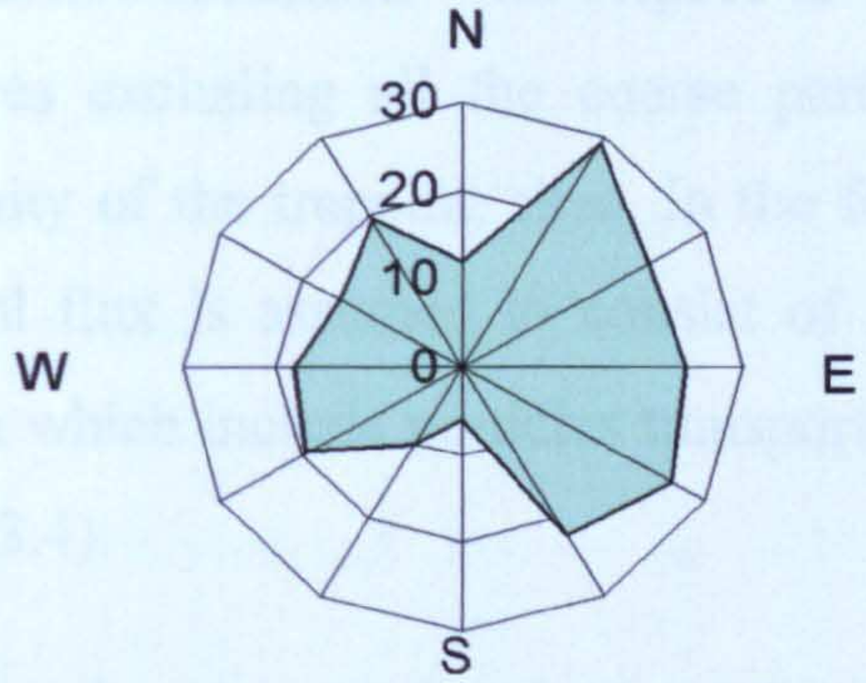

Figure 6.40 Prevailing winds at Sebha during April based on all wind velocities

The April samples contained more clay mineral than the samples of the other months with the highest percentage of kaolinite (12.5 %). The mineralogical analysis of bulk dust sediments collected during the Haramattan storms period from 1985 until 1989, which were deposited at two sites in Niger, were mainly composed of quartz with small amount of kaolinite and traces of feldspar and mica whereas the clay fraction was dominated by kaolinite. It is suggested that these sediments were originated at Bilma-Faya Largeau alluvial plain (Drees *et al*, 1993). Therefore, aerosol sediments deposited in the southern region during April can mainly be linked to the Libyan Desert and the Bodele Depression.

The wind roses (based on all wind velocities) show that winds ranging from northeast to southeast dominated throughout most of the year except during the winter season which was mainly influenced by winds from south west drawing the highest percentages of palygorskite during December (5.1 %) which can be linked to the Ahaggar region in southern Algeria.

6.7. VERTICAL FLUX COMPONENT VERSUS TOMS AAI DATA

6.7.1. Vertical sediment weight calculation

The persistent presence of sand in all the trapped samples shows the significance of the near trap surface in emission of sand and contribution to the total dust samples. In order to link deposition to source, a separation of the total flux into vertical and horizontal appears to be necessary. Assessment of spatial distribution of deposited sediments with respect to the spatial distribution of TOMS data requires excluding all the coarse particles entrained from the surface in the vicinity of the trapping sites. In the following calculations and analysis the vertical flux is assumed to consist of all deposited particles of smaller than 70 μm which include particles transported in short and long term suspension (Figure 3.4).

Since the physical density of matter is calculated from the following equation:

$$\rho = m / V \qquad [6.1]$$

where

ρ is density

m is mass

V is volume

Since the differences in the density of most of the dominant minerals (light and clay) are small enough to be neglected (Pye, 1994), we assume that the average density of the sediments deposited vertically is approximately equals the average density of the bulk sediment. Therefore, the mass of sediments transported in vertical mode can be calculated as follows:

Since $\rho_v = \rho_t \qquad [6.2]$

$$m_v / V_v = m_t / V_t \qquad [6.3]$$

Then

$$m_v = m_t (V_v / V_t) \qquad [6.4]$$

Where the subscripts v and t represent vertical and total flux respectively.

Finally, the masses of the vertically transported and deposited sediments are calculated from the particle size distribution data of each sample using equation (6.4) and a list of these results are provided in Appendix II.

6.7.2. Spatial variation of vertical flux

The spatial distributions of the vertically transported sediments vary from one month to another in their agreement with TOMS AAI spatial distributions. A comparison of the two sets of data reveals the seasons of high emission in the Sahara and higher AAI values for the study regions coincide with an increase in deposition across the study regions through the vertical flux mode, however, the monthly sets of data range from complete agreement to a lack of agreement. A locally derived vertical flux is evident during the winter months which can only be attributed to the wadis, sabkhas, oceanic aerosols and anthropogenic dust sources.

6.7.2.1. Summer months

Transport of suspended dust during the summer months occurred under a dominant influence of northern to easterly winds in the north, north easterly winds in the south and alternating wind direction between northwest and south east in the central region. The contour maps in (Figures 6.41 –6.43) show that deposition in the northern region during June, July and August appear to be derived from the Chotts in northeastern Algeria, despite the fact that the prevailing wind directions on the ground are in the opposite direction. Dust plumes which originated at the Chotts terminate in the western fringes of the northern region with the highest AAI value 0f 0.4 during July. The vertical deposition in the northern region reached very high rates (> 0.3 t/ha) competing with the central region that experienced higher aerosol loadings during the same months.

The central region appears to be the region which is most affected by the vertical flux of transported sediment from the Libyan Desert. The meteorological data for this region is recorded at Hun Station, which is located in a narrow inter-mountainous corridor oriented in the same direction of the prevailing winds and is therefore not necessarily representative of the regional conditions in the central area. Among the four sites in this region three sites are

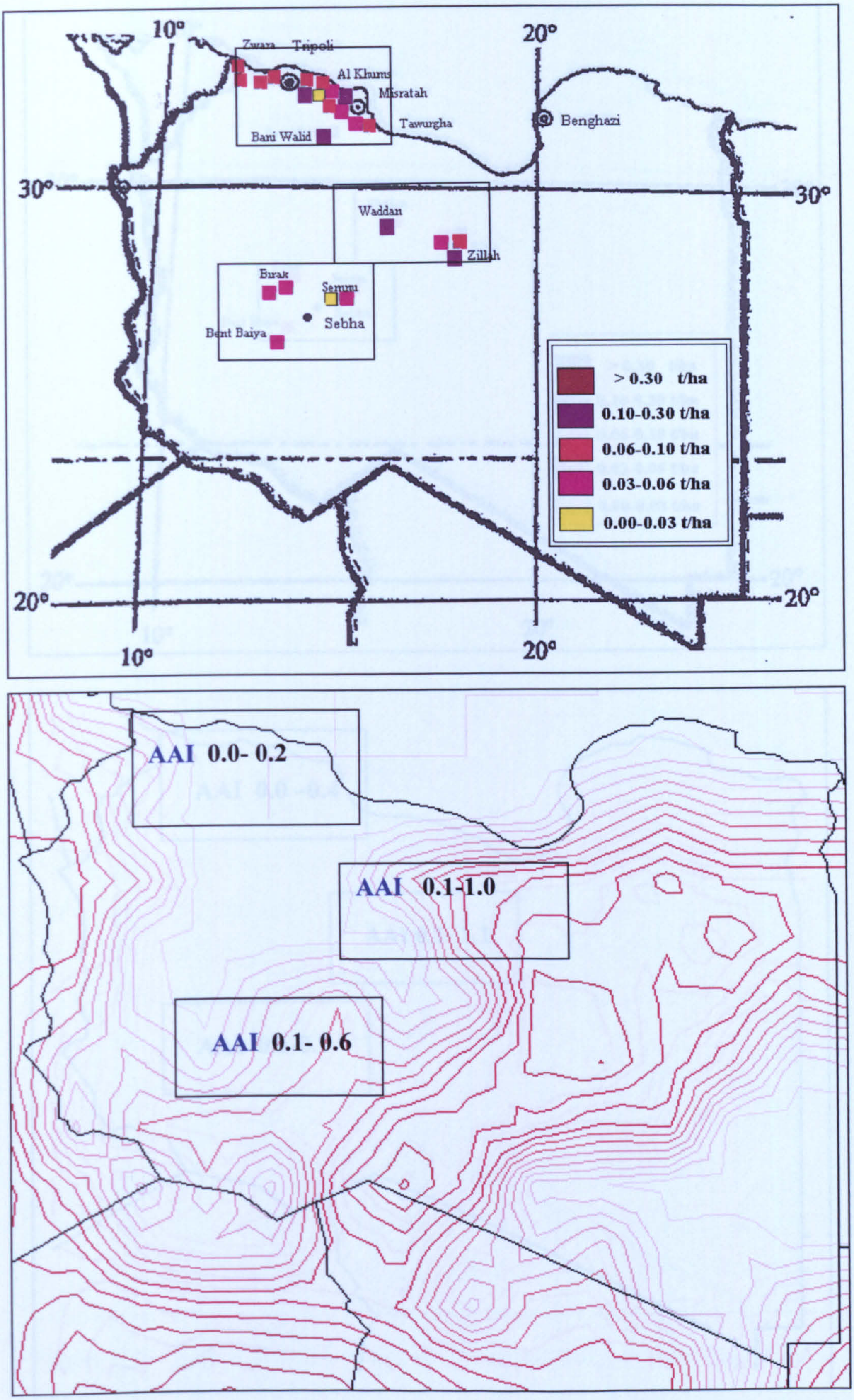

Figure 6.41 Vertical deposition versus TOMS aerosol index for June 2000

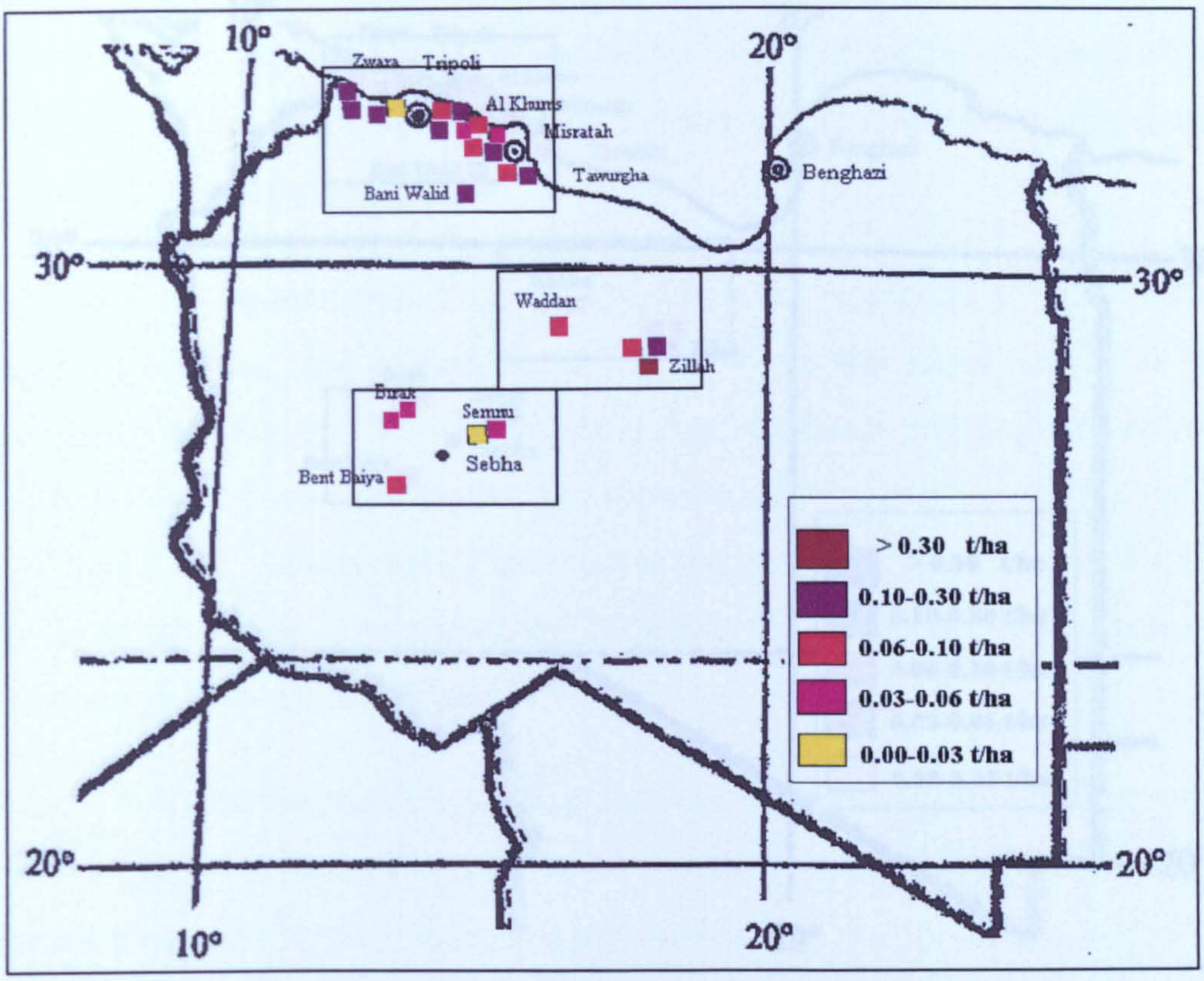

Figure 6.42 Vertical deposition versus TOMS aerosol index for July 2000

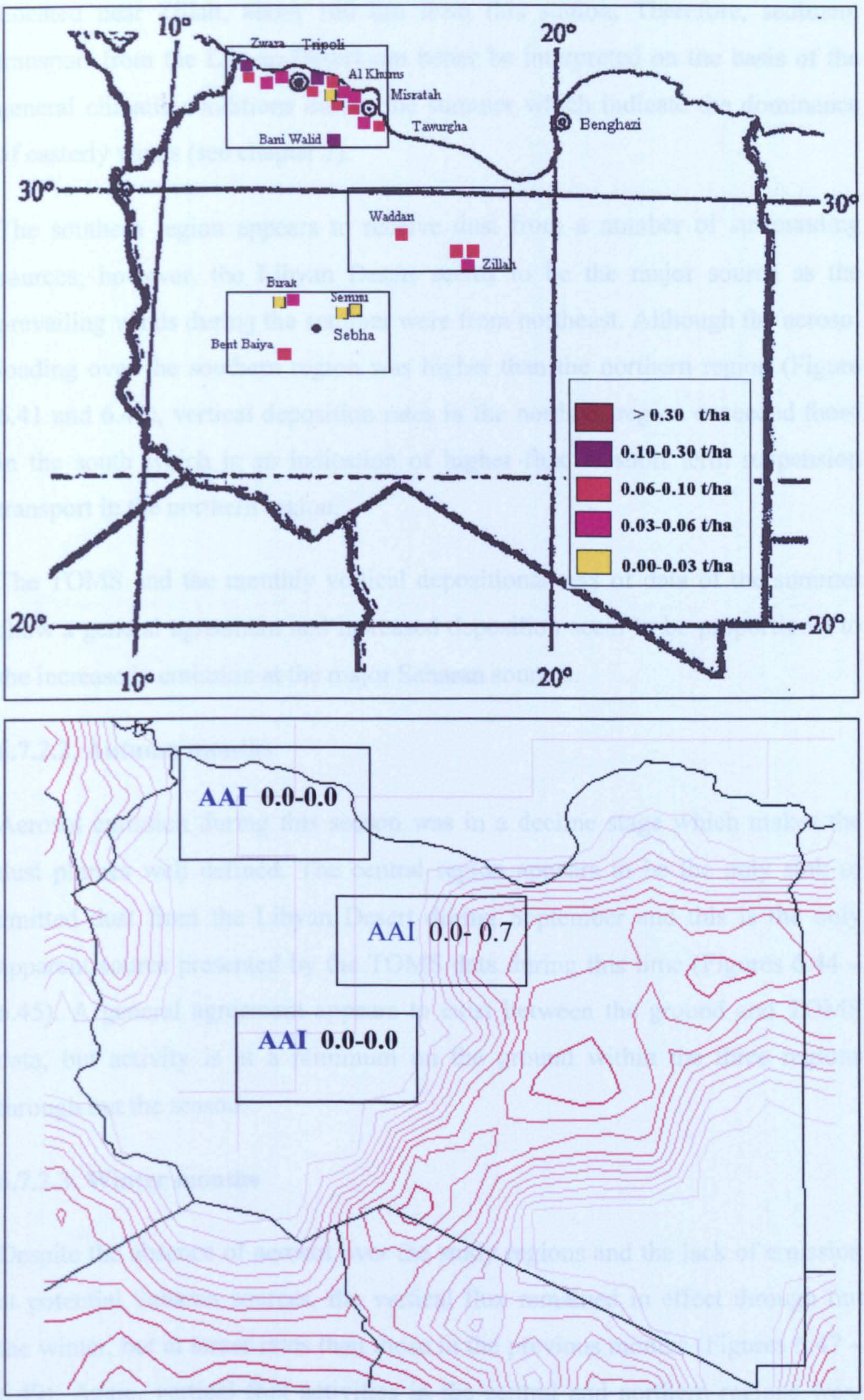

Figure 6.43 Vertical deposition versus TOMS aerosol index for August 2000

Located near Zillah, about 160 km from this station. Therefore, sediment transport from the Libyan Desert can better be interpreted on the basis of the general climatic conditions during the summer which indicate the dominance of easterly winds (see chapter 2).

The southern region appears to receive dust from a number of surrounding sources; however, the Libyan Desert seems to be the major source as the prevailing winds during the summer were from northeast. Although the aerosol loading over the southern region was higher than the northern region (Figure 6.41 and 6.42), vertical deposition rates in the northern region exceeded those in the south which is an indication of higher flux of short term suspension transport in the northern region.

The TOMS and the monthly vertical depositional sets of data of the summer show a general agreement and increased deposition seem to be proportional to the increase in emission at the major Saharan sources.

6.7.2.2. Autumn months

Aerosol emission during this season was in a decline stage which makes the dust plumes well defined. The central region appears to be the only sink of emitted dust from the Libyan Desert during September and this is the only apparent source presented by the TOMS data during this time (Figures 6.44 – 6.45). A general agreement appears to exist between the ground and TOMS data, but activity is at a minimum on the ground within the three regions through out the season.

6.7.2.3. Winter months

Despite the absence of aerosol over the study regions and the lack of emission at potential Saharan sources, the vertical flux remained in effect through out the winter, but at lesser rates than those in the previous months (Figures 6.47 – 6.49). Again, vertical flux activities in the central and northern regions were higher than those in the southern region. Precipitation may have had an important role in depositing short-term suspended sediments in the northern region.

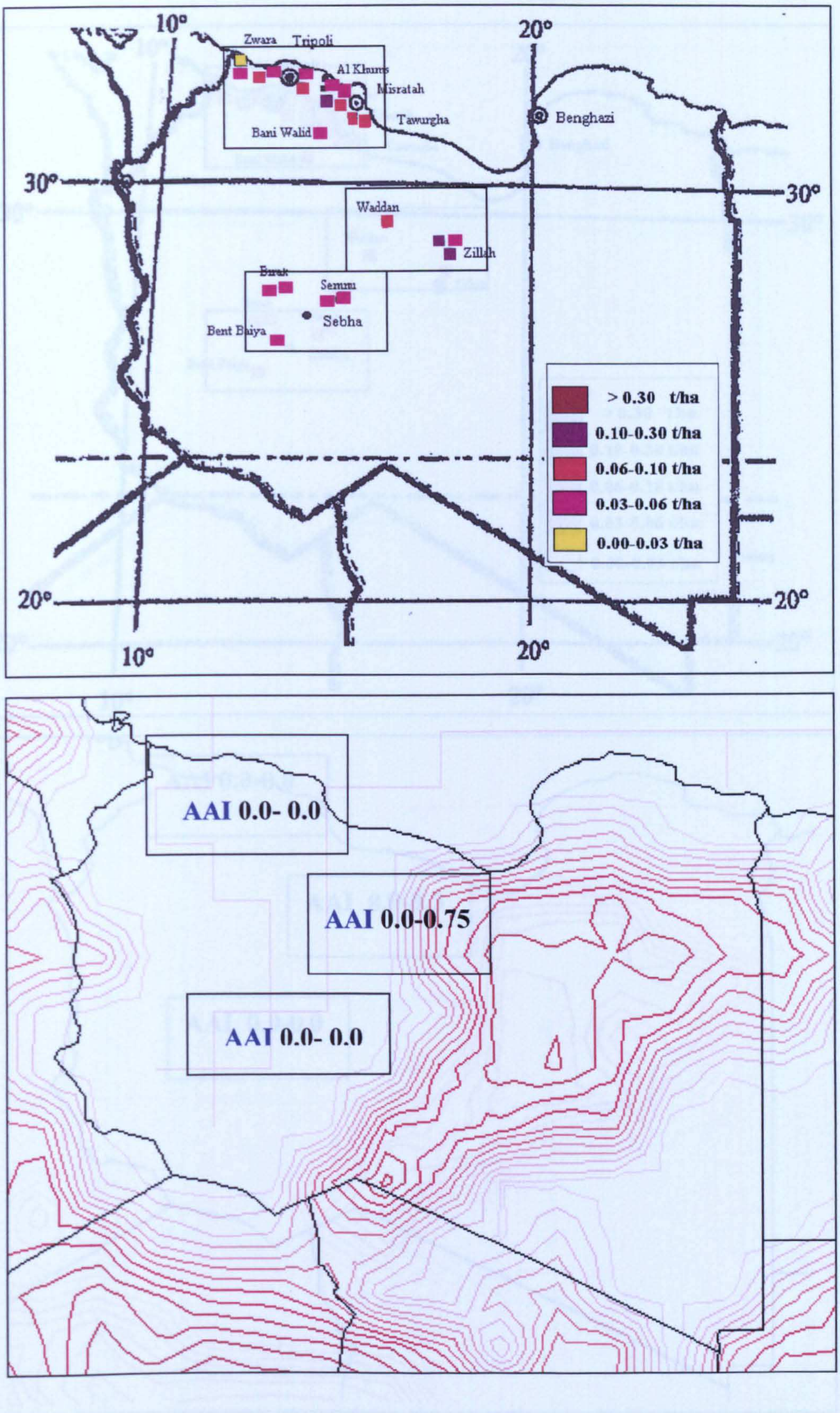

Figure 6.44 Vertical deposition versus TOMS aerosol index for September 2000

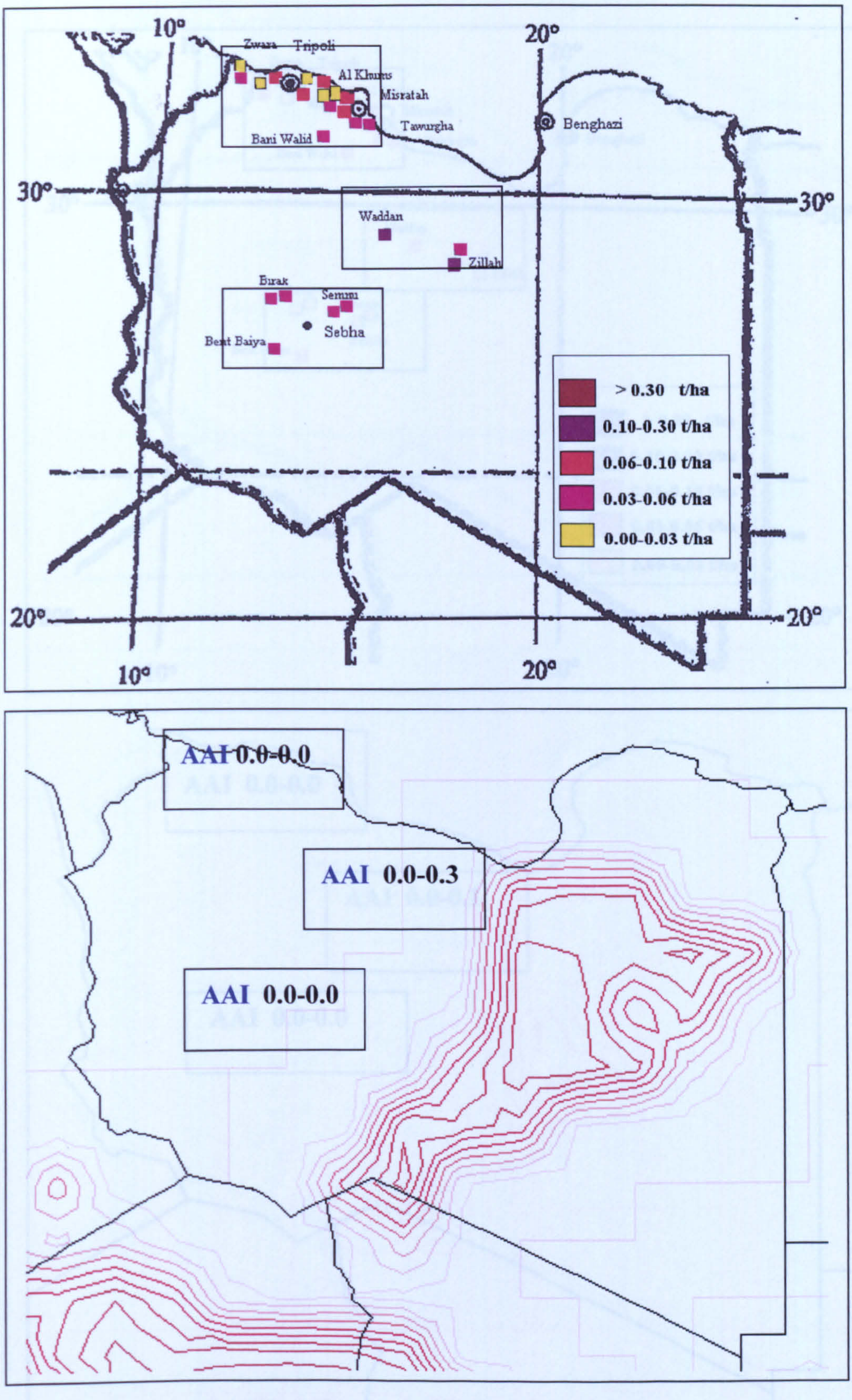

Figure 6.45 Vertical deposition versus TOMS aerosol index for October 2000

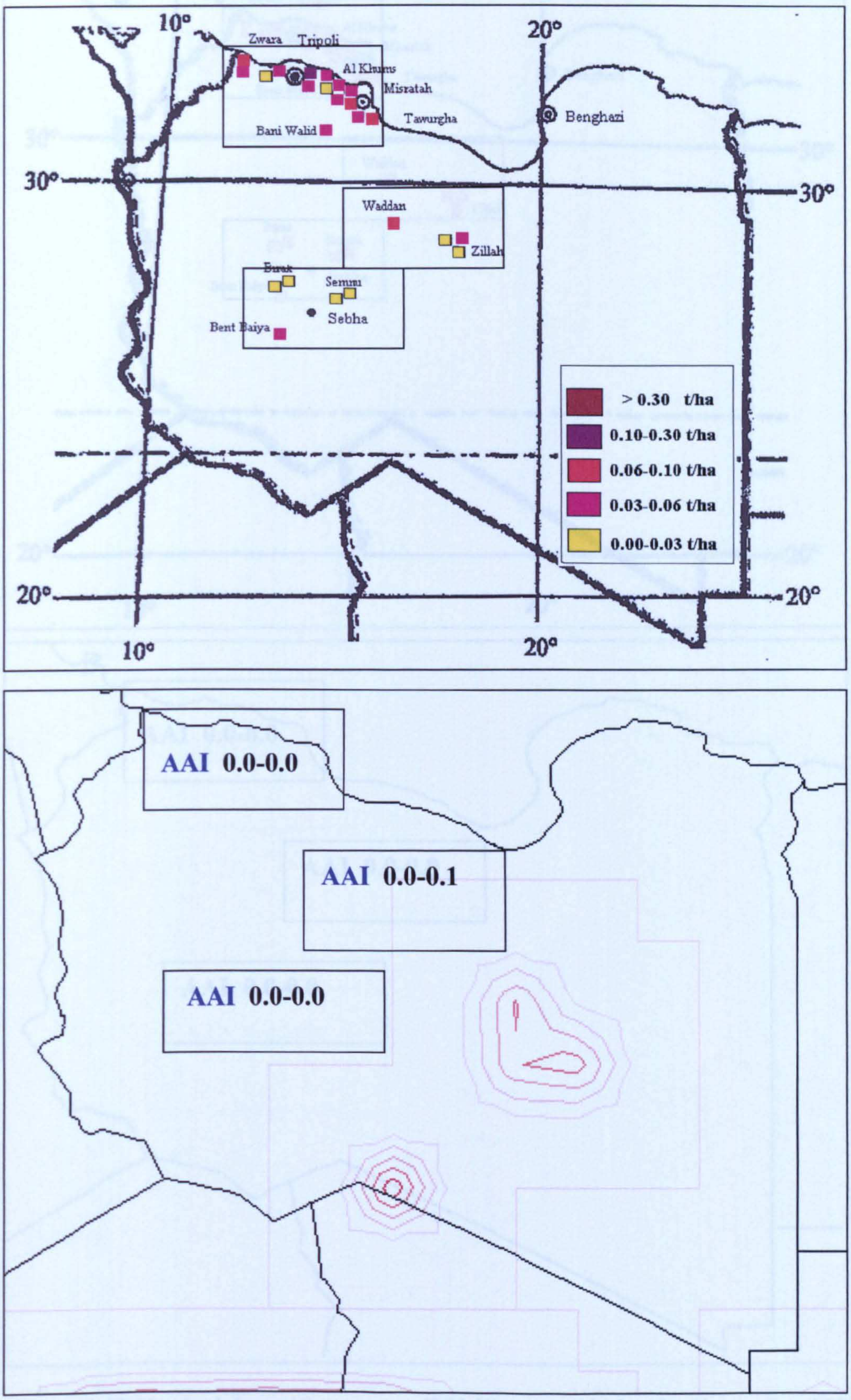

Figure 6.46 Vertical deposition versus TOMS aerosol index for November 2000

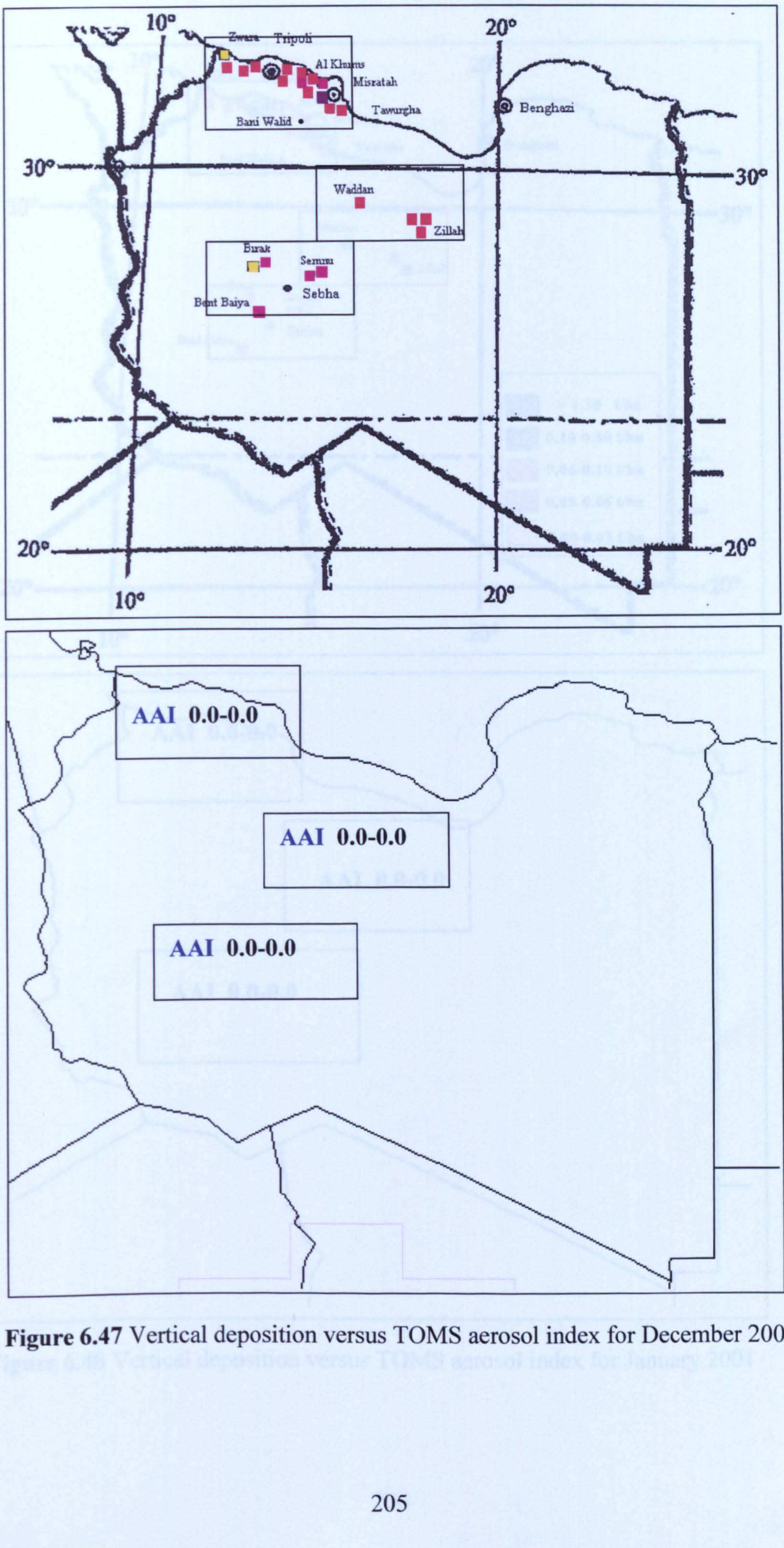

Figure 6.47 Vertical deposition versus TOMS aerosol index for December 2000

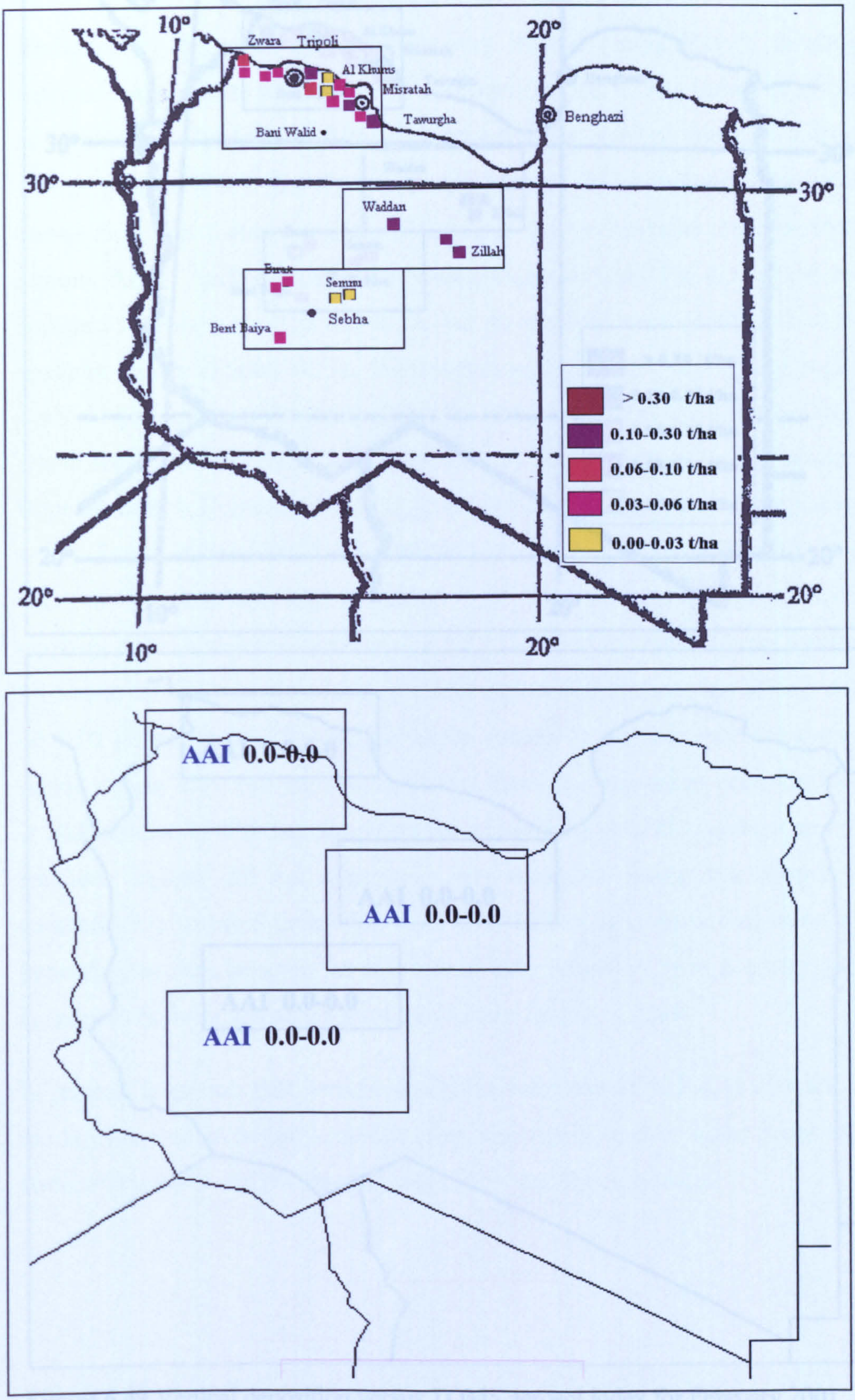

Figure 6.48 Vertical deposition versus TOMS aerosol index for January 2001

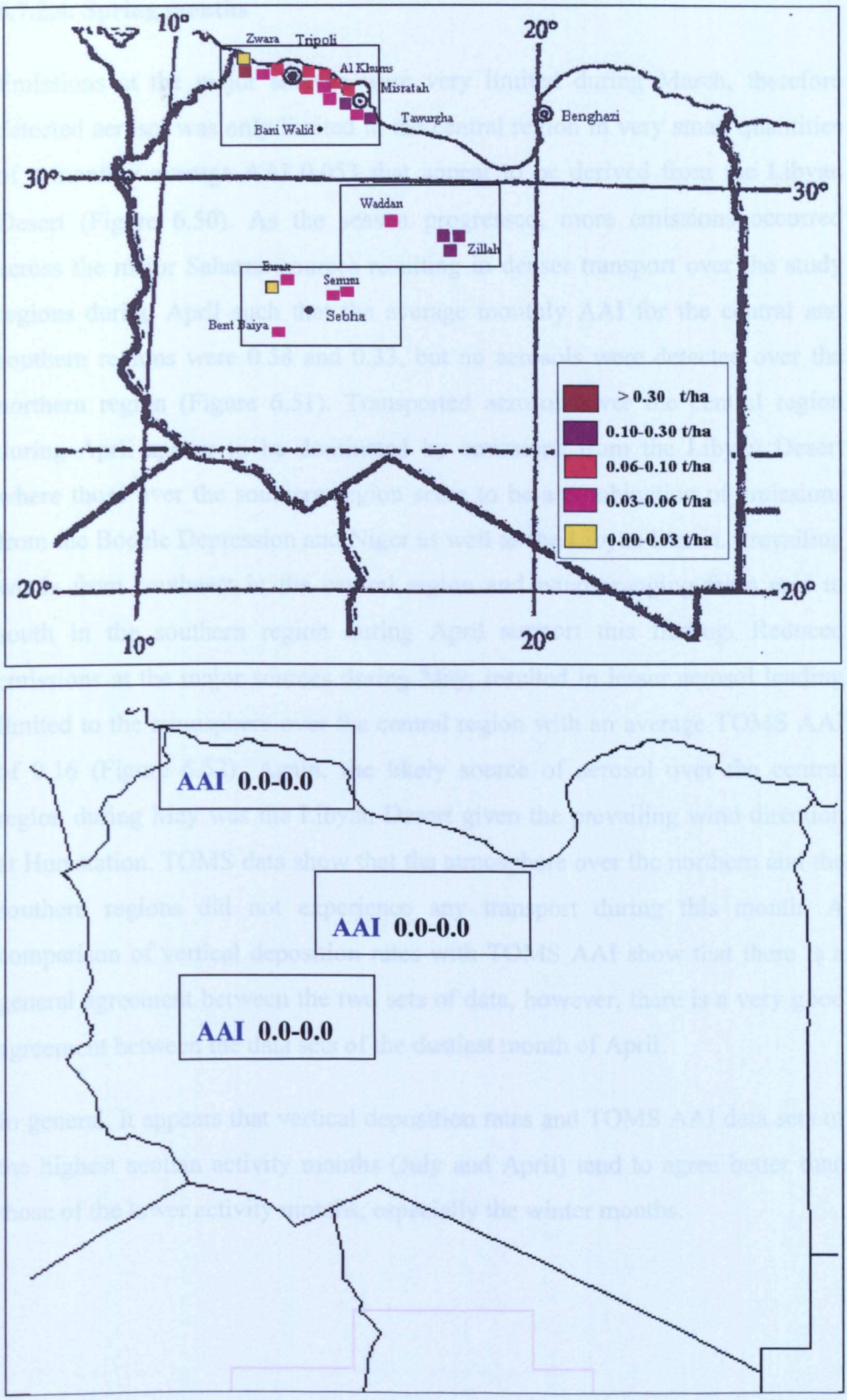

Figure 6.49 Vertical deposition versus TOMS aerosol index for February 2001

6.7.2.4. Spring months

Emissions at the major sources were very limited during March, therefore detected aerosol was only limited to the central region in very small quantities of a monthly average AAI 0.053 that appear to be derived from the Libyan Desert (Figure 6.50). As the season progressed, more emissions occurred across the major Saharan sources resulting in denser transport over the study regions during April such that the average monthly AAI for the central and southern regions were 0.58 and 0.33, but no aerosols were detected over the northern region (Figure 6.51). Transported aerosols over the central region during April appear to be dominated by emissions from the Libyan Desert where those over the southern region seem to be a combination of emissions from the Bodele Depression and Niger as well as the Libyan Desert. Prevailing winds from southeast in the central region and winds ranging from east to south in the southern region during April support this finding. Reduced emissions at the major sources during May, resulted in lesser aerosol loading limited to the atmosphere over the central region with an average TOMS AAI of 0.16 (Figure 6.52). Again, the likely source of aerosol over the central region during May was the Libyan Desert given the prevailing wind direction at Hun station. TOMS data show that the atmosphere over the northern and the southern regions did not experience any transport during this month. A comparison of vertical deposition rates with TOMS AAI show that there is a general agreement between the two sets of data, however, there is a very good agreement between the data sets of the dustiest month of April.

In general, it appears that vertical deposition rates and TOMS AAI data sets of the highest aeolian activity months (July and April) tend to agree better than those of the lower activity months, especially the winter months.

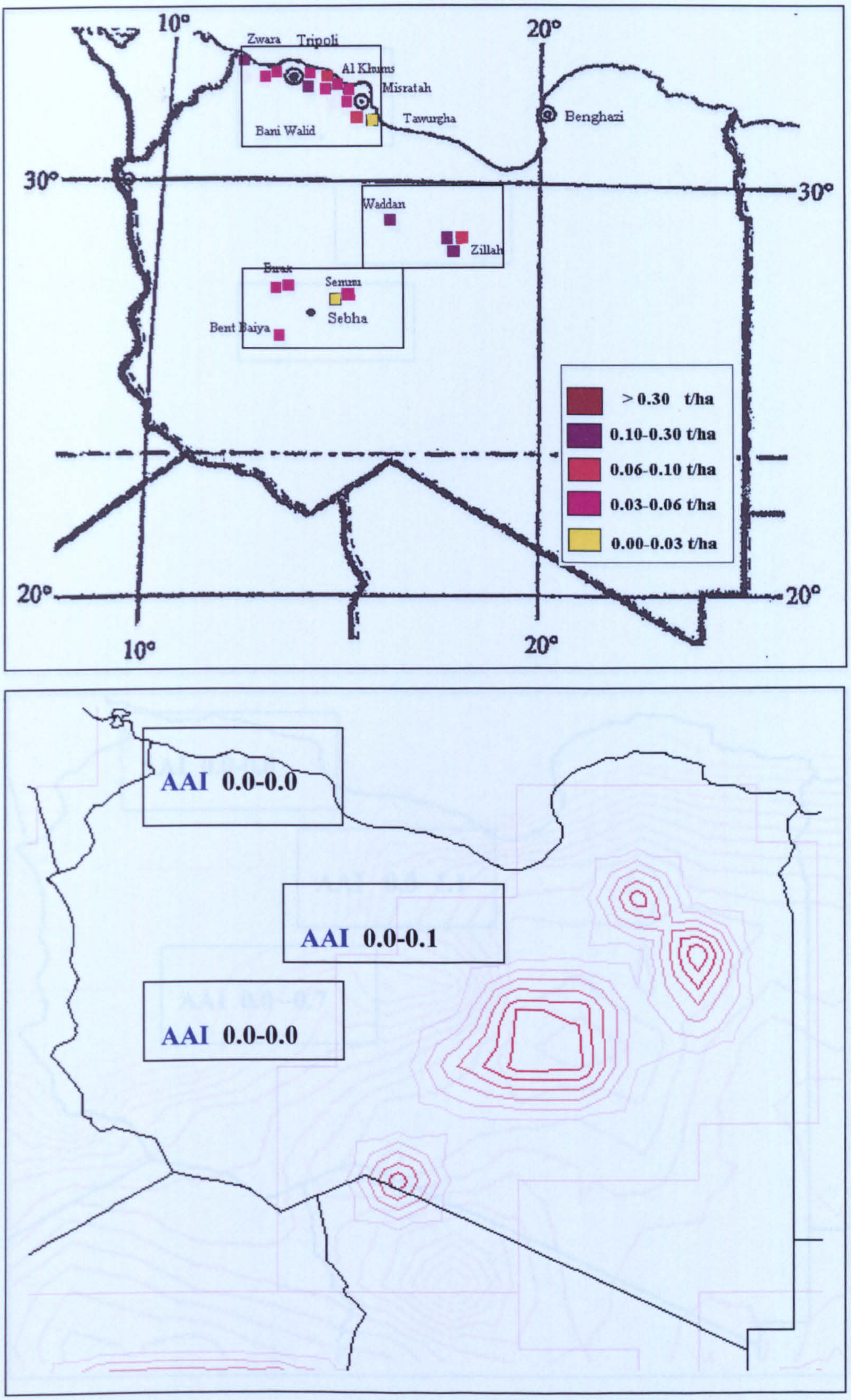

Figure 6.50 Vertical deposition versus TOMS aerosol index for March 2001

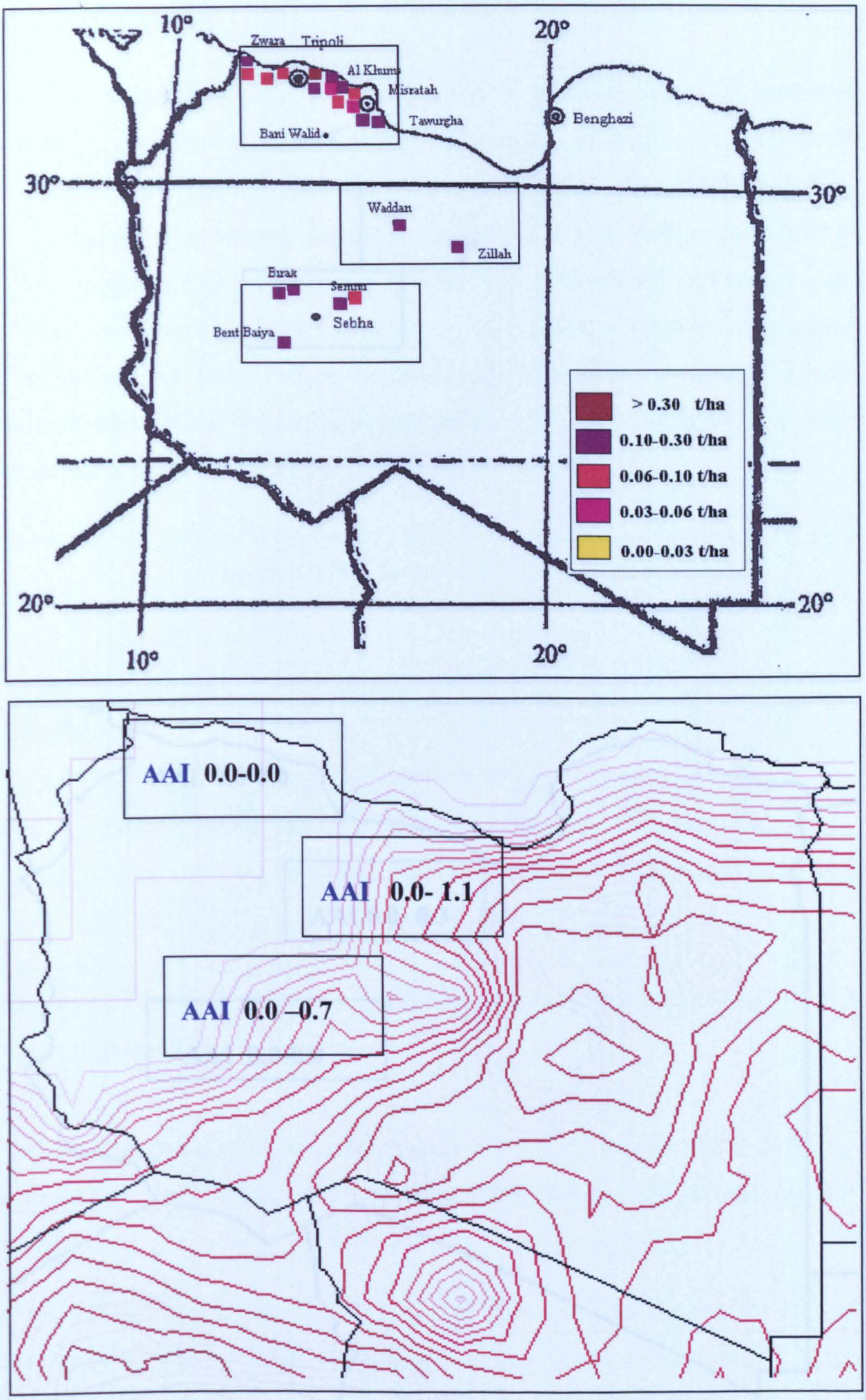

Figure 6.51 Vertical deposition versus TOMS aerosol index for April 2001

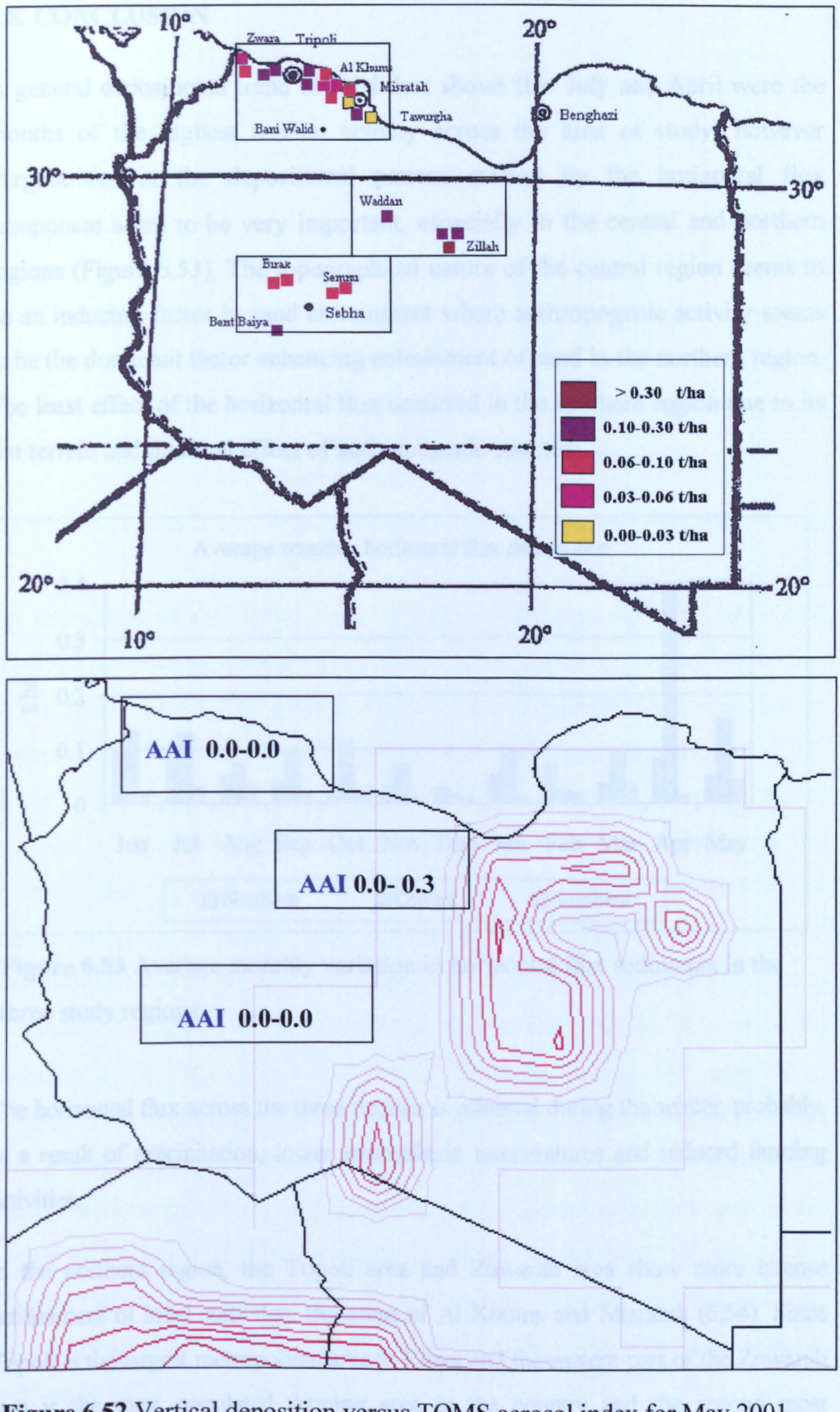

Figure 6.52 Vertical deposition versus TOMS aerosol index for May 2001

6.8. CONCLUSION

A general depositional trend of total dust shows that July and April were the months of the highest aeolian activity across the area of study, however irregularities in the depositional pattern created by the horizontal flux component seem to be very important, especially in the central and northern regions (Figure 6.53). The topographical nature of the central region seems to be an inducing factor in sand entrainment where anthropogenic activity seems to be the dominant factor enhancing entrainment of sand in the northern region. The least effect of the horizontal flux occurred in the southern region due to its flat terrain and minimal effect of anthropogenic sources.

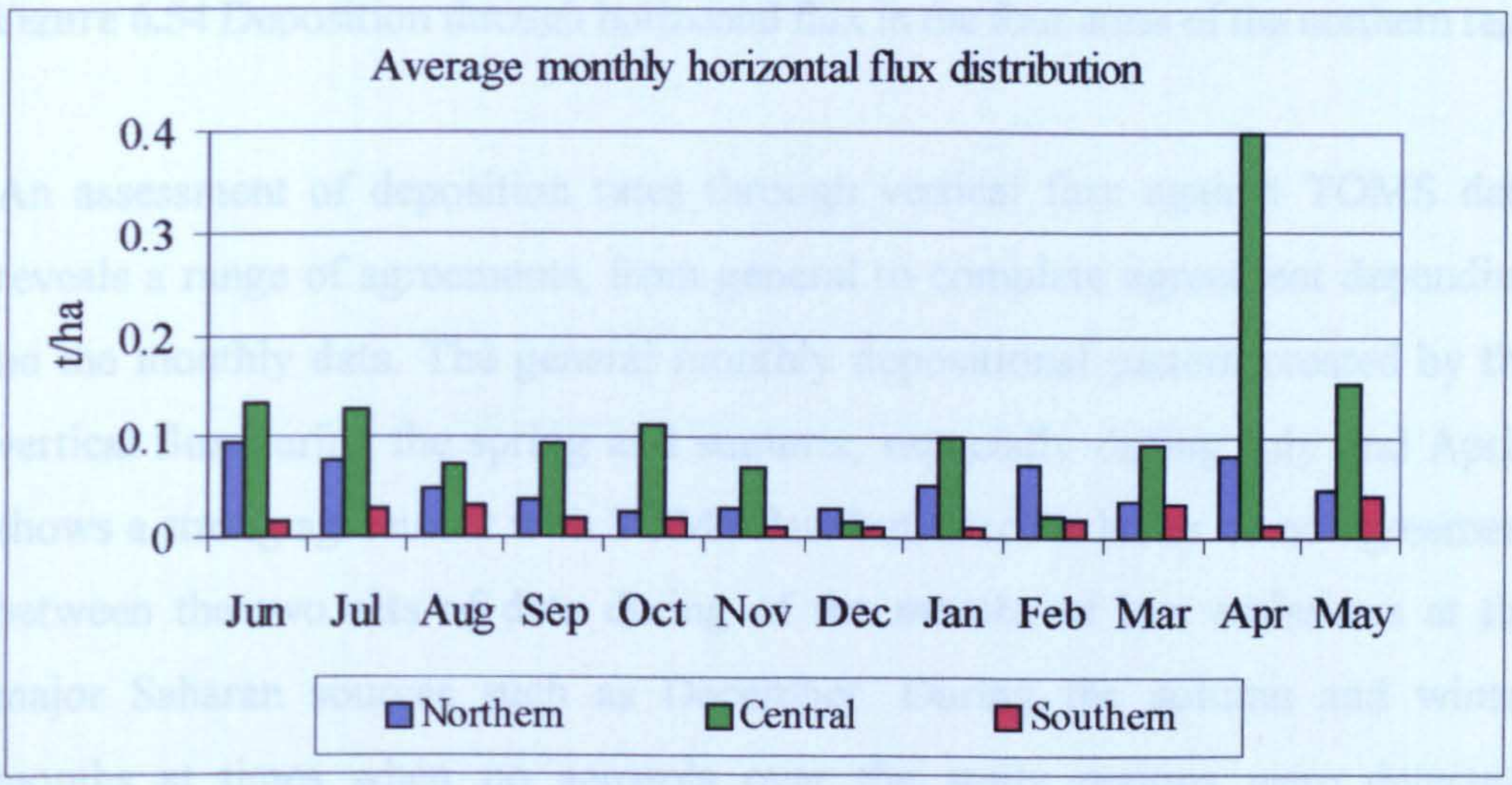

Figure 6.53 Average monthly variation in horizontal flux sediments in the three study regions

The horizontal flux across the three regions is minimal during the winter, probably, as a result of precipitation, lower atmospheric temperatures and reduced farming activities.

In the northern region, the Tripoli area and Zuwarah area show more intense entrainment of local soils than the areas of Al Khums and Misratah (6.54). Since Tripoli is the largest metropolitan area in Libya and the eastern part of the Zuwarah area is the most populated farming area in the country and the second most populated in the northern region, the excessive and irregular effects of the horizontal flux in these two areas can only be attributed to anthropogenic sources.

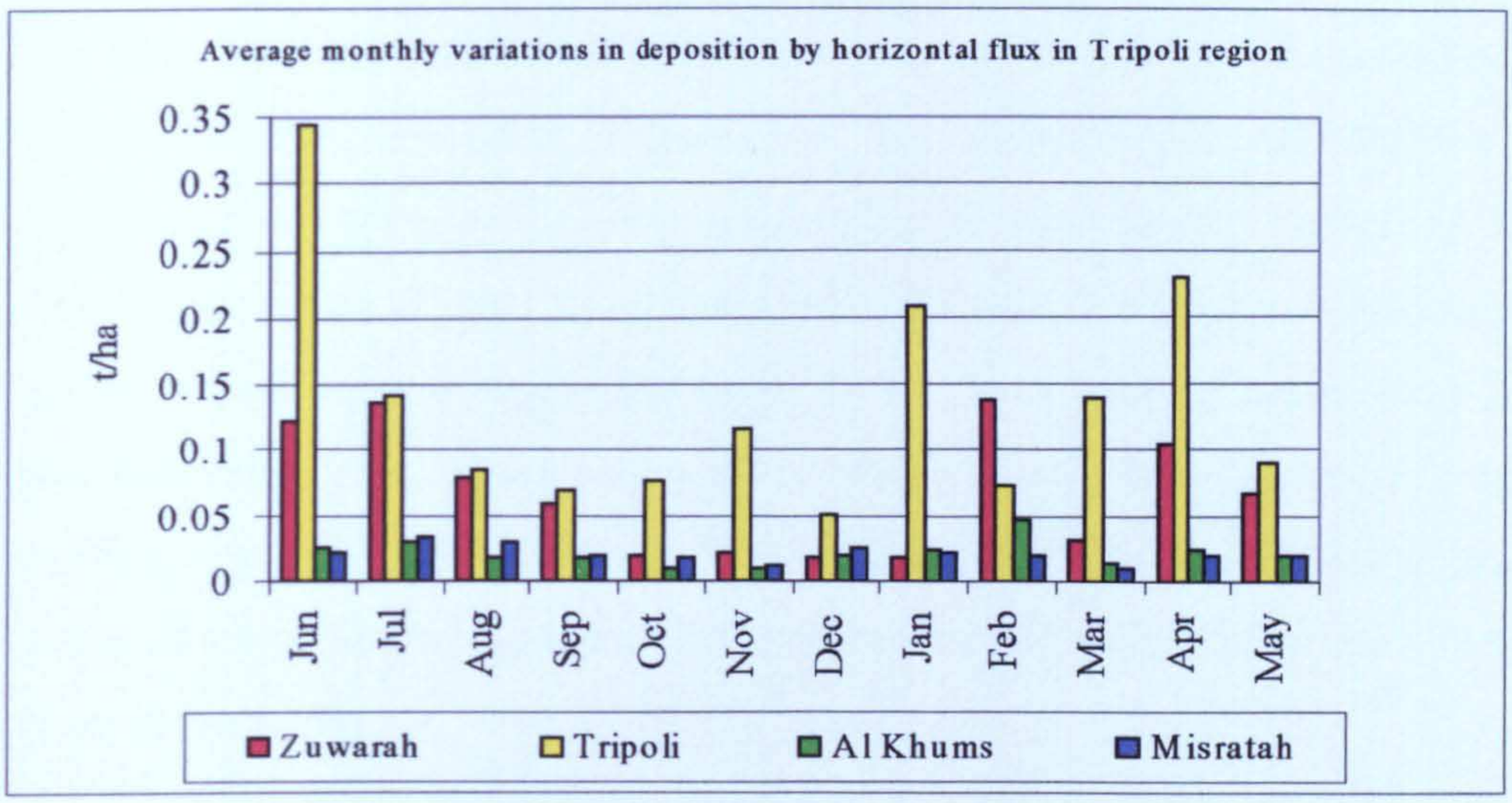

Figure 6.54 Deposition through horizontal flux in the four areas of the northern region

An assessment of deposition rates through vertical flux against TOMS data reveals a range of agreements, from general to complete agreement depending on the monthly data. The general monthly depositional pattern created by the vertical flux during the spring and summer, especially during July and April, shows a strong agreement with TOMS data but, there is lesser or no agreement between the two sets of data during of the months of low emissions at the major Saharan sources such as December. During the autumn and winter months at times when no aerosols over the study regions were detected, vertical dust fluxes were lower, but always present. It appears that transport in short-term suspension of particles sizes smaller than 70 μm is a persistent character of the aeolian activities within the study regions. The intensity of these activities in the northern and central regions seems to be higher than that in the southern region. These activities can be attributed to local natural sources such as wadis and sabkhas as well as industrial emissions such as the cement factories in the northern region. It appear that the likely sources of dust affected the study area are mainly the Libyan Desert during Summer 2000 and the Libyan Desert, Bodélé Depression during Spring 2001 given the prevailing wind directions.

CHAPTER 7

AEOLIAN DEPOSITION IN LIBYA: LOCAL VERSUS REGIONAL DUST FLUX

7.1. SOURCES AND SINKS

The three regions under investigation show a considerable spatial and temporal variation in dust deposition (Figure 7.1). The central region experienced the highest rates of deposition under an influence of what largely appears to be a local wind regime created by its hilly local terrain where the northern region comes second under a significant effect of disturbed soils by human activities and emissions from wadis and sabkhas and exposed lime stones. The least monthly deposited rates occurred in the southern region where the local terrain is free of any major topographic obstacles and human activities are far less than those in the north.

The three regions experienced the highest deposition during the month of April 2001 at times which were dominated by winds ranging from eastern to northern along the coast and from north eastern to south eastern inland. However, southern and south western winds were frequent in the north especially within the speed range of less than 6.5 m/s. March and May were some of the dustiest months of the year under persistent winds from southern directions affecting all three regions of study. Traditionally, increased deposition rates in the spring were associated with prevailing southern winds. Increased deposition in the spring is largely attributed to tropical air drawn from the south toward the north under the effect of the Saharan depression south of the Atlas Mountains (Algeria). The Saharan depression moves eastward creating a low pressure belt and often draws continental tropical air from the south northward as warm and dusty winds known as Sirocco or ghibli (Barry & Chorley, 1987). The coastal districts experience a relatively hotter weather and dusty ghibli winds from March to June. These winds come from the desert raise temperatures in the north up to 50° C for up to four days and carry dust up to high levels crossing the Mediterranean to Europe (Pearce and Smith, 1993). Temperatures recorded in the north during May 2001 reached 45.5° C.

During the summer months, dust was mainly transported to these areas along eastern trajectories. Collected samples in the southern region appear to be, on the one hand more of deposits of a moving aerosol over the region that settled on the surface under the effect of gravity during calm weather conditions and

on the other hand lesser entrainment of sand particle from the local terrain if compared with the northern and central regions. Despite the perturbation in the deposition trend introduced by local dust, deposition appears to be directly proportional to the atmospheric temperatures. This can be better concluded from data obtained from sites exposed to the minimal amount of saltating particles as those in the south. Wash out by rain does not correlate to a significant increase in dust deposition may be because of the overwhelming contribution of local dust, however, recorded precipitation during the winter in the northern and central regions may have had a role in cementing topsoil resulting in a lesser effect of the horizontal particle flux. Due to absence the of rain in the southern region during the winter months, the reduction in deposition rates can only be a result of low wind frequencies of winds ≥ 6.5 m/s.

In general, increased aeolian activities correlate with drought. Drought experienced along the coastal region during the peak of the rainy season, specifically during December 2000, was dominated by winds from southwestern directions resulting in a tri-modal deposition distribution in all of the northern areas and the southern region (Figure 7.1). Dominant wind direction during winter is usually from north and northwest rather than from southwest; therefore December 2000 was unrepresentative of most years (see chapter 1).

The variations in the monthly average TOMS AAI over the regions of study (Figure 7.2) indicates that aerosols derived from the main Saharan sources were denser and more frequent over the central region whereas the troposphere over the northern region experienced the least amount of aerosol loading. Although wind directions at low elevation are unrepresentative of the wind regime in the upper layers of the atmosphere and since the prevailing winds from east during the summer represent a general trend across Libya at times of pronounced emissions from the Qattara Depression and the narrow corridor east of Al Haruj Al Asuad in the Libyan Desert, this source seems to be the main supplier of minerals to western Libya during summer 2000. The aerosol

density is higher over the nearer study region from the source; therefore the central region must have received the largest amounts of aerosol.

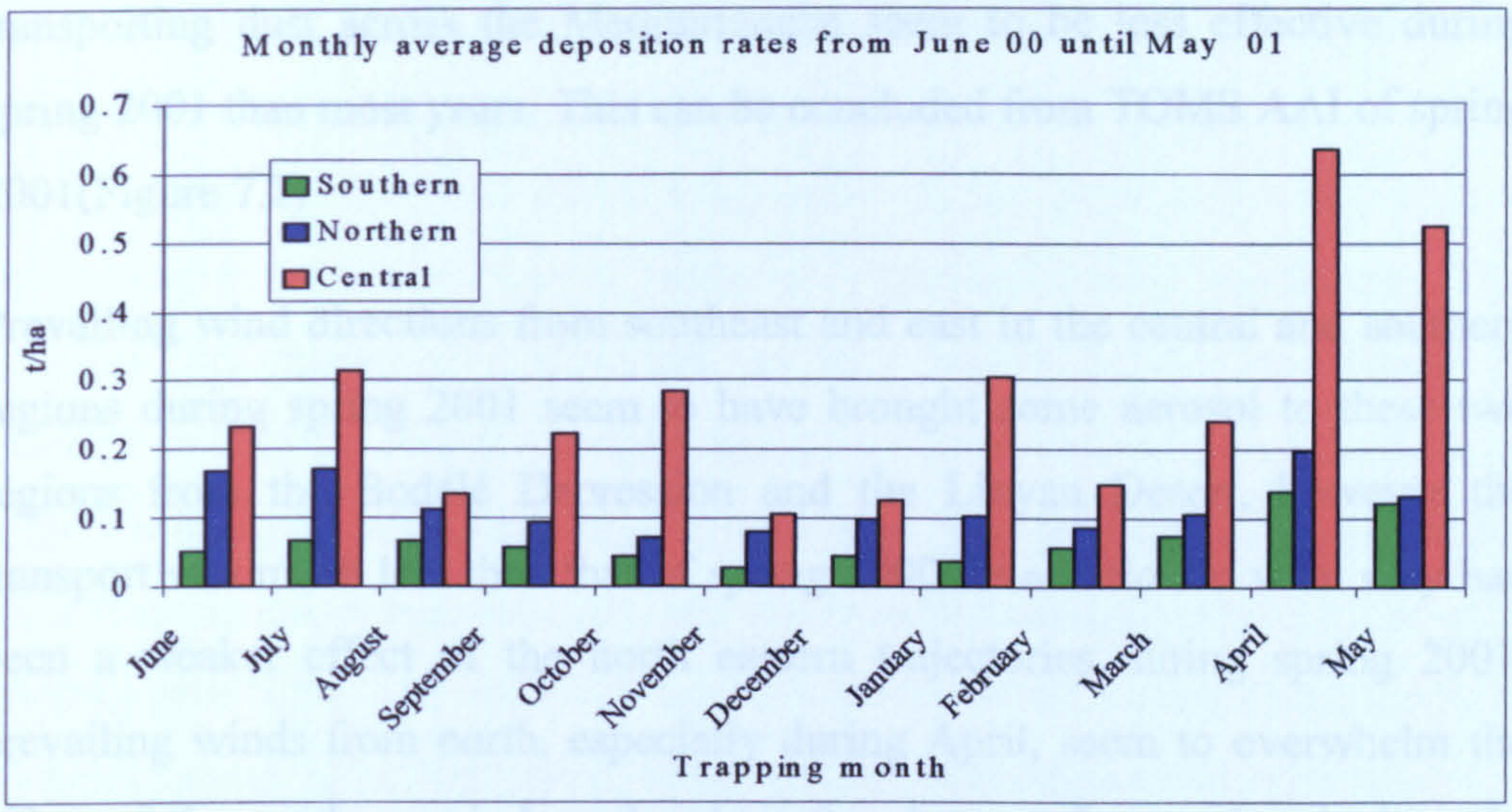

Figure 7.1 Monthly average total deposition rates in three regions of study

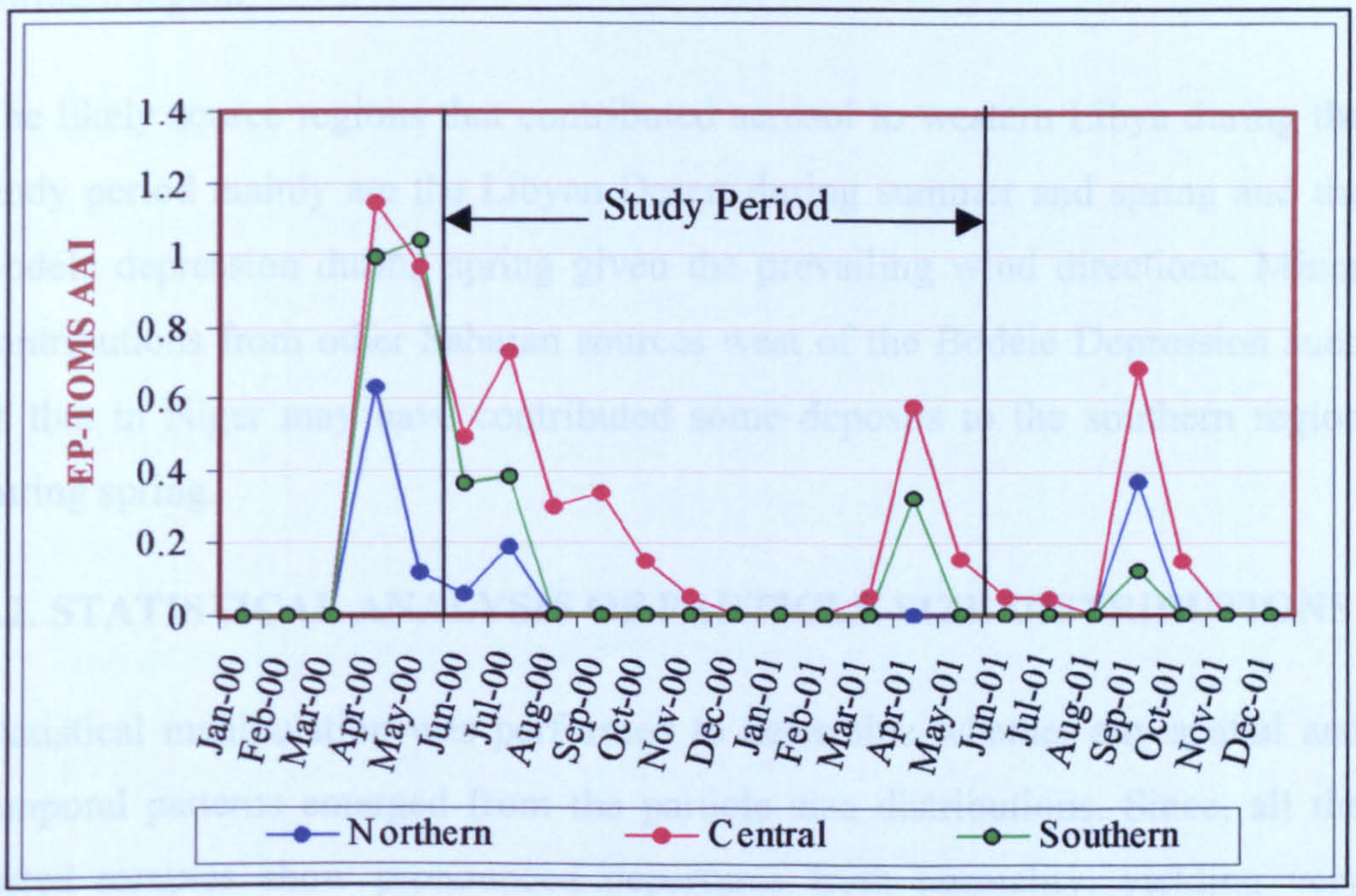

Figure 7.2 Monthly variations in EP-TOMS AAI monthly average values for each region

Aerosol transported during the spring of 2001 does not seem to follow the general trend of the main seasonal trajectories concluded from TOMS data of previous years as presented by Goudie (2003) and shown in Figure 1.5. The northern and north eastern trajectories induced by the Saharan depression transporting dust across the Mediterranean seem to be less effective during spring 2001 than most years. This can be concluded from TOMS AAI of spring 2001(Figure 7.2)

Prevailing wind directions from southeast and east in the central and southern regions during spring 2001 seem to have brought some aerosol to these two regions from the Bodélé Depression and the Libyan Desert, however the transport was much less than that of spring 2000. In addition to what may had been a weaker effect of the north eastern trajectories during spring 2001, prevailing winds from north, especially during April, seem to overwhelm the effect of the southern winds and reduce the chance of aerosol arrival to the northern region.

The likely source regions that contributed aerosol to western Libya during the study period mainly are the Libyan Desert during summer and spring and the Bodélé depression during spring given the prevailing wind directions. Minor contributions from other Saharan sources west of the Bodélé Depression such as that in Niger may have contributed some deposits to the southern region during spring.

7.2. STATISTICAL ANALYSIS OF PARTICLE SIZE DISTRIBUTIONS

Statistical manipulation was performed to determine whether any spatial and temporal patterns emerged from the particle size distributions. Since, all the tested samples show pronounced departures from normality, yielding very skewed multimodal distributions, it seems that any objective statistical analysis must be based on skewness and kurtosis of the particle size distribution data. Skewness and kurtosis account for sorting in the central portion as well as sorting in the tails of the skewed distributions. Skewness measures the extent to which the bulk of the values in a distribution are concentrated to one side or the other of the mean. If the bulk of the values are less than the mean, the

distribution is positively skewed but, if they are greater than the mean, the distribution is negatively skewed (Ebdon, 1996). Kurtosis measures the ratio between the sorting in the skewed portions and the sorting in the central portion of the distribution curve (Folk and Ward, 1957). Therefore, a normal distribution has a Kurtosis =0.0 and known as mesokurtic. If the distribution has a higher and sharper peak than the normal curve, then it has a larger kurtosis value (>0.0) and called leptokurtic. If the peak is broader than a normal curve, then the kurtosis value is (<0.0) and called platokurtic. The statistical parameters are calculated, as they would be for the frequency distribution with the number percent in a certain size channel being analogous to the frequency of occurrence of a certain value. Particle sizing channels in the LS-200 are spaced logarithmically, and are therefore increasingly wider in span toward larger sizes. The statistical calculations are based on logarithmic centre of each channel. Skewness and Kurtosis are determined geometrically from the following equations (Coulter Corporation, 1994):

$$g_1 = \sum [n_c (\log x_{gc} - \log x_g)^3] / SD_g{}^3 \sum n_c \qquad (7.1)$$

$$g_2 = \sum [n_c (\log x_c - \log x_g)^4] / SD_g{}^4 \sum n_c \qquad (7.2)$$

Where,

g_1 = Skewness

g_2 = Kurtosis

n_c = Percentage of particles in the C'th channel.

x_c = Weighted centre of the C'th channel in μm^3.

x_g = Geometric mean = antilog [[$\sum(n_c \times \log x_c)$] / $\sum n_c$].

SD_g = Geometric standard deviation = antilog [$\sum [n_c (\log x_c - \log x_g)^2] / \sum n_c]^{1/2}$

The frequency distributions of the monthly dust samples and their corresponding topsoil particle size distribution plots provide an appropriate visual insight of the monthly variations in dust grain size distributions and a quick comparison with the surface samples distributions. The extent of local

soil contribution to a dust sample is more pronounced as a dust sample plot becomes more identical in peakedness and skewness to that representing the soil sample at the same trapping sites.

The skewness-kurtosis data for each dust sample are plotted on six graphs representing the four areas in the north, central and southern regions under study (Figures 7.3-7.8). If traced in a clockwise direction, the data points plotted in the second, third and forth quadrants of the coordinate axis, would demonstrate an increase in grain median sizes. For example, the southern samples show dominant fraction of clay and fine silt (Figure 7.8) whereas the Tripoli area samples are dominated by sand (Figure 7.4). On the skewness-kurtosis scatter plots, extreme high and low values of kurtosis indicate that different parts of the sediments achieved their sorting in different geographical regions. Poorest sorting is found in multimodal sediments and those have the lowest kurtosis such as the Semnu samples (Figure 7.8). Kurtosis is highest in those samples where one mode dominates and the other is subordinate such as the Tripoli sediments (Figure 7.4). The sediments trapped at the southern sites show lower kurtosis values as an indication of their pronounced bimodality and probable multimodality and poorer sorting. This implies that each sample consists of a mixture of sediments, retaining their individual characteristics and the resulting mixture is of less effective sorting (departing from unimodality).

Topsoil samples taken from the local terrain do not represent unimodal distributions, but they rather display a dominant fraction of a single mode of fine and medium size sand. Soil samples at each trapping site display higher kurtosis values if compared with the trapped samples as an indication of one dominant mode. Some of the point coordinates representing dust samples appear to be either identical or the same as those representing the local soil sample at the same site, however, this is an indication of a similar modality rather than a similarity in grain size distribution contents.

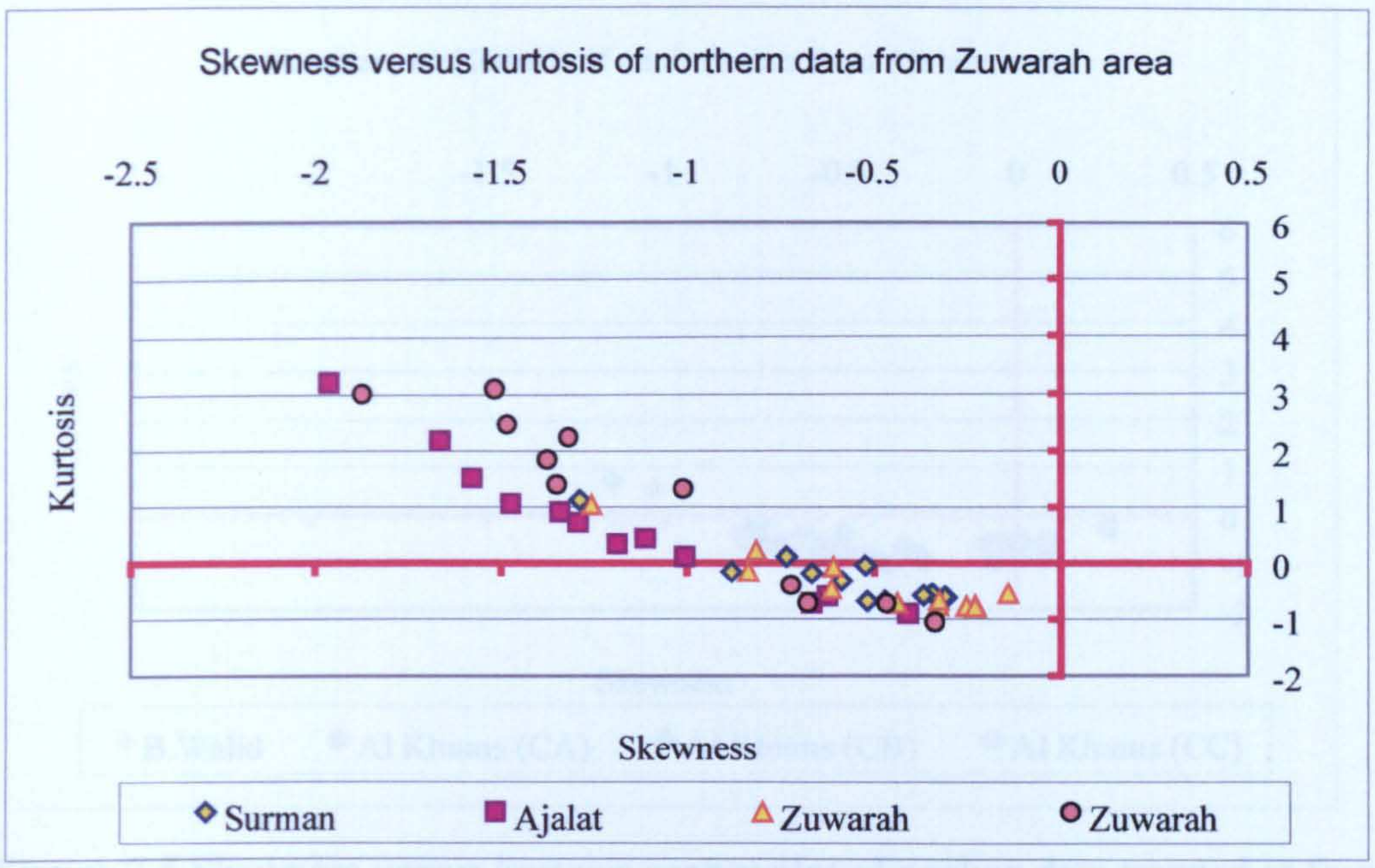

Figure 7.3 Skewness versus kurtosis scatter plot of aeolian data trapped at four sites in the northern region (Zuwarah area)

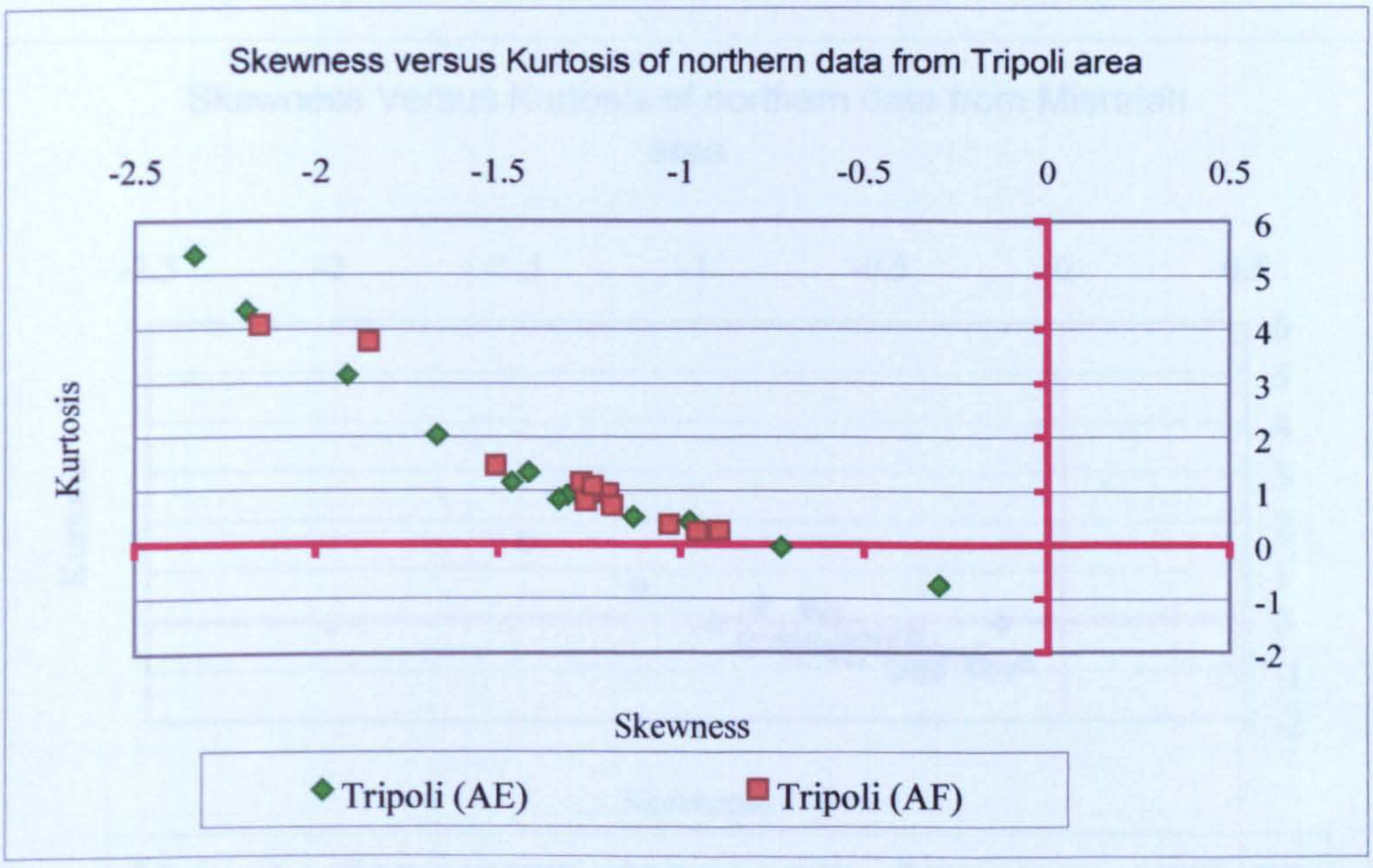

Figure 7.4 Skewness versus kurtosis scatter plot of aeolian data trapped at two sites in the northern region (Tripoli area)

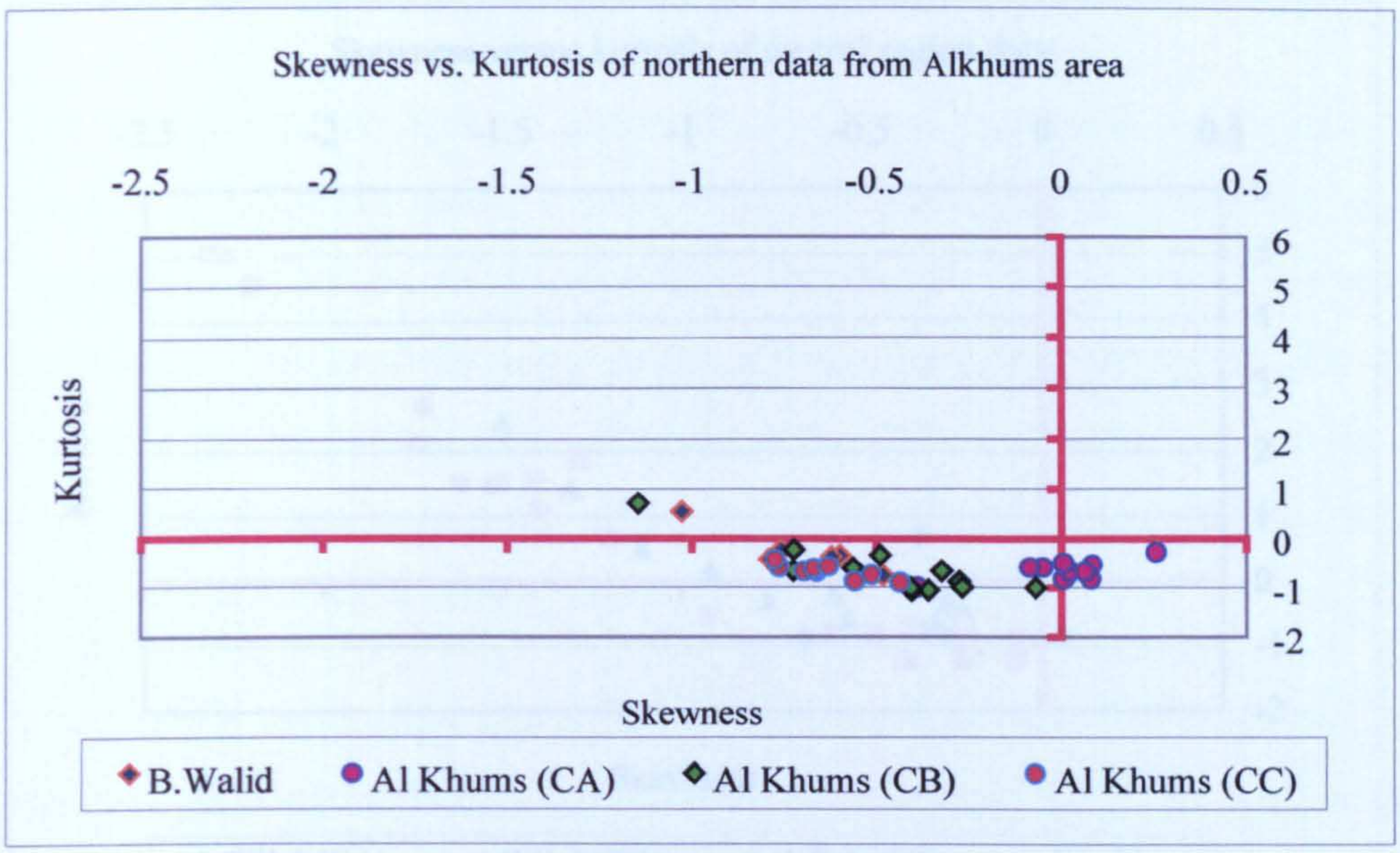

Figure 7.5 Skewness versus kurtosis scatter plot of aeolian data trapped at four sites in the northern region (Al Khums area)

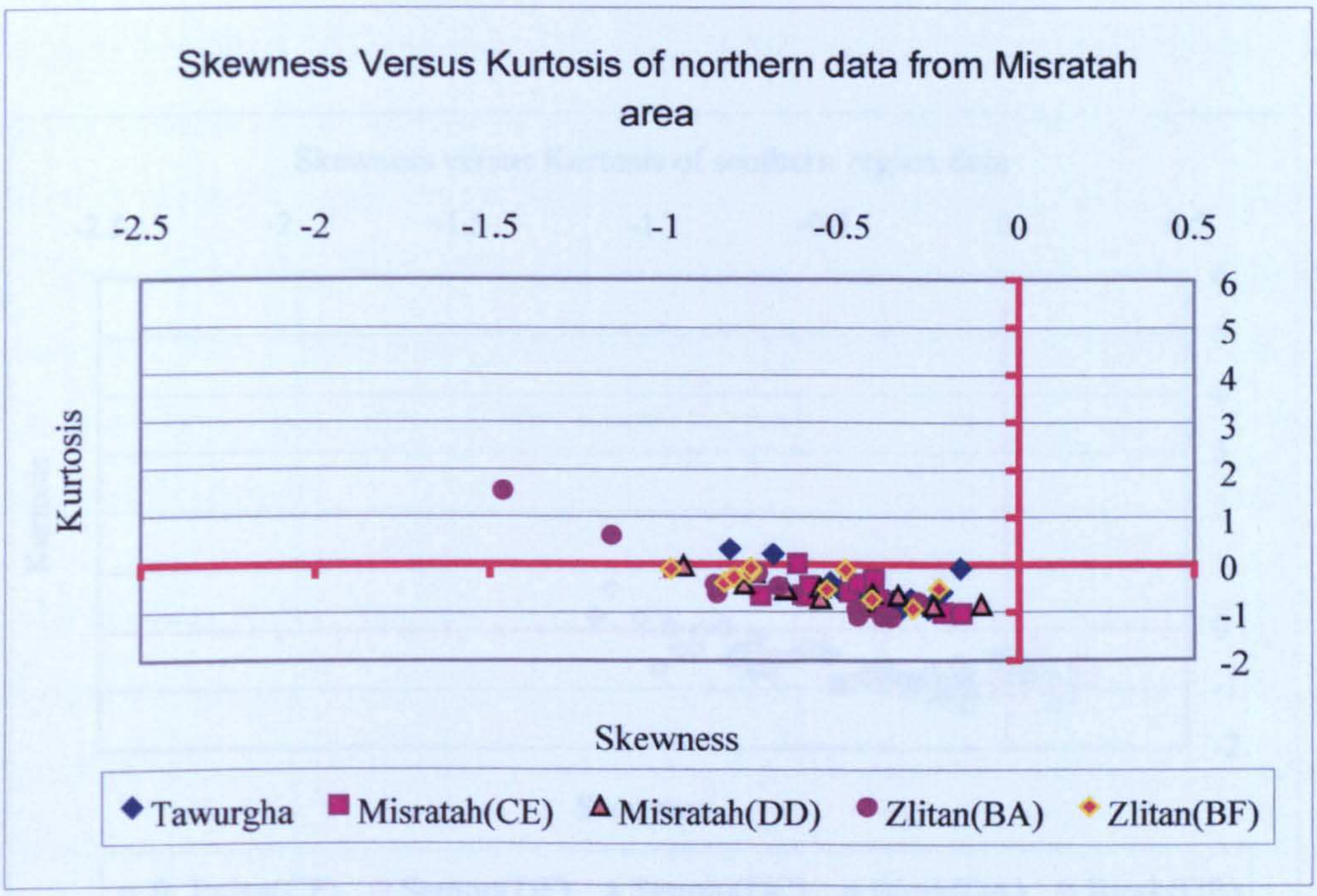

Figure 7.6 Skewness versus kurtosis scatter plot of aeolian data trapped at five sites in the northern region (Misratah area)

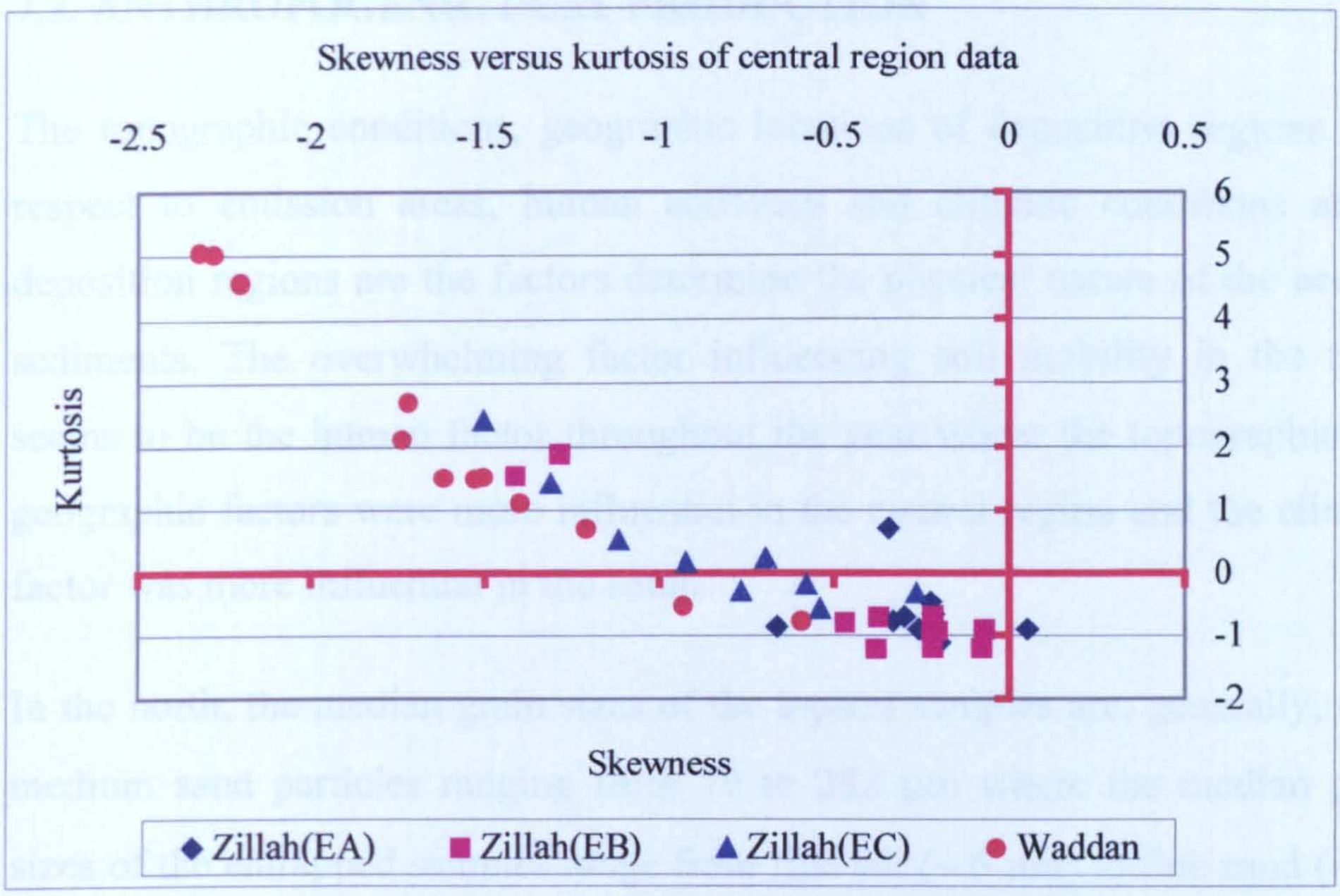

Figure 7.7 Skewness vs. Kurtosis scatter plot of aeolian data trapped at four sites in the central region

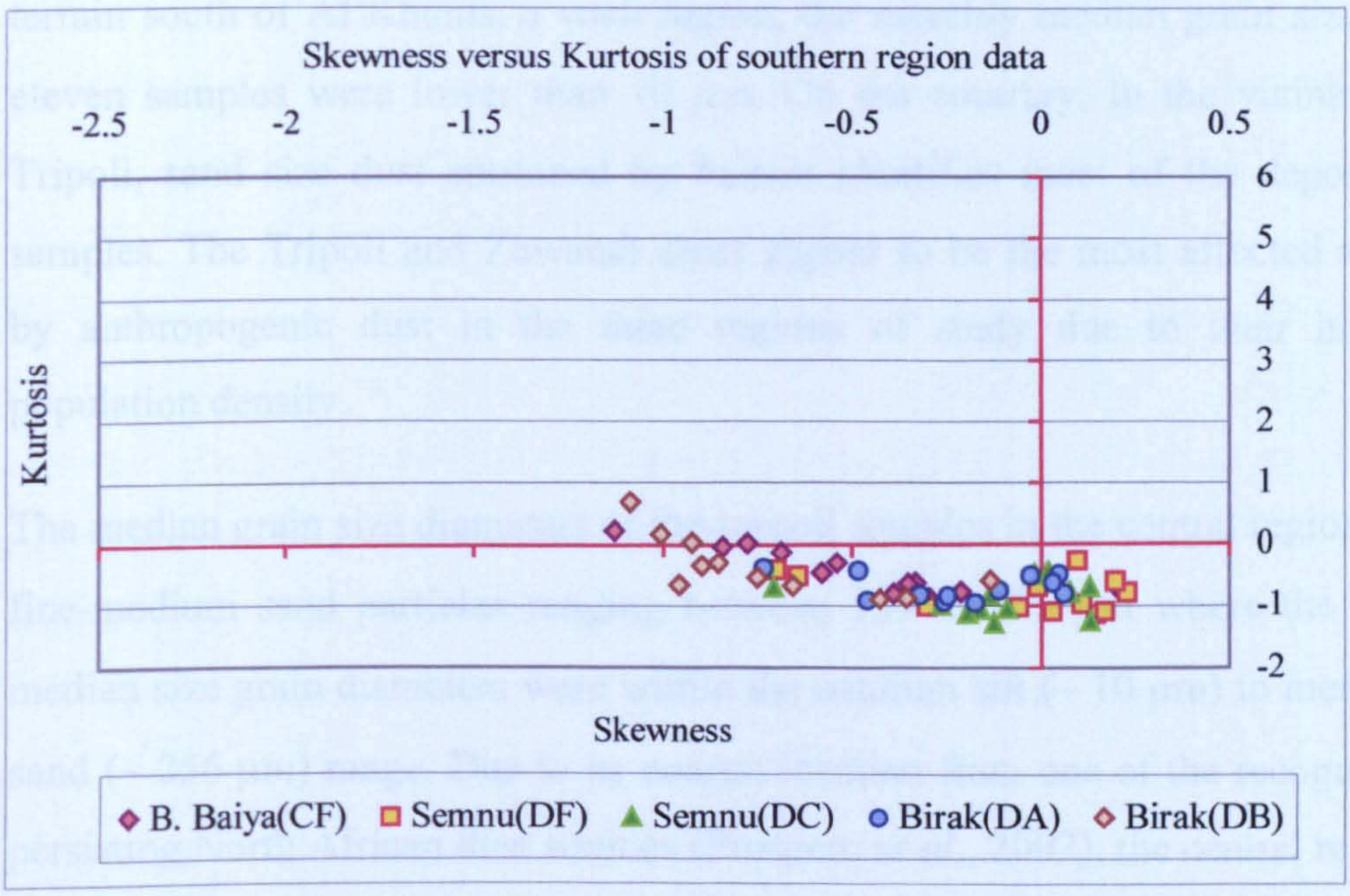

Figure 7.8 Skewness vs. Kurtosis scatter plot of aeolian data trapped at five sites in the southern region

7.3. ANTHROPOGENIC DUST PRODUCTION

The topographic conditions, geographic locations of deposition regions with respect to emission areas, human activities and climatic conditions at the deposition regions are the factors determine the physical nature of the aeolian sediments. The overwhelming factor influencing soil mobility in the north seems to be the human factor throughout the year where the topographic and geographic factors were more influential in the central region and the climatic factor was more influential in the south.

In the north, the median grain sizes of the topsoil samples are, generally, fine-medium sand particles ranging from 79 to 282 μm where the median grain sizes of the entrapped samples range from fine silt (~ 6 μm) to fine sand (~115 μm) depending on the trapping site locations, the dominant geomorphologic features and the local atmospheric conditions at each site. Sites in the proximities of sabkhas and wadis, regardless the climatic conditions, contained higher fractions of fine dust. At a typical site, in that sense, erected on a hilly terrain south of Al Khums, a wadi region, the monthly median grain sizes of eleven samples were lower than 10 μm. On the contrary, in the vicinity of Tripoli, sand size dust entrained by human identifies most of the deposited samples. The Tripoli and Zuwarah areas appear to be the most affected areas by anthropogenic dust in the three regions of study due to their higher population density.

The median grain size diameters of the topsoil samples in the central region are fine-medium sand particles ranging between 133 to 295 μm where the dust median size grain diameters were within the medium silt (~ 10 μm) to medium sand (~ 256 μm) range. Due to its nearest location from one of the recognized persisting North African dust sources (Prospero *et al.*, 2002), the central region seems to receive considerable amounts of a wide range of grain size sediments from the northern and western areas of the Libyan Desert. In addition, the central study region acts as a natural trap by accumulating large amounts of sand nested within its hilly terrain. This region experienced the most pronounced dust activities represented by the highest deposition rates of the

widest range of grain size distributions as an indication of strong activities through both modes of transport, horizontal and vertical. The grain size analysis shows that the southern region is the least affected by transport through horizontal flux, seemingly, due to the absence of any topographical obstacles and limited human activities.

7.4. MINERAL COMPOSITION VERSUS SOURCE

The mineralogical analysis of collected dust samples in the northern and the southern regions show that they were dominated by quartz ranging from 30 to 80 %. The northern coastal sites contained higher percentages of halite, calcite and dolomite, probably, due to the effects of salt aerosol originated in the Mediterranean and the coastal Sabkhas and exposed limestones which are rich in calcite and dolomite in the region. The southern samples are better identified by a higher presence of Kaolinite reaching a maximum percentage of 12.5 % per weight in the sample of May 2001. In general, increased Kaolinite in deposited dust correlated with southwestern and southeastern winds, indicating that this mineral was largely originated in the Bodele Depression and Erg du Djourab in Chad and the vicinity of the Ahaggar Mountains in southern Algeria. Gypsum rates found in the southern samples were slightly higher than those in the northern samples. More gypsum was deposited in the north and the south during the summer and the spring which can mainly be attributed to the calcareous soils in the central part of Libya at Al Hammada Al Hamrah, the region to north of the Great Sand Sea and around Al Haruj Al Asuad which are reported to contain gypsum (The Secretary of Planning, 1978). Other minerals such as albite, anorthite, orthoclase, illite, chlorite, palgorskite were present in small quantities in most of the tested samples but they yielded no clear trend.

7.5. CONCLUSIONS

- An emerging general trend of variations in deposition rates across the northern and the southern regions manifest itself in a tri-modal distribution with two major modes corresponding to the summer 2000 and spring 2001 where the highest deposition rate corresponds with the month of April. The deposition pattern in the central region neither

follows a clear trend nor lend it self to a direct interpretation. The central region seems to undergo irregular deposition of sand dislodged from the surface under the influence of local wind regimes created by its undulating terrain and wind funnelling effects created by the inter-mountainous corridors in this region. Therefore, the central region has experienced the highest monthly deposition rates (Figure 7.1).

- Although winds below the threshold velocity of 6.5 m/s were more frequent, entrained sand from topsoil have constituted the dominant fraction of the deposited sediments. This is concluded from a persistent significant presence of sand size particles in every dust sample and the dominant quartz in their mineral composition. On dry and bare soils a wind threshold of 6.5 m/s seems to appropriate in interpreting the variations in deposition data. Precipitation during the rainy months seems to play a significant role in reducing the effects of the horizontal flux by cementing the topsoil in the northern and central regions. Since the southern region received no rainfall, reduced effect of the horizontal flux during the winter seems to result from the lowest frequency of winds above the threshold velocity.
- The particle size analysis reveals that deposition in the northern region was largely influenced by anthropogenic dust that can be attributed to farming, automobiles driving and civil constructions. The frequency plots of the dust samples entrapped in the Tripoli area, the most populated city; seem to mimic those of the corresponding topsoil at the same area.
- The main dust sources that have contributed to deposition in the study area seem to be the eastern Libyan Desert during the summer months and a number of other Saharan sources, mainly the Bodele Depression and the eastern Libyan Desert. Natural emissions from local sources within the regions of study are mainly present in the northern region which include sabkhas and wadis.
- The lack of any aerosol over the north western coastal region and the low aerosol index values over the central and southern regions during the spring 2001 makes the sampling year low dust transport year.

Therefore, the sampling period cannot be regarded as a representative year of the general trend of transport and deposition.

7.6. LIMITATIONS AND RECOMMENDATIONS

This study provides the first field-based test of TOMS data, but it is temporally limited. The year 2000-2001 was not a year of major dust storms as the aerosol index was very low during the traditionally high emission and transport season of spring. The north eastern Saharan dust trajectories during spring dominating most of Libya, as illustrated in Figure (1.5), were not as effective during the spring 2001 as most years. For example, the monthly average AAI of April 2000 over the central region reached 1.15 about double the intensity of AAI for April 2001 (AAI=0.58). Therefore, the sampling year does not represent a general trend of transport over Libya and consequently deposition of clay minerals in study regions is also unrepresentative of most years.

The choice of an Astroturf trap for dust monitoring was made on qualitative basis such as the environmental conditions in the field of work, the feasibility of servicing a large number of traps in a sporadically inhabited part of the world and trap cost. In theory, a less polarized trap sites distribution would yield a more representative data, however, in reality there are vast regions in Libya that are not inhabited at all. The shortage of the Meteorological ground stations is another limiting factor for any large scale studies in the Saharan countries. Therefore, we have assumed that meteorological conditions at each trapping site are identical to those at the nearest station which may not necessarily be representative. Moreover, lack of information on the atmospheric conditions influencing aerosol transport in the upper atmosphere limit the exploitation of the TOMS data contour maps that can lead to better understanding of prevailing direction of aerosol movement and help linking deposited minerals to their emission sources.

The findings of this research lay the ground for any further dust trapping studies in Libya and North Africa in general as well as studies explaining dust effects on human health and the environment. Future studies should cover other areas in the eastern part of the country and target emissions from the eastern

Libyan Desert, the dominant source during summer and an influential source during spring. In a representative year the north eastern trajectories over Libya are product of number of Saharan sources including those in southern Algeria, Mali, Niger and Chad.

Since the period of study was very low in aerosol, the mineralogical testing was only based on the remainder from grain size distribution testing of the bulk samples. In order to utilize the mineral composition of entrapped dust, future studies should focus on mineral suits on the clay fraction to be better able to link deposited clay minerals to source areas. Grain size distribution analysis should be excluded so sufficient clay for XRD testing can be retrieved from the samples.

Trapping efficiency of Astroturf is internally consistent with an average error of 4.3 %, but it needs to be determined more accurately and compared with other traps (e.g. marbles) under similar environmental conditions.

7.7. IMPLICATIONS

This study concludes that large proportions of emissions within the study regions are local dust and their health impacts are also localised, therefore a direct study is possible. The implication of halite on soil fertility is one of the environmental problems that need to be studied in a country of limited agricultural lands. Aeolian sediments rich in sodium emitted from the coastal sabkhas and the long range transported aerosols that seem to be emitted, mainly, from playa regions are likely to be hazard affecting the chemical balance of fertile soils. Sodium chloride content reached 28.2 and 21% in April and May samples in the vicinity of Sabkhat Tawurgha where its content in the topsoil is only 0.1 %. It is likely that the soluble-salt component of dust is more efficiently moved downward into the soils because it is more easily dissolved by the infrequent rains.

REFERENCES

Alpert, P., and Ganor, E., 1993. A jet stream associated with heavy dust storm in the western Mediterranean. *J. Geophys. Res.*, 98D, 7339-7349.

Amit, R. and Gerson, R., 1986. The evolution of Holocene reg (gravely) soils in deserts-an example from the Dead Sea region. *Catena*, 13, 59-79.

Anketell, J. M., 1989. Quaternary Deposits of Northern Libya-Lithostratigraphy and correlation. *Libyan Studies*, 20, 1-29.

Aren, S. M., and Van der Lee, G. E. M., 1995. Saltation sand traps for the measurement of aeolian transport into the foredunes. *Soil Technology*, 8, 61-74.

Arimoto, R., 2001. Eolian dust and climate: relationships to sources, tropospheric chemistry, transport and deposition. *Earth-Science Reviews*, 54, 29-42.

Armandi, R., 1976. Libya, *In*: Committee for the World Atlas of Agriculture, ed. *World Atlas of Agriculture*, Volume 4. Novara, Italy: Institute Geogrphico De Agostini S.P.A., 1976, pp. 296-308.

Assallay, A. M., Rogers, C. D. F., Smalley, I. J., and Jefferson, I. F., 1998. Silt: 2-62 μm, 9-4 φ. *Earth-Sci. Rev.*, 45, 61-88.

Assalley, A. M., Rogers, C. D. F., and Smalley, I. J., 1996. Engineering properties of loess in Libya. *J. Arid Env.*, 32, 373-386.

Augusti, G., Borri, C., and Niemann, H., 2001. Is Aeolian risk as significant as other environmental risks? *Reliability Engineering and System Safety*, 74, 227-237.

Bagnold, R. A., 1941. *The Physics of Blown Sand and Desert Dunes.* London: Methuen & Co. Ltd.

Barry, R. G., and Chorley, R. J., 1998. *Atmosphere, Weather and Climate*. 7th ed. London: Routledge.

Belly, P. Y., 1964. Sand movement by wind. *US Army Corps of Engineers, Coastal Engineering Research Centre, Tech. Memo. No. 1*, pp.1-38.

Bergametti, G., Gomes, L., Ramoudaki, E., Desbois, M., Martin, D., and Buat-Menard, P., 1989. Present transport and deposition patterns of African dust to the north-eastern Mediterranean. *In*: M. Leinen, and M., Sarntheim, eds. *Paleoclimatology and Paleometeorology*: *Modern and Past Patterns of Global Atmospheric Transport*. Dordrecht: Kluwer, 1989, pp. 227-252.

Bisal, F., and Hsieh, J., 1966. Influence of moisture on erodibility of soil by wind. *Soil Sci.* 102, 143-146.

Bisal, F., and Nielsen, K. F., 1962. Movement of soil particles in saltation. *Can. J. Soil. Sci.*, 42, 81-86.

Blake, G., Dewdney, J., and Mitchell, J., 1987. *The Cambridge Atlas of The Middle East and North Africa*. Cambridge: Cambridge University Press.

Brooks, N., 1999. *Dust-climate interactions in the Sahel-Sahara zone of northern Africa, with particular reference to late twentieth century Sahelian drought* [online]. UK: University of East Anglia. Available at: <http://www.rdg.ac.uk/~sgs99npb/thesis.html> [Accessed 21/11/2001].

Bruins, H. J., and Lithwick, H., 1998. *The Arid Frontier: Interactive Management of Environment and Development*. Dordrecht, Netherlands: Kluwer Academic Press.

Buhrke, V. E., Jenkins, R., and Smith, D. K., 1998. A Practical Guide for the *Preparation of Specimens for X-Ray Fluorescence and X- Ray Diffraction Analysis*. New York: Wiley-VCH.

Callot, Y., Marticorena, B. and Bergametti, G., 2000. Geomorphologic approach for modelling the surface features of arid environments in a model of dust emissions: application to the Sahara desert. *Geodinamica Acta*, 13(5), 245-270.

Carbon Dioxide Information Analysis Center, 1990. *Carbon Dioxide and Climate Glossary*. Oakridge National Laboratory, ORNL/CDIAC-39.

Central Intelligence Agency, 2002. *The World Fact book 2002 - Libya* [online]. Available at: <http://www.odci.gov/cia/publications/factbook/geos/ly.html#Intro> [Accessed 09/12/2002].

Chepil, W. S., 1945. Dynamics of wind erosion: IV. The translocating and abrasive action of wind. *Soil Sci.*, 61, 169-177.

Chepil, W. S., 1956. Influence of moisture on erodibility of soil by wind. *Soil Sci. Soc. Am. Proc.*, 20, 288-292.

Chepil, W. S., 1959. Equilibrium of soil grains at the threshold of movement by wind. *Soil Sci. Soc. Am. Proc.*, 23, 422-428.

Chepil, W. S., and Milne, R. A., 1941. Wind erosion of soil in relation to size and nature of exposed area. *Sci. Agric.*, 19, 279-287.

Choa, S. C., and Xing, J. M., 1982. Origin and development of the Shano (sandy deserts) and the Gobi (sandy deserts) of China. *Striae*, 17, 79-91.

Claquin, T., Schulz, M., and Balkanski, Y. J., 1999. Modelling the mineralogy of atmospheric dust sources. *J. Geophys. Res.*, 104(D18), 22,243-22,256.

Clement, T., Stone, R. O., Mann, J. F., and Eymann, J. L. 1963. A study of borne - wind sand and dust in desert areas. *US Army Natick Laboratories, Earth Sci. Div., Tech. Rep. ES8*, 61pp.

Cooke, R., Warren, A. and Goudie, A., 1993. *Desert Geomorphology*. London: UCL Press.

Corbett, S. W., 1996. Asthma exacerbations during Santa Ana Winds in southern California. *Wilderness and Environmental Medicine*, 4, 304-311.

Coulter Corporation, 1994. *Product Manual, Coulter LS Series, PN 4237214A.* Coulter Corporation, Miami, USA.

D'Almeida, G. A., 1986. A model for Saharan dust transport. *J. Climate. Appl. Met.*, 25, 903-916.

Darby, D. A., Buckle, L. H., and Clark, D. L., 1974. Airborne dust on Arctic pack ice: Its composition and fallout rate. *Earth Planet Sci. Lett.*, 24, 166-172.

Dayan, U., Heffter, J., Miller, J., and Gutman, G., 1991. Dust intrusion events into the Mediterranean Basin. *J. Appl. Met.*, 30, 1185-1199.

deMenocal, P.M. and Rind, D., 1993. Sensitivity of Asian and African climate to variations in seasonal insolation, glacial ice cover, sea-surface temperature, and Asian orography. *J. Geophys. Res.*, 98(4), 7265-7287.

deMenocal, P.M., 1995. Plio-Pleistocene African Climate. *Science*, 270, 53-59.

Drees, L. R., Manu, A., and Wilding, L. P., 1993. Characteristics of aeolian dust in Niger, West Africa. *Geoderma*, 59, 213-233.

Ebdon, D., 1996. *Statistics in Geography*. 2nd ed. Oxford: Blackwell.

Erell, E., and Tsoar, H., 1999. Spatial variations in the aeolian deposition of dust - the effect of a city in Be'er-Sheva, Israel. *Atmospheric Environment*, 33, 4049-4055.

Fairall, C.W>, Davidson, K.L. and Schacher, G.E., 1983. An analysis of surface production of sea-salt aerosol. *Tellus*, 35B, 31-39.

FAO, 1984. *Agroclimatological Data for Africa*, Vol. 1. Rome: FAO.

Fennelly, P.F., 1976. The origin and influence of airborne particulates. *Am. Scient.*, 64, 46-56.

Fisher, W. B., 2003. Libya - physical and social geography. *In*: J. Maher, ed. *Regional Survey of The World - The Middle East and North Africa.* 49th ed. London: Europa Publications Ltd.

Folk, R. L., and Ward, W. C., 1957. Brazos River Bar: A study in the significance of grain size parameters. *J. Sed. Petrol.*, 27, 3-26.

Fookes, P. G., and Gahir, J. S., 1995. Engineering performance of some coarse-grained arid soils in the Libyan Fezzan. *Quarterly J. Eng. Geology*, 28(2), 105-130.

Fryrear, D. W., 1986. A field dust sampler. *J. Soil and Water Conservation*, 41, 117-120.

Ganor, E., and Mamane, Y., 1982. Transport of Saharan dust across the eastern Mediterranean. *Atmos. Env.*, 16(3), 581-587.

Genthon, C., 1992. Simulations of desert dust and sea salt aerosols in Antarctica with a general circulation model of the atmosphere. *Tellus*, 44 (B4), 371-389.

Gerson, R., Amit, R. and Grossman, S. 1985. *Dust availability in desert terrain - A study of the desert of Israel and Sinai.* Report to the US Army Research, Development and Standardisation Group, UK, Contract No. DAJA 45-83-C-0041.

Gerson, R., and Amit, R. 1987. Rates and modes of dust accretion and deposition in an arid region-the Negev, Israel. *In*: L. Frostick, and L. Reid, eds. *Desert Sediments: Ancient and Modern*, Special Publication of the Geological Society, 35, 157-169.

Gillette, D. A., 1978a. A wind tunnel simulation of the erosion of soil: effect of soil texture, sandblasting, wind speed, and soil consolidation on wind production. *Atmos. Env.*, 12, 1735-1743.

Gillette, D. A., 1979. Environmental factors affecting dust emission by wind erosion. *In*: C. Morales, ed. *Saharan Dust – Mobilization, Transport, Deposition.* Chichester: Wiley, 1979, pp. 71-91

Gillette, D. A., 1981. Production of dust that may be carried great distances. *Geol. Soc. Am. Spec. Pap.*, 186, 11-26.

Gillette, D. A., 1999. A quantitative geophysical explanation for "hot spot" dust emitting source regions. *Contrib. Atmos. Physics*, 72, 67-77.

Gillette, D. A., Adams, J., Endo, L., and Smith, D., 1980. Threshold velocities for input soil particles into the air by desert soils. *J. Geophys. Res.*, C85, 5621-5630.

Gillette, D. A., Adams, J., Muhs, D. R., and Kihl, R., 1982. Threshold friction velocities and rupture moduli for crushed desert soils for the input of soil particles into the air. *J. Geophys. Res.*, 87(C11), 9003-9015.

Gillette, D. A., Blifford, I. H., and Fryear, D. W., 1974. The influence of wind velocity on the size distributions of aerosols generated by the wind erosions of soils. *J. Geophys. Res.*, 79, 4068-4075.

Gillette, D. A., Marticorena, B., and Bergametti, G., 1998. Change in the aerodynamic roughness height by saltating grains: Experimental assessment, test of theory, and operational parameterisation. *J. Geophys. Res.*, 103, 6203-6210.

Gillette, D.A., 1978b. Tests with a portable wind tunnel for determining wind erosion threshold velocities. *Atmos. Env.*, 12, 2309-2313.

Glaccum, R. A., and Prospero, J. M., 1980. Saharan aerosol over the tropical North Atlantic: mineralogy. *Marine Geology*, 37, 295-321.

Goossens, D., 1995. Field experiments of Aeolian dust accumulation on rocky fragment substrata. *Sedimentology*, 42, 391-402.

Goossens, D., 2000. Dry Aeolian dust accumulation in rocky deserts: A medium-term field experiment based on short-term wind tunnel simulations. *Earth Surface Process and Landforms*, 25, 41-57.

Goossens, D., and Offer, Z. Y., 1994. An evaluation of the efficiency of some eolian dust collectors. *Soil Technology*, 7, 25-35.

Goossens, D., and Offer, Z. Y., 2000. Wind tunnel and field calibration of six Aeolian dust samplers. *Atmo. Env.*, 34(7), 1043-1057.

Goudie, A. S. and Middleton, N.J., 2001. Saharan Dust Storms: nature and consequences. *Earth-Sci. Rev.*, 56, 179-204.

Goudie, A. S., 2003. *Great Warm Deserts of the World.* Oxford: Oxford University Press.

Goudie, A. S., Allchin, B., and Hegde, K. T. M., 1973. The former extensions of the Great former Indian Desert. *Geog. J.*, 139, 243-257.

Goudie, A., 2000. *The Human Impact On The Natural Environment.* 5th. ed. Oxford: Blackwell Publishers.

Green, H. L., and Lane, W. R., 1964. *Particulate Clouds: Dusts, Smokes and Mists*. London: Spon.

Hall, F. F., 1981. Visibility reductions from soil dust in western United States. *Atmos. Env.*, 15, 1929-1933.

Hamonou, E., Chazette, P., Balis, D., Dulac, F., Schneider, X., Gaalani, E., Ancellet, G., and Papayannis, A., 1999. Characterization of the vertical structure of Saharan dust export to the Mediterranean basin. *J. Geophy. Res.*, 104 (D18), 22,257-22,270.

Handy, R.L. and Davidson, D.T., 1953. On the curious resemblance between fly ash and meteoric dust. *Proc. Iowa Acad. Sci.*,60,373-379.

Harrison, S. P., Kohfeld, K. E., Roelandt, C. and Claquin, T., 2001. The role of dust in climate changes today, at the last glacial maximum and in the future. *Earth-Science Reviews*, 54, 43-80.

Harrison, S.P., Kohfeld, K.E., Roelandt, C. and Claquin, T., 2001. The role of dust in climate changes today, at the last glacial maximum and in the future. *Earth-Science Reviews*, 54 (1-3), 43-80.

Hasan, A.M.T., 1997. *The Geomorphological History of The Gebel Al Akhdar Valleys, North-Eastern Libya.* Ph.D. thesis, University of Nottingham, Nottingham.

Haub, C., and Yanagishita, M., 1996. *World Population Datasheet.* Washington D.C., USA, Population Reference Bureau.

Heathershaw, A.D., 1974. Bursting phenomena in the sea. *Nature*, 248, 394-395.

Helgren, D. M., and Prospero, J. M., 1987. Wind velocities associated with dust deflation events in the Western Sahara. *J. Climate and Appl. Met.*, 26(9), 1147-1151.

Herman, J. R., Bhartia, P. K., Torres, O., Hsu, C., Seftor, C., and Celarier, E., 1997. Global distribution of UV-absorbing aerosols from Nimbus-7/TOMS data. *J. Geophys Res.*, 102, 16,911-16,922.

Herrmann, L., 1996. *Staubdeposition auf Böden West-Afrikas*. Hohenheimer Bodenkundliche Hefte 36, Stuttgart. 239 pp.

Hidy, G. M. and Brock, J. R., 1971. An assessment of the global sources of tropospheric aerosols. *Proceedings of the Second Clean Air Congress*, Washington DC, 1088-1097.

Horikawa, K., and Shen, H. W., 1960. Sand movement by wind action. *US Army,* Corps *of Engineers, Beach Erosion Board Tech. Memo. No.119*, 51 pp.

Horikawa, K., Hotta, S., and Kubota, S., 1982. Experimental study of blown sand on a wetted sand surface. *Coastal Eng. Jap.*, 25, 177-195.

Hotta, S., Kubota, S., Katori, S. and, Horikawa, K., 1985. Sand transport by wind on a wet surface. *Proc. 19th Coastal Eng. Conf. Houston*, 1265-81.

Illenberger, W. K., and Rust, I. C., 1986. Venturi-compensated aeolian sand trap for field use. *J. Sed. Petrol.*, 56, 541-543.

Jackson, D. W. T., 1996. A new instantaneous aeolian sand trap design for field use. *Sedimentology*, 43, 791-796.

Jaenicke, R., and Schutz, L., 1978. Comprehensive study of the chemical and physical properties of the surface aerosol in the Cape Verde Island regions. *J. Geophys. Res.*, 83, 3585-3599.

Johnson, D. L., 1973. *Jabal Al akhdar, Cyrenaica: A historical geograpyh of settlements and livelihood.* Department of Geology, University of Chicago, Research Paper No. 148.

Joussaume, S., 1990. Three-dimensional simulations of the atmospheric cycle of desert dust particles using a general circulation model. *J. Geophys. Res.*, 95(D2), 1909-1941.

Joussaume, S., 1993. Paleoclimatic tracers: An investigation using an atmospheric general circulation model under ice age conditions. 1. Desert dust. *J. Geophys. Res.*, 98(D2), 2767-2805.

Kendrew, W.G., 1953. *The Climates of the Continents*. 4th ed. London: Oxford University Press.

Kennedy, S. K., Meloy, T. P., and Gurney, T. E., 1985. Sieve data size and shape information. *J. Sed. Petrol.*, 55, 356-360.

Kezeiri, S. K., 1987. Problems of Urban Water Supply in Libya. *Libyan Studies*, 18, 103-113.

Khalaf, F. I., al-Kadi, A., and al-Saleh, S., 1985. Mineralogical composition and potential sources of dust fallout deposits in Kuwait, northern Arabian Gulf. *Sed. Geol.*, 42, 255-278.

Kohfeld, K. E. and Harrison, S. P., 2001. DIRTMAP: the geological record of dust. *Earth-Science Reviews*, 54 (1-3), 81-114.

Komar, P.D., and Cui, B., 1984. The analysis of grain size measurements by settling tube techniques. *J. Sed. Petrol.*, 54, 603-614.

Krolak, E., 2000. Heavy metals in falling dust in eastern Mazowieckie Province. *Polish Journal of Environmental Studies*, 9(6), 517-522.

Kubota, S., Horikawa, K., and Hotta, S., 1983. Blown sand on beaches, *Proceedings of the 18th International Conference on Coastal Engineering.* ASCE, New York, 1181-1198.

Larney, F. J., Bullock, M. S., Janzen, H. H., Ellert, B. H., and Olsen, E. C. S., 1997. Soil nutrient redistribution by wind erosion. *CAESA, Soil Quality Program*, Agricultural and agri-food Canada, Lethbridge Research Centre, Research Factsheet CSQ05.

Larney, F. J., Bullock, M. S., McGinn, S. M., and Fryrear, D. W., 1995. Quantifying wind erosion on summer fallow in southern Alberta. *J. Water and Soil Cons.*, 50(1), 91-95.

Lawless, R. I., 1989. Population Geography and Settlement Studies. *Libyan Studies*, 20, 251-258.

Leather, C. R., 1981. Plant components in desert dust in Arizona and their significance for man. *Geological Society of America, Special Paper* 186, 191-206.

Leatherman, S. P., 1978. A new aeolian sand trap design. *Sedimentology*, 25, 303-306.

Li, Z. S. and Ni, J. R., 2003. Sampling efficiency of vertical array aeolian sand traps. *Geomorphology*, 52, 243-252.

Littmann, T., 1991. Recent African dust deposition in West Germany - sediment characteristics and climatological aspects. *Catena supplement*, 20, 57-73.

Livingstone, I., and Warren, A. 1996. *Aeolian Geomorphology: An Introduction.* England: Addison Wesley Longman Ltd.

Lyles, L., and Krauss, R. K., 1971. Threshold velocities and initial particle motion as influenced by air turbulence. *Trans. Am. Soc. Agr. Eng.*, 17, 134-139.

Macleod, N. H., 1998. *The Role of Airborne Sahelian Dust in the Frequency and Intensity of Hurricanes Formed in the Eastern Atlantic Ocean* [online]. Washington D.C.: Third World Foundation. Available at: <http://216.239.53.100/search?q=cache:Ec8uAIqRPlcC:www.prospect-tech.com/r3g/role.doc+atmospheric+dust+and+soil+fertility+&hl=en&ie=UTF-8> [Accessed 28/02/2003].

Mahowald, N. M., Bryant, R. G., Corral, J., and Steinberger, L., 2003. Ephemeral lakes and desert dust sources. *Geophys. Res. Letters*, 30(2), 1074, 46-1-46-4.

Mainguet, M., 1968. Le Borkou, aspects d' un modelé éolien. *Ann. Géog.*, 77, 296-322.

Mainguet, M., 1998. *Aridity: drought and human development.* Heidelberg, Germany: Springer-Verlag.

Malina, F. J., 1941. Recent developments in the dynamics of wind erosion. *Trans. Am. Geophys. Un. 1941*, 262-284.

Marticorena, B., Bergametti, G., Aumont, B., Callot, Y., N' Doumé, C., and Legrand, M., 1997. Modelling the atmospheric dust cycle: 2, Simulations of Saharan dust sources. *J. Geophys. Res.*, 102, 4387-4404.

McLachlan, K., 1989. Libya's Oil Resources. *Libyan Studies*, 20, 243-250.

McPeters, R., 2002. *TOMS* [online]. NASA. Available at: <http://jwocky.gsfc.nasa.gov/> [Accessed 20/9/2002].

McTainsh, G., 1980. Harmattan dust deposition in Northern Nigeria. *Nature*, 286, 587-588.

Middelton, N. J., and Goudie, A. S., 2001. Saharan dust: sources and trajectories. *Transactions of the Institute of British Geographers* [online], 26(2). Available at: <http://swets2.nesli.ac.uk/link/access_db?issn=0020-2754> [Accessed 20/11/2001].

Middelton, N., and Thomas, D., eds., 1997. *World Atlas of Desertification.* 2nd ed. London: United Nations Environmental Programme.

Miller, R., and Tegen, I., 2003. *Desert dust, dust storms and climate* [online]. Goddard Institute for Space Studies. Available at: <http://www.giss.nasa.gov/research/intro/miller_01/> [Accessed 28/02/03].

Milligan, P. J. M., Brabin, B. J., Kelly, Y. J., Pearson, M. G., Mahoney, G., Dunne, E. Heaf, D., and Reid, J., 1998. Association of spatial distribution of childhood respiratory morbidity with environmental dust pollution. *Journal of Toxicology and Environment Health*, 55(A), 101-116.

Nalpanis, P., 1985. Saltating and suspended particles over flat and sloping surfaces. II. Experiments and numerical simulations. *In*: O. E. Barndorff-Nielsen, J. T. Moller, K. R. Rasmussen and B. B. Willetts, eds. *Proceedings of the international workshop on the physics of blown sand*, 37-66. Dept. Theoretical Statistics, Institute of Mathematics, Univ. Aarhus, Mem. 8.

NASA, 2000a. *Scientific Visualization Studio, Libyan Dust Storm* [online]. NASA. Available at:<http://svs.gsfc.nasa.gov/vis/a000000/a002200/a002238/> [Accessed 17/12/02].

NASA, 2000b. *Visible Earth, TOMS Aerosol Index* [online]. NASA. Available at: <http://visibleearth.nasa.gov/cgi-bin/viewrecord?7069> [Accessed 1/12/02].

NASA, 2001. *Dust Begets Dust* [online]. Marshall Space Flight Center. Available at: <http://www.science.nasa.gov/headlines/y2001/ast22may_1.htm> [Accessed 14/04/03].

Nickling, W. G., 1983. Grain size characteristics of sediment transported during dust storms. *J. Sed. Petrol.*, 53, 1011-1024.

Nickling, W. G., 1988. The initiation of particle movement by wind. *Sedimentology*, 31, 111-117.

Nickling, W. G., 1994. Aeolian sediment transport and deposition. *In*: K. Pye, ed. *Sediment Transport and Depositional Processes*. Oxford: Blackwell, 1994, pp. 293-350.

Nickling, W. G., and Gillies, J. A., 1989. Emission of fine –grain particulates from desert soils. *In*: M. Leinen, and M., Sarnthein, eds. *Paleoclimatology and Paleometeorology*: *Modern and Past Patterns of Global Atmospheric Transport*. Dordrecht: Kluwer, 1989, pp. 227-252.

O'Brien, M. P., and Rindlaub, B. D., 1936. The transportation of sand by wind. *Civil Eng.*, 6, 325-327.

O'Hara, S. L., Wiggs, G. F. S., Wegerdt, J., van der Meer, J., Small, I., Falzon, D., and Hubbard, R., 2001. Dust exposure and respiratory health amongst children in the environmental disaster zone of Karakalpakstan, Central Asia: preliminary findings of the ASARD project. *In*: C. A. Brebbia and, D. Fajzieva, eds. *Environmental Health Risk*. UK: WIT Press, 2001, pp. 71-82.

Owen, J. S., 1927. The movement of sand by wind. *The Engineer*, 143, 377.

Péwé, T. L., 1981. Desert dust: an overview. *Geol. Soc. Am. Spec. Pap.*, 186, 1-10.

Pearce, E. A., and Smith, C. G., 1993. *The World Weather Guide*, 3rd ed. Oxford: Helicon Publishing Ltd.

Penner, J. E., Hegg, D., and Leaitch, R., 2001. Unravelling the role of aerosol in climate change. *Env. Sci. and Tech.*, 35 (1 August), 332A-340A.

Perkins, S., 2001. Dust, the Thermostat, How tiny airborne particles manipulate global climate. *Science News*, 160(13), 200-202.

Perry, K. D., Cahill, T. A., Eldred, R. A., Dutcher, D. D., and Gill, T. E., 1997. Long-range transport of North African dust to the eastern United States. *J. Geophys. Res.*, 102,11225-11238.

Peterson, J. T. and Junge, C. E., 1971. Source of particulate matter in the atmosphere. *In*: W. Matthews, W. Kellog and G.D. Robinson, eds. *Man's Impact on Climate*. Cambridge, Mass: MIT Press, 1971, pp. 310-320.

Pope, C. A., 1996. Adverse health effects of air pollutants in a non-smoking population. *Toxicology*, 111, 149-155.

Prodi, F., and Fea, G., 1979. A case of transport and deposition of Saharan dust over the Italian peninsula and southern Europe. *J. Geophys. Res.*, 84C, 6951-6960.

Prospero, J. M., Bonatti, E., Schubert, C., and Carlson, T. N., 1970. Dust in the Caribbean atmosphere traced to an African dust storm. *Earth Planet. Sci. Lett.*, 9, 287-293.

Prospero, J. M., Ginoux, P., Torres, O., Nicholson, S. E., and Gill, T. E., 2002. Environmental characterization of global sources of atmospheric soil dust identified with the NIMBUS 7 Total Ozone Spectrometer (TOMS) Absorbing Aerosol Product. *Reviews of Geophysics*, 40(1), 2-1-2-31.

Pye, K., 1987. *Aeolian Dust and Dust Deposits*. London: Academic Press Ltd.

Pye, K., 1989. Process of fine particle formation, dust source regions, and climatic changes. *In*: M. Leinen, and M. Sarnthein, eds. *Paleoclimatology and Paleometeorology: Modern and Past Patterns of Global Atmospheric Transport*. Dordrecht: Kluwer, 1989, pp. 3-30.

Pye, K., 1992. Aeolian dust transport and deposition over Crete and adjacent parts of the Mediterranean Sea. *Earth Surface Processes and Landforms,* 17, 271-288.

Pye, K., 1994. Properties of sediment particles. *In*: K. Pye, ed. *Sediment Transport and Depositional Processes*. Oxford: Blackwell, 1994, pp. 1-24.

Pye, K., and Tsoar, H., 1990. *Aeolian Sand and Sand Deposits*. London: Unwin Hyman Ltd.

Rabenhorst, M. C., Wilding, L. P., and Girdner, C. L., 1984. Airborne dust in the Edwards Plateau region of Texas. *Soil Sci. Soc. Am. J.*, 48, 621-627.

Rahn, K. A., Borys, R. D., and Shaw, G. E., 1977. The Asian source of Arctic haze bands. *Nature*, 268, 712-714.

Rahn, K. A., Borys, R.D., and Shaw, G. E., 1981. Asian desert dust over Alaska: Anatomy of an Arctic haze episode. *Am. Geol. Soc. Spec. Pap.*, 186, 37-70.

Raloff, J., 2001. III Winds, Dust storms ferry toxic agents between countries and even continents. *Science News*, 160 (14), 218-220.

Ramsperger, B., Peinemann, N., and Stahr K., 1998. Deposition rates and characteristics of aeolian dust in the semi-arid and subhumid regions of the Argentinean Pampa. *J. Arid Env.*, 39, 467-476.

Reed International Books Ltd., 1993. *Philip's Atlas of The World.* 3rd ed. London: Reed International Books Ltd.

Reheis, M., and Kihl, R., 1995. Dust deposition in southern Nevada and California, 1984-1989: Relations to climate, source area, and source lithology. *J. Geophys. Res.*, 100(D5), 8893-8918.

Reid, I., 1994. Rivers and their deposits-Cinderellas of the arid realm. *In*: P. G. Fookes, and R. H. G. Parry, eds. *Engineering Characteristics of Arid Soils, Proceedings of the 1st International Symposium on Engineering Characteristics of Arid Soils, London.* Balkema, Rotterdam, 41-46.

Reynolds, R., Belnap, J., Reheis, M., Lamothe, P., and Luiszer, F., 2001. *Aeolian dust in Colorado Plateau soils: Nutrient inputs and recent change in source* [online]. USA: USGS and University of Colorado. Available at: < http://www.unlv.edu/faculty/debelle/bio495/Sept28.pdf> [Accessed 28/05/03].

Richards, A. L., Hyams, K. C., Douglas, M. W., Rozmajzl, P. J., Woody, J. N., and Merrell, B. R., 1993. Respiratory disease among military personnel in Saudi Arabia during Operation Desert Shield. *American Journal of Public Health*, 83(9), 1326-1329.

Riley, D., and Spolton, L., 1982. *World Weather and Climate*. 2nd ed. Cambridge: Cambridge University Press.

Rubio, A. O., Naranjo, A., Nieto, A., Arguelles, C., Salinas, F., Aguilar, R. and, Romero, H., 1998. Suspended particles in atmosphere and health respiratory problems at La Paz City, Baja California Sur, Mexico. *J. Env. Biology*, 19(4), 381-387.

Schmidt, L. J., 2001. *From the Dust Bowl to the Sahel* [online]. Distributed Active Archive Center (DAAC) Alliance. Available at: <http://earthobservatory.nasa.gov/Study/DustBowl/> [Accessed 01/03/03].

Schütz, L., 1980. Long range transport of desert dust with special emphasis on the Sahara. *Ann. N.Y. Acad. Sci.*, 338, 515-532.

Secretary of Planning, 1978. *National Atlas of Libya*. 1st ed. Sweeden: Essellete. (Arabic).

Shütz, L., 1980. Long range transport of desert dust with special emphasis on the Sahara. *Ann. N.Y. Acad. Sci.*, 388, 515-532.

Simonson R. W., 1995. Airborne dust and its significance to soils. *Geoderma*, 65, 1-43.

Sivall, T., 1957. Sirocco in the Levant. *Geografiska Annaler*, 39, 114-142.

Smalley, I. J., and Vita-Finzi, C., 1968. The formation of fine particles in sandy deserts and the nature of desert loess. *Journal of Sedimentary Petrology*, 38(3), 766-774.

Smith, D., 2003. *MODIS Fire and Thermal Anomalies* [online]. USA: NASA. Available at: <http://modis-fire.gsfc.nasa.gov/rationale.asp> [Accessed 20/08/2003].

Smith, R. M., Twiss, P. C., Krauss, R. K., and Brown, M. J., 1970. Dust deposition in relation to site, season and climatic variables. *Soil Sci. Soc. Am. Proc.*, 34, 112-117.

Stetler, L. D., and Saxton, K. E., 1996. Saltation and PM_{10} emissions from agricultural fields on the Columbia Plateau. *Earth Surface Processes and Landforms*, 21, 673-685.

Stiles, D., 1995. *Social Aspects of Sustainable Dryland Management.* Wiley & Sons, Chichester: Wiley & Sons.

Stout, J. E., and Zobeck, T. M., 1996. The Wolfforth field experiment: A wind erosion study. *Soil Sci.*, 161, 616-632.

Svasek, T. N., and Terwindt, J. H., 1974. Measurement of sand transport by wind on a natural beach. *Sedimentology*, 21, 311-322.

Tegen, I. and, Fung, I., 1994. Modelling of mineral dust in the atmosphere: sources, transport and optical thickness. *J. Geophys. Res.*, 99(D11): 22897-22914.

Tegen, I., and Fung, I., 1995. Contribution to the atmospheric mineral aerosol load from land surface modification. *J. Geophys. Res.*, 100, 18,707-18,726.

Thomas, D. S. G., Goudie, A., Dunkerley, D., Meadows, M., Balling, R., Sherman, D., and Abrahams, A., 2000. *The Dictionary of Physical Geography*, 3rd ed. Oxford: Blackwell Publishers Ltd.

Tiedemann, R., Sarnthein, M. and Shackleton, N.J., 1994. Astronomic timescale for Pliocene Atlantic d18O and dust flux records of ODP Site 659. *Paleoceanography*, 9(4), 619-638.

Torres, O., Bhartia, P. K., Herman, J. R., Ahmed, Z., and Gleason, J., 1998. Derivation of aerosol properties from satellite measurements of backscattered ultraviolet radiation: Theoretical basis. *J. Geophys. Res.*, 103, 17,099-17,110.

Torres, O., Bhartia, P. K., Herman, J. R., Sinyuk, A., Ginoux, P., and Holben, B., 2002. A long–term record of aerosol optical depth from TOMS observations and comparison to AERONET measurements. *J. Atmos. Sci.*, 59, 398-413.

Tsoar, H., and Møller, J. T., 1986. The role of vegetation in the formation of linear sand dunes (analysis of the case of Negev-Sinai borderline). *In*: W.G. Nickling, ed. *Aeolian Geomorphology*. New York: Allen and Unwin, 1986, pp. 75-95.

Tsoar, H., and Pye, K., 1987. Dust transport and the question of desert loess formation. *Sedimentology*, 34, 139-153.

United Nations Environmental Programme, 1997. *World Atlas of Desertification*, 2nd ed. London: Arnold.

Unluata, U., 2001. *The IOC Pacific Cruise* [online]. IMS Newsletter. Available at: <http://ioc.unesco.org/iocweb/news/items2001/item017.htm> [Accessed 20/12/2002].

USDA and ARS, 2000. *The Wind Erosion Problem* [online]. USA: US Department of Agriculture and Agriculture Research Service of Kansas State University. Available at:<http://www.weru.ksu.edu/new_weru/problem/problem.shtml> [Accessed 14/12/2002].

USGS, 1962. *Topographic Map of Libya,* Washington D.C., USA.

USGS, 1998. *Coral Mortality and African Dust* [online]. USGS. Available at:<http://coastal.er.usgs.gov/projects98/7242-32912.html> [Accessed 23/12/2002].

USGS, 2000. *African Dust Causes Widespread Environmental Distress* [online]. USGS. Available at: <http://coastal.er.usgs.gov/african_dust/dust-infosheet.pdf> [Accessed 13/12/2002].

USGS, 2002. *Coral Mortality and African Dust, Satellite Images of African Dust* [online]. USGS. Available at: <http://coastal.er.usgs.gov/african_dust/satellite.html> [Accessed 15/12/2002].

USGS, 2002. *Coral Mortality and African, Dust: Barbados Dust Record: 1965-1996.* [online]. USGS. Available at: <http://coastal.er.usgs.gov /african dust/barbados.html > [Accessed 23/12/2002].

USGS, 2002. *EarthExplorer* [online]. Earth Resources Observation System Data Centre. Available at:<http//edcsns17.cr.usgs.gov/ EarthExplorer/> [Accessed 01/12/2002].

Wake, C. P., Mayewski, P. A., Durham, N. H., Han, Z., L., J. and, Qin, D., 1994. Modern eolian dust deposition in Central Asia. *Tellus*, 46B, 220-233.

Walker, A. S., 1982. Deserts of China. *Am. Scient.*, 70, 366-376.

Wang, P., and Kraus, N. C., 1999. Horizontal water trap for measurement of aeolian transport. *Earth Surface Processes and Landforms*, 24, 65-70.

Whalley, W. B., Marshall, J. R., and Smith, B. J., 1982. Origin of desert loess from some experimental observations. *Nature*, 300, 433-435.

Whalley, W. B., Smith, B. J., McAlister, J. J., and Edwards, A., 1987. Aeolian abrasion of quartz particles and the production of silt size fragments, preliminary results and some possible implications for loess and silcrete formation. *In*: L. E. Frostick, and I. Reid, eds. *Desert Sediments: Ancient and Modern.* Geol. Soc. Lond. Spec. Pub. 35, Oxford, Blackwell, 1987, pp. 129-138.

Wiggs, G. F. S. and O'Hara, S. L. A simple dust deposition trap design for use in dryland environments. *Earth Surface Processes and Landforms*, (in review).

Wiggs, G.F.S., 1997. Sediment mobilisation by the wind. *In*: D. S. G. Thomas, ed. Arid Zone Geomorphology-Process, Form and Change in Drylands. 2nd ed. Wiley, 1997, pp. 351-372.

Williams, M. A. J., 2001. Interactions of desertification and climate: Present understanding and Future research imperatives. *Arid Lands* [online], 49. Available at: <http://www.ag.arizona.edu/OALS/ALN/aln49/williams.html# desertimpact> [Accessed 27/10/2001].

Wilshire, H. G., 1980. Human causes of accelerated wind erosion in California's deserts. *In*: D. R. Coates, and J. D. Vitek, eds. *Thresholds in Geomorphology.* London: Allen and Uwin, pp. 415-434.

World Resources Institute, 2001. *Disappearing Land: Soil Degradation* [online]. Available at: <http://www.wri.org/wri/trends/soilloss.html> [Accessed 14/12/2002].

Yaalon, D. H., 1969. Origin of desert loess. *Etudessur le quarternaire dans le monde Quarter., 8th International Association for Quaternary Research (INQUA) Congeress.* (Paris) 2, 755.

Yaalon, D. H., 1997. Comments on the source, transport and deposition scenario of Saharan dust to southern Europe. *Journal of Arid Environments*, 36, 193-196.

Yaalon, D. H., and Ganor, E., 1973. The influence of dust on soils during the Quaternary. *Soil Sci.*, 116, 146-155.

Yaalon, D. H., and Ganor, E., 1979. East Mediterranean trajectories of dust-carrying storms from the Sahara and Sinai. *In*: C. Morales, ed. *Saharan Dust – Mobilization, Transport, Deposition.* Chichester: Wiley, 1979, pp. 187-193.

Zingg, A. W., 1951. A portable wind tunnel and dust collector developed to evaluate the erodibility of field surfaces. *Agron. J.*, 43, 189-191.

APPENDIX I

MONTHLY WIND ROSES

I.1. WIND ROSES BASED ON WIND SPEEDS ≥ 6.5 m/s

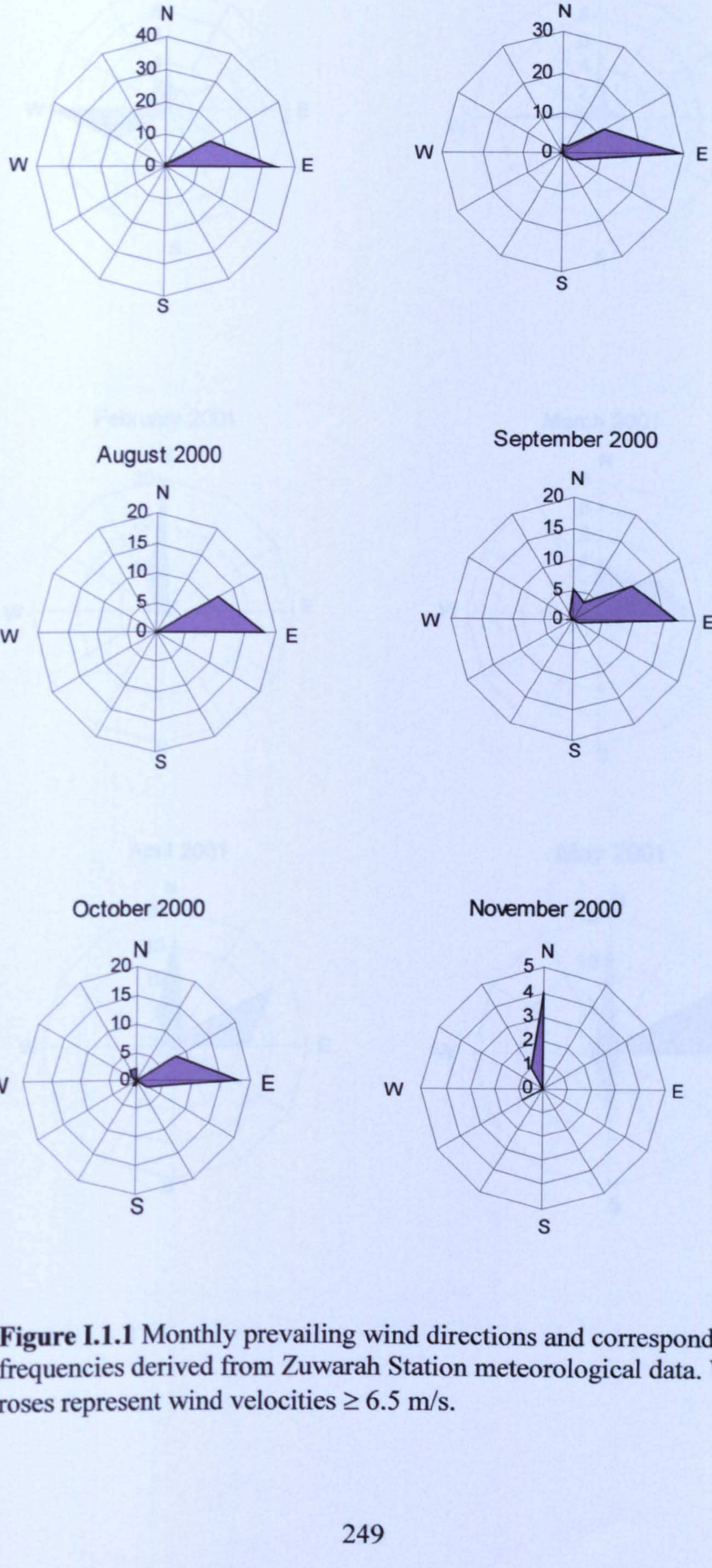

Figure I.1.1 Monthly prevailing wind directions and corresponding frequencies derived from Zuwarah Station meteorological data. Wind roses represent wind velocities ≥ 6.5 m/s.

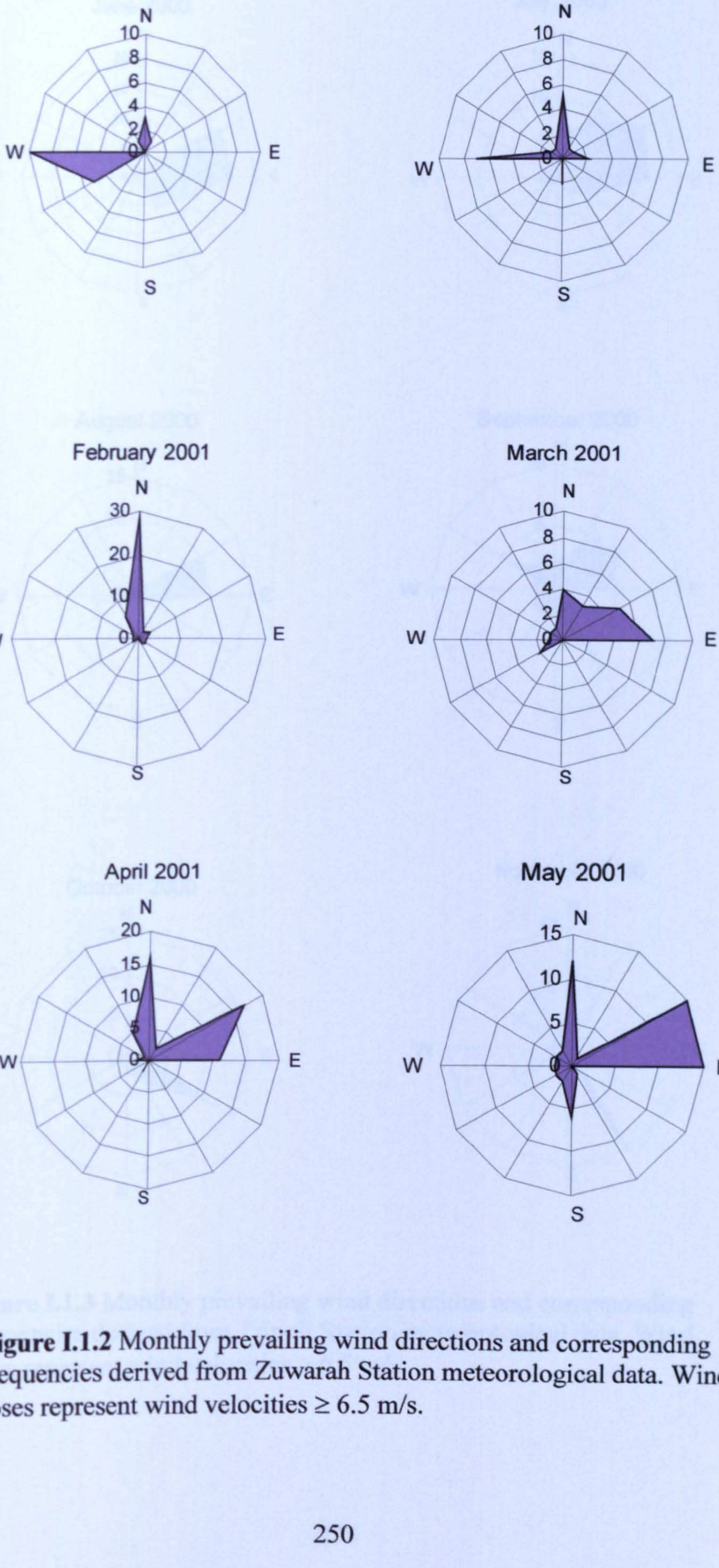

Figure I.1.2 Monthly prevailing wind directions and corresponding frequencies derived from Zuwarah Station meteorological data. Wind roses represent wind velocities ≥ 6.5 m/s.

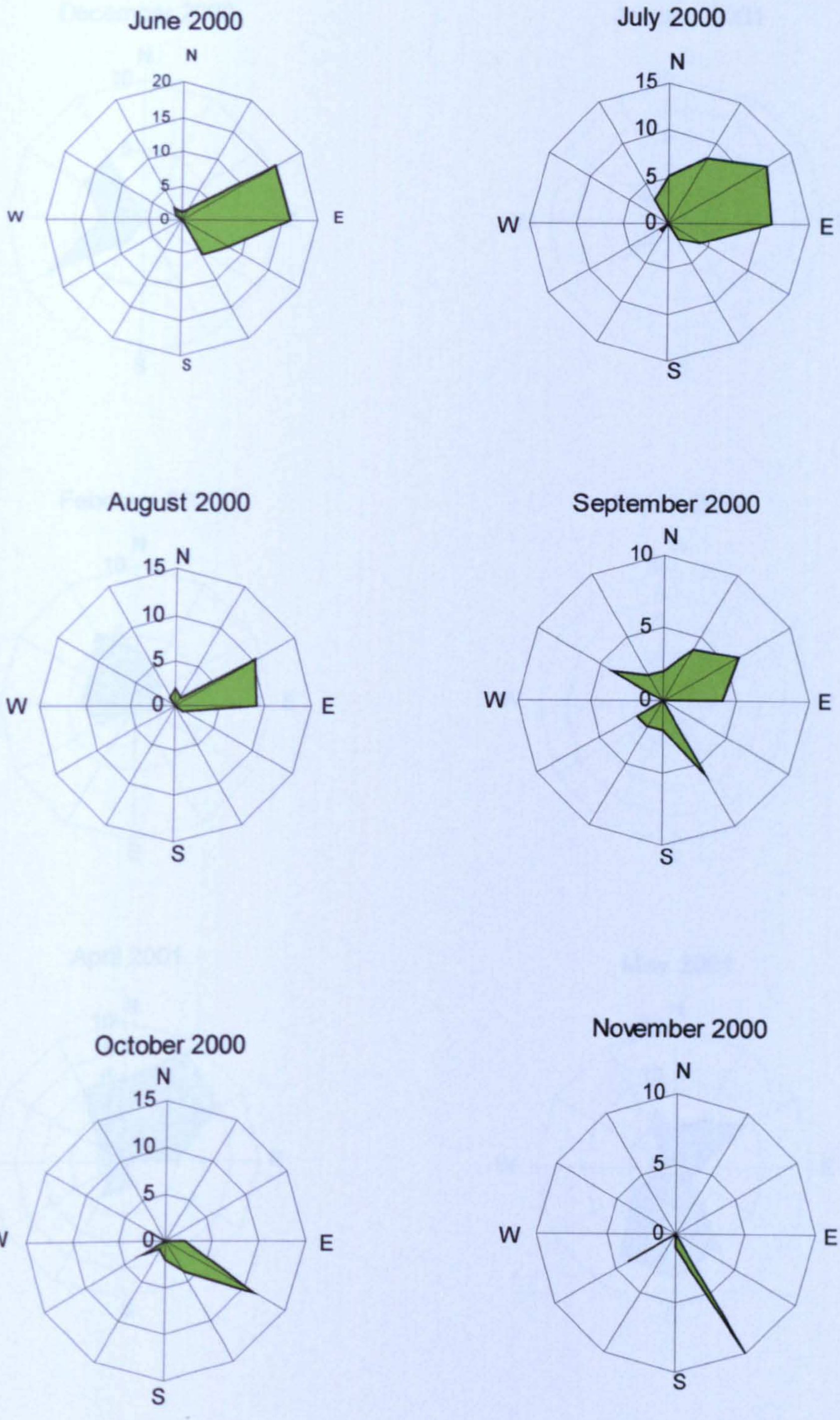

Figure I.1.3 Monthly prevailing wind directions and corresponding frequencies derived from Tripoli Station meteorological data. Wind roses represent wind velocities ≥ 6.5 m/s.

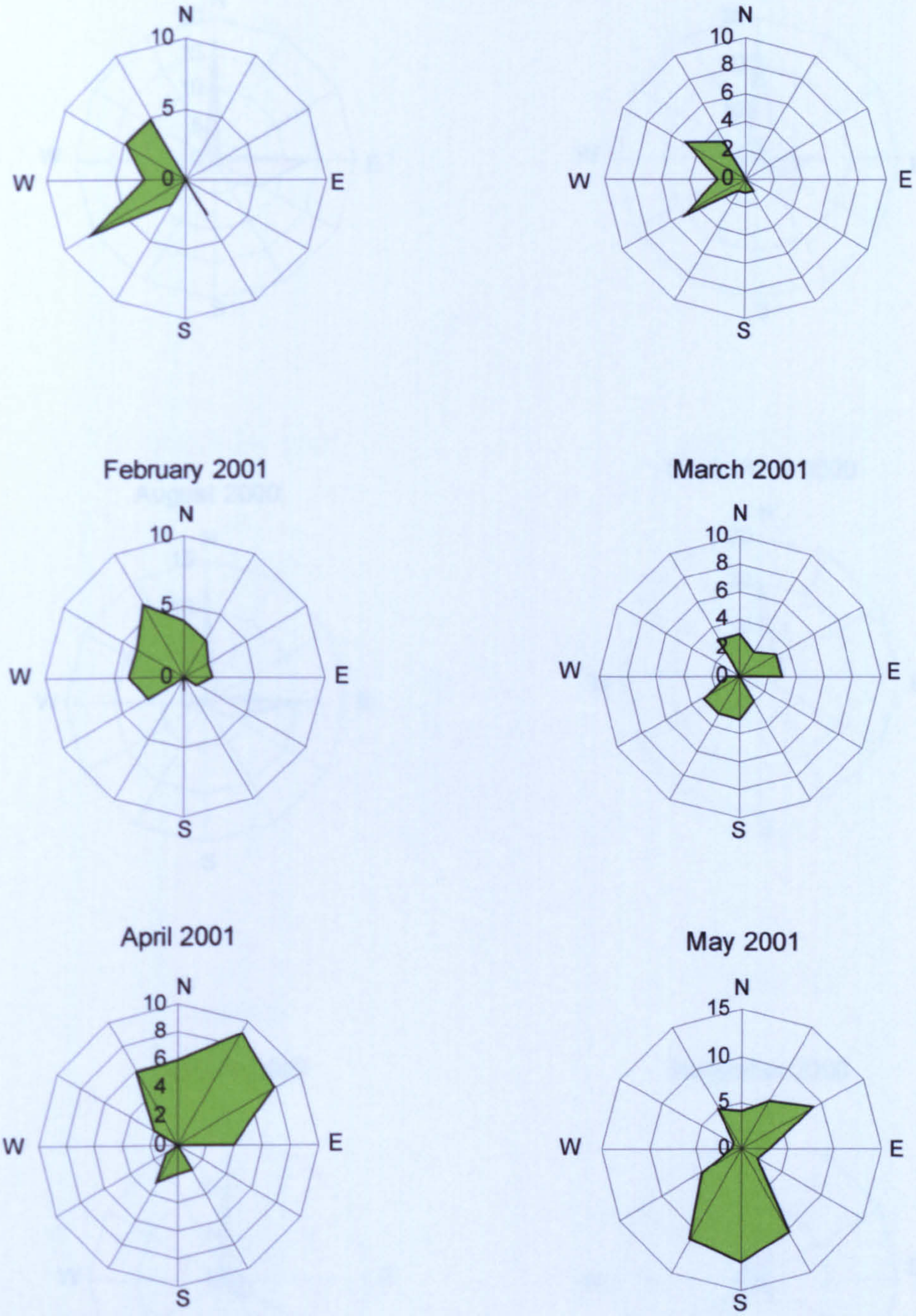

Figure I.1.4 Monthly prevailing wind directions and corresponding frequencies derived from Tripoli Station meteorological data. Wind roses represent wind velocities ≥ 6.5 m/s.

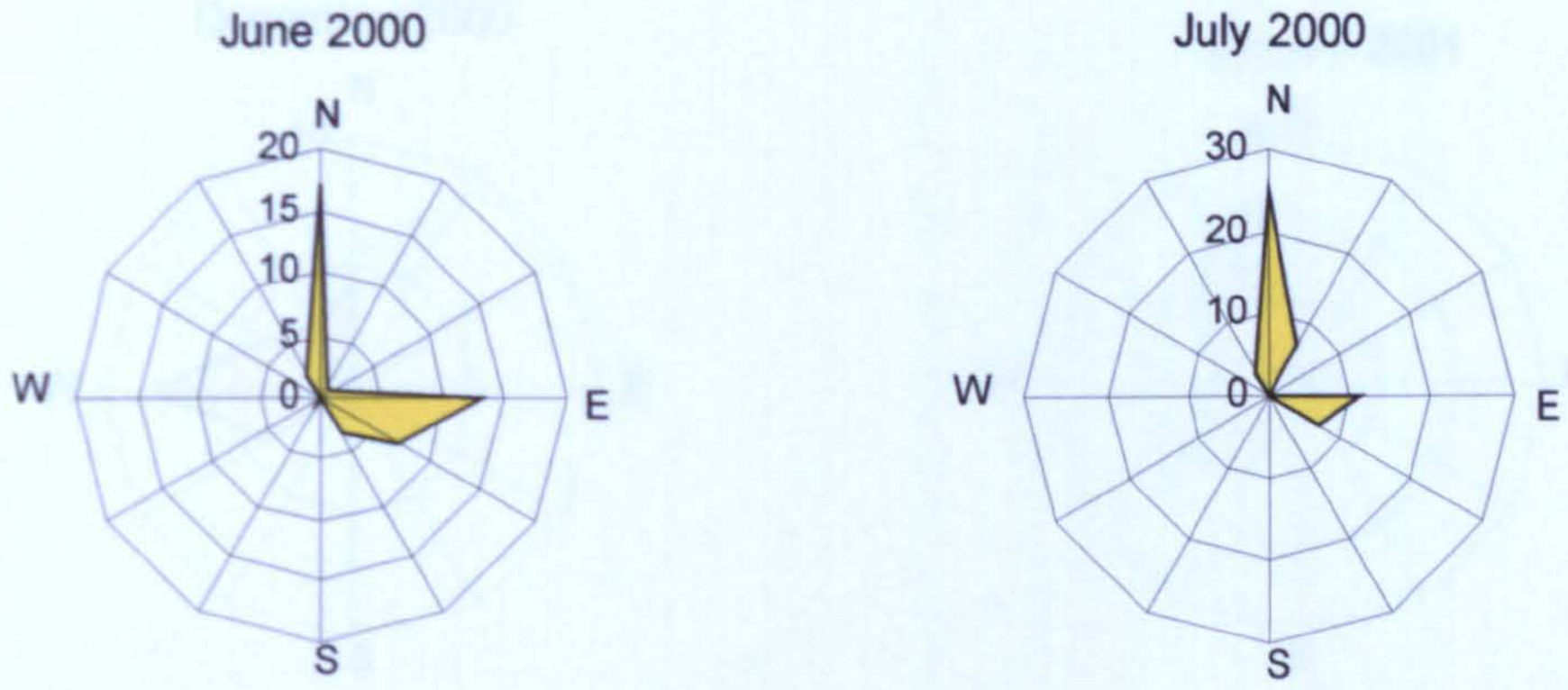

Figure I.1.5 Monthly prevailing wind directions and corresponding frequencies derived from Al Khums Station meteorological data. Wind roses represent wind velocities ≥ 6.5 m/s.

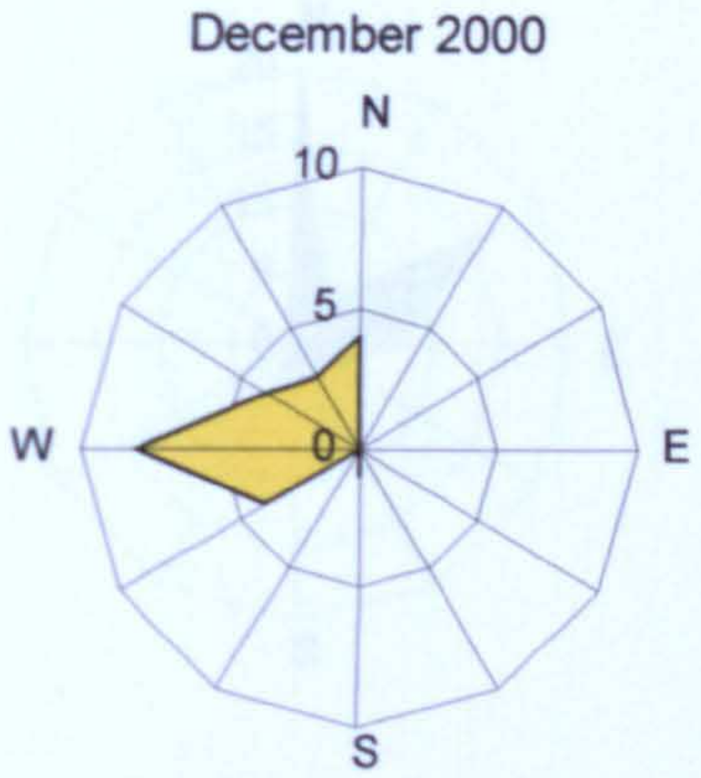

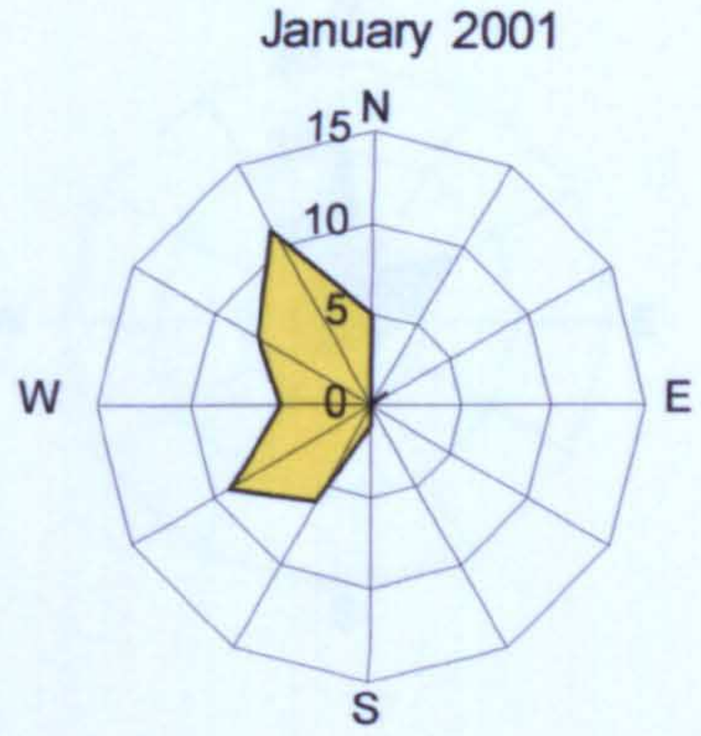

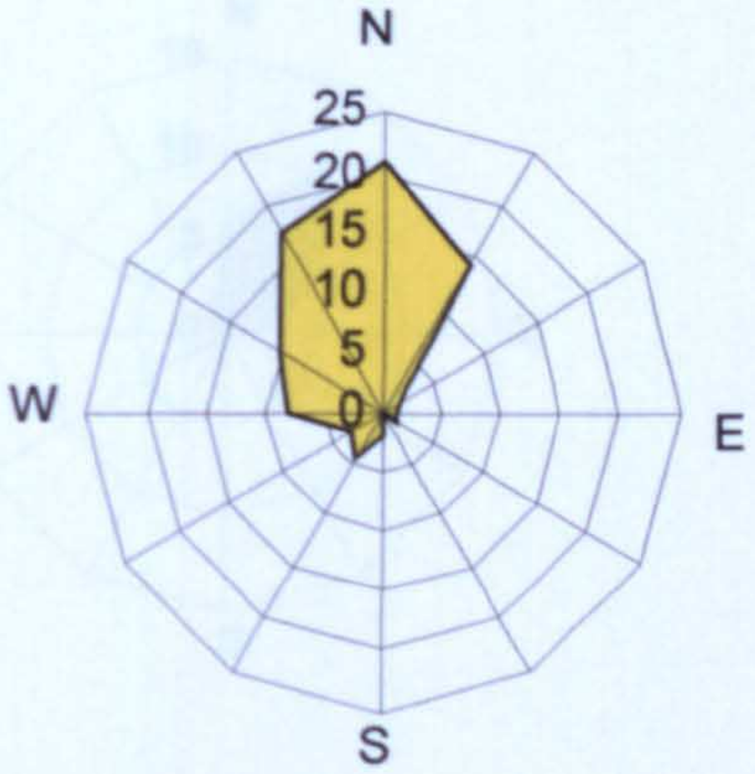

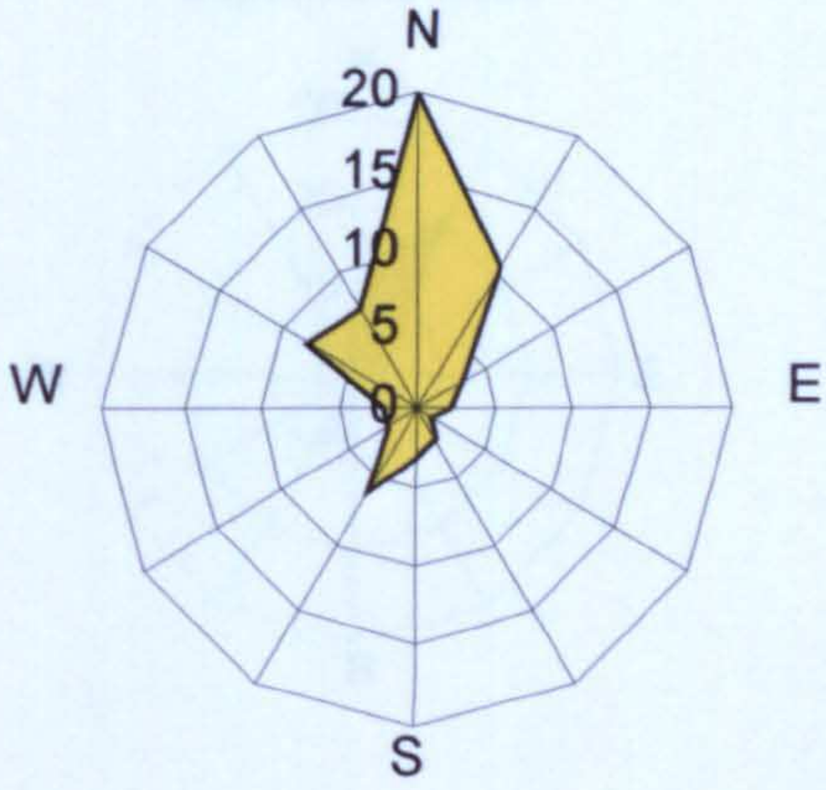

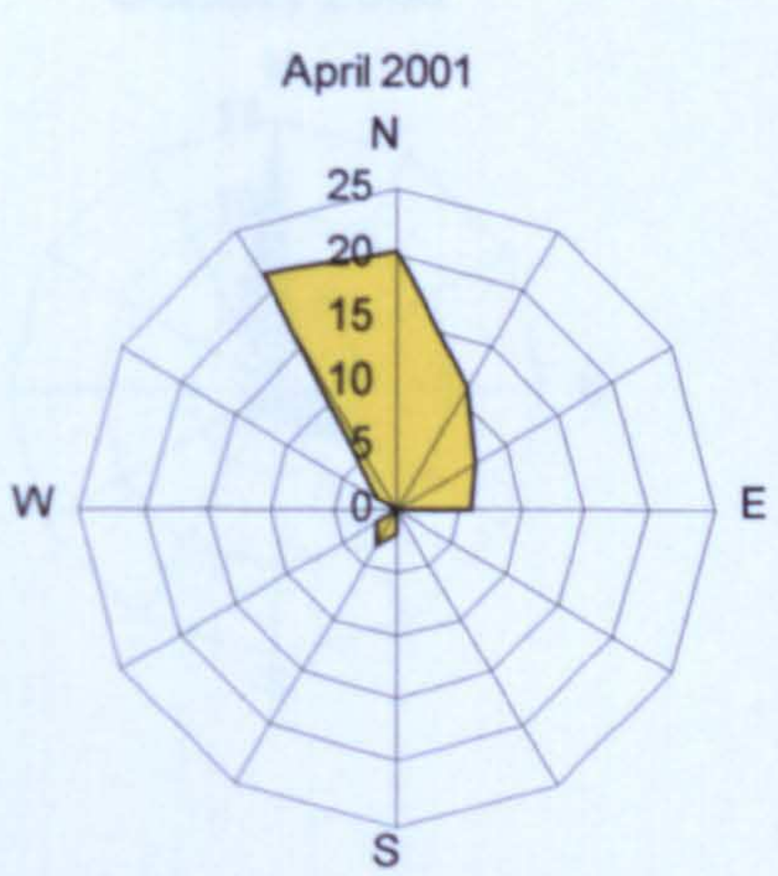

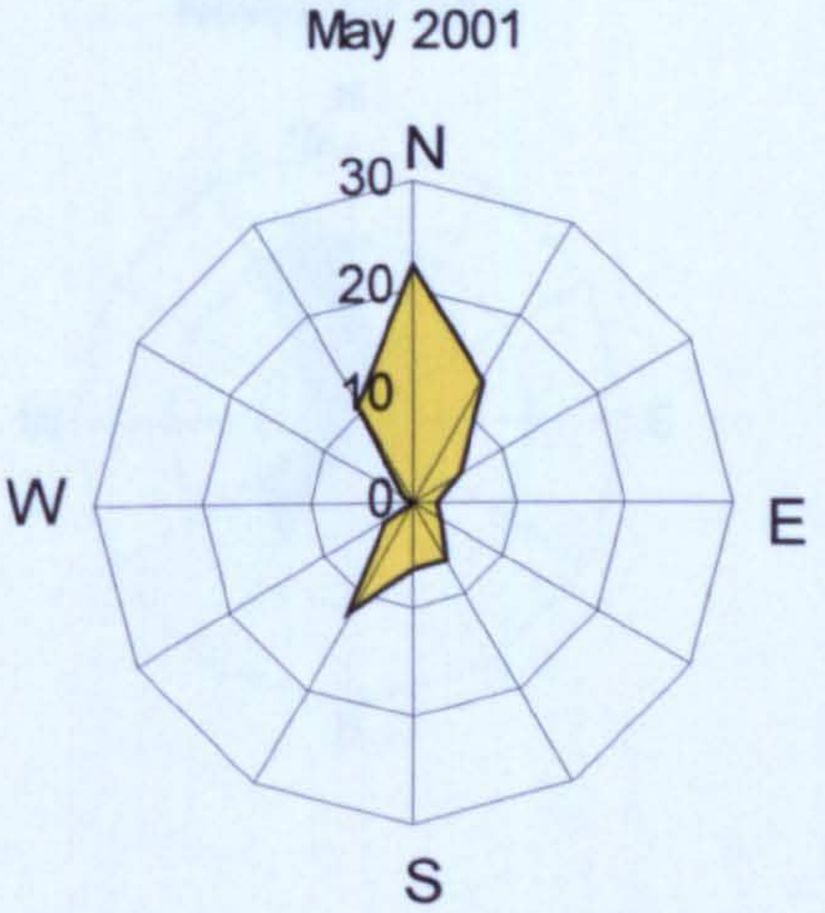

Figure I.1.6 Monthly prevailing wind directions and corresponding frequencies derived from Al Khums Station meteorological data. Wind roses represent wind velocities ≥ 6.5 m/s.

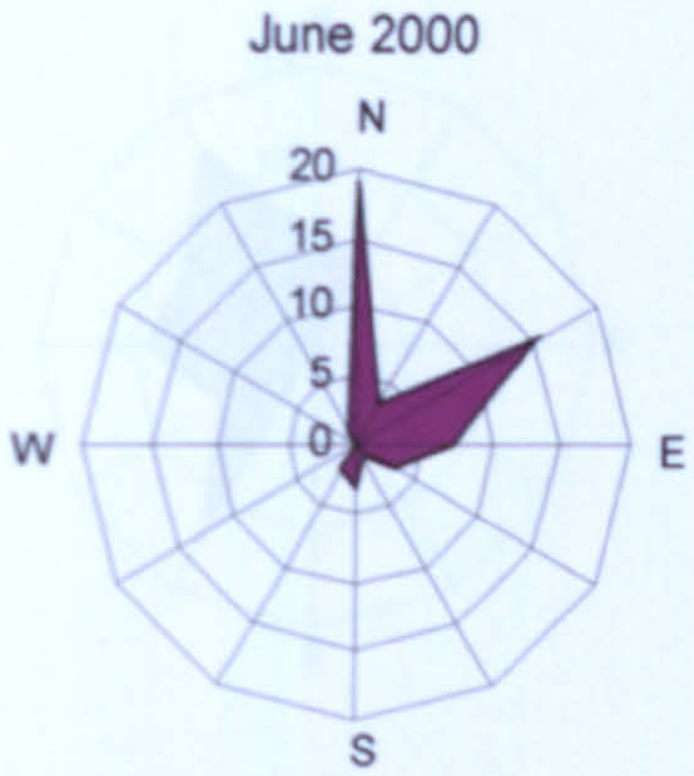

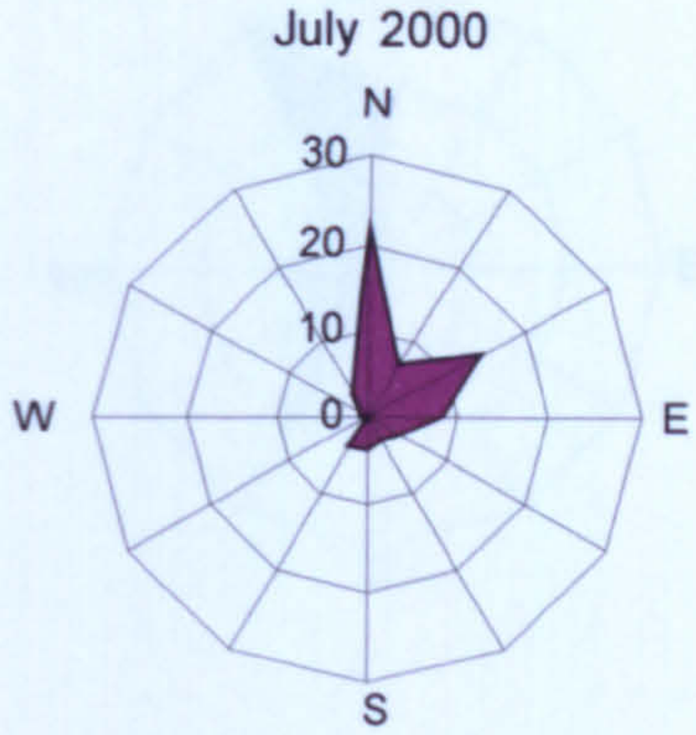

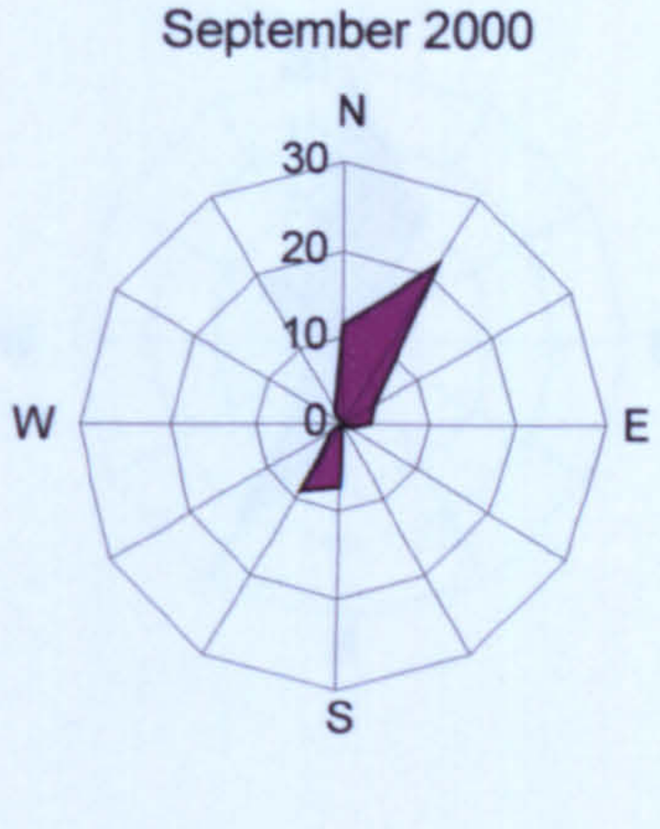

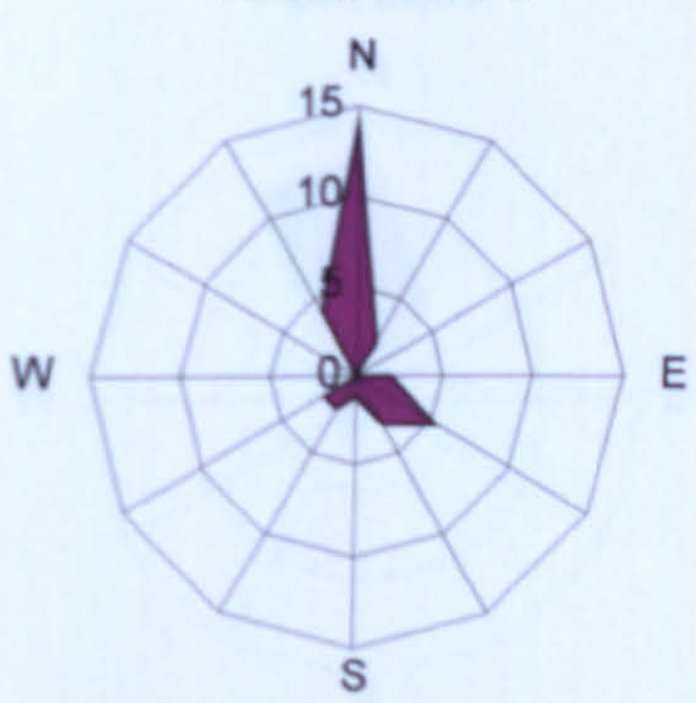

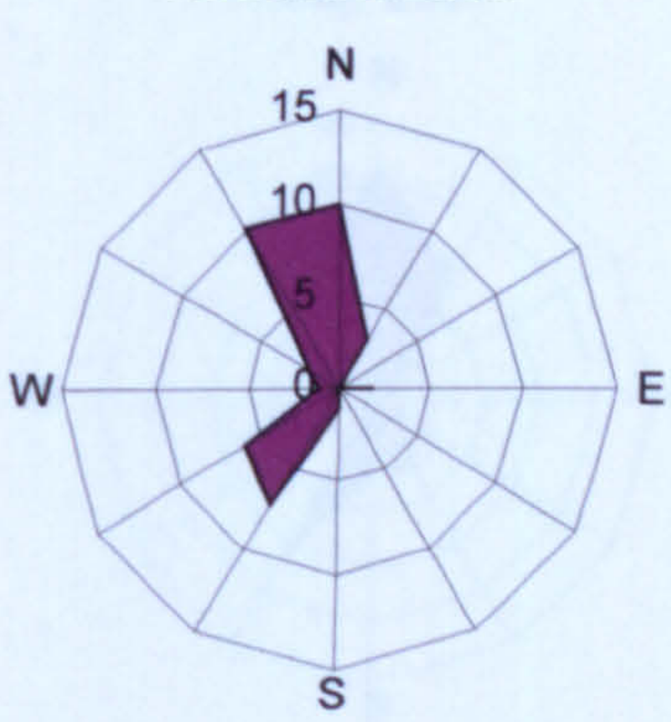

Figure I.1.7 Monthly prevailing wind directions and corresponding frequencies derived from Misratah Station meteorological data. Wind roses represent wind velocities ≥ 6.5 m/s.

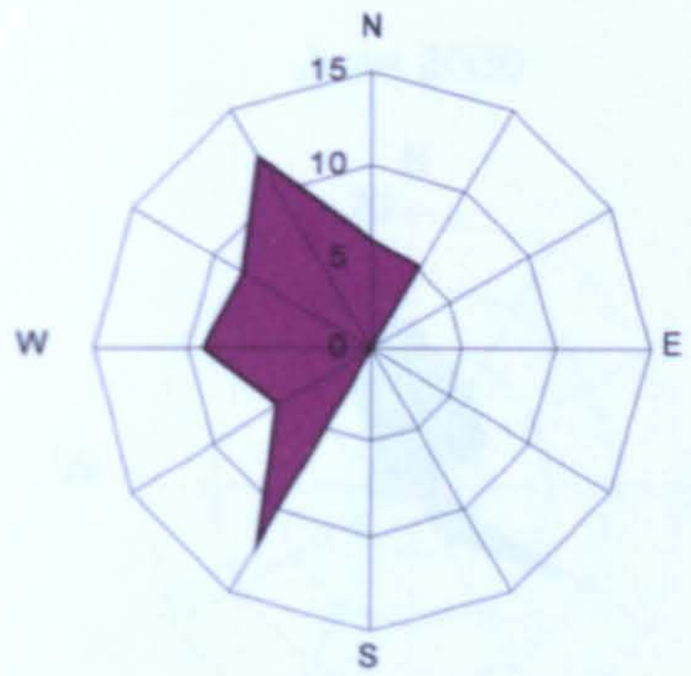

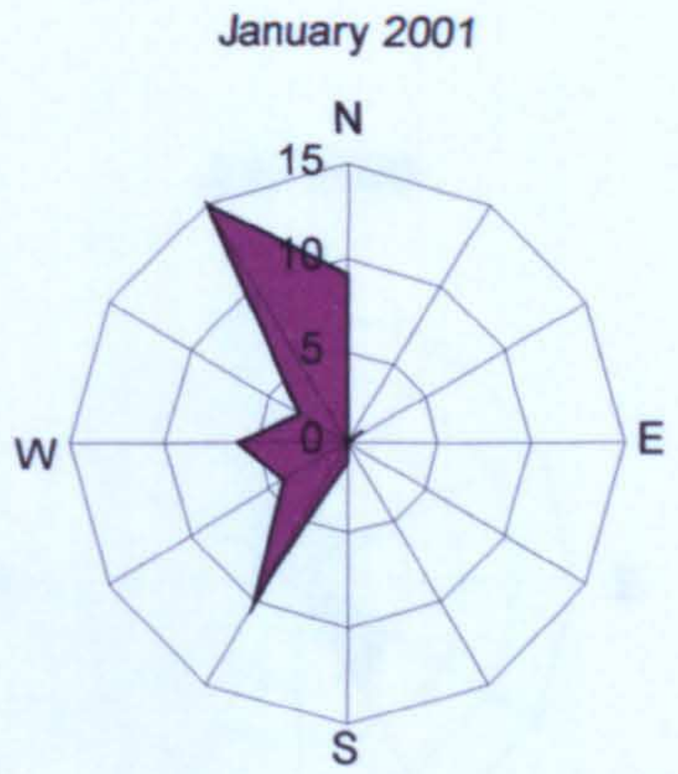

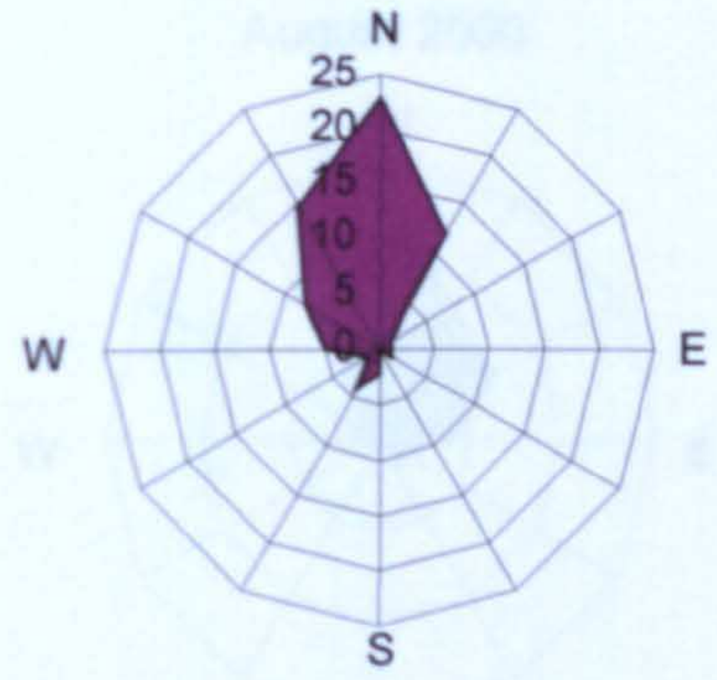

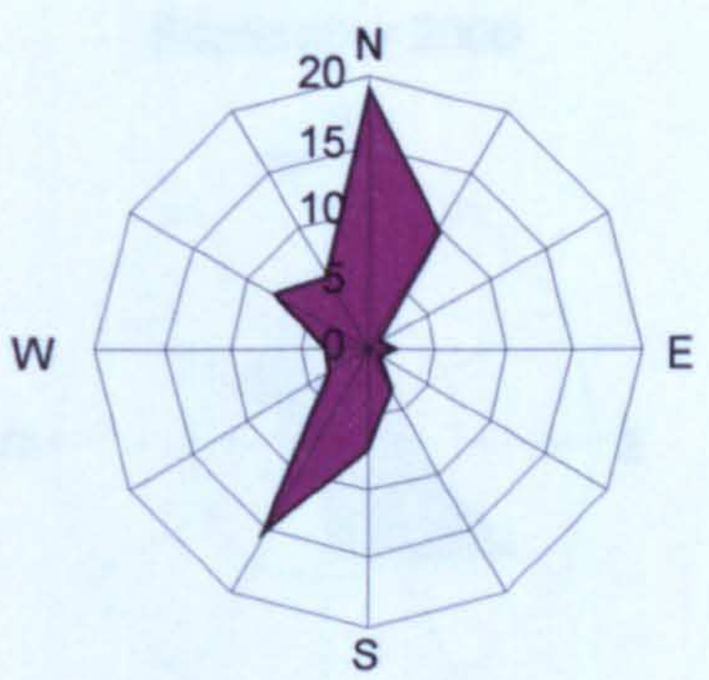

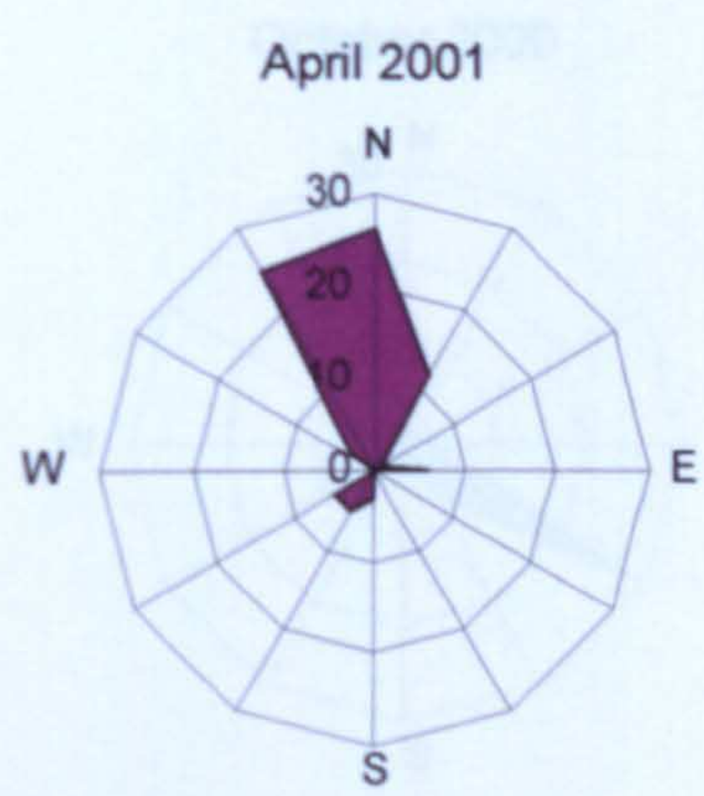

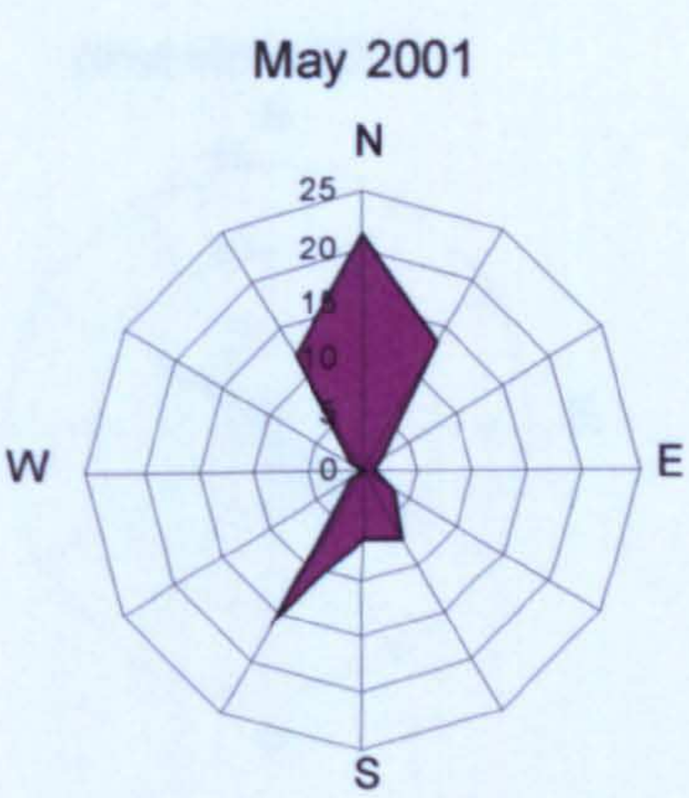

Figure I.1.8 Monthly prevailing wind directions and corresponding frequencies derived from Misratah Station meteorological data. Wind roses represent wind velocities ≥ 6.5 m/s.

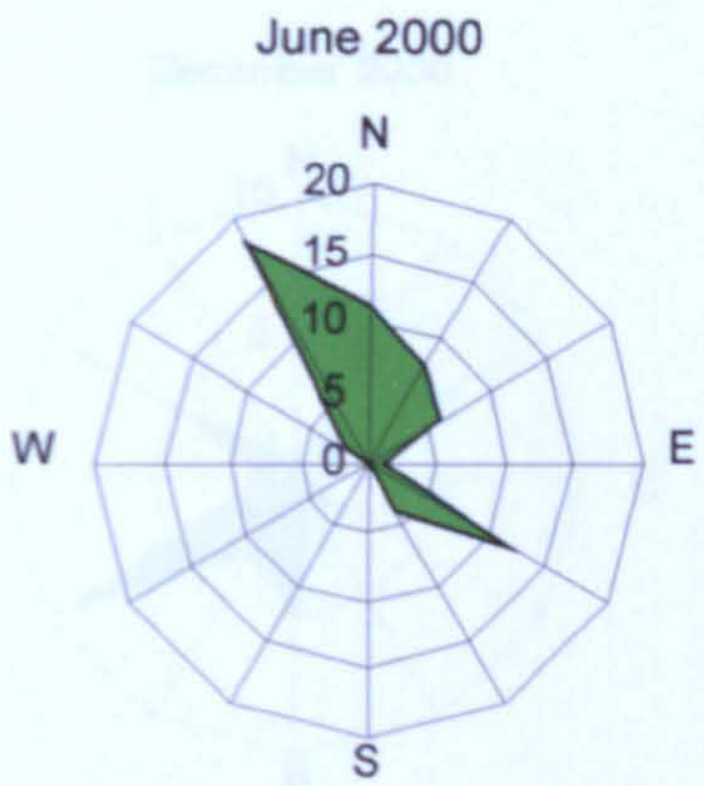

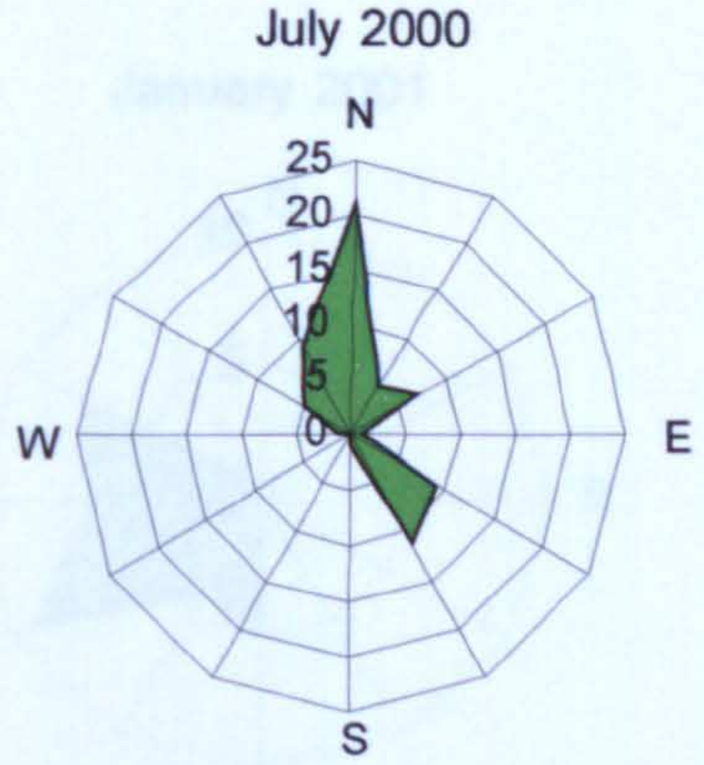

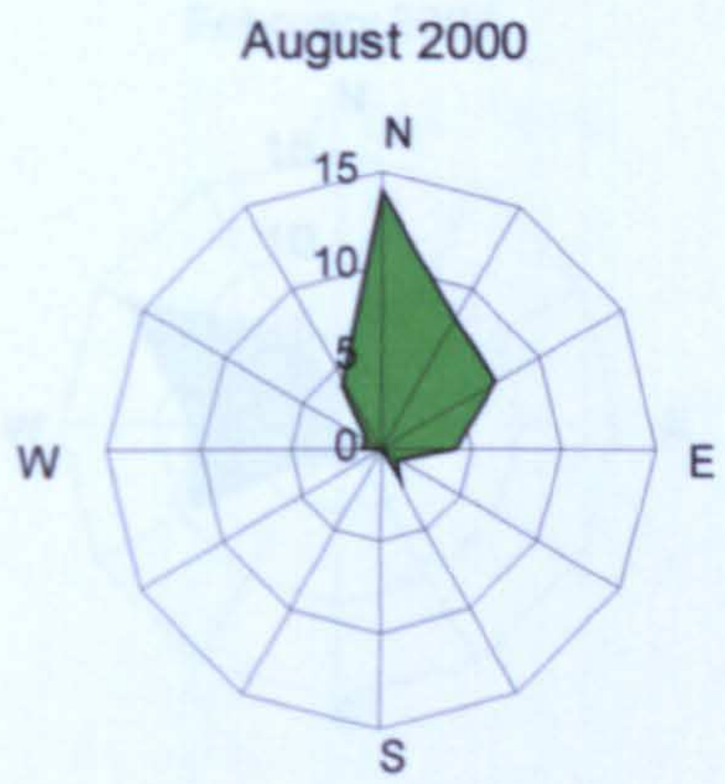

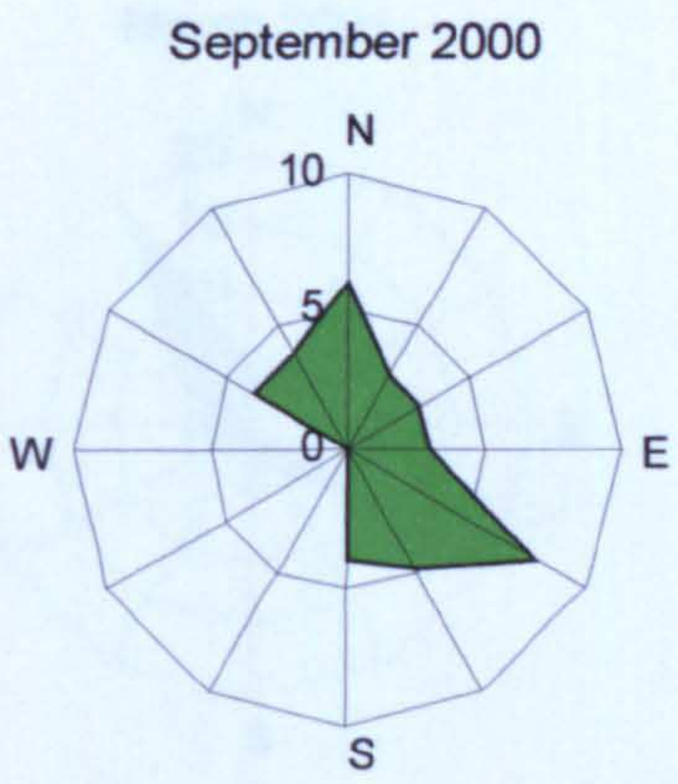

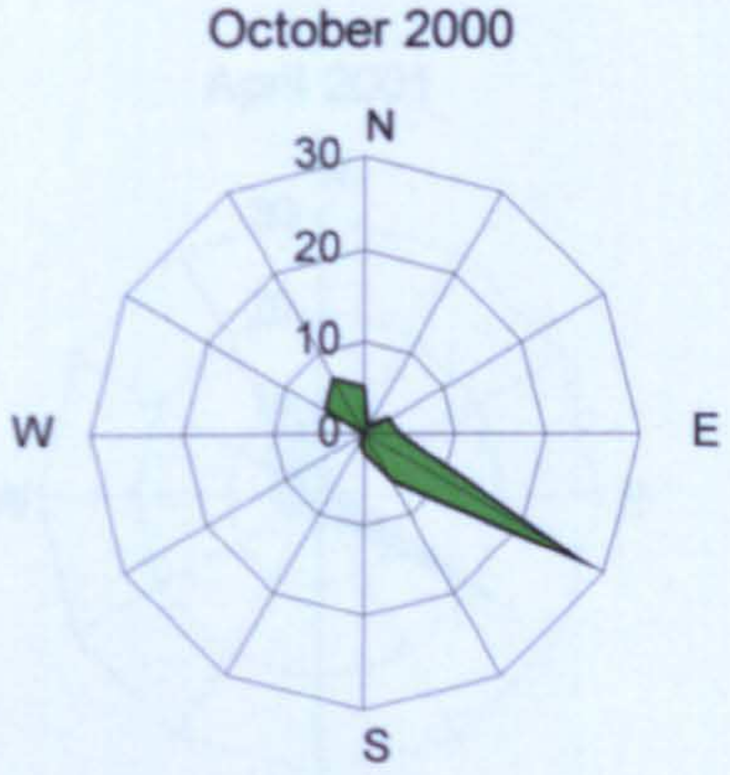

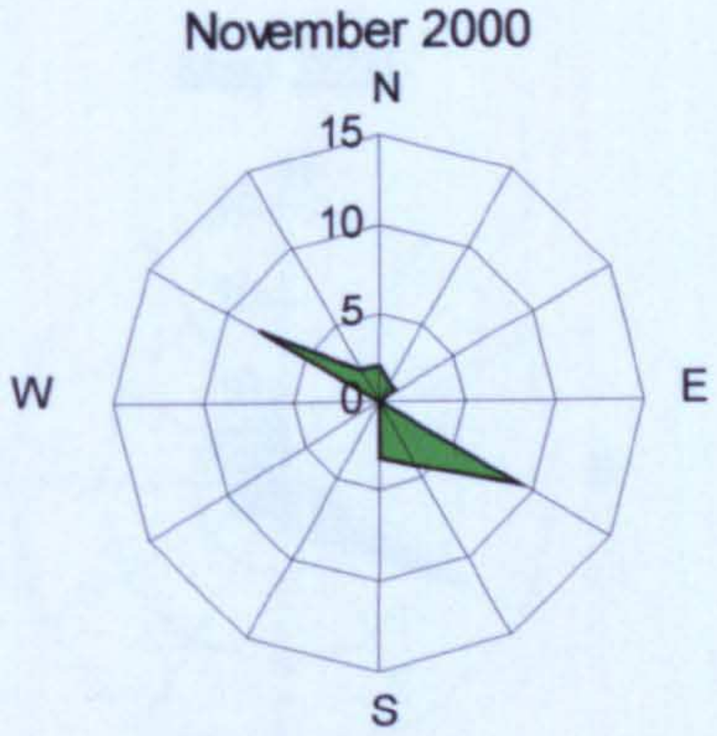

Figure I.1.9 Monthly prevailing wind directions and corresponding frequencies derived from Hun Station meteorological data. Wind roses represent wind velocities ≥ 6.5 m/s.

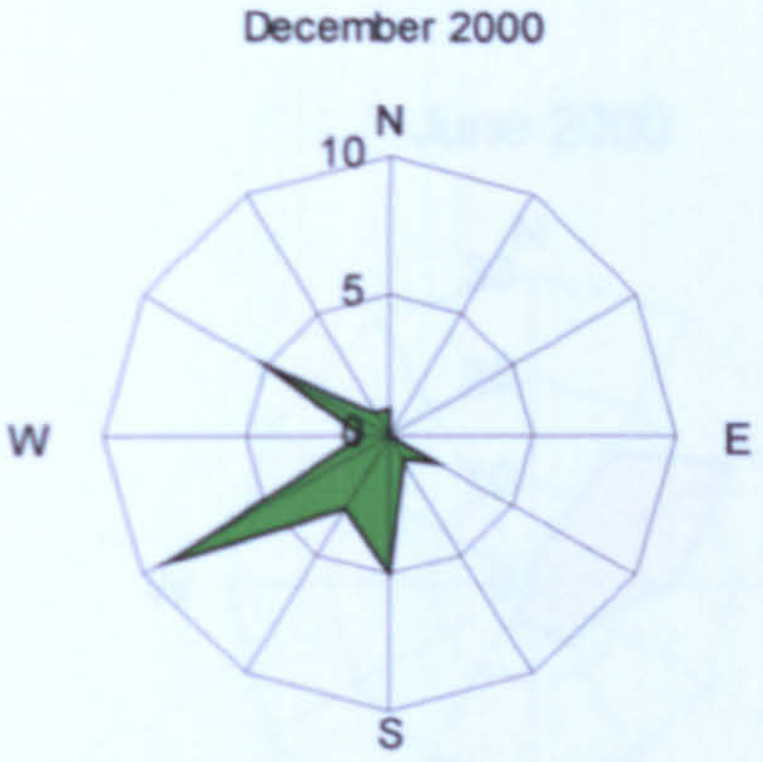

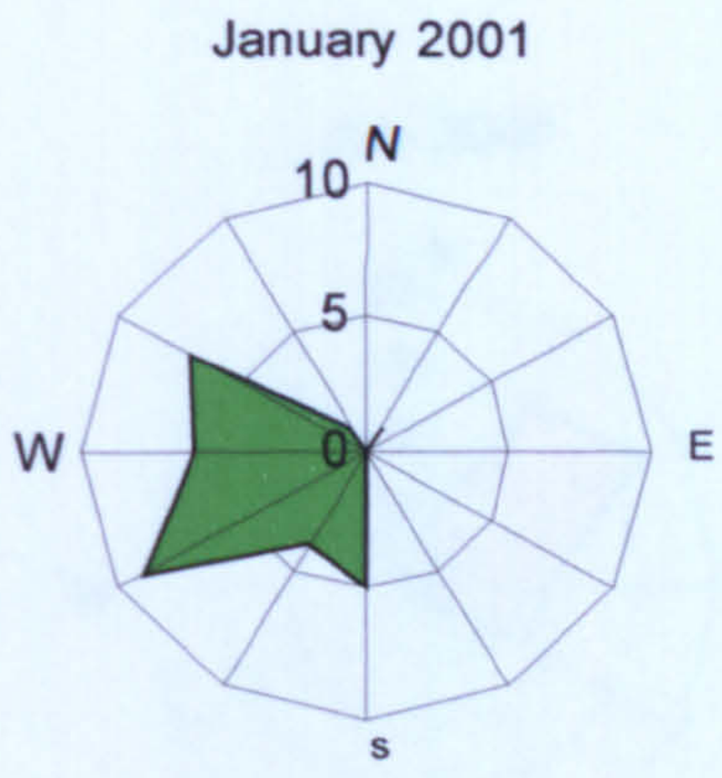

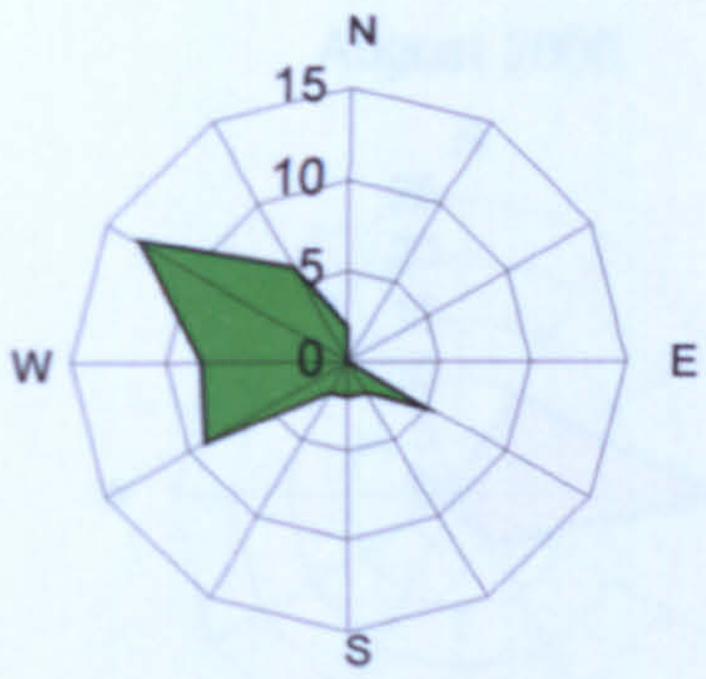

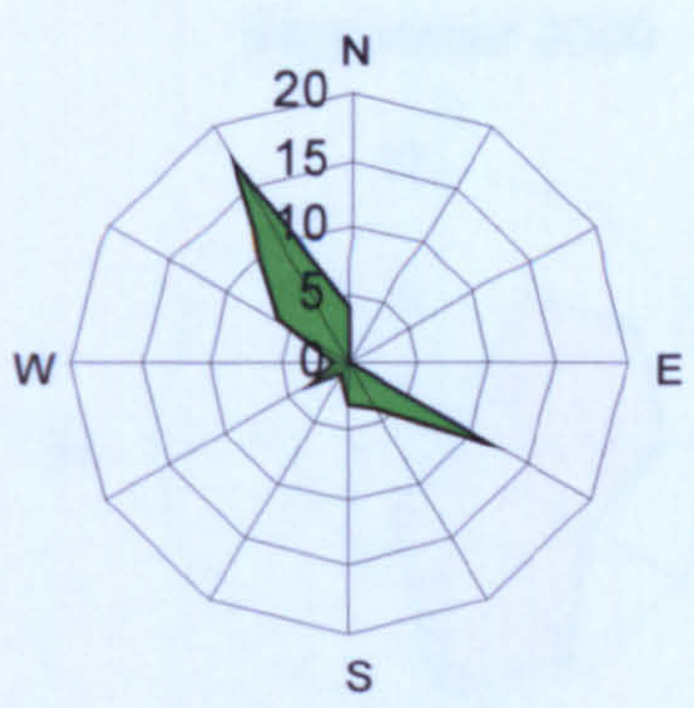

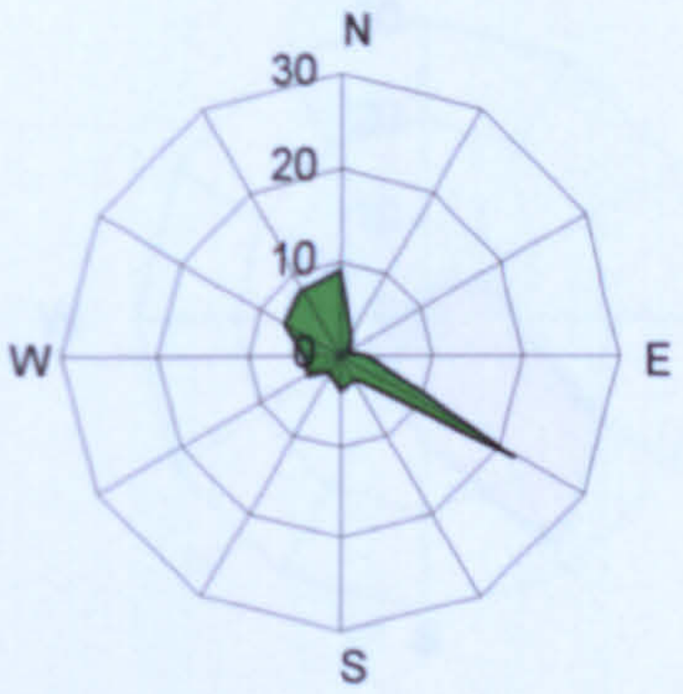

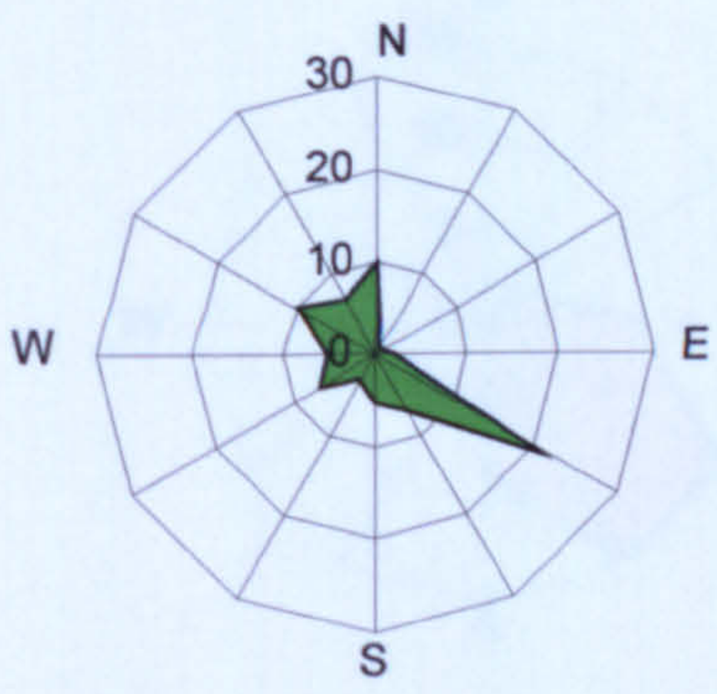

Figure I.1.10 Monthly prevailing wind directions and corresponding frequencies derived from Hun Station meteorological data. Wind roses represent wind velocities ≥ 6.5 m/s.

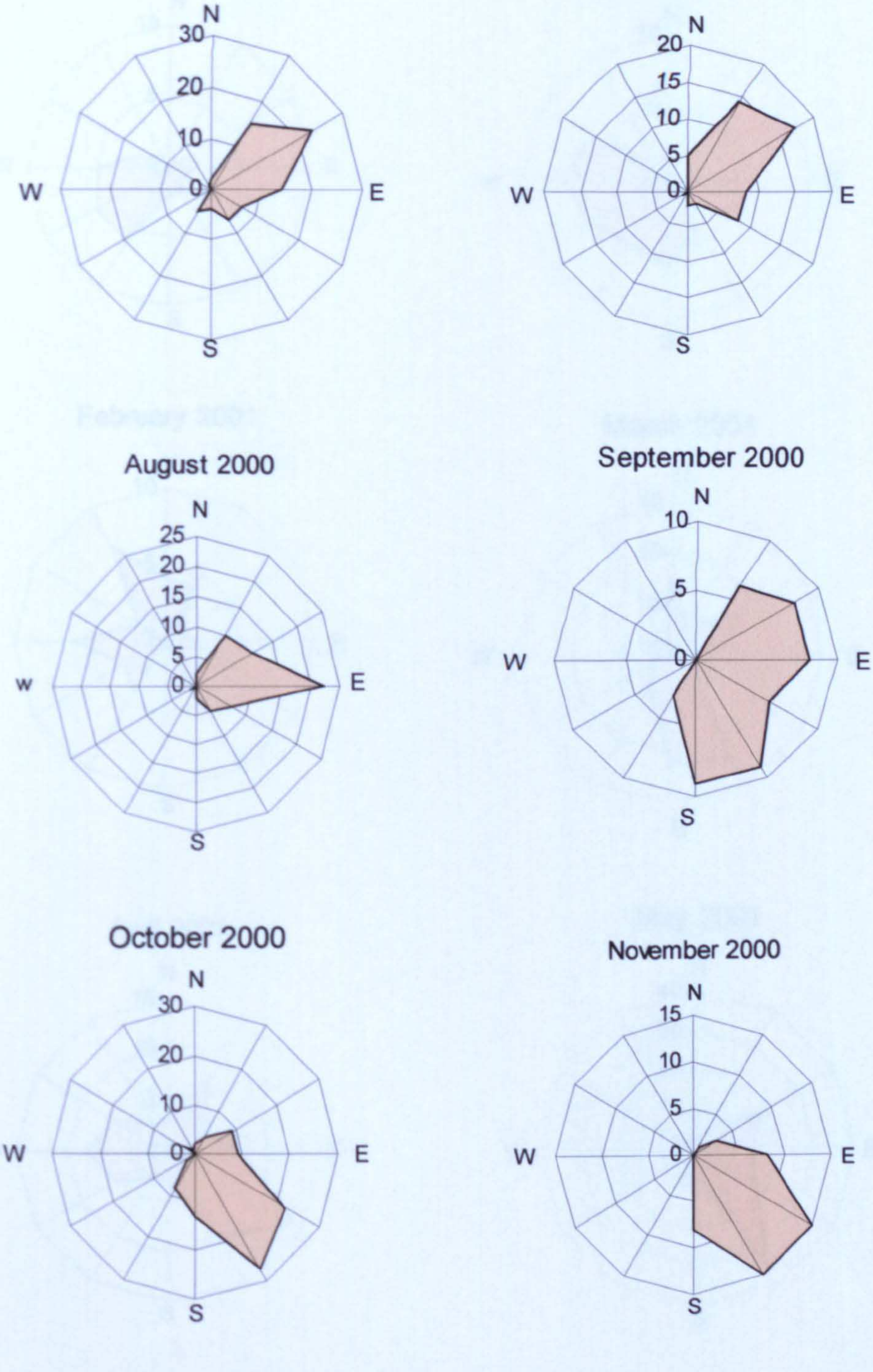

Figure I.1.11 Monthly prevailing wind directions and corresponding frequencies derived from Sebha Station meteorological data. Wind roses represent wind velocities > 6.5 m/s.

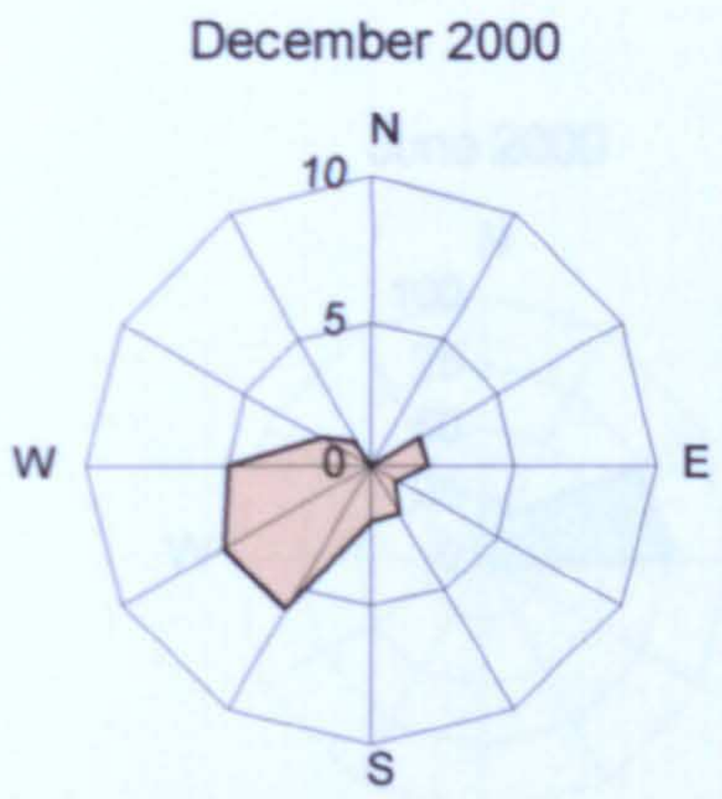

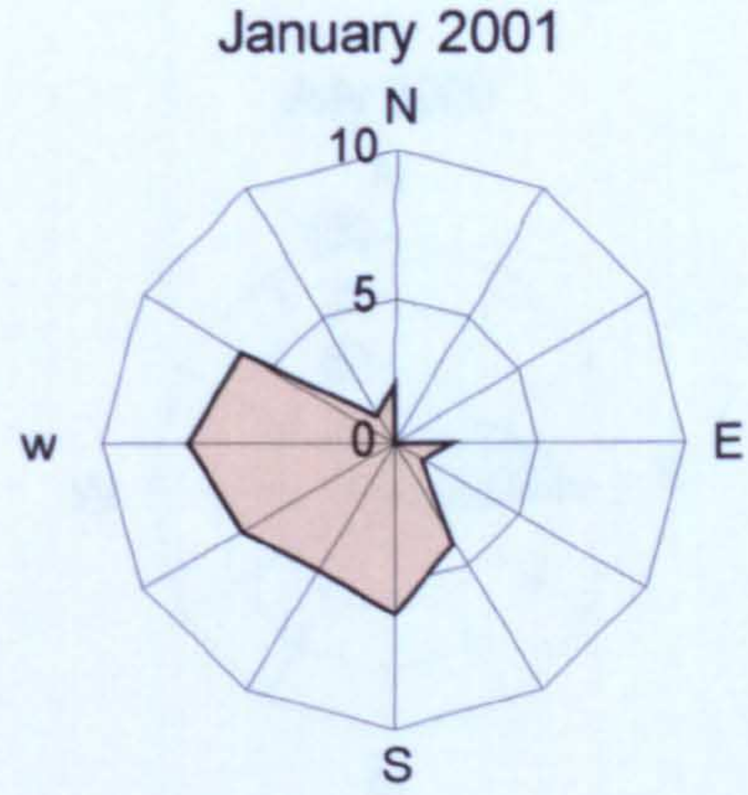

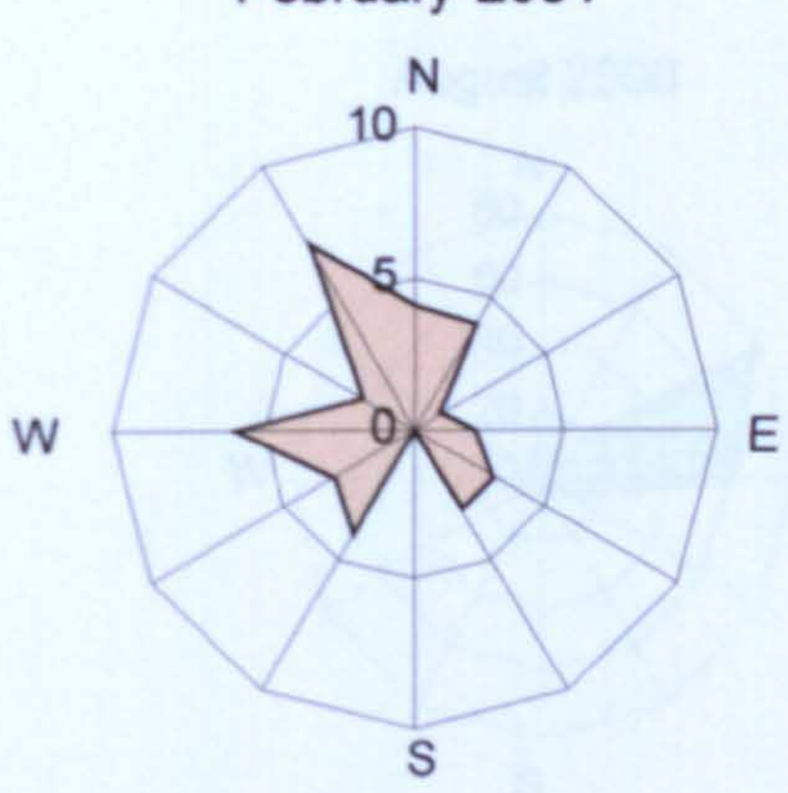

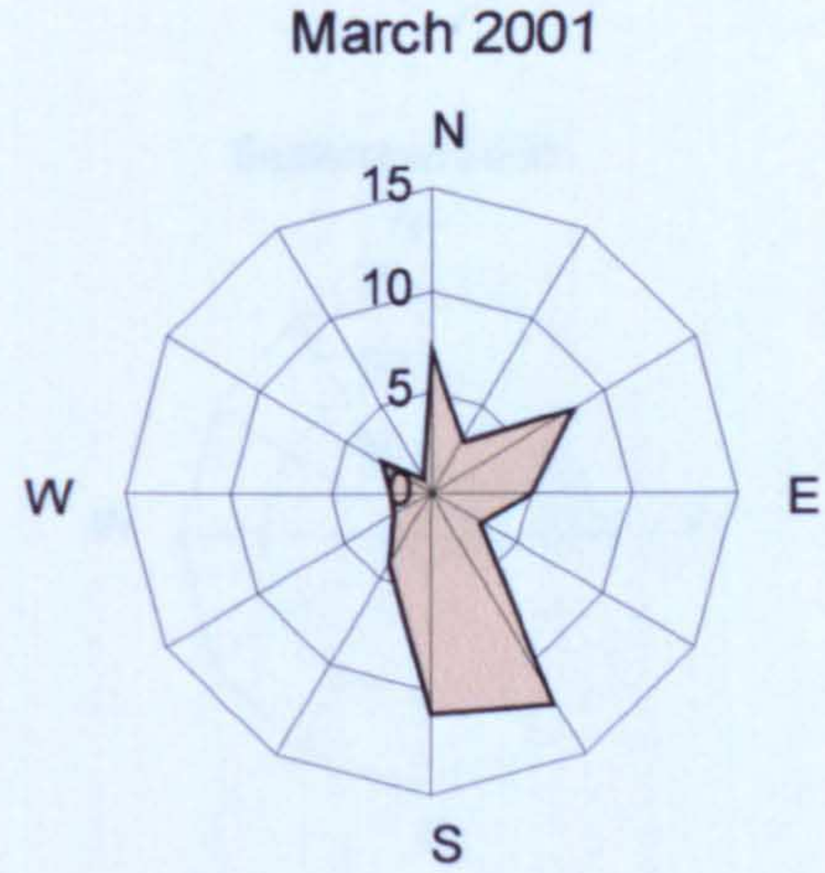

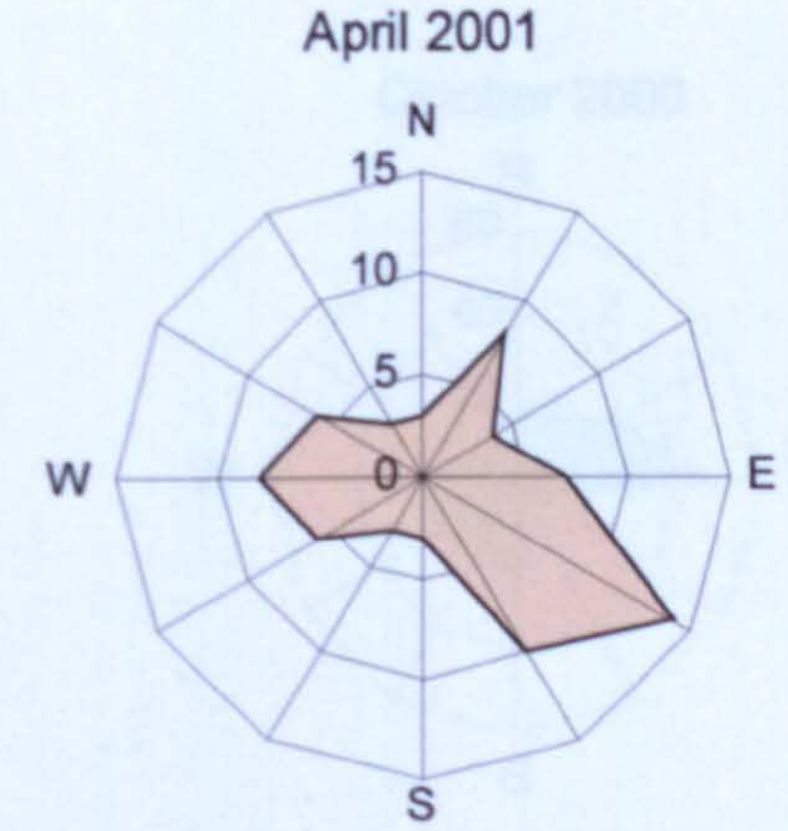

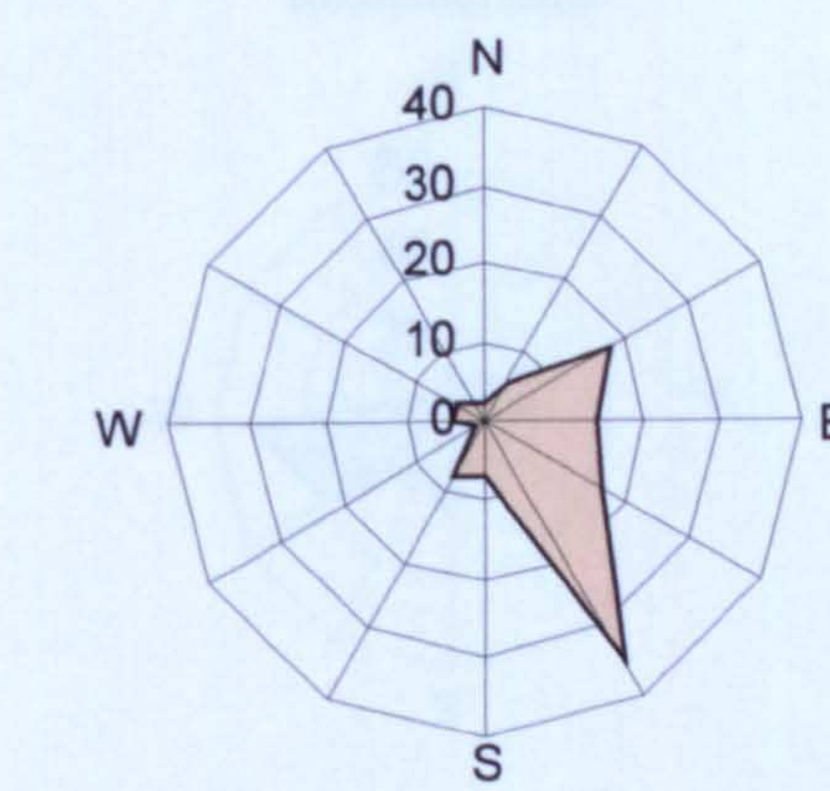

Figure I.1.12 Monthly prevailing wind directions and corresponding frequencies derived from Sebha Station meteorological data. Wind roses represent wind velocities ≥ 6.5 m/s.

I.2. WIND ROSES BASED ON ALL WIND SPEEDS

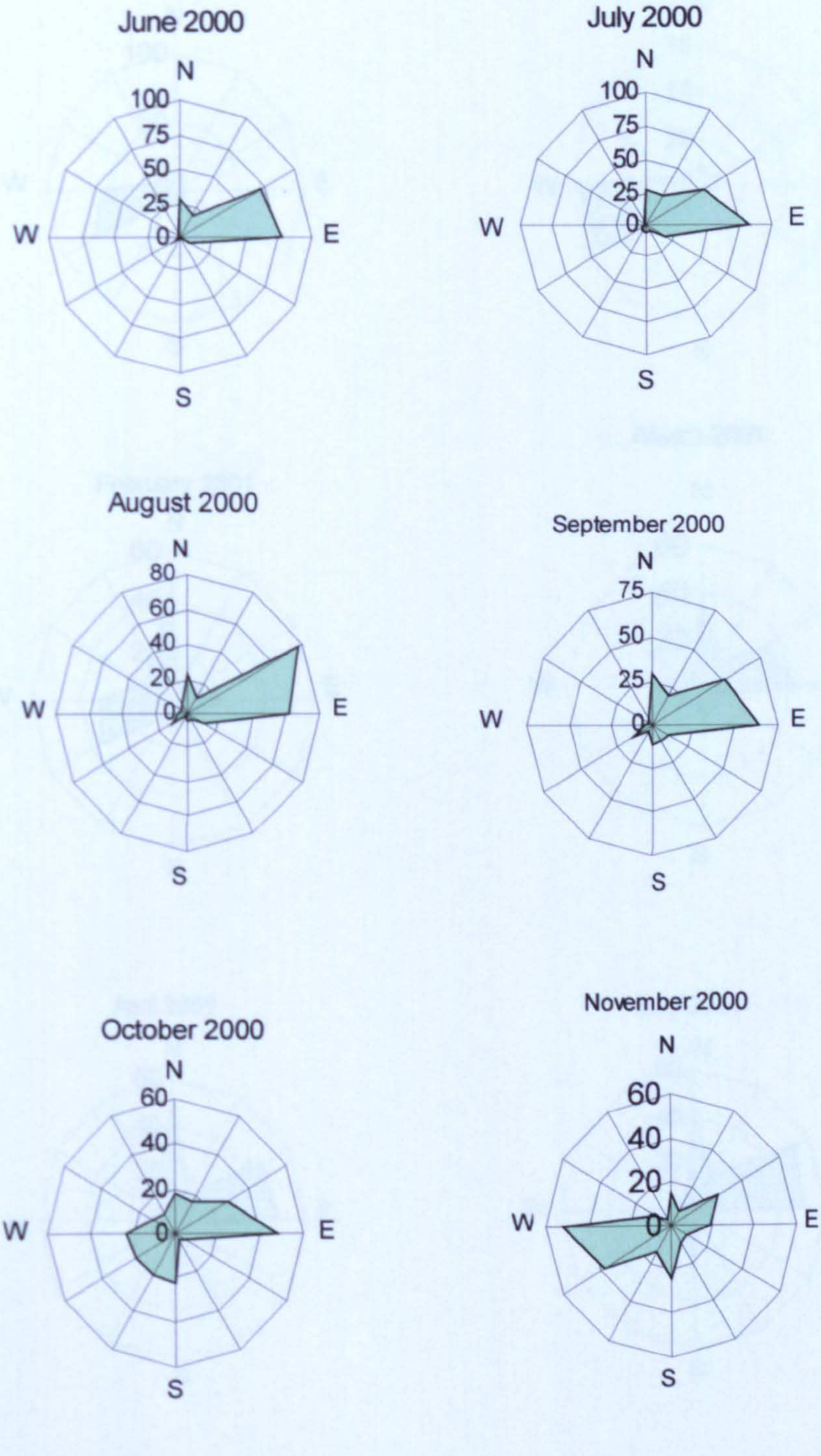

Figure I.2.1 Monthly prevailing wind directions and corresponding frequencies derived from Zuwarah Station meteorological data. Wind roses represent all wind velocities

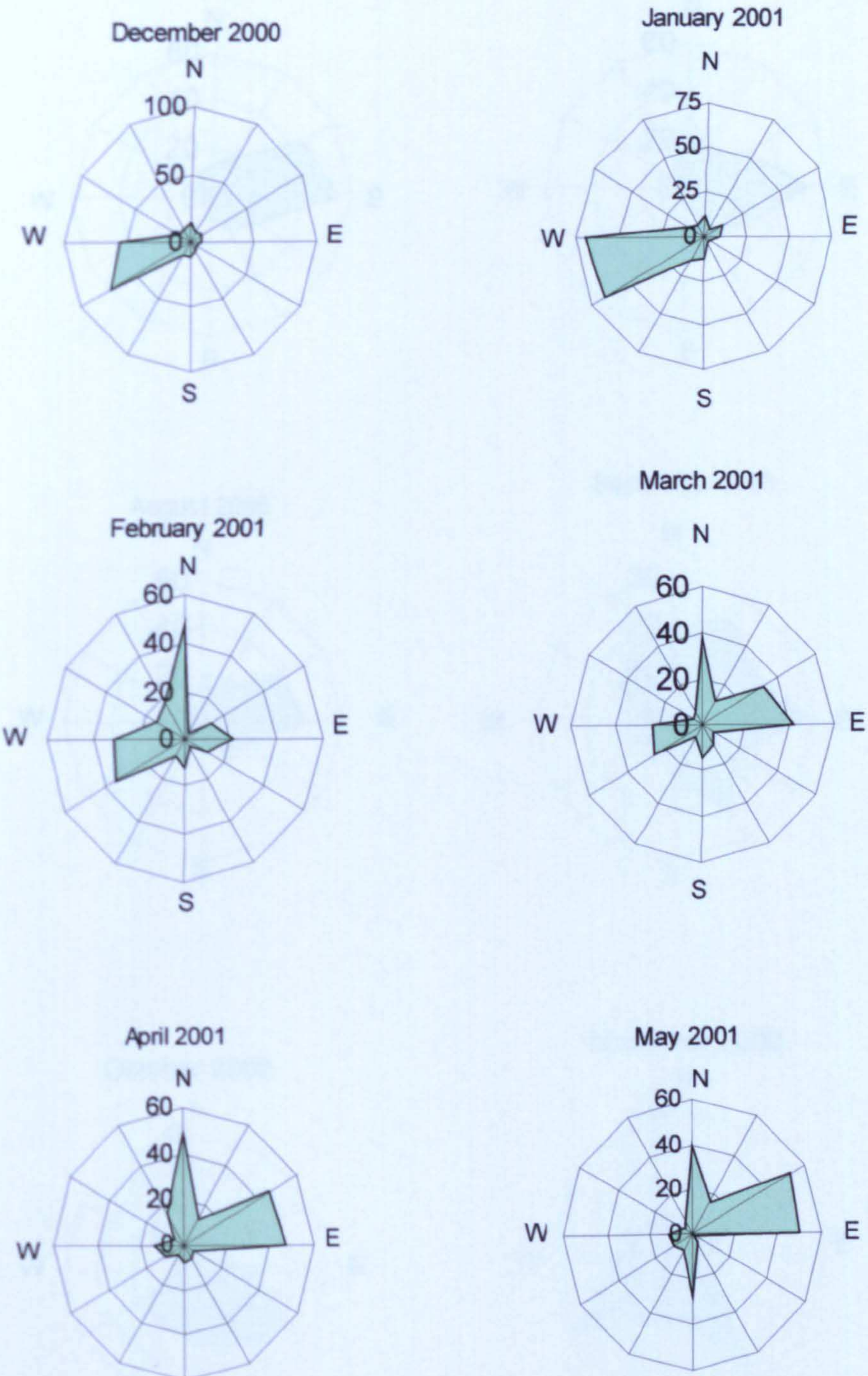

Figure I.2.2 Monthly prevailing wind directions and corresponding frequencies derived from Zuwarah Station meteorological data. Wind roses represent all wind velocities

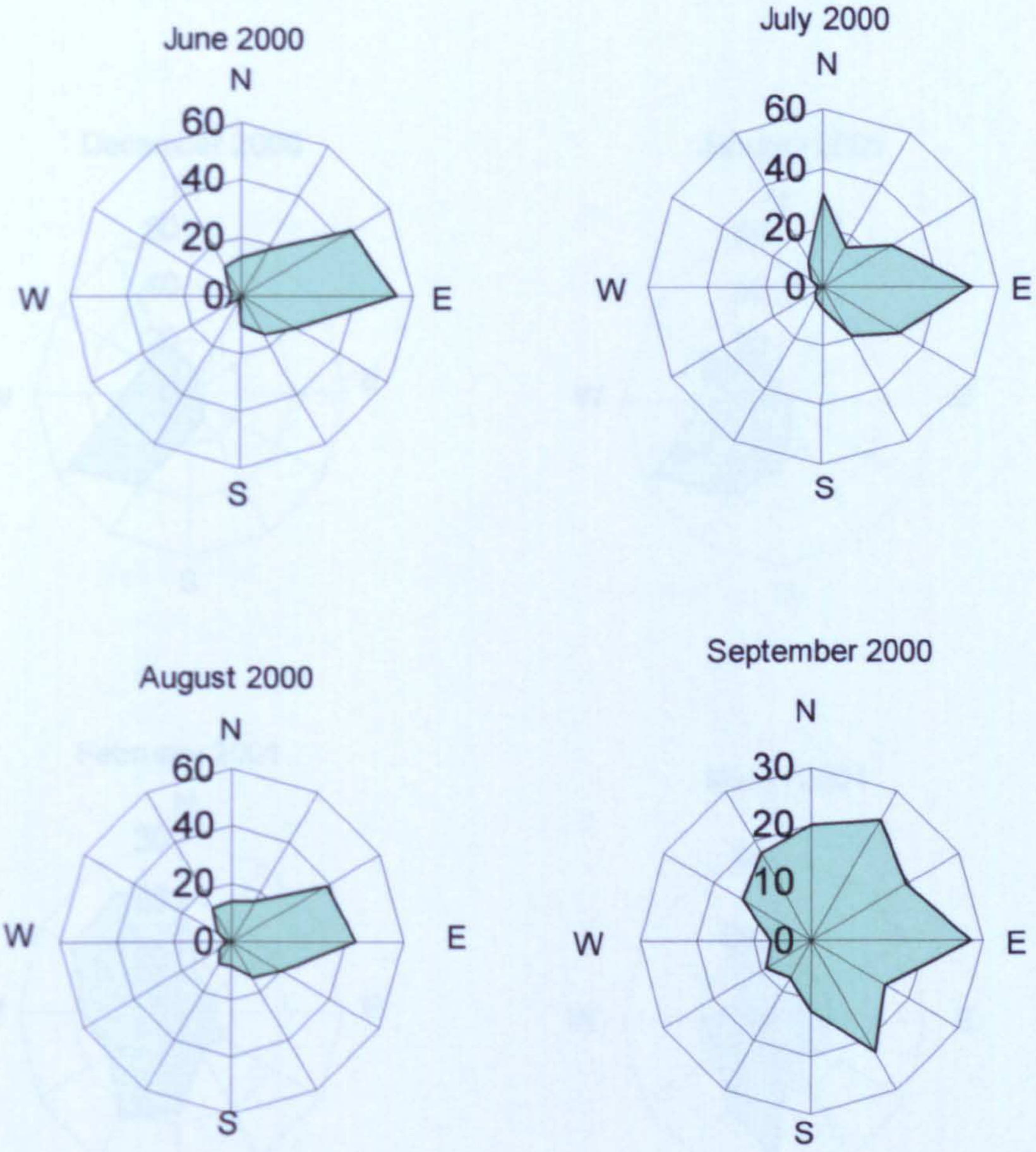

Figure I.2.3 Monthly prevailing wind directions and corresponding frequencies derived from *Tripoli* Station meteorological data. Wind roses represent all wind velocities

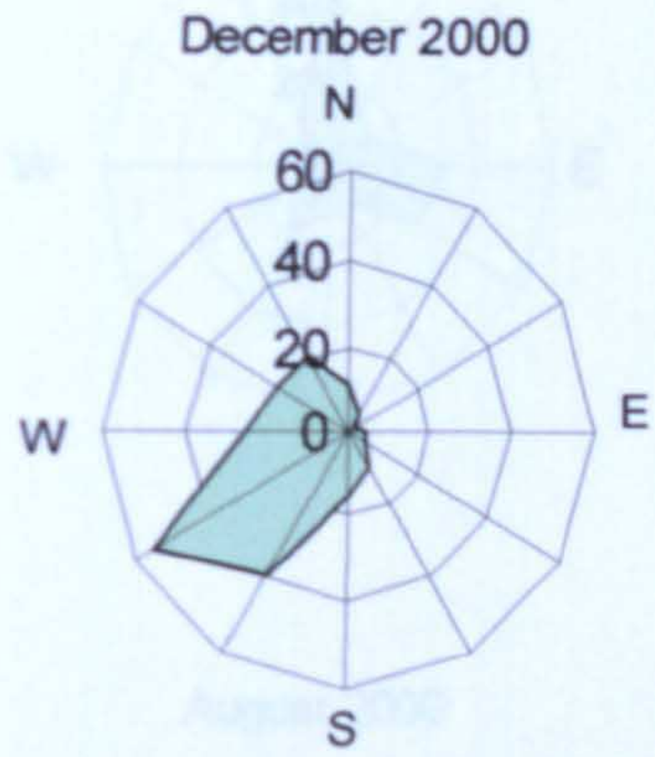

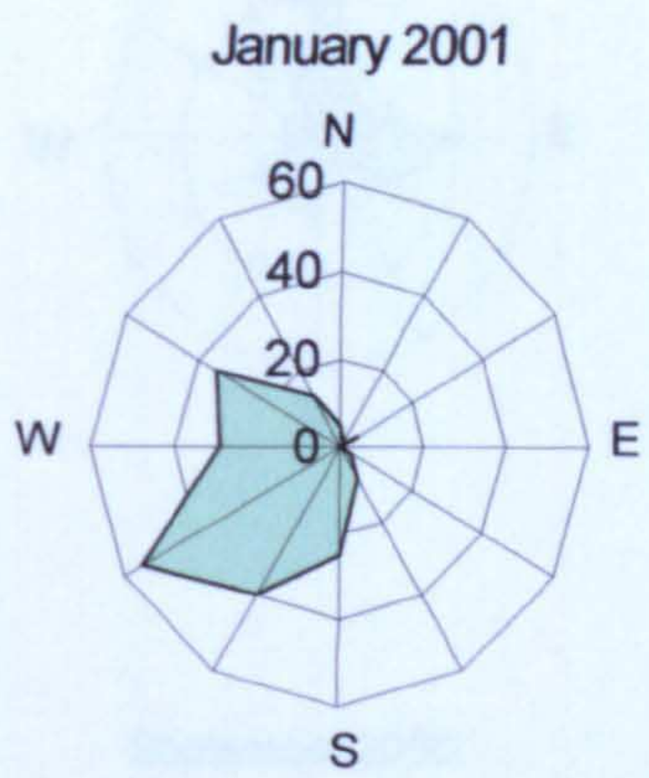

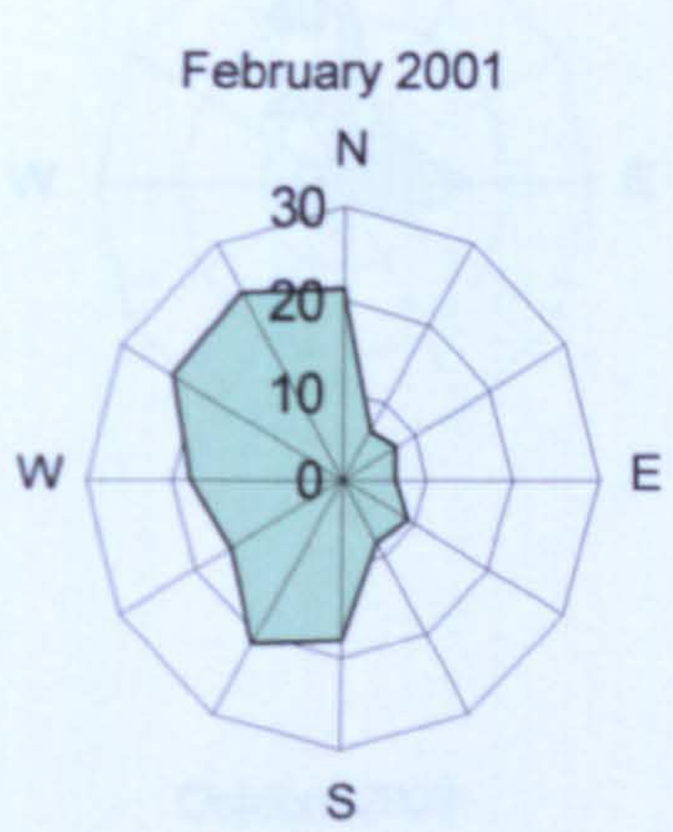

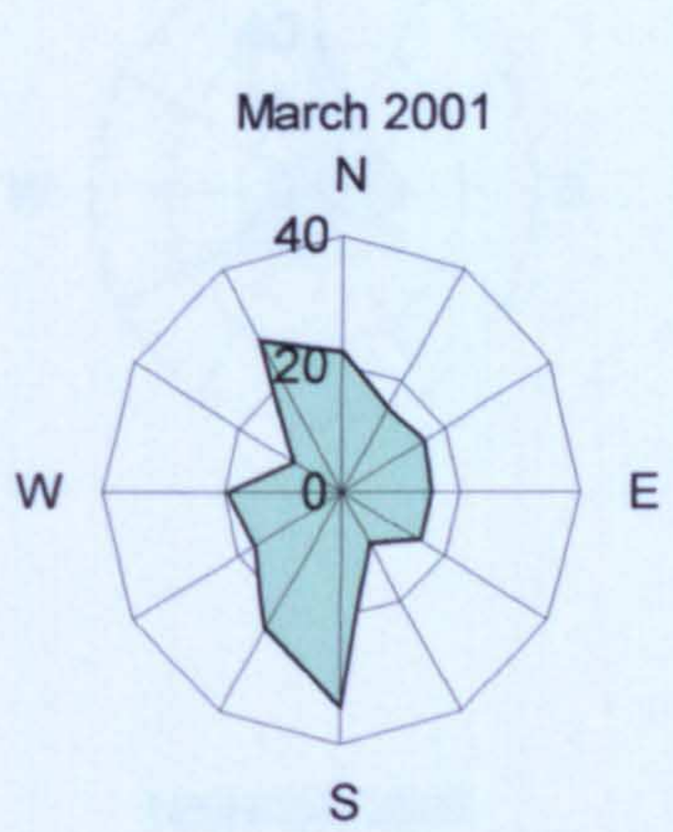

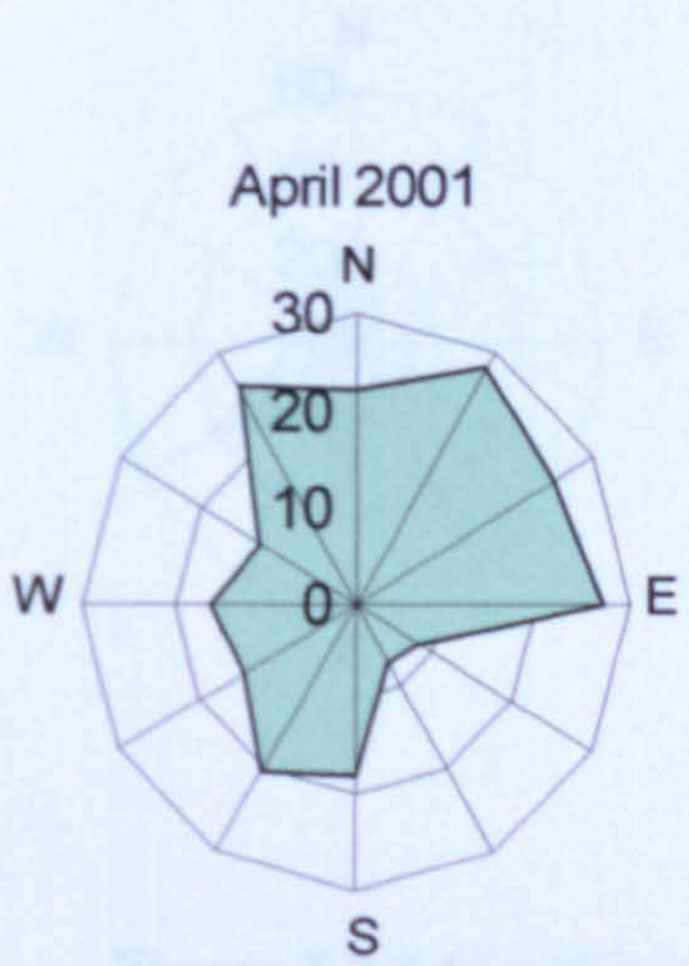

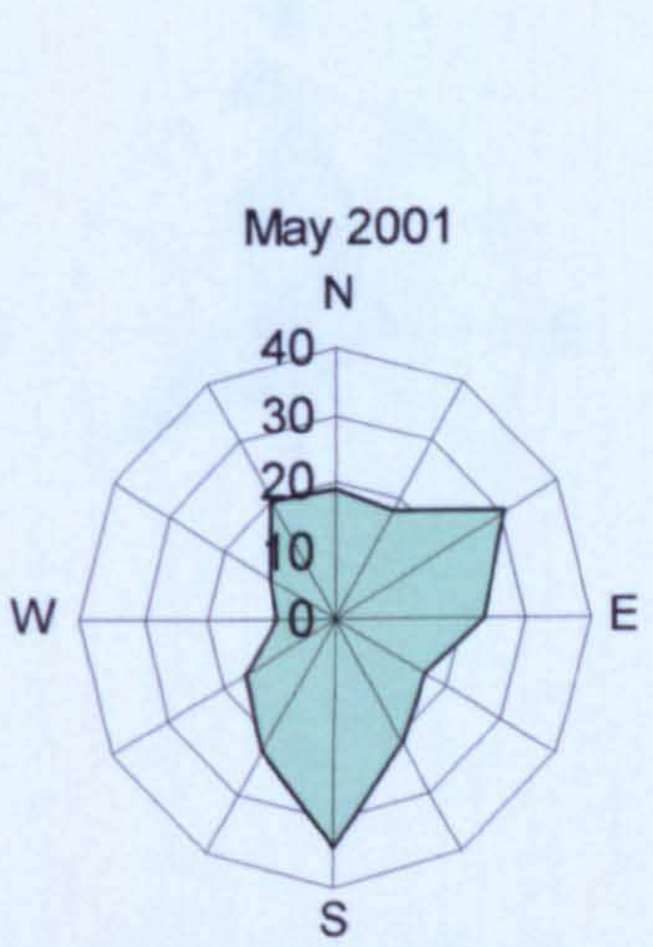

Figure I.2.4 Monthly prevailing wind directions and corresponding frequencies derived from Tripoli Station meteorological data. Wind roses represent all wind velocities

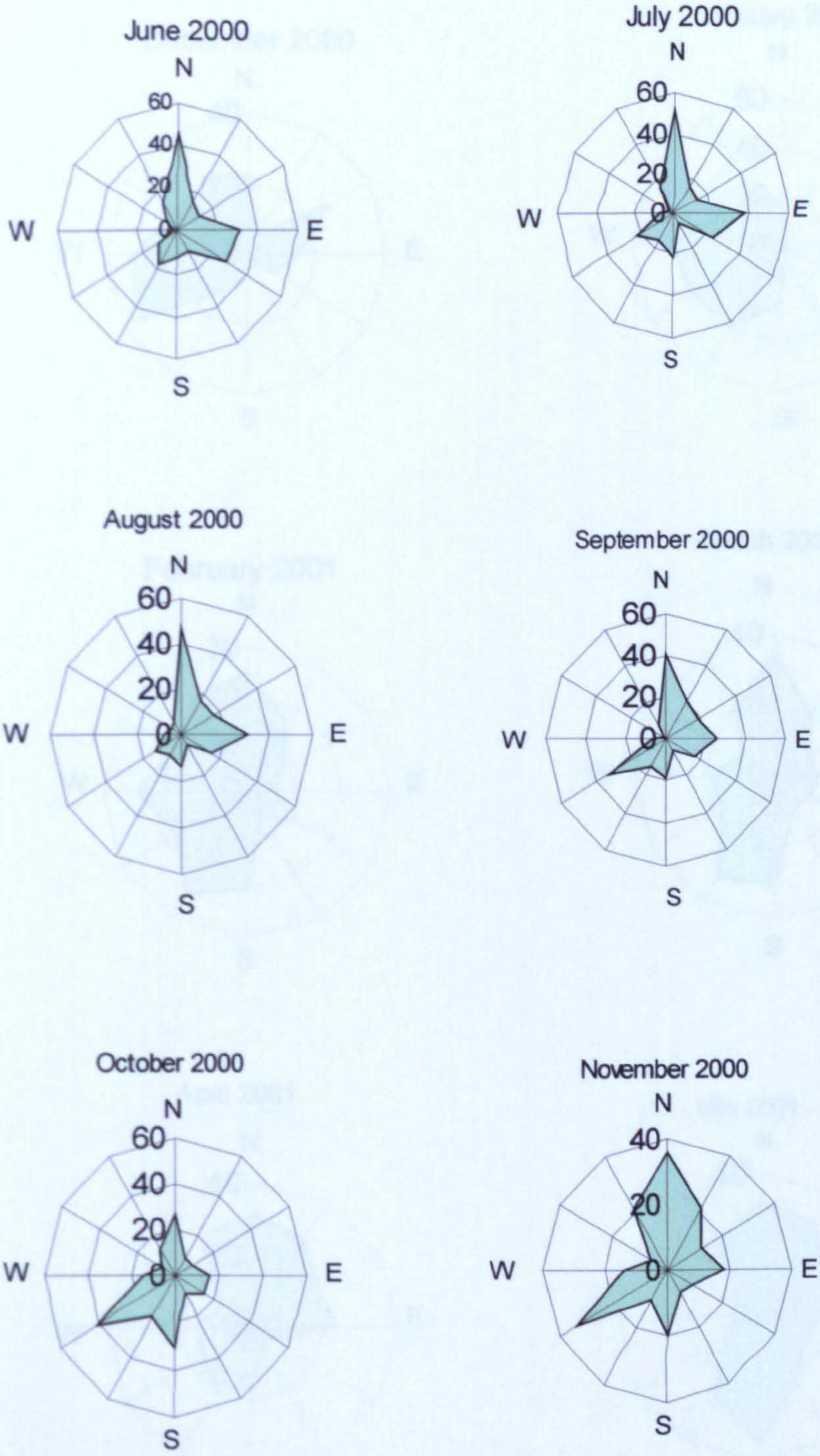

Figure I.2.5 Monthly prevailing wind directions and corresponding frequencies derived from Al Khums Station meteorological data. Wind roses represent all wind velocities

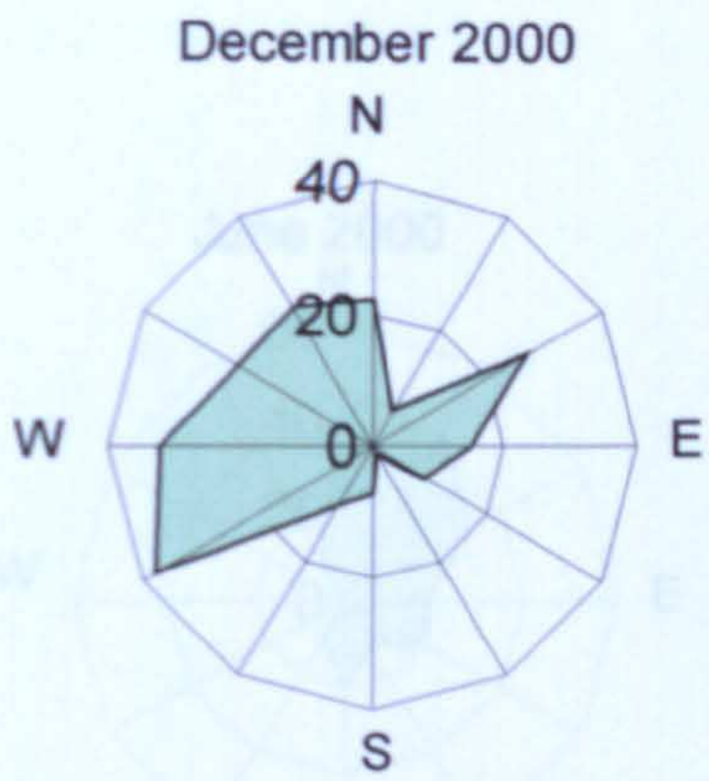

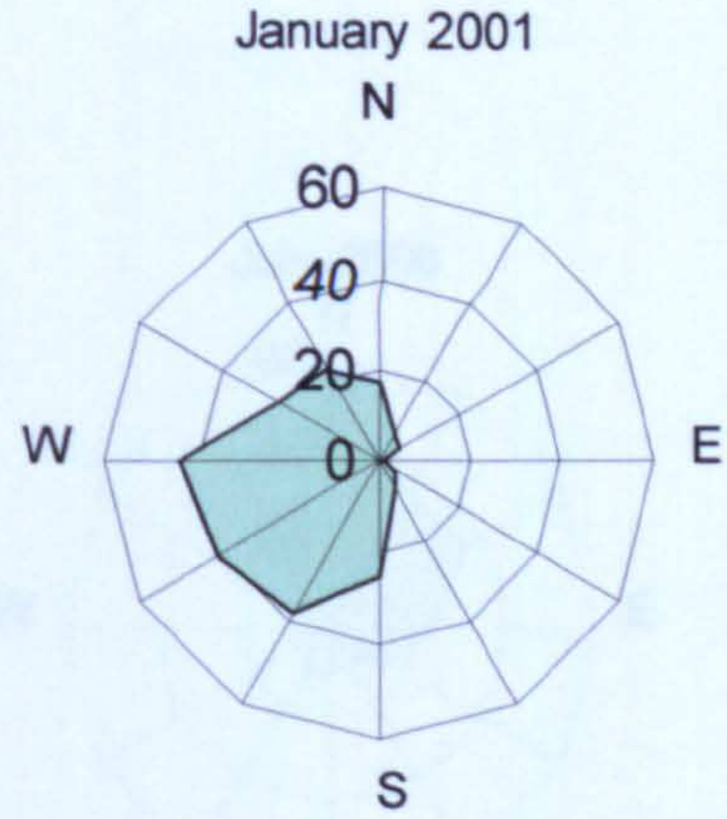

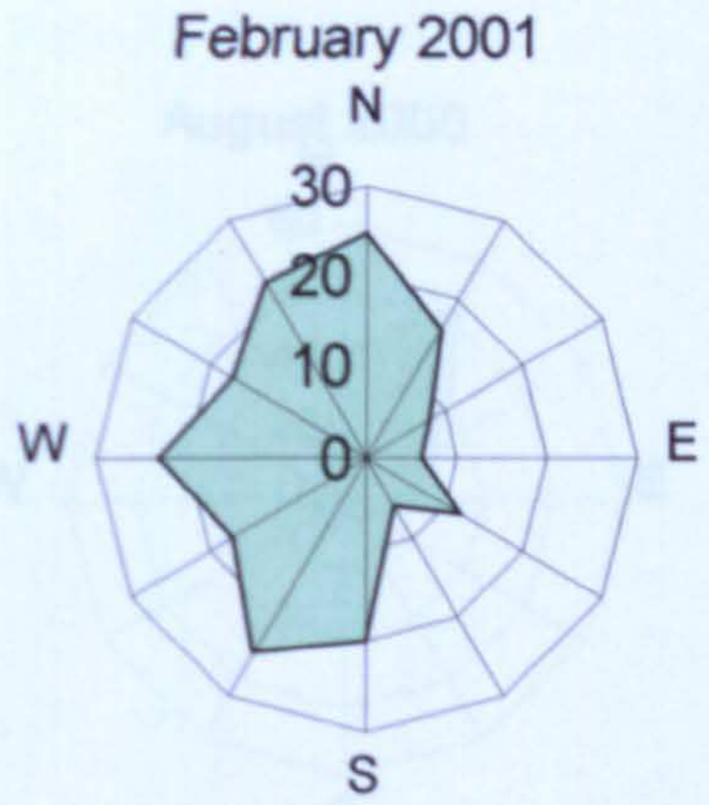

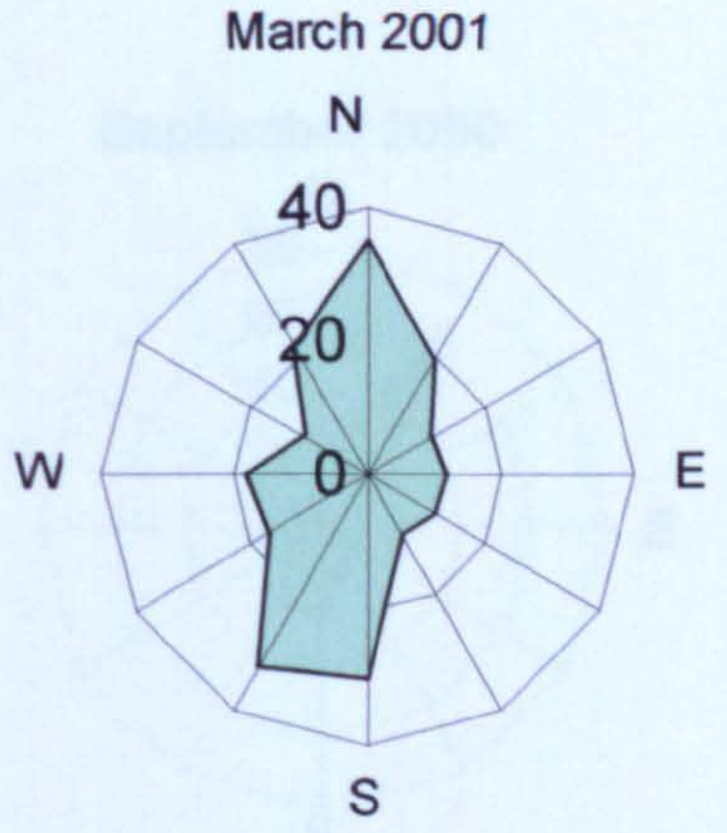

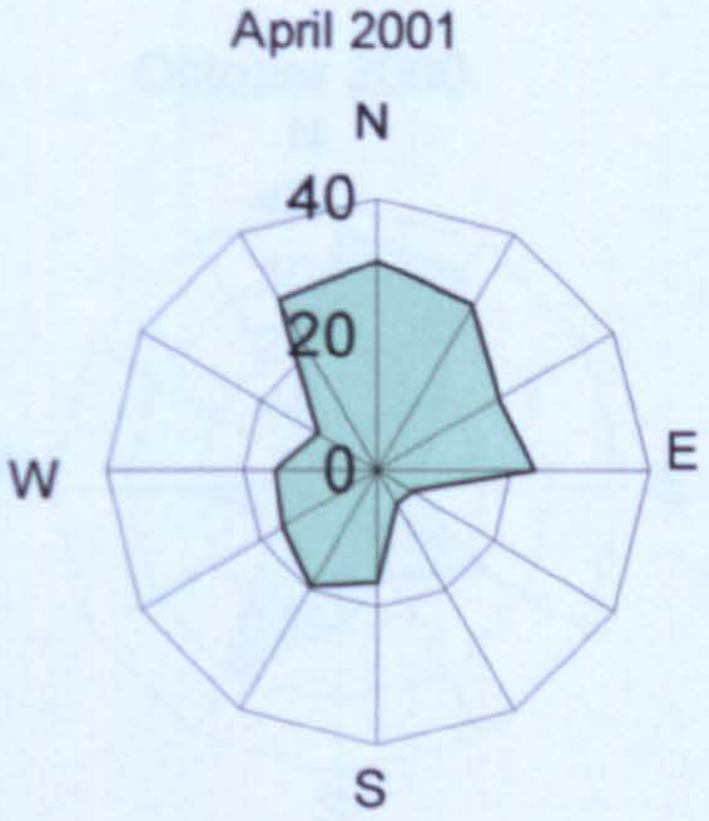

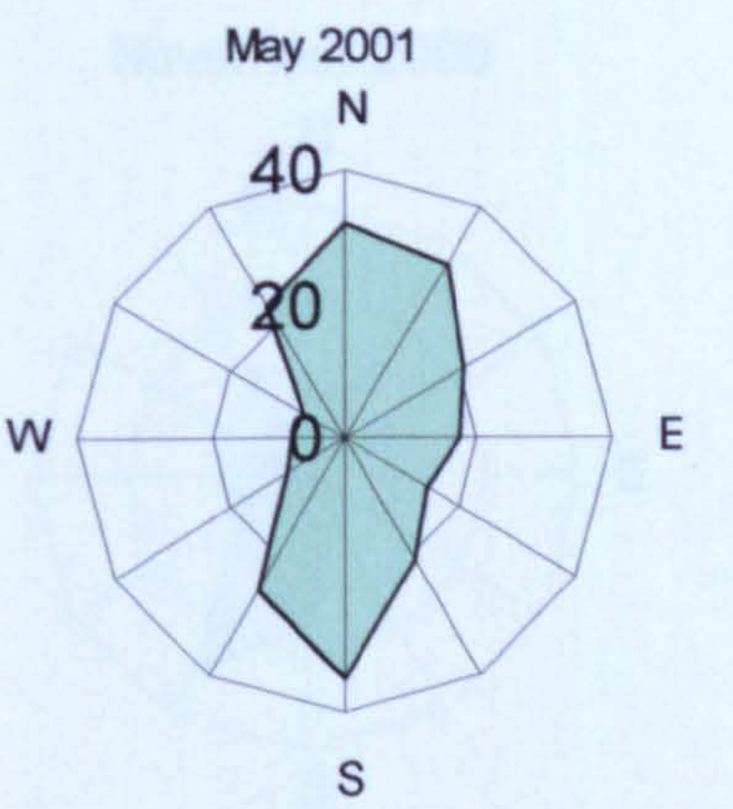

Figure I.2.6 Monthly prevailing wind directions and corresponding frequencies derived from Al Khums Station meteorological data. Wind roses represent all wind velocities

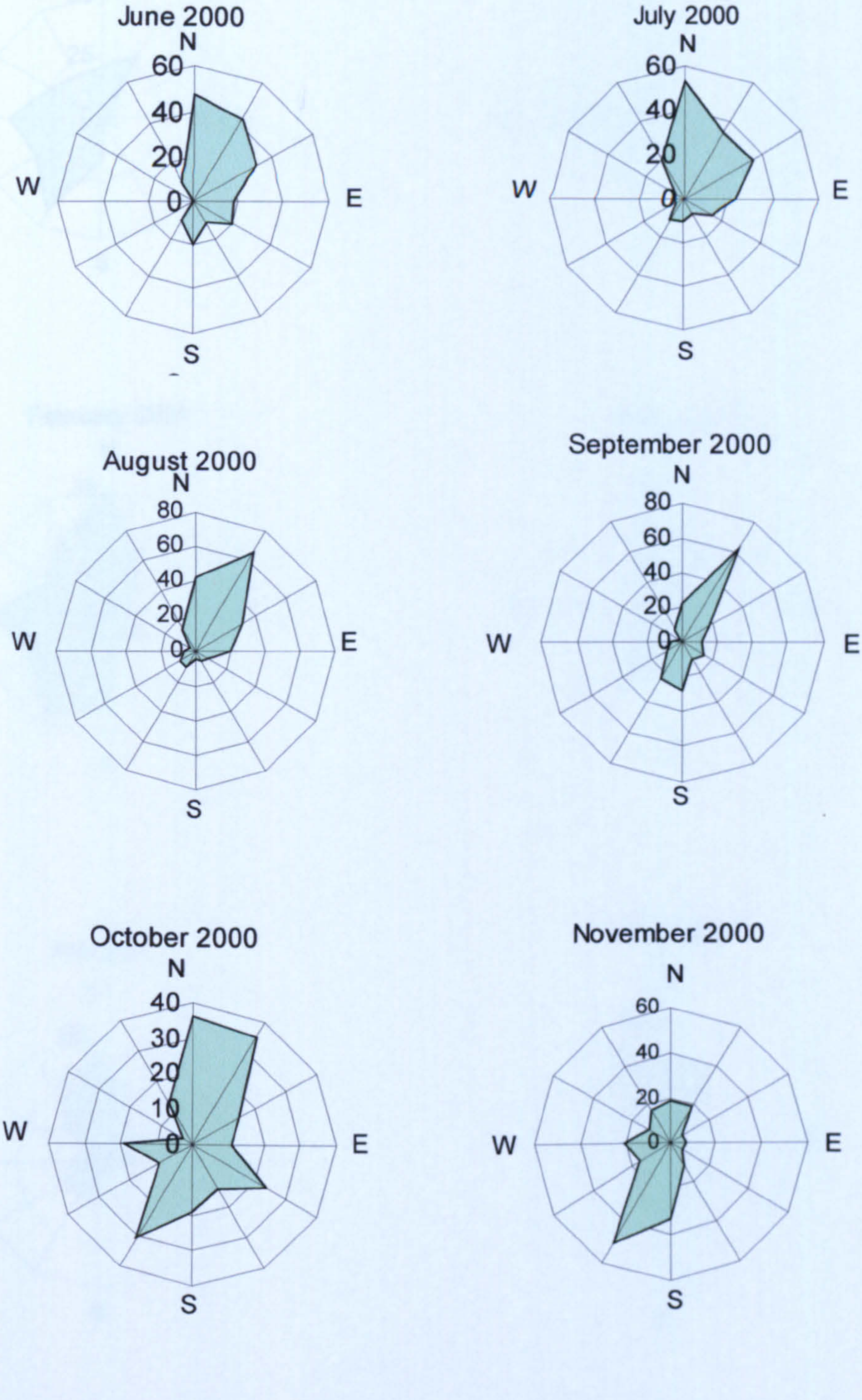

Figure I.2.7 Monthly prevailing wind *directions* and corresponding frequencies derived from *Misratah* Station meteorological data. Wind roses represent all wind velocities

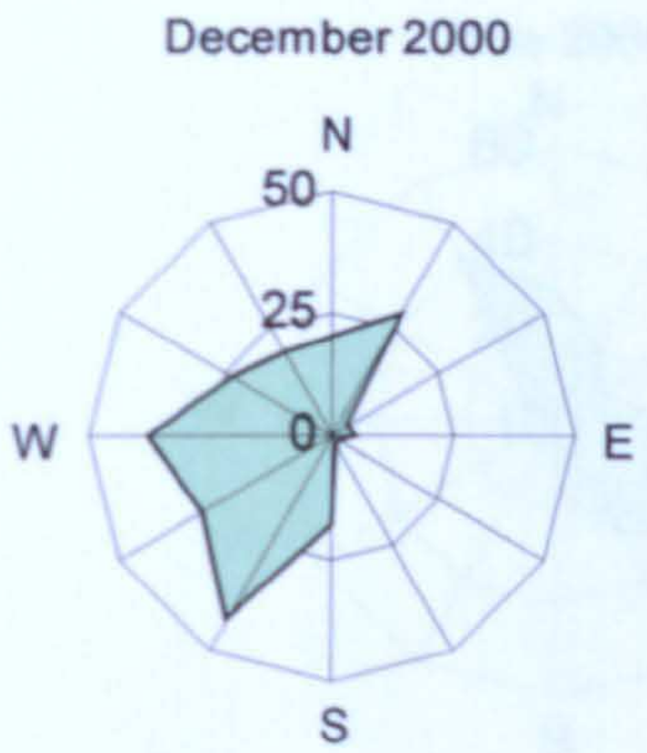

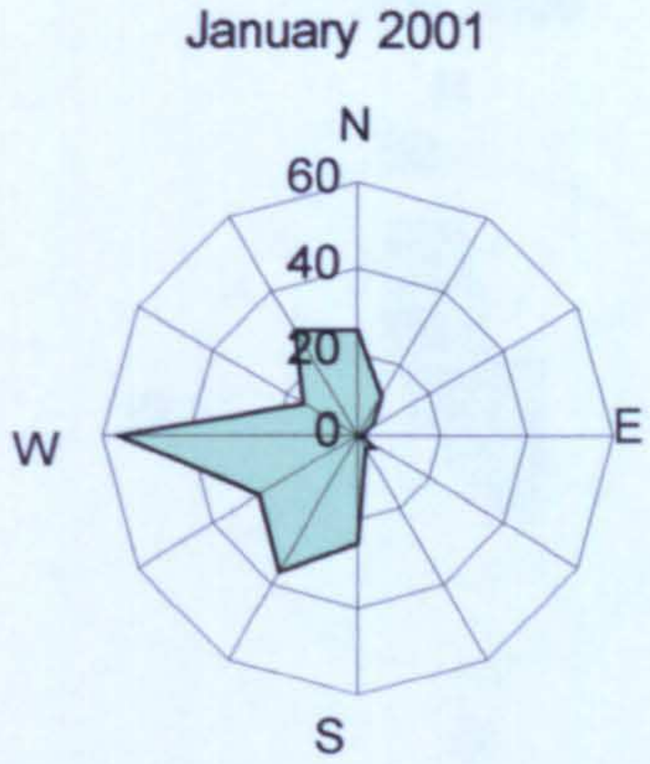

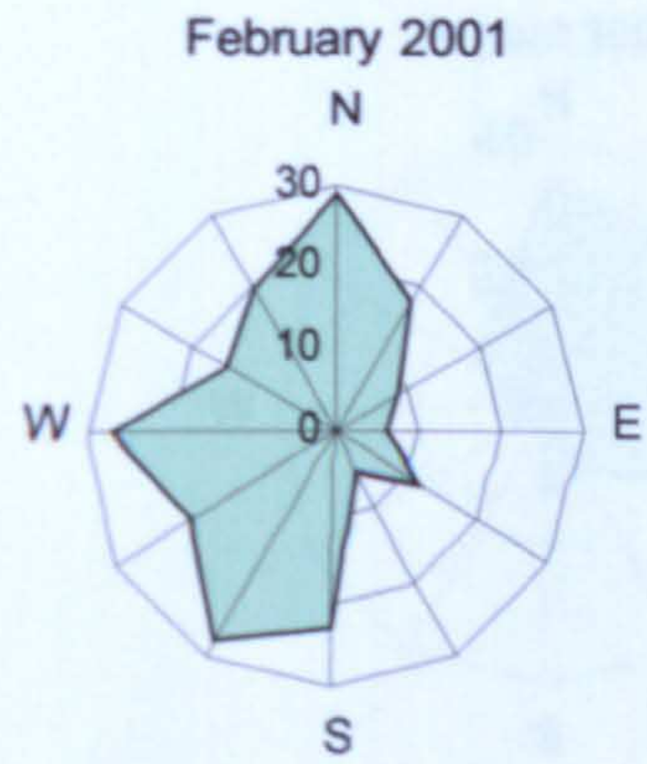

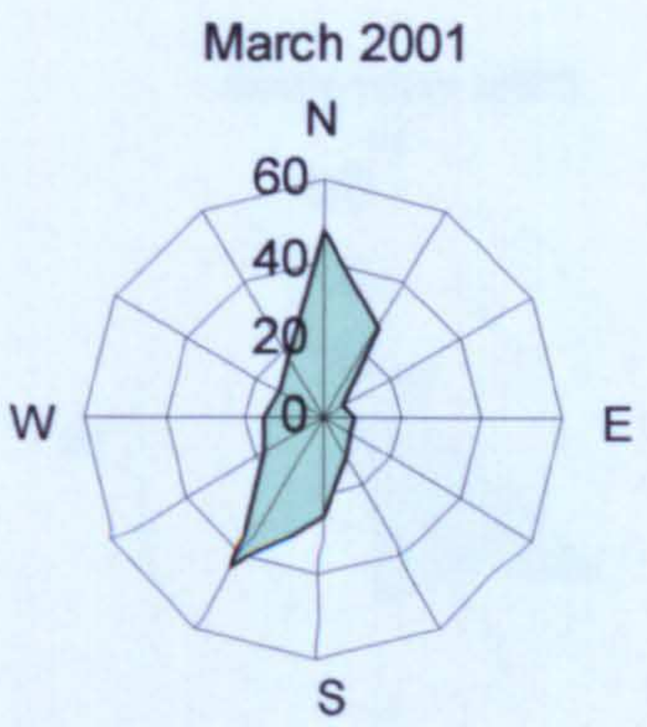

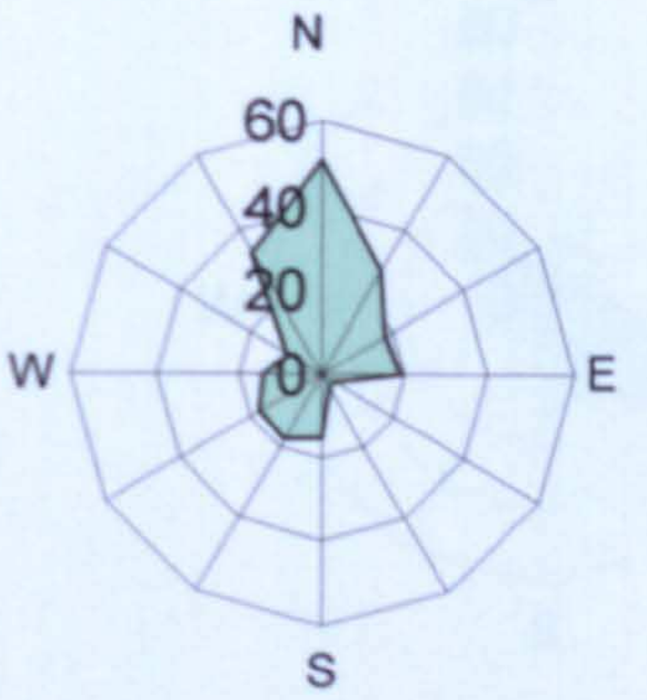

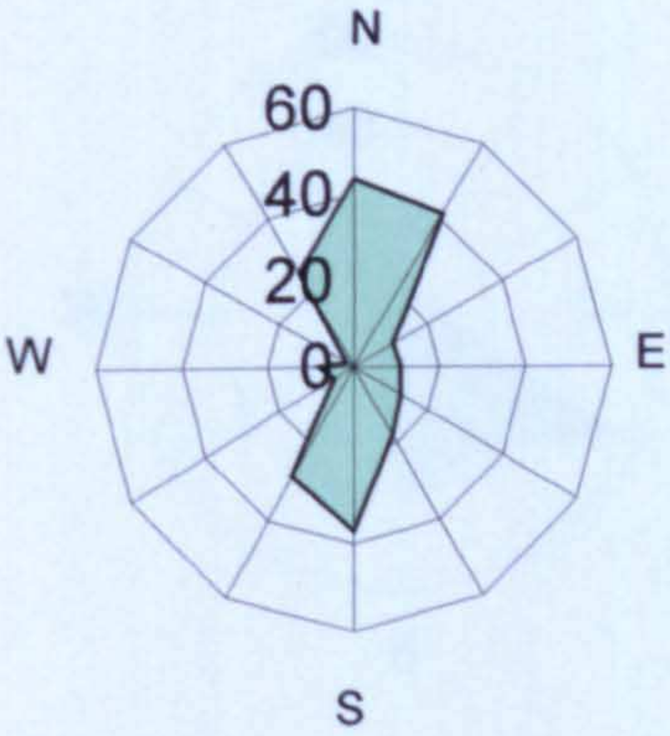

Figure I.2.8 Monthly prevailing wind directions and corresponding frequencies derived from Misratah Station meteorological data. Wind roses represent all wind velocities

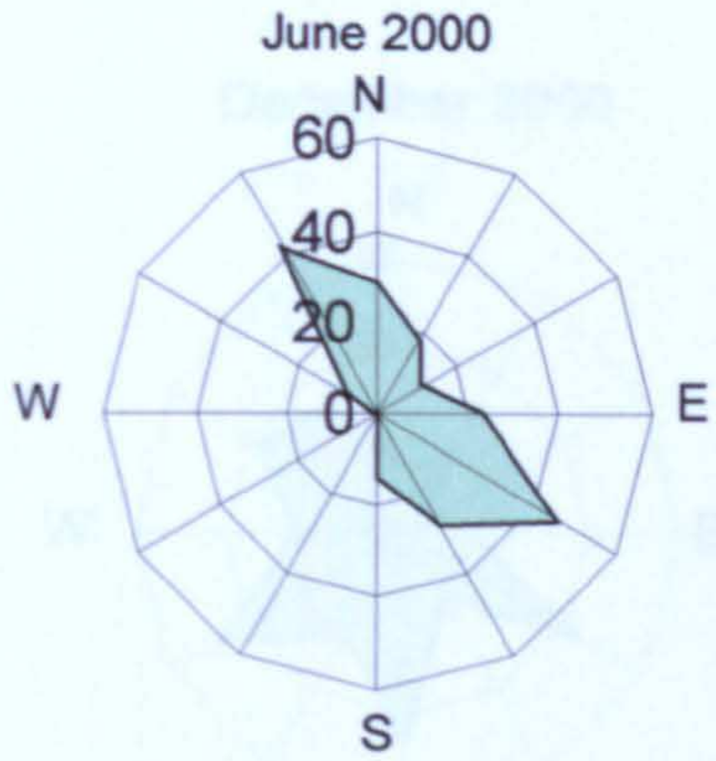

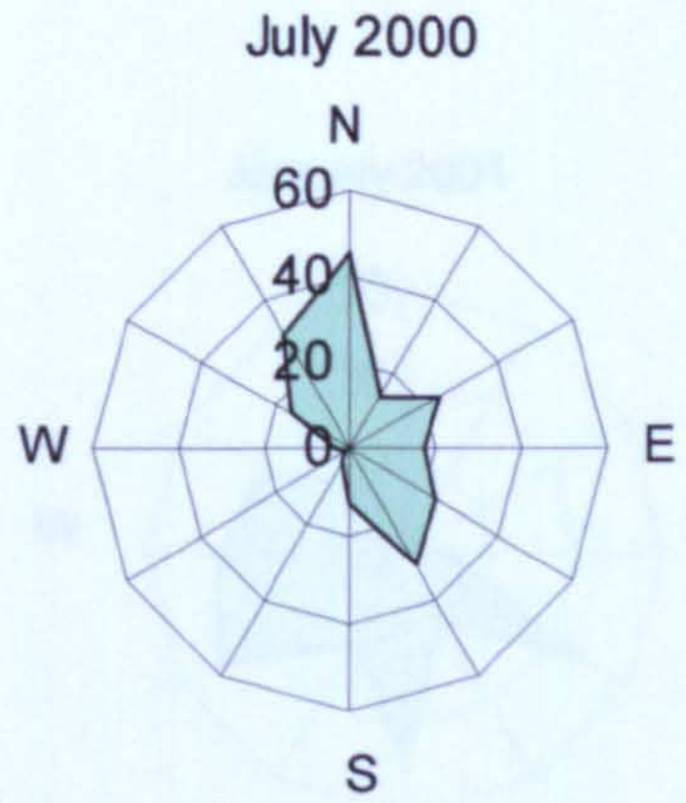

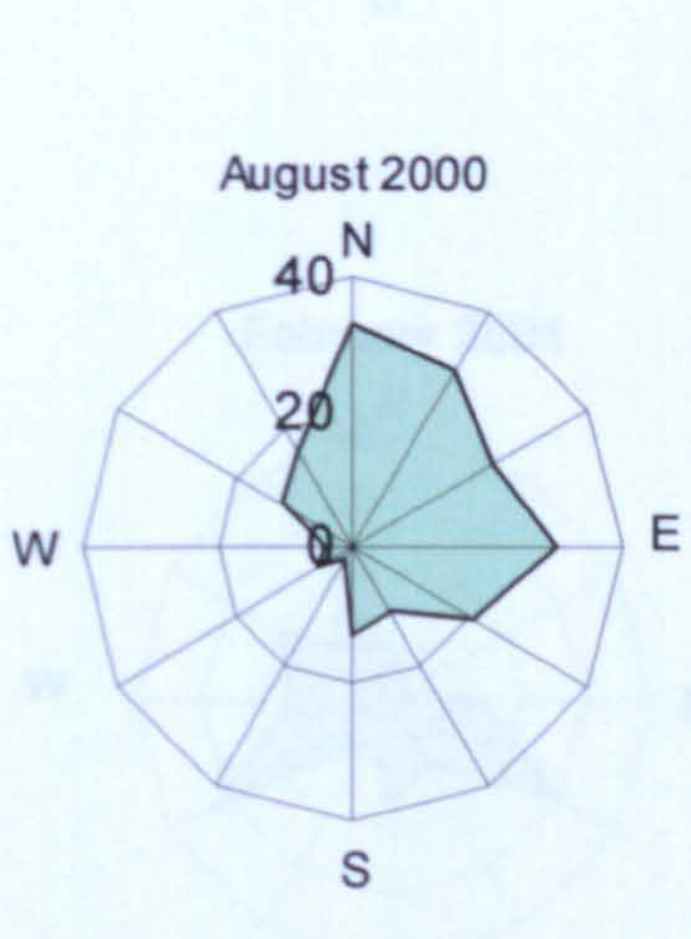

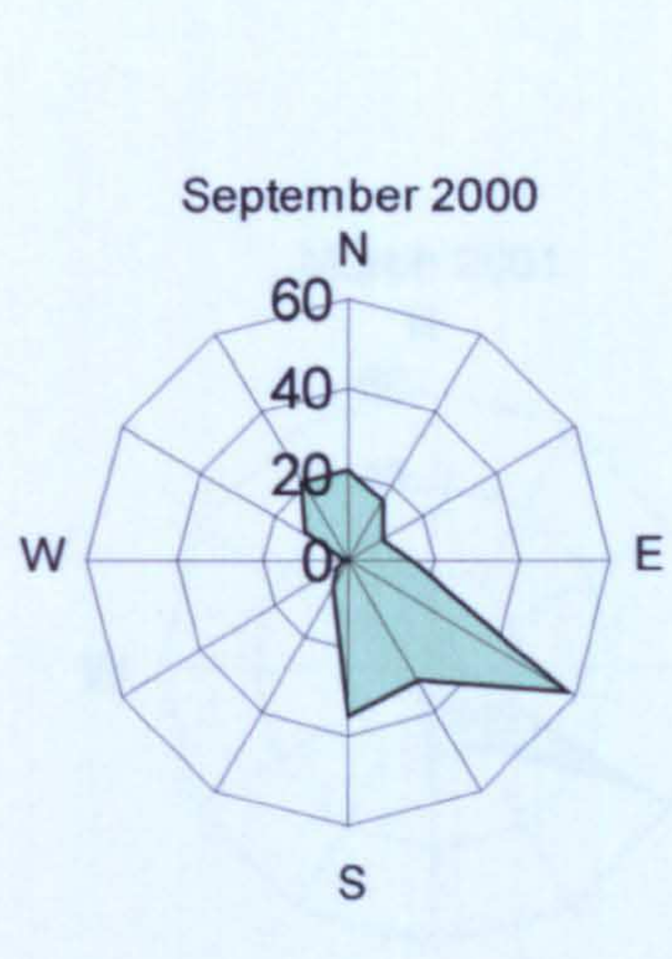

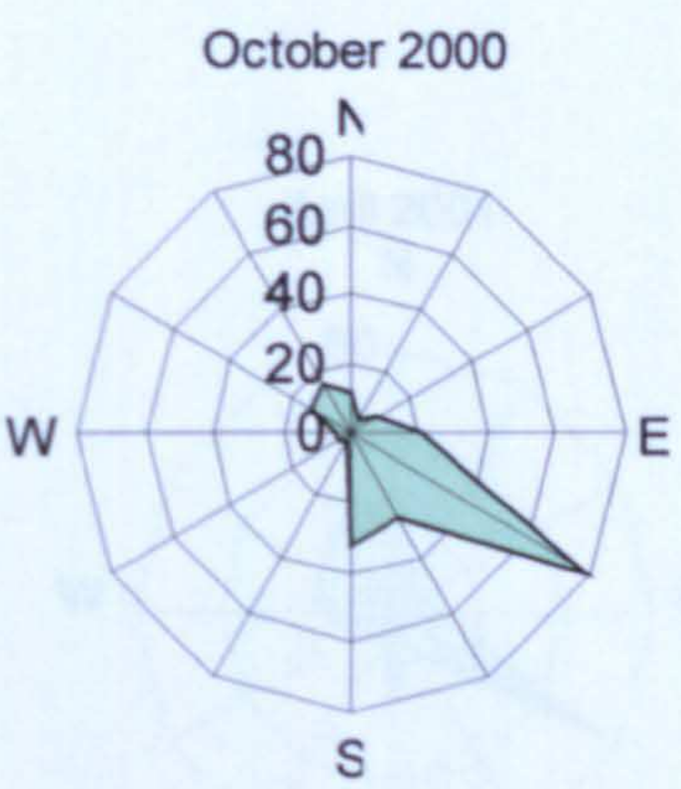

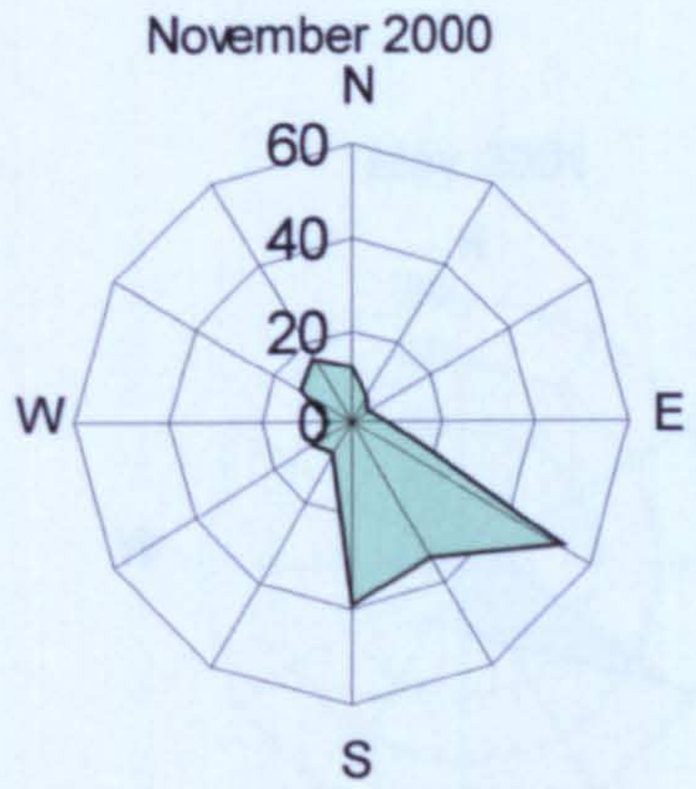

Figure I.2.9 Monthly prevailing wind directions and corresponding frequencies derived from Hun Station meteorological data. Wind roses represent all wind velocities.

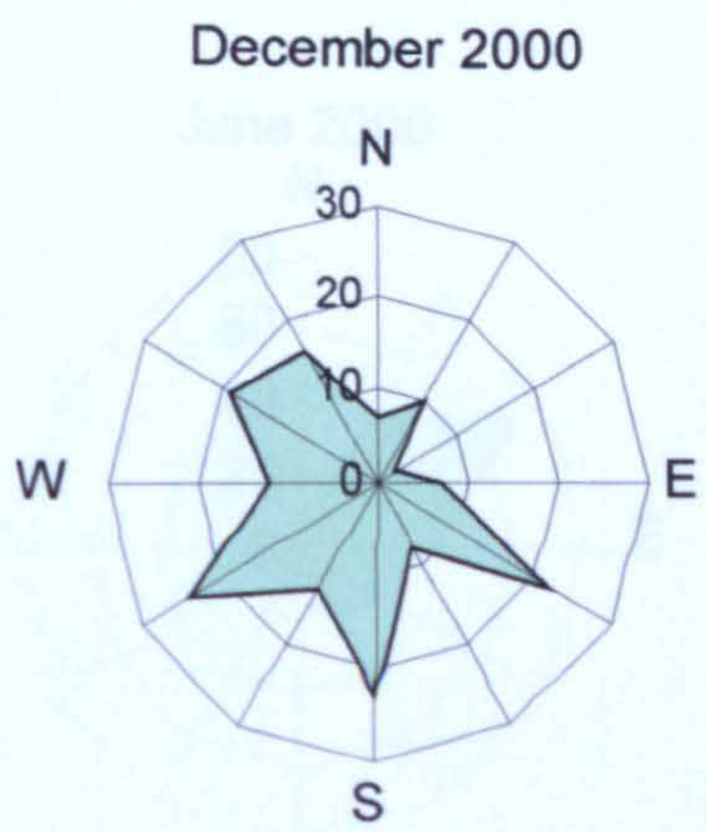

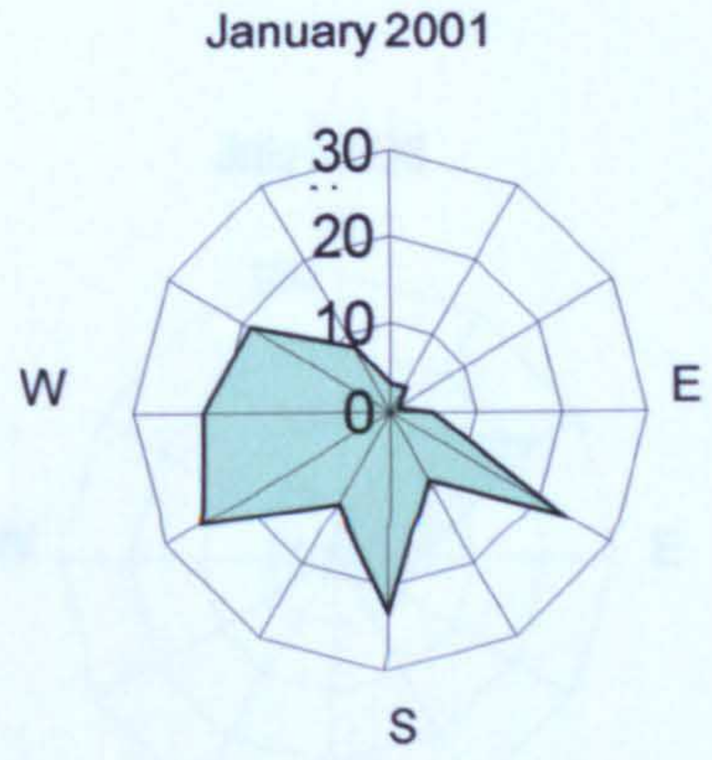

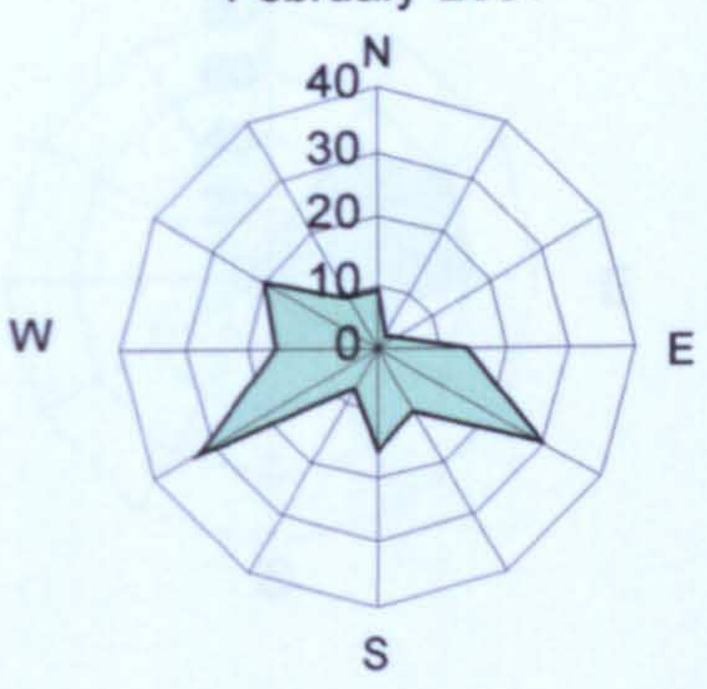

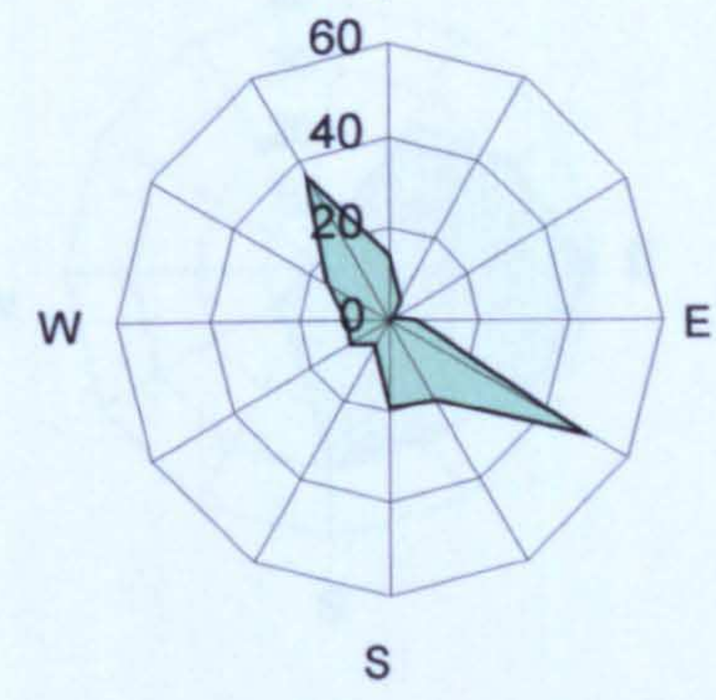

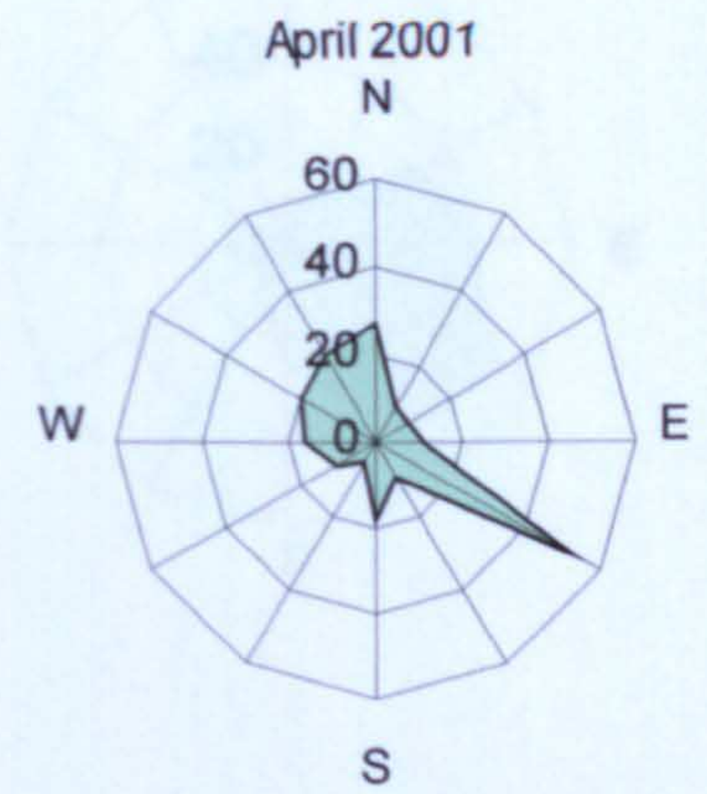

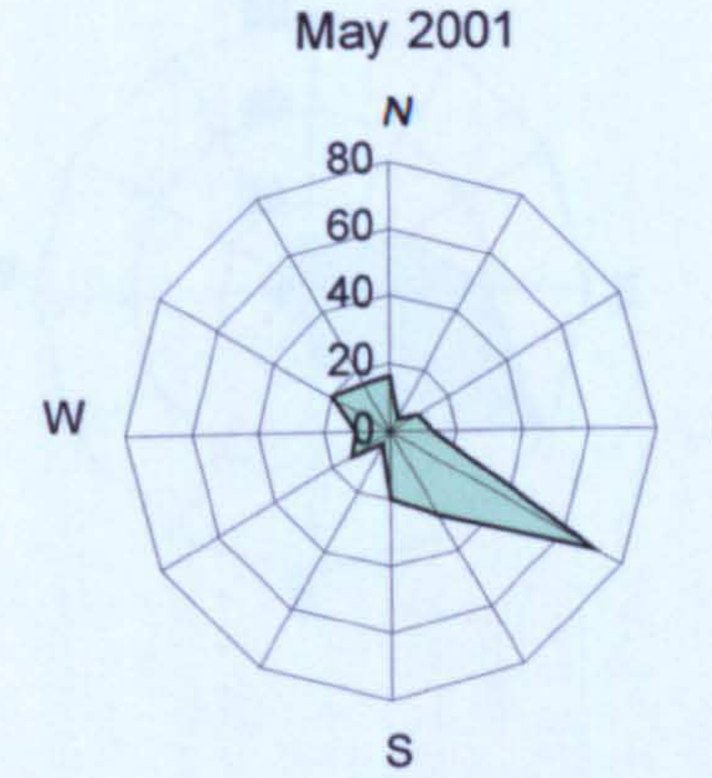

Figure I.2.10 Monthly prevailing wind directions and corresponding frequencies derived from Hun Station meteorological data. Wind roses represent all wind velocities.

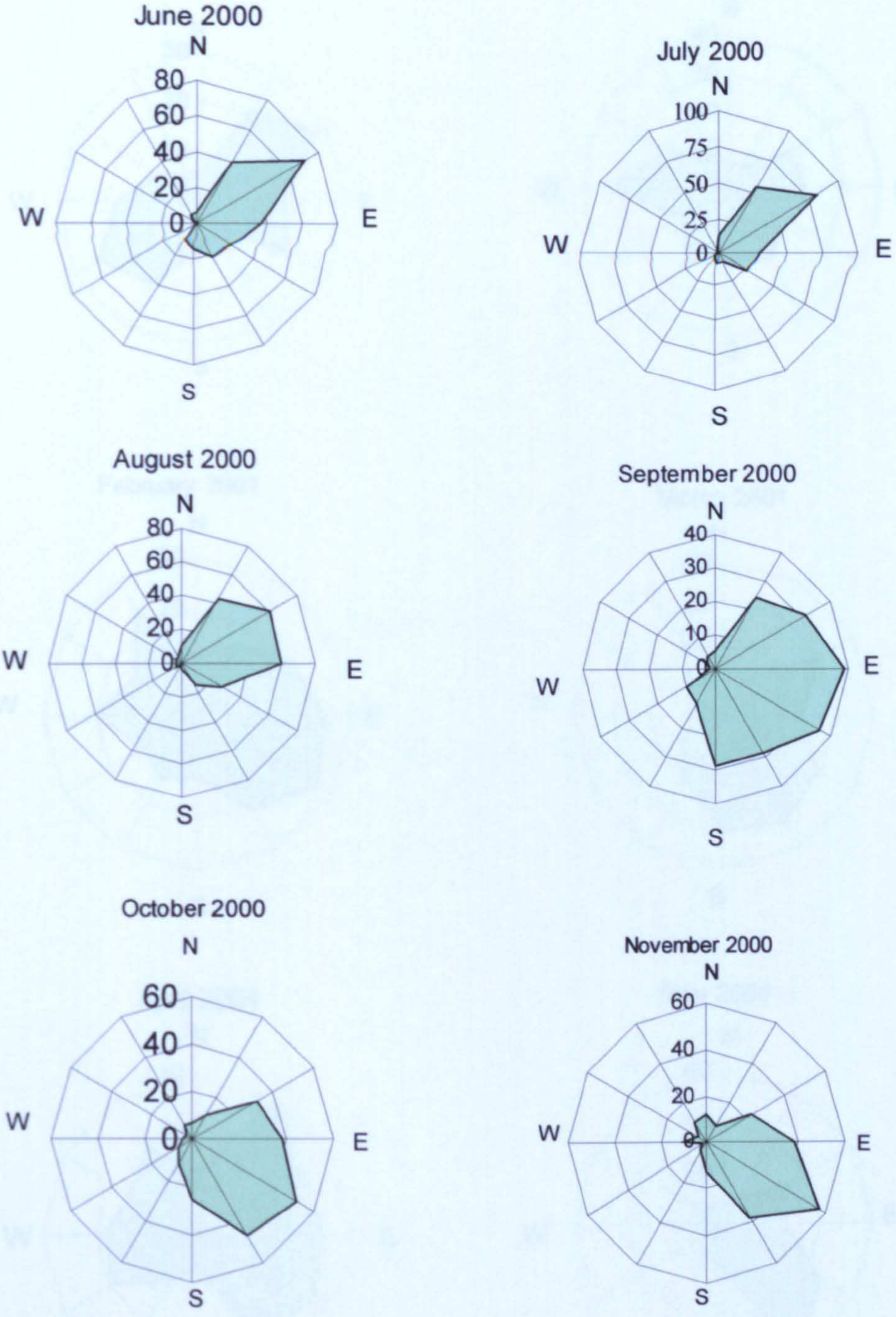

Figure I.2.11 Monthly prevailing wind directions and corresponding frequencies derived from Sebha Station meteorological data. Wind roses represent all wind velocities.

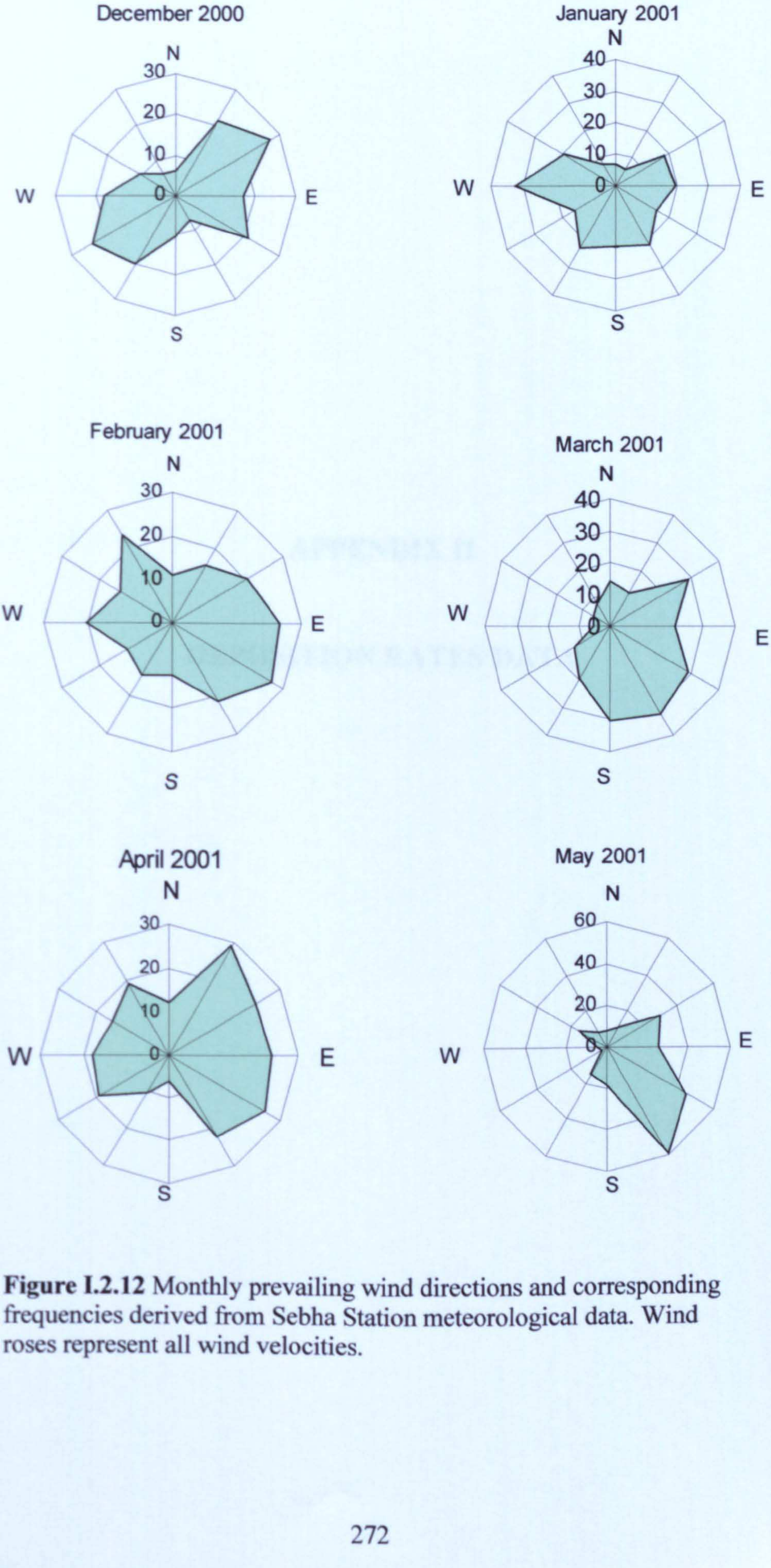

Figure I.2.12 Monthly prevailing wind directions and corresponding frequencies derived from Sebha Station meteorological data. Wind roses represent all wind velocities.

APPENDIX II

DEPOSITION RATES DATA

II.1. DEPOSITION RATES – NORTHERN REGION

II.1.1. Zuwarah area

Month	Total deposition (t/ha)	Vertical Flux (t/ha)	Horizontal Flux (t/ha)
Jun	0.08477707	0.061334854	0.023442216
Jul	0.164394904	0.137712461	0.026682444
Aug	0.144426752	0.125741425	0.018685327
Sep	0.037165605	0.030483304	0.006682301
Oct	0.021210191	0.020959168	0.000251023
Nov	0.127165605	0.092344483	0.034821122
Dec	0.022038217	0.020227887	0.001810329
Jan	0.095700637	0.084854511	0.010846126
Feb	0.028821656	0.026834824	0.001986832
Mar	0.249968153	0.212589415	0.037378738
Apr	0.330605096	0.171928271	0.158676825
May	0.087802548	0.048660453	0.039142095

Table II.1 Deposition data of site AA

Month	Total deposition (t/ha)	Vertical Flux (t/ha)	Horizontal Flux (t/ha)
Jun	0.354681529	0.087990812	0.266690716
Jul	0.394522293	0.115263239	0.279259054
Aug	0.273917197	0.060557614	0.213359583
Sep	0.187993631	0.055817377	0.132176254
Oct	0.09044586	0.054326215	0.036119645
Nov	0.058025478	0.041136582	0.016888896
Dec	0.118566879	0.071699052	0.046867827
Jan	0.070031847	0.04994705	0.020084798
Feb	0.855859873	0.351359577	0.504500296
Mar	Lost		
Apr	0.201528662	0.060525103	0.141003559
May	0.181369427	0.083319664	0.098049763

Table II.2 Deposition data of site AB

Month	Total deposition (t/ha)	Vertical Flux (t/ha)	Horizontal Flux (t/ha)
Jun	0.267898089	0.080443367	0.187454723
Jul	0.346847134	0.112200539	0.234646595
Aug	0.107993631	0.034129864	0.073863766
Sep	0.159171975	0.068781234	0.09039074
Oct	0.054299363	0.023450299	0.030849065
Nov	0.049076433	0.026656601	0.022419832
Dec	0.081210191	0.063020156	0.018190035
Jan	0.066146497	0.047799602	0.018346895
Feb	0.09589172	0.054619396	0.041272324
Mar	0.078089172	0.030223633	0.047865539
Apr	0.202420382	0.09437907	0.108041312
May	0.253726115	0.161511642	0.092214473

Table II.3 Deposition data of site AC

Month	Total deposition (t/ha)	Verticle Flux (t/ha)	Horizontal Flux (t/ha)
Jun	0.080923567	0.067666069	0.013257498
Jul	0.033949045	0.02757264	0.006376405
Aug	0.05433121	0.043886089	0.010445121
Sep	0.062006369	0.05519466	0.00681171
Oct	0.086719745	0.071768221	0.014951525
Nov	0.040477707	0.030624866	0.009852841
Dec	0.090254777	0.083348382	0.006906395
Jan	0.063280255	0.038822538	0.024457717
Feb	0.074745223	0.06508971	0.009655513
Mar	0.065987261	0.058758396	0.007228865
Apr	0.086210191	0.07343278	0.012777411
May	0.15544586	0.113244905	0.042200955

Table II.4 Deposition data of site AD

II.1.2. Tripoli area

Month	Total deposition (t/ha)	Verticle Flux (t/ha)	Horizontal Flux (t/ha)
Jun	0.105541401	0.064750958	0.040790443
Jul	0.142229299	0.080134547	0.062094752
Aug	0.227929936	0.133772488	0.094157449
Sep	0.113375796	0.057552933	0.055822863
Oct	0.033821656	0.020660364	0.013161292
Nov	0.352707006	0.131804351	0.220902655
Dec	0.275318471	0.191268698	0.084049774
Jan	0.475509554	0.152443608	0.323065946
Feb	0.126719745	0.065473723	0.061246023
Mar	0.080127389	0.043174392	0.036952997
Apr	0.709171975	0.373505277	0.335666697
May	0.336433121	0.220761796	0.115671325

Table II.5 Deposition data of site AF

Month	Total deposition (t/ha)	Verticle Flux (t/ha)	Horizontal Flux (t/ha)
Jun	0.890764331	0.243873459	0.646890873
Jul	0.370828025	0.147962644	0.222865381
Aug	0.153535032	0.075886378	0.077648653
Sep	0.182165605	0.099502497	0.082663108
Oct	0.213057325	0.070936371	0.142120954
Nov	0.04455414	0.032115872	0.012438268
Dec	0.095031847	0.076203472	0.018828375
Jan	0.159171975	0.065363971	0.093808003
Feb	0.159649682	0.076126077	0.083523605
Mar	0.356910828	0.112701732	0.244209096
Apr	0.301528662	0.178603297	0.122925366
May	0.183343949	0.118364653	0.064979296

Table II.6 Deposition data of site AE

II.1.3. Al Khums area

Month	Total deposition (t/ha)	Verticle Flux (t/ha)	Horizontal Flux (t/ha)
Jun	0.030127389	0.02175568	0.008371708
Jul	0.037515924	0.036330233	0.001185691
Aug	0.024649682	0.023308788	0.001340893
Sep	0.03611465	0.033492401	0.002622249
Oct	0.008821656	0.008706375	0.000115281
Nov	0.019267516	0.017855091	0.001412425
Dec	0.03633758	0.033950564	0.002387016
Jan	0.02044586	0.019460656	0.000985204
Feb	0.03522293	0.032882895	0.002340035
Mar	0.032834395	0.031527051	0.001307344
Apr	0.059872611	0.054112303	0.005760308
May	0.045541401	0.042352091	0.00318931

Table II.7 Deposition data of site CE

Month	Total deposition (t/ha)	Verticle Flux (t/ha)	Horizontal Flux (t/ha)
Jun	0.052707006	0.043034094	0.009672912
Jul	0.08133758	0.064455143	0.016882436
Aug	0.047929936	0.037721478	0.010208458
Sep	0.054649682	0.045280864	0.009368818
Oct	0.021242038	0.013980163	0.007261875
Nov	0.04888535	0.038257783	0.010627568
Dec	0.151401274	0.126067602	0.025333672
Jan	0.048407643	0.045410479	0.002997164
Feb	0.112388535	0.066970788	0.045417747
Mar	0.063025478	0.05494471	0.008080768
Apr	0.134299363	0.102504257	0.031795106
May	0.061178344	0.051644164	0.00953418

Table II.8 Deposition data of site CB

Month	Total deposition (t/ha)	Verticle Flux (t/ha)	Horizontal Flux (t/ha)
Jun	0.115605096	0.07679959	0.038805506
Jul	0.175191083	0.122889099	0.052301984
Aug	0.096910828	0.068657087	0.028253741
Sep	0.153375796	0.106723908	0.046651888
Oct	0.077611465	0.061432928	0.016178537
Nov	0.07566879	0.053157741	0.022511049
Dec	0.107866242	0.077894959	0.029971283
Jan	0.079363057	0.011190191	0.068172866
Feb	0.165414013	0.072396255	0.093017758
Mar	0.110700637	0.076835187	0.03386545
Apr	0.133184713	0.101275547	0.031909166
May	0.143471338	0.095876472	0.047594866

Table II.9 Deposition data of site CC

Month	Total deposition (t/ha)	Verticle Flux (t/ha)	Horizontal Flux (t/ha)
Jun	0.161974522	0.112942635	0.049031888
Jul	0.203312102	0.152856565	0.050455537
Aug	0.145254777	0.116552304	0.028702473
Sep	0.053280255	0.04151752	0.011762735
Oct	0.076974522	0.059639968	0.017334555
Nov	0.064745223	0.056268888	0.008476335
Dec	Unavailable		
Jan	Unavailable		
Feb	Unavailable		
Mar	Unavailable		
Apr	Unavailable		
May	Unavailable		

Table II.10 Deposition data of site BD

II.1.4. Misratah area

Month	Total deposition (t/ha)	Verticle Flux (t/ha)	Horizontal Flux (t/ha)
Jun	0.069076433	0.046631013	0.02244542
Jul	0.117133758	0.089548289	0.027585469
Aug	0.113980892	0.075991061	0.037989831
Sep	0.043853503	0.029247129	0.014606374
Oct	0.045923567	0.032234211	0.013689356
Nov	0.051528662	0.040828401	0.010700262
Dec	0.113535032	0.09947902	0.014056012
Jan	0.060987261	0.04809242	0.012894842
Feb	0.063630573	0.052031108	0.011599465
Mar	Lost	Lost	Lost
Apr	0.087993631	0.075343261	0.012650369
May	0.107165605	0.078728676	0.028436929

Table II.11 Deposition data of site BF

Month	Total deposition (t/ha)	Verticle Flux (t/ha)	Horizontal Flux (t/ha)
Jun	0.107165605	0.06398794	0.043177665
Jul	0.168630573	0.122182968	0.046447605
Aug	0.111305732	0.077584436	0.033721296
Sep	0.09589172	0.074831127	0.021060593
Oct	0.08156051	0.065988706	0.015571803
Nov	0.072388535	0.063358912	0.009029623
Dec	0.338184713	0.248598873	0.089585841
Jan	0.229745223	0.201076465	0.028668758
Feb	0.229745223	0.201076465	0.028668758
Mar	0.064936306	0.038596971	0.026339334
Apr	0.073471338	0.046662381	0.026808956
May	0.015573248	0.014518893	0.001054356

Table II.12 Deposition data of site BA

Month	Total deposition (t/ha)	Verticle Flux (t/ha)	Horizontal Flux (t/ha)
Jun	0.020987261	0.016209177	0.004778084
Jul	0.067547771	0.050813689	0.016734082
Aug	0.076273885	0.035587869	0.040686016
Sep	0.071178344	0.057484342	0.013694002
Oct	0.096050955	0.076863817	0.019187139
Nov	0.056624204	0.047950452	0.008673752
Dec	0.064617834	0.054345408	0.010272426
Jan	0.037356688	0.030795445	0.006561243
Feb	0.08455414	0.066039658	0.018514482
Mar	0.055828025	0.048511355	0.00731667
Apr	0.107133758	0.086495404	0.020638354
May	0.119585987	0.084355728	0.035230259

Table II.13 Deposition data of site CE

Month	Total deposition (t/ha)	Verticle Flux (t/ha)	Horizontal Flux (t/ha)
Jun	0.069585987	0.049983197	0.01960279
Jul	0.107101911	0.07621372	0.030888191
Aug	0.045	0.03047778	0.01452222
Sep	0.08388535	0.062883814	0.021001536
Oct	0.085700637	0.057398601	0.028302035
Nov	0.06133758	0.046904755	0.014432824
Dec	0.073471338	0.067092356	0.006378981
Jan	0.069968153	0.056516636	0.013451517
Feb	0.073216561	0.058048798	0.015167762
Mar	0.076082803	0.065627724	0.010455078
Apr	0.15410828	0.134124905	0.019983375
May	0.137101911	0.105335184	0.031766727

Table II.14 Deposition data of site DD

Month	Total deposition (t/ha)	Verticle Flux (t/ha)	Horizontal Flux (t/ha)
Jun	0.097070064	0.080808207	0.016261857
Jul	0.176847134	0.130172931	0.046674203
Aug	0.089267516	0.065104138	0.024163378
Sep	0.117388535	0.088598762	0.028789773
Oct	0.056910828	0.047346804	0.009564024
Nov	0.094267516	0.074412948	0.019854568
Dec	0.117070064	0.109483795	0.007586269
Jan	0.236942675	0.194072945	0.04286973
Feb	0.188598726	0.166185531	0.022413195
Mar	0.033503185	0.027033897	0.006469287
Apr	0.210031847	0.19388822	0.016143627
May	0.028694268	0.021446179	0.007248088

Table II.15 Deposition data of site DE

II.2. DEPOSITION RATES – CENTRAL REGION

Month	Total deposition (t/ha)	Verticle Flux (t/ha)	Horizontal Flux (t/ha)
Jun	0.061687898	0.03382403	0.027863868
Jul	0.117643312	0.097661478	0.019981834
Aug	0.110605096	0.085957414	0.024647682
Sep	0.252006369	0.220179981	0.031826388
Oct	Lost	Lost	Lost
Nov	0.034840764	0.025057094	0.00978367
Dec	0.182898089	0.169845567	0.013052522
Jan	0.185955414	0.169483855	0.016471559
Feb	0.18477707	0.171687278	0.013089792
Mar	0.195859873	0.181289465	0.014570408
Apr	0.189426752	0.173928461	0.015498291
May	0.150859873	0.132479558	0.018380314

Table II.16 Deposition data of site EA

Month	Total deposition (t/ha)	Vertical Flux (t/ha)	Horizontal Flux (t/ha)
Jun	0.375955414	0.170717594	0.20523782
Jul	0.636528662	0.445986417	0.190542245
Aug	0.155700637	0.041807334	0.113893303
Sep	0.341210191	0.21823292	0.122977271
Oct	0.467834395	0.360143128	0.107691267
Nov	0.098121019	0.028687446	0.069433573
Dec	0.090477707	0.083898014	0.006579693
Jan	0.210254777	0.191578644	0.018676133
Feb	0.195350318	0.180125945	0.015224373
Mar	0.203152866	0.188547922	0.014604944
Apr	Lost	Lost	Lost
May	1.299859000	1.008690000	0.291168000

Table II.17 Deposition data of site EB

Month	Total deposition (t/ha)	Vertical Flux (t/ha)	Horizontal Flux (t/ha)
Jun	0.121433121	0.063697416	0.057735705
Jul	0.24111465	0.118928451	0.122186199
Aug	0.11366242	0.069316672	0.044345748
Sep	0.142229299	0.033638083	0.108591217
Oct	0.085095541	0.049041326	0.036054215
Nov	0.17156051	0.031404838	0.140155672
Dec	0.111624204	0.107506387	0.004117817
Jan	Lost	Lost	Lost
Feb	0.112101911	0.101136315	0.010965596
Mar	0.089012739	0.075161493	0.013851246
Apr	Lost	Lost	Lost
May	0.175477707	0.15585386	0.019623847

Table II.18 Deposition data of site EC

Month	Total deposition (t/ha)	Verticle Flux (t/ha)	Horizontal Flux (t/ha)
Jun	0.370828025	0.1280929	0.242735126
Jul	0.268089172	0.093797163	0.174292009
Aug	0.169171975	0.061188996	0.107982979
Sep	0.197324841	0.086133674	0.111191166
Oct	0.305031847	0.11629391	0.188737937
Nov	0.125477707	0.063328222	0.062149485
Dec	0.125477707	0.086360785	0.039116922
Jan	0.513152866	0.24984592	0.263306946
Feb	0.103630573	0.056837701	0.046792872
Mar	0.476528662	0.145951199	0.330577464
Apr	1.078407643	0.296626806	0.781780837
May	0.48133758	0.157768018	0.323569561

Table II.19 Deposition data of site EF

II.3. DEPOSITION RATES – SOUTHERN REGION

Month	Total deposition (t/ha)	Verticle Flux (t/ha)	Horizontal Flux (t/ha)
Jun	0.046815287	0.031904711	0.014910575
Jul	0.054299363	0.03368701	0.020612353
Aug	0.036974522	0.02790763	0.009066892
Sep	0.051019108	0.038381063	0.012638045
Oct	0.041656051	0.033445602	0.008210449
Nov	0.02044586	0.016823385	0.003622475
Dec	0.068535032	0.056813965	0.011721067
Jan	0.033343949	0.029802001	0.003541948
Feb	0.037929936	0.031573941	0.006355995
Mar	0.085191083	0.056289096	0.028901986
Apr	0.104012739	0.095086137	0.008926602
May	0.117420382	0.069638389	0.047781994

Table II.20 Deposition data of site DF

Month	Total deposition (t/ha)	Verticle Flux (t/ha)	Horizontal Flux (t/ha)
Jun	0.041528662	0.028567575	0.012961087
Jul	0.049936306	0.03763989	0.012296416
Aug	0.039363057	0.028365373	0.010997684
Sep	0.050095541	0.035961134	0.014134407
Oct	0.037261146	0.020594236	0.016666911
Nov	0.013312102	0.009624445	0.003687657
Dec	0.064968153	0.041711503	0.02325665
Jan	0.035031847	0.029225802	0.005806045
Feb	0.044936306	0.037547294	0.007389012
Mar	0.033917197	0.028343924	0.005573274
Apr	0.110159236	0.107612817	0.002546419
May	0.147579618	0.096996114	0.050583504

Table II.21 Deposition data of site DC

Month	Total deposition (t/ha)	Verticle Flux (t/ha)	Horizontal Flux (t/ha)
Jun	0.044044586	0.031099133	0.012945453
Jul	0.057898089	0.039283159	0.01861493
Aug	0.078248408	0.037893075	0.040355333
Sep	0.050573248	0.034690467	0.015882782
Oct	0.045700637	0.036736868	0.008963769
Nov	0.011815287	0.010299492	0.001515795
Dec	0.051878981	0.044718281	0.0071607
Jan	0.035254777	0.031001852	0.004252925
Feb	0.056178344	0.048193323	0.007985021
Mar	0.064745223	0.045839987	0.018905236
Apr	0.150764331	0.133951952	0.016812379
May	0.087261146	0.070257352	0.017003794

Table II.22 Deposition data of site DA

Month	Total deposition (t/ha)	Verticle Flux (t/ha)	Horizontal Flux (t/ha)
Jun	0.053757962	0.0323802	0.021377762
Jul	0.060063694	0.030823335	0.02924036
Aug	0.046847134	0.025173776	0.021673358
Sep	0.066273885	0.040931686	0.025342199
Oct	0.071242038	0.046449182	0.024792856
Nov	0.01888535	0.012324712	0.006560639
Dec	0.002388535	0.002388535	0
Jan	0.038375796	0.030286677	0.008089119
Feb	0.036401274	0.02429978	0.012101494
Mar	0.083216561	0.035327128	0.047889433
Apr	0.182006369	0.178506387	0.003499982
May	0.077452229	0.060996729	0.016455501

Table II.23 Deposition data of site DB

Month	Total deposition (t/ha)	Verticle Flux (t/ha)	Horizontal Flux (t/ha)
Jun	0.068025478	0.047966322	0.020059156
Jul	0.120286624	0.061224701	0.059061923
Aug	0.14066879	0.072582409	0.068086381
Sep	0.074745223	0.050254876	0.024490347
Oct	0.075732484	0.04305316	0.032679324
Nov	0.075477707	0.04587369	0.029604017
Dec	0.041305732	0.030881777	0.010423956
Jan	0.053025478	0.033456955	0.019568522
Feb	0.11089172	0.056016287	0.054875433
Mar	0.109968153	0.047485482	0.062482671
Apr	0.157707006	0.136355528	0.021351478
May	0.181146497	0.105021493	0.076125004

Table II.24 Deposition data of site CF